FINAL COPY

Technical Report Documentation Page

1. Report No. FHWA/TX-05/0-1700-2	2. Government Accession No.	3. Recipient's Catalog No.:

4. Title and Subtitle Temperature Control During Construction to Improve the Long Term Performance of Portland Cement Concrete Pavements	5. Report Date May 2002
	6. Performing Organization Code
7. Author(s) Anton K. Schindler, Terry Dossey, and B. F. McCullough	8. Performing Organization Report No. 0-1700-2
9. Performing Organization Name and Address Center for Transportation Research The University of Texas at Austin 3208 Red River, Suite 200 Austin, TX 78705-2650	10. Work Unit No. (TRAIS)
	11. Contract or Grant No. Research Study 0-1700
12. Sponsoring Agency Name and Address Texas Department of Transportation Research and Technology Implementation Office P.O. Box 5080 Austin, TX 78763-5080	13. Type of Report and Period Covered: Technical Report, September 2001 through August 2004
	14. Sponsoring Agency Code

15. Supplementary Notes
Project conducted in cooperation with the Texas Department of Transportation and the Federal Highway Administration.

16. Abstract

The study developed mitigation techniques to control the in place temperature development of early-age concrete. Longer lasting PCC pavements will be produced if the assumptions made during design are achieved in the field. This study proposes a method to integrate the design assumptions to the construction process by means of an end-result temperature control specification.

A general hydration model for cementitious materials and a model to predict the temperature gain in hardening concrete is developed and calibrated. The temperature prediction model was calibrated for field conditions with data collected from seven concrete paving projects. The model accounts for different pavement thicknesses, mixture proportions, cement chemical composition, cement fineness, amount of cement, mineral admixtures, material types, climatic conditions, and different construction scenarios. The temperature prediction model will enable the development of performance based specifications to guard against premature concrete failures. This model will further provide the designer, contractor, and specification developer with the means to evaluate and quantify the effect of most of the various complex interactions that affect the concrete temperature development during early-ages.

A model to predict initial and final setting of hardening concrete is presented, and calibrated, with data collected under laboratory and field conditions. The effects of concrete temperature, different cements, and mineral admixtures on the initial and final times are characterized.

Finally, an innovative temperature control specification is presented, which encourages contractor innovation and focuses on material selection for the particular location and environmental conditions. This approach accounts for the impact of modern paving materials, and will ensure improved concrete performance under hot weather placement conditions.

17. Key Words PCC, Concrete Pavements, temperature control, hydration, performance-based specifications.	18. Distribution Statement No restrictions. This document is available to the public through the National Technical Information Service, Springfield, Virginia 22161; www.ntis.gov

19. Security Classif. (of report) Unclassified	20. Security Classif. (of this page) Unclassified	21. No. of pages 538	22. Price

Form DOT F 1700.7 (8-72) Reproduction of completed page authorized

TEMPERATURE CONTROL DURING CONSTRUCTION TO IMPROVE THE LONG TERM PERFORMANCE OF PORTLAND CEMENT CONCRETE PAVEMENTS

by

Anton K. Schindler
Terry Dossey
and
B. Frank McCullough

Research Report Number 0-1700-2

Research Project 0-1700
Improving Portland Cement Concrete Paving

Conducted for the

TEXAS DEPARTMENT OF TRANSPORTATION

in cooperation with the

Federal Highway Administration

by the

CENTER FOR TRANSPORTATION RESEARCH
Bureau of Engineering Research
THE UNIVERSITY OF TEXAS AT AUSTIN

May 2002

DISCLAIMERS

B. Frank McCullough , P.E. (Texas No. 19924)
Research Supervisor

ACKNOWLEDGEMENTS

The author would like to express their gratitude to the Texas Department of Transportation (TxDOT) for their support, without which this study would not have been possible. The assistance and guidance of George Lantz, the TxDOT project director is appreciated. The members of the project monitoring committee members have all provided valuable contributions to this project. These members included: Dr. Moon Won, Gray Graham, Gerald Lankes, Jim Hunt, David Head, Thomas Saenz, Dr. German Claros, Angela Batiz, Charles Gaskin, James Kosel, Susan Chu, Ned Finney (Jobe Concrete), Dennis Warren (ACPA), Gene Marter (ACPA), and Mark Brown (Zachary Construction).

Part of this study required laboratory and field work. Special thanks to the many individuals at the Construction Materials Research Group whom contributed. Without the help supplied by Mike Rung, Kerry Rothenbach, and Dave Figurski much of this work would not have been possible, and to those individuals we would like to extend our sincere gratitude. The contribution of the following individuals is appreciated: Dave Whitney, Sherian Williams, Cruz Carlos, Patricia "Pat" Campbell, Marie Martinez, Zeeshan Arshad, Moses Ogolla, Guy Dudley, Zack Pannier, and Oliver Salgado.

Research performed in cooperation with the Texas Department of Transportation and the
U.S. Department of Transportation, Federal Highway Administration.

Executive Summary

Findings from past research efforts have demonstrated that the concrete temperature development during the first 24 to 72 hours has a major impact on long-term pavement performance. The development of excessive portland cement concrete (PCC) temperatures may result in reduced pavement performance. These factors emphasize that concrete temperature control during construction in hot weather conditions is essential to improve the durability of PCC pavements.

The primary objective of this study is to develop mitigation techniques to control the in place temperature development of early-age concrete, as this will improve the performance of PCC pavements constructed under hot weather conditions. Longer lasting PCC pavements will be produced if the assumptions made during design are achieved in the field. This study proposes a method to integrate the design assumptions to the construction process by means of an end-result temperature control specification.

During this study, a general hydration model for cementitious materials and a model to predict the temperature gain in hardening concrete is developed and calibrated. The temperature prediction model was calibrated for field conditions with data collected from seven concrete paving projects. The model accounts for different pavement thicknesses, mixture proportions, cement chemical composition, cement fineness, amount of cement, mineral admixtures, material types, climatic conditions, and different construction scenarios. The temperature prediction model will enable the development of performance based specifications to guard against premature concrete failures. This model will further provide the designer, contractor, and specification developer with the means to evaluate and quantify the effect of most of the various complex interactions that affect the concrete temperature development during early-ages.

A model to predict initial and final setting of hardening concrete is presented, and calibrated, with data collected under laboratory and field conditions. The effects of concrete temperature, different cements, and mineral admixtures on the initial and final times are characterized.

Finally, an innovative temperature control specification is presented, which encourages contractor innovation and focuses on material selection for the particular location and environmental conditions. This approach accounts for the impact of modern paving materials, and will ensure improved concrete performance under hot weather placement conditions.

Table of Contents

List of Tables

List of Figures

Chapter 1

Introduction

The economy and way of life of the American public is dependent on the state of their transportation infrastructure and its ability to move people and goods in an efficient manner from one destination to another. The nearly 45,000 mile long interstate highway system was launched in 1956 and has been hailed as one of the greatest engineering public works projects of the past century (NAE, 2000). It is estimated that approximately 60% of the interstate system is built with portland cement concrete (PCC). Concrete commonly serves 20 to 30 years without needing major repair, while asphalt typically lasts only 8 to 12 years before resurfacing or significant repair is required (PCA, 2002). Many portions of the interstate have aged and currently require repair, replacement, and/or expansion.

Concrete pavements are constructed with an intended design life of twenty or more years; however, cases do occur where poor performance due to premature distresses reduces the pavement's intended design life. Examples of such distress and failures are shown in Figure 1-1. In many cases, major pavement repair activities are required within a short period (less than 5 years) after construction has been completed. Combined with the current high traffic volumes on highways, major congestion occurs during such rehabilitation and repair activities. The costs associated with these repairs are in some cases being included in the economic feasibility study as life cycle costs, in order to determine which type of pavement structure is appropriate for use (Wilde, 1999). This approach is considered most appropriate, since it reflects the return in investment the public receives from their tax dollars invested in their infrastructure.

Repairs to newly constructed pavements are currently being questioned by the ever-increasing awareness of the public. The stage has been reached where the influence and knowledge of the public has prompted various state transportation departments to investigate and develop means to improve pavement performance, and thus the design life of pavements.

In 1993, the SHRP-C-321 Study, “A Guide to Evaluating Thermal Effects in Concrete Pavements,” reported that the effects of temperature and moisture early in the life of concrete strongly influence early strength development and long-term durability. Research findings from the Center for Transportation Research (CTR) demonstrated that the concrete temperature development during the first 24 to 72 hours after placement has a major impact on long-term pavement performance (Hankins et al., 1991; Dossey et al., 1994; and McCullough et al., 1998). The HIPERPAV program sponsored by the Federal Highway Administration (FHWA) was specifically developed to address early-age concreting problems during fast-track concrete construction

(McCullough and Rasmussen, 1999). These findings emphasize that concrete temperature control during construction in hot weather conditions may be necessary to improve the long-term performance of PCC pavements.

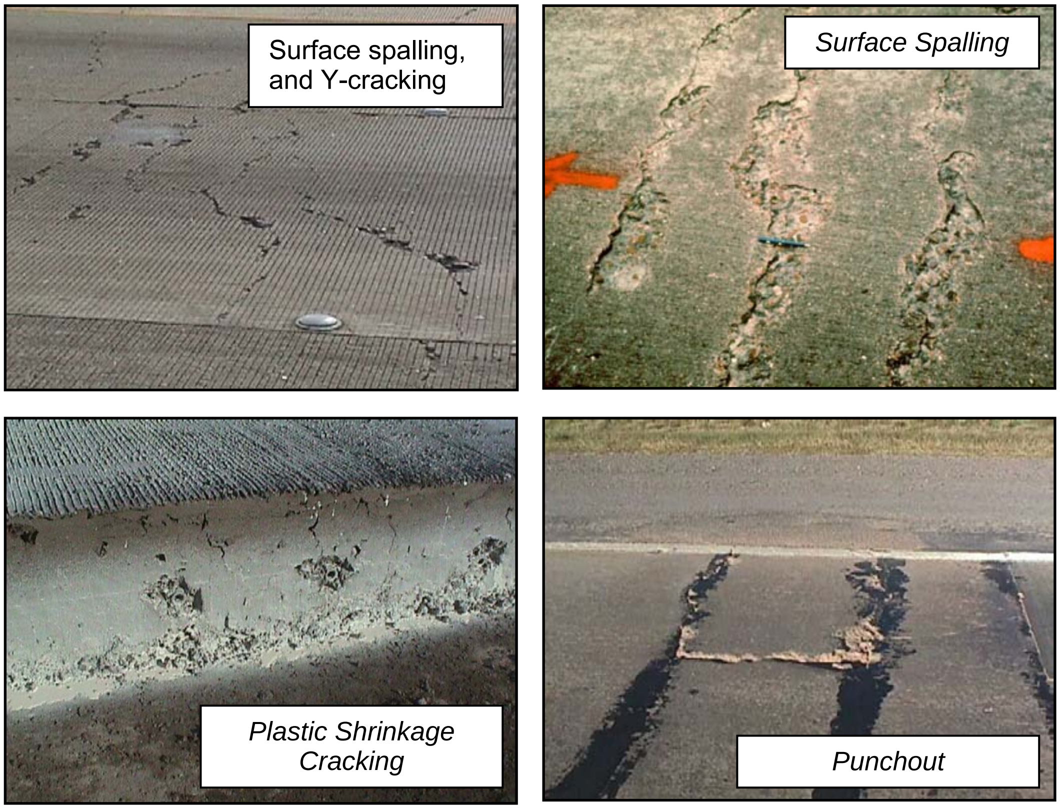

Figure 1-1: Distresses in portland cement concrete pavements

The overall goal of this study is to develop techniques for the concrete paving industry to mitigate against the detrimental long-term effects of high concrete temperatures that occur during early-ages. This Chapter provides background on the origin for the work undertaken during this study. The objectives and scope of the report is presented, along with the research approach taken to accomplish the goals of the study.

1.1 BACKGROUND

Continuously reinforced concrete (CRC) pavements are designed without transverse contraction joints, and transverse cracks are allowed to occur naturally. Under normal conditions, cracks tend to develop at intervals of 3 to 6 feet. The reinforcement content in CRC pavements range between 0.5 to 0.7% and it is designed to control the crack width and the spacing of cracks that develop over time. Figure 1-2 presents the reinforcement layout for a typical CRC pavement just prior to concrete placement. Figure 1-3 presents a typical concrete placement process, which has been shown to have a significant influence on the long-term pavement performance. In CRC pavements, the transverse crack spacing is one of the key indicators of the pavement's future performance, since cracks spaced below 3 feet frequently lead to punchouts and reduced performance (McCullough et al., 1998). Punchouts are the most detrimental CRC pavement distress, and an example of a punchout is shown in Figure 1-1.

Figure 1-2: Typical reinforcement layout of a CRC pavement prior to paving

Figure 1-3: A typical concrete placement process where a slipform paver is used

In Texas, the overwhelming choice of concrete pavement type is currently CRC pavements. Texas constructed its first experimental CRC pavement in Fort Worth in 1951 and has constructed more CRC pavements than any other state. Due to the high truck traffic volumes on Texas Interstates, 85% of the concrete paving that has been done on the interstate system has been CRC pavements. It is currently estimated that approximately 80% of the concrete paving projects that are contracted are CRC pavements. In 2001, the Dallas District placed about 544,000 cubic yards of concrete in pavements, at a cost of around 54.6 million dollars, of which the majority was CRC pavements. From 1993 through 2001, an annual average of about 419,000 tons of cement has been used in the Texas concrete paving industry.

TxDOT Research Project 3925 evaluated the primary variables that affect pavement performance based on 23 years of data collection and analysis undertaken in Texas (McCullough et al., 1998). These variables were ranked based on state-wide concrete pavement performance observations. It was concluded that the four most important variables affecting the performance of CRC pavements are (McCullough et al., 1998):

1. Aggregate type used in the concrete mixture,
2. Season in which construction occurs,
3. Concrete placement above ambient temperatures of 90°F (32.2°C), and
4. Prevailing evaporation rate that occurred during construction.

It was recommended that performance-based specifications for PCC pavements be developed to improve the overall level of PCC pavement performance in Texas. The items that should first be included in such a specification are those that address the control of the most significant variables listed previously. It was recommended that the following factors be included as special provisions to the PCC pavement construction specification (McCullough et al., 1998):

1. Control should be placed on the pavement for concrete placement with ambient air temperature greater than 90°F (32.2°C) to ensure this concrete does not develop excessive hydration temperatures.
2. The evaporation rate on every project should be monitored in real time and for use by the contractor to adjust the curing conditions of placed pavements to ensure a desirable set of conditions are realized.
3. The thermal coefficient of the portland cement concrete and, specifically, the coarse aggregate should be included in the specification so that various design levels (and in some instances crack control) may be established by the designer for various conditions experienced in the field.

In order to develop a performance-based specification, the agency has to be able to quantify the effect of different controllable and uncontrollable parameters on the pavement response and performance. For example, should one select a different type of cement, or use mineral admixtures in the cementitious system; the effect of these materials on the concrete temperature, and ultimately the concrete performance, need to be quantified. There are currently few tools available to the concrete industry to predict the in place concrete temperature. In 1996, the HIPERPAV program was developed in cooperation with the Federal Highway Administration (FHWA) (McCullough and Rasmussen, 1999). This program internally predicts the concrete temperature for use in stress and strength prediction, but does not provide the user with concrete temperatures. The effect of cement chemical composition, mineral admixtures, and different cement finenesses cannot be addressed with the current HIPERPAV program.

Thus, there is a critical need to develop a temperature prediction model that characterizes and quantifies the early-age temperature development in hardening concrete. This model may be used as a tool during specification development and as an aid during pre-construction planning to guard against the development of concrete temperatures that exceed the design conditions. However, once the in place concrete temperatures are predicted, the model has a number of applications during early ages and in the long-term. These applications could include the following:

1. ***Early-age and long-term pavement behavior:*** Fluctuations in temperature produce expansion and contraction movements in concrete pavements, which lead to the development of stresses that may significantly affect the pavement's long-term performance. This aspect will be covered in more detail in this report.
2. ***Strength prediction:*** Through the application of the maturity method (Carino, 1991), the strength development of in place concrete can be predicted from the calculated in place temperatures. Once the in place strength is predicted, it can be used among other applications to evaluate causes for distress, earliest sawcutting time, opening to traffic time, and risk of crack formation.
3. ***Risk of plastic shrinkage cracking:*** Calculation of the prevailing evaporation rate from a water surface is a function of concrete temperature, wind speed, air temperature, and relative humidity (ACI 305R, 2000). With the concrete temperature prediction model, the evaporation rate can be determined and mitigation measures to prevent plastic shrinkage cracking (shown in Figure 1-1) can be evaluated prior to the occurrence of undesirable conditions.
4. ***Temperature gradients:*** The thermal gradients at final set, in accordance with the definition provided by ASTM C 403, can be determined with the concrete temperature and hydration prediction model that is developed in this report. It has been reported that the initial thermal gradient at setting (built-in curling), plays a major role in the long-term performance of jointed concrete pavements (Yu et al., 1998). Measures can be evaluated to control the gradient at set, or even to design for the gradient that may develop under different conditions.

In concrete pavements, temperature and moisture changes cause volumetric changes to occur, which, depending on the amount of restraint, may lead to the development of stresses. In the following section, the development of thermal stresses is discussed. Thereafter, the effects of high concrete temperatures are presented.

1.1.1 Development of Thermal Stresses

The magnitude of the thermal stress (σ_T) is dependant on the magnitude of the temperature change (ΔT) the pavement is subjected to. For an accurate estimate of the thermal stresses, stress relaxation due to creep effects during early-ages and over the pavement life should be accounted for as shown in Equation 1-1 (Metha and Monteiro, 1991).

$$\sigma_T = \Delta T \cdot \alpha_c \cdot E_c \cdot K_r$$ *Equation 1-1*

where, ΔT = concrete temperature change (°C),

α_t = concrete coefficient of thermal expansion (strain/°C),

E_c = creep adjusted modulus of elasticity (Pa), and

K_r = degree of restraint factor.

Figure 1-4 presents the development of early-age concrete temperatures and thermal stresses over time, in a fully restrained specimen. The displayed temperature development is typical for concrete placed under hot weather field conditions. The concrete is plastic at placement and stresses do not start to develop until enough hydration products have formed to cause final setting, which occurs at time t_{fs}. The hydration of cement with water is exothermic in nature, and this causes the concrete temperature to increase beyond the setting temperature. The restrained expansion of the concrete caused by the temperature leads to the development of compressive stresses until the peak temperature ($\mathbf{T_{max}}$) is reached at time t_a. During this phase, the hydrating paste is still developing structure, the strength is low, and most of the early-age compressive stresses are relaxed (Springenschmid and Breitenbücher, 1991, Westman, 1999).

As a decline in concrete temperature starts to occur, the compressive stresses are relieved until the concrete temperature drops below the zero-stress temperature ($\mathbf{T_{zs}}$). This condition is reached at time t_{zs}, where the stress condition changes from compression to tension for the first time. The zero-stress temperature is generally significantly higher than the final-set temperature, due to the relaxation of early-age compressive stresses and the rapid gain in concrete stiffness during early-ages. If the temperature continues to decrease, additional tensile stresses will develop, and when these tensile stresses exceed the tensile strength, cracking will occur at time t_c. The effective temperature change that caused cracking is the difference between the zero-stress temperature and the temperature at cracking.

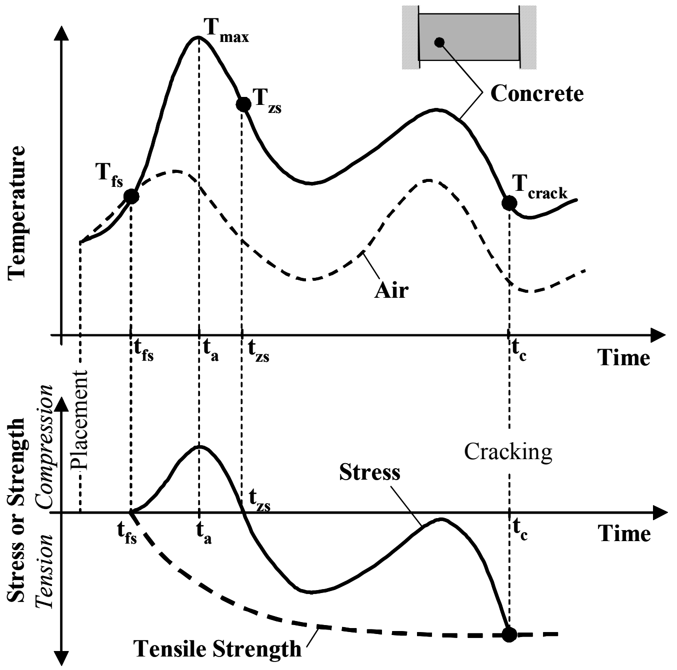

Figure 1-4: The development of early-age concrete thermal stresses and strength

The behavior of the concrete temperature development after placement is a complex problem. It is primarily affected by the temperature of the concrete at placement, the ambient temperature, the type and quantity of the cementitions materials, the solar radiation intensity, and the boundary conditions of the pavement. Figures 1-5 and 1-6 present temperatures measured on two different CRC paving projects in Dallas, Texas. Figure 1-5 presents the concrete temperatures for a pavement placed in **hot** weather conditions, since the average ambient temperature during the day of placement was above 30°C (86°F). This figure indicates that a rapid initial rise in temperature occurs due to the rapid heat generation in the concrete. This concrete mixture used five sacks of Type I cement with no mineral admixtures. The concrete was placed at a temperature of 32°C (90°F) and a maximum temperature of 62°C (143°F) occurred only 5.5 hours after placement.

Figure 1-6 presents the temperature rise for a section that was placed in weather conditions that is considered **normal** weather placement conditions, since the average ambient temperature during the day of placement was approximately 20°C (68°F). This concrete mixture used 5.5 sacks of a Type I cement with a 20% by volume replacement with Class F fly ash. The concrete was placed at a temperature of 22°C (72°F) and a maximum temperature of 39°C (102°F) occurred 7.5 hours after placement. The difference between the peak concrete temperatures was approximately 23°C (41°F) for the section placed under hot versus normal paving conditions.

The difference in temperature histories of the two CRC pavements, shown in Figures 1-5 and 1-6, will have a direct impact on the amount of thermal stress the pavement will be subjected to. The zero-stress temperature for the section placed under the hot weather conditions will be much higher than for the section cast under normal paving temperatures. To produce improved performance of concrete pavement placed all year around, sections constructed under high ambient temperature conditions require mitigation techniques to reduce the temperature development in the concrete.

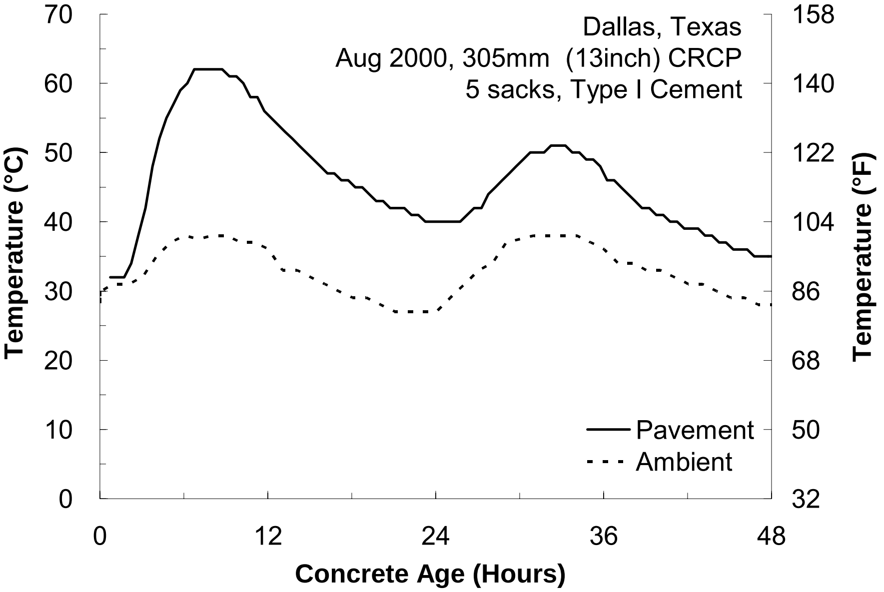

Figure 1-5: The development of concrete temperatures under hot temperature placement conditions (T_{air} > 30°C (86°F))

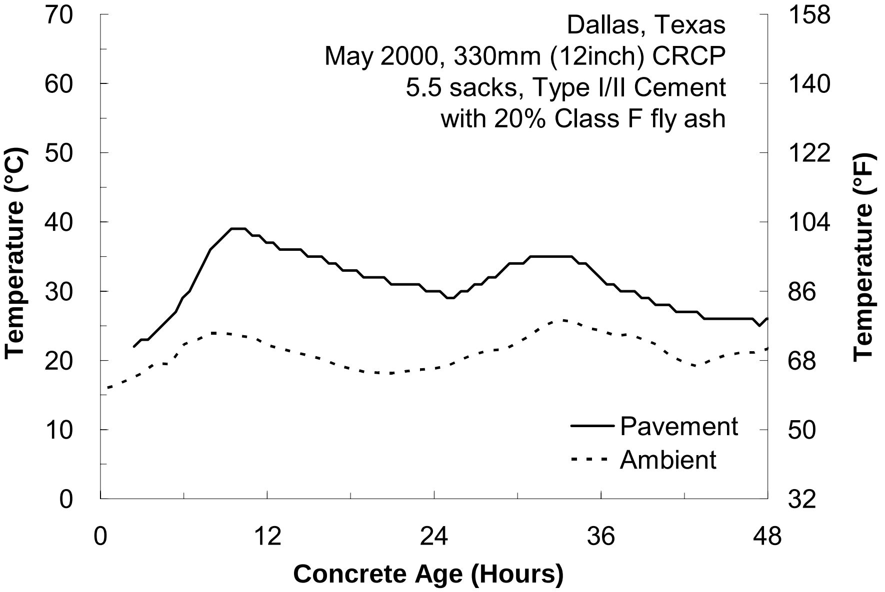

Figure 1-6: The development of concrete temperatures under normal temperature placement conditions (T_{air} < 25°C (77°F))

1.1.2 Effects of High Concrete Temperatures

In this section, the detrimental effects of high concrete temperatures on the long-term performance of concrete pavements will be introduced. The hydration of a concrete mixture is a process that liberates heat and the rate of heat generation is accelerated with an increase in concrete temperature. Concrete is a poor conductor of heat, and the rate of heat evolution due to the hydration process is, therefore, much greater than the rate of heat dissipation. Consequently, the temperature inside the concrete rises during early hydration stages. In this regard, Soroka (1993) elaborates by stating that: "It can be realized that this problem of thermal cracking is further aggravated by the accelerating effect of temperature on the rate of hydration. This effect results in a higher rate of heat evolution which, in turn, brings about a higher rise in concrete temperature."

As expressed in Equation 1-1, the magnitude of thermal stresses that develop in a restrained concrete pavement is proportional to the change in temperature it is subjected to during it design life. Higher concrete temperatures during hydration, therefore, produce higher thermal stress in the pavement. Through this mechanism, the concrete temperature at placement has a significant influence on the magnitude of the thermal stress the pavement is subjected to. This is confirmed by the SHRP-C-321 study (1993), which reported that the effects of temperature and moisture changes early in the life of concrete strongly influence early strength development and long-term durability.

The problems with high concrete temperatures are nationally recognized, and it is reported by ACI committee 305 (2000) that problems in hot weather conditions could be experienced in both fresh and hardened concrete. In the fresh state, problems with the use of chemical admixtures have been reported, since some chemicals become incompatible and are less effective at higher temperatures. ACI 305 (2000) further comments that:

> "Potential problems for concrete in the freshly mixed state are likely to include:
> - Increased water demand;
> - Increased rate of slump loss and corresponding tendency to add water at the job site;
> - Increased rate of setting, resulting in greater difficulty with handling, compacting, and finishing, and a greater risk of cold joints;
> - Increased tendency for plastic shrinkage cracking; and
> - Increased difficulty in controlling entrained air content."

> "Potential deficiencies to concrete in the hardened state may included:
> - Decreased 28-day and later strengths resulting from either higher water demand, higher concrete temperature, or both at time of placement or during the first several days;
> - Increased tendency for drying shrinkage and differential thermal cracking from either cooling of the overall structure, or from temperature differentials within the cross section of the member;
> - Decreased durability resulting from cracking;
> - Greater variability of surface appearance, such as cold joints or color difference, due to different rates of hydration or different water-cementitious material ratios (*w/cm*);
> - Increased potential for reinforcement corrosion – making possible the ingress of corrosive solutions; and

- Increased permeability as a result of high water content, inadequate curing, carbonation, lightweight aggregates, or improper matrix-aggregate proportions."

Two aspects caused by high concrete temperatures at placement that may have a significant impact on the behavior and long-term performance of concrete pavements are: (1) an increased rate of hydration, and (2) a decreased 28-day or long-term concrete strength. Due to their importance, both of these issues will be discussed in more detail.

Increased rate of hydration at high temperatures:

Samarai et al. (1975) reported that elevated temperatures in hot climates cause rapid setting. "The higher the curing temperature is, the faster are the reactions between cement and water, and consequently the shorter becomes the setting time." The reaction of cement with water is accelerated to such an extent, that there is a perceived increase in water demand (Mather, 1996). From Figure 1-7, one of the inherent problems associated with concrete placement under high temperature conditions is clearly identifiable. The heat of hydration increases rapidly above curing temperatures of around 25 to 30°C (77 to 86°F). It should be emphasized that this graph was developed through the studying of the hydration of C_3S, which is the major compound found in cement. For typical Type I cements in the United States, C_3S contributes about 54% of the cement particle composition (Gebhardt, 1995).

Concrete mixtures currently used in highway construction may contain mineral and/or chemical admixtures, which could significantly change the rate of the hydration and heat development. The effect of adding fly ash to a concrete mixture can be seen in Figure 1-8, which presents the rate of heat development for two different mixes tested by isothermal calorimetry (Ma et al., 1994). The vertical axis of Figure 1-8 presents the rate of heat development in terms of milliwatts per gram (mW/gram). Note that the mixture with Type I cement (Figure 1-8a) reached a rate of heat evolution of around 20 mW/gram at a mixing temperature of 55°C (131°F). The mixture with 17% Type F fly ash replacement (Figure 1-8b) only reached a rate of heat evolution of around 13 mW/gram. This indicated for this case that the use of fly ash significantly reduces the rate of heat development.

Experimental results have shown that a change in initial mixture temperature significantly affects the rate of heat development (Komonen and Penttala, 1997; ACI 207, 1995). The higher the fresh concrete temperature becomes the higher and more rapid the rate of hydration. In fact, Komonen and Penttala (1997) concluded that the "…mixing temperature was the most significant variable. The higher the mixing temperature was the earlier the heat gain took place."

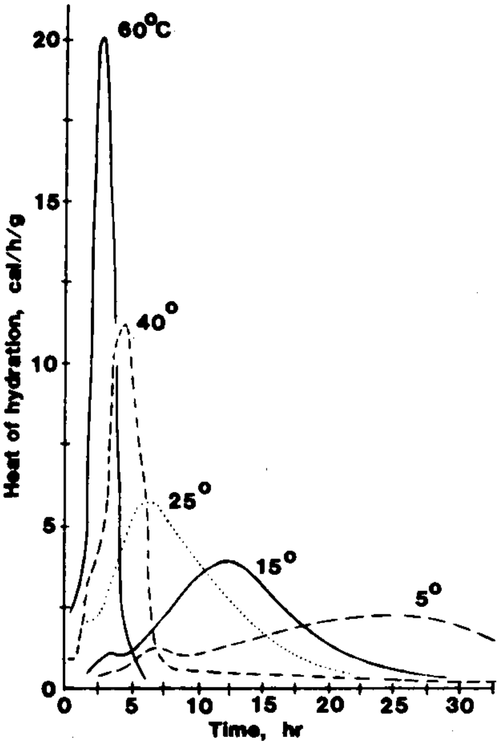

Figure 1-7: Heat of hydration for Tricalcium Silicate (C_3S) under different curing temperatures (Samarai et al., 1975)

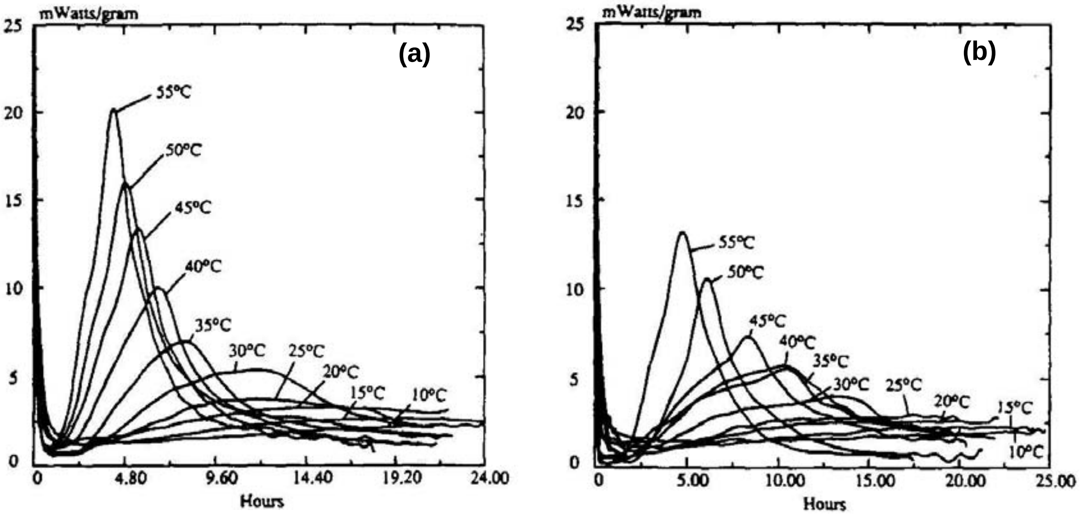

Figure 1-8: Heat of hydration: (a) Type I Cement, (b) Type I Cement with 17% Class F Fly Ash (Ma et al., 1994: Reprinted, with permission, copyrighted ASTM International.)

The higher the initial rate of hydration becomes the higher the development of in place concrete temperatures. In Section 1.1.1, it was shown that this directly affects the magnitude of thermal stresses the pavement is subjected to over its design life. The increased rate of hydration at high temperatures, therefore, subjects the pavement to higher thermal stresses. If the thermal stresses exceed those used during the initial design, the long-term performance and pavement life may not be as intended during its design.

Concrete strength as affected by high curing temperatures:

Concrete mixed, placed, and cured at elevated temperatures normally develops higher **early** strengths, than concrete produced and cured at lower temperatures. However, at 28 days and later, strengths are generally lower (Neville, 1996; Emborg, 1989; USBR, 1995). Data are available which indicate that low placement temperatures followed by normal curing will lead to higher concrete strengths as compared to concrete placed at high temperatures (Verbeck, and Helmuth, 1968). Furthermore, high curing temperatures will lead to a reduced later-age concrete strength, as compared to samples cured at lower temperatures. Figure 1-9 is an example of the effect of curing temperatures on the development of concrete strength. This figure presents the result of specimens cured at different isothermal temperatures and a long-term strength loss of about 12% as compared to curing at room (20°C) temperatures.

Verbeck and Helmuth (1968) presented an explanation for the reduced long-term strength for concretes cured at high temperatures. They suggested that a higher initial temperature results in more than a proportional increase in the initial rate of hydration. Therefore, during the early stage of curing, when there is rapid strength development, the strength of concrete cured at the higher temperature is greater than that of concrete cured at the lower temperature. However, with rapid hydration, hydration products do not have time to become uniformly distributed within the pores of the hardening paste. In addition, "shells" made up of low permeability hydration products build up around the cement grains. The non-uniform distribution of hydration products leads to more large pores, which reduce strength, and the shell impedes hydration of the unreacted portion of the grains at later ages. This theory was later validated by means of backscattered electron imaging, which provides a direct means of examining the uniformity of distribution of hydration products (Kjellsen et al, 1991). It was found that "…the sample hydrated at 50°C had dense hydration shells surrounding the cement grains …", and that an increased curing temperature resulted in an increased porosity.

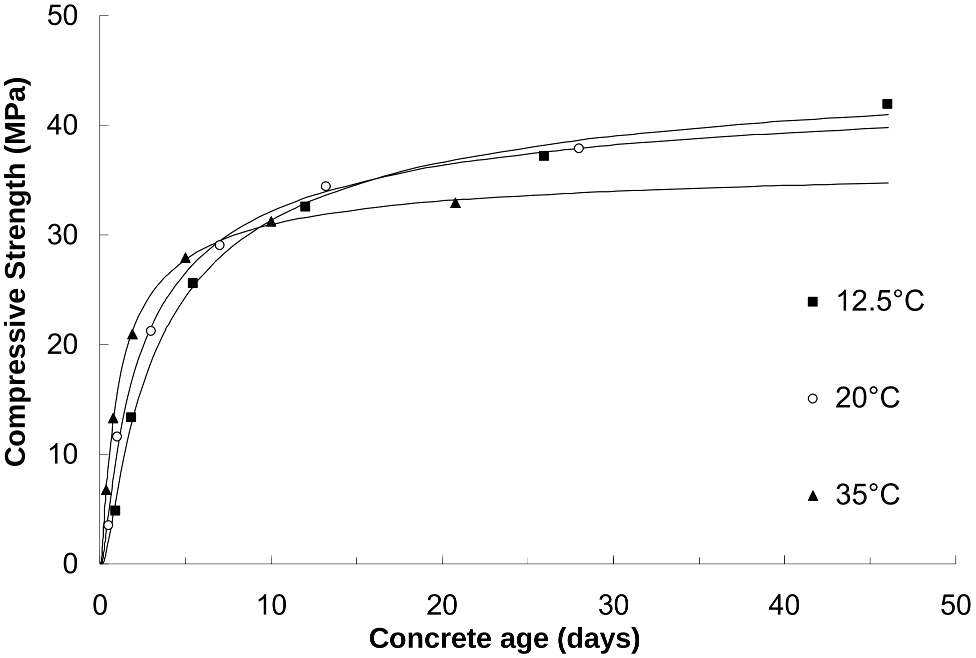

Figure 1-9: Compressive strength development for mortar (Carino, 1981)

Irrespective of the cause of strength loss associated with concrete placed at high temperatures, this strength loss will directly affect long-term pavement performance. Concrete pavements are designed for fatigue failures by ensuring that enough pavement depth is provided to keep the stress to strength ratio to an acceptable level. When the long-term strength of the concrete is reduced, the capacity of the pavement to withstand the intended fatigue life is reduced and the pavements performance is decreased.

Figure 1-10 schematically summarizes the primary reasons that contribute to reduced pavement life, when high concrete temperatures are experienced in actual pavements. If one combines the effect of the increased thermal stress development associated with the high concrete temperatures, and the lower long-term strength, it may be understood why some sections constructed during hot weather conditions may exhibit poor performance.

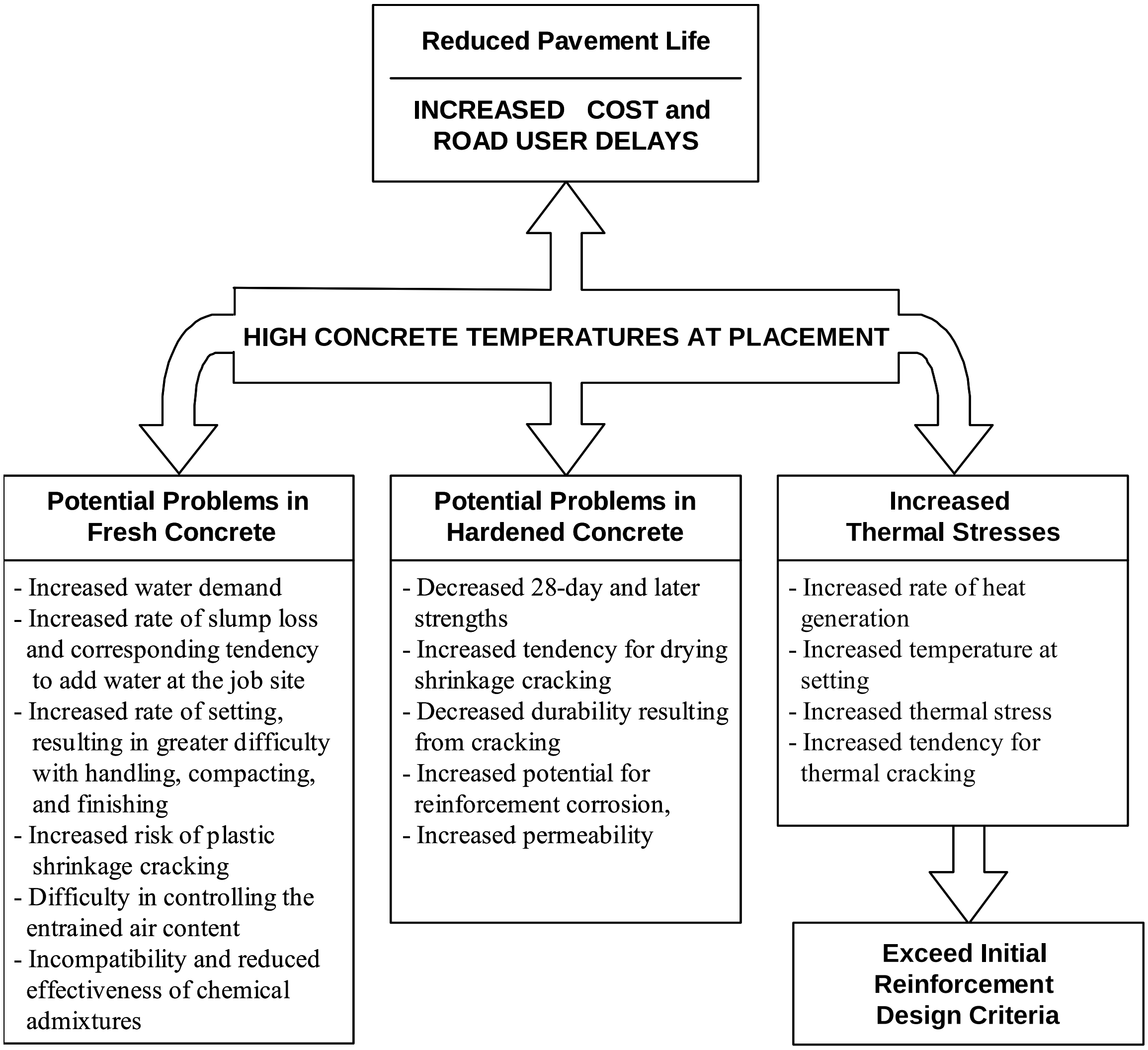

Figure 1-10: Impact of high concrete temperatures

1.2 RESEARCH APPROACH

The focus of this work is to develop procedures to improve the long-term performance of concrete pavements, especially when constructed under hot weather conditions. This section outlines the research undertaken during the course of this study. In this section, the objectives of this study, the significance of the work, and the research plan for this study are presented.

1.2.1 Study Objectives

The primary objective of this study is to develop procedures to improve the long-term performance of concrete pavements, especially when constructed under hot weather conditions. In order to achieve the primary objective, several secondary objectives were required during this study. These secondary objectives are as follows:

1. Quantify the effects of mineral admixtures on the heat of hydration of concrete,
2. Develop a procedure to quantify the early-age temperature development of PCC pavements constructed under field conditions. Account for:
    - ambient conditions,
    - cement chemistry,
    - the use of mineral admixtures,
    - concrete temperature at placement,
    - subbase conditions, and
    - curing method.
3. Quantify the effect of curing temperature on concrete hydration, setting, and early-age stress development,
4. Quantify the relationship between the concrete development of early-age concrete temperatures and thermal stresses, and
5. Recommend procedures to ensure improved long-term performance of PCC pavements when constructed under hot weather conditions.

1.2.2 Research Significance

The importance of temperature control has been realized for many years. Even back in the 1930s, great attention was paid during the selection of the most appropriate materials and construction practices to construct the Hoover Dam (Blanks et al., 1938). ACI 305 states that in general types of construction in hot weather, "… it is impractical to recommend a maximum limiting ambient or concrete temperature because circumstances vary widely. A limit that would serve a specific case might be unsatisfactory in others." The report by the ACI committee concludes on this subject that "…at some temperature between about 70 F and 100 F (24 and 38 C) there is a limit that will be found to be most favorable for best results in each hot weather operation, and such a limit should be determined for the work."

Most states specify a maximum concrete temperature at placement, and the limit remains the same irrespective of the type of mineral or chemical admixtures used. In modern paving operations, the use of mineral admixtures has become common practice, and under certain conditions, these admixtures could mitigate some of the problems associated with hot weather placement. The specification of a concrete placement temperature limit to prevent these problems might be applicable to some conditions, but unnecessary in others.

The recommendation and models from this study will directly be applicable to help the concrete industry to construct longer lasting concrete pavements under hot weather conditions. The key element of this research strategy involves the development of a temperature prediction program to characterize and quantify the early-age temperature development of hardening concrete. This study will provide a means to quantify the most appropriate limit of ambient or fresh concrete temperature. It will further provide the means to select the most appropriate materials and construction practices to ensure good performance. The proposed approach will encourage contractor innovation and the use of improved materials.

1.2.3 Research Strategy

The temperature prediction program developed in this study will allow pavement designers and contractors to quantify and evaluate the effect of various controllable and uncontrollable parameters on the in place temperature development. In order to ensure that the program accurately predicts the in place concrete temperatures, the program will be calibrated based on the following two stages of experimental data collection:

1. ***Materials characterization phase:*** The objective of this stage was to determine what effect a change in mixture proportion has on the heat of hydration development. During this phase, a standard cement source was chosen, and then mineral admixtures used with the cement were changed. By using different replacement levels of fly ash and ground granulated blast furnace slag, the effect of these materials on the hydration of the total cementitious system was evaluated. General hydration models were developed to account for the effect of cement chemical composition, cement fineness, mineral admixtures (fly ash, and ground granular blast furnace slag), mixture proportions, and concrete properties.
2. ***Field work phase:*** The objective of this phase was to collect data from actual paving projects to use during the calibration of the temperature prediction program. Seven projects were instrumented across the state of Texas. In place concrete temperatures were measured, along with all the necessary variables required for the temperature prediction phase. Raw materials and mixture proportions were collected from each project.

In order to investigate the hydration characteristics of typical Texas paving mixtures, different concrete paving mixtures were tested by semi-adiabatic calorimeter testing. A database of test results and all the known variables was developed for these mixtures, which was then evaluated to characterize the hydration of different cementitious systems.

The overall research strategy is schematically outlined in Figure 1-11. The approach will involve the development of an end-result type specification, which limits the maximum in place concrete temperature of the hydrating concrete. The specified values should be based on the amount of reinforcement provided in the section, the project location, and the type of coarse aggregate used in the concrete mixture. This practice would thus link the design conditions to the actual construction conditions experienced on site. The temperature prediction program functions as a tool for contractors and designers to evaluate and compare different options that might lower the in place concrete temperature.

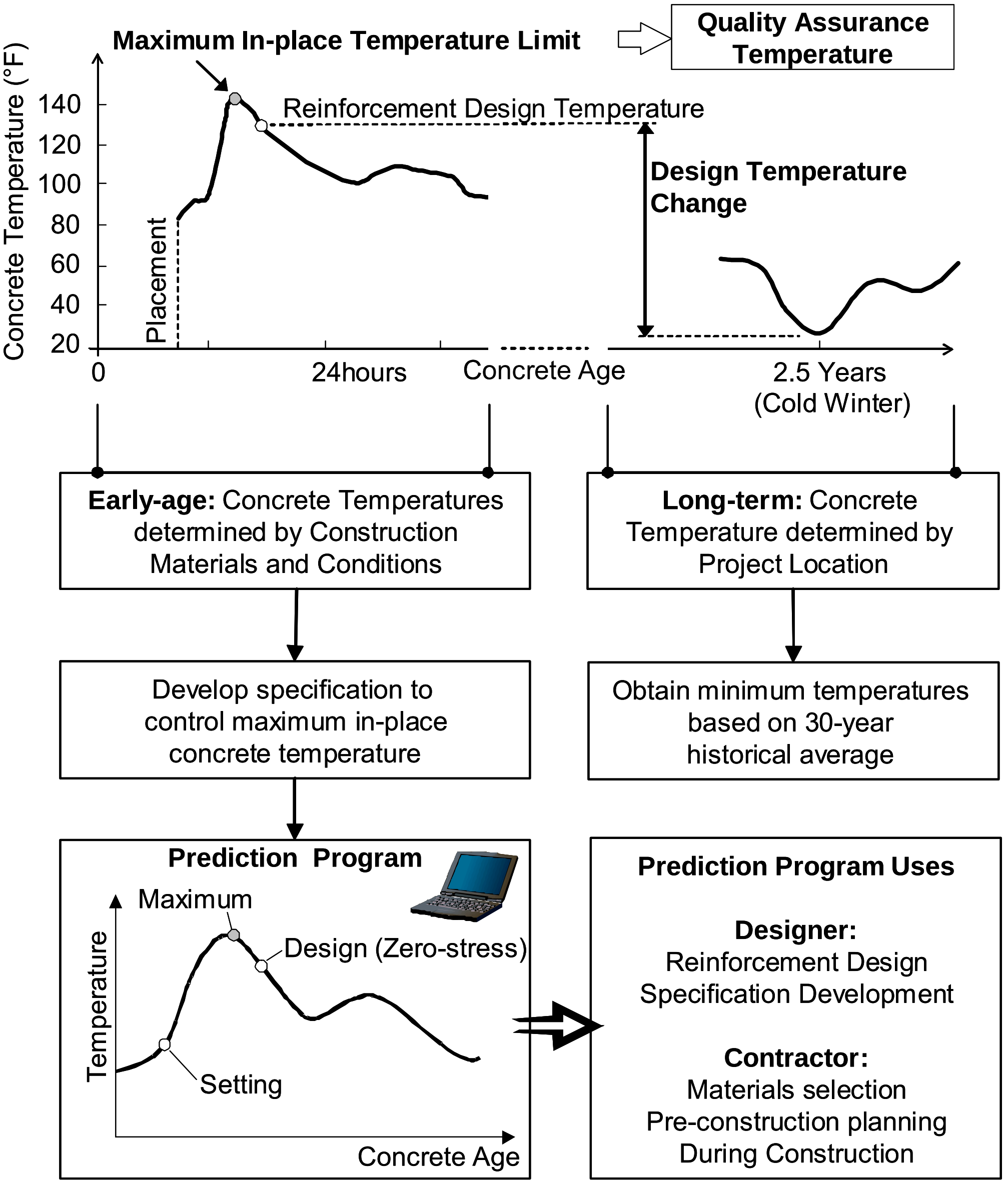

Figure 1-11: Overview of research strategy

This approach will allow contractor innovation during the selection of the mixture constituents and their proportions. The contractor will now be able to consider and optimize the cost of cooling the mixture versus the use of mineral and/or chemical admixtures during hot weather placement conditions. Furthermore, the contractor is in the position to schedule the paving activity at different times of the day, and this may influence the development of concrete temperatures.

Due to the advances in modern technology, inexpensive devices are currently available to monitor the temperature of the in place concrete. It is recommended that the use of such devices, installed at specified intervals, be considered for quality assurance purposes in a concrete temperature control specification.

1.3 REPORT SCOPE AND OUTLINE

This scope of the report is to document the information relevant to the work undertaken during the development of the procedure to produce long life pavements even when constructed under hot weather paving conditions. Early-age thermal cracking may affect the long-term performance of concrete pavements. Early-age cracking can be controlled by procedures that asses the risk of cracking by comparing the early-age strength gain and stress development (McCullough and Rasmussen, 1999; Bernander, 1998). The scope of this study is limited to the control of long-term thermal stresses, which can be achieved by ensuring that the design temperature change is not exceeded. Although many of the models developed during this study predict early-age behavior, the control of early-age thermal cracking is beyond the scope of this study

For quick reference purposes, Figure 1-12 graphically presents a chart of the basic elements and scope of this report. Chapter 2 contains a literature review, which serves to provide the necessary background and terminology on concrete technology. The chemical composition and hydration process of different cementitious systems will be reviewed. The factors that influence concrete hydration and the development of concrete temperatures will also be reviewed. This section will further provide a summary of current construction practices to mitigate the detrimental effects of high concrete temperatures.

Chapter 3 provides a review of different algorithms to model the concrete hydration, temperature development, heat transfer, setting and mechanical properties at early-ages. Various models will be evaluated and reasons for the selection of the recommended models are provided. A key element of the temperature prediction model is the heat transfer to the environment. The heat transfer mechanisms of thermal conduction, convection (including evaporative cooling), solar radiation, and irradiation are reviewed and mathematical models to quantify their effect on the in place concrete are developed. Due to the constantly changing cement hydration and environmental effects, the heat transfer problem is transient in nature, and solutions to this problem are introduced.

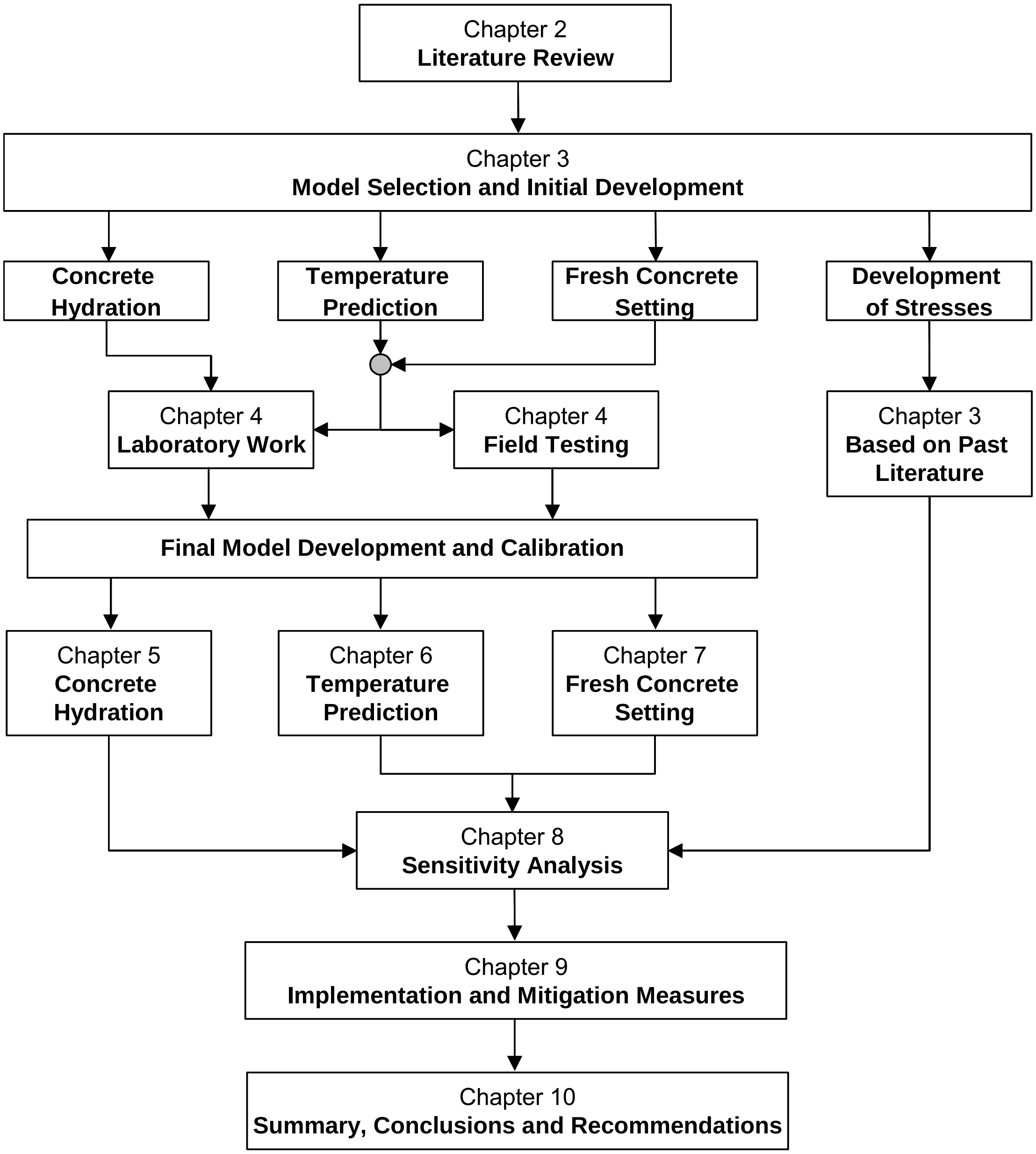

Figure 1-12: Report layout and structure of contents

Chapter 4 summarizes the information collected during the field testing phase of this study. The materials information for the different paving mixtures are all presented. In this Chapter, the detail of the laboratory work under taken is described. All the test procedures are listed and the design of the experimental program is documented.

The final development and calibration of general hydration models are covered in Chapter 5. The effect of temperature on the rate of hydration is defined by means of the equivalent age maturity method. With this method, the temperature sensitivity of the mixture is defined by the activation energy. A model is proposed to determine the activation energy of different cementitious systems. Both the development of the temperature sensitivity and generic hydration models are based on a multivariate regression analysis approach. In each case, the goodness of fit and the sensitivity of the proposed models are presented.

Chapter 6 describes in detail the final model selection and calibration of the temperature prediction model. The model is first calibrated under controlled laboratory conditions and then further with the data collected during the field testing phase. The accuracy of the temperature prediction is assessed.

Chapter 7 provides the data analysis and models developed to predict the initial and final setting times of the in place concrete. The model is calibrated based on the laboratory results and validated against the field measured setting times.

In order to determine which parameters should be controlled and added to the computer based temperature prediction program, a sensitivity analysis was performed for each of the parameters in the models. The results of the sensitivity analyses are presented in Chapter 8. Recommendations are made about the variables that need to be included in the temperature prediction program.

The proposed mitigation approach was briefly discussed in this Chapter since it provides the reader with the necessary direction for this study. However, Chapter 9 will discuss the proposed mitigation measures in more detail. Based on the work documented in this report, a computer based application is developed to assist with the calculation involved with the heat transfer process and the computation of early-age stresses. Chapter 9 closes with the proposed temperature control specification, and a proposed special provision to the current TxDOT construction specification is supplied.

Finally, Chapter 10 provides a summary of the work undertaken, overall conclusions of this study and recommendations are offered for future research. Several appendices are included at the end of the report, which contain most of the experimental data, miscellaneous graphs, and statistical analysis results obtained during the model development stages.

Chapter 2

Literature Review

In Chapter 1, it was shown that the development of high concrete temperatures could cause a number of effects that may be detrimental to long-term concrete performance. High concrete temperatures increase the rate of hydration, thermal stresses, the tendency for drying shrinkage cracking, permeability, and decrease long-term concrete strengths, and durability because of cracking. Current practices to prevent hot weather concreting problems will be reviewed in this chapter.

The hydration reaction of cement is an exothermic process, in which heat is liberated during the reaction of the cement with water. Based on work performed at Luleå University of Technology in Sweden, Emborg (1989) stated that the balance between the heat generation in the concrete and heat transfer to the environment is influenced by the following factors:

- the heat of hydration of the cement (i.e. type and amount of cement)
- the possible use of cement replacement material
- the thermal characteristics of the concrete (transmissivity and specific heat)
- the fresh concrete placement temperature
- the size of the structure
- the boundary conditions of the studied body, formwork and insulation, ambient temperature and wind.

The factors cited above indicate that there are many variables and interaction to consider when the concrete temperature is to be predicted. This chapter contains a literature review, which serves to provide the necessary background in concrete technology, and presents the chemical composition and hydration process of different cementitious systems. The factors that influence concrete hydration and the temperature development are evaluated based on results obtained in previous research efforts. This chapter further covers current measures used to guard against the problems associated with hot weather concreting. This state-of-the-art review will not be limited to paving applications, since applications such as bridges and mass concrete construction is covered.

The results of previous studies have been incorporated wherever appropriate to substantiate facts, findings, or conclusions made throughout this review. Many of the effects cited in this document have been repeated; as redundant as this may seem, the repetition is necessary to emphasize the effect they could have on the development of concrete temperatures at early-ages.

2.1 BACKGROUND ON CEMENTITIOUS MATERIALS COMPOSITION AND HYDRATION

The chemical composition and type of cementitious materials affect the heat released during hydration. General models to characterize the hydration development of cement based materials will, therefore, be developed during this study. An understanding of the hydration process and the basic constituents of cement is an essential pre-requisite for this study. The composition and hydration of cement and other cementitious materials (mineral admixtures) will, therefore, be reviewed in this section.

2.1.1 Cement Composition

The process of cement manufacturing can be simplified by stating that cement is produced through the chemical interaction of limestone (calcium) and clay (silica) materials at temperatures of 2550 to 2900°F to form primarily calcium silicates (Mindess and Young, 1981). After the burning process, a clinker is obtained, which is ground to a fine powder to produce cement. During the grinding process, gypsum (or other sources of sulfates) is added to the process to control the early reaction of the cement.

Portland cement primarily consists of various calcium compounds, but its chemical composition is normally reported in terms of oxides. This practice is followed since the chemical composition of cement can routinely be determined, whereas the determination of the compounds is complex and requires expensive equipment and well trained staff. The chemical composition of cement is traditionally written in an oxide notation, which gives rise to a universally accepted shorthand notation listed in Table 2-1. The use of this shorthand is adopted throughout this report.

Table 2-1: Typical oxide composition of portland cement (Mindess and Young, 1981)

Oxide	Shorthand Notation	Common Name	Typical Weight Percent
CaO	C	Lime	63
SiO_2	S	Silica	22
Al_2O_3	A	Alumina	6
Fe_2O_3	F	Ferric oxide	2.5
MgO	M	Magnesia	2.6
K_2O	K	Alkalies[a]	0.6
Na_2O	N		0.3
SO_3	$\bar{S}$	Sulfur trioxide	2.0
H_2O	H	Water	-

Note: [a] The two alkalies are normally combined into an equivalent alkali content.
Equivalent Alkalies = $Na_2O + 0.658K_2O$ (ASTM C 150, 2000)

The individual oxides can be combined into principle compounds, which can be used to characterize the hydration and behavior of the cement. By using the oxides determined from routine tests, the compound composition can be determined by Bogue calculations (Bogue, 1947). The compounds typically found in cement and their shorthand are presented in Table 2-2. The behavior of cement can be modified by changing the compound composition and fineness of the cement. The degree of hydration development during the hydration for each of the cement compounds are shown in Figure 2-1.

Table 2-2: Typical compound composition of portland cement (Bogue, 1947)

Chemical Name	Chemical Formula	Shorthand Notation
Tricalcium silicate	$3CaO \cdot SiO_2$	C_3S
Dicalcium silicate	$2CaO \cdot SiO_2$	C_2S
Tricalcium aluminate	$3CaO \cdot Al2O_3$	C_3A
Tetracalcium Aluminoferrite	$4CaO \cdot Al_2O_3 \cdot Fe2O_3$	C_4AF
Calcium sulfate dihydrate (Gypsum)	$CaSO_4 \cdot 2H_2O$	$C\bar{S}H_2$

From Figure 2-1, it may be seen that C_3A and C_3S contribute the most to the early-age hydration, whereas C_2S reacts much more slowly. It was mentioned earlier that gypsum is added to the grinding process, and its effect can clearly be seen in Figure 2-1. The presence of gypsum slows the early hydration of C_3A, which prevents flash set and allows the cement to be workable long enough for proper placement. The amount of gypsum is thus expected to influence the hydration process.

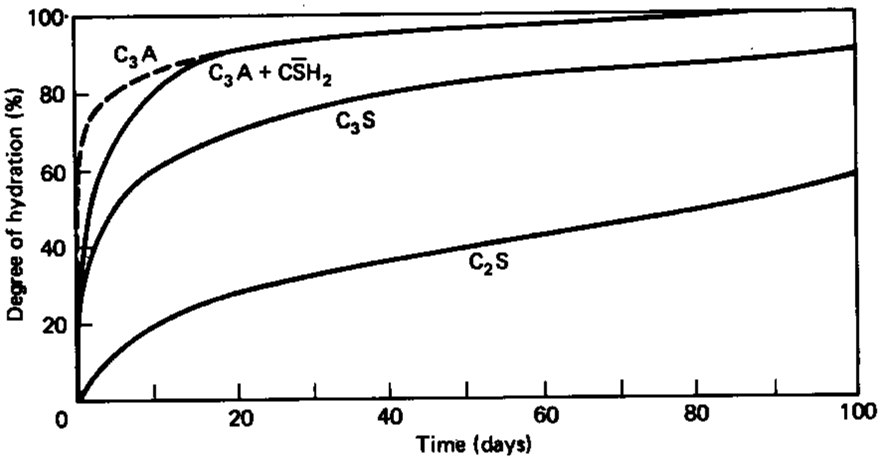

Figure 2-1: Degree of hydration development for the different cement compounds (Mindess and Young, 1981: Reprinted by permission of Pearson Education, Inc.)

In this study, the cement types commonly used in the paving industry will be considered. ASTM C 150 (2000), “Standard Specification for Portland Cement”, is the governing specification in the United States to designate different cement types. ASTM C 150 classifies portland cement into five primary classes.

ASTM Type I portland cement is the most common cement used in the concrete industry, is widely available, and is the least expensive of the five classes. ASTM Type II cements are for use when moderate sulfate resistance or moderate heat of hydration is desired. If a more rapid rate of hardening is desired for applications that require high early-age strength, or concreting at low temperatures is expected, Type III cement can be used. Cement Type III can be manufactured by increasing the C_3S content, but it is common practice is to grind the cement particles finer. By grinding the cement particles finer, the surface area is increased, which increases the rate of hydration and results in more rapid strength development. However, since this increases the rate of hydration, it produces more heat during the very early stages of hydration.

Thermal cracking was a frequent problem during the construction of earlier dams, and this problem was addressed by the development of ASTM Type IV cement, which produces low heat of hydration. However, Type IV cement is not commonly used today and is generally not commercially available. Type V cement is for use when high sulfate resistance is desired as it has a limit on the maximum amount of C_3A. The standard chemical and physical requirements for the different cement types are listed in Tables 2-3 and 2-4.

Table 2-3: Relevant ASTM C 150 (2000) chemical requirements for different cement types

Chemical Compound	**Cement Type**				
	I	**II**	**III**	**IV**	**V**
SiO_2 (Min,%)	-	20	-	-	-
Al_2O_3 (Max, %)	-	6	-	-	-
Fe_2O_3 (Max, %)	-	6	-	6.5	-
MgO (Max, %)	6	6	6	6	6
SO_3 (Max %) when:					
C_3A is 8% or less	3		3	2.3	2.3
C_3A is more than 8%	3.5	-	0.75	-	-
C_3S (Max, %)	-	-	-	35	-
C_2S (Min, %)	-	-	-	40	-
C_3A (Max, %)	-	8	15	-	5
C_4AF + 2(C3A), (Max, %)	-	-	-	-	25

In 1994, the Portland Cement Association gathered cement characteristics from all 108 U.S. cement manufacturing plants (Gebhardt, 1995). The ranges of potential compound composition for different cement types are shown in Table 2-5. During this study, the composition of cements used in Texas was determined based on the cement certificates from 1999 to 2000. The ranges of potential compound composition for different cements in Texas are shown in Table 2-6.

Table 2-4: Relevant ASTM C 150 (2000) physical requirements for different cement types

Requirement	Cement Type				
	I	II	III	IV	V
Fineness, Specific surface (m^2/kg)					
- Turbidimeter test, (Min)	160	160	160	160	160
- Air permeability test, (Min)	280	280	280	280	280
Time of setting: Gillmore test:					
- Initial set, not less than	60 min	60 min	60 min	60 min	60 min
- Final set, not more than	600 min	600 min	600 min	600 min	600 min
Time of Setting, Vicat test:					
- Time of setting, not less than	45 min	45 min	45 min	45 min	45 min
- Time of setting, not more than	375 min	375 min	375 min	375 min	375 min

Table 2-5: Range of compound composition of North American Cements (Gebhardt, 1995)

Cement Type	C_3S	C_2S	C_3A	C_4AF	Blaine Fineness (m^2/kg)
I (Min – Max)	40 – 63	9 – 31	6 – 14	5 – 13	300-421
(Mean)	54	18	10	8	369
II (Min – Max)	37 – 68	6 – 32	2 – 8	7 – 15	318-480
(Mean)	55	19	6	11	337
III (Min – Max)	46 –71	4 – 27	0 – 13	4 – 14	390-644
(Mean)	55	17	9	8	548
V (Min – Max)	43 – 70	11 – 31	0 – 5	10 – 19	275-430
(Mean)	54	22	4	13	373

Table 2-6: Range of compound composition of Texas cement between 1999-2000

Cement Type	C_3S	C_2S	C_3A	C_4AF	SO_3	Blaine Fineness (m^2/kg)
I (Min – Max)	57 – 65	9.3 – 18	8 – 12.6	5.5 – 10.3	2.6 – 3.5	347-504
(Mean)	62.2	13.5	9.9	7.5	3.0	380
II (Min – Max)	55 – 69	6.3– 19.0	3.5 – 6.3	9.0 – 12.0	1.9 – 3.5	333-398
(Mean)	60.2	13.0	6.1	10.9	2.7	372
III (Min – Max)	53 –64	11 – 16	5 – 13	7 – 12	3.4 – 4.4	492-537
(Mean)	59.5	13.2	8.9	9.8	3.9	523

Calcium silicates (C_3S and C_2S) account for 72-76% of a portland cement and are responsible for its cementitious qualities. From Tables 2-5 and 2-6, it may be seen that on average the compound composition for the different cement types are very similar. The largest difference between different cement types is the cement fineness, and the C_3A content. The C_3A content for Type II cements are under 8%, since this is required by ASTM C 150 (see Table 2-3). Comparisons of the Blaine values indicate that the Type III cement is considerably finer than any other cement type. According to Table 2-5, the Blaine index of Type III cements is on average 48% finer than that of a Type I cement. From Table 2-6, note that the SO_3 (sulfates) content increases along with the reactivity level of the cement. The Type III cement has the highest SO_3 content, and the Type II cement the lowest.

A comparison of the values in Tables 2-5 and 2-6 reveals that the chemical composition of the cements found in Texas is somewhat different to that represented by the national average. On average, Texas cements contain a higher amount of C_3S and less C_2S, but the total amount of calcium silicates remain around 75%. Since C_3S has a higher contribution to early-age heat generation, it may be concluded that cements typically used in Texas will have a higher rate of early-age heat generation as compared to the national average.

2.1.2 Mineral Admixtures

Mineral admixtures are generally added to concrete to replace some of the cement in the system. In some instances, they are obtained as by-products from other industries, and if readily available, their use could lead to cost savings. Mineral admixtures may enhance the workability of fresh concrete, and may decrease the permeability of the hardened concrete. This leads to improved durability of concrete against sulfate attack, and alkali-silica reaction. Improved performance in corrosive environments can be achieved due to the increased densification of the pore structure, which slows the rate of chloride penetration into the concrete element.

Currently in Texas, two types of mineral admixtures are being used in pavement construction. These are fly ashes and ground granulated blast furnace (GGBF) slag, and both will be briefly introduced in the following two sections.

2.1.2.1 *Fly ash*

Fly ash is a by-product and is obtained by collecting the ash precipitated from the exhaust gasses from coal-fired power plants. Due to the rapid cooling process, the fly ash particles are spherical and very fine. Figure 2-2 presents a close-up view of flyash particles and their round shape can easily be identified. The chemical composition of fly ash is, therefore, determined from the type of coal burned during its production. The source of the coal provides insight to differences in performance from one fly ash to another.

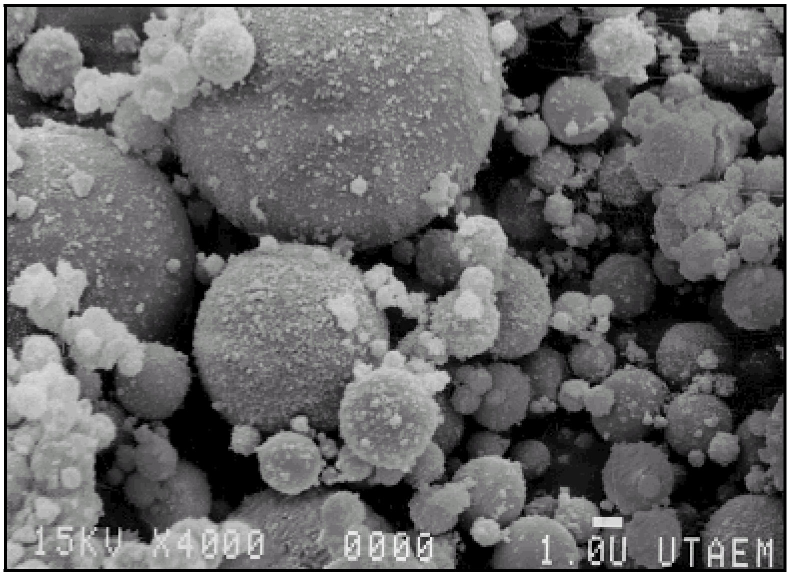

Figure 2-2: A close-up of fly ash particles (ACI 232.2R, 1996: Reprinted by permission of the American Concrete Institute)

Fly ashes are classified in accordance with ASTM C 618 (1994), and in Texas, both Class F and C fly ashes are used in the Texas concrete paving industry. Class F ashes are normally obtained from burning bituminous and anthracite coals (Metha and Monteiro, 1993). Bituminous and anthracite coal fly ashes rarely contain more than 15 percent lime (CaO) content, and generally only contribute to the pozzolanic reaction (See Section 2.1.3). In Texas, the CaO content of Class F fly ashes vary between 9 and 15%.

Type C fly ash is obtained from burning sub-bituminous coal and lignite, and typically has a high lime content contain more than 20 percent calcium oxide. In Texas the CaO content of Class C fly ashes vary between 22 and 29%. Due to the high-lime content of Class C fly ashes, they may have some cementitious properties of their own, but they additionally have some pozzolanic properties (ACI 232.2R, 1996). Table 2-7 presents some typical ranges of chemical compositions for the two fly ash types. TxDOT specifications allow the use of 20 to 35 percent fly ash replacement of cement in terms of volume of the original cement (TxDOT, 1993). Special Provisions to the current construction specification allows a maximum fly ash content of 40% for Type IP blended cements.

2.1.2.2 *Ground Granulated Blast-Furnace Slag*

Ground granulated blast-furnace (GGBF) slag is a by-product from the production of iron. Unlike fly ash, which can be used directly after collection from the stack, GGBF slag has to be ground to the desired fineness before it can be used as a cementitious material. In the United States, GGBF slag is specified according to ASTM C 989, which provides for three grades of GGBF slags, depending on their respective mortar strengths when blended with an equal mass of portland cement.

The classifications are Grades 120, 100, and 80. In Texas, only Grade 120 GGBF slag is currently available. Although GGBF slag is classified as a mineral admixture, it does react as a pozzolan. In fact the hydration products formed are essentially the same as the principal product (C-S-H) formed when portland cement hydrates (ACI 233R, 1995). However, when GGBF slag reacts with water no calcium hydroxide is produced. When GGBF slag is mixed with water, the initial hydration is much slower than when portland cement is mixed with water, and this affects the heat of hydration.

Table 2-7: Typical range of chemical composition of fly ash (Roy et al., 1986)

Oxide	**Range of Chemical Compositions (% by Weight)**	
	Class F Fly Ash	**Class C Fly Ash**
SiO_2	38 – 65	33 – 61
Al_2O_3	11 – 63	8.0 – 26
Fe_2O_3	3.0 – 31	4.0 – 10
CaO	**0.6 - 13**	**14 – 37**
MgO	0.0 – 5.0	1.0 – 7.0
Na_2O	0.0 – 3.1	0.4 – 6.4
K_2O	0.7 – 5.6	0.3 – 2.0
SO_3	0.0 – 4.0	0.5 – 7.3

2.1.3 Hydration of Cement

The degree of hydration is a measure of the quantity of cement gel (hydration products) formed and is, therefore, linked to the heat of hydration development. During the hydration process, the degree of hydration (α) is defined as the ratio between the quantity of hydrated cementitious material and the original quantity of cementitious material. The degree of hydration is a function of time, with α varying between 0.0, at the start of hydration, and 1.0 when hydration is fully completed. In reality, not all of the cementitious material always hydrates, and an α of 1.0 may never be reached. After investigating the hydration of a range of different cementitious materials, Mills (1966) stated that, “In most, if not all, cement pastes hydration stops before the cement is totally consumed.” In Chapter 3, models to estimate the ultimate degree of hydration will be presented in more detail.

Hardening in cement is caused by chemical reactions between the cement clinker components and water. Tikalsky and Carrasquillo (1988) presented the following sequence to briefly explain the complex chemical reactions of portland cement and fly ash. When water is added to portland cement, the first reaction to take place is one that forms the binding characteristics of concrete. As expressed in Reactions 1 and 2, the formation of calcium silicates hydrates (C-S-H) can form with the addition of water to either tricalcium silicate or dicalcium silicate. C-S-H accounts for about 50 to 60% of the volume of the hydrated paste and is strong, stable and durable under most conditions and controls the strength and durability of the hardened concrete. Reactions 1 and 2 shown below are referred to as “**cementitious**” reactions. During the cementitious reaction, calcium hydroxide ($Ca(OH)_2$) is formed, which is less dense and relatively weak as compared to C-S-H, and may become unstable when exposed to acids.

C_3S + Water → C-S-H + $Ca(OH)_2$ *Reaction 1*

C_2S + Water → C-S-H + $Ca(OH)_2$ *Reaction 2*

The calcium hydroxide ($Ca(OH)_2$) formed during the cementitious reaction, will react in the presence of water with the fly ash particles to form more calcium silicate hydrates as expressed in Reaction 3. This reaction is referred to as a “**pozzolanic**” reaction. From a durability standpoint the benefit of the pozzolanic reaction is that it converts more $Ca(OH)_2$ into C-S-H, which results in a denser less permeable concrete. However, the pozzolanic reaction develops slowly, and good curing practices are required to provide sufficient water to ensure continued hydration.

Fly Ash + $Ca(OH)_2$ + Water → C-S-H *Reaction 3*

The second series of reactions involves tricalcium aluminate, C_3A. Portland cement contains gypsum ($C\bar{S}H_2$), which has been added to control the setting of hydrating portland cement. As water is added, Reaction 4 is first to take place.

C_3A + Gypsum + Water → Ettringite *Reaction 4*

Reaction 4 will continue until the gypsum, the source of sulfate, is exhausted. As shown in Reaction 5, the ettringite now becomes unstable and starts to react with the remaining C_3A to form the stable product, monosulfoaluminate.

C_3A + Ettringite + Water → Monosulfoaluminate *Reaction 5*

In Reaction 5, the ettringite is converted back to monosulfoaluminate, and there may still be unused C_3A available in the clinker. The remaining C_3A will hydrate as shown in Reaction 6, to form a calcium aluminate hydrate, C-A-H.

C_3A + Water → C-A-H *Reaction 6*

The third series of reactions is the hydration process of tetracalcium aluminoferrite, C_4AF, in portland cement. The reaction of C_4AF, is similar to the reaction of C_3A, and is expressed in Reaction 7.

C_4AF + Water → Monosulfoaluminoferrite *Reaction 7*

The hydration process of a typical concrete mixture can be grouped into different stages. Byfors (1980) and Mindess et al. (1981) presented similar material in which they subdivided the heat development cycle into five stages, and these are graphically presented in Figure 2-3. In terms of heat release and temperature development, the third stage is the most important and numerous factors influence the hydration process at this stage. It is important to know to what extent some factors influence the hydration process.

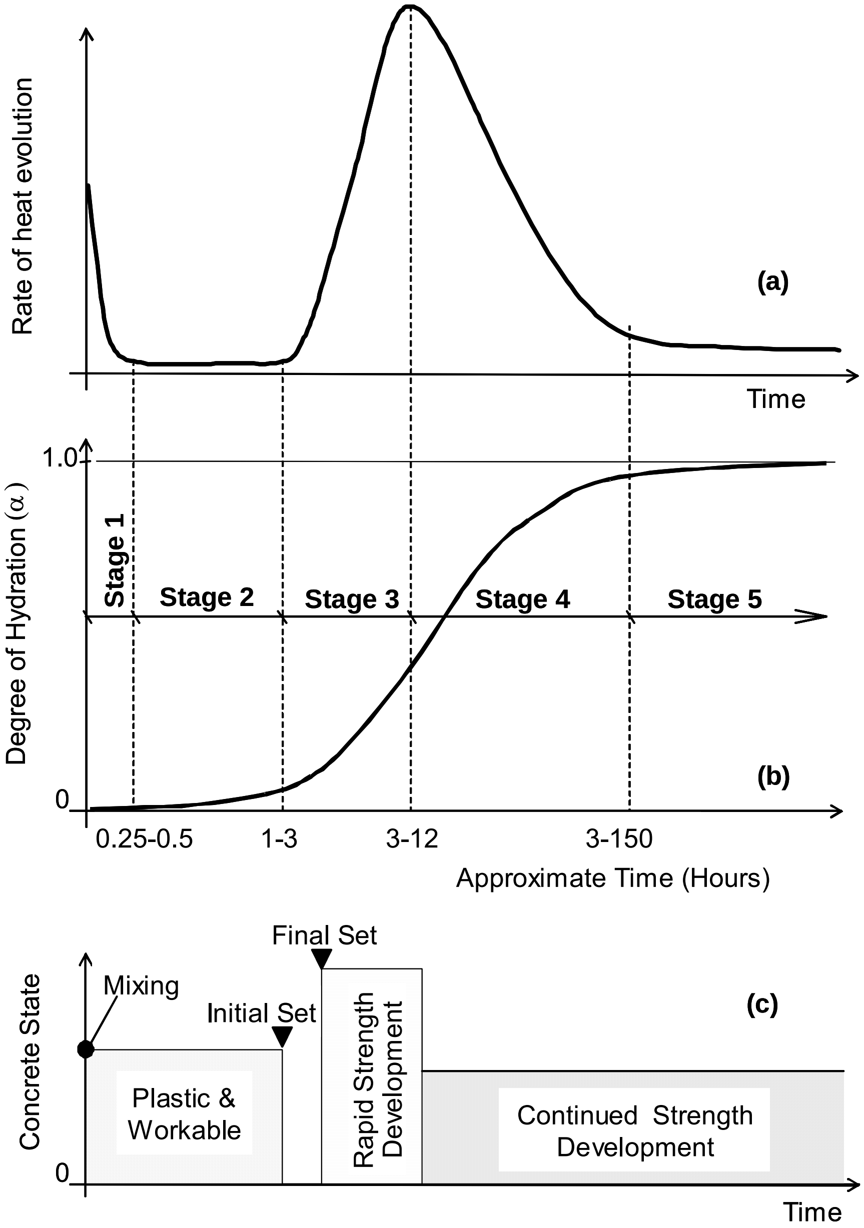

Figure 2-3: Stages during the hydration process (adapted from Byfors, 1980)

Stage 1: *Period of rapid heat evolution*

This stage occurs immediately after water is first added to the cement, and a period of rapid heat evolution occurs. The initial high heat of hydration is caused by the reaction of C_3A and gypsum, to form ettringite, as shown in Reaction 4. During this stage, the alkalinity of the paste is rapidly increased to over a pH of 12. The formation of ettringite slows down the hydration of C_3A, the reaction rate is rapidly slowed down, and the dormant stage is reached. During this stage, Reactions 1 and 2 are activated, although initially at a much slower rate as compared to the reaction of C_3A. This stage generally only lasts 15 to 30 minutes. Since this stage occurs in the batch plant or concrete mixer and the concrete is still in a plastic state, its only effect on the in place concrete temperature is to affect the temperature of the fresh concrete as delivered to site.

Stage 2: *The dormant stage*

During this stage, there is a period of relative inactivity, since the rate of reaction is slowed down through the dormant period. This can be seen in the continued degree of hydration shown in Figure 2-3(b). This is the stage that permits the placing and handling of portland cement since it is still in a plastic state. Prior to initial set, bleeding could occur. Bleeding is the phenomenon where some of the water in the mixture rises to the surface. This occurs since water has the lowest specific gravity of the mixture components, and the heavier particles tend to settle. At room temperatures, this stage can last between 1 to 3 hours. Initial set generally occurs at the end of this phase, and the paste starts to stiffen considerably. When the calcium and hydroxide concentrations reach a critical value, the reaction of C_3S and C_3A proceeds at a rapid rate and the acceleration stage is reached.

Stage 3: *Acceleration stage*

The stage during which C_3S (Reaction 1) accelerate to a very high level of activity, and the maximum rate of heat evolution is reached during this stage. During this stage, acceleration of the C_3A occurs (Reaction 4), ettringite is formed and the heat of hydration of the C_3A compound adds to the total heat evolution. The exact stage at which Reaction 5 and 6 will develop will be determined by the amount of gypsum added during the cement manufacture. The more gypsum in the system, the longer the ettringite will remain unstable. Final set is reached at some point just after the start of this stage, the concrete starts to harden, and the onset of strength and stiffness development follows. This stage can last anywhere from 3 to 12 hours depending on the cement composition and the curing temperature. During this phase, the paste is still developing structure and is subjected to high amount of creep (relaxation) should it be subjected to early-age loading (Westman, 1999). This stage is accelerated by the presence of alkalies and by an increase in cement fineness (Neville, 1996).

Stage 4: *Deceleration stage*

The stage during which the rate of reaction slows down and the majority of the hydration process will be completed. Reactions 2 and 7 generally occur at this stage, since they progress very slowly and little heat is developed. The slow reaction rate of Reaction 2 (C_2S) can be seen in Figure 2-1. This stage can last anywhere from 4 to 150 hours.

Stage 5: *Steady stage*

During this stage, all the reactions are completed and the concrete has reached its long-term strength. The pozzolanic reaction may still be converting $Ca(OH)_2$ into C-S-H over the course of this stage.

2.2 FACTORS THAT INFLUENCE CONCRETE HYDRATION

There are several factors that affect the hydration of concrete, and the interactions of all these factors are quite complex. This section will present some of the factors that influence the hydration process and, therefore, the amount and rate of heat generation. In Section 1.1.2, it was shown that the curing temperature has a significant effect on the rate of hydration. The higher the concrete temperature, the faster the rate of hydration, and the more rapid heat is generated in the concrete element. This effect can be seen in Figures 1-7 and 1-8. In the remainder of this section, the effect of the following factors on the hydration of concrete will be discussed: cement type, water-cement ratio, admixtures, and member thickness.

2.2.1 Cement Type

It is important to note that the higher the cement content, the greater the potential temperature rise in the concrete. The cement influences the hydration process through its chemical composition and fineness, and both of these aspects will be addressed in remainder of this section.

2.2.1.1 *Chemical composition of the cement*

The effect of chemical composition can by identified by evaluating the rate of hydration of the different compounds, and their individual contribution to the total heat of hydration of the cement. In Table 2-8, the heat of hydration contribution of each compound when it is fully hydrated is presented (Bogue, 1947). If the typical composition of the average Texas Type I cement is considered, it may be concluded that the C_3S and C_3A content provide the largest contribution to the heat of hydration of the cement. C_3S and C_3A contribute, respectively, about 62% and 17% of the total heat of hydration of the cement.

Table 2-8: Evaluation of heat of hydration contribution of the different cement compounds

Property	**C_3S**	**C_2S**	**C_3A**	**C_4AF**	**MgO**	**Free CaO**	**SO_3**
Heat of Hydration of individual compounds(J/g) (Bogue, 1947)	500	260	866	420	850	1168	624
Texas Type I Average Composition (%)	62.2	13.5	9.9	7.5	1.3	0.8	3.0
Compound contribution to heat of cement (J/g)	311	35	86	32	11	9	19
Compound contribution to heat of cement (J/g)	62%	7%	17%	6%	2%	2%	4%

Figures 2-4 and 2-5 present the heat of hydration development for pastes, with different C_3A and C_3S contents (Lerch and Bogue, 1934). Figure 2-4 presents that an increase in C_3A content will produce an increase in rate and amount of heat generated. The hydration of C_3A occurs rapidly after the initial dormant stage, and it reaches the steady stage within 16 hours regardless of the C_3A content. A similar conclusion can be made from Figure 2-5 concerning the hydration of C_3S, and it appears that the steady stage is reached even earlier, at around 12 hours.

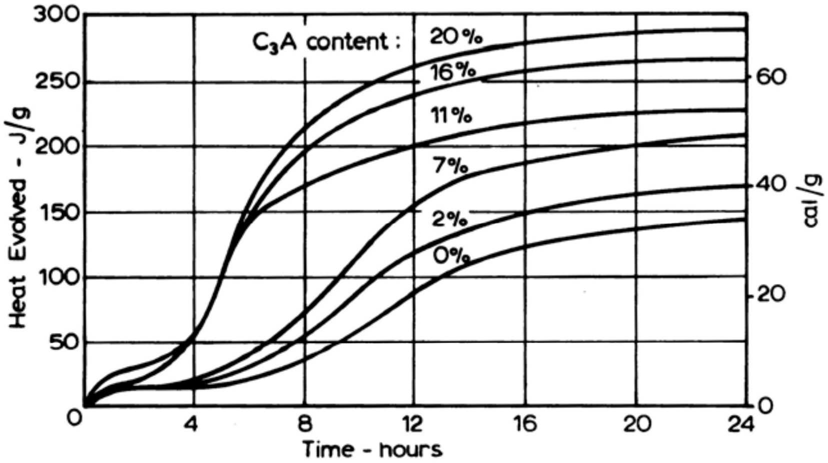

Figure 2-4: Effect of C_3A content ($C_3S \approx$ constant) on heat of hydration (Lerch and Bogue, 1934)

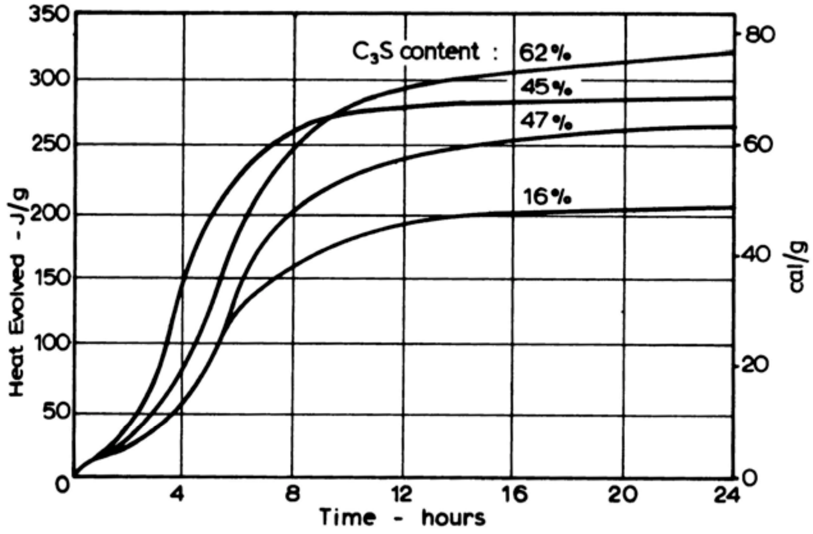

Figure 2-5: Effect of C_3S content ($C_3A \approx$ constant) on heat of hydration (Lerch and Bogue, 1934)

Figure 2-6 is an example of the adiabatic temperature rise for different cement types. Due to the differences in chemical composition, the rate of hydration and the total temperature rise (heat of hydration) are very different from one cement type to another.

The previous discussions reveal that the amount of C_3A and C_3S compounds affect both the early-age rate of hydration and the total heat of hydration. This is substantiated by the results presented in Figure 2-1, which indicated that the C_3A and C_3S clinker compounds react rapidly after water is added. Mindess and Young (1981) provide the following relevant comments:

> Since C_3S and C_3A are responsible for most of the early liberation of heat, reduction in the amounts of these compounds substantially reduces the amount of heat produced.

From Table 2-6, it may be seen that the C_3A content in Texas cements can vary between 3.5 and 13%, whereas the C_3S content varies between 53 and 69%. From this, it may be concluded that the heat of hydration may vary significantly from one cement source to another depending on the chemical composition of the cement. These effects need to be accounted for during this study, since they could influence the heat development, and thus the development of thermal stresses in concrete pavements. In order to control the maximum in place concrete temperature, the use of cements with low heats of hydration should be explored.

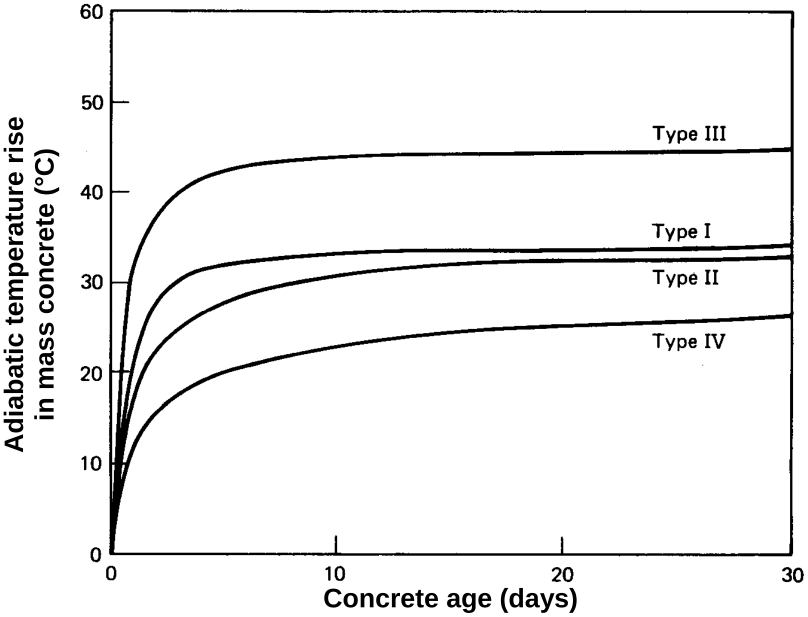

Figure 2-6: Rate of heat evolution for mass concrete stored under adiabatic conditions (Mindess and Young, 1981: Reprinted by permission of Pearson Education, Inc.)

2.2.1.2 *Cement Fineness*

Fineness of cement is usually measured in terms of its specific area. The specific area is the total surface area of all the grains contained in a unit weight of cement. Based on this principle, it can be found that larger surface area values correspond to an increase in the fineness of the cement particles. Although cements of quite different particle sizes can have the same specific area, the use of the specific area method still provides a useful measure of the cement fineness. ASTM C 150 recognizes both the Wagner turbidimeter and Blaine air permeability test to characterize the cement fineness in terms of specific surface area. In this study, the specific area results from the Blaine air permeability test will be used since these are readily available and commonly used. The values in Table 2-6 indicate that average Texas Type I cement has a Blaine value of 380 m^2/kg, whereas Type III cement has a value of 523 m^2/kg.

The more finely ground the cement, the more surface area is exposed to react with water. Therefore, the more finely ground the cement the more rapidly the heat development. This is confirmed by the following statement from the U.S. Bureau of Reclamation (USBR, 1975), " ...higher fineness increases the rate at which cement hydrates, causing greater early strength and more rapid generation of heat." According to Mindess and Young (1981) finely ground cements increase the hydration rate, but the total heat of hydration at very late ages is not particularly affected. This is also confirmed by work done at the National Institute of Standards and Technology, where cements of different particle size distribution (PSD) were tested to determine their total heat of hydration (Bentz et al., 1999). They concluded that cements with finer particles hydrate more rapidly, which results in a higher initial rate of heat release. However, the total heat of hydration is unaffected by the cement fineness, and this can be seen in Figure 2-7. In Figure 2-7, the mean particle size of the cement is provided. The fine and coarse cement has a mean particle size of, respectively, 5 and 30 microns.

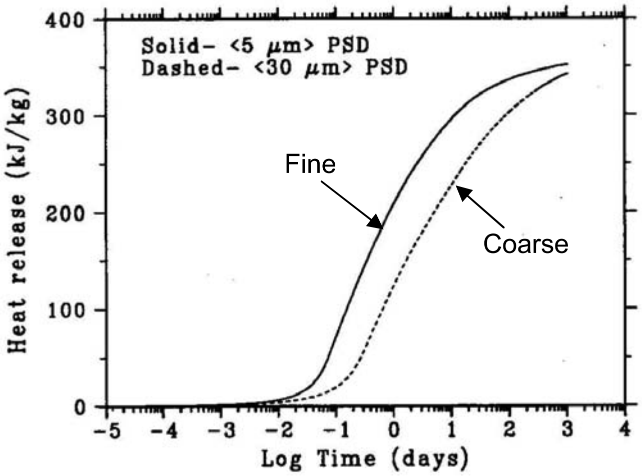

Figure 2-7: The effect of cements with different particle size distributions (PSD) on the heat released during hydration (Bentz et al., 1999)

2.2.2 Water-Cement Ratio

The water-cement ratio provides an indication of the amount of water relative to the cement present in the mixture. In Section 2.1.3, it was discussed, that complete hydration seldom occurs in concrete mixtures. Many references have addressed this issue, and in general the degree of hydration is accepted to be related to the water-cement ratio of the mixture (Mills, 1966; Hansen, 1986; van Breugel, 1997). Figure 2-8 presents the effect of change in water-cement ratio on the chemically bound water per gram of cement (Taplin, 1959). The ratio of chemically bound water per gram of cement has been shown to be a good indicator of the degree of hydration development. Note as the water-cement ratio increases, the maximum amount of chemically bound water (degree of hydration) decreases. Based on these test results, Byfors (1980) reported that the water-cement ratio does not affect the rate of hydration at early ages. However, at later ages the rate of hydration decreases as the water-cement ratio decreases.

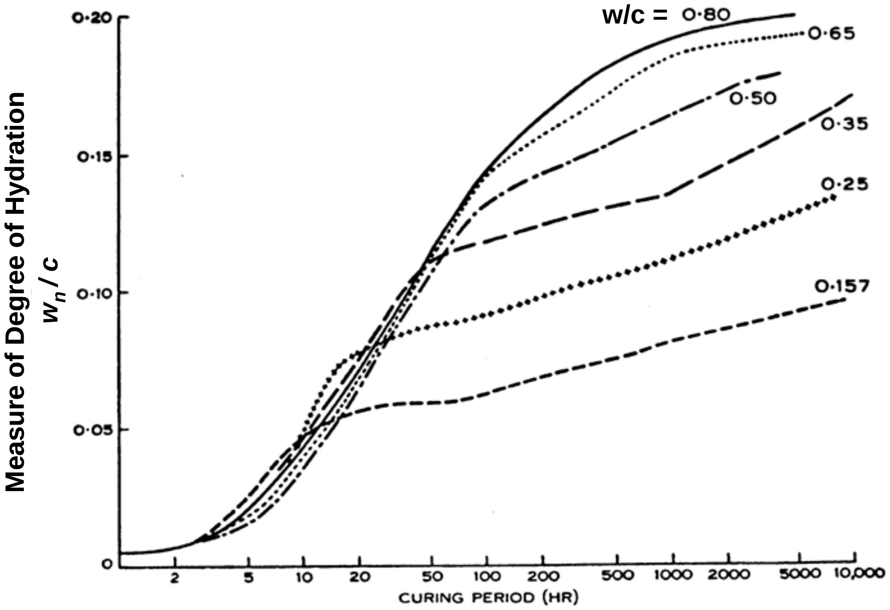

Figure 2-8: Ratio of chemically bound water per gram of cement versus log curing age (adapted from Taplin, 1959)

The ultimate degree of hydration will directly affect the amount of heat that is released during hydration, and for that reason, it has to be accounted for in the model that predicts the heat of hydration for different mixtures. The effect that different water-cement ratios have on the maximum heat of hydration can clearly be identified on Figure 2-9. The reason for the decrease in maximum degree of hydration is related to the fact that hydration can only continue to develop if the following conditions are reached:

1. **Sufficient space is available for all hydration products:**
   During hydration, cementitious grains react with free water to form hydration products. The volume of the hydration products is approximately equal to the volume of the cement plus volume of the water (Metha and Monteiro, 1993). Therefore, during hydration the hydration products gradually fill the voids initially occupied by the mixing water. When no more capillary space is available, the hydration reaction ceases, since there is no longer room for the formation of hydration products (Hansen, 1986).

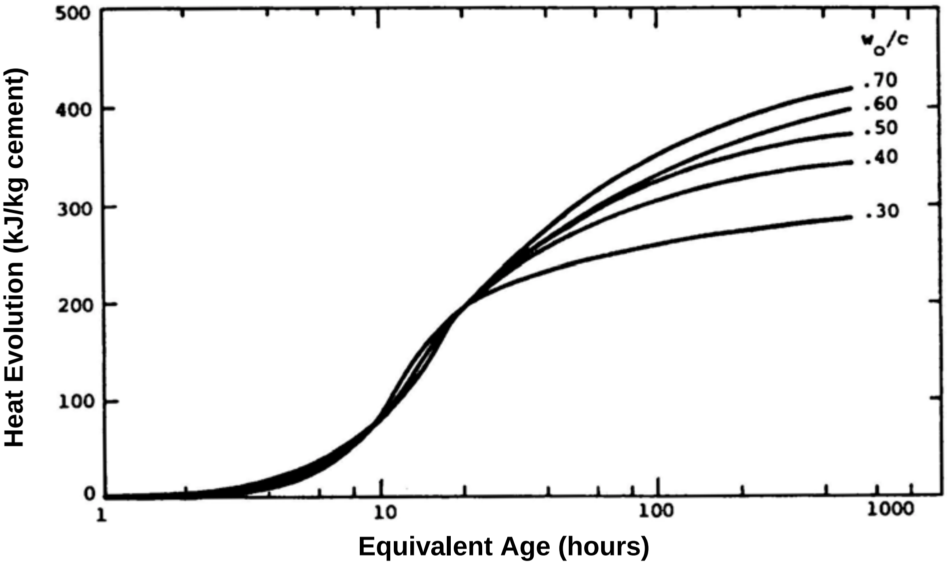

Figure 2-9: Adiabatic heat evolution for concretes with different w/c ratio (RILEM 42-CEA, 1984)

2. **Sufficient free water is available for the hydration reaction:**

   Free capillary water is required for the hydration process to continue. Hansen (1986) describes the requirements for this process and states that: “Excess water must therefore be available for the chemical process, beyond which is required in order to satisfy the requirements of sufficient space for the hydration products.” If additional water can enter the concrete from outside, then requirement (1) will determine the maximum degree of hydration. However, Hansen (1986) states that:

   > ... this is only the case for small specimens, permanently stored in water. In larger specimens of cement paste and in most concretes this excess water must be present as mixing water when fresh paste is cast, or the process will stop before all cement has hydrated.

3. **Extremely slow diffusion rate:**

   Verbeck (1960) elegantly describes this process by the following statement:

   > The hydration of cement requires the diffusion of water through hydrated products to the surface of the unhydrated cement and the diffusion of reacted material away from the reaction site. The hydration product which is laid down in the liquid surrounding the unhydrated cement serves to retard the diffusion of these materials and hence retard the hydration of the cement. At a particular water-cement ratio the retardation of hydration should increase as hydration proceeds due to the increasing amounts (concentrations) of hydration products present.

Due to the significant effect of water-cement ratio on the ultimate degree of hydration and, therefore, on the heat of hydration, this effect should be accounted for when the heat of hydration model is developed. The most appropriate formulation will be determined based on the test results obtained from this study.

2.2.3 Mineral Admixtures

In Section 2.1.2, fly ash and ground granulated blast furnace (GGBF) slag were discussed, and it was mentioned that both are used in Texas paving applications. The use of mineral admixtures are recommended for use under hot weather applications since they potentially could reduce the rate of hydration, which in turns could reduce the in place concrete temperature, the rate of setting, and even the rate of slump loss (ACI 305, 2000). This section will review the influence of using both fly ash and GGBF slag in terms of their effect on the heat of hydration and temperature development.

2.2.3.1 *Fly Ash*

It was shown earlier that during the pozzolanic reaction (Reaction 3), fly ash reacts with calcium hydroxide, which is produced by hydration of clinker minerals. Various researchers have investigated the effect of adding fly ash to concrete mixtures. In some instances, it was found that they reduce the total heat of hydration, and the rate of hydration. This effect was previously noted in Figure 1-8, where Class F fly ash, with a low CaO content (3.6%) was used. Barrow and Carrasquillo (1988) found that partial replacement with Texas Type A fly ash (comparable to ASTM Class F), results in a reduction in the peak temperature rise in concrete. From Figure 2-10, it may be seen that cement replacement with Texas Type B (comparable to ASTM Class C) fly ash did not reduce the peak temperature significantly, but it did prolong the time until the peak temperature was reached.

This effect can also be seen in Figure 2-11(b), which indicates that the peak heat of hydration is reduced when higher a dosage of fly ash is used. From the results of their tests in Figure 2-11(b), Kishi and Maekawa (1995) concluded that fly ash retards the hydration of portland cement, especially at early ages. The fly ash used to obtain the results shown in Figure 2-11(b), had a CaO content of 8.8%, which indicates that it has little cementitious nature and that it could be classified as a Class F fly ash. The data reviewed in this section show that fly ash could possibly be used to reduce the temperature development in PCC pavements constructed under hot weather conditions. The use of these mineral admixtures should further be explored for inclusion in mitigation measures developed throughout this study.

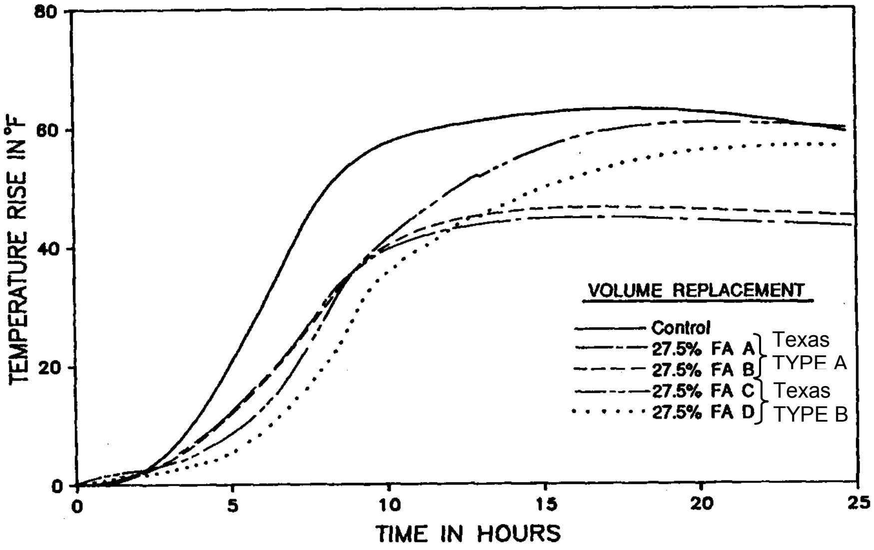

Figure 2-10: The effect of different Texas fly ashes on the heat development in beam specimens (Barrow and Carrasquillo, 1988)

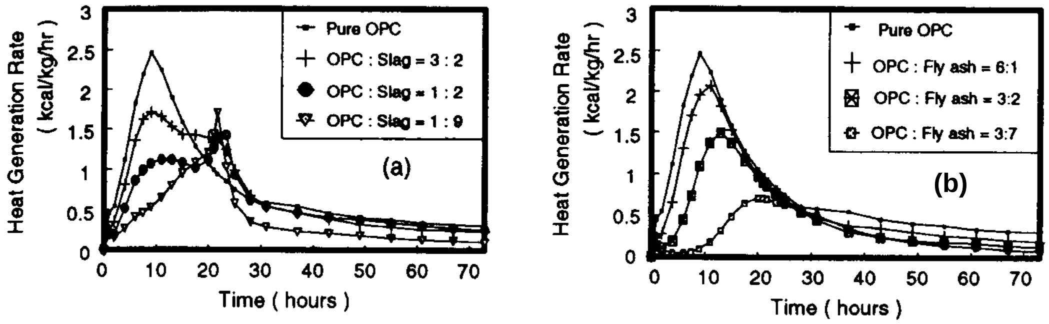

Figure 2-11: The effect of (a) GGBF slag and (b) fly ash on the hydration of cement (Kishi and Maekawa, 1995)

2.2.3.2 *Ground Granulated Blast-Furnace Slag*

Typical heat generation rates for cements with different slag replacement levels are shown in Figure 2-11(a) (Kishi and Maekawa, 1995). From Figure 2-11(a), it may be seen that the addition of slag reduces the total heat generation rate. This figure further presents that two peaks are generated and that the magnitude of the second peak seems unaffected by the slag content. The first peak occurs at the same time the peak for ordinary portland cement (OPC) occurred, and from this data it may be concluded that slag does not retard the normal hydration of the portland cement contained in the mixture. Based on the their results, Kishi and Maekawa concluded that:

> ... slag can react independently under a condition where calcium hydro-oxide is sufficiently released from cement, but at the higher replacement of slag, the reaction of slag is stagnant because of shortage of calcium hydro-oxide in pore solution.

The effect of adding GGBF Slag to a mixture can be seen in Figure 2-12, which presents the rate of heat development for two different mixes tested by isothermal calorimetry (Ma et al., 1994). These results are part of the information previously shown in Figure 1-8. Note that the mixture with Type I cement (Figure 2-12a) reaches a rate of heat evolution of around 20 mW/gram at a mixing temperature of 55°C (131°F). The mixture with 65% GGBF slag replacement (Figure 2-12b) only reaches a rate of heat evolution of about 7 mW/gram, which amounts to a 65% reduction in heat. This indicates that the use of GGBF slag would significantly reduce the heat of hydration for this mixture.

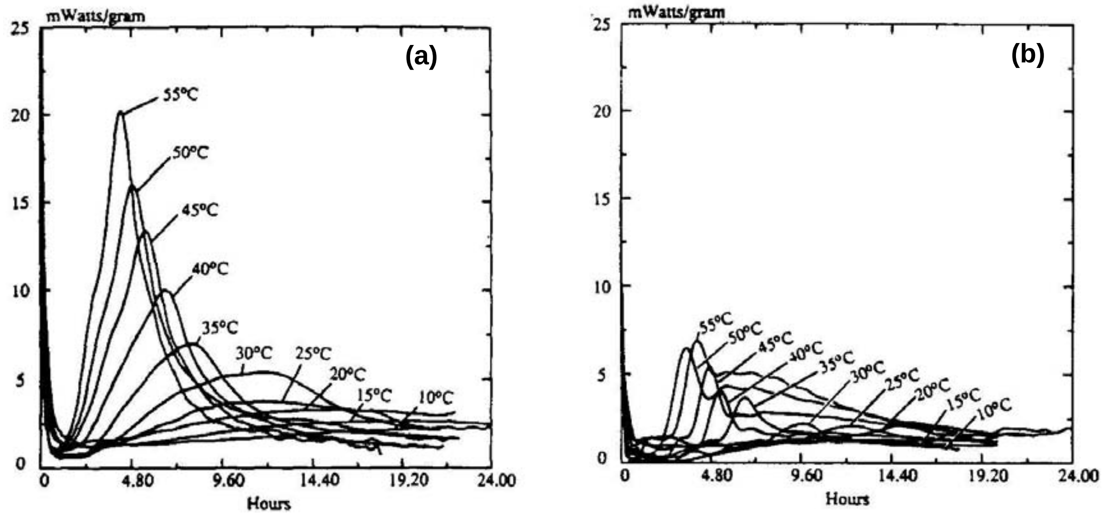

Figure 2-12: Heat of hydration: (a) Type I Cement, (b) Type I Cement with 65% GGBF Slag (Ma et al., 1994: Reprinted, with permission, copyrighted ASTM International.)

It has been reported that the total cumulative heat of hydration of GGBF slag is greater than that of normal cement (ACI 233R, 1995). Kishi and Maekawa reported a total heat of hydration of 461 J/g for GGBF Slag, which is similar to that of cement. Since the use of slag obviously influences the concrete temperature development, the effect of GGBF Slag will further be investigated in this study.

2.2.4 Chemical Admixtures

Chemical admixtures may impart dramatic modifications to the cement reaction rate and rate of heat generated. In the United States, most of the chemical admixtures used are classified under ASTM C 494 (1984). In this document, seven types of admixtures are listed:

Type A:	Water-reducing admixtures
Type B:	Retarding admixtures
Type C:	Accelerating admixtures
Type D:	Water-reducing and retarding admixtures
Type E:	Water-reducing and accelerating admixtures
Type F:	High-range water-reducing admixtures (Superplasticizers)
Type G:	High-range water reducing and retarding admixtures

Accelerating admixtures (Type C & E) primarily accelerate early strength development and the setting of concrete. These admixtures are most effective when used during cool weather since they greatly increase the rate of reaction. According to Neville (1996), the use of accelerators at high temperatures may result in too high a rate of heat development and shrinkage cracking may develop.

Water-reducing admixtures (Type A) generally serve the purpose of permitting the use of a lower water-cement ratio while retaining a desired workability or, alternatively, to improve the workability of a mixture with a given water-cement ratio. Water-reducing admixtures have little effect on the reaction rate unless increased dosages are used, then they usually become retarders. The effect of water-reducing admixtures is indirectly brought forward if the mixture proportions are known.

Retarders (Type B & D) delay the setting of the cement paste, and depending on the dosage have the ability to affect the reaction rate of portland cements (Tritsch, 1994). Neville (1996) comments that retarders are useful in hot weather conditions, however in some cases high concrete temperatures may even shorten normal setting times. Barrow and Carrasquillo (1988) concluded from their experimental results presented in Figure 2-13 that the use of retarders did not produce much change in peak temperature, but the time to peak temperature was altered. In Figure 2-13, it may be noted that the use of 5 oz of retarder caused the peak temperature to occur 5 hours later. This was true regardless of the cement type used.

High-range water-reducers, also referred to as superplasticizers, are admixtures that are water reducing, but to a greater extent than water-reducing admixtures. It has been reported (Tritsch, 1994) that some high-range water-reducing admixtures (Type F) and high-range water reducing and retarding admixtures (Type G) can provide significant benefits under hot weather conditions. From the data presented in Figure 2-13, Barrow and Carrasquillo (1988) further concluded that “regardless of the cement type, the superplasticizer also did not have a significant effect on the peak temperature rise of mixes containing either class of fly ash.”

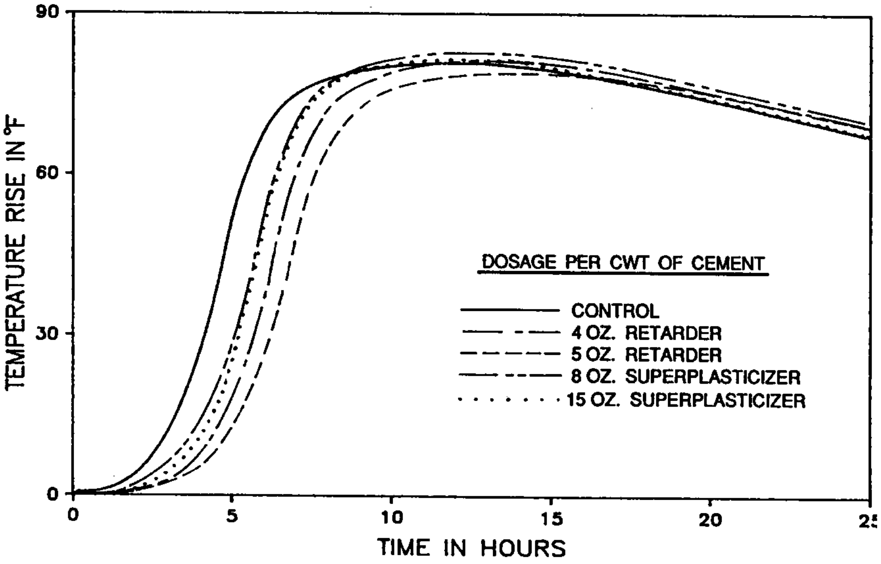

Figure 2-13: The effect of chemical admixtures on the heat development in beam specimens (Barrow and Carrasquillo, 1988)

2.2.5 Member Thickness

The temperature development of the in place concrete member is determined by heat transfer principles. The thicker the slab, the longer it will take the heat to be dissipated into the environment. In thin sections, the temperature even at middle of the element might be affected by changes in ambient conditions. In thick sections, the temperature development at the middle of the element will resemble fully adiabatic condition, since little heat losses to the environment occurs. Currently in the state of Texas, interstate PCC pavements have been placed at thicknesses ranging from 12 to 15 inches. Figures 1-4 and 1-6 present the development of concrete temperatures under typical concrete paving conditions. These figures indicate that the concrete temperature is strongly influenced by the environmental conditions and that the thickness of the slab needs to be considered during the development of the temperature prediction program.

2.3 MITIGATION MEASURES: CURRENT PRACTICE

One of the possible measures to minimize the potential problems associated with hot weather concreting can be to control the concrete mixture temperature (Samarai et al., 1975; Komonen et al., 1997; McCullough et al., 1998; and ACI 305, 2000). An effort should be made to keep the concrete temperature as low as economically practical. The Bureau of Reclamation presents guidelines on hot weather precautions for mass concrete structures. The USBR (1975) requires that " ...concrete, as deposited, shall have a temperature no higher than a stipulated value - usually 80 °F for concrete to be placed in hot arid climates and 90 °F for most other concretes."

In 1998, the American Concrete Paving Association (ACPA) compiled a database of current state practices from surveys of state departments of transportations (DOTs) (ACPA, 1998). When using the data, one has to keep in mind that the data were obtained by survey and that the data are those generally used in the state. Table 2-9 presents a summary of the practices of different state DOTs concerning the specified limit of the concrete temperature at placement. Note that it is not clear whether the states that have no maximum concrete placement temperature, do not specify one, or did not respond to the survey. Note that 50% of the concrete producing states place a limit of 90 °F on the concrete placement temperature. At the time of the survey, the state of Texas had no limit on the concrete placement temperature. This table reveals a national recognition of problems associated with concrete placement under high temperature conditions.

Table 2-9: Maximum concrete temperature at placement limit for all U.S. states (ACPA, 1998)

State	Maximum Concrete Temperature at Placement (°F)
Alabama	
Alaska	
Arizona	90
Arkansas	90
California	
Colorado	
Connecticut	90
Delaware	90
Florida	85
Georgia	90
Hawaii	90
Idaho	80
Illinois	90
Indiana	
Iowa	
Kansas	90
Kentucky	90
Louisiana	95
Maine	
Maryland	90
Massachusetts	
Michigan	90
Minnesota	90
Mississippi	95
Missouri	
Montana	
Nebraska	90
Nevada	
New Hampshire	85
New Jersey	
New Mexico	
New York	90
North Carolina	95
North Dakota	90
Ohio	90
Oklahoma	90
Oregon	
Pennsylvania	90
Rhode Island	
South Carolina	90
South Dakota	
Tennessee	
Texas	
Utah	90
Vermont	
Virginia	
Washington	
West Virginia	90
Wisconsin	
Wyoming	

At the start of this study in 1999, Texas had no specification that limited the maximum concrete temperature at placement for paving applications (as shown in Table 2-9). As result of the effort undertaken in this study, modifications were made to the state-wide concrete pavement construction specification. Initially a 32°C (90°F) limit was proposed for all concrete pavement construction; however, 35°C (95°F) was finally approved for state-wide use. The following amendments to the state-wide construction specification are currently in effect (TxDOT SP 360-035, 2000):

> **Article 360.8. Concrete Mixing and Placing, Subarticle (3) Placing.** The first paragraph and the Temperature-Time Requirements Table is voided and replaced by the following:
> **(3) Placing**. At time of placement, the concrete temperature shall not exceed 95 F. The temperature of the concrete will be measured at the time of discharge at the paving operation in accordance with Test Method Tex-422-A. Immediate corrective action shall be taken by the Contractor when the concrete at time of placement exceeds the specified 95 F or the Contractor shall stop production activities. The Contractor will be allowed to transport and place all concrete produced up to the time of being notified of the high concrete temperature.

As part of NCHRP Report 380 (Krauss and Rogalla, 1996), the effect of high concrete temperatures on the performance of **bridge decks** was investigated. They commented that by reducing placement and peak concrete temperatures relative to ambient temperatures, the cracking of bridge decks can be reduced. In bridge decks, "…to prevent excessive thermal gradients within the concrete, the concrete should have acceptable peak and placement temperatures; however, the transportation agencies do not agree on appropriate placement and peak temperatures." In NCHRP 380, it is mentioned that some DOTs recommend the use of retarders, since this may reduce the temperature rise. If proper curing is not maintained caution is expressed to the use of retarders since this may lead to increased plastic shrinkage cracking. Krauss and Rogalla further recommended that the concrete be cast 10 to 20°F lower than the ambient temperature. When ambient temperatures are below 60°F, it is recommended that the concrete be cast at the ambient temperature.

In Item 420.11, Subarticle (1), the Texas Department of Transportation (TxDOT, 1993) currently limits the temperature of cast-in place concrete in **bridge slabs** to 85°F when it is placed. It is worth noting that bridge decks tend to cool faster than pavements, since they are in most cases exposed to air on both sides of the deck.

The temperature of the fresh concrete can be regulated by controlling the temperature of the ingredients (ACI 305, 1991). Equations that may be used to estimate the temperature of the fresh concrete based on the temperature of its ingredients, are presented in Chapter 3, Section 3.4. The following are techniques that could be used to lower the temperature of fresh concrete (USBR, 1975; ACI 305, 2000):

- the use of cold mixing water,
    - add large quantities of ice,
    - the injection of liquid nitrogen,

- cooling of the mixed concrete with liquid nitrogen injection,
- avoid the use of hot cement, i.e. cement that has not cooled since its production,
- insulate water-supply lines and tanks,
- cool coarse aggregates with refrigerated water or with cold air blasts,
- insulate mixer drums or cool them with water sprays or wet burlap coverings, and
- shade materials and facilities not otherwise protected from the heat.

Other than to limit the maximum concrete placement temperature, other precautions can be taken to avoid or reduce potential problems during hot weather concreting. The following are a few examples of such methods (USBR, 1975; ACI 305, 2000):

- use the minimum cement content that will still permit the concrete to reach the required design strength,
- use a concrete consistency that allows rapid placement and effective consolidation at high temperatures,
    - trial batches to determine fresh concrete properties should be made at the air temperatures anticipated during placement,
- use concrete materials and proportions with satisfactory records in field use under hot weather conditions,
    - use cement that hydrates at a slower rate,
    - use coarse ground cement,
    - use mineral admixtures such as fly ash and slag,
- use chemical admixtures,
- keep the subgrade and forms moist to help keep their temperatures down,
- schedule placement activities during the times of the day or night when the weather conditions are favorable,
    - Work during night times, since this will offset the peak heat of hydration with that of the incoming solar radiation,
- minimize the time to transport, place, consolidate, and finish the concrete, and
- to minimize the potential for plastic shrinkage cracking, and decreased strengths caused by surface moisture loss, the concrete should be protected from moisture loss at all times during placement and during the curing period,
    - This is especially important when mineral admixtures are used, since they require moisture over a longer period to ensure continued hydration (Neville, 1996).

Construction practices in Germany involve the use of reflective white pigment curing compounds and the spraying of additional water onto the surface in warm summer months

(Springenschmid and Fleischer, 2001). By spraying water on the surface, evaporative cooling occurs, which cools the surface. This practice is followed to reduce the risk of early-age longitudinal cracking, since it reduces the development of high temperatures on the concrete surface due to solar radiation effects. In Germany, reflective white pigment curing compounds have recently been developed, which reflect more solar radiation and reduce the heat development of the concrete surface (Springenschmid and Fleischer, 2001).

2.3.1 Discussion of Current Mitigation Practices

The production of cooled concrete under hot weather summer conditions can be very expensive. Depending on the location, ambient temperatures in the Texas summer may exceed 100°F during 45 days of the year. Ambient temperatures above 90°F are generally expected to occur between the months of April and October. Contractors would be required to have large refrigerating units, ice making machines, insulated mixing water storage units, or liquid nitrogen supply vessels on site. Many contractors do not have access to such equipment, and all these methods increase the unit cost of the concrete placed.

On a national level, ACI 305 (2000) states that in general types of construction in hot weather a "...maximum ambient or concrete temperature that will serve a specific case may be unrealistic in others." The ACI committee advises on this subject that:

> …at some temperature between approximately 75 F and 100 F (24 and 38 C) there is a limit that will be found to be most favorable for best results in each hot weather operation, and such a limit should be determined for the work.

In modern paving operations, the use of mineral admixtures has become common practice, and under certain conditions, these admixtures could mitigate some of the problems associated with hot weather paving. The specification of a limiting concrete temperature at placement might be applicable to some conditions, but unnecessary in others. The limits selected by most states were chosen based on mixture designs that contain no mineral or chemical admixtures that may be effective in reducing the rate of heat evolution. Furthermore, the limits do not account for the use of mineral admixtures, and the same limit applies to cement with or without mineral admixtures. The use of the maximum placement limit does not account for changes to the time of paving, such as nighttime placement, which has been shown to reduce the temperature development of the in place concrete.

It has been well documented that the use of mineral admixtures such as fly ash or ground granulated blast furnace (GGBF) slag can significantly slow down the rate of heat evolution (Ma et al, 1994). The current practice is thus prohibitive and does not encourage the use of mineral admixtures during hot weather applications. In order to encourage the use of mineral admixtures, specifications should differentiate between mixtures that have different heat evolution rates.

The development of high concrete temperatures at early-ages has been shown to be detrimental to long-term pavement performance. Due to the current lack of means to quantify the effect of various mitigation techniques, specification cannot be developed to account for the wide variety of constructions materials and climatic conditions commonly encountered today. During this study an early-age concrete temperature program will be developed that will be able to predict the influence of different mitigation techniques on the in place concrete temperature development. With this program, a new innovative temperature control specification will be developed, which will encourage the contractor to use innovation and materials that will reduce the early-age heat of hydration under hot weather conditions. This approach should account for the impact of modern paving materials and will ensure improved concrete performance under all placement conditions.

2.4 SUMMARY AND CONCLUSIONS

The heat development in hydrating concrete is a complex phenomenon, which is influenced by many factors. It was shown that the amount of C_3A and C_3S compounds affect both the early-age rate of hydration and the total heat of hydration. Depending on the chemical composition of the cement, the heat of hydration may vary significantly from one cement source to another. Cements with finer particles hydrate more rapidly, which results in a higher initial rate of heat release. However, the total heat of hydration is unaffected by the cement fineness. The water-cement ratio will affect the ultimate degree of hydration. This impacts the amount of heat that is released during hydration, and this phenomenon should be included in the temperature prediction model. The most appropriate formulation will be determined from the test results obtained under this research effort.

The data reviewed in this chapter indicate that the use of fly ash may reduce and retard the peak heat of hydration. The use of these mineral admixtures should be explored further to be included in the mitigation measures developed throughout this study. Data are shown that indicates that the use of GGBF slag could significantly reduce the heat of hydration.

All the factors mentioned will be evaluated and their effect on the development of concrete temperatures assessed. These effects need to be accounted for during this study, since they could influence the heat development, and thus the development of thermal stresses in concrete pavements. In modern paving operations, the use of mineral admixtures has become common practice, and under certain conditions, these admixtures could mitigate some of the problems associated with hot weather construction. The specification of a fresh concrete temperature limit, to prevent these problems, might be applicable to some conditions, but overly prohibitive in others.

Throughout the U.S., specifications to limit the placement temperature of the fresh concrete have been used in the areas of bridge, dam, and highway construction to minimize the maximum temperature reached during hydration. This emphasizes the fact that problems associated with concrete placement under high temperature conditions are recognized on a national level. ACI 305, states that in general types of construction in hot weather, "… it is impractical to recommend a maximum limiting ambient or concrete temperature because circumstances vary widely. A limit that would serve a specific case might be unsatisfactory in others." The report by the ACI committee concludes on this subject that "…at some temperature between about 70 F and 100 F (24 and 38 C) there is a limit that will be found to be most favorable for best results in each hot weather operation, and such a limit should be determined for the work."

In order to produce specifications that encourage the use of contractor innovation and improved materials, modern specifications need to account for these materials, which will ensure good concrete performance under all conditions. Damage due to high concrete temperatures can be mitigated by planning and integrating the selection of appropriate materials, concrete batching procedures, and concrete placement techniques. One of the objectives of this study is to develop a concrete temperature prediction program. This program should have the flexibility to account for all the factors that have a significant impact on the development of concrete temperatures. With this program developed, the effects of different mitigation techniques to improve concrete pavement performance under hot weather placement conditions can be developed and implemented in a practical specification.

Chapter 3

Modeling of Early-Age Behavior, and Temperature Development

This chapter documents the assembly of all the models necessary to predict the in place temperature development, setting, and stresses of concrete at early-ages. Models were selected to simulate the factors that influence the development of concrete temperatures, and the hydration of cementitious material. During the selection of the models, compatibility was kept in mind in order to ensure that the overall model can be developed.

It is essential with any mechanistic empirical model, that local materials are tested and the models be calibrated for local conditions. It is proposed that the models be calibrated with laboratory data in a controlled environment, and with field measurements. The final step should be the validation of the model based on another set of independent field measurements. This chapter first introduces the overall modeling concept (Section 3.1), and then covers the following components of the overall model:

- hydration of cement based materials (Section 3.2),
- temperature prediction and heat exchange with the environment (Section 3.3),
- calculation of the fresh concrete temperature (Section 3.4),
- initial and final set models (Section 3.5), and
- development of early-age thermal stresses and calculation of the zero-stress temperature (Section 3.6).

3.1 OVERALL MODELING CONCEPT

The development of temperatures in hydrating concrete can be determined from the transient heat balance with respect to distance (x, y), and time (t), as governed by the following Fourier law (Jonasson, 1995):

$$\frac{d}{dx}\left(k \cdot \frac{dT}{dx}\right) + \frac{d}{dy}\left(k \cdot \frac{dT}{dy}\right) + Q_H = \rho \cdot c_p \cdot \frac{dT}{dt} \qquad \textit{Equation 3-1}$$

where, T = temperature (°C),
k = thermal conductivity (W/m/°C),
Q_H = rate of heat generation (W/m^3),
ρ = density (kg/m^3), and

c_p = specific heat capacity (J/kg/°C).

During hydration of concrete under field conditions, the concrete temperature development is determined by the balance between heat generation from the cementitious materials and heat exchange with the structure and its surroundings. The surroundings could either be an additional source of heat or at a lower temperature than the hydrating concrete. Figure 3-1 presents a simplification of the process used to predict concrete temperatures under field conditions, which is categorized into the following three components:

I. **Concrete Heat of Hydration:** Numerous factors influence the concrete heat of hydration and the interaction of these factors are very complex. The cement composition, cement fineness, amount of cement, water-cement ratio, presence of mineral and chemical admixtures, and the temperature of hydration primarily influence the heat of hydration. Models to include all these aspects will be evaluated and selected in this chapter. More details will be provided on the models selected to model the concrete heat of hydration.

II. **Environmental Effects:** As is the case with most chemical reactions, the hydration of cement is strongly affected by its current temperature and moisture state. Environmental conditions fluctuate through diurnal cycles, and parameters such as ambient air temperature, wind speed, relative humidity, solar radiation, and cloud cover have constantly changing values. This causes the hydration behavior under field conditions to be very different from hydration under laboratory conditions. Conditions imposed during laboratory tests are often adiabatic or isothermal, which do not reflect the in place hydration environment. This necessitates that the environmental effects encountered during construction and curing be accounted for when the in place properties of concrete structures are predicted. Models to include these environmental effects will be selected in this chapter.

III. **Heat Exchange:** In concrete placed under field conditions, heat will be transferred to and from the surroundings. Heat transfer mechanics have to be considered to model the transient heat exchange. As shown in Figure 3-1, the effects of various parameters including base temperature, curing methods, type of support materials, aggregate type used, slab thickness, and concrete surface color should all be accounted for in the heat transfer model used in this study.. Details of the heat transfer models selected for this study will be covered in Section 3.4.

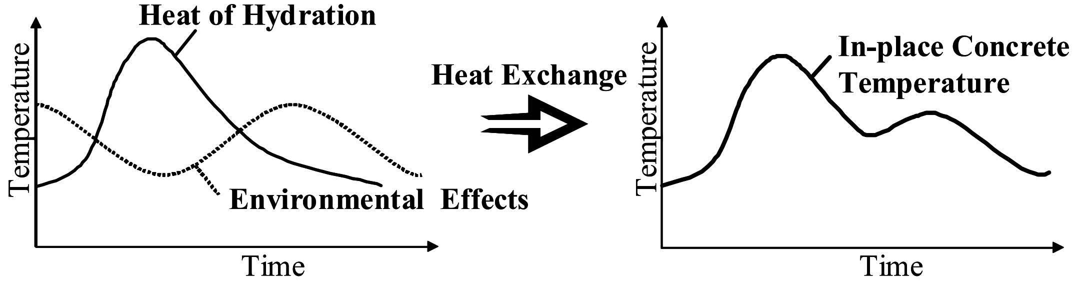

FACTORS CONSIDERED

Heat of Hydration	Environmental Effects	Heat Exchange
Cement Composition	Air Temperature	Base Temperature
Cement Fineness	Wind Speed	Curing method
Amount of cement	Relative Humidity	Support material
w/cm ratio	Solar Radiation	Aggregate type
Admixtures	Atmospheric Pressure	Slab Thickness
Mix Temperature	Cloud Cover	Surface color

Figure 3-1: Overview of primary model components and the variables considered

3.2 MODELING THE HYDRATION OF CEMENT BASED MATERIALS

This section document and discusses all the proposed components required to model the hydration of cement based materials. For some of the models, preliminary results of the analysis will be presented. The following components are covered:

- equivalent age maturity method (Section 3.2.1),
- activation energy values (Section 3.2.2),
- ultimate heat of hydration (Section 3.2.3),
- methods to determine the degree of hydration (Section 3.2.4),
- modeling the degree of hydration development (Section 3.2.5),
- physical interpretation of the degree of hydration (Section 3.2.6),
- ultimate degree of hydration (Section 3.2.7), and
- modeling the heat generation and associated temperature (Section 3.2.8).

3.2.1 Equivalent Age Maturity Method

The maturity method is an approach used to account for the combined effect of temperature and time on the development of concrete mechanical properties and the development of hydration. Some maturity equations also consider the effect of moisture, since the availability of moisture may have a significant effect on the development of hydration and strength (Baźant and Najjar, 1972; Jonasson et al., 1995). In this study, it will be assumed that good curing practices are followed and that adequate moisture is available for hydration.

Traditional maturity methods include both maturity functions recommended by ASTM C 1074; (1) the Nurse-Saul function, which is used to determine the time-temperature factor, (2) the Arrhenius formulation, from which an equivalent curing age relative to a reference temperature is calculated. The question becomes; which of these functions are most accurate? Byfors (1980) and Niak (1985) demonstrated that the maturity function based on the Arrhenius function was best able to account for the effects of different temperatures on the strength gain. After an investigation by the National Bureau of Standards (Carino, 1991), it was concluded "…a nonlinear function, such as the Arrhenius equation, can better represent the effect of temperature on strength development over wide temperature ranges."

The equivalent age approach is a convenient method for accommodating a variety of proposed maturity functions. In the equivalent time approach, the curing time intervals at known temperatures are converted to equivalent time intervals at a selected reference temperature. In this study, the nonlinear Arrhenius formulation of the maturity function will be used to determine the temperature sensitivity of the cementitious materials.

In the Arrhenius equivalent age function, the activation energy defines the temperature sensitivity of a concrete mixture, and it is used to determine the rate of hydration at any specific temperature relative to a reference temperature. In this section, the original Arrhenius theory for chemical reactions and the first use of this concept for maturity calculations in concrete will be reviewed. Thereafter, activation energy values as recommended by other authors will be reviewed.

3.2.1.1 The Original Arrhenius Definition of Rate Processes

In order to obtain a better understanding of what the activation energy means and the intent of the Arrhenius equation, the original concept as proposed by Arrhenius in 1889 will be reviewed. Due to equilibrium between inert and active species it may be shown that, "... the variation of the specific rate of the reaction with temperature should be expressed by an equation of the form" Glasstone et al. (1941):

$$\ln(k) = \ln(A) - \frac{E}{R \cdot T} \quad \text{or equivalently} \quad k = A \cdot \exp\left(\frac{-E}{R \cdot T}\right) \qquad \textit{Equation 3-2}$$

where, k = specific rate of reaction,

A = parameter that is independent or varies little with temperature,

E = activation energy (J/mol),

T = Absolute reaction temperature (°K), and

R = Universal gas constant J/(mol K).

Glasstone et al. (1941) continues by stating the activation energy should actually be called the “experimental activation energy” since it can be obtained “ ... from the linear plot of the observed values of *ln(k)* against *1/T*, in accordance with the requirements ... ” of Equation 3-2. An example of this concept, as implemented on concrete compressive strength results, is shown in Figure 3-2.

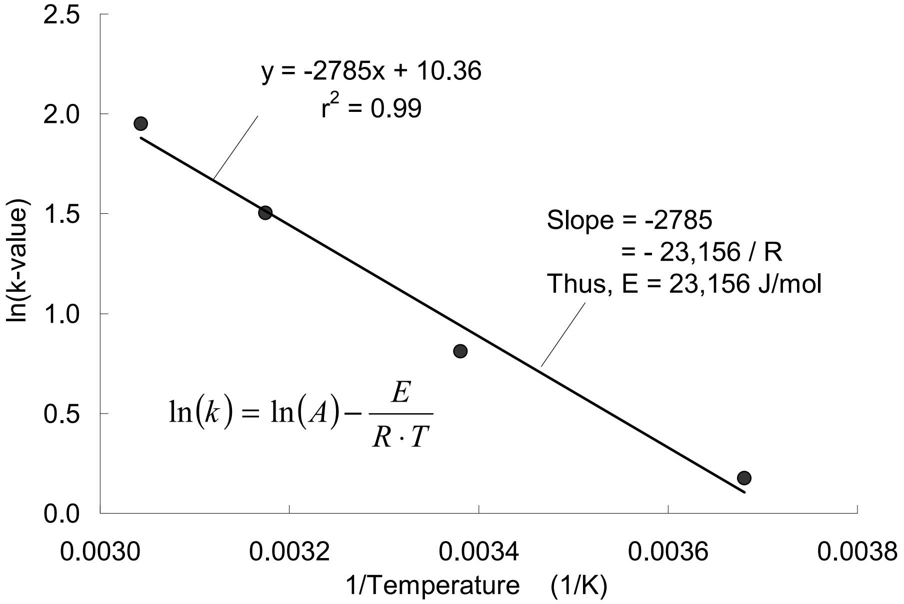

Figure 3-2: Experimental calculation of activation energy

3.2.1.2 Equivalent Age Maturity Method

The original use of the equivalent age Arrhenius formulation for concrete applications is credited to Freiesleben Hansen and Pedersen (FHP) who documented this concept in Danish in 1977. FHP presented an expression based on the Arrhenius equation in order to express the real time concrete curing age in terms of an equivalent age when cured at a reference temperature. Equation 3-3 presents their definition, and it is commonly referred to as the **Arrhenius equation** due its dependence of the Arrhenius rate concept:

$$t_e(T_r) = \sum_0^t \exp\left(\frac{E}{R}\left(\frac{1}{273+T_r} - \frac{1}{273+T_c}\right)\right) \cdot \Delta t \qquad \textit{Equation 3-3}$$

where, $t_e(T_r)$ = equivalent age at the reference curing temperature (hours or days),

T_c = average concrete temperature during the time interval, Δt, (°C),

T_r = reference temperature (°C),

E = activation Energy (J/mol), and

R = universal gas constant (8.3144 J/mol/K).

Freiesleben Hansen and Pedersen (1977) recommended a formulation for the activation energy that is most commonly used in Europe when the equivalent age maturity concept is applied. This relationship was obtained after applying the maturity method to compressive strength tests performed at different isothermal curing temperatures. Freiesleben Hansen and Pedersen presented the following empirical determined activation energy relationship that is a function of the concrete temperature (T_c) and is generally referent to as the FHP formulation:

for $T_c \geq 20°C$ (68°F): $E(T_c) = 33{,}500$ J/mol,
for $T_c < 20°C$ (68°F): $E(T_c) = 33{,}500 + 1{,}470\,(20 - T_c)$ J/mol *Equation 3-4*

where, T_c = average concrete temperature (°C).

Equation 3-5, presents the age conversion factor, $f(T_c)$, associated with the Arrhenius Equation. Carino (1991) explained the physical meaning of the age conversion factor, as: "it converts a curing interval (Δt) to the equivalent curing interval at the standard reference temperature." Should the temperature over the curing interval be larger than the reference temperature, then the age conversion factor will be greater than one. Conversely, if the temperature over the curing interval is less than the reference temperature, then the age conversion factor will be less than one.

$$f(T_c) = \exp\left(\frac{E}{R}\left(\frac{1}{273+T_r} - \frac{1}{273+T_c}\right)\right) \qquad \textit{Equation 3-5}$$

Figure 3-3 is a graphical comparison of the age conversion factor with a reference temperature of 20°C, as computed with the Arrhenius function presented in Equation 3-5. The age conversion factor is plotted for two different activation energy values, and for the activation energy formulation proposed by Freiesleben Hansen and Pedersen (1977).

Several observations can be made from Figure 3-3. In accordance with the definition of the equivalent age maturity method, the age conversion factor is equal to unity at the reference temperature of 20°C regardless of the activation energy value. For temperatures below 20°C (68°F), the age conversion factor is less than unity, and visa versa. Figure 3-3 indicates that the Arrhenius definition produces a nonlinear relationship between the age conversion factor and the curing temperature. It is for this reason that after investigation by the National Bureau of Standards, it was concluded "…a nonlinear function, such as the Arrhenius equation, can better represent the effect of temperature on strength development over wide temperature ranges" (Carino, 1991).

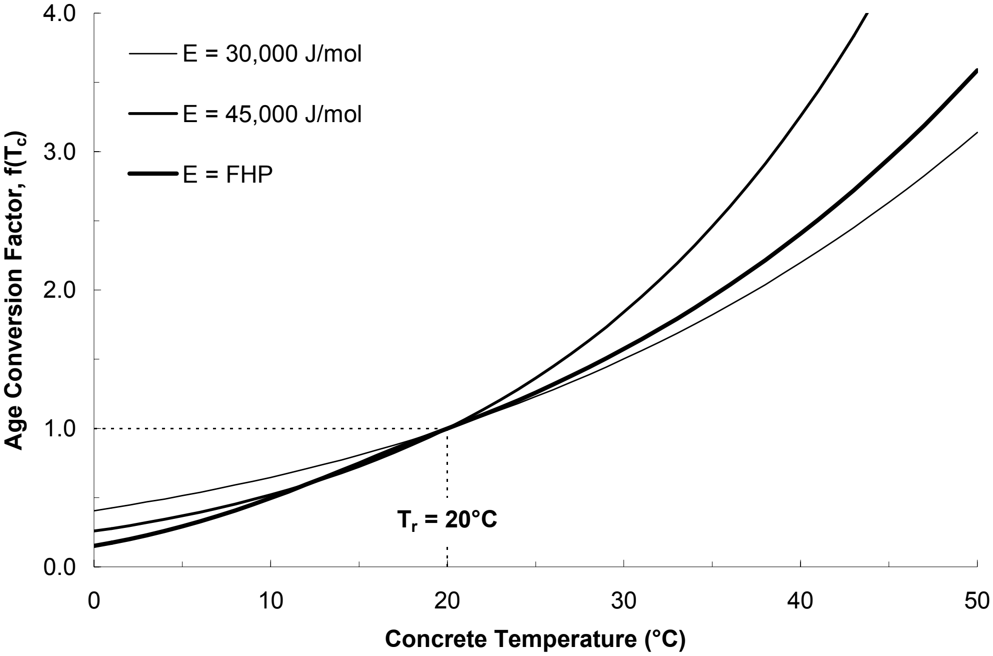

Figure 3-3: Age conversion factor as determined by different activation energy values

The derivation of Freiesleben Hansen and Pedersen (1997) provides further insight to the meaning of the activation energy in the application to the equivalent age maturity method. FHP developed their maturity concept based on physical chemistry as defined by the Arrhenius theory. The rate of hydration ($d\alpha/dt$) for a cement paste at a specific degree of hydration (α) was defined solely as a function of the rate constant (k) at the current reaction temperature (T_c). In order to define the equivalent age of curing at the isothermal reference temperature (T_r), the hydration rate at a different curing temperature (T_c) is compared to that at that the reference temperature (T_r), at the same degree of hydration. In doing so, the fundamental formulation of the traditional equivalent age (t_e) maturity formulation was obtained, as shown in Equation 3-6:

$$t_e(T_r) = \int_0^t \frac{k(T_c)}{k(T_r)} \cdot dt = \int_0^t f(T_c) \cdot dt \qquad \textit{Equation 3-6}$$

where, $t_e(T_r)$ = the equivalent age at isothermal reference temperature, T_r,
$k(T_c)$ = rate constant at concrete temperature, T_c,
$k(T_r)$ = rate constant at the isothermal reference temperature, T_r, and
$f(T_c)$ = the age conversion factor (also termed the affinity ratio).

Freiesleben Hansen and Pedersen defined the rate constant based on the Arrhenius theory as shown in Equation 3-2. Due to introduction of the Arrhenius definition of the rate process, all temperatures have to be defined in the absolute scale (Kelvin). If the Arrhenius definition (Equation 3-2) is substituted into Equation 3-6, the following can mathematically be determined:

$$t_e(T_r) = \int_0^t \frac{A \cdot \exp\left(\frac{-AE}{R \cdot (273 + T_c)}\right)}{A \cdot \exp\left(\frac{-AE}{R \cdot (273 + T_r)}\right)} \cdot dt$$

$$= \int_0^t \exp\left(\frac{AE}{R} \cdot \left(\frac{1}{273 + T_r} - \frac{1}{273 + T_c}\right)\right) \cdot dt \qquad \textit{Equation 3-7}$$

Equation 3-7 is now in the familiar form used to define the maturity in terms of equivalent age (see Equation 3-3). The reference temperature should be taken as the isothermal temperature at which the hydration or mechanical properties under evaluation are known. The reference temperature in European practice is generally taken as 20°C (68°F), as standard specimens are cured at this temperature. In American practice, the ASTM strength specification requires a standard curing temperature of 22.8°C (73°F), however, in some instances a value of 20°C is used. Nothing prohibits the use of a higher reference temperature, provided that the hydration or mechanical properties are evaluated at that temperature.

Figure 3-4 presents some of the analysis results presented by Freiesleben Hansen and Pedersen. Based on the best fit formulation obtained for strength tests (mechanical behavior), over a temperature range of -10°C to 80°C, FHP proposed the activation energy formulation as shown in Equation 3-4. The FHP activation energy is, therefore, developed to produce the best fit strengths as predicted with the equivalent age method.

Figure 3-4 reveals some key points that are worth highlighting. The strength results for the heat curing (20 to 80°C) are shown only up to 30 hours (1.25 days) and any later age strength loss that might have occurred, due to curing at high temperatures, are not included in this graph. At a temperature of 20°C, results are shown for up to about 96 hours (4 days), and for the lower temperature range of -10°C to 20°C the results are shown for up to 168 hours (7 days). In terms of equivalent age, the results cover a period of 96 hours (4 days) or less. From the data presented by FHP, it appears that their activation energy definition is applicable to specifically early-age strength applications.

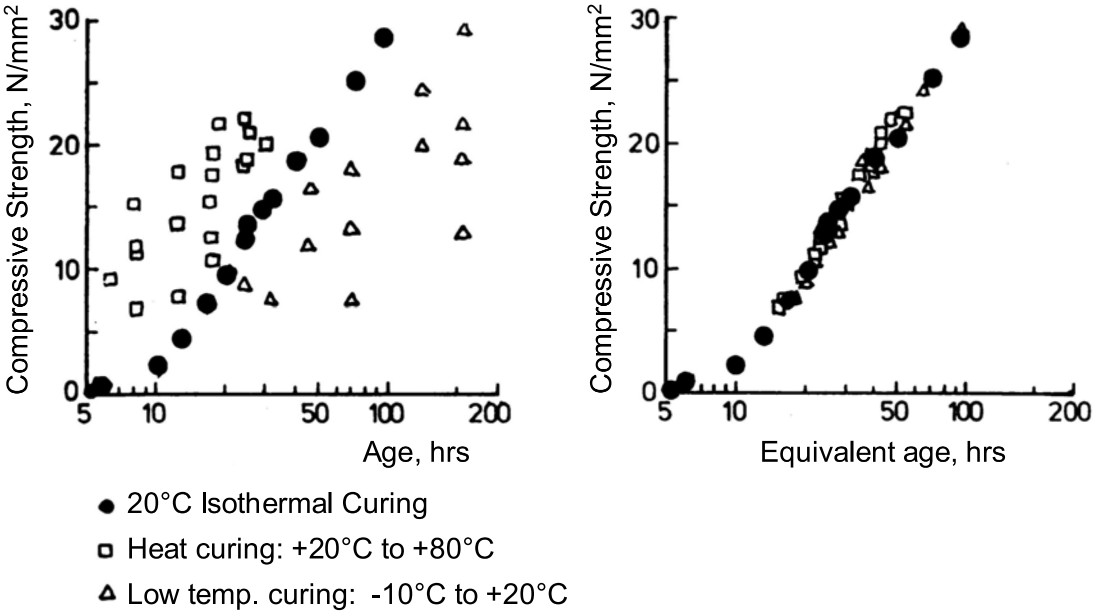

Figure 3-4: Results obtained by Freiesleben Hansen and Pedersen (1977), converting strength data at various temperatures and actual ages (a) into equivalent ages (b).

3.2.2 Activation Energy Values Recommended in Literature

The FHP formulation for the activation energy is one of the most commonly used definitions, and it is used in the equivalent age maturity method to account for the temperature sensitivity of the hydration reaction, specifically for degree of hydration or heat of hydration prediction calculations. In many cases the FHP formulation is used, irrespective of the cement type or mineral admixtures (fly ash, GGBF slag, and/or silica fume) used in the mixture (Radjy and Vunic, 1994; Yang, 1996; and Tritsch, 1994). Carino (1991) reports that the value of the activation energy depends on the cement chemistry, cement fineness, type and quantity of cement replacements, and admixtures used in the mixture. Other authors have indicated that the activation energy is a function of the water-cement ratio, but it has been shown that it does not have a consistent effect on the activation energy (Jonasson et al., 1995).

Currently, there are irregularities in literature about how the activation energy should be determined and which formulation is applicable for use in a particular situation. The activation energy can be measured through a number of methods. Table 3-1 lists some of the activation energy values as proposed by different research efforts. These values range from 26,700 J/mol to 67,000 J/mol, and seem to vary depending on the type of materials used in the mixture. Contrary to the FHP activation energy definition shown in Equation 3-4, all these values are constant and independent of the reaction temperature. This is in agreement with the Arrhenius formulation reviewed in Section 3.2.1.1.

Table 3-1: Activation energy (E) values proposed by various research efforts

Cement Type	Type of Test	Specimen type	E (J/mol)	Reference
OPC[a] OPC[a] + 70% GGBFS[b]	Heat of Hydration	Paste	42,000–47,000 56,000	Gauthier(1982)
OPC[a] RHC[c]	Chemical Shrinkage	Paste	61,000 57,000	Geiker (1983)
OPC[a]	Chemical Shrinkage	Paste	67,000	Roy (1982)
Type I	Strength	Mortar Mortar Concrete	42,000 44,000 41,000	Carino (1981)
Type I/II Type I/II + 50% GGBF	Heat of Hydration	Paste	44,000 49,000	Barnes (1977)
Type I Type I+17% F Fly Ash Type 1+7.5% SF [d] Type I+65% GGBFS [b]	Isothermal calorimetry (Heat of Hydration)	Blended Pastes	39,000 26,700 30,400 49,300	Ma et al., 1994

Note: [a] OPC = ordinary portland cement
[b] GGBFS = Ground granulated blast furnace slag
[c] RHC = rapid hardening cement
[d] SF = silica fume

In ASTM C 1074 (1998), “Standard practice for estimating concrete strength by the maturity method,” an activation energy in the range of 40,000 to 45,000 J/mol is recommended for a Type I cement when no admixtures are used. Should any other cement types or admixtures be used, ASTM provides no further guidelines to select the appropriate activation energy values. However, a test method to determine the materials activation energy based on the development of compressive strength at different temperatures is provided.

Activation energy values obtained from ***strength*** development that are most representative of U.S. cements and combinations of cements with fly ash, slag, accelerators, and retarders is documented in the dissertation of Tank (1988). Tank conducted an extensive study of the isothermal strength development in concrete and mortar specimens made with different cementitious systems and having two water-cement ratios. Specimens in this study were cured at 50, 73, and 104°F, and strength tests were performed at regular age intervals. Table 3-2 summarizes the experimental activation energy values obtained by Tank. Based on these results, Tank concluded that the activation energy for a concrete mixture could be obtained from the strength gain data of mortar cubes. The values proposed by Tank (1988) vary with a change in water-cement ratio; however, the effect of a change in the water-cement ratio is unclear. For some mixtures, there was no effect when the water-cement ratio was changed. However, with Type I and Type II cements, the low water-cement ratio mixtures showed significant higher activation energy values. On the other hand, the mortar mixture with Type I cement plus 50% GGBF slag had higher values for the high water-cement ratio. This table further indicates how the addition of admixtures may alter the activation energy for a particular cement type.

Table 3-2: Activation energy values proposed by Tank (1988) based on strength testing

Cement Type	**Activation Energy, E (J/mol)**			
	w/c ratio = 0.45		**w/c ratio = 0.60**	
	Concrete	**Mortar**	**Concrete**	**Mortar**
Type I	61,000	62,000	46,000	44,000
Type II	51,000	55,000	43,000	42,000
Type III	44,000	40,000	43,000	42,000
Type I + 20% Fly Ash	30,000	32,000	31,000	36,000
Type I + 50% Slag	46,000	44,000	44,000	51,000
Type I + Accelerator	46,000	54,000	49,000	51,000
Type I + Retarder	39,000	42,000	39,000	34,000

During the initial development of the FHWA HIPERPAV program (McCullough and Rasmussen, 1999), the Activation Energy values listed in Table 3-3 were selected for use. These activation energies were used to perform the temperature correction of the degree of hydration development at temperatures other than the reference temperature. Note that these activation energies were selected to be a function of the cement type and independent of the concrete temperature. These values were selected based on engineering judgment and values recommended in literature. It was reasoned that Type III cements have higher C_3A content and fineness and, therefore, should have an increased rate of reaction associated with an increase in concrete temperature.

Jonasson et al. (1995) proposed the formulation in Equation 3-8 to model the activation energy of Standard Swedish cements, and this definition was adopted by Emborg (1999). This formulation is similar to the FHP definition, since it is a function of temperature and degreases with an increase in curing temperature.

$$E(T_c) = 44{,}066 \times (30/(10+T_c))^{0.45} \qquad \text{Equation 3-8}$$

Table 3-3: Activation energies for different cement types (McCullough and Rasmussen, 1999)

Type of Cement	Activation Energy, E (J/mol)
Type I	41,750
Type IP	41,750
Type II	39,050
Type III	44,150
Type V	36,350

In a recent RILEM documentation on the following test method, "Adiabatic and Semi-Adiabatic Calorimetry to Determine the Temperature Increase in Concrete due to Hydration Heat of Cement," values for the activation energy were recommended (RILEM 119-TCE, 1999). The RILEM recommendations are shown in Equations 3-9 and 3-10. It should be re-emphasized that this definition of the activation energy is recommended to define the temperature sensitivity of the ***hydration*** process when the equivalent age maturity function is used. Note that the same activation energy definition is recommended irrespective of the cement type.

For portland cement:

for $T_c \geq 20°F\ (68°C)$ $\quad E(T_c) = 32{,}536$ J/mol, *Equation 3-9*

for $T_c < 20°F\ (68°C)$ $\quad E(T_c) = 32{,}536 + 1{,}455\,(20-T_c)$ J/mol.

For slag cements:

for all T_c $\quad E = 48{,}804$ J/mol

Equation 3-10

Figure 3-5 provides a comparison of the different concrete temperature dependent activation energy formulations as recommended, by Freiesleben Hansen and Pedersen (Eq. 3-4), RILEM Technical Committee 119-TCE (Eq. 3-9), and Jonasson (Eq. 3-10). From Figure 3-5 it may be seen that the RILEM Technical Committee 119-TCE formulation for cement is nearly identical to the original FHP activation energy formulation.

3.2.2.1 Concluding Remarks on the Activation Energy Value

In the activation energy formulation shown in Figure 3-5, the activation energy is a function of the concrete temperature, which is inconsistent with the original Arrhenius definition (thermo-dynamic/physical) point of view. In Section 3.2.1.1, the original Arrhenius definition was briefly reviewed, and the activation energy can be obtained as indicated in Figure 3-2, by taking the slope of the ***linear*** plot of *ln(k)* against *1/T*. If the activation energy was a function of the temperature, the Arrhenius plot would not yield a straight line.

Tables 3-1, 3-2, and 3-3 presented in Section 3.2.2 list numerous activation energy values that were proposed by various authors. All these activation energies are consistent with the original Arrhenius definition of rate processes since they are independent of the concrete temperature.

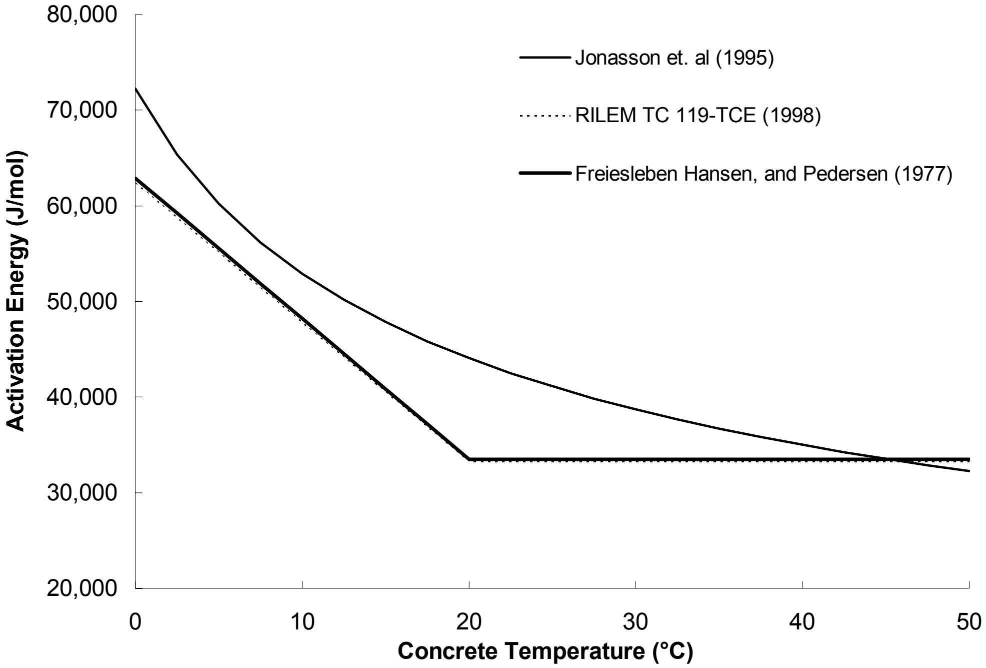

Figure 3-5: A comparison of different concrete temperature dependent activation energy models

After all the above factors are considered, the disparity that exists in the literature concerning the appropriate choice of the appropriate activation energy may be observed. The primary points of disparity will be investigated and addressed in Chapter 5, and can be summarized with the following three key questions:

1. ***Should the same activation energy be used for the prediction of mechanical properties and the development of hydration?***
2. ***Does the activation energy change as a function of temperature or degree of hydration?***
3. ***Should the same activation energy be used irrespective of the type of cementitious materials?***

3.2.3 Ultimate Heat of Hydration Modeling

In Section 2.2.1.1, it was discussed that the heat of hydration varies greatly with the cement composition, with C_3A and C_3S being primarily responsible for high heat evolution. The use of mineral admixtures may affect the ultimate heat of hydration. The four clinker minerals have different characteristics with regard to the development of heat. The ultimate heat of hydration (H_T), when all of the cement particles have reached 100% hydration, can be determined through knowledge of the total cementitious materials content, and the heat of hydration (H_u) per unit weight of all the cementitious materials.

Models are available to characterize the heat of hydration contribution of each of the primary cement compounds. The ultimate heat development (H_u) can be estimated directly from the cement chemistry (Bogue, 1947), and the composition of the mineral admixtures (Kishi and Maekawa, 1995). Cement constituents have been found to have a unique heat of hydration. A method of estimating the maximum heat of hydration of cement (H_{cem}) is to determine the percentage of the total mass of each constituent and multiply these by the heat of hydration of the respective components as shown in Equation 3-11.

$$H_{cem} = \sum \left(h_i \cdot p_i \right) \qquad \textit{Equation 3-11}$$

where, H_{cem} = ultimate heat of hydration of the cement (J/g),

h_i = heat of hydration of individual *i-th* component (J/g), and

p_i = mass ratio of i-th component ito total cement content.

The accuracy of the estimated ultimate heat of hydration depends on the accuracy by which the clinker composition has been determined. Other proposals have been made to calculate the composition of cements, and it has been reported that the Bogue composition underestimates the C_3S content (Taylor, 1989). However, Bogue's calculations are generally used and are recommended by ASTM C 150 (1998). In the case of cement, the values for the heat of hydration of each of the components are available, and Table 3-4 lists some values recommended by previous research efforts.

In this study, the heat of hydration values as recommended by Bogue will be used, since this will provide compatibility with the use of Bogue's calculations to determine the cement compounds. The accuracy of this method will be re-evaluated once test data on local cements have been obtained. The ultimate heat of hydration (at 100% hydration) for the portland cement in the system, can thus be determined as follows:

Table 3-4: Heat of hydration of individual cement components

Component	**Heat of hydration of individual component (J/g)**			
	Mindess and Young (1981)	SHRP-C-321 (1993)	Bogue (1947)	Kishi and Maekawa (1995)
C_3S	490	500	500	502
C_2S	225	256	260	260
C_3A	1160	721	866	865
C_4AF	375	302	420	419
Free Lime	-	-	1165	-
MgO	-	-	850	-
SO_3			624	

Previously, $H_{cem} = \sum (h_i \cdot p_i)$

$$H_{cem} = 500 \cdot p_{C_3S} + 260 \cdot p_{C_2S} + 866 \cdot p_{C_3A} + 420 \cdot p_{C_4AF} + \qquad \textit{Equation 3-12}$$

$$624 \cdot p_{SO_3} + 1186 \cdot p_{FreeCaO} + 850 p_{MgO}$$

where, p_i = mass ratio of i-th component in terms of total cement content.

In this study, the effect of using mineral admixtures such as fly ash and GGBF slag will be evaluated and their contribution to the total heat of hydration need to be incorporated. Little data were found in published literature to characterize the total heat contribution of the added fly ash or GGBF slag. Kishi and Maekawa (1995) provided a formulation similar to that shown in Equation 3-12, with additional terms to incorporate the effect of fly ash and GGBF slag. Based on typical materials found in Japan, their recommendations were as follows:

- Fly ash: h_{FA} = 209 J/g, with CaO = 8.8%, SiO_2 = 48.1%, and specific gravity = 2.33
- GGBF Slag: h_{SLAG} = 461 J/g, CaO = 43.3%, SiO_2 = 31.3%, and specific gravity = 2.89

Bensted (1981) reported total heat of hydration values between 355 and 440 J/g for GGBF slag. Since the heat contribution of fly ashes in Texas could vary significantly from that obtained by Kishi and Maekawa (1995), the fly ash ultimate heat of hydration will be determined based on the laboratory test results obtained from this study. The ultimate heat of hydration obtained by Kishi and Maekawa (1995) for GGBF slag will be selected for the initial model, and the use of this value will be re-evaluated based on the laboratory test results of Texas slags. In Section 2.1.2.1, it was mentioned that the CaO content is an indicator of the cementitious nature of the fly ash. It is recommended to account for the difference in heat of hydration of different fly ash sources based on their CaO content.

This approach is taken, since Class F ashes are generally produced from coals, which rarely contain more than 15 percent calcium oxide, and Class C fly ashes generally contain more than 20 percent of CaO (ACI 232.2R, 1996).

The total ultimate heat of hydration of the concrete (H_T), which incorporates both cement and mineral admixtures, will be modeled thought the use of Equation 3-13. The applicability of this model will be evaluated with test data collected from cements, fly ashes, and GGBF slags typically used in Texas.

$$H_T = H_u \cdot C_c \qquad \textit{Equation 3-13}$$

where, H_T = total ultimate heat of hydration of the concrete (J/m^3),

C_c = cementitious materials content (g/m^3), and

H_u = ultimate heat of hydration of cementitious materials at 100% hydration (J/g), defined as follows:

$$H_u = H_{cem} \cdot p_{cem} + 461 \cdot p_{SLAG} + \cdot h_{FA} \cdot p_{FA} \qquad \textit{Equation 3-14}$$

where, H_{cem} = heat of hydration of the cement (J/g), defined with Eq. 3-12,

p_{cem} = cement mass ratio ito total cementitious content,

p_{SLAG} = slag mass ratio ito total cementitious content,

p_{FA} = fly ash mass ratio ito total cementitious content, and

h_{FA} = heat of hydration of fly ash (J/g).

3.2.4 Methods to Determine the Degree of Hydration Development

The degree of hydration (α) is a measure of how far the reactions between the cementitious materials and the water have developed, and is defined as the ratio between the quantity of hydrated cementitious material and the original quantity of cementitious material. The degree of hydration for a concrete mixture can experimentally be determined by a number of techniques, some direct and others indirect. In direct methods, the quantity of hydration products that has formed is determined, but as stated by RILEM Commission 42-CEA (1984), it is "... almost impossible to make a direct determination of the quantity of cement gel formed or the quantity of hydrated cement."

Note that the use of strength to estimate the degree of hydration is not recommended, since the relationship between the degree of hydration and mechanical properties is strongly influenced by the curing temperature. This statement will be supported by the work document in Chapter 5. Two indirect methods commonly used to determine the degree of hydration are described in the following sections.

3.2.4.1 Amount of Chemically Bound Water

The most frequently used indirect method is to determine the amount of chemically bound water, and then the degree of hydration can be calculated as follows (Byfors, 1980):

$$\alpha(t) = \frac{w_n(t)/c}{(w_n/c)_{\max}}$$ *Equation 3-15*

where, $\alpha(t)$ = degree of hydration at time, t,

$w_n(t)$ = quantity of chemically bound water at time, t, (g),

c = quantity of cementitious material (g), and

$(w_n/c)_{max}$ = maximum mass ratio of (w_n/c) at complete hydration (g/g).

Different maximum mass ratio of w_n/c have been reported (van Breugel, 1997), but a value of 0.25 as proposed by Powers and Brownyard (1948) is generally used (Taplin, 1959; Byfors, 1980; Kjellsen and Detwiler, 1991). With the maximum ratio of w_n/c known, the degree of hydration can be determined by measuring the chemically bound water during the hydration process.

The chemically bound (non-evaporatable) water (w_n) is defined as the part of the total water content that has chemically reacted with the cement. It can be measured as the quantity of water emitted from a dried (105°C) specimen when it is subjected to ignition, which occurs at about 1050°C (Byfors, 1980). There are other methods to determine the amount of chemically bound water, which is beyond the scope of this study.

3.2.4.2 Amount of Heat Generated During Hydration

A more practical indicted method to determine the degree of hydration is as shown in Equation 3-16, where heat development that occurs during hydration is compared to the maximum possible at 100% complete hydration.

$$\alpha(t) = \frac{H(t)}{H_u}$$ *Equation 3-16*

where, $\alpha(t)$ = degree of hydration at time, t,

$H(t)$ = total heat development at time, t, (J/g), and

H_u = maximum heat development (at 100% complete hydration) (J/g).

This method has been shown to provide an accurate measure of the degree of hydration (van Breugel, 1991; RILEM Technical Committee 119-TCE, 1981; Radjy et al., 1994). A linear correlation has been reported between the heat of hydration and the amount of non-evaporable water, from which it is concluded that these two methods are equivalent to indirectly reflect the extent of hydration (van Breugel, 1997). Some commonly used methods to determine the heat released include:

1) **Conduction Calorimetry:** In this method, the heat flux from a small sample of cement paste hydrating at a constant temperature is measured. The total heat evolution can be determined by the summation of the measured heat over time. The disadvantage of this method is that small paste samples are used, and not concrete. This method can only be used to determine the heat of hydration at early ages (72 hrs). Currently no standardized ASTM method exists for this procedure.
2) **Heat of Solution Calorimetry:** This test method covers the determination of the heat of hydration of cement by measuring the heat of solution of the dry cement and the heat of solution of a separate portion of the cement that has been partially hydrated, the difference between these values being the heat of hydration. The method involves dissolving cement in an acidic mixture within a calorimeter. The test is performed at selected intervals and produces results that are comparable to those obtained form conduction calorimetry. This test is typically suited to estimate the heat of hydration over extended periods (months). The disadvantage of this method is that small paste samples are used and not concrete samples. This method is covered by ASTM C 186, "Standard test method for heat of hydration of hydraulic cement."
3) **Adiabatic Calorimetry:** In this method, the specimen is sealed in a chamber and no heat loss is permitted to occur. When concrete is sealed in such a manner, the heat of hydration is completely converted into temperature. Therefore, hydration increasingly occurs at a higher temperature, which in turn affects the hydration rate. Due to the high temperatures reached during hydration, full hydration can be reached in a short period of time (7 days). In order to convert these test data into degree of hydration at an isothermal reference temperature, information about the temperature sensitivity (activation energy) is required. The disadvantage of this method is that the degree of hydration has to be computed based on heat transfer principles. The result can thus be affected by inaccurate assumptions of activation energy (temperature sensitivity) and material properties such as thermal conductivity, specific heat, and density. The advantage of this method is that the heat evolution of an actual concrete mixture can be determined. No standardized ASTM test method is currently available for this procedure, but a RILEM draft test procedure has been proposed (RILEM 119-TCE, 1999).
4) **Semi-Adiabatic Calorimetry:** This method is similar to the adiabatic method described above, except that a known amount of heat loss is allowed to occur over time. The temperature development is, therefore, not as high as with the fully adiabatic calorimeter test. In some instances, this might be an added advantage, since hydration occurs at lower temperatures, and less temperature correction is required for the conversion to an isothermal curing temperature. Currently no standardized ASTM test method exists for this procedure,

but a RILEM draft test procedure has been proposed (RILEM 119-TCE, 1999). A commercial version of this test is currently available in the U.S. An additional disadvantage of this method is that the true adiabatic heat development has to be determined from the test results, and the losses associated with the test have to be accounted for.

In this study, semi-adiabatic calorimeter test were performed to determine the degree of hydration for various mixtures typically used in concrete paving projects in the state of Texas. This test was selected due to the major advantage that actual concrete specimens can be tested. The semi-adiabatic procedure was preferred over the adiabatic procedure, due to fact that the temperature development in pavements is closer in magnitude to those experienced under semi-adiabatic testing conditions. Adiabatic calorimeter test results are more likely to reflect the temperature levels in mass concrete elements, such as dam structures and bridge piers. Figure 3-6 presents calculated results for a Type I/II cement with 20% class F fly ash, which presents the temperature rise in a standard 6x12 inch concrete cylinder cured under adiabatic and semi-adiabatic conditions. A maximum temperature of 62°C and 46°C is respectively reached under adiabatic and semi-adiabatic conditions. Figure 3-7 presents the temperature rise measured during the construction of a 13 inch thick continuously reinforced concrete pavement, together with the adiabatic and semi-adiabatic calorimeter test data shown in Figure 3-6. The data from this particular field site indicate that the temperature **range** measured in place is similar to that measured under semi-adiabatic conditions.

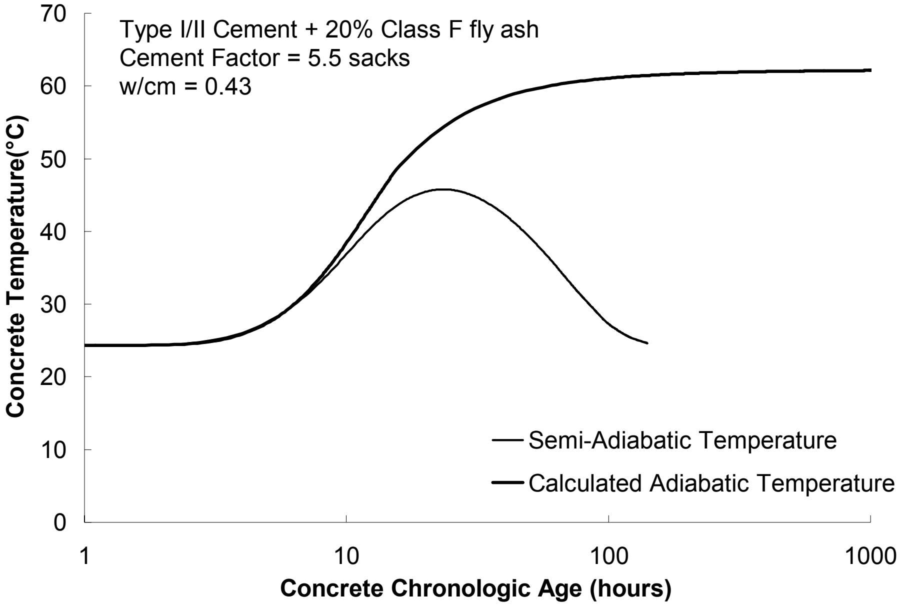

Figure 3-6: Calculated temperature rise in a standard 6x12-inch concrete cylinder cured under adiabatic and semi-adiabatic conditions.

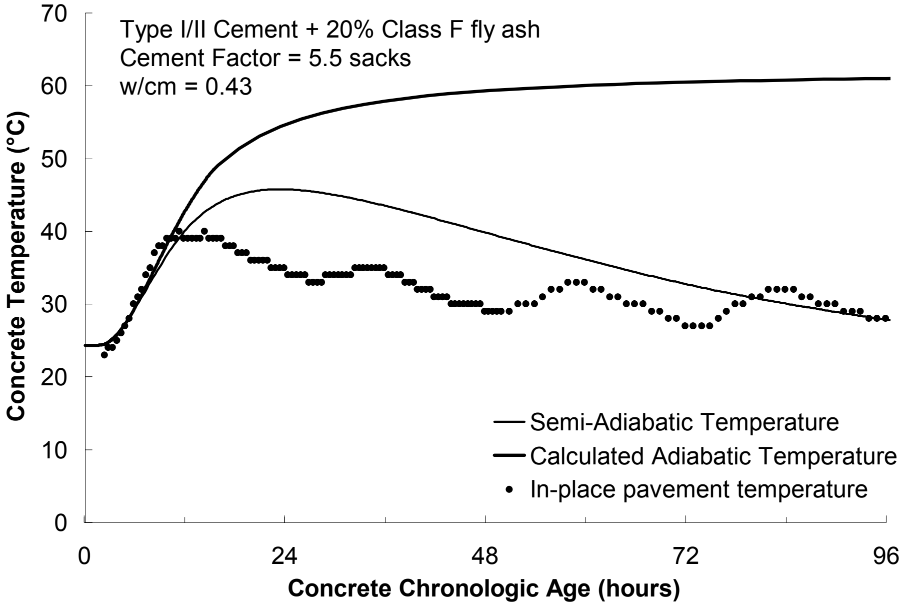

Figure 3-7: A comparison on the temperature rise of concrete cured under different conditions

3.2.5 Modeling the Degree of Hydration Development

The rate of cement hydration and the temperature development of a hydrating concrete mixture is dependent upon the concrete temperature, cement composition, cement fineness, admixtures used, aggregate type, water-cement ratio, etc. (ACI 305, 1991; De Sitter and Ramler, 1991).

Furthermore, during the hydration of cement, each of the Bogue compounds has different rates of hydration (shown in Figure 2-1). The simultaneous combination of these combined with the effect of mineral and chemical admixtures represent the development of hydration over time. In Section 2.2.1, it was shown that the heat of hydration is influenced by the chemical composition and fineness of the cement. It was further shown that the chemical composition of cement and mineral admixtures may vary significantly depending on the source they are processed from.

The development of hydration is affected by the size of the cement particles. For a given volume of cement, the smaller the particle size, the faster the rate of reaction will become. The reason being related to the fact that more surface area is in contact with free water; hence the dissolution process is more rapid. A further complication is caused by the fact that it has been shown that the chemical composition between different cement particle sizes are different. This would bring about different rates of reaction, depending on the compounds in each cement particle. All the aspects mentioned above are very complex to model with a pure mechanistic approach, and limited success has been reached in the past for plain cementitious systems. This becomes an even more daunting task when mineral and chemical admixtures are added into the system.

Therefore, it is a rather complicated task to incorporate all these factors in a mechanistic model that will accurately predict the hydration development. Pure mechanistic models that account for all the possible interactions are not available. It is for this reason that the hydration development is best determined by a testing procedure, and the problem is overcome by submitting the concrete to an adiabatic calorimeter test.

The test data from the adiabatic calorimeter test provide a means to determine the heat of hydration development as the hydration of the mixture progresses (van Breugel, 1991; RILEM 119-TCE, 1981; Radjy et al., 1994). It has been shown and is widely accepted that the ratio of the heat development heat as compared to the maximum heat available in the system is an accurate practical method to quantify the degree of hydration. The degree of hydration (α) is actually defined as the ratio between the quantity of hydrated cementitious material and the original quantity of cementitious material. Figure 3-8 presents the physical meaning of the degree of hydration, since it provides a method to quantify the progress of hydration for a specific concrete mixture. Since the degree of hydration is influenced by all the factors above, it becomes a unique "signature" of the concrete mixture. Any change in mixture proportions, source of cementitious materials, aggregate type, and the like, will result in a different degree of hydration, which will need to be re-determined.

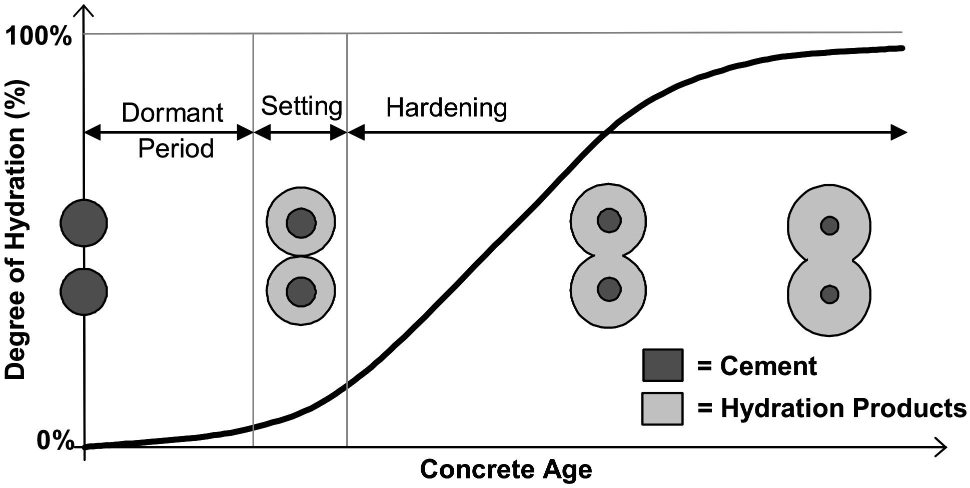

Figure 3-8: Physical meaning of the degree of hydration development

One of the objectives of this study is to develop a general model to characterize the degree of hydration, and heat of hydration development of concrete. With the predicted degree of hydration of a specific concrete mixture, one can predict the concrete temperature development under adiabatic conditions. The models should be general in nature and consider the effect of all the factors that have been shown in Section 2.2 to influence the heat of hydration. These factors include the effect of mixture proportions, cement chemical composition, cement fineness, and mineral admixtures.

3.2.5.1 Mathematical Formulation of the Degree of Hydration Development

Once test data of the degree of hydration development with equivalent age have experimentally been determined, the best-fit mathematical model of the data needs to be determined. Many mathematical forms of the hydration-maturity relationship have been proposed in past publications. Table 3-5 lists some of the mathematical formulations that have been used in the past. Equation 3-17 represents the **exponential** function used by Freiesleben Hansen and Pedersen (1985).

Figure 3-9 presents the degree of hydration curves that can be obtained by Equations 3-17, 3-18 and 3-19 as listed in Table 3-5. With any of these equations, one would be able to obtain a reasonable fit of the degree of hydration curve. It would be beneficial to use the same form of relationship to predict both strength and degree of hydration development. In Chapter 6, it will be shown that the exponential formulation is suited for use to model the strength-maturity relationship (Carino, 1991). The exponential model as defined in Equation 3-17 will, therefore, be selected to model the degree of hydration development over time. This expression requires the use of two parameters, whereas Equation 3-18 uses three parameters. The two parameters have distinctive physical meanings, which will be covered in the following section.

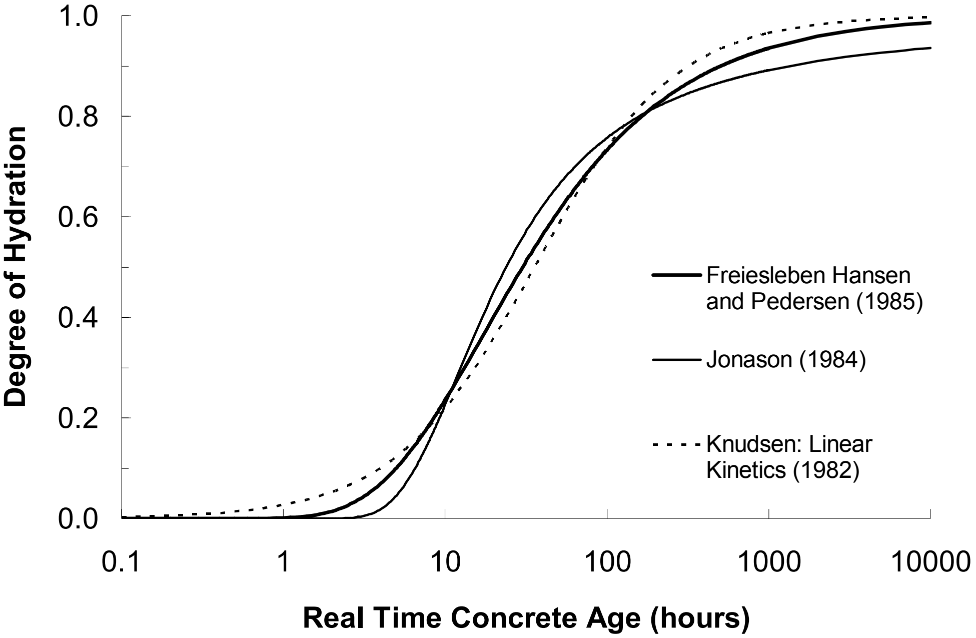

Figure 3-9: Comparing different hydration-maturity functions using Equations 3-17 to 3-19

Table 3-5: Different hydration-maturity relationships

Hydration-Maturity Relationship	**Numbering**
$\alpha(t_e) = \exp\left(-\left[\frac{\tau}{t_e}\right]^{\beta}\right)$ where, $\alpha(t_e)$ = degree of hydration at equivalent age, t_e, t_e = equivalent age at reference temperature (hrs), τ = hydration time parameter (hrs), and β = hydration slope parameter. *References:* Freiesleben Hansen and Pedersen (1985), Radjy and Vunic (1994), Kjellsen and Detwiler (1993)	*Equation 3-17*
$\alpha(t_e) = \exp\left[-\lambda_1\left(\ln\left(1+t_e/t_1\right)\right)^{-\kappa_1}\right]$ where, the parameters are as defined in Equation 14, except for: λ_1 = hydration shape parameter, κ_1 = hydration slope parameter, and t_1 = time parameter (hour). *References:* Byfors (1980), Jonasson(1984), and McCullough and Rasmussen (1999)	*Equation 3-18*
$\alpha(t_e) = \frac{t_e}{t_e + 1/C}$ where, the parameters are as defined in Equation 14, except for: C = Hydration shape parameter dependant on the particle size distribution and rate constant. *References:* Knudsen(1982), referred to as the dispersion model.	*Equation 3-19*
$\alpha(t_e) = 1 - \exp\left[-\gamma \cdot t_e\right]$ where, the parameters are as defined in Equation 14, except for: γ = Hydration shape parameter. *References:* Nakamura et al. (1999)	*Equation 3-20*

3.2.6 Physical Interpretation of the Degree of Hydration Formulation

In the Section 3.2.5.1, it was recommended to use the exponential formulation to characterize the degree of hydration development. The following exponential function will be used throughout this study to represent the degree of hydration development:

$$\alpha(t_e) = \alpha_u \cdot \exp\left(- \left[\frac{\tau}{t_e} \right]^{\beta} \right) \qquad \textit{Equation 3-21}$$

where, $\alpha(t_e)$ = the degree of hydration at equivalent age, t_e,

τ = hydration time parameter (hrs),

β = hydration slope parameter, and

α_u = ultimate degree of hydration.

Equation 3-21 is similar to Equation 3-17, except that an additional parameter (α_u) has been introduced to account for the phenomenon that complete hydration seldom occurs (discussed in Section 2.2.2). With experimental data available, the best fit hydration parameters, to calibrate the model to test data, can be determined by regression analysis. The degree of hydration can be determined at temperatures other than the reference temperature by using the equivalent age maturity method. With this method, only the hydration time parameter is adjusted and the degree of hydration is translated with respect to time. The physical effect and meaning of the hydration parameters (τ, β, and α_u) is shown in Figures 3-10 to 3-12, and the effect of each parameter will be discussed next.

Due to the formulation of the exponential model, the hydration time parameter (τ) corresponds to the time at which 37% of the degree of hydration has progressed. The earlier the hydration time parameter, the more rapid the hydration. From Figure 3-10, it may be seen that a change in τ causes a time shift in the hydration curve. Higher values of τ is, therefore, anticipated for more reactive cementitious materials such as Type III cements, whereas, lower τ values are expected for cements that contain fly ash or GGBF slag.

In Figure 3-11, it may be seen that a change to the hydration slope parameter, β, predominantly changes the slope of the hydration curve, however, the hydration time is additionally affected. An increase in β is associated with more reactive cementitious materials; however, because the hydration time is simultaneously delayed, a coinciding change in the τ parameter is also required.

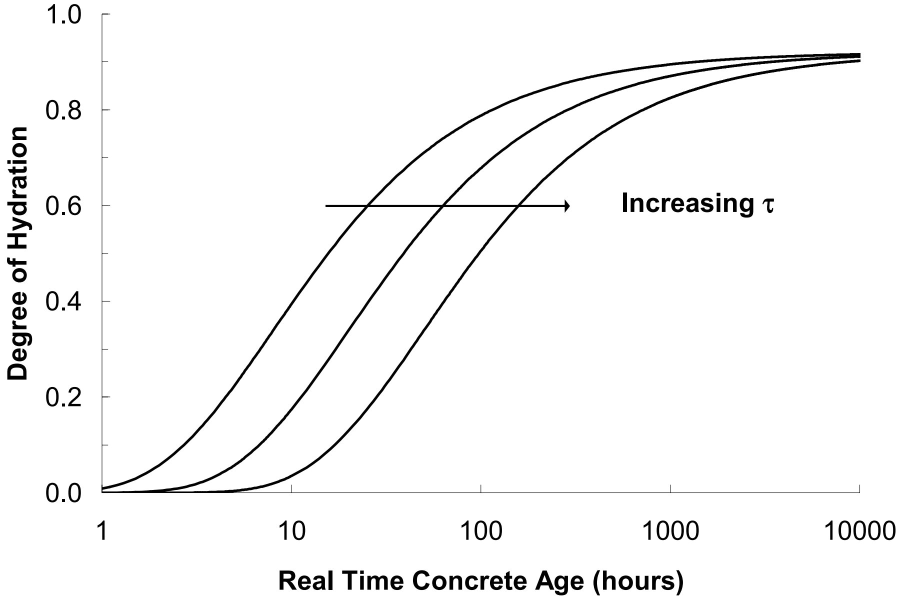

Figure 3-10: Effect of change in hydration time parameter (τ) on the degree of hydration development

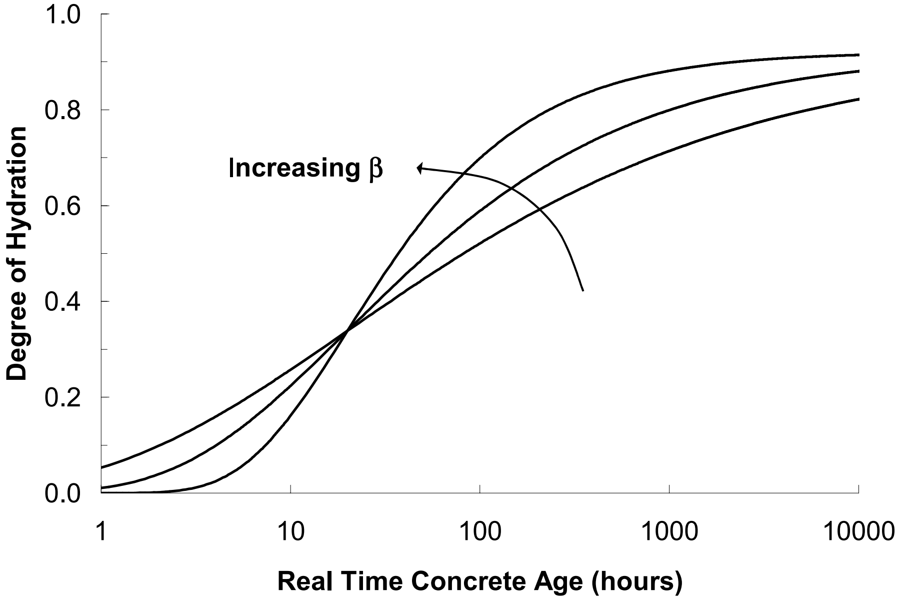

Figure 3-11: Effect of change in hydration slope parameter (β) on the degree of hydration development

Figure 3-12 presents the effect of a change in the ultimate degree of hydration parameter on the degree of hydration curve. It may be seen that a change in α_u affects the magnitude of the degree of hydration, since it is a constant multiplied with the degree of hydration development. The higher α_u, the higher the final degree of hydration will become, and additional total heat will become available for the hydration process.

The effect of the ultimate degree of hydration parameter is not truly similar to the actual effect of the water-cement ratio. This can be seen if the behavior in Figure 3-12 is compared to that of experimental results shown in Figure 2-9. From the experimental results, it appears as if the effect of the water-cement ratio only emerges after 10 to 20 hours of hydration. The use of the ultimate degree of hydration parameter will be evaluated based on experimental results.

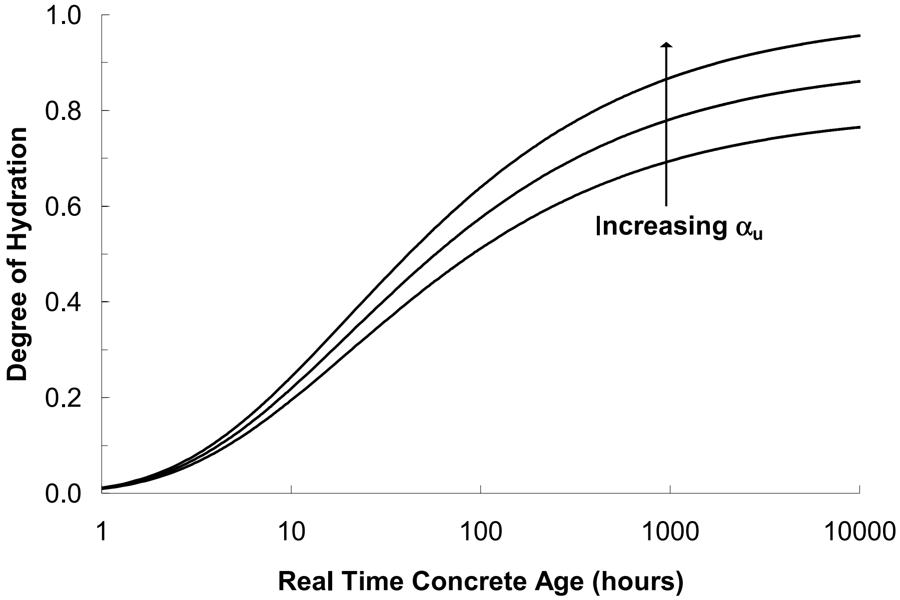

Figure 3-12: Effect of change in ultimate degree of hydration (α_u) on the degree of hydration development

3.2.7 Ultimate Degree of Hydration

In Equation 3-21, a parameter (α_u) has been introduced to characterize the ultimate extent of the hydration reaction. The use of this parameter is necessary, since in Section 2.2.2 it was indicated that complete hydration seldom occurs in concrete mixtures. The effect of the water-cement ratio on the degree of hydration and heat evolution can be seen in Figure 2-8 and 2-9. After investigating the hydration of a range of different cementitious materials, Mills (1966) stated that, “In most, if not all, cement pastes hydration stops before the cement is totally consumed.”

The reason of the decrease in maximum degree of hydration is related to the fact that that hydration can only continue to develop if certain conditions are reached. In Section 2.2.2, these conditions were discussed, and they can be modeled as follows:

1. **Sufficient space is available for all hydration products:**

   During hydration, the hydration products gradually fill the voids initially occupied by the mixing water. When no more capillary space is available, the hydration reaction ceases. From this requirement, it may be concluded that the lower the water-cementitious ratio, the less water per unit volume, and the lower the ultimate degree of hydration. This requirement can be quantified as follows (Hansen, 1986):

   $$\alpha_u = \frac{w/c}{0.36} \leq 1.0 \qquad \textit{Equation 3-22}$$

2. **Sufficient free water is available for the hydration reaction:**

   Free capillary water is required for the hydration process to continue. Based on properties of typical portland cements, Hansen (1986) recommended the following fromulation for air-entrained paste:

   $$\alpha_u = \frac{w/c}{0.42} \leq 1.0 \qquad \textit{Equation 3-23}$$

In order to quantify the effects of the factors discussed above, Mills (1966) performed numerous tests to determine the maximum degree of hydration by measuring the amount of chemically bound water (see Section 3.2.4.1) after hydration is completed. Based on experimental results, calculations, and various physical properties recommended by Powers, Mills (1966) recommend that the ultimate degree of hydration for saturated concrete be calculated as follows:

$$\alpha_u = \frac{0.261 \cdot w/c}{(w_n/c)_{\max} \cdot (0.194 + w/c)} \qquad \textit{Equation 3-24}$$

where, α_u = ultimate degree of hydration, and

$(w_n/c)_{max}$ = maximum mass ratio of (w_n/c) at complete hydration (g/g).

Maximum mass ratio of w_n/c is as discussed in Section 3.4.2.1, and Mills recommends the use of the following:

- Cement: $(w_n/c)_{max}$ = 0.253, (Powers and Brownyard (1948) additionally found 0.253)
- Cement with 50% GGBF Slag: $(w_n/c)_{max}$ = 0.261

If the recommended $(w_n/c)_{max}$ of 0.253 for cement is used, Equation 3-24 can be simplified to Equation 3-25, which is recommended for use by van Breugel (1997) and Cervera (1999). When GGBF slag is used, Equation 3-26 presents the form recommended by Mills. The effect of water-cement ratio on the ultimate degree of hydration as determined by Equations 3-23, 3-25 and 3-26 are shown in Figure 3-13. This figure indicates that there is a large difference in the calculated ultimate degree of hydration as per the calculations of Mills and Hansen. The most appropriate formulation will be determined from the testing performed under this program.

For Cement:

$$\alpha_u = \frac{1.031 \cdot w/c}{0.194 + w/c} \qquad \text{Equation 3-25}$$

For Cement with 50% GGBF Slag:

$$\alpha_u = \frac{w/c}{0.194 + w/c} \qquad \text{Equation 3-26}$$

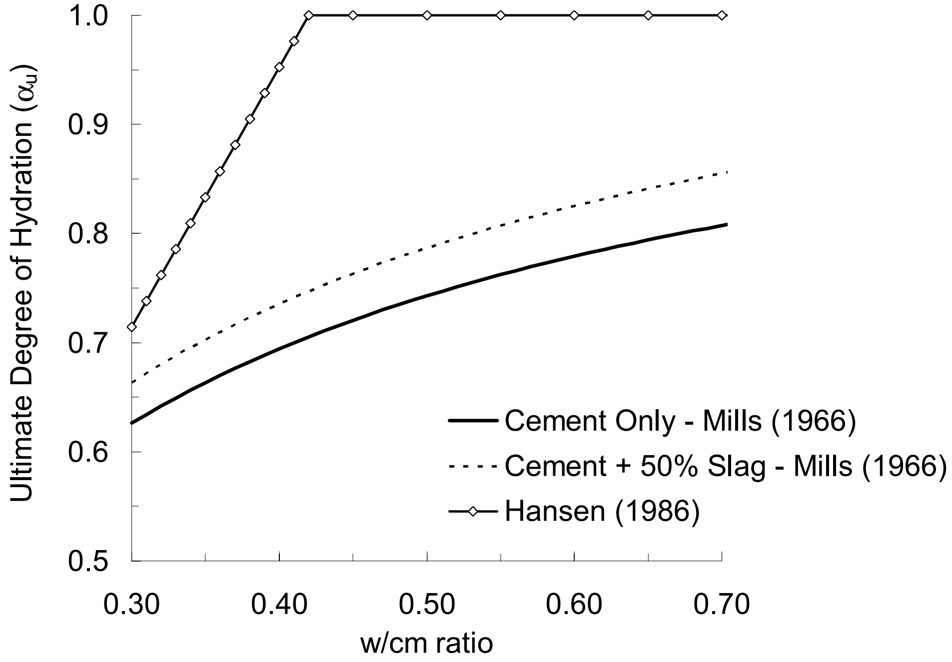

Figure 3-13: Comparing the effect of water-cementitious ratio on the ultimate degree of hydration predicted by Equations 3-23, 3-25 and 3-26

The ultimate degree of hydration is unaffected by the curing temperature. Kjellsen et al. (1991) confirmed that the maximum extent of the hydration is unaffected by the curing temperature. They stated that based "... on a variance analysis it appears that the amount of unhydrated cement was independent of the curing temperature. This was also the case for the chemically bound water content. This implies that the ratio of the chemically bound water to the degree of hydration is not significantly influenced by the temperature within this range."

3.2.8 Modeling the Heat Generations and the Associated Temperature

The temperature destitution in concrete specimen curing under adiabatic conditions, where there is no heat transfer to the environment, can be determined with Equation 3-1. From Equation 3-1, the temperature development of hydrating concrete can be determined as follows:

$$\frac{dT}{dt} = \frac{Q_H}{\rho \cdot c_p} = \frac{dH}{dt}\left(\frac{1}{\rho \cdot c_p}\right) \qquad \textit{Equation 3-27}$$

where, T = temperature of the concrete (°C),
ρ = concrete density (kg/m^3),
c_p = concrete specific heat capacity (J/kg/°C),
Q_H = rate of heat generation (W/m^3), and
H = total heat of hydration of the concrete (J/m^3).

The specific heat of hardening concrete is influenced by the unbound water in the concrete and changes over time. A model for the specific heat is covered in Section 3.2.8.1. In Equation 3-1, the thermal conductivity of the concrete will be required if heat transfer to the environment occurs. Section 3.2.8.2, provides a discussion on the calculation of the thermal conductivity of hardening concrete. The rate of heat generation heat, Q_H, is dependent on the degree of hydration:

$$Q_H = \frac{dH}{dt} \qquad \textit{Equation 3-28}$$

where, H = total heat of hydration of the concrete (J/m^3), defined as:
= $H_u \cdot C_c \cdot \alpha$
and H_u = ultimate heat of hydration of cementitious materials at 100% hydration (J/kg), as defined in Equation 3-14,
C_c = cementitious materials content (kg/m^3), and
α = degree of hydration, as defined in Equation 3-21.

The degree of hydration is a function of the time and temperature history, which can be calculated, by the equivalent age maturity function. With this approach, the concrete temperature can be evaluated at discrete times after batching of the specimen. When Equation 3-28 is calculated in terms of the chronologic age, the age conversion factor as defined in Equation 3-6 can be used and the rate of heat generation, at time, t, can be determined as follows:

$$Q_h(t) = H_u \cdot C_c \cdot \left(\frac{\tau}{t_e}\right)^{\beta} \cdot \left(\frac{\beta}{t_e}\right) \cdot \alpha(t_e) \cdot \frac{E}{R}\left(\frac{1}{273+T_r} - \frac{1}{273+T_c}\right) \qquad \textit{Equation 3-29}$$

Figure 3-14 provides an indication of how a change in placement temperature is accounted for with the proposed model. Note that the nonlinear behavior of increased hydration is captured with the Arrhenius equation. The modeled nonlinear behavior is similar to that experimentally determined and shown in Figure 1-7.

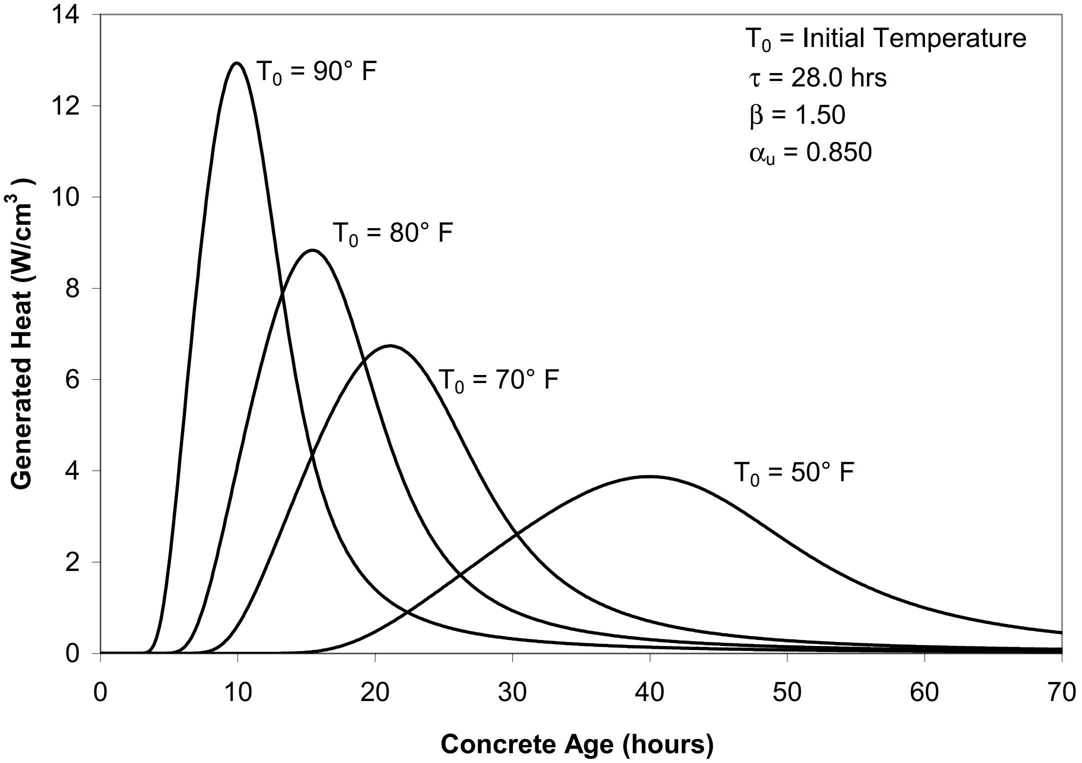

Figure 3-14: The effect of different initial mixture temperatures on the temperature development during adiabatic conditions as predicted with Equation 3-29

3.2.8.1 Specific Heat of Hardening Concrete

The specific heat of a material can be defined as the ratio of the amount of heat required to raise a unit weight of a material 1°C, to the amount of heat required to raise the same weight of water by 1°C (Janna, 2000). The temperature of the concrete and the water has a significant impact on the specific heat of the mixture (Scanlon et al., 1994; Khan et al., 1998). Based on test performed on hardening concrete, it is reported that the heat capacity is linear with the logarithm of time, which for common cement types is similar to a linear decline with the degree of hydration (De Shutter and Taerwe, 1995; Khan et al., 1998). Test data from De Shutter and Taerwe (1995) show a 13% decrease in concrete specific heat during hardening. The following model, developed by van Breugel (1997), is recommended for use in this study, since it accounts for the effect of temperature, mixture proportions, and decreases during hardening:

$$c_p = \frac{1}{\rho} \cdot (W_c \cdot \alpha \cdot c_{cef} + W_c \cdot (1-\alpha) \cdot c_c + W_a \cdot c_a + W_w \cdot c_w) \qquad \textit{Equation 3-30}$$

where, c_p = current specific heat of the concrete mixture (J/kg/ºC),

ρ = unit weight of concrete mixture (kg/m^3),

W_c, W_a, W_w = amount by weight of cement, aggregate, and water (kg/m^3),
c_c, c_a, c_w = specific heats of cement, aggregate, and water (J/kg/ºC),
c_{cef} = fictitious specific heat of the hydrated cement (J/kg/ºC),
= $8.4 \cdot T_c + 339$ (J/kg/ºC),
α = degree of hydration, and
T_c = current concrete temperature (ºC).

Based on literature, the following specific heat values are recommended for cement, aggregate, and water:

Table 3-6: Typical specific heat values for concrete constituents

Material	**Specific heat (J/kg/ºC)**	**Reference**
Cement	1140	Mindess and Young, 1981
Water	4187	Scanlon et al., 1994
Limestone / Dolomite	910	Trinhztfy et al., 1982
Sandstone	770	
Granite / Gneiss	780	
Siliceous River Gravel	770	
Basalt	900	

The proposed specific heat model was evaluated with the mixture proportions of a typical paving mixture. The mixture proportions per cubic meter consisted of 380 kg cement, 154 kg water, and 1631 kg of coarse and fine aggregate, which provided a unit weight of 2224 kg/m^3. Figure 3-15 was developed based with the model shown in Equation 3-30. It may be concluded that the model provides an adequate estimate of the specific heat since it fulfills the following requirements:

- the calculated values are between the recommended range of 800 and 1200 J/kg/°C,
- the specific heat decreases linearly with an increase in degree of hydration,
- there is 8 to 14 % difference in specific heat of the mature and hardened concrete,
- the specific heat increases with an increase in concrete temperature, and
- the model accounts for the effect of mixture proportions.

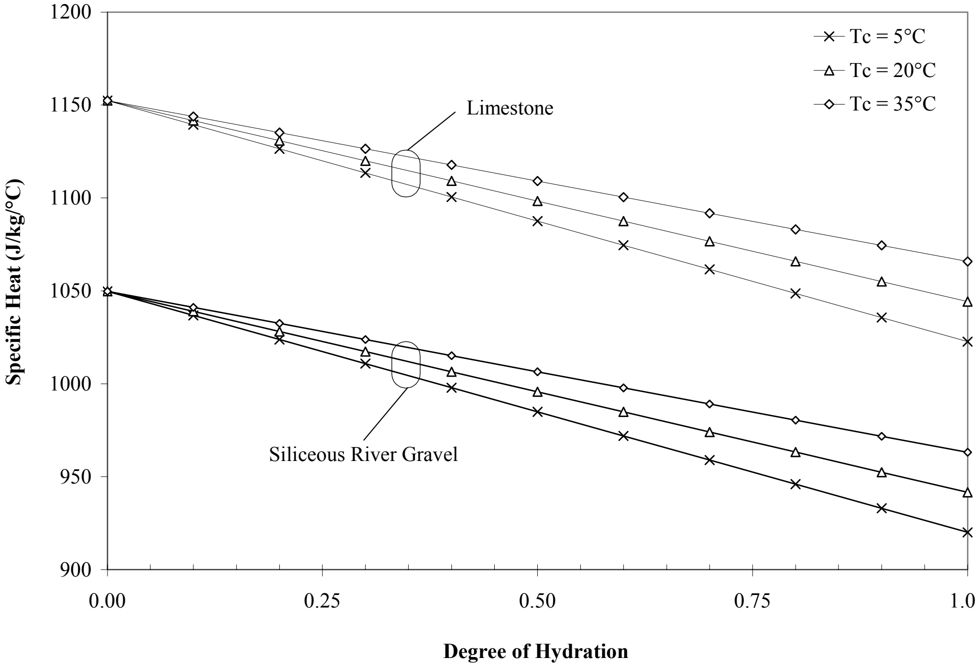

Figure 3-15: Concrete specific heat as influenced by the mixture proportions, temperature, and degree of hydration calculated by Equation 3-30

3.2.8.2 Thermal Conductivity of Hardening Concrete

Thermal conductivity of concrete (*k*) provides an indication of concrete's ability to transfer heat and is defined as the ratio of the rate of heat flow to the temperature gradient (Janna, 2000). The thermal conductivity is of great importance since it determines the rate of penetration of heat into the concrete and hence the magnitude of temperature gradients and thermal stresses (Mindess and Young, 1981).

It is reported that the water content, density, and temperature of the concrete may significantly influence the thermal conductivity (Scanlon et al., 1994). The thermal conductivity of ordinary concrete depends on its composition and especially the aggregate type used. Typical values for the thermal conductivity of concrete are listed in Table 3-7.

Values, similar to those shown in Table 3-7, are recommended by ACI Committee 207 (1995). Contrary to the values reported above, Khan et al. (1998) reported for normal strength concrete, thermal conductivity values for maturing concrete of 1.72-1.74 W/m/ºC and values of 1.14-1.17 W/m/ºC for hardened concrete. These values are significantly lower than those that are listed in Table 3-7. Khan et al. concluded that, on average the thermal conductivity of maturing concrete is 33 percent higher than that of hardened concrete. This value is in agreement with that obtained by others (De Shutter and Taerwe, 1995), which showed a 21 percent decrease in thermal conductivity from the maturing state to the hardened state.

Table 3-7: Thermal conductivity of moist mature concrete (Scanlon et al., 1994).

Aggregate Type	**Moist Density of Concrete**		**Thermal Conductivity**	
	(kg/m^3)	**(lbs/ft^3)**	**(W/m/ºC)**	**(Btu/h/ft/°F)**
Quartzite	2350-2440	147-152	4.1-3.1	2.33-1.75
Dolomite	2500	156	3.3	1.9
Limestone	2450-2440	153-151	3.2-2.2	1.83-1.25
Sandstone	2400-2130	150-133	2.9	1.7
Granite	2420	151	2.6	1.5
Basalt	2520-2350	158-157	2.0-1.9	1.17-1.08

From this information, assuming that the decline in this parameter is linear with the logarithm of time, which for common cement types is very similar to a linear decline with degree of hydration, a relationship that considers these initial and final values could be expressed as:

$$k(\alpha) = k_u \cdot (1.33 - 0.33 \cdot \alpha) \qquad \textit{Equation 3-31}$$

where, $k(\alpha)$ = the current thermal conductivity (W/m/ºC),

k_u = ultimate thermal conductivity of mature concrete (W/m/ºC), and

α = the degree of hydration.

3.3 TEMPERATURE PREDICTION AND HEAT EXCHANGE WITH THE ENVIRONMENT

In concrete placed under field conditions, heat will be transferred to and from the surroundings, and the temperature development in the concrete structure is determined by the balance between heat generation in the concrete and heat exchange with the environment. The surroundings could either be an additional source of heat or at a lower temperature than the hydrating concrete. The transient heat balance as governed by Fourier's law is as defined in Equation 3-1.

Different numerical techniques are available to provide approximations for the time and space dependent heat-transfer problem. Both finite element and finite difference techniques may be used. It is proposed to use a transient one-dimensional finite difference model, since it requires less solution time without losing any accuracy during the heat transfer computation (Incorpera et al., 1990). The disadvantage of this method is that stability of the solution needs to be insured. To overcome this shortcoming, it is proposed to develop the temperature prediction program to choose appropriate element sizes to insure conversion of the finite difference method.

With this approach, the concrete slab, subbase, and subgrade are divided into finite layers and the number of layers will be determined to provide the necessary accuracy. The boundary conditions are specified in terms of heat fluxes, and these have to be converted into temperatures.

The one-dimensional relationship between flux, temperature, and time in the unsteady state, can be expressed as (Chapra and Canale, 1998):

$$-\frac{q_z}{dz} = -\rho \cdot c_p \cdot \frac{dT}{dt} \qquad \text{Equation 3-32}$$

Where, q_z = heat flux in the z-direction (W/m^2), and
all other terms as defined previously.

From the above relationship, the change in temperature at the boundary of a discrete system can be calculated as follows:

$$\Delta T = \frac{q_z}{\rho \cdot c_p} \cdot \frac{\Delta t}{\Delta z} \qquad \text{Equation 3-33}$$

Where, ΔT = the change in temperature (°C),
Δt = the time increment (s), and
Δz = the distance increment (m).

Different thermal conditions may exist at the boundaries of the system. The boundary conditions can be either a fixed temperature, or a heat flux. An example of a fixed temperature condition occurs at the bottom of the soil profile where the soil temperature is governed by the constant deep ground temperature. Radiation and convection are examples where heat is exchanged through a heat flux.

A finite difference model will be developed to include the heat of hydration of the cementitious materials and the heat transfer mechanisms of thermal conduction, convection (including evaporative cooling), solar radiation, and irradiation. Figure 3-16 illustrates the role of each of these heat exchange methods in the case of a concrete slab. Figure 3-16 shows that the amount of solar radiation will be influenced by the prevailing cloud cover and by the reflectivity of the pavement surface. The heat exchange models will be based on those developed by previous research projects; however, the models will be calibrated to ensure accurate predictions of the in place concrete temperature. In the following sections, each of these heat transfer mechanisms and models will be presented and discussed.

3.3.1 Conduction

Thermal conduction is defined as heat transport in a material by transfer of heat between portions of the material that are in direct contact with each other (Janna, 2000). In a pavement system, conduction occurs between the pavement layers, and between the slab surface and the surface protection (insulation) used at early-ages. Conduction models for heat transfer to the support material and surface coverings will be covered in the remainder of this section.

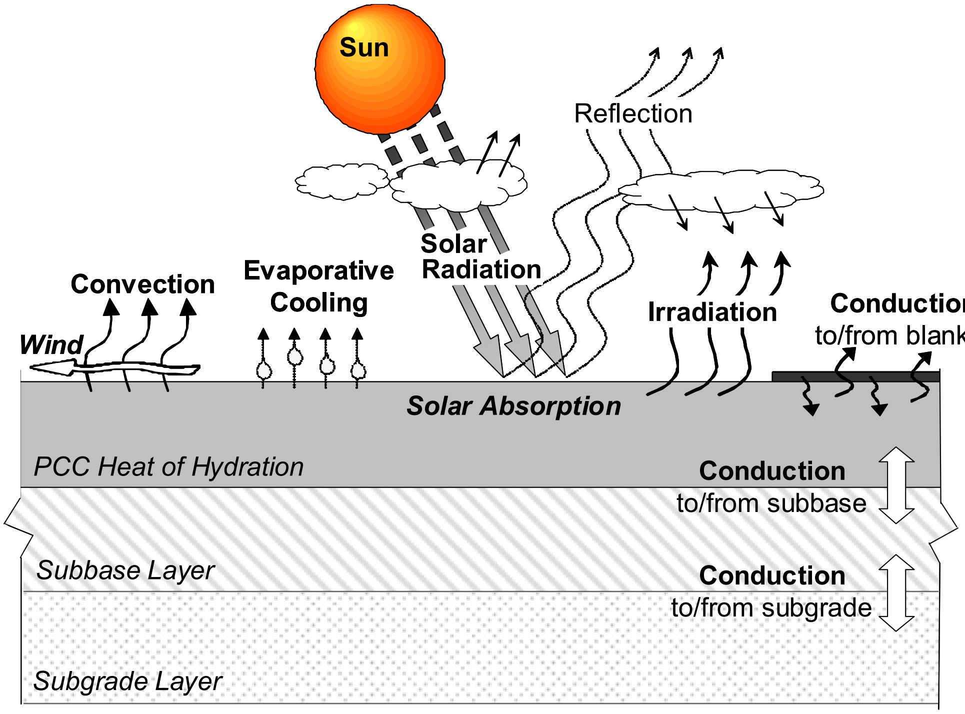

Figure 3-16: Heat transfer mechanisms between the concrete pavement and its surroundings

3.3.1.1 Conduction to Supporting Layers

The governing equation (Equation 3-33) for thermal conduction reveals that heat transfer is a function of the thermal conductivity, density, and specific heat of the materials in contact. The temperature and properties of the base underlying the concrete could have a significant influence on the temperature development of the hardening concrete. For example, in Texas, concrete pavements are frequently placed over an asphalt concrete stress relief layer. During this study, an asphalt surface temperature of 142°F was measured at around 1:30 pm during the month of August. Subbase temperatures of this magnitude will increase the bottom concrete temperature. Tables 3-8 and 3-9 present typical thermal characteristics of some commonly used base materials.

3.3.1.2 Conduction to Surface Protection

Conduction further transpires between the concrete surface covering and the concrete slab. These covering include insulation blankets, curing compound, plastic sheets, foams, and other patented products. Insulation blankets are often used to provide a uniform temperature gradient, to prevent concrete freezing under cold weather conditions and in applications where very rapid strength gain is required (FHWA SP 201, 1994). The use of blankets in cold weather conditions will increase the strength gain considerably, since some of the heat generated during hydration is trapped, which allows hydration at increased temperatures. It is reported that when a period of less than 16 hours is required for early opening to traffic the use of blankets become beneficial (FHWA SP 201, 1994). These blankets should be placed after the sawing operation and near the time the slab temperature begins to decrease from the peak temperature. The steady state heat transfer to the surrounding (excluding any radiation effects) can be expressed as follows (McAdams, 1954):

$$q = h_0 \cdot (T_s - T_a) \qquad \text{Equation 3-34}$$

where, q = Heat flux (W/m^2),
h_0 = overall heat transfer coefficient (W/m^2/°C),
T_s = surface temperature (°C), and
T_a = air temperature (°C).

Table 3-8: Material properties of characteristics of various base materials (SHRP-C-321, 1993; and Thompson et al., 1998)

Base Material	**Density (kg/m^3)**	**Thermal Conductivity (W/m/ºC)**	**Specific Heat (J/kg/ºC)**
Gravel, dry	1703	0.52	838
Gravel, moist	1898	2.42	1047
Asphalt	2302	1.38	1047
Stabilized Base	2,339	3.32	1,005
Cohesive Subgrade	2,066	1.59	1,214

Where more that one layer of insulation is used, an overall heat transfer coefficient can be calculated, which is a single coefficient that defines the thermal resistance of all the materials. The overall heat transfer coefficient can be calculated with the formulation shown in Equation 3-35 (McAdams, 1954). Table 3-9 contains thermal conductivity values of various insulation materials that could be encountered during construction operations.

$$h_0 = \left(\frac{d_1}{k_1} + \frac{d_2}{k_2} + \ldots + \frac{d_n}{k_n} \right)^{-1} \qquad \text{Equation 3-35}$$

where, h_0 = overall heat transfer coefficient (W/m^2/°C),
$d_1, d_2, \ldots d_n$ = thickness of n successive layers (m), and
$k_1, k_2, \ldots k_n$ = thermal conductivity of n successive layers (W/m/ºC).

3.3.2 Convection

Thermal convection is the heat transferred from a surface to a gas (or fluid), where convection is the movement of a mass of gas (or liquid) due to the temperature difference, and physical contact of the gas (or liquid) is the actual method of heat transfer. Convection is, therefore, the mechanism of heat transfer of heat between the concrete surface and the environment. Figure 3-16 illustrates that convection includes the effect of wind and evaporation on the heat transfer process. The effect of evaporative cooling will be discussed in Section 3.3.2.1.

Table 3-9: Thermal characteristics of various materials

Surface Covering Material	**Thermal Conductivity (W/m/ºC)**	**Reference**
Plastic sheet	0.043	ASHRAE, 1993
Water	2.168	
Blankets: Mineral Fiber (ρ = 0.4-2 lb/ft^3)	0.039	
Organic Fiber: ρ = 0.75-1.5 lb/ft^3	0.043	
ρ = 1.5-3 lb/ft^3	0.033	
Polyurethane foam	0.035	Turner, 1981
Blanket: Glass Fibers (ρ = 1-2 lb/ft^3)	0.055	
Blanket: Cotton Wool Mats (ρ = 5 lb/ft^3)	0.042	McAdams, 1954
Blanket: Mineral Wool: ρ = 9.4 lb/ft^3	0.039	
ρ = 19.7 lb/ft^3	0.042	

For flat surfaces such as concrete pavements, the wind velocity across the concrete surface determines whether convection is forced or free. In the case of free convection, the transport of heat is the result of temperature gradients between the body and the air. In this study, the convective heat transfer is modeled with the following equation (McAdams, 1954):

$$q_c = h_c \cdot (T_s - T_a) \qquad \textit{Equation 3-36}$$

where, q = convection heat flux (W/m^2),
h_c = surface convection coefficient (W/m^2/°C),
T_s = surface temperature (°C), and
T_a = air temperature (°C).

The rate of heat flow from a horizontal surface is controlled by the magnitude of the temperature difference, the speed of the air flow, and the surface texture of the member. Since heat is transferred from the warmer horizontal plate to the adjacent air, the air is heated, its density becomes less, and it has a tendency to rise. As the heated air rises, it is replaced by cooler air, which in turn is heated, rises, and this recurring process continues until the heat balance is eliminated. This complex phenomenon has been thoroughly investigated by numerous researches in the heat transfer field. From combinations of experimental work from Heilman (1929) and Langmuir (1981), a model is available for use on a smooth horizontal surface that is valid for both forced and free convection (ASHRAE, 1993). However, this model does not include any modification due to surface roughness and it is recommended that the surface convection coefficient above be increased by 6% to account for this effect (McAdams, 1954). Therefore, the following model is recommended for use to determine the surface convection coefficient:

$$h_c = 3.727 \cdot C \cdot \left(0.9 \cdot \left(T_s + T_a\right) + 32\right)^{-0.181} \cdot \left(T_s - T_a\right)^{0.266} \cdot \sqrt{1 + 2.857 \cdot w} \qquad \textit{Equation 3-37}$$

where, h_c = surface convection coefficient (W/m^2/°C),
C = constant depending on the shape and heat flow condition,
= 1.79, when surface is warmer than the air,
= 0.89, when surface is cooler than the air,
T_s = surface temperature (°C),
T_a = air temperature (°C), and
w = wind speed (m/s).

In some heat transfer models for concrete structures (Germann Instruments, 1988; Digital Site Systems, Inc., 1988; Yang, 1996; McCullough and Rasmussen, 1999), the following formulation has been used to determine the magnitude of the convection coefficient:

$$\begin{aligned} &\text{If } w \le 5 \text{ m/s}, && \text{then } h_c = 20 + 14 \cdot w \\ &\text{If } w > 5 \text{ m/s}, && \text{then } h_c = 25.6 \cdot w^{0.78} \end{aligned} \qquad \textit{Equation 3-38}$$

where, h_c = surface convection coefficient (kJ/m^2/h/°C), and
w = wind speed (m/s).

This equation was obtained from experimental data for the flow of air at room temperature parallel to a smooth ***vertical*** copper plate (McAdams, 1954). The original equation presented by McAdams (1954) is very similar to the form of Equation 3-38 and once converted to equivalent units is as follows:

$$\begin{aligned} &\text{If } w \le 4.87 \text{ m/s}, && \text{then } h_c = 20.24 + 14.08 \cdot w \\ &\text{If } w > 4.87 \text{ m/s}, && \text{then } h_c = 25.82 \cdot w^{0.78} \end{aligned} \qquad \textit{Equation 3-39}$$

These equations do not incorporate the fact that the surface convection coefficient is influenced by the magnitude of the temperature difference, since the tests were all performed at room temperature (70°F). McAdams (1954) acknowledged this relationship, and recommended that the wind speed in the above equations be modified by a multiplier to account for this effect. In the convection formulation in Equation 3-37, incorporates this effect.

The use of the convection equation shown in Equation 3-38 is, therefore, more appropriate for use to determine the effect of convection on vertical elements such as columns, beam webs, or retaining walls. However, the multiplier to the winds speed needs to be incorporated when the air temperatures is above room temperature and the effect of a rough concrete surface as apposed to a smooth plate should be incorporated.

Figure 3-17 provides a comparison of the surface convection coefficient associated with a vertical (Equation 3-38) and horizontal plate (Equation 3-37) as presented in this section. Note that a vertical surface has a significant higher amount of heat loss that is transferred as the wind speed is increased.

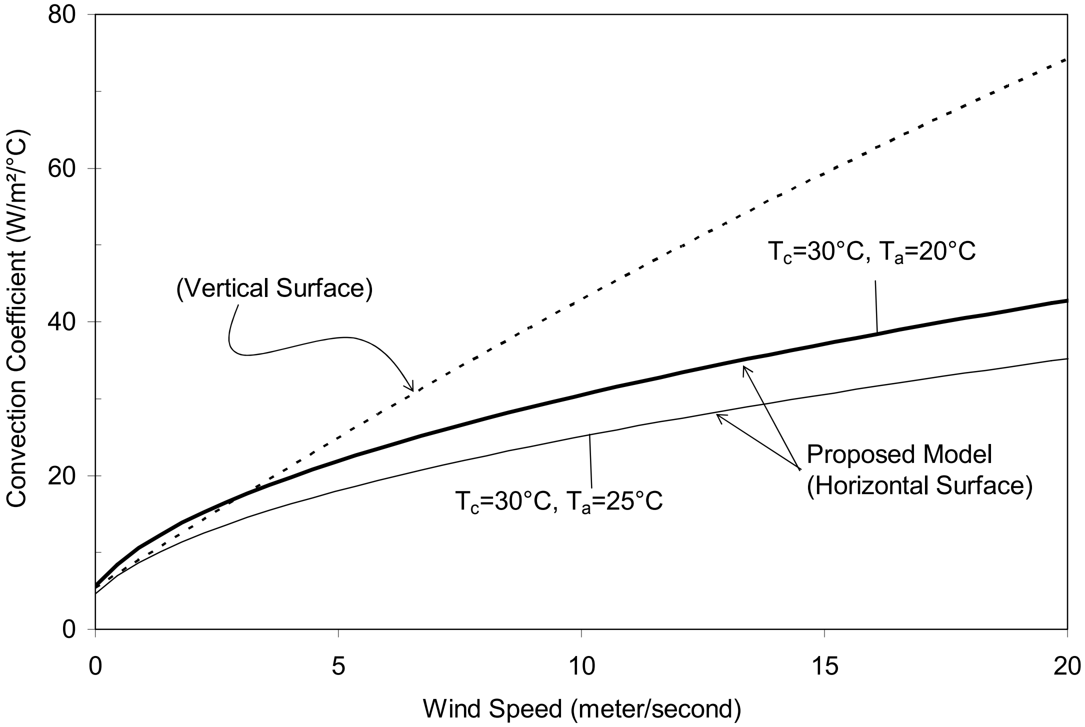

Figure 3-17: Comparison of different convection coefficients as influenced by wind speed

Since heat transfer due to convection could simultaneously occur with the presence of surface insulations, the overall heat transfer coefficient has to be determined that includes both these effects. The overall heat transfer coefficient can be calculated as follows (with all parameters as defined previously) (McAdams, 1954):

$$h_0 = \left(\frac{1}{h_c} + \frac{d_1}{k_1} + \frac{d_2}{k_2} + \ldots + \frac{d_n}{k_n} \right)^{-1} \qquad \textit{Equation 3-40}$$

3.3.2.1 Heat Transfer due to Evaporative Cooling

Prior to initial set, most concrete mixtures bleed. Bleeding is the phenomenon where some of the water in the mixture rises to the surface. This occurs as water has the lowest specific gravity of the mixture components, and the heavier particles tend to settle. Bleed water will accumulate on the surface and will evaporate over time. Figure 3-18 presents a freshly paved concrete pavement and the accumulation of surface water may be seen.

Figure 3-18: The accumulation of bleed water on the surface of a newly paved section

In some cases, liquid-curing membranes, water fogging of the pavement surface, or other coverings are used as curing methods. When evaporation of water from a surface occurs, the energy associated with the phase change is the latent heat of vaporization, which causes evaporative cooling. This effect is well known to man, as the human body cools itself at high temperatures by producing perspiration, which evaporates to produce a cooling effect. The amount of energy dissipated through evaporative cooling can be determined as follows (ASHRAE, 1993):

$$q_{evap} = -E_c \cdot h_{lat} \qquad \textit{Equation 3-41}$$

where, q_{evap} = heat flux due to evaporative cooling (W/m^2),

E_c = evaporation rate of water from concrete surface (kg/m^2/s), and

h_{lat} = latent heat of vaporization (J/kg).

In metric units, the latent heat of vaporization is the quantity of heat, in joules, required to evaporate 1 gram of water. The latent heat of vaporization is a function of the surface water temperature and can be approximated as follows (ASHRAE, 1993):

$$h_{lat} = 2{,}500{,}000 + 1859 \cdot T_{sw} \qquad \textit{Equation 3-42}$$

where, h_{lat} = latent heat of vaporization (J/kg), and
T_{sw} = temperature of surface water (°C).

Where curing membranes and water fogging is used, the duration of latent heat development can be determined from the evaporation rate per unit area and by knowing the thickness of the membranes. Most states specify the curing compound application rate, and ASTM C 309 (1998) recommends a rate of application of 200 ft^2/gal (5m^2/liter).

The evaporation rate of water from free surfaces (E_w) is driven by the difference in vapor pressure between the air and the evaporating water. Menzel was the first to publish a graphical solution to predict evaporation from lakes and other bodies of water (Menzel, 1954). ACI Committee 305 (2000) recommends a version of Menzel's nomograph to calculate evaporation rate of water from free surfaces as indicator to evaluate the risk of plastic shrinkage cracking. The rate of water evaporation from a concrete surface (E_c) is equal to the evaporation rate of water from free surfaces (E_w) only when the concrete surface is covered with bleed water (Al-Fadhala and Hover, 2001). It has been shown that the amount of water that evaporates from the concrete surface is dependent on the bleeding rate, the concrete surface texture, and the curing method used (Rochefort, 2000; Al-Fadhala and Hover, 2001). The bleeding rate for a specific mixture is a complex issue that is currently not well understood. It has been shown to be influenced by the water-cement ratio, cement content, concrete degree of hardening, and type of cementitious materials used (Al-Fadhala and Hover, 2000; Almusallam et al., 1998).

After laboratory tests, Al-Fadhala and Hover (2001) presented the formulation in Equation 3-43 to determine the rate of water loss from a concrete surface as compared to the water loss from a free surface. Figure 3-19 presents the development of the E_c/E_w ratio from Equation 3-43. Note that there is a rapid reduction in the concrete and mortar evaporation rate as the concrete hardens over time.

$$\frac{E_c}{E_w} = \exp\left(-\left(\frac{t}{a}\right)^{1.5}\right) \qquad \textit{Equation 3-43}$$

where, E_c = evaporation rate from a concrete surface (kg/m^2/h),

E_w = evaporation rate from a free water surface (kg/m^2/h),

t = concrete age (hours), and

a = time constant, defined as follows:

= 3.75 hours for concrete, and 6.16 hours for mortar.

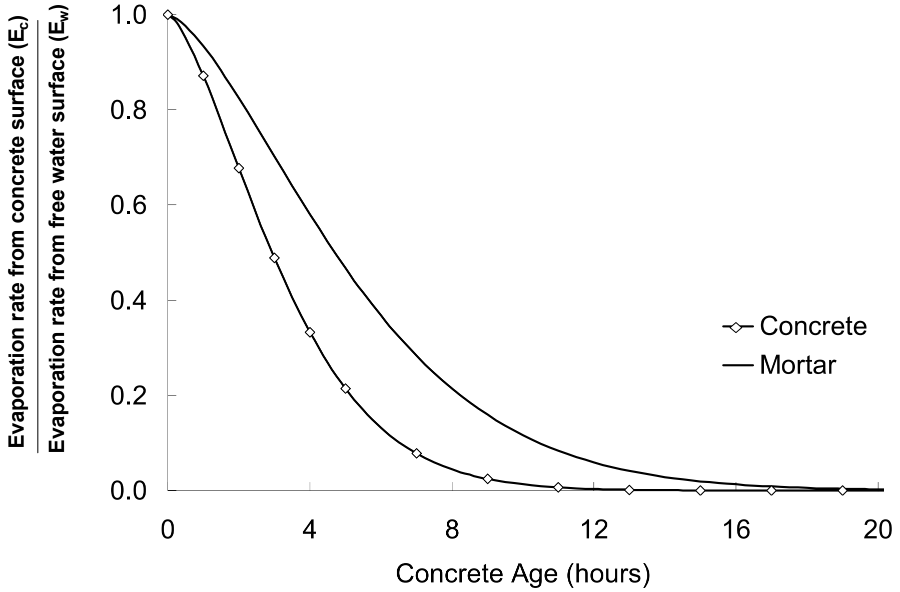

Figure 3-19: Al-Fadhala and Hover's (2001) recommended E_c/E_w development with time

The formulation shown in Equation 3-43, was developed from test data obtained from concrete specimens 60mm deep, and a Type I cement was used. The formulation does not account for the effect of surface texture or different curing methods. It was recommended that the time constant, a, be determined for a given mixture. Evaporative cooling may occur even at low evaporation rates. It has been noted that plastic shrinkage cracks occur at evaporation rates ranging from 0.2 to 0.7 kg/m^2/h, as opposed to the threshold value of 1 kg/m^2/h suggested by ACI Committee 305 (2000). Due to the limited information available on the subject, the formulation above will be evaluated during the course of this study. The accuracy of the model will be evaluated during the calibration of the temperature prediction program.

3.3.3 Solar Absorption

Solar absorption is the flux absorbed by the pavement surface through exposure to incoming solar radiation. During the development of the FHWA's HIPERPAV program, Equation 3-44 was used to account for solar absorption (McCullough and Rasmussen, 1999).

$$q_{sol} = -\beta_s \cdot I_f \cdot q_{solar} \qquad \text{Equation 3-44}$$

where, q_s = solar absorption heat flux (W/m^2),

I_f = intensity factor to account for angle of sun during a 24-hour day,

β_ε = solar absorptivity, and

q_{solar} = instantaneous solar radiation, (W/m^2) as defined in Table 3-10.

Table 3-10: Solar radiation values (McCullough and Rasmussen, 1999)

Sky Conditions	Solar Radiation, J, (W/m^2)
Sunny	1,000
Partly Cloudy	700
Cloudy (Overcast)	300

Note that in Table 3-10, the solar radiation is a function of the cloud cover. Even when overcast conditions exist, some of the longer wavelengths can still penetrate the sky and be a source of heat. During nighttime, the solar radiation is negligible. During daytime, the intensity of solar radiation (I_f) is assumed to follow a sinusoidal distribution.

Figure 3-20 presents different hourly solar radiation intensities for Houston and El Paso during the months of January and August. The values are the hourly 30-year average, calculated over 1961 to 1990, as obtained from the CR-Rom of the National Climatic Data Center (NCDC, 1996). In this study, it is recommended to obtain hourly instantaneous solar radiation values (q_{solar}) based on the 30-year historical average at the location under consideration. This approach is taken since the solar intensity varies by location, day and time.

The solar absorptivity of portland cement concrete is a function of the surface color, with typical values ranging from 0.5 to 0.6. An ideal white-body would have a value of 0.0, and an ideal black-body would have a value of 1.0. Table 3-11 provides further solar absorptivity and emissivity values for different surfaces. Table 3-11 presents how the effect of white curing compound could be helpful to reduce the concrete temperature. A white concrete surface will have a lower solar absorptivity as compared to a concrete surface where the curing compound has been worn off. The reason why asphalt surface temperatures become so high when exposed to solar effects can be explained with the values listed in Table 3-11. With a solar absorptivity of 0.90, the black asphalt surface absorbs most of the solar radiation.

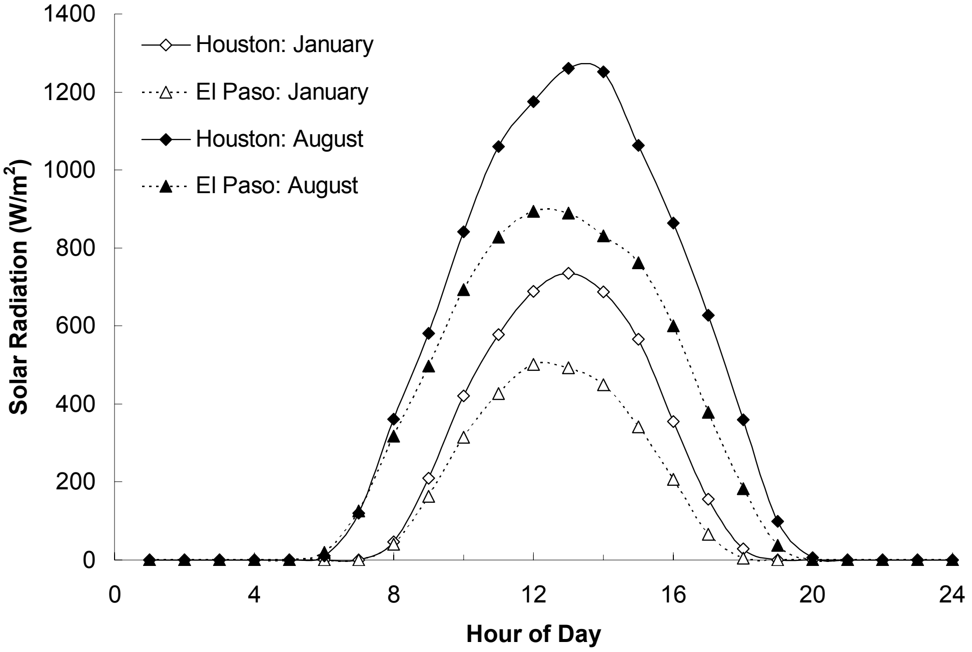

Figure 3-20: A comparison of hourly solar radiation values in Houston and El Paso

Table 3-11: Absorptivity and emissivity values for different surfaces (Janna, 2000)

Surface Material	Emissivity [a]	Solar Absorptivity
White, nonmetal surfaces	0.70 - 0.90	0.10 - 0.35
Dark-colored nonmetals	0.70 - 0.90	0.45 - 0.80
Black paint, asphalt, water	0.85 - 0.95	0.70 - 0.90

Note: [a] Emissivity is covered in Section 3.3.4.

3.3.4 Irradiation

Irradiation is the reason that frost occurs on a clear night even though the air temperature remains well above the freezing point (Bliss, 1961). Irradiation heat transfer affects the pavements surface boundary and is the heat transfer that is accomplished by electromagnetic waves between a surface and its surroundings (see Figure 3-16). The Stefan-Boltzmann law is commonly used for this type of heat transfer, which is defined as follows (McAdams, 1954):

$$q_r = -\varepsilon \cdot \sigma \cdot \left(T_c^4 - T_\infty^4\right) \qquad \textit{Equation 3-45}$$

where, q_r = heat flux from the surface (W/m^2),

σ = Stefan-Boltzmann radiation constant (5.67x10^{-8} W/m^2/°C^4),

ε = surface emissivity of concrete,

T_c = concrete surface temperature (°C), and

T_∞ = surrounding air temperature (°C).

The surface emissivity is a function of the concrete's surface color. An "idealized" black surface would have a value of 1.0. A value of 0.88 has been recommended for concrete surfaces (McCullough and Rasmussen, 1999). It should be noted that in the above equation, T_∞ is the temperature of the ***surrounding environment***. This value cannot arbitrarily be assumed equal to the ambient temperature. This assumption would be valid for use in enclosed spaces, but where long wave radiation towards the open sky is involved, the use of this assumption requires an appropriate estimate of the effective surrounding air temperature in terms of the atmosphere's ability to reflect and absorb the radiation. In Figure 3-21, an idealized thermally black body, with a surface temperature (T_s) equal to the air temperature, is receiving and absorbing solar energy at a rate, q_r (Bliss, 1961). Because the plate is at the same temperature as the air, there will be no heat transfer through convection, but the plate will exhibit a radiation loss due to irradiation. The loss rate (R) is defined as the difference between the black-body radiation emitted by the surface ($\sigma \cdot T_s^4$) and the incoming long wave atmospheric radiation (A_R) which is striking the surface (Bliss, 1961).

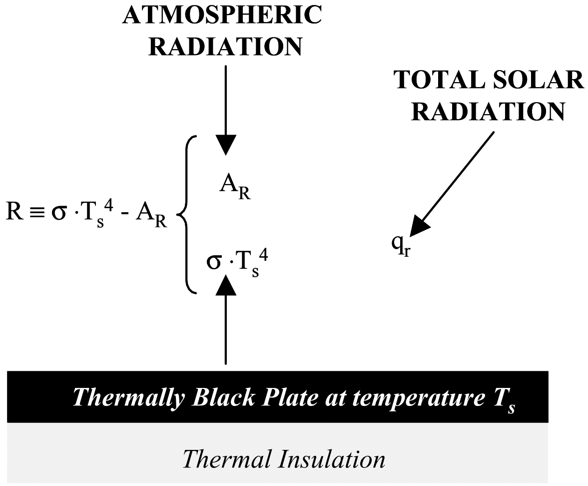

Figure 3-21: Radiant energy exchanges between the sky and an exposed thermally black plate (Adapted from Bliss, 1961)

Atmospheric radiation originates from gasses in the air. When radiation at the ground level is of concern, only water vapor, and carbon dioxide are the primary contributors, with water vapor being the most important (Bliss, 1961). It is interesting to note that it is only the presence of these small gases, which prevents the atmosphere from being completely transparent in the far infrared. Therefore, in order to accurately model the radiation from the atmosphere to the surface, it is essential to determine the radiation of the mixture of water vapor and carbon dioxide. The fact that the composition, temperature, and pressure of these mixtures vary with height above ground level should be considered.

The emissivity of a particular radiating gas is a function of the number of molecules in the column of air under investigation. At a given temperature, the number of molecules of the radiating gas is linearly proportional to the density-length product, $m_g \equiv p_g L_g$., where p_g is the density of the gas and L_g is the length of the gas column (Bliss, 1961). The total emissivity (ε_w) of a column of water vapor and non-radiating gas is primarily a function of the following: the density-length product (m_w) of the water vapor, the partial pressure (P_w) of the water vapor, the total pressure (P_T) of the mixture, and the temperature of the mixture (Bliss, 1961). However, the total emissivity is not significantly influenced by either the partial pressure of the moisture or the temperature of the mixture.

When carbon dioxide is added to the gas mixture, the radiative behavior of the gas column is only slightly changed. Based on the established work of Hottel and Egbert (1942), Bliss (1961) expressed the total emissivity of moist atmospheric air as a function of m_w and the ratio of carbon dioxide to water vapor concentrations at a total pressure of one atmosphere and a temperature of 20°C. Part of the data was presented in a graph, which was converted by the author to obtain the following mathematical form:

$$\varepsilon_{atm} = \left(1.009 + \frac{0.2191}{\sqrt{m_w}} + \frac{1.547\times10^{-5}}{(m_w)^{1.5}}\right)^{-1} + \\ 0.185\cdot\left(\exp(-3.060\cdot m_w) - \exp\left(-1.8\cdot m_w\left(1.7 + 50\cdot\frac{\rho_c}{\rho_w}\right)\right)\right) \qquad \text{Equation 3-46}$$

where, ε_{atm} = total atmospheric emissivity (unitless),

m_w = density-length product of the water vapor ($m_w \equiv p_g L_g$ = g/cm^2), and

ρ_c / ρ_w = ratio of carbon-dioxide density to water vapor density.

In Equation 3-46 above, the first term accounts for the emissivity of water vapor (moist air) and the second term accounts for the added emissivity caused by the presence of carbon dioxide. Figure 3-22 presents the individual contribution of the water vapor and carbon dioxide to the calculated emissivity of moist air. Note that the presence of carbon dioxide adds a maximum of only 0.185 to the overall emissivity. This figure further presents the effect of water vapor in the air on the atmospheric emissivity. As the concentration of water vapor becomes less (dry air) the atmospheric radiation (total emissivity) decreases.

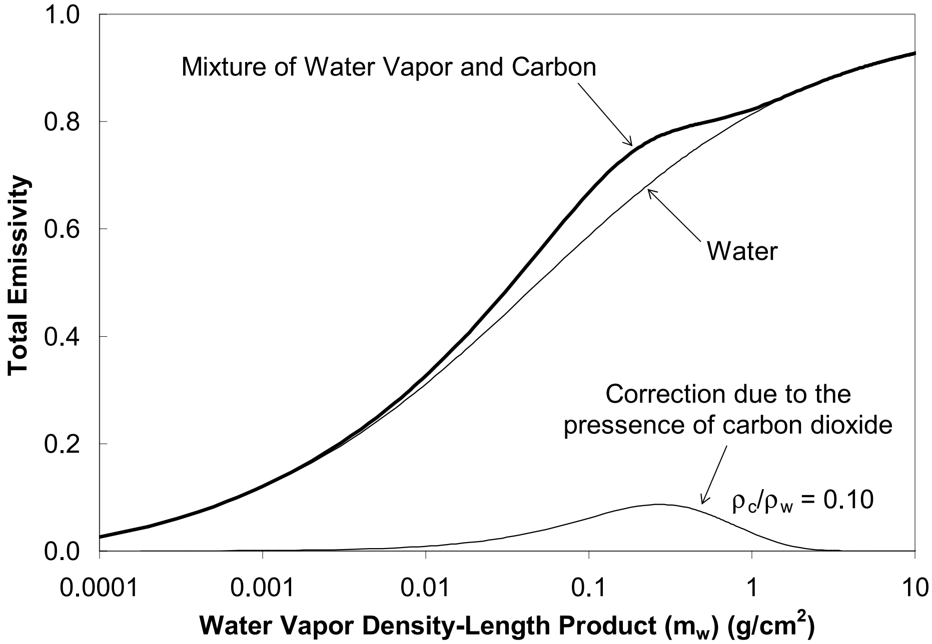

Figure 3-22: Emissivity of moist air at a total pressure of 1 atmosphere and a temperature of 20°C (Adapted from Bliss, 1961)

The nature of the earth's atmosphere is that pressure and temperature decreases with altitude, which due to gas equilibrium principles causes a change in the moisture condition of the body of gas (Bliss, 1961). Therefore, in order to determine the total atmospheric emissivity, the earth's atmosphere is considered as several layers, all at different temperatures, pressures, and moisture conditions. The composition of the atmosphere varies significantly, but it varies with height in typical ways. It can be shown that the variation of pressure with altitude can be determined by the following relationship (Bliss, 1961):

$$P_z = P_i \cdot \exp\left(-1.2\times10^{-4} \cdot z\right) \qquad \textit{Equation 3-47}$$

where, P_z = atmospheric pressure at height z (atm),
P_i = atmospheric pressure at ground level (atm), and
z = height above ground level (m).

As the total pressure is decreased, the emissivity of the gas decreases. Equation 3-46 provided the total atmospheric emissivity at a pressure of 1 atmosphere, and by determining an adjusted density-length product of the water vapor the effect of different pressures can be incorporated. The adjusted density-length product of the water vapor (m'_w) can be determined as follows (Bliss, 1961):

$$m'_w = m_w \cdot \frac{P_z}{P_0} \qquad \textit{Equation 3-48}$$

where, P_z = actual pressure of the moist air (atm), and
P_0 = pressure of the know emissivity versus water vapor relationship (1 atm).

The variation of temperature with height is non-uniform, but it is reported that at heights above a few meters off the ground, it often obeys the following relationship (Bliss, 1961):

$$T_z = T_i - 0.006 \cdot z \qquad \textit{Equation 3-49}$$

where, T_z = atmospheric temperature at height z (°C),
T_i = atmospheric temperature at ground level (°C), and
z = height above ground level (m).

As the total energy of a moist air column changes with a change in temperature, a temperature correction needs to be applied to the calculated total atmospheric emissivity. The total energy radiated by a gas of specified water-vapor content is a function of its temperature only, and is directly proportional to the fourth power of its absolute temperature (Bliss, 1961). The temperature adjustment factor (T_f), which can be multiplied to the emissivity determined at a temperature different than the actual condition, can be determined as follows (Bliss, 1961):

$$T_f = \left(\frac{T_i + 273}{T_0 + 273} \right)^4 \qquad \textit{Equation 3-50}$$

where, T_i = actual temperature of the moist air (°C), and
T_0 = assumed temperature during calculation of the emissivity (°C).

The water-vapor density is variable with height and the total precipitable water contained below a certain height (z) can be determined with the following relationship (Bliss, 1961):

$$\int_0^z dm'_w = \frac{p_{wi}}{5.7 \times 10^{-6}} \left(1 - \exp\left[-z \cdot 5.7 \times 10^{-6}\right]\right) \qquad \textit{Equation 3-51}$$

where, $\int_0^z dm'_w$ = total precipitable water contained below a height z (g/cm^2),

p_{wi} = water-vapor density at ground level (g/cm^2), and

z = height above ground level (m).

In the temperature prediction program, the climatic conditions are defined in terms of the relative humidity and the dry-bulb temperature, and through the use of established gas relationships, the water-vapor density can be determined. The water vapor saturation pressure for a given dry-bulb temperature can be determined as follows (ASHRAE, 1993):

For dew-point range of -100 to 0°C:

$$\ln(p_{ws}) = C_1 / T_R + C_2 + C_3 \cdot T_R + C_4 \cdot T_R^2 + C_5 \cdot T_R^3 + C_6 \cdot T_R^4 + C_7 \cdot \ln(T_R) \quad \text{Equation 3-52}$$

where, p_{ws} = the water-vapor saturation pressure (psi),

T_R = the dry-bulb temperature, (°R = °C *1.8+491.67),

C_1 = -10214.165, C_2 = -4.8932428,

C_3 = -0.0053765794, C_4 = -1.9202377×10^{-7},

C_5 = 3.5575832×10^{-10}, C_6 = -9.0344688×10^{-14}, and

C_7 = 4.1635019.

For dew-point range of 0 to *200°C:*

$$\ln(p_{ws}) = C_8 / T_R + C_9 + C_{10} \cdot T_R + C_{11} \cdot T_R^2 + C_{12} \cdot T_R^3 + C_{13} \cdot \ln(T_R) \quad \text{Equation 3-53}$$

where, C_8 = -10440.397, C_9 = -11.29465,

C_{10} = -0.027022355, C_{11} = -1.289036×10^{-5},

C_{12} = -2.4780691×10^{-9}, C_{13} = 6.5459673.

Once the water vapor saturation pressure is determined, the water vapor pressure of the moist air can be determined from the known relative humidity (*RH*) as shown below.

$$p_w = RH \cdot p_{ws} \quad \text{Equation 3-54}$$

With the information above, we have all the required information to determine the apparent atmospheric emissivity with the following variables: surface atmospheric pressure (atm), dry-bulb temperature (°C), relative humidity, and the ratio of carbon dioxide to water vapor. The atmosphere is divided into different layers, and by using a stepwise procedure, the emissivity can be accumulated from each layer. Once the apparent emissivity (ε_{app}) is determined, the intensity of atmospheric radiation (A_R) can be determined by (Figure 3-21):

$$A_R = \varepsilon_{app} \cdot \sigma \cdot T_a^4 \quad \text{(W/m}^2\text{)} \qquad \textit{Equation 3-55}$$

Now with the intensity of atmospheric radiation determined, the apparent surrounding air temperature (T_∞) can be solved from the following:

$$T_\infty = \left(A_R / \cdot \sigma\right)^{0.25} - 273 \qquad \textit{Equation 3-56}$$

Since the apparent surrounding air temperature is now determined, the Stefan-Boltzmann law can be used to determine the heat transfer by irradiation (Equation 3-45). Once the open sky irradiation is determined, corrections can be made to account for the effect of cloud cover. Figures 3-23 to 3-25 illustrate the sensitivity of the effective surrounding temperature to all the various input variables with the following parameters as base-line values for the analysis: atmospheric pressure = 750 millibars, dry-bulb temperature 30°C, relative humidity = 20%, ratio carbon dioxide to water vapor = 1.0. Under the conditions investigated, there is a significant reduction in the apparent surrounding temperature associated with a decrease in total pressure and relative humidity. A change in the carbon dioxide content appears to have a minimal impact on the apparent surrounding temperature and a ratio of 0.1 should be sufficient for most conditions (Bliss, 1961).

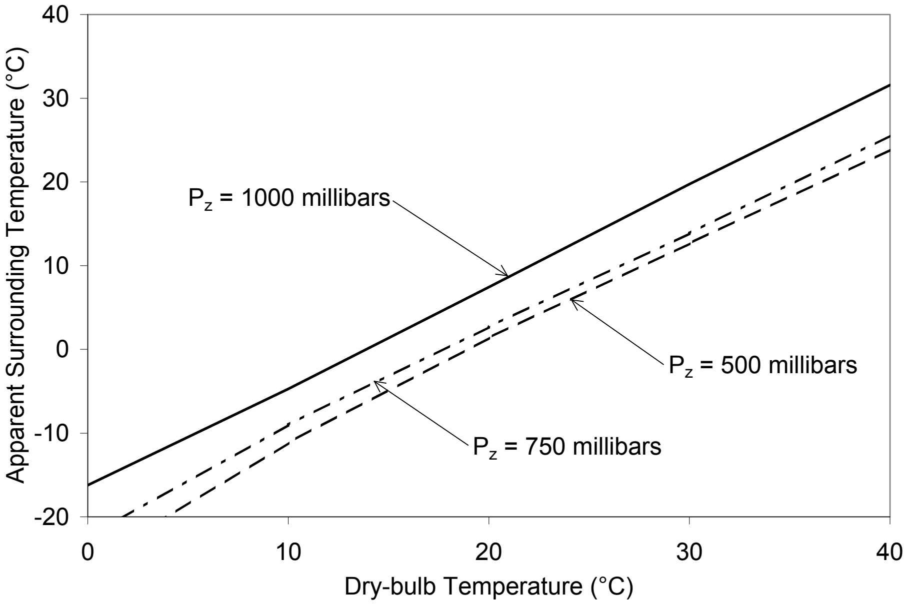

Figure 3-23: Sensitivity of the apparent surrounding temperature to changes in atmospheric pressure

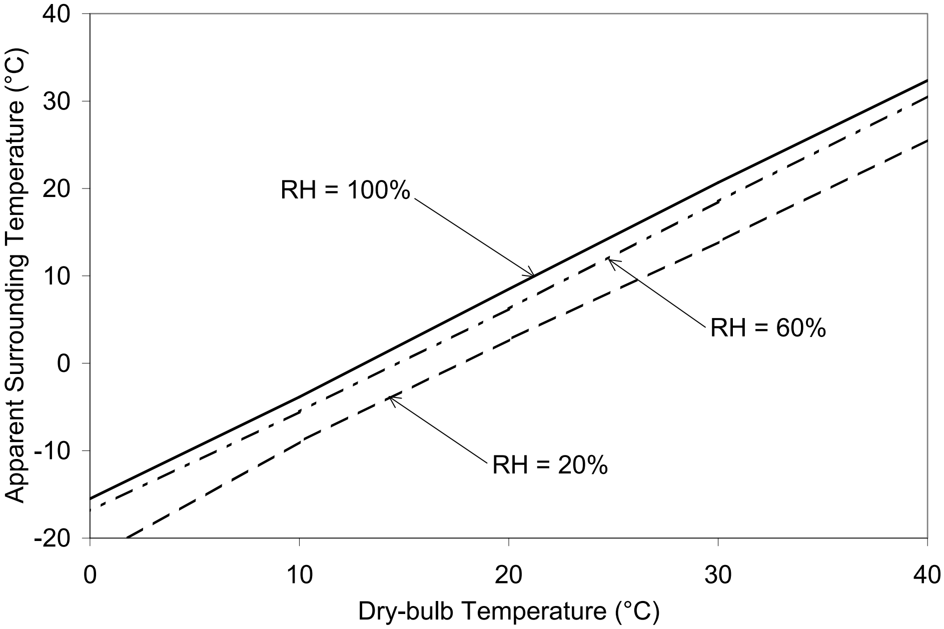

Figure 3-24: Sensitivity of the apparent surrounding temperature to changes in relative humidity

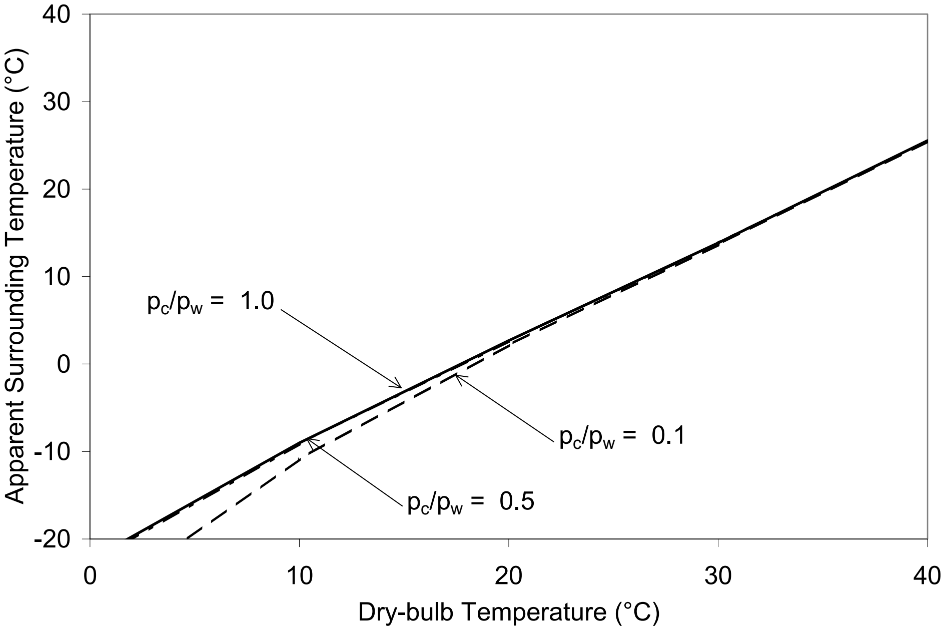

Figure 3-25: Sensitivity of the apparent surrounding temperature to changes in carbon-dioxide content in air

3.3.5 Finite Difference Heat Transfer Method

Different numerical techniques are available to provide approximations for the time and space dependent heat transfer problem. The explicit centered forward finite difference technique can be used to solve the heat-transfer problem. In one-dimension, the forward finite difference equation shown in Equation 3-57 can be used to compute the temperature at nodal point *i* at time (*t*+*Δt*) (Chapra and Canale, 1998). The nodes addressed in the procedure above are presented in Figure 3-26.

$$T_{(i,t+\Delta t)} = T_{(i,t)} + \left(\frac{k}{\rho \cdot c_p} \right) \cdot \left(\frac{\Delta t}{\Delta z^2} \right) \cdot \left(T_{(i+1,t)} - 2 \cdot T_{(i,t)} + T_{(i-1,t)} \right) \qquad \textit{Equation 3-57}$$

where, Δt = the time increment (s), and

Δz = the distance increment (m).

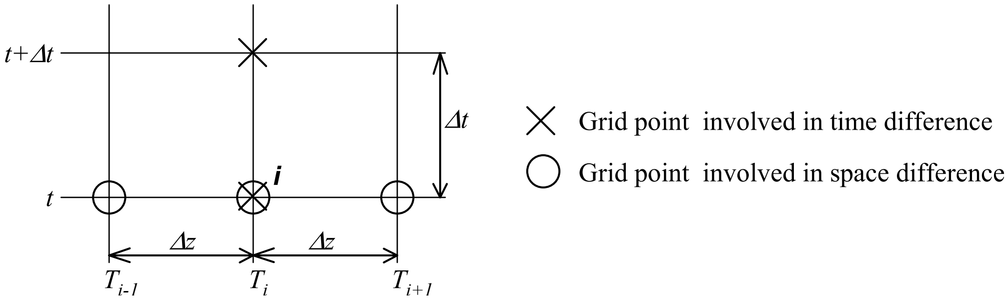

Figure 3-26: Layout of the nodes involved in the finite difference model (Chapra and Canale, 1998)

3.3.5.1 Incorporating Boundary Conditions with Finite Difference Method

Different thermal conditions may exist at the boundaries of the system. The boundary conditions can be either a fixed temperature or a heat flux. An example of a fixed temperature condition occurs at the bottom of soil profile where the soil temperature is governed by the constant deep ground temperature. Radiation and convection are examples where heat exchange occurs though a heat flux. Boundary conditions can readily be incorporated into the finite difference method by adding fictitious exterior nodes at the boundaries, as shown in Figure 3-27.

Through these exterior nodes, the boundary conditions can now be applied. The boundary shown in Figure 3-27 can be incorporated as follows:

$$T_{(0,t+\Delta t)} = T_{(0,t)} + \left(\frac{k}{\rho \cdot c_p} \right) \cdot \left(\frac{\Delta t}{\Delta z^2} \right) \cdot \left(T_{(1,t)} - 2 \cdot T_{(0,t)} + T_{(-1,t)} \right) \qquad \textit{Equation 3-58}$$

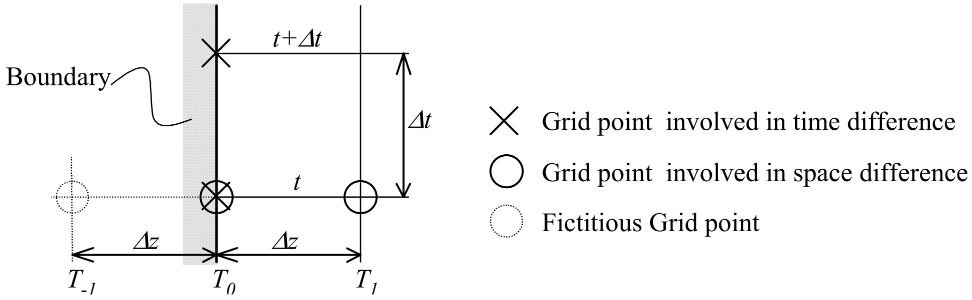

Figure 3-27: Layout of the nodes at system boundary

3.3.5.2 Convergence and Stability of the Finite Difference Method

The numerical procedure associated with the finite difference method is straight-forward, but care has to be taken to ensure that the method provides reasonable results. The finite difference method is both convergent and stable when (Chapra and Canale, 1998):

$$\Delta t \le 0.25 \cdot \left(\frac{\rho \cdot c_p}{k} \right) \cdot \Delta z^2 \qquad \textit{Equation 3-59}$$

The requirement above places a strong limitation on the explicit finite difference method. In the analysis of a pavement system, the mesh size and the material thermal properties should be evaluated to determine the magnitude of the analysis time step. For example, if the mesh size is halved to prevent instability, the time step must be quartered to maintain convergence and stability. Thus, to perform the analysis, the time steps must be increased by a factor of four, which may prove to be a computational burden. Due to the presence of a heat flux at the surface boundary condition, stability of the surface node additionally needs to ensured (Price and Slack, 1952).

3.3.5.3 Initial Temperature Profile

In order to utilize the finite difference method, an initial temperature profile has to be determined prior to the start of the analysis. During the early-ages, the concrete placement temperature, concrete heat of hydration, and the initial subbase temperature govern the initial pavement temperature distribution. In the long term, the temperature distribution is based on the equilibrium of the pavement system and climatic conditions. The temperature at the bottom of the pavement system will be assumed to be equal to the deep ground temperature, as obtained from non-thermal wells at depths of 30 to 60 feet (Lytton et al., 1993). In Texas, these temperatures vary from 72°F at the coast, to 62°F in the Texas plains. The subgrade layer depth will be finalized after a sensitivity analysis is performed. A linear relationship will be assumed from the deep ground temperature to the temperature at the bottom of the subbase layer. The initial temperature profile of the subbase layer will be determined by the closed form solution proposed by Barber (1957).

Barber (1957) developed a method to estimate the temperature distribution based on standard weather conditions. The 24-hour cyclic temperature (*T*) of a semi-infinite mass in contact with the air at temperature $T_M + T_V \cdot \sin(0.262 \cdot t)$ can be calculated as follows (Barber, 1957):

$$T = T_M + T_V \cdot \left(\frac{H \cdot \exp(-z \cdot C)}{\sqrt{(H+C)^2 + C^2}} \right) \cdot \sin\left(0.262 \cdot t - z \cdot C - \arctan \frac{C}{H+C} \right) \qquad \textit{Equation 3-60}$$

where, T = temperature of the mass (°F),
T_M = mean effective temperature air temperature (°F),
= $T_A + R$ for all $T \geq T_A$ (°F),
= $T_A + 0.5 \cdot R$ for all $T < T_A$ (°F),
T_A = actual mean air temperature (°F),
R = solar radiation contribution (Langleys/day = 3.68 BTU/ft^2/day),
= $0.67 \cdot b \cdot 3.69 \cdot L / 24$ (Langleys/day),
L = solar radiation (Langleys/day),
T_V = maximum variation in temperature from mean (°F),
= $0.5 \cdot T_R + 3 \cdot R$ for all $T \geq T_A$ (°F),
= $0.5 \cdot T_R$ for all $T < T_A$ (°F),
T_R = daily temperature range (°F),
t = time from beginning of cycle (hours),
z = depth below surface (°F),
H = constant = h / k,
h = surface coefficient (BTU/ft^2/h),
= $1.3 + 0.62 \cdot v^{0.75}$ BTU/ft^2/h
v = wind velocity (mph),
k = thermal conductivity (BTU/ ft^2/h·°F/ft),
C = $\sqrt{0.131}$ per c,
= diffusivity (ft^2·h),
= $k / (s \cdot \rho)$,
s = specific heat capacity (BTU/lb/°F), and
ρ = density (lb/ft^3).

In the above formulation the effects of solar radiation and wind speed on surface temperatures has already been included to calculate the effective air temperature.

3.4 FRESH CONCRETE TEMPERATURE PREDICTION MODELS

One possible measure to minimize the potential problems associated with hot weather concreting can be to control the concrete mixture temperature. An effort should be made to keep the concrete temperature as low as economically practical. The temperature of the fresh concrete can be regulated by controlling the temperature of the ingredients (ACI 305, 2000; Samarai et al., 1975). The contribution of each constituent is determined by its temperature, specific heat, and weight fraction. This is the basis of Equation 3-61, which can be used to estimate the temperature of freshly mixed concrete (Tc) as follows:

$$T_c = \frac{H(T_a W_a + T_c W_c) + T_a W_{wa} + T_w W_w}{H(W_a + W_c) + W_{wa} + W_w} \qquad \textit{Equation 3-61}$$

where, H = specific heat of cement and aggregate, (Average ≈ 0.22 Btu/lb·°F)
T_a = temperature of aggregate (°F),
T_c = temperature of cement (°F),
T_w = temperature of mixing water (°F)
W_a = dry weight of aggregate (lbs),
W_c = dry weight of cement (lbs),
W_w = weight of water (lbs), and
W_{wa} = weight of free and absorbed moisture of the aggregate (lbs).

When ice is added to the mixture, Equation 3-61 is modified to take the following form:

$$T_c = \frac{H(T_a W_a + T_c W_c) + T_a W_{wa} + T_w W_w - F_i W_i}{H(W_a + W_c) + W_{wa} + W_w + W_i} \qquad \textit{Equation 3-62}$$

where, F_i = latent heat of fusion (Average ≈112 Btu/lbs), and
W_i = weight of ice (lbs).

ACI 305 (2000) used the relationships above, together with concrete of usual proportions to calculate the effectiveness of cooling each of the mixture components. It was determined that the concrete temperature can be reduced by 1°F, if any of the following adjustments are made to the raw material temperatures:

- 8°F reduction in cement temperature,
- 4°F reduction in water temperature, or
- 2°F reduction in aggregate temperature.

The effectiveness of cooling the water is due to its high specific heat, which offsets its small weight fraction. The aggregate constitutes the largest portion of the concrete and a reduction in aggregate temperature, therefore, brings about the greatest change in concrete temperature. High concrete placement temperature mitigation measures such as shading, sprinkling or cooling of the aggregates, should be fully investigated, since it may prove to be cost effective measures. It can further be seen that a change in temperature of the cement has little effect on the concrete temperature.

3.5 INITIAL AND FINAL SET MODELING

One of the objectives of this study is to predict when thermal stresses, stiffness, and strength start to develop in the in place concrete. Hewlett (1998) defines the term "setting" as "… a rather sudden loss of plasticity of the original paste and its conversion to a solid material with a barely measurable strength." The transition from liquid to solid is a gradual process, and the definition of any point at which the paste is considered set, is somewhat arbitrary (Neville, 1996). In terms of ASTM C 403 (1999), setting of the concrete is defined in terms of initial and final set. A mortar sample is obtained from concrete by passing it through a number four (4.75 mm) sieve. In this test, the maximum force required to penetrate needles of different sizes to a depth of 25 mm over a 10-second period is measured. As the concrete stiffens, the size of needles is progressively reduced. At a penetration resistance of 500 psi, initial setting occurs, which was chosen to correspond with the time when the concrete can no longer be vibrated (Tuthill and Cordon, 1955). Tuthill and Cordon further determined that at a penetration resistance of 4000 psi the concrete has reached a compressive strength of around 80 psi, and it could carry some measurable loads.

Pinto and Hover evaluated how different temperatures affected the setting time in terms of the penetration resistance method described by ASTM C 403. It was shown that for any given mixture, final set occurs when a specific level of microstructure development has occurred, and, therefore, that a specific degree of hydration has been reached. In their study, numerous tests were performed at different temperatures and different activation energy values were determined to provide agreement with their test results. Figure 3-8 presents that the degree of hydration provides an indication of the amount of hydration products that are formed, and once the degree of hydration of the cementitious materials are known, this information can be used to estimate initial and final set.

Byfors (1980) defined the term "critical degree of hydration" (α_{cr}) as the degree of hydration that has to be reached before any strength gain will occur. Byfors concluded that the critical degree of hydration is dependent on the water-cement ratio and presented the following expression:

$$\alpha_{cr} = k_s \cdot (w/c) \qquad \textit{Equation 3-63}$$

where, k_s = constant that varies between 0.4 and 0.46, and
w/c = water-cement ratio

It is proposed that initial and final set as defined by ASTM C 403, be modeled with the approach shown in Equation 3-63. However, as the "arbitrary" definition of set used by ASTM C 403 and that used by Byfors originate from different requirements, the appropriate k_s values should be based on tests performed on local materials. In this study, the critical degree of hydration will be determined for both initial setting and final set.

3.6 DEVELOPMENT OF EARLY-AGE THERMAL STRESSES

As shown in Figure 1-4, the zero-stress temperature is the point at which tensile stresses begin to develop the first time after the initial compression stage. Initial compression in a slab is caused by continued hydration and rapid heat development after initial set has occurred and due to a restraint of movement. One of the objectives of this task is to predict the zero-stress temperature, as this temperature will be used to calculate the long-term thermal stress. In Equation 1-1, the long-term temperature change was defined as the difference between the zero-stress temperature and the minimum long-term concrete temperature. In the pavement performance prediction programs developed at the Center for Transportation Research, CRCP-8 and JRCP-6, the zero-stress temperature is the temperature that is used to calculate the long-term temperature differential the pavement is subjected to.

The point of zero-stress should not be confused with the time of final set as presented in Section 3.5. In the concrete technology industry, the time of setting is determined in terms of tests performed on setting concrete.

In Figure 1-4, it may be seen that the temperature at which the zero-stress condition is reached (T_{zs}) is higher than the temperature at which final set (T_{fs}) initially occurred. This implies that there is a rapid gain in concrete stiffness at this stage, and it has been found that most of the initial compressive stresses are relaxed between the time of final set (t_{fs}) and the time when the zero-stress condition is reached for the first time (t_{zs}). From this effect, it has been concluded that the development of early-age thermal stresses are generally not proportional to the temperature variations, since the development of early-age mechanical behavior in concrete has to be accounted for (Emborg, 1989). This "relaxation" phenomenon exhibited by early-age concrete has been thoroughly researched in Sweden (Emborg, 1989; and Westman, 1999) and Germany (Springenschmid and Breitenbücher, 1991).

From Figure 1-4, it may be noticed that it would be ***nonconservative*** to neglect the early-age stress relaxation, since relaxation in compressive stresses would cause the zero-stress temperature to occur at a higher temperature.

Three fundamental types of deformations may occur when young concrete is subjected to loading: elastic, plastic and viscous deformations (Emborg, 1989). When describing time-dependent deformations of uncracked concrete, it is convenient to use strain-time relations, as presented in Figure 3-28. From this figure, it can be seen that elastic and delayed elastic deformations are recoverable when the load is removed. The delayed elastic deformation may be considered as a form of creep. The elastic and time-dependent behavior of ***hardened*** concrete has been well researched and documented (Baźant, 1972; CEB-FIP, 1978; ACI 209, 1992; Emborg, 1989). However, up until the 1990s little work has been done on the elastic and time-dependent behavior of concrete in the ***early-ages*** (Emborg, 1989).

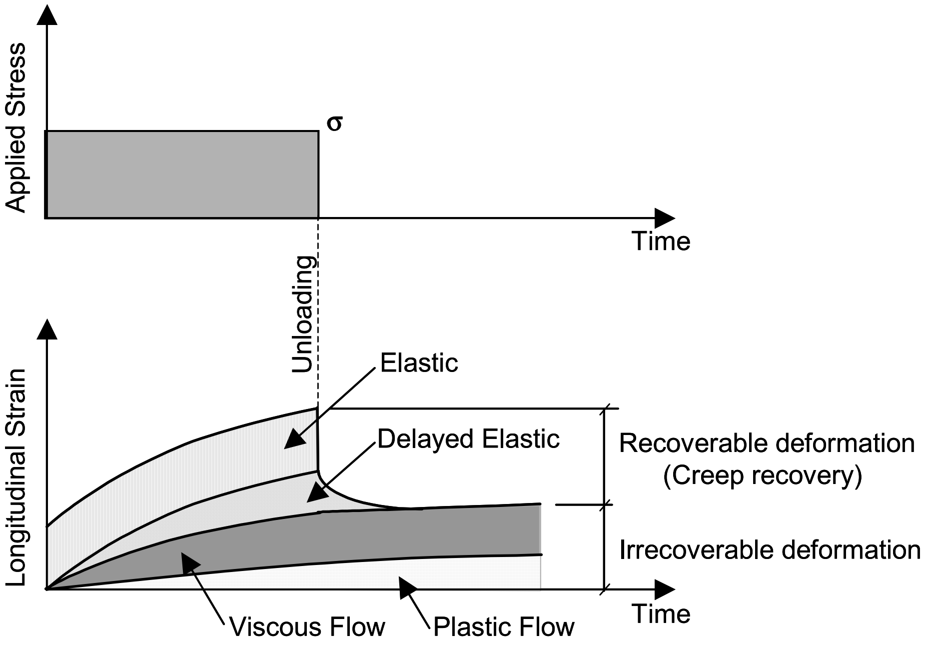

Figure 3-28: Typical stain-time curves showing fundamental types of deformations under loading and unloading (Emborg, 1989)

The viscous flow component is irrecoverable and may be defined as the time-dependent deformation occurring at normal working stress levels. It has been suggested that plastic flow in concrete might be due to low-stress "microcracking flow." In the work Emborg (1989) presented, the term viscoelastic deformation was used to cover all the elastic, delayed elastic and viscous flow components according to Figure 3-28. Knowledge of the nonlinear creep behavior at high tensile stresses is of paramount importance when estimating stresses, and, therefore, the time at which zero-stresses occur in concrete at early-ages (Westman, 1999).

3.6.1 Background to Creep Models

When load is applied (at time t_0) to a concrete member, it responds with immediate elastic deformation (ε_{el}) followed by a time-dependent creep response (ε_{cr}), which is shown in Figure 3-29. In the modeling of time dependent deformation, the use of the creep compliance formulation is commonly used. In this method, the total linear time dependent deformation, $\varepsilon(t)$, at time, t, is expressed as mathematically shown in Equation 3-64 and illustrated in Figure 3-29. If the specific creep ($\varphi(t,t_0)$) is known, the instantaneous and time dependant components of the total deformation can be separated as shown in Equation 3-65.

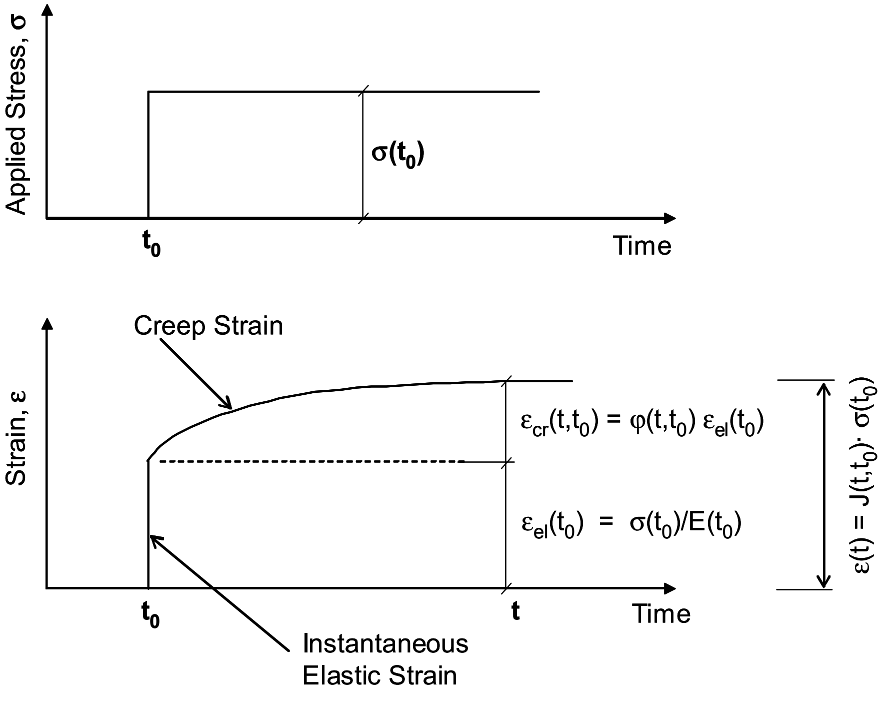

Figure 3-29: Time dependant deformation at time t, for a loading at time t0 (Westman, 1999)

$$\varepsilon(t) = J(t,t_0) \cdot \sigma(t_0) \qquad \textit{Equation 3-64}$$

where, $J(t,t_0)$ = creep compliance defined as the response at time t after loading at time t_0, and
$\sigma(t_0)$ = applied stress at time t_0.

$$J(t,t_0) = \frac{1 + \varphi(t,t_0)}{E(t_0)} = \frac{1}{E_{eff}} \qquad \textit{Equation 3-65}$$

where, $E(t_0)$ = the instantaneous modulus of elasticity at time t_0,
$\varphi(t,t_0)$ = is the creep coefficient (ratio of creep to elastic strain), and
E_{eff} = is the effective modulus of elasticity at time, t.

3.6.2 Selection of Creep Model

Few models are available to model the time dependent deformation and creep compliance of concrete at early-ages. It is recommended that the Extended Triple Power Law as developed by Westman (1999) at the University of Luleå, Sweden, be used to account for early-age relaxation effects. This model is recommended, since it was developed specifically to account for the early-age creep effects, and combines the early-age effect, with the well-recognized work on hardened concrete as developed by Baźant and Chern (1985).

This model is developed from the Double Power Law (Baźant and Panula, 1978) and the Triple Power Law (Baźant and Chern, 1985). The Double Power Law is perhaps the most well know compliance function, and has been used by many authors because it is based on extensive laboratory test results. The Triple Power Law was developed to provide an accurate description of the long-term creep. As is commonly done, it will be assumed that the creep in tension is equal to the creep in compression.

Neither the Double nor the Triple Power Laws was calibrated for loading at early ages, and their use was not intended to predict creep for young concrete (Emborg, 1989). Westman (1999) estimated that the Double or Triple Power Laws are only valid for loading ages more than about 2 days. Therefore, the Triple Power Law was adjusted first by Emborg (1989) and then by Westman (1999) to account for loading at ages less than about 2 days. The Extended Triple Power Law as documented by Westman (1999) provides good agreement with early-age test data and accounts for the following factors that could influence the time dependent deformation:

- concrete age at setting,
- concrete age at loading (which is most important),
- applied stress level, and

- the influence of varying temperature on concrete properties.

Since the Double Power Law and the Triple Power Law are used by the Extended Triple Power Law, the necessary components of both these models will be presented in the following sections. The presentation of these models will be based on the documentation provided by Westman (1999).

3.6.3 **Double Power Law** (Bazant and Panula, 1978)

With the Double Power Law (DPL), creep of concrete at constant moisture and temperature conditions is defined by power curves for load duration (t-t_0), and by inverse power curves to account for the effect of the loading age t_0. The creep compliance according to the double power law can be calculated through the following formulation presented by Bazant and Panula (1978):

$$J(t,t_0) = \frac{1}{E_0} + \frac{\varphi_1}{E_0}\left(t_0^{-m} + \alpha\right)\left(t - t_0\right)^n \qquad \textit{Equation 3-66}$$

where, t_0 = the loading age (days),

E_0 = the “negative asymptotic modulus” of elasticity at time t_0 (psi)

(E_0 may be determined from the 28-day modulus, $E_0 \approx 1.5 \cdot E_{28}$)

$$\frac{1}{E_0} = 0.09 + \left[1.7 \cdot \left(0.00005 f_c^{'} \rho^2\right)^2\right]^{-1} \qquad \textit{Equation 3-67}$$

where, f'_c = the 28-day cylinder compressive strength (ksi), and

ρ = the concrete unit weight (lb/ft^3).

$$\varphi_1 = \frac{10^{3n}}{2\left(28^{-m} + \alpha\right)} \qquad \textit{Equation 3-68}$$

$$m = 0.28 + (f_c^{'})^{-2}\text{, and} \qquad \textit{Equation 3-69}$$

$$\alpha = \frac{1}{40(w/c)} \qquad \textit{Equation 3-70}$$

where, *w/c* = the water-cement ratio, and if x > 4, $n = 0.12 + \dfrac{0.07 \cdot x^6}{5130 + x^6}$ *Equation 3-71*

if x ≤ 4, $n = 0.12$ *Equation 3-72*

with, $x = \left[2.1 \dfrac{(a/c)}{(s/c)^{1.4}} + 0.1 \left(f_c'\right)^{1.5} (w/c)^{1/3} (a/g)^{2.2} \right] \cdot a_1^{-4} - 4$ *Equation 3-73*

where, *a/c* = total aggregate/cement ratio,

s/c = sand/cement ratio,

a/g = total aggregate/coarse aggregate ratio,

a1 = 1.00 for Type I or II cement,

= 0.93 for Type III cement, or

= 1.03 for Type IV cement.

The dependence of creep on different curing temperatures that are constant for the time of interest may be modeled with the coefficients n_T and φ_T instead of n and φ_1, as follows:

$$n_T = \beta_T \cdot n$$ *Equation 3-74*

where, $\beta_T = \dfrac{0.25}{1 + (74/(T - 253.2))^7} + 1$ *Equation 3-75*

with, T = concrete temperature (Kelvin),

$$\varphi_T = \varphi_1 (1 + C_T)$$ *Equation 3-76*

where, $C_T = C_{T1} \cdot \tau_T \cdot C_0$ *Equation 3-77*

$$C_{T1} = \frac{19.40}{1 + (100/(T - 253.2))^{3.5}} - 1$$ *Equation 3-78*

$\tau_T = \dfrac{1}{1 + (60/t_{oT})^{0.69}} + 0.78$, and *Equation 3-79*

$$C_0 = 0.125 \cdot (w/c)^2 (a/c) \cdot a_1$$ *Equation 3-80*

where, t_{0T} = the age of the concrete when the temperature, *T* is applied, (days)

The age of the concrete is expressed in terms of the maturity method. Since the parameters of the model was calibrated with the maturity function shown in Equations 31- and 3-82, these will be used during the development of this model. The maturity of the concrete at time of loading, t_0, is expressed as follows:

$$t' = t'_e = \int_o^{t'} \beta'_T \left(t''\right) dt'' \qquad \textit{Equation 3-81}$$

where, t'_e = the equivalent hydration period, and

$$\beta'_T = \exp\left(\frac{4000}{T_0} - \frac{4000}{T}\right) \qquad \textit{Equation 3-82}$$

where, T_0 = the reference temperature (293 K)

3.6.4 Triple Power Law (Bazant and Chern, 1985)

The triple power law was developed to improve the predicted long-term creep. The double power law was modified with a binomial function ***B(t,t$_0$;n)*** to provide a more accurate description of long-term creep. The creep compliance according to the triple power law is as follows:

$$J(t,t_0) = \frac{1}{E_0} + \frac{\varphi_1}{E_0}\left(t_0^{-m} + \alpha\right)\left[\left(t - t_0\right)^n - B\left(t,t_0;n\right)\right] \qquad \textit{Equation 3-83}$$

In which E_0, $\varphi 1$, m, n, and α have the same values as defined in the Double Power law. $B(t,t_0;n)$ is a binomial integral and may be evaluated by the power series shown in Equation 3-84. Emborg (1989) states that the power series converges fast as long as n is large and when $t\text{-}t_0 \geq 0.1$.

$$B\left(t,t_0;n\right) = n \cdot t_0^n \left[\frac{\beta^{-n} - 1}{n} + \ln\beta + \sum_{k=1}^{\infty} \binom{n-1}{k} \left(-1\right)^k \left(\frac{\beta^{k-n} - 1}{n-k} - \frac{1-\beta^k}{k}\right)\right] \qquad \textit{Equation 3-84}$$

where, β = t_0/t.

3.6.5 Extended Triple Power Law (Bazant and Chern, 1985)

Both the double or triple power laws were not calibrated for loading at early ages, and their use was not intended to predict creep for young concrete (Emborg, 1989). Westman (1999) estimated that the double or triple power laws are only valid for loading ages greater than approximately 2 days. In Figure 3-30, test results are compared with computations with the triple power law, and it can be seen that for loading ages greater than 2 days, the amount of creep is closely predicted by the triple power law. However, at early ages the computed creep compliance is much less than predicted by the triple power law, and the early-age viscous behavior seems to be underestimated for very early loading by the triple power law. Therefore, the triple power law was adjusted first by Emborg (1989) and then by Westman (1999) to account for loading at ages less than 2 days.

In 1989, Emborg extended the triple power law with additional functions, which Westman modified in 1999 to $\Psi_1(t_0)$ and $\Psi_2(t,t_0)$. The purpose of the two new terms, $\Psi_1(t_0)$ and $\Psi_2(t,t_0)$, are shown schematically in Figure 3-31. For loading ages less than approximately 2 days, the function $\Psi_1(t_0)$ models the age dependence of the instantaneous deformation and $\Psi_2(t,t_0)$ models the increase of creep when the load has been applied. The creep compliance according to the extended triple power law is as shown in Equation 3-85.

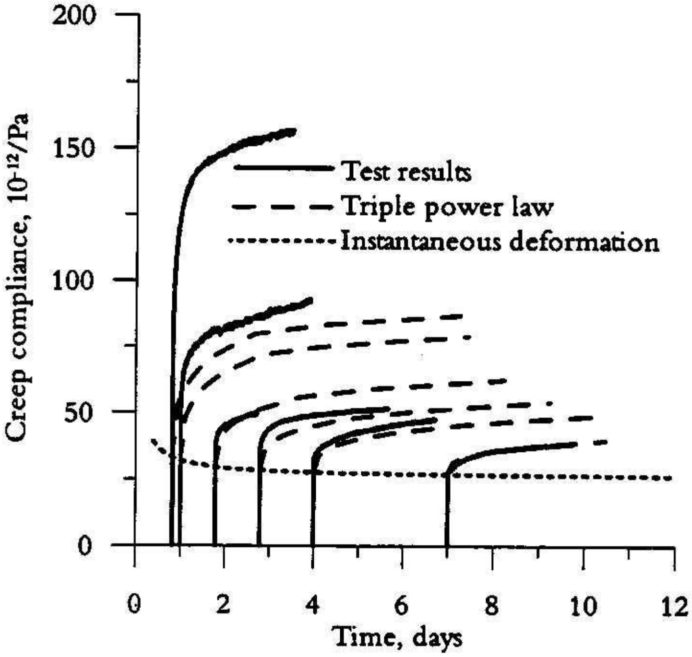

Figure 3-30: Comparison of different power laws compared to test results (Westman, 1999)

$$J(t,t_0) = \frac{1}{E_0} + \frac{\varphi_1}{E_0}\left(t_0^{-m} + \alpha\right)\left[(t-t_0)^n - B(t,t_0;n)\right] + \frac{\Psi_1(t_0)}{E_0} + \frac{\Psi_2(t,t_0)}{E_0} \qquad \textit{Equation 3-85}$$

Where, E_0, $\varphi 1$, m, n, α, and $B(t,t_0;n)$ have the same definition as defined in the Triple Power law, and where:

$$\Psi_1(t_0) = \gamma_1 \cdot \left(\frac{t_1 - t_0}{t_1 - t_s}\right)^{a_1} \quad \text{for all } t_0 \le t_1 \text{, and} \qquad \textit{Equation 3-86}$$

$$\Psi_1(t_0) = 0 \quad \text{when } t_0 > t_1$$

$$\Psi_2(t,t_0)=\gamma_2\cdot\left[1-\exp\left(-\left(\frac{t-t_0}{t_2}\right)^{a_2}\right)\right]\left(\frac{t_1-t_0}{t_1-t_s}\right)^{a_3} \quad \text{for all } t_0 \le t_3$$

Equation 3-87

and

$$\Psi_2(t,t_0)=0 \qquad \text{when } t_0 > t_3$$

where, t_0 = the equivalent age when the load is applied (days),

t_s = the apparent setting time of the concrete (days),

t_1 , t_3 = time limits for adjustment at early ages (days),

t_2 , a_2 = parameter for the development of the time function (days),

t - t_0 = actual time period after loading (days),

γ_1 = initial value of function $\Psi_1(t_0)$ at $t_0 = t_s$,

γ_2 = initial value of function $\Psi_2(t,t_0)$ at $t_0 = t_s$,

a_1 = parameter modifying the shape of $\Psi_1(t_0)$, and

a_2 = parameter modifying the end value of $\Psi_2(t,t_0)$.

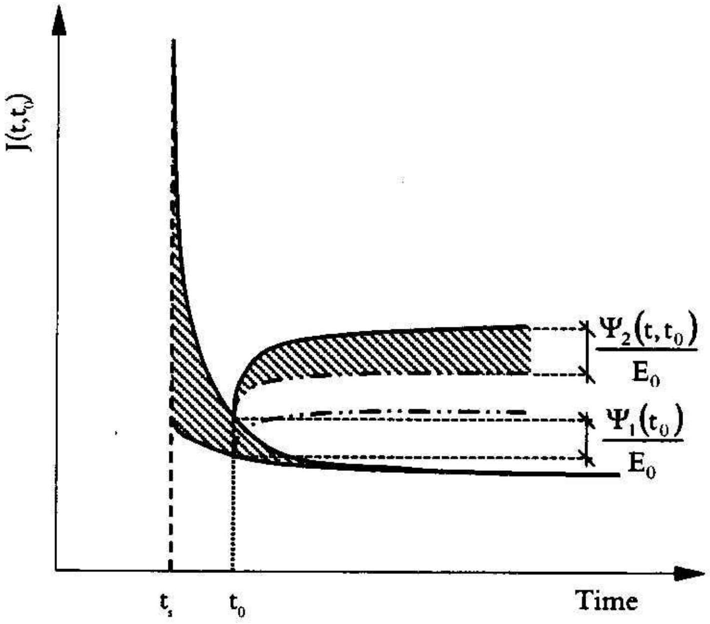

Figure 3-31: A schematic of the additional $\Psi_1(t_0)$ and $\Psi_2(t,t_0)$ functions used to extend the triple power law for the early-age creep response (Westman, 1999)

In the documentation provided by Westman (1999), the necessary values for each of the parameters listed in this section is provided as to allow the implementation of this model. Based on the characteristics of the different mixtures tested by Westman, the mixture corresponding to a typical pavement mixture was selected. The characteristics of this mixture (LTU 20) are as follows: w/c = 0.40, 557 lb/yd^3 cement (6.0 sacks), 5.6% air content, and a 28-day compressive strength of around

6850 psi. Based on the test results with this mixture proportions, it is recommended that the following parameters for the Extended Triple Power Law be used:

t_1 = 1.5 days, γ_1 = 10.0,
t_3 = 1.5 days, γ_2 = 18.0,
t_2 = 0.02 days, a_1 = 5.0,
a_2 = 0.2, and a_3 = 5.0.

3.6.6 Implementation of Proposed Creep Model

In the implementation of creep compliance formulation, there are two possible approaches, and both methods have their advantages and disadvantages. The methods can briefly be described as follows (Emborg ,1989):

1. The simplest method "… is to assume the stress history is a series of sudden (discontinuous) stress increments and then solve the algebraic equations resulting from the superposition of creep responses due to all the individual stress increments," (Baźant, 1972). The error involved with this numerical procedure is of the second time step, however, the result obtained by Emborg (1989) and others show good agreement with test data. The disadvantage of this method is that large storage space could be required to store the complete history of stresses for all the elements in the structure.
2. The second method requires the conversion of the creep compliance values into relaxation values. For this process, the Maxwell chain model is most often used in the conversion process. This procedure requires good selection of parameters for the Maxwell elements, and in some instances convergence of the conversion could require user intervention. It is reported that for very long load durations, negative relaxation values could develop and adjustments of the creep curves are necessary to prevent this problem from occurring (Westman, 1999). After the relaxation values are determined, further curve fitting is also required to obtain a smooth representation of the concretes behavior.

In this study, it is recommended that the method of superposition be used, since run time and storage problems will be less of a problem in the case of very-early age analysis. This is the case since the analysis only needs to be performed until the zero-stress temperature is reached, and only a few concrete elements has to be considered in a slab element. The following sections will provide further details on the solution to this procedure.

3.6.6.1 Relaxation Formulation of Creep Deformations based on the Principle of Superposition

Using the principle of superposition (Baźant, 1972), the strain history ε(t) caused by an arbitrary history of applied stress σ(t), can be determined by assuming the stress history is composed of infinitesimal step functions as shown in Figure 3-32. The total strain can be calculated as shown in Equation 3-88 (Baźant, 1972; and Emborg, 1989). This equation is a general uniaxial constitutive relation defining concrete as an aging viscoelastic material.

$$\varepsilon(t) = \int_0^t J(t,t_0)\cdot d\sigma(t_0) + \varepsilon_0(t) \qquad \textit{Equation 3-88}$$

where, $J(t,t_0)$ = creep compliance defined as the response at time t after loading at time t_0,

$d\sigma(t_0)$ = stress increment at time t_0, and

$\varepsilon_0(t)$ = stress-independent strain increment at time t.

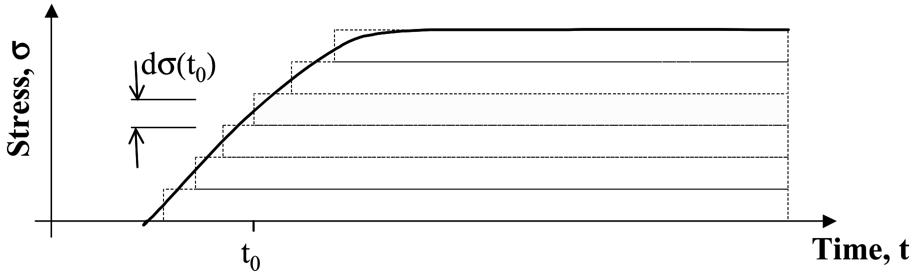

Figure 3-32: Decomposition of stress history into stress steps

When the history of strain is prescribed, Equation 3-88 can be solved by a step-by-step numerical solution (Baźant, 1972), where time is subdivided into discrete time steps, t_r (r=0,1,2, … n) with time steps, $\Delta t_r = t_r - t_{r-1}$. A schematic for the numerical solution is shown in Figure 3-33, and the steps for the algorithm are as follows:

STEP 1: At time t_r, determine the equivalent age te_r, and the change in equivalent age as follows:

$$\Delta te_r = te_r - te_{r-1} \qquad \textit{Equation 3-89}$$

STEP 2: Determine the applied strain, ε_r, and calculate the incremental strain as follows:

$$\Delta\varepsilon_r = \varepsilon_r - \varepsilon_{r-1} \qquad \textit{Equation 3-90}$$

STEP 3: Determine the incremental elastic modulus:

$$E''_r = 1 / J(r, r-½) \qquad \textit{Equation 3-91}$$

where, subscript r, refer to the discrete time te_r, and $J(r,r-½)$ may be interpreted as follows: $J(te_r, te_r - \Delta te_r/2)$

STEP 4: Determine the incremental strain, $\Delta\varepsilon''_r$:

$$\Delta\varepsilon''_r = \sum_{s=1}^{r-1} \Delta J_r \cdot \Delta\sigma_s + \Delta\varepsilon_r^0 \qquad \textit{Equation 3-92}$$

where, $\Delta\sigma_s = \sigma_s - \sigma_{s-1}$
$\Delta\varepsilon^0_r = \varepsilon^0_r - \varepsilon^0_{r-1}$
$\Delta J_r = J(r,s-½) - J(r-1,s-½)$

STEP 5: Finally, the stress increment ($\Delta\sigma_r$) for the time step, Δt_r can be determined as follows:

$$\Delta\sigma_r = E''_r \cdot (\Delta\varepsilon_r - \Delta\varepsilon''_r) \qquad \textit{Equation 3-93}$$

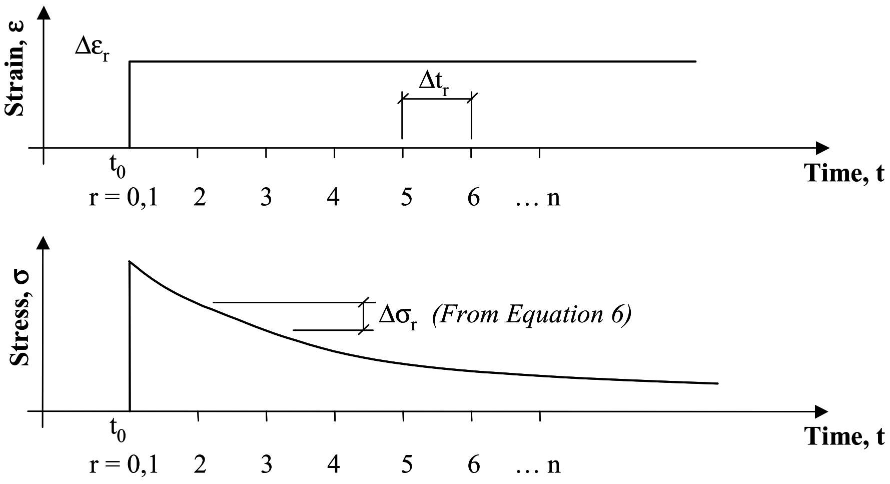

Figure 3-33: Discreet subdivision of time for numerical creep analysis

NOTE: Due to the nature of the summation required in Equation 3-92, and the fact that the value *J(x,x)* is not singular, the start of the numerical iteration (r=0, and r=1) requires some initial calculations other than those presented above. Iteration interval r=0, should be taken to occur at time, $t = t_0$, and r=1 should be taken to occur at time, $t = t_o + 0.01$ (hours). The following calculations are necessary for r=0, and r=1 (Baźant, 1972):

At r = 0: $\Delta\sigma_r = 0$, and $t = t_0$ (days)

At r = 1: $\Delta\varepsilon''_r = 0$, $t = (t0 + 0.01)/24$ (days)

$E''_r = 1 / J(r, r-0.1)$, and $\Delta\sigma_r = E''_r \cdot (\Delta\varepsilon_r)$

Figure 3-34 presents a schematic of how strains could be superimposed to account for strain levels of varying intensities. Is should be noted that creep recovery at unloading could be overestimated by this principle, since the plastic flow component of the irrecoverable time dependent deformation is not accounted for (Westman, 1999). However, at very-early ages this effect should be insignificant.

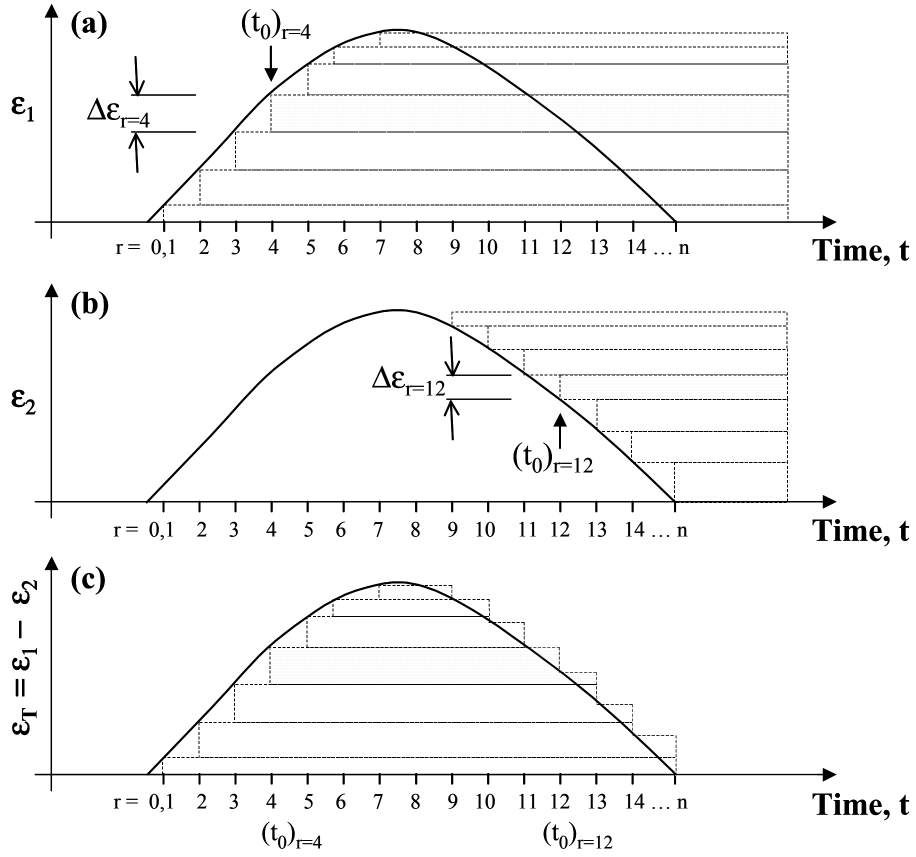

Figure 3-34: Superposition of various strains intensities: (a) Loading, (b) Unloading, (c) Net applied strains

3.6.7 Sample results from the Proposed Creep Model

The creep model proposed and analysis algorithm outlined in this section, was used to evaluate the behavior obtained by the model. Based on typical mixture proportions, an thermal coefficient of expansion of 9.34 microstrain/°C, and the temperature history as shown in Figure 3-35, strains were calculated for a 305 mm thick concrete pavement. A fully restrained condition for the uncracked concrete pavement was assumed at early-ages. The development of strain due to the early-age thermal effects is plotted on the secondary y-axis of Figure 3-36. The numerical procedure outlined above was programmed into FORTRAN, and the development of thermal stresses is shown in Figure 3-36.

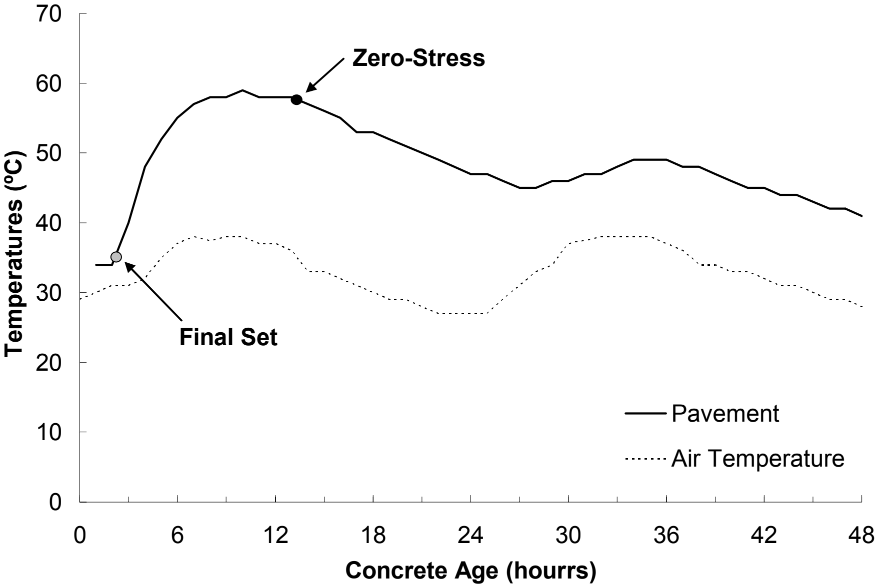

Figure 3-35: Concrete and air temperatures used for relaxation calculations

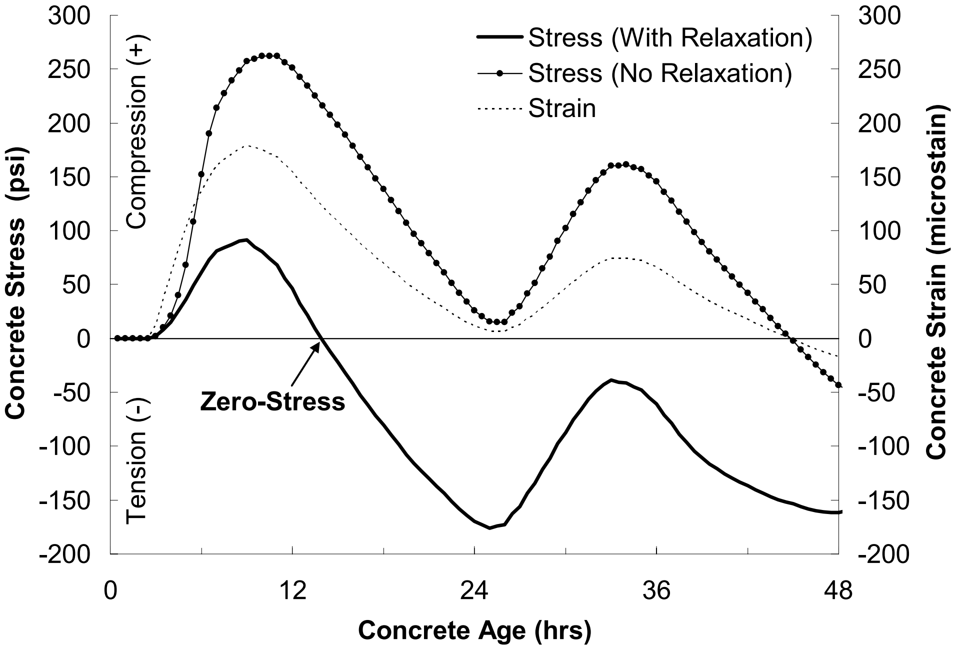

Figure 3-36: Comparison of the results of the relaxation model and model without relaxation

Final set occurred after 3 hours and without the incremental strain approach and relaxation effects, strains and stresses cross the zero-stress level at the same time (time ≈ 45 hours). However, when the effects of relaxation is accounted for, the stress at early-ages are significantly less, due to the effect of relaxation, and the zero-stress level occurs much earlier at an age of about 14 hours. The locations of the final set and zero-stress conditions are shown on Figure 3-35. Because much of the early compression has been “relaxed”, tensile stresses occur earlier, and it can be seen that it will be nonconservative to disregard these early-age relaxation effects.

3.7 SUMMARY AND CONCLUDING REMARKS

The work documented in this chapter presents mechanistic models to determine the heat transfer from the pavement system to the environment. A number of models are presented in detail and the models will be calibrated later in this report. It is recommended that the models be evaluated for implementation into the temperature prediction program.

The early-age temperature development of concrete could be estimated from knowledge of cement the composition, cement fineness, the presents of admixtures, thermal characteristics of the concrete (aggregate type) and surroundings, the slab thickness, and the prevailing environmental conditions. Numerous factors are involved and the fact that most of these factors do not influence the concrete temperature independent of each other, and the use of adiabatic testing will be necessary to determine the internal heat generated by local concretes.

Models were selected to characterize the factors that have the most significant influence on the development of concrete temperatures. The most applicable models were selected, and compatibility of all the available models was kept in mind in order to ensure that the overall model can be developed. The proposed model could account for the following factors: cement composition, water-cement ratio, cement fineness, mineral admixtures, initial concrete temperature at placement, environmental conditions, subbase temperature, and slab thickness.

Techniques are available from literature to predict the heat transfer from the concrete to the surroundings; however, the development of a computer program to facilitate the computing process will be required. Heat transfer through, conduction, convection, irradiation, and solar absorption can account for the effects of different in place conditions.

High zero-stress temperatures will increase the thermal stresses the pavement is subject to over its intended life. Temperature control in pavements is thus related to the control and minimization of excessive zero-stress temperatures, which have been shown to produce poor long-term pavement performance.

Few models are available to characterize the time dependent deformation and creep compliance of concrete at very early-age (less than 2 days). It is recommended that the Extended Triple Power Law as developed by Westman (1999) be developed and evaluated to account for early-age relaxation effects. This model is recommended since it accounts for the following factors that could influence the time dependent deformation: concrete age at setting, concrete age at loading (including ages less than 2 days), applied stress level, and the influence of varying temperature on concrete properties.

Based on the information reviewed and presented in this document, it is evident that many models are available to predict the concrete temperature. However, due to the nature of any mechanistic model, and the fact that most of the literature available was conducted outside of the United States, calibration for local conditions and materials will be an essential phase to ensure that the models are valid under the intended conditions.

Chapter 4

Experimental Program

In Chapter 3, models were selected to predict the in place temperature, setting, and stresses of concrete pavements. Numerous factors affect the development of the in place concrete temperatures, and it is essential with any mechanistic model that local materials are tested to calibrate it for local conditions. The calibration requires actual test data, and the more detailed and comprehensive this data set, the higher the confidence in the calibrated model. In this study, the models will be calibrated based on experimental data collected from the three stages of experimental work. These phases will be covered in this chapter, and they are as follows:

Phase I: Field Work

The objective of this phase was to collect data from actual paving projects, which will be used during the calibration of the temperature prediction program. Seven projects were instrumented across the state of Texas. At each field site, quantities of the all raw materials were gathered to enable the reproduction of the field mixtures during the laboratory testing phase of this project.

Phase II: **Materials Characterization**

During the laboratory test phase, the hydration behavior of the field mixtures were determined for use during the calibration of the temperature and setting prediction models. The additional objective of the laboratory phase was to characterize the hydration of different cementitious materials. During this phase, a standard cement source was chosen, and the effect of using different dosages of various mineral admixtures was evaluated.

Phase III: **Concrete Hydration under Controlled Conditions**

During this phase, small insulated concrete slabs were cured in environmental chambers and their temperature development monitored. This process minimizes the impact climatic conditions such as fluctuating wind speeds, cloud cover, air temperatures, and relative humidity. The data from this phase were used during the initial calibration of the hydration and heat transfer models.

4.1 PHASE I: FIELD WORK

This section will present the field work plan undertaken as part of this project. Seven projects were instrumented across the state, as shown in Figure 4-1. The sections were selected to be representative of the range of concrete placement conditions, and materials commonly used in

Texas. Data were collected from three different locations in Texas: Dallas, Houston, and El Paso. Since the primary objective of this project is to provide measures to improve the long-term performance of concrete pavements constructed under hot weather conditions, three of the field sites were instrumented in the summer of 2000. No sections were instrumented under cold weather construction conditions.

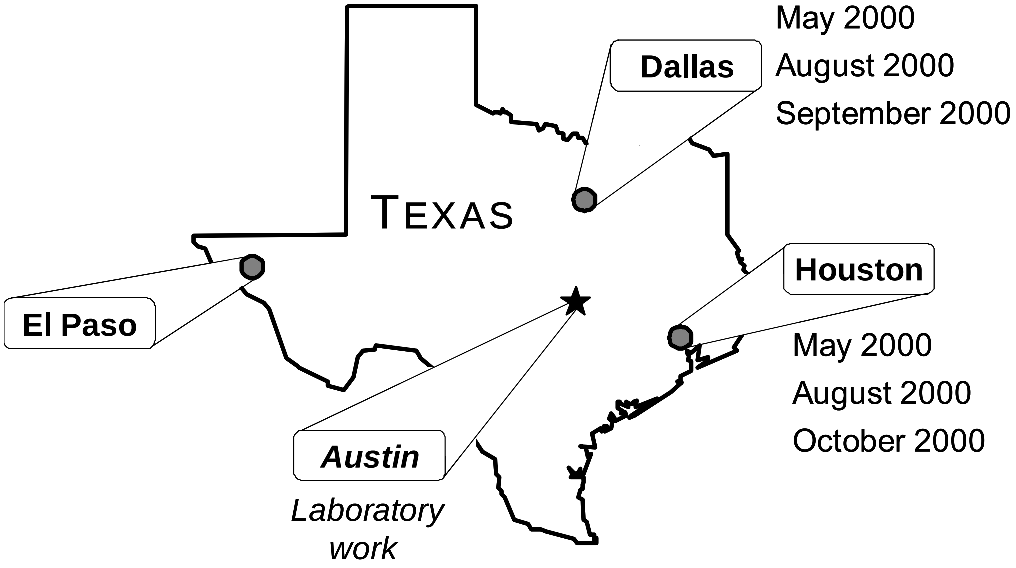

Figure 4-1: Location of the field sites across the state of Texas

4.1.1 Data Collection Plan

The monitoring plan was developed to characterize all the variables that possibly affect the temperature development in freshly placed concrete. Additional variables that are required as inputs for the models developed in Chapter 3 were collected. The variables collected include: mixture design properties, concrete properties, concrete temperature history, environmental conditions during placement, pavement thickness, subbase type, subbase temperature, and curing methods used.

At four of the seven sites, the pavement was instrumented to monitor and record the temperature development at two different concrete placement times. At the other sites, only one location was instrumented due to unscheduled changes in the construction process during the intended instrumentation period. The mixture proportions used in each of the instrumentation sections were obtained and samples of the raw materials were taken to reproduce the mixture for laboratory testing. The following data were collected at each site:

4.1.1.1 *Concrete Temperature History*

The temperatures at slab mid depth, one-half inch from the top and one-half inch from the bottom were recorded at half hour intervals, over a 72-hour period. Thermo couples were used to measure and log the concrete from the time of placement. The positioning and fastening of the thermocouples can be seen in Figure 4-2. The thermocouple wires were fastened to wire that was tensioned between vertically positioned reinforcement bars. These bars were fastened to the slab reinforcement to prevent movement during placement. Attention was given to keep the thermocouple ends away from surrounding rebar, since the temperature of the reinforcement could affect the reading. The initial mixture temperature at time of placement was measured with a thermometer. The temperature of the subbase was measured with infra-red temperature sensor, as shown in Figure 4-3.

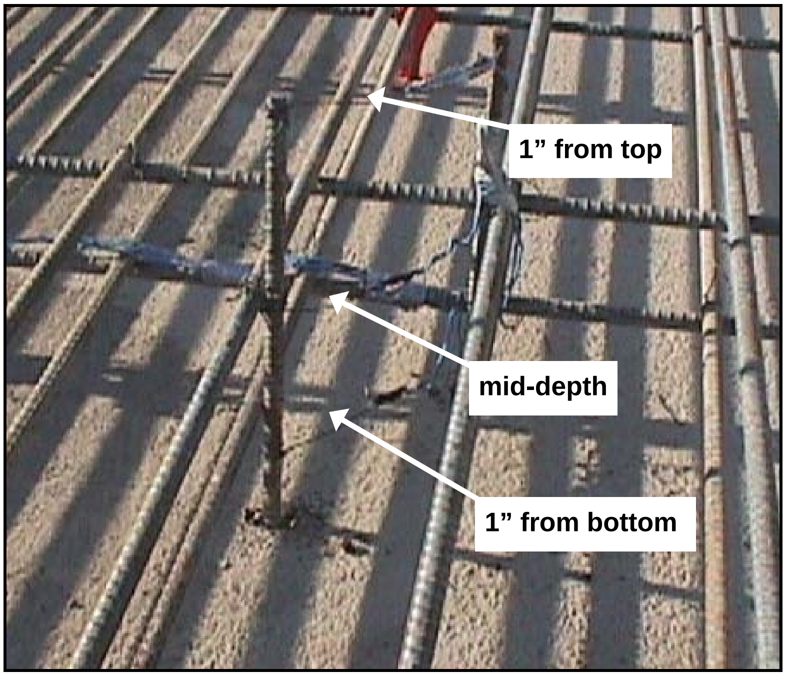

Figure 4-2: Fastening of thermocouples prior to concrete placement

Figure 4-3: Handheld infrared thermometer used during the field work

4.1.1.2 *Mixture Properties*

Changes in mixture properties, such as the cement type, cement grind, water-to-cement ratio, etc. are some of the primary causes for excessive heat development in concrete pavements. In order to determine which of the mixture properties contribute to the significant differences in the concrete temperature and strength the following parameters were collected during the detailed monitoring:

a. Mixture proportions,
b. Coarse aggregate type,
c. Cement composition from cement certificate,
    - Bogue compounds, sulfate content (SO_3), alkali content, free Lime (CaO) content, and magnesium oxide (MgO) content.
d. Cement fineness,
e. Fly ash Composition (if used on the project), and
f. GGBF slag composition (if used on the project).

4.1.1.3 *Concrete Initial and Final Setting (ASTM C 403)*

The time of initial and final set was determined through ASTM C 403, "Time of Setting of Concrete Mixtures by Penetration Resistance." This method requires that a mortar sample of the fresh concrete be obtained by sieving the concrete through a 4.75-mm sieve. Initial attempts to sieve the very stiff paving concrete (slump = 0.75 inch) were unsuccessful. Based on this experience, a decision was made to use a vibration table to separate the paste from the coarse aggregate. The equipment used for the test is shown in Figure 4-4. Setting data were not collected for the two field sites visited during May 2000. However, for the remaining sites a portable vibration table was obtained, which was used to separate the paste from the coarse aggregates.

4.1.1.4 *Concrete Properties*

In order to characterize the concrete as delivered to site, the 7-day flexural strength of the concrete was determined by the project personnel. Additional concrete properties were determined on the mixture prepared in the laboratory. These properties are presented in Section 4.2.1.

Figure 4-4: Vibration table and Pentrometer used on site

4.1.1.5 *Environmental Conditions*

The concrete temperature development is affected by the climatic conditions that occur during placement. Environmental conditions were monitored by an on-site weather station. The following parameters were collected: air temperature, wind speed, and relative humidity. The status of the cloud cover that prevailed during the 72-hour instrumentation period was evaluated through visual observations. The cloud cover will be characterized in terms of the estimated percentage of cloud cover: that is 100% for totally overcast, and 0% for clear sky. The purpose of this will be to account for the impact of solar radiation on the temperature gain in the slab. The solar radiation was not measured on site, and was obtained from the nearby weather station. The on-site weather station was used to collect the necessary parameters to calculate the evaporation rate associated with the free water surface.

4.1.1.6 *Miscellaneous Parameters*

The following additional parameters were collected as all of them could affect the temperature development of freshly placed concrete:

a. Pavement thickness,
b. Subbase type and temperature prior to placement, and
c. Method of curing: The type of curing compound used and the time at which it was applied were documented.

4.1.2 Mixture Proportions and Materials for the Field Sites

Table 4-1 provides a summary of cementitious materials, and the water cementitious ratios used for each of the field sites. The detailed mixture proportions and sources of raw materials are provided in Appendix A. Table 4-2 summarizes the chemical and physical properties of all the cements, and Table 4-3 provide the chemical properties of the mineral admixtures. In most cases, a slip form concrete paver was used to place the concrete, and all the mixtures had low slumps. Note that the level of replacement for the mineral admixtures was done on a volume basis, which is the practice in the state of Texas. (In most part of the U.S. replacement is done on a weight basis.)

Table 4-1: Summary of concrete mixtures used during the field work phase

Mix No.	Description	Cementitious Materials	Cement Factor	w/cm
1	Dallas: 05/2000	Type I/II + 20% Class F fly ash	5.5 sacks	0.39
2	Houston: 05/2000	Type I/II + 25% Class C fly ash	6.0 sacks	0.44
3	Dallas: 08/2000	Type I	5.0 sacks	0.46
4	Houston: 08/2000	Type I/II + 35% Class C fly ash	6.0 sacks	0.41
5	El Paso: 08/2000	Type I/II + 50% GGBF Slag	5.0 sacks	0.54
6	Dallas: 09/2000	Type I/II + 20% Class F fly ash	5.0 sacks	0.50
7	Houston: 10/2000	Type I/II + 25% Class C fly ash	6.5 sacks	0.41

Table 4-2: Chemical and physical properties of cements tested during this project

Mix No.	Cement Type	Bogue Compounds (%)				Chemical Composition (%)				Blaine (m^2/kg)
		C_3S	C_2S	C_3A	C_4AF	SO_3	Free CaO	MgO	Alkalies[a]	
1	Type I/II	53	23	6	10	2.81	0.77	0.95	0.57	374
2	Type I/II	60	14	5	10	2.34	0.80	4.00	0.51	365
3	Type I	56	16	11	7	3.36	2.3	0.98	0.63	342
4	Type I/II	60	14	6	10	2.37	0.8	3.58	0.51	359
5	Type I/II	57	18	6	10	2.79	2.0	2.00	0.55	367
6	Type I/II	53	21	5	12	3.20	1.02	1.20	0.46	350
7	Type I/II	60	14	6	10	2.27	0.7	3.72	0.49	362

Note: [a] Equivalent Alkalies = $Na_2O + 0.658 \cdot K_2O$, according to ASTM C 150

Table 4-3: Chemical properties and source of the mineral admixtures used in the field sites

Mix No.	Mineral Admixture	Chemical Composition (%)		
		CaO	SiO_2	Alkalies
1	Class F fly ash	10.6	57.3	0.30
2	Class C fly ash	24.7	32.7	1.22
3	None used	-	-	-
4	Class C fly ash	25.3	39.6	1.18
5	GGBF Slag	-	-	-
6	Class F fly ash	10.8	58.2	0.40
7	Class C fly ash	25.4	32.4	1.61

4.1.3 Data Collected at Each Field Site

This section reports project specific information for each of the seven field sites visited. The measured concrete temperatures and concrete setting information are also presented.

4.1.3.1 *Field Site 1: Dallas, May 2000*

The instrumented pavement was a 13-inch thick CRC pavement located on Interstate 45, South of Dallas. The pavement instrumented was placed on Friday May 5, 2000. The section was part of the northbound inside lane, and started 980 ft before the southern expansion joint of the Dowdy Ferry Road bridge crossing right in front of the Hutchins District Office. The contractor on the project was Granite Construction. The properties collected during the fieldwork are summarized in Table 4-4.

Placement was scheduled to occur on Thursday May 4, 2000, but was delayed to the next day due to heavy thunderstorms that occurred during most of the day. Construction started early Friday morning at around 8:10am, but only 510 ft was placed as construction was forced to stop at around 11:00am due to heavy rainfall. Figure 4-5 provides a picture of the construction operations. Only a morning placement was, therefore, instrumented on this project. As shown in Figure 4-6, the freshly paved concrete was covered with black polyethylene sheets to prevent damage due to rain.

The concrete temperatures measured for this project are shown in Figure 4-7. The maximum temperature in concrete was 39.0°C (102°F).

Table 4-4: Summary of variables collected on IH 45, Dallas, May 2000

Parameters		Values		
Pavement design and materials				
Measured pavement thickness		13.25 inch (330 mm)		
Reinforcement layout		#6 bars at 6-inch c/c		
Cement factor		5.5 sacks		
Control strength		555 psi flexural at 7-days		
Coarse aggregate type		1.5” Crushed limestone		
Subbase type		Hot mix asphalt		
Environmental conditions		***Day 1***	***Day 2***	***Day 3***
Air temperature (°C)	Minimum	18.6	21.1	21.2
	Maximum	25.8	29.2	30.2
Relative humidity (%)	Daytime	74	59	58
	Nighttime	91	88	89
Wind speed (mph)	Daytime	2.6	8.5	6.6
	Nighttime	13.3	15.2	13.4
Maximum Solar Radiation (W/m^2) [a]		1286	1309	1394
Cloud cover	Daytime	70%	60%	30%
	Nighttime	60%	30%	30%
Rainfall	Daytime	9:30am–1pm	-	-
	Nighttime	-	-	-
Construction operations		May 5, 2000		
Construction time		8:10 am		
Fresh concrete temperature		72°F (22.4°C)		
Initial subbase temperature		74°F (23.3°C)		
Time of surface texturing		9:45 am		
Time of curing application		10:00 am		
Curing method		Single layer white curing compound, black plastic sheet during 3-24 hours Sheets were placed at 11am		
Approximate Haul time		≈ 20 minutes with dump trucks		

Note: [a] Obtained from nearest weather station, and does not incorporate cloud cover.


Figure 4-5: Photograph of construction operations on IH 45 in Dallas, May 2000


Figure 4-6: Newly paved pavement protected against rainfall, Dallas, May 2000

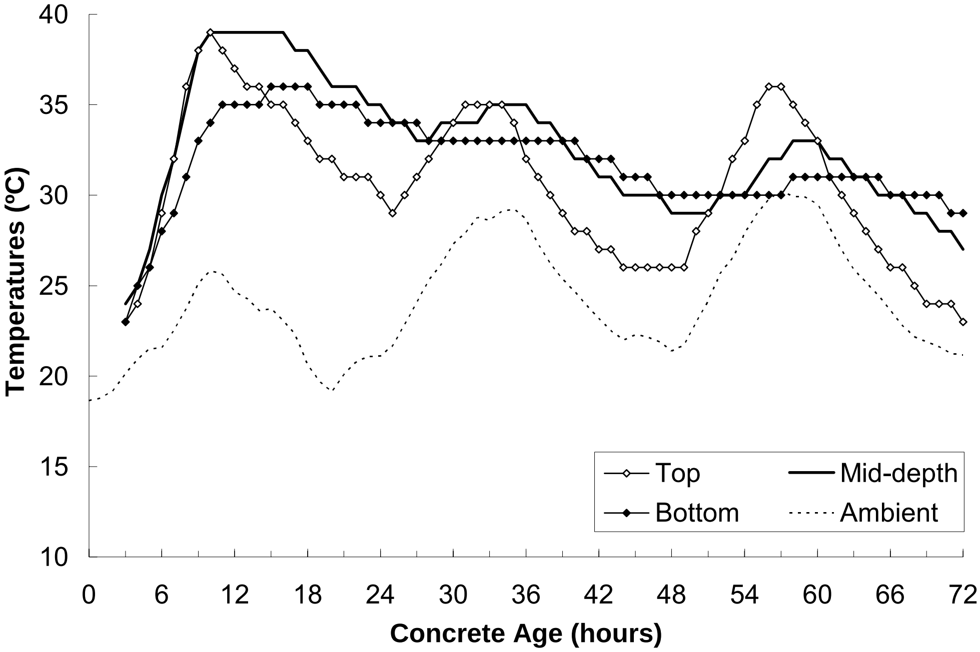

Figure 4-7: Ambient and in place concrete temperatures measured on in Dallas, May 2000

4.1.3.2 *Field Site 2: Houston, May 2000*

The instrumented pavement was a 13-inch thick CRC pavement, located on US 59, southwest of downtown Houston, and southwest of the intersection of US 59 and Beltway 8. The section was part of the southbound outside shoulder and was started 160 feet before the southern expansion joint of the Kirkwood Road Bridge. The contractor was H.B. Zachary Construction.

Construction started at 8:00am on May 11, 2000, and about 1500 feet was constructed during a full day of placement. Since the section was located between the barrier wall and an existing part of pavement, the slip form paver was used in a cantilever configuration, as can be seen in Figure 4-8. The properties collected during the fieldwork are summarized in Table 4-5.

Table 4-5: Summary of variables collected on US 59, Houston, May 2000

Parameters		**Values**		
Pavement design and materials				
Measured pavement thickness		13.0 inch (330 mm)		
Reinforcement layout		2 layers of #6 bars at 12-inch c/c		
Cement factor		6.0 sacks		
Control strength		555 psi flexural at 7-days		
Coarse aggregate type		1.5" Crushed limestone		
Subbase type		Hot mix asphalt		
Environmental conditions		***Day 1***	***Day 2***	***Day 3***
Air temperature (°C)	Minimum	25.6	20.6	19.4
	Maximum	29.4	30.6	27.8
Relative humidity (%)	Daytime	70	69	63
	Nighttime	88	96	84
Wind speed (mph)	Daytime	8.1	0.0	4.6
	Nighttime	16.1	15.0	16.1
Maximum Solar Radiation (W/m^2) [a]		1225	1231	1330
Cloud cover	Daytime	30%	70%	50%
	Nighttime	70%	100%	80%
Rainfall	Daytime	-	-	-
	Nighttime	-	5pm–11pm	-
Construction operations		May 11, 2000		
Construction day and times		8:45 am		3:10pm
Fresh concrete temperatures		88°F (31.1°C)		86°F (30.0°C)
Initial subbase temperatures		86°F (30.0°C)		93°F (33.9°C)
Times of surface texturing		10:15 am		3:52pm
Times of curing application		10:30 am		3:55pm
Curing method		Single layer white curing compound		
Approximate Haul time		≈ 30 minutes with dump trucks		

Note: [a] Obtained from nearest weather station, and does not incorporate cloud cover.

Figure 4-8: Photograph of construction operations used on IH 45 in Dallas, May 2000

Two locations were instrumented, the first at 8:45am and the second at 3:10pm. The concrete temperatures measured for this project are shown in Figures 4-9 and 4-10. The maximum concrete temperature was measured to be 44.0°C (111°F) for the 8:45am placement, and 42.0°C (108°F) for the 3:10pm placement.

The air temperature, wind speed, and relative humidity were initially collected by an onsite weather station. However, after the data were retrieved, it was discovered that the weather station malfunctioned. Therefore, for this section, the climatic conditions were based on hourly data obtained from the nearby Houston Hobby Airport.

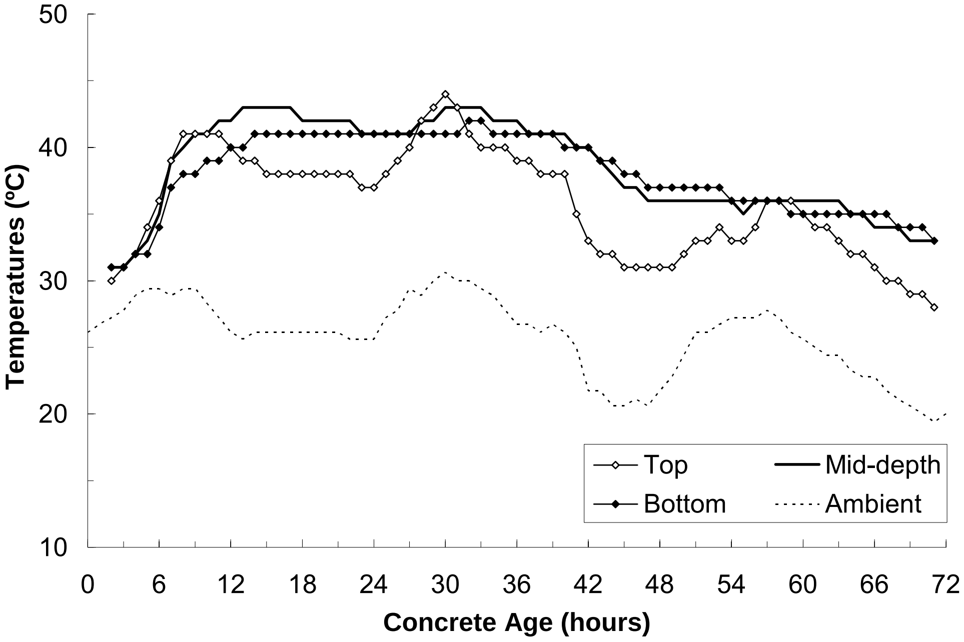

Figure 4-9: Ambient and in place concrete temperatures for the 8:45am placement in Houston, May 2000

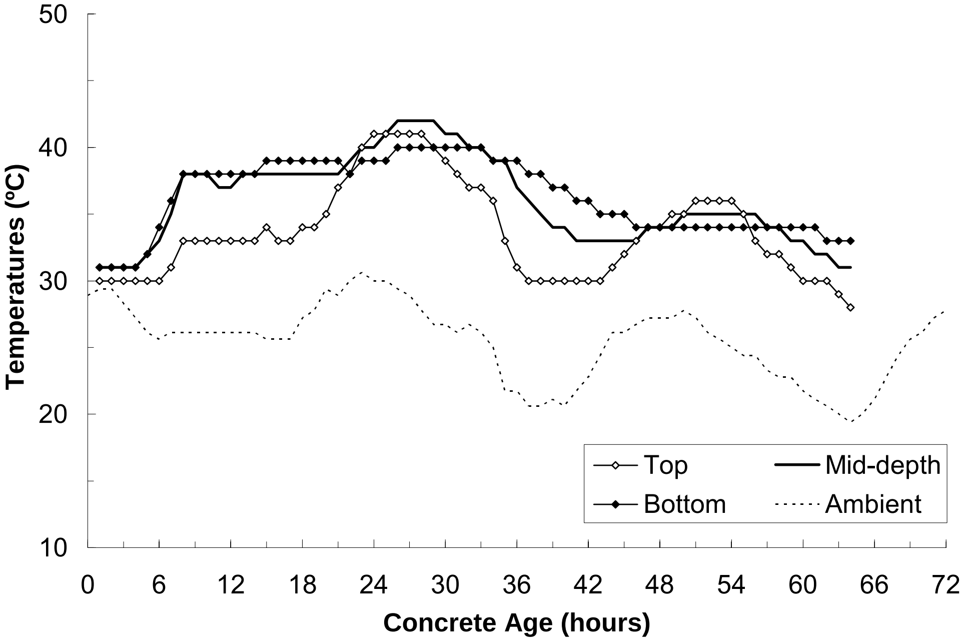

Figure 4-10: Ambient and in place concrete temperatures for the 3:10pm placement in Houston, May 2000

4.1.3.3 *Field Site 3: Dallas, August 2000*

This section reports on the fieldwork performed and the data collected in Dallas on a 12-inch thick CRCP section constructed on SH 190; known as the President George Bush Turnpike. The section formed part of the eastbound main lanes. This project was not under TxDOT's supervision, since it is a toll road and falls under the North Texas Turnpike Authority. The pavement was placed at 7:05am in the morning on Friday August 4, 2000. Figure 4-11 presents a photograph of the curing operation used on this project.

Construction started early Friday morning at around 3:00am, and about 500 ft was placed up until 9:30am when construction was stopped due to an unscheduled shortage of coarse aggregates. This limited the instrumentation to one location for this site. The properties collected during the fieldwork are summarized in Table 4-6.

Figure 4-11: Photograph of construction operations used on SH 190 in Dallas, August 2000

The air temperatures during this field project exceeded 100°F, and numerous hot weather placement problems were experienced. The concrete temperatures measured for this project are shown in Figure 4-12. This figure indicates that there is a very steep rise in concrete temperature at around 3 hours after placement and the peak concrete temperature of 62.2°C (144°F) occurred at around 8 hours after placement. Note that this section was placed in the morning (7:05am) and still very high concrete temperatures occurred. From Figure 4-12, it may be seen that a considerable temperature gradient developed between the top and the bottom of the slab.

Table 4-6: Summary of variables collected on SH 190 Dallas, August 2000

Parameters		Values		
Pavement design and materials				
Measured pavement thickness		12.0 inch (305 mm)		
Reinforcement layout		#6 bars at 6-inch c/c		
Cement factor		5.0 sacks		
Control strength		555 psi flexural at 7-days		
Coarse aggregate type		Crushed limestone		
Subbase type		Hot mix asphalt		
Environmental conditions		***Day 1***	***Day 2***	***Day 3***
Air temperature (°C)	Minimum	27.0	27.0	28.0
	Maximum	38.0	38.0	39.0
Relative humidity (%)	Daytime	28	27	28
	Nighttime	67	67	63
Wind speed (mph)	Daytime	5.8	9.2	10.4
	Nighttime	15.0	19.6	17.3
Maximum Solar Radiation (W/m^2) [a]		1267	1289	1187
Cloud cover	Daytime	15%	5%	5%
	Nighttime	5%	5%	5%
Construction operations		August 4, 2000		
Construction time		7:05 am		
Fresh concrete temperature		93°F (22.4°C)		
Initial subbase temperature		88°F (23.3°C)		
Time of surface texturing		8:15 am		
Time of curing application		9:20 am		
Curing method		Single layer white curing compound		
Approximate Haul time		≈ 15 minutes with dump trucks		

Note: [a] Obtained from nearest weather station, and does not incorporate cloud cover.

The time of final set was estimated through the penetration resistance method described in ASTM C 403. The penetration resistance test results are plotted in Figure 4-13, and ASTM C 403 defines initial setting to occur at a pressure of 500 psi and final set at a pressure of 4000 psi. An equation of the form recommended by ASTM C 403, was fitted through the data as presented in Figure 4-13. From this figure, it may be seen that there is only 43 minutes between initial set and final set, which were calculated to be as follows:

- Time of initial set = 2 hours 34 min
- Time of final set = 3 hours 17 minutes

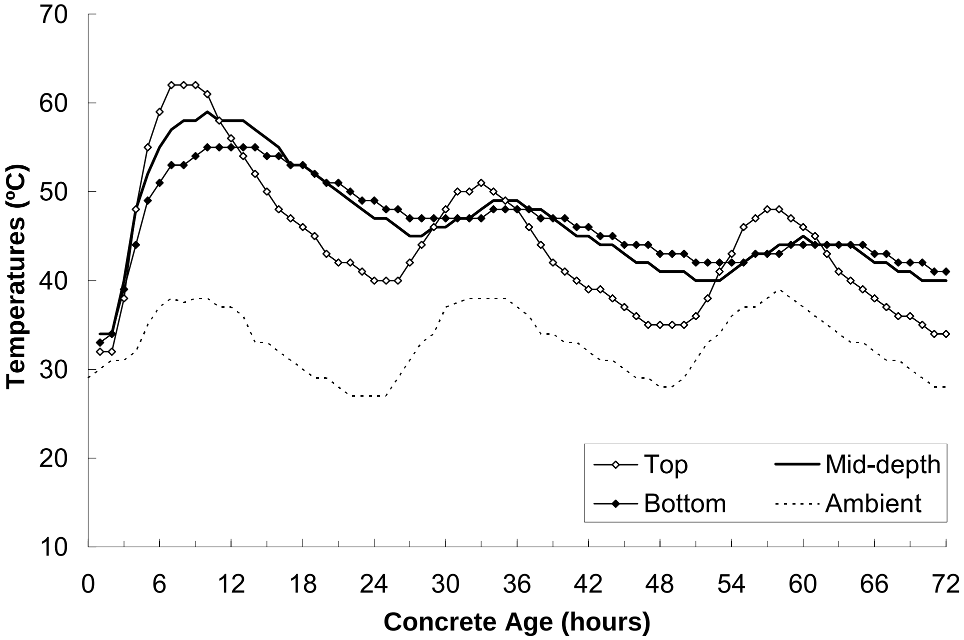

Figure 4-12: Ambient and in place concrete temperatures measured on SH 190 in Dallas, August 2000

Additional Comments on Hot Weather Concreting Problems on this Site

While on site, the author observed some adverse effects that can probably be attributed to the high concrete temperatures experienced on site. Some of these observations were noticed on the specific section instrumented, and some on other sections placed during the 3 day observation time following the construction of the instrumented section. The following temperatures were recorded on 8/4/00 at 1:30 pm:

- Asphalt base surface = 142 °F
- Reinforcement = 132 °F

Figure 4-14 shows some concrete debris on the surface caused by the tining operation that was applied too late, since setting of the surface had already occurred. The tining was very shallow and in some places, only slight lines were drawn on the concrete.

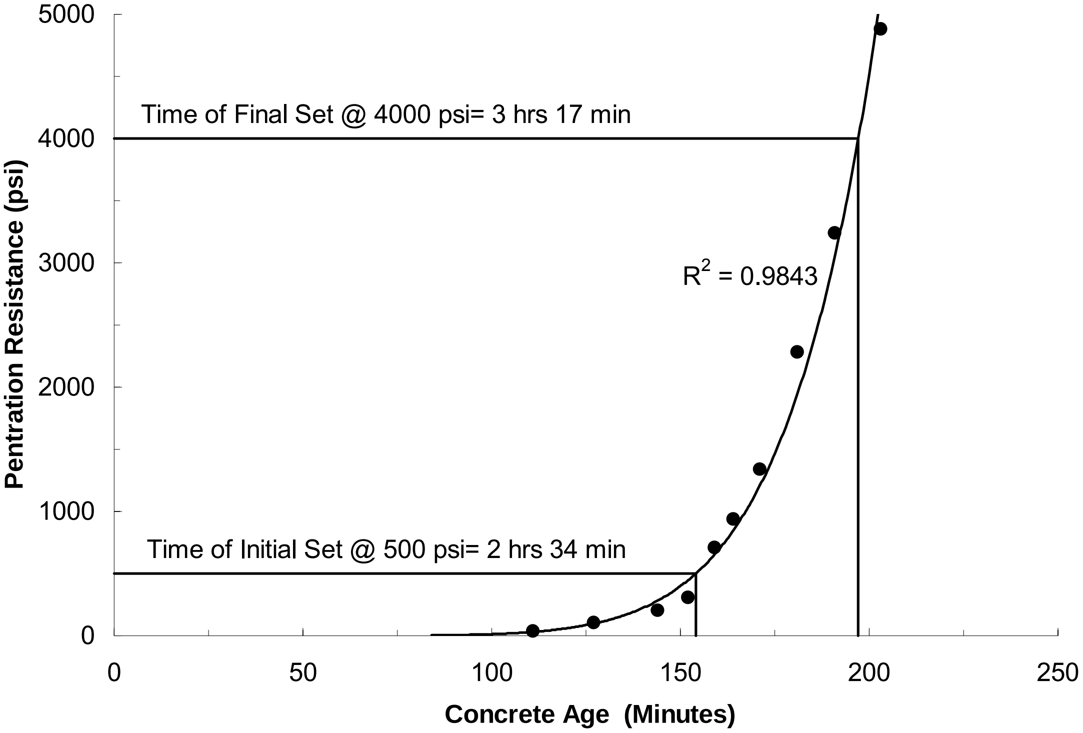

Figure 4-13: Time of setting by penetration resistance on SH 190 in Dallas, August 2000

Figure 4-14: Concrete debris caused by tining over an already set concrete surface

Figure 4-15 presents the evaporation rate that occurred during placement, and all the values were extremely high and well above the critical value of 0.2 lb/ft^2/hr (ACI 305, 2000). Under these conditions, it is likely that plastic shrinkage will develop if extra precautions are not taken to provide adequate curing.

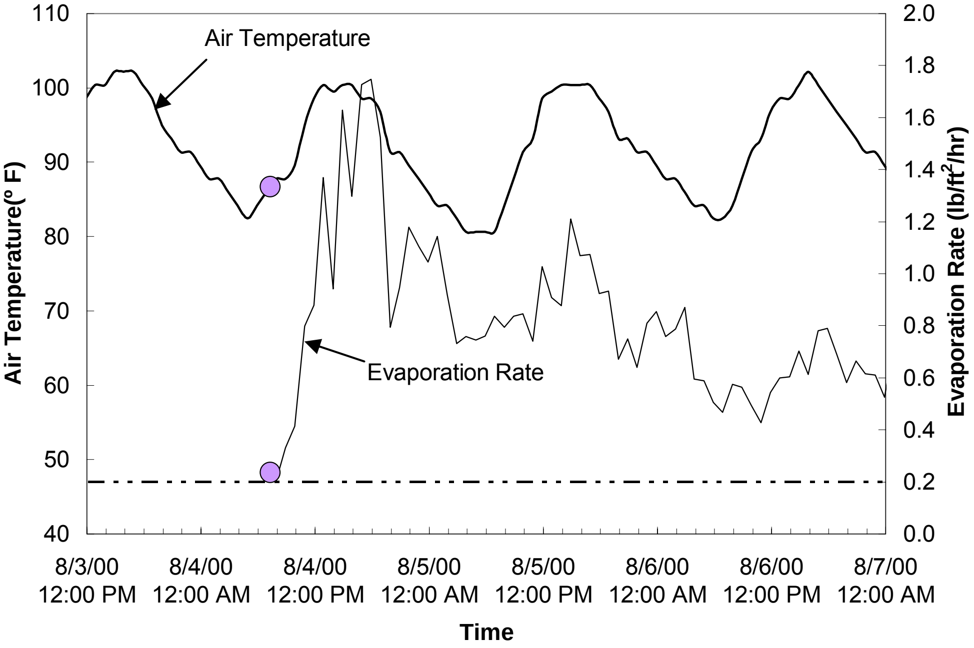

Figure 4-15: Air temperature and evaporation rate that prevailed during construction

Figure 4-16 presents an edge view of the concrete that was not cured for an extended period during these hot weather conditions. Note that this picture is **not** representative of the majority of the concrete placed, but was taken on the last 50 feet of concrete placed on 8/7/00. This picture indicates the extent of plastic shrinkage cracking that occurred due to the extremely high evaporation rates experienced during placement. It is noticeable that the widths of some of the cracks are extremely wide. An excessive amount of voids can be seen, which may indicate that the concrete was already setting up by the time of vibration.

Figure 4-16: Cracking in the fresh concrete on the edge of the section placed on 8/7/00

4.1.3.4 *Field Site 4: Houston (August 2000)*

The instrumented section was 10-inch thick CRC pavement constructed on FM 529, north of Houston. The mixture design included the use of 35% Class C fly ash replacement. The pavement was placed on August 25, 2000 and during placement, two locations were instrumented. The first was instrumented at 9:30am and the second at 2:45pm. The section started 350 ft east of Ridgeway Drive, and paving continued east towards Texas Highway 6. During the paving day, 2100 linear feet of 12 feet wide concrete pavement was placed. The two instrumentation locations were 1450 feet apart. The contractor was Pate and Pate Construction. The properties collected during the fieldwork are summarized in Table 4-7. Figure 4-17 presents the construction operations for this project.

The concrete temperatures measured for this project are shown in Figures 4-18 and 4-19. The maximum temperature in concrete was measured to be 49.0°C (120°F) for the 9:30am placement, and 51.0°C (124°F) for the 2:45pm placement.

Table 4-7: Summary of variables collected on FM 529, Houston, August 2000

Parameters		**Values**		
Pavement design and materials				
Measured pavement thickness		10.0 inch (255 mm)		
Reinforcement layout		#6 bars at 8.5-inch c/c		
Cement factor		6.0 sacks		
Control strength		555 psi flexural at 7-days		
Coarse aggregate type		Crushed limestone		
Subbase type		Hot mix asphalt		
Environmental conditions		***Day 1***	***Day 2***	***Day 3***
Air temperature (°C)	Minimum	23.2	22.9	23.4
	Maximum	39.4	40.8	40.6
Relative humidity (%)	Daytime	44	41	35
	Nighttime	100	97	97
Wind speed (mph)	Daytime	0.4	0.4	0.4
	Nighttime	6.7	7.1	7.2
Maximum Solar Radiation (W/m^2) [a]		1169	1244	1174
Cloud cover	Daytime	60%	40%	40%
	Nighttime	40%	40%	40%
Construction operations		August 25, 2000		
Construction day and times		9:30 am		2:45pm
Fresh concrete temperatures		90°F (31.9°C)		96°F (35.6°C)
Initial subbase temperatures		92°F (33.3°C)		110°F (43.3°C)
Times of surface texturing		9:45 am		2:55pm
Times of curing application		9:56 am		3:15pm
Curing method		Double layer white curing compound		
Approximate Haul time		≈ 30 minutes with dump trucks		

Note: [a] Obtained from nearest weather station, and does not incorporate cloud cover.

Figure 4-17: Photograph of construction operations used on FM 529 in Houston, August 2000

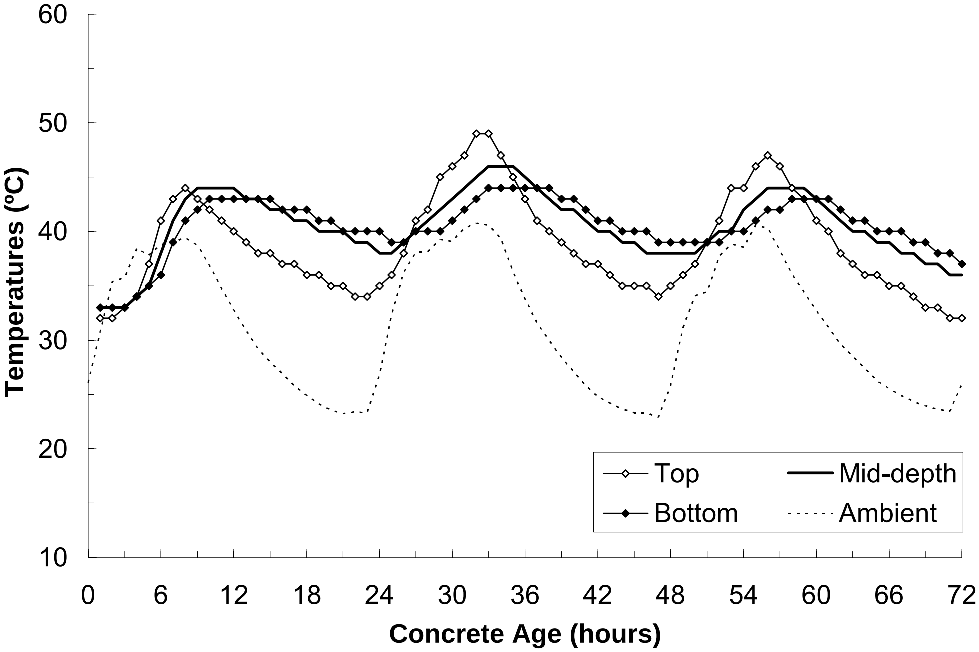

Figure 4-18: Ambient and in place concrete temperatures for the 9:30am section in Houston, August 2000

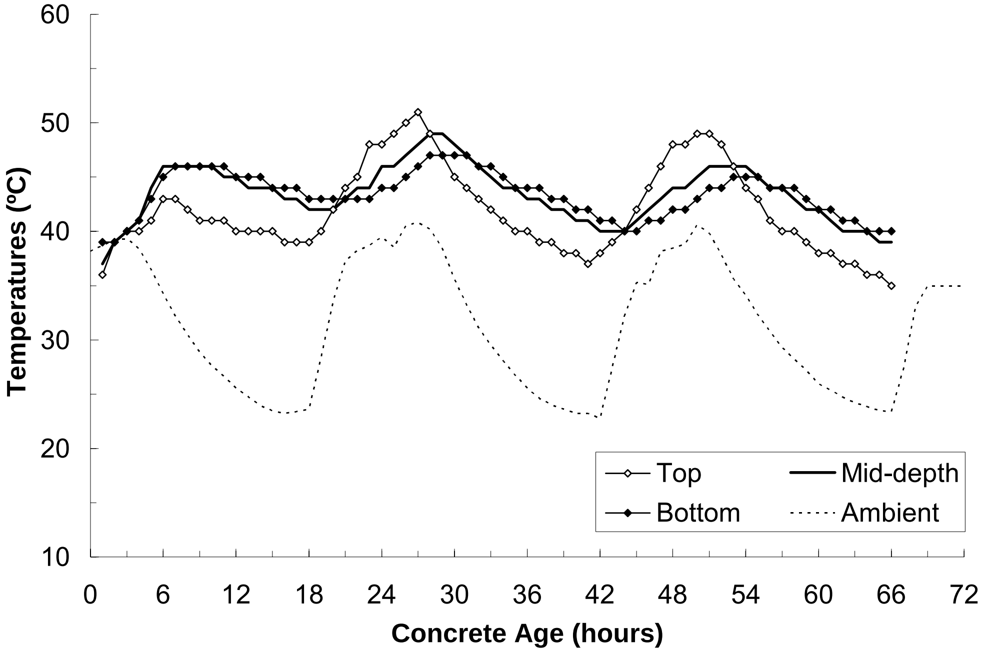

Figure 4-19: Ambient and in place concrete temperatures for the 2:45pm section in Houston, August 2000

The time of final set was estimated through the penetration resistance method described in ASTM C 403. The penetration resistance test results for concrete sampled in the morning and the afternoon are plotted in Figure 4-20. The setting values from this figure are as follows:

9:30am Placement:

- Time of initial set = 4 hours 23 min
- Time of final set = 5 hours 25 minutes

2:45pm Placement:

- Time of initial set = 3 hours 21 min
- Time of final set = 4 hours 40 minutes

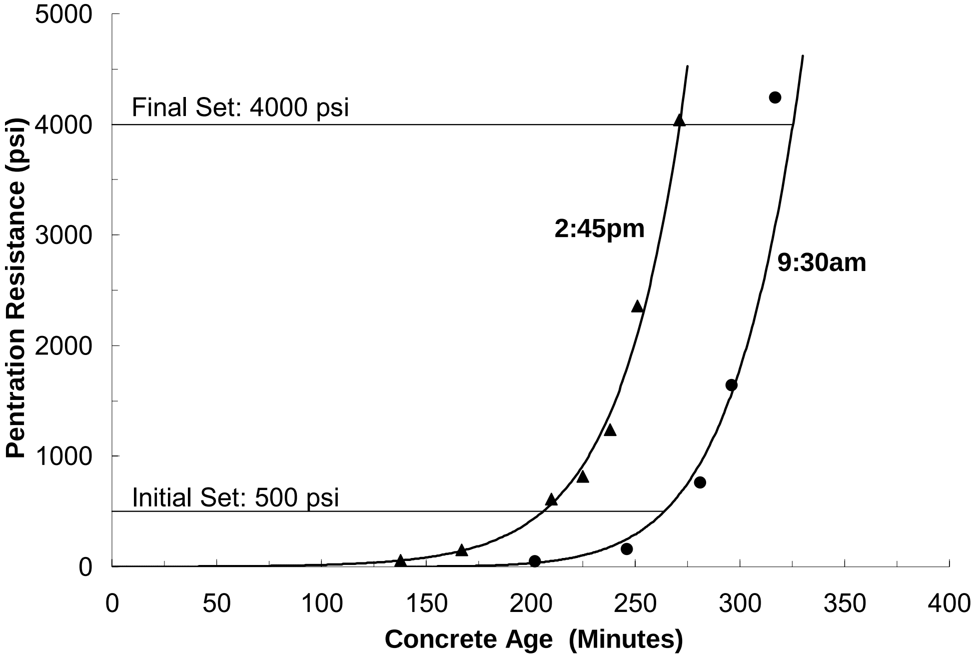

Figure 4-20: Time of setting by penetration resistance on FM 529 in Houston, August 2000

4.1.3.5 *Field Site 5: El Paso, August 2000*

This section reports on the fieldwork performed and the data collected in El Paso on an 11-inch thick CRC pavement section constructed on Loop 375 (Americas Avenue), southeast of downtown El Paso. During the day of instrumentation, a section, 24 foot wide and 540 foot long, of the southbound main lanes was paved. The section ended at the southern transition with the Alameda Road bridge crossing. The mixture design included the use of 50% GGBF Slag replacement. The instrumented pavement was placed on August 17, 2000. The contractor on the project was J.D. Abrams and the concrete was supplied by Jobe Concrete. The properties collected during the fieldwork are summarized in Table 4-8.

Figure 4-21 presents a photograph of the paving operation used on this project. Data was collected from a late morning 10:30am placement. The concrete temperatures measured for this project are shown in Figure 4-22, and a maximum concrete temperature of 43.0°C (109°F) was measured.

Table 4-8: Summary of variables collected on Loop 375 in El Paso, August 2000

Parameters		**Values**		
Pavement design and materials				
Measured pavement thickness		11.0 inch (280 mm)		
Reinforcement layout		#6 bars at 6-inch c/c		
Cement factor		5.0 sacks		
Control strength		555 psi flexural at 7-days		
Coarse aggregate type		1.5" Crushed limestone		
Subbase type		Hot mix asphalt		
Environmental conditions		***Day 1***	***Day 2***	***Day 3***
Air temperature (°C)	Minimum	19.2	23.0	23.2
	Maximum	32.6	38.6	38.3
Relative humidity (%)	Daytime	56	28	24
	Nighttime	93	68	66
Wind speed (mph)	Daytime	1.1	0.4	0.4
	Nighttime	7.8	7.1	5.6
Maximum Solar Radiation (W/m^2) [a]		1127	1220	1292
Cloud cover	Daytime	70%	35%	35%
	Nighttime	90%	35%	35%
Rainfall	Daytime	7-8am	-	-
	Nighttime	5-6pm	-	-
Construction operations		August 17, 2000		
Construction time		10:30 am		
Fresh concrete temperature		90°F (32.2°C)		
Initial subbase temperature		85°F (29.4°C)		
Time of surface texturing		1:15 pm		
Time of curing application		2:20 pm		
Curing method		Single layer white curing compound		
Approximate Haul time		≈ 20 minutes with dump trucks		

Note: [a] Obtained from nearest weather station, and does not incorporate cloud cover.

Figure 4-21: Photograph of construction operations on Loop 375 in El Paso, August 2000

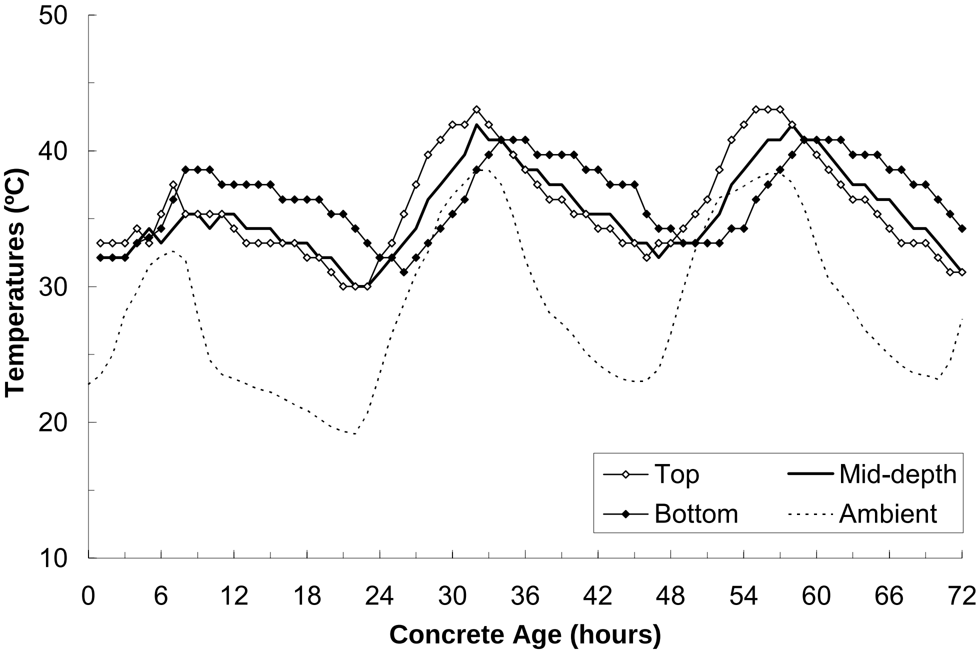

Figure 4-22: Ambient and in place concrete temperatures measured in El Paso, August 2000

The time of final set was estimated through the penetration resistance method described in ASTM C 403. The penetration resistance test results for concrete sampled in the morning and the afternoon are plotted in Figure 4-23. The setting values from the figure are as follows:

10:30am Placement:

- Time of initial set = 2 hours 52 min
- Time of final set = 4 hours 07 minutes

2:40am Sample:

- Time of initial set = 3 hours 31 min
- Time of final set = 5 hours 23 minutes

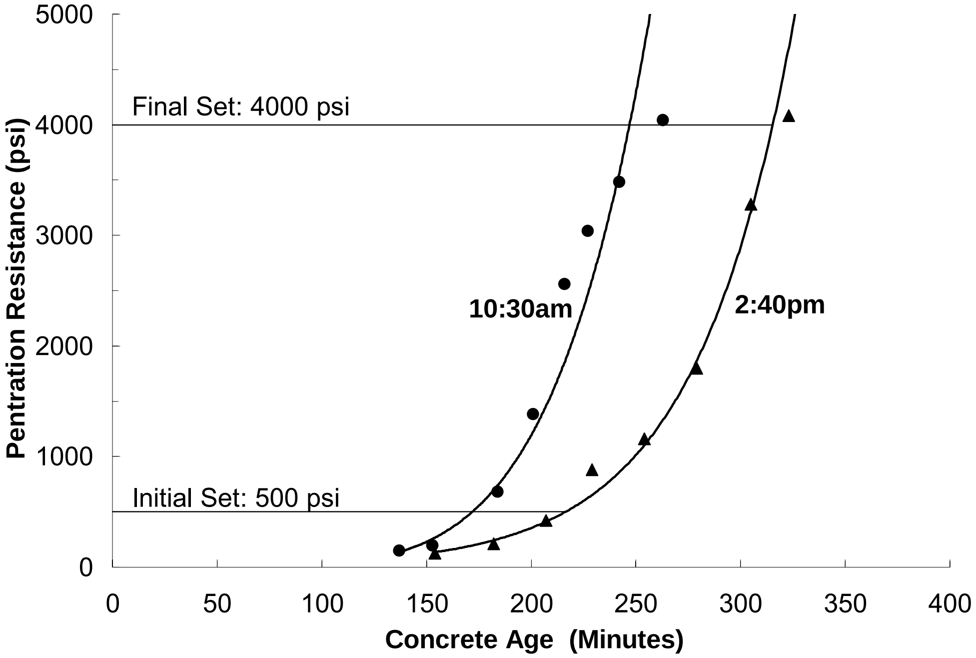

Figure 4-23: Time of setting by penetration resistance on Loop 375 in El Paso, August 2000

4.1.3.6 *Field Site 6: Dallas, September 2000*

The instrumented section was a 13-inch thick CRC pavement, constructed on the eastbound inside shoulder of Interstate 30, east of Dallas. The pavement was placed on September 29, 2000, and two locations were instrumented. Construction started late and the first section was instrumented at 12:20pm and the second at 2:30pm. The section started at Station 30+750, west of the bridge at Belt Line Road. The contractor was H.B. Zachary. Table 4-9 present the properties collected during the fieldwork. Figure 4-24 presents a photograph of construction operations used on this project.

The concrete temperatures measured for this project are shown in Figures 4-25 and 4-26. The maximum temperature in concrete reached 37.0°C (98.6°F) for the 12:20pm placement, and 40.0°C (104°F) for the 2:30pm placement.

Table 4-9: Summary of variables collected on IH 30, Dallas, September 2000

Parameters		Values		
Pavement design and materials				
Measured pavement thickness		13.25 inch (335 mm)		
Reinforcement layout		2 layers of #6 bars at 10.0-inch c/c		
Cement factor		5.0 sacks		
Control strength		555 psi flexural at 7-days		
Coarse aggregate type		1.5 inch crushed limestone		
Subbase type		Hot mix asphalt		
Environmental conditions		***Day 1***	***Day 2***	***Day 3***
Air temperature (°C)	Minimum	13.5	17.8	20.7
	Maximum	29.7	32.4	32.7
Relative humidity (%)	Daytime	20	16	18
	Nighttime	74	62	86
Wind speed (mph)	Daytime	0.4	0.4	0.5
	Nighttime	3.5	3.1	11.1
Maximum Solar Radiation (W/m^2) [a]		1161	1201	1078
Cloud cover	Daytime	40%	60%	60%
	Nighttime	30%	50%	50%
Construction operations		September 29, 2000		
Construction day and times		12:20 pm		2:30pm
Fresh concrete temperatures		81°F (27.3°C)		87°F (30.7°C)
Initial subbase temperatures		86°F (27.8°C)		100°F (37.8°C)
Times of surface texturing		2:20 pm		3:58pm
Times of curing application		3:15 pm		4:02pm
Curing method		Single layer white curing compound		
Approximate Haul time		≈ 30 minutes with dump trucks		

Note: [a] Obtained from nearest weather station, and does not incorporate cloud cover.

Figure 4-24: Photograph of construction operations on IH 30, Dallas, September 2000

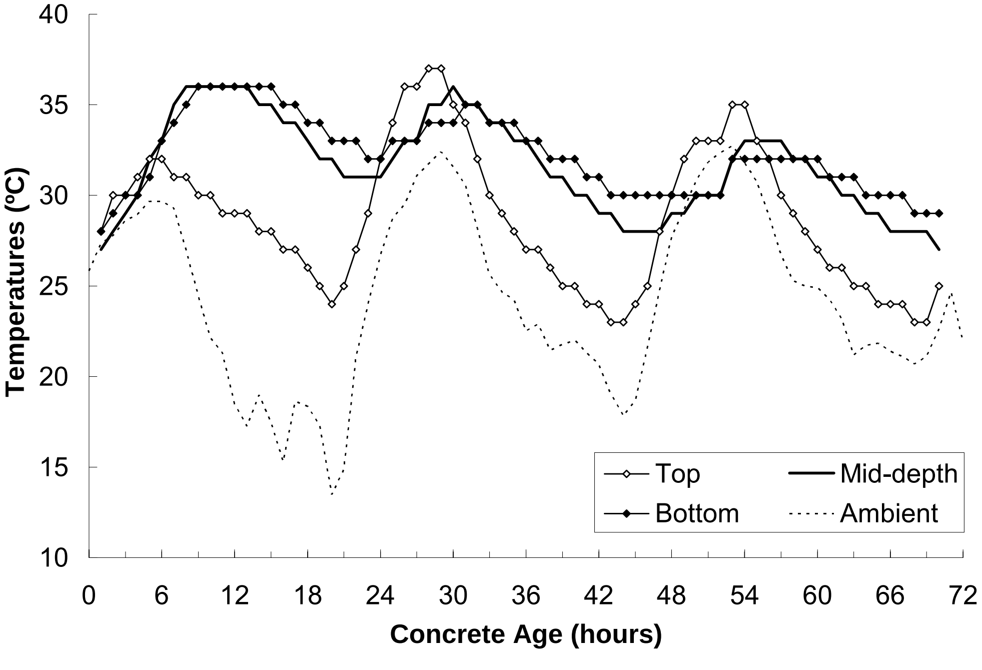

Figure 4-25: Ambient and in place concrete temperatures for the 12:20pm section on IH 30, Dallas, September 2000

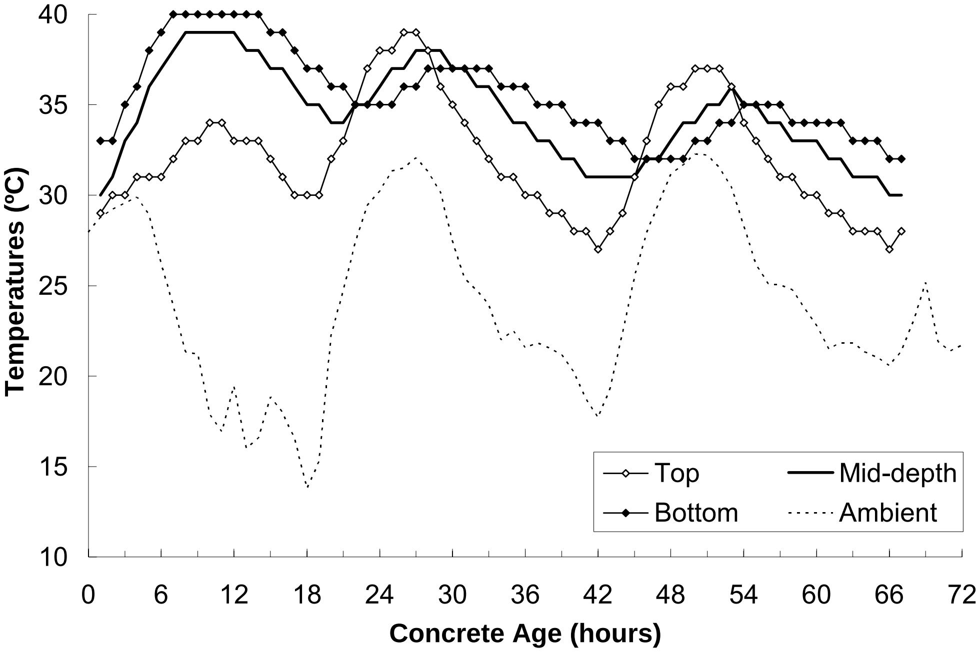

Figure 4-26: Ambient and in place concrete temperatures for the 2:30pm placement on IH 30, Dallas, September 2000

The time of final set was estimated through the penetration resistance method described in ASTM C 403. The penetration resistance test results for concrete sampled in the afternoon are plotted in Figure 4-27. The setting values from the figure are as follows:

- Time of initial set = 3 hours 16 min
- Time of final set = 4 hours 14 minutes

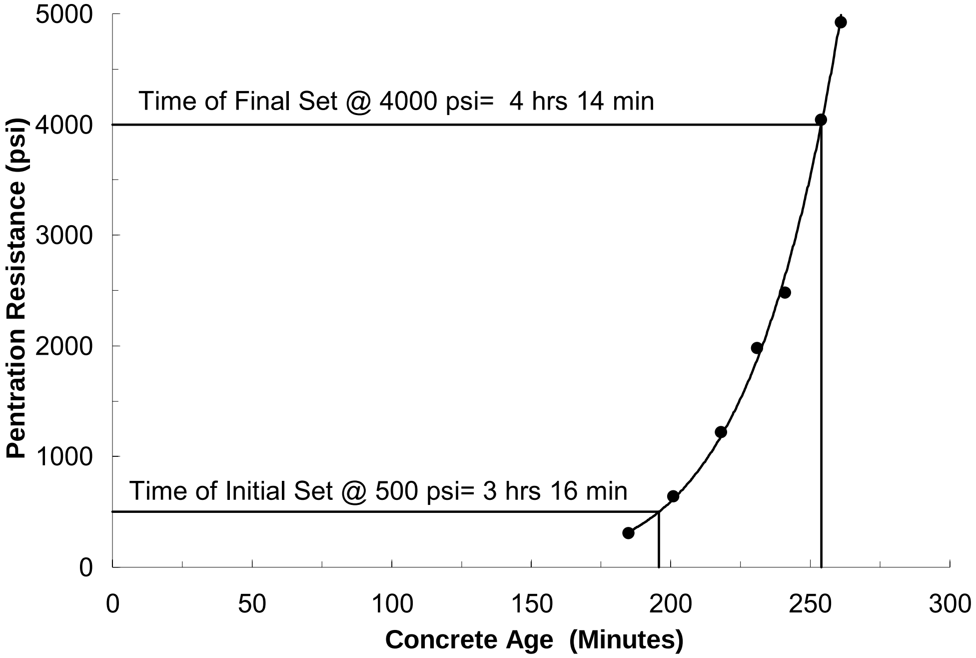

Figure 4-27: Time of setting by penetration resistance on IH 30, Dallas, September 2000

4.1.3.7 *Field Site 7: Houston, October 2000*

The instrumented section was 15-inch thick CRC pavement constructed on southbound inside lane of US 59, north of Houston. The pavement was placed on October 19, 2000, and two locations were instrumented. Construction started at 7:30am, and the first section was instrumented at 10:00am and the second at 2:45pm. The section started at station 1076+00 and ended at station 1063+00. The contractor was Williams Brothers. Table 4-10 present the properties collected during the fieldwork. Figure 4-28 presents the construction operations of this project.

The concrete temperatures measured for this project are shown in Figures 4-29 and 4-30. A maximum concrete temperature of 40.0°C (104.0°F) was measured at both locations.

Table 4-10: Summary of variables collected on US 59, Houston, October 2000

Parameters		**Values**		
Pavement design and materials				
Measured pavement thickness		15.00 inch (380 mm)		
Reinforcement layout		2 layers of #6 bars at 6.5-inch c/c		
Cement factor		6.5 sacks		
Control strength		555 psi flexural at 7-days		
Coarse aggregate type		1.5 inch crushed limestone		
Subbase type		Hot mix asphalt		
Environmental conditions		***Day 1***	***Day 2***	***Day 3***
Air temperature (°C)	Minimum	16.3	20.2	20.9
	Maximum	27.7	28.2	27.1
Relative humidity (%)	Daytime	32	32	60
	Nighttime	89	90	95
Wind speed (mph)	Daytime	0.4	0.4	0.7
	Nighttime	3.7	4.1	5.9
Maximum Solar Radiation (W/m^2) [a]		1085	1042	1010
Cloud cover	Daytime	40%	60%	60%
	Nighttime	30%	50%	50%
Construction operations		October 19, 2000		
Construction day and times		10:00 am		2:45pm
Fresh concrete temperatures		80°F (26.6°C)		84°F (28.6°C)
Initial subbase temperatures		85°F (29.4°C)		105°F (40.6°C)
Times of surface texturing		10:35 pm		3:48pm
Times of curing application		12:30 pm		4:10pm
Curing method		Single layer white curing compound		
Approximate Haul time		≈ 25 minutes with dump trucks		

Note: [a] Obtained from nearest weather station, and does not incorporate cloud cover.

The time of final set was estimated through the penetration resistance method described in ASTM C 403. The penetration resistance test results for concrete sampled in the afternoon are plotted in Figure 4-31. The setting values are as follows:

- Time of initial set = 5 hours 20 min
- Time of final set = 6 hours 42 minutes

Figure 4-28: Photograph of construction operations on US 59, Houston, October 2000

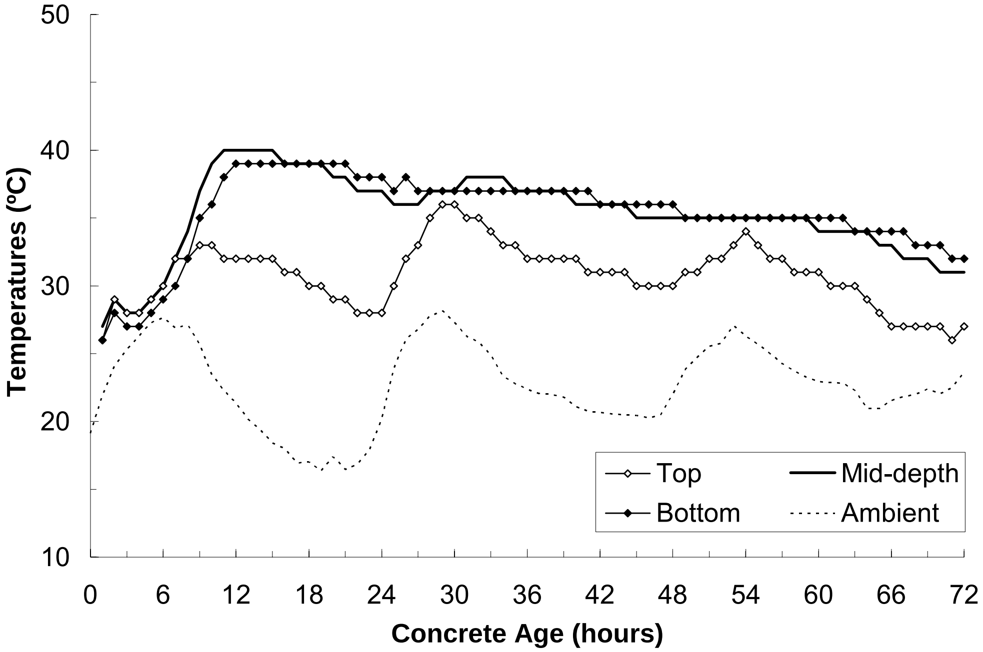

Figure 4-29: Ambient and in place concrete temperatures for the 12:20pm section on US 59, Houston, October 2000

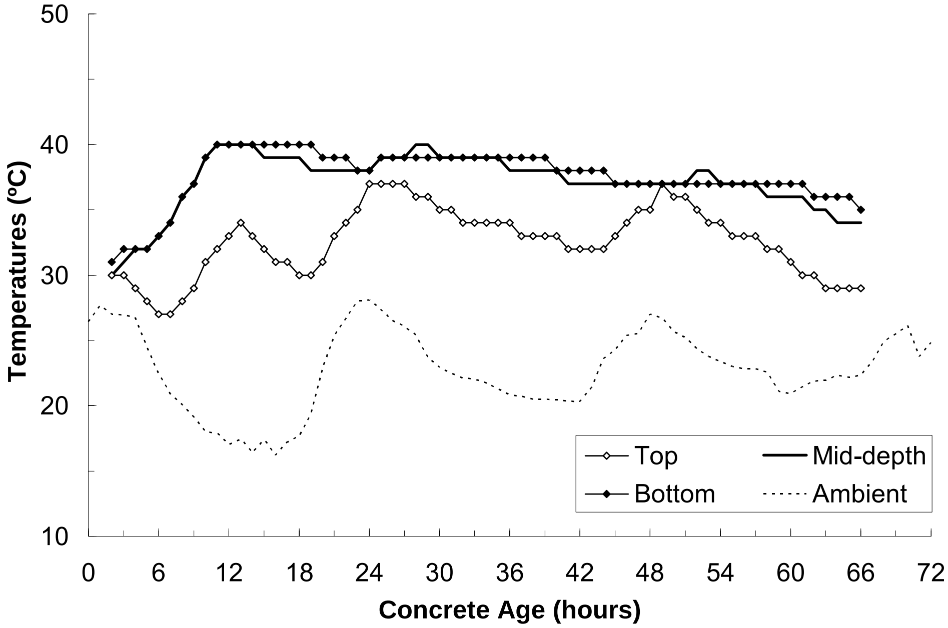

Figure 4-30: Ambient and in place concrete temperatures for the 2:30pm placement on US 59, Houston, October 2000

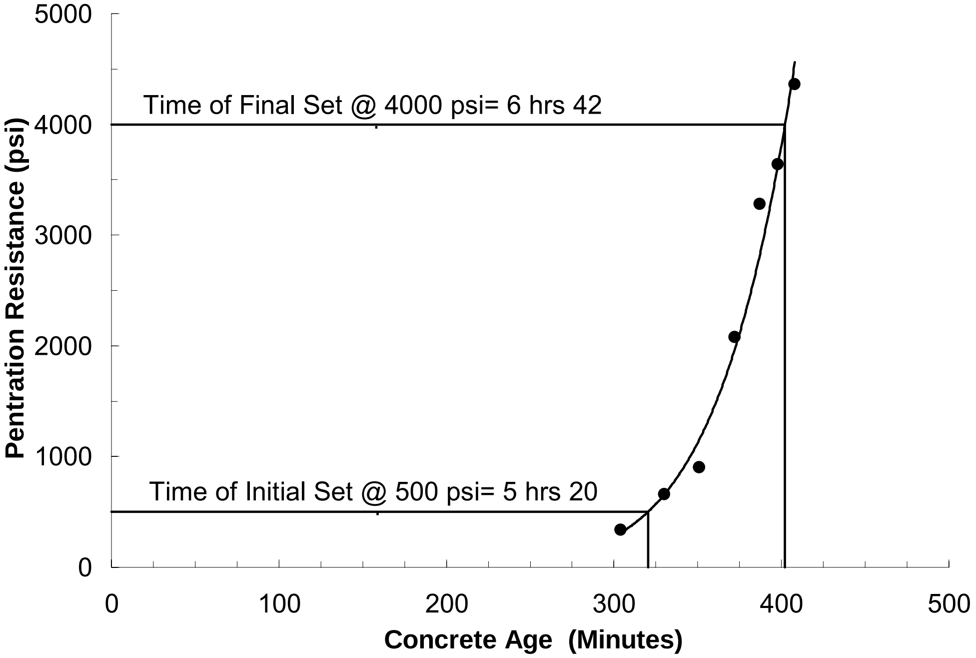

Figure 4-31: Time of setting by penetration resistance on US 59, Houston, October 2000

4.2 PHASE II: MATERIALS CHARACTERIZATION

During the laboratory test phase, the hydration behavior of the seven field mixtures was determined for use during the calibration of the temperature and setting prediction models. The additional objective of the laboratory phase was to characterize the hydration of different cementitious materials. During this phase, a standard cement source was chosen, and the effect of using different mineral admixtures on the hydration development was then evaluated.

During the materials characterization phase, an additional 13 mixture proportions were obtained from two stages of data collection. A standard cement source was chosen, and the type and dosage level of the mineral admixtures used with the cement were changed. Two additional cement sources were tested. The following combinations of mineral admixtures were used:

- 15%, 25%, 35%, and 45% ASTM C 618 Class C Fly Ash
- 15%, 25%, 35%, and 45% ASTM C 618 Class F Fly Ash
- 30%, and 50% ASTM C 989 Grade 120 GGBF Slag

All tests were performed at the facilities of The University of Texas at Austin located at the J.J. Pickle Campus. Most of the mixing and testing was done by the author, and help was provided by the staffs of the Construction Materials Research Group (CMRG) which form part of the Civil Engineering Department at the University of Texas at Austin.

4.2.1 Testing Plan

The laboratory tests consisted of testing the concrete mixtures from the field sites, and the mixtures developed to characterize the hydration behavior.

4.2.1.1 *Testing of Field Mixtures*

In order to characterize the seven concrete mixtures used at each field site, laboratory tests were performed on these mixtures. The mixture proportions of all the field sites are presented in Appendix A.

The tests conducted in the laboratory are summarized in Table 4-11. Fresh concrete tests such as slump, air content and unit weigh was determined on all concrete batched. Some of these tests are routine quality control tests; however, the activation energy, semi-adiabatic calorimetry, and time of setting tests were specifically chosen to characterize the hydration development and setting. Section 4.2.2 will provide more information on the procedure used for these three tests.

Table 4-11: Tests performed to characterize the concrete mixtures obtained from the field

Test	Specification	Material Type	Concrete Age (days)	Specimen Type
Compressive Strength	ASTM C 39	Concrete	7,28	6”∅ x 12” Cyl
Splitting Tensile	Tex 421-A	Concrete	7,28	6”∅ x 12” Cyl
Flexural Strength	ASTM C 78	Concrete	7,28	6” x 6” Beam
Modulus of Elasticity	ASTM C 469	Concrete	7,28	6”∅ x 12” Cyl
Concrete CTE [a]	AASHTO TP 60	Concrete	7	6”∅ x 12” Cyl
Semi-Adiabatic Calorimetry	None	Concrete	0.1 to 7	6”∅ x 12” Cyl
Time of Initial and Final Set	ASTM C 403	Mortar	Early-age	6”∅ x 6” Cyl
Activation Energy	ASTM C 1074	Mortar	1,2,4,7,14,28d[b]	2x2x2” Cube

Note: [a] Concrete coefficient of Thermal Expansion

[b] Testing times at lowest testing temperature.

4.2.1.2 *Testing to Characterize Hydration Behavior*

Table 4-12 presents the tests that were performed during this phase, and it can be seen that Activation energy and semi-adiabatic calorimetry tests were performed on the concrete mixtures selected to characterize the hydration of cementitious materials in Texas. Section 4.2.2 will provide more information on the procedure used for these three tests. The mixture proportions of these mixtures are presented in Appendix B. Table 4-12 provides a summary of concrete mixtures used during the **materials characterization phase**. Note that Mixture No. 8 was a mixture obtained from a previous project on US 290 in Hempstead. This mixture was tested to provide results for another part of the overall project.

Table 4-12: Tests performed to characterize the hydration of cementitious material

Test	Specification	Material Type	Concrete Age (days)	Specimen Type
Semi-Adiabatic Calorimetry	None	Concrete	0.1 to 7	6”∅ x 12” Cyl
Activation Energy	ASTM C 1074	Mortar	1,2,4,7,14,28d	2x2x2” Cubes

Table 4-13: Summary of concrete mixtures used for the **materials characterization phase**

Mix No.	Description	Cement Factor	w/cm
	CEMENT ONLY		
9	Type I Cement [a] (No admixtures)	6.0 sacks	0.37
	CLASS C FLY ASH		
10	15% Fly Ash	6.0 sacks	0.37
11	25% Fly Ash		0.38
12	35% Fly Ash		0.38
13	45% Fly Ash		0.39
	CLASS F FLY ASH		
14	15% Fly Ash	6.0 sacks	0.38
15	25% Fly Ash		0.39
16	35% Fly Ash		0.40
17	45% Fly Ash		0.41
	GGBF SLAG		
18	30% GGBF Slag	6.0 sacks	0.38
19	50% GGBF Slag		0.38
	ADDITIONAL CEMENT SOURCES		
21	Capitol Type I [b]	5.5 sacks	0.50
22	Alamo Type I [c]		

Note: [a] Cement source: Texas Lehigh Cement Company, Buda plant (April 2000)
[b] Cement source: Capitol Cement, San Antonio (July 2000)
[c] Cement source: Alamo Cement Company, San Antonio (May 2000)

Note that for all cases, the mineral admixtures level of replacement was done on a volume basis, which is the practice in the state of Texas. (In most of the U.S., replacement is done on a weight basis). This is the reason why the water-cementitious ratios do not remain constant in the last column of Table 4-13. The mixtures proportions of the materials characterization phase were selected to be representative of pavement mixtures; hence a low water-cement ratio was used. The mixture proportions for all these mixtures are in Appendix B.

Table 4-14 provides a summary of the chemical and physical properties of all the cements tested during this project. Since all combinations of mineral admixtures can not be tested, the following three different mineral admixtures were chosen to evaluate their effect on the hydration of portland cement:

- Class C fly ash is more frequently used in Texas, and locally its composition has a CaO content of 22-29%, and a SiO_2 content of 35-40%. The Class C Fly ash source supplied by Boral Materials from their Deely plant was chosen, since its chemical composition is representative of most Class C fly ash sources in the state. The Deely fly ash was obtained in July 2000, and its CaO content was 24.3%, SiO_2 content 35.8%, available alkalies 1.4%, and specific gravity 2.75.

- Class F fly ash is not a frequently used in Texas, and locally it has a CaO content of 9-15%, and a SiO_2 content of 50-60%. Type F fly ashes typically found along the U.S. east coast might have CaO content as low as 3-5%. The Class F Fly ash source supplied by Boral Materials from their Rockdale plant was chosen for this project. The Rockdale fly ash was obtained in July 2000, and its CaO content was 10.8%, SiO_2 content 54.1%, available alkalies 0.3%, and specific gravity 2.33.
- Ground granulated blast-furnace (GGBF) slag has been used in El Paso, and its use is becoming more common in paving applications. Most of the GGBF slag used in Texas is supplied by Lone Star Industries, from their New Orleans facility. This source was selected for this project. The GGBF slag was obtained in July 2000, and was a Grade 120 with a specific gravity of 2.91.

Table 4-14: Chemical and physical properties of cements tested during this project

Mix No.	Cement Type	Bogue Compounds (%)				Chemical Composition (%)				Blaine (m^2/kg)
		C_3S	C_2S	C_3A	C_4AF	SO_3	Free CaO	MgO	Alkalies[a]	
9 to 19	Type I	57	14	10	8	3.5	2.9	1.3	0.69	358
20	Type I	63	12	10	6	2.9	1.0	1.4	0.52	354
21	Type I	64	9	8	10	3.3	0.8	0.6	0.67	367

Note: [a] Equivalent Alkalies = $Na_2O + 0.658 \cdot K_2O$, according to ASTM C 150

4.2.2 Laboratory Tests Performed

Many routine quality control tests were performed in accordance with the relevant ASTM standard. These tests will not be discussed further. Due to their unique characteristics, the following tests are discussed in this section: activation energy, semi-adiabatic calorimetry, and time of setting.

4.2.2.1 *Activation Energy Testing: ASTM C 1074*

Mortar specimens, 2-inch x 2-inch x 2-inch in dimension, were made in accordance with ASTM C 109, “Standard Test Method for Compressive Strength of Hydraulic Cement Mortar.” The cubes were cured in lime saturated water kept at constant temperatures of 8°C, 23°C, and 40°C. Since casting and curing temperatures are some of the most important variables in this study, all the raw materials were brought to the curing temperature before batching.

The ASTM C 1074 method is used to evaluate the strength gain for mortar specimens cured at different temperatures. It was found that mortar test data may be used for this purpose, since the objective is to compare the rate of strength gain at different temperatures (temperature dependence), thus the absolute value of the mortar strength is not of importance. Tank and Carino (1991) evaluated the activation energy results obtained from both concrete and mortar specimens and demonstrated that comparable results are obtained. An equivalent mortar is obtained by proportioning the mortar to have a cement-fine aggregate ratio equal to the cement-coarse aggregate ratio of the concrete.

Cubes were cured by keeping them immersed in water bathes saturated with calcium hydroxide at controlled temperatures. When cubes were moved to be tested, drying of the surfaces and cooling of the specimen was prevented by transporting the cubes in containers filled with water obtained from that particular curing bath. At each curing temperature, three cubes were tested at six different ages. ASTM C 1074 recommends that the first set of cubes be tested at approximately twice the time of final setting, and that tests thereafter be performed at about twice the age of the previous test. This would require different testing times for each type of cement, and combination of mineral admixtures.

Due to the large magnitude of this testing program, this process was simplified and standard testing times were chosen for each curing temperature. The testing times were determined based on the equivalent age approach with an assumed activation energy of 40,000 J/mol. The objective was to test at equivalent maturities for the specimens cured at the three different temperatures. Table 4-15 presents the approximate testing ages used for all the different mixtures. After the data was analyzed, it was noticed that for some mixtures (high early strength), the age of the first test at the higher curing temperature was critical. This was because most of the strength development happened early. Therefore, earlier test data was required to determine an accurate representation of the strength development. Where these cases occurred, the testing program was modified as shown in Table 4-15. Note that the earliest test for curing at 40°C was 9 hours after batching, and for curing at 8°C it was 24 hours after batching.

Table 4-15: Approximate testing ages used for different curing temperatures

Isothermal Batching and Curing Temperature	**Approximate testing ages (days)**					
	Set 1 (hrs)	Set 2 (hrs)	Set 3 (days)	Set 4 (days)	Set 5 (days)	Set 6 (days)
8°C	24	48	4	8	14	28
23°C	12	40	3	6	11	22
40°C	16 (9[a])	24	2	4	6	11

Note: [a] Used for high-early strength mixtures.

4.2.2.2 *Semi-Adiabatic Calorimetry and Data Analysis Process*

Semi-adiabatic tests were performed to define the degree of hydration for each mixture design. The semi-adiabatic testing equipment used during this project was supplied by Digital Site Systems, Inc., 4516 Henry Street, Suite 315, Pittsburgh, Pennsylvania. The Qdrum™ calorimeter shown in Figure 4-32 was used together with a data logger to record the test data. The calorimeter consisted of an insulated steel drum that can contain a 6x12-inch concrete cylinder, with probes to record the concrete temperature, heat loss through the calorimeter wall, and air temperature surrounding the test setup. The heat loss through the calorimeter was determined by a calibration test. Heated water was used for the calibration test, since it has a known thermal conductivity. Heated water with a known mass was placed into the chamber of the calorimeter at around 45°C. The data logger was then used to monitor the decrease in water temperature and the heat lost through the wall of the calorimeter over time. Based on the data obtained from this test, the heat loss of the calorimeter at different temperatures was estimated and a calibration factor determined.

Once the concrete was batched, 6x12-inch cylinders were made according to the usual ASTM procedures for making laboratory specimens. The weight of concrete was determined and the sample was inserted into the chamber of calorimeter as soon as possible. Once the chamber was sealed, the data logger recorded all the necessary information over approximately 7-days. The within-test repeatability with this equipment is reported to be within 1% to 3%.

Morabito(1998) investigated the variability associated with the semi-adiabatic test procedure by conducting a round robin study. Standard materials and mixture proportions were provided. It was reported that the test repeatability between different organization varied between -4.8 % and 4.8% after 72 hours of testing. Jonasson (1995) concluded that the results obtained from semi-adiabatic testing may be described by the coefficient of variation in the order 10%.

Figure 4-32: Semi-adiabatic equipment used for this project

Currently there is no standardized procedure to analyze the data obtained from the semi-adiabatic test procedure. However, in a recent technical RILEM recommendation, "Adiabatic and Semi-Adiabatic Calorimetry to Determine the Temperature Increase in Concrete due to Hydration Heat of Cement," (RILEM Technical Committee 119-TEC, 1999) a standardized approach is recommended to analyze the data obtained from both adiabatic and semi-adiabatic tests.

In order to analyze the data, the mixture proportions and thermal characteristics of the raw materials used during the semi-adiabatic test need to be known. The hydration dependant nature of properties such as the specific heat and thermal conductivity of the fresh concrete needs to be considered. The temperature sensitivity (activation energy) of the mixture is required, in order to back-calculate the true adiabatic temperature rise of the mixture. This is necessary, because under semi-adiabatic conditions, the sample is hydrating at a lower temperature, as compared to subjecting it to full adiabatic conditions. Therefore, it is not sufficient to account for only the loss in temperature associated with the semi-adiabatic curing conditions. The loss of additional concrete hydration, should the sample have been at the higher adiabatic temperature, needs to be included to obtain the true adiabatic temperature.

This effect is discussed by Van Breugel (1997), who recommended that the change in hydration be accounted for by the Arrhenius rate constant. In this project, this approach was followed throughout the analysis of the semi-adiabatic test results, and the semi-adiabatic temperature development was determined by modeling the actual hydration and measured losses over time. The temperature sensitivity was accounted for by the activation energy model developed in Chapter 5 (see Equation 5-17). If this effect is not considered, a "false-adiabatic temperature" will be determined from the semi-adiabatic test setup, which will always be less than the "true" adiabatic temperature development.

Figures 4-33 and 4-34 present the effect of not considering that the mixture would actually have been hydrating at a higher temperature for two of the mixtures tested during this project. Figure 4-33 presents the results where a Type III cement with an activation energy of 52,865 J/mol was tested. It may be seen that when the additional hydration at the actual adiabatic temperature is not incorporated, the difference in back-calculated adiabatic temperature rise is around 2°C. Figure 4-34 presents the results for a Type I/II cement with 35% Class C fly ash, with an activation energy value of 38,375 J/mol. In this instance, the back-calculated temperature difference between the true and false adiabatic temperature rise is around 6°C, which becomes significant.

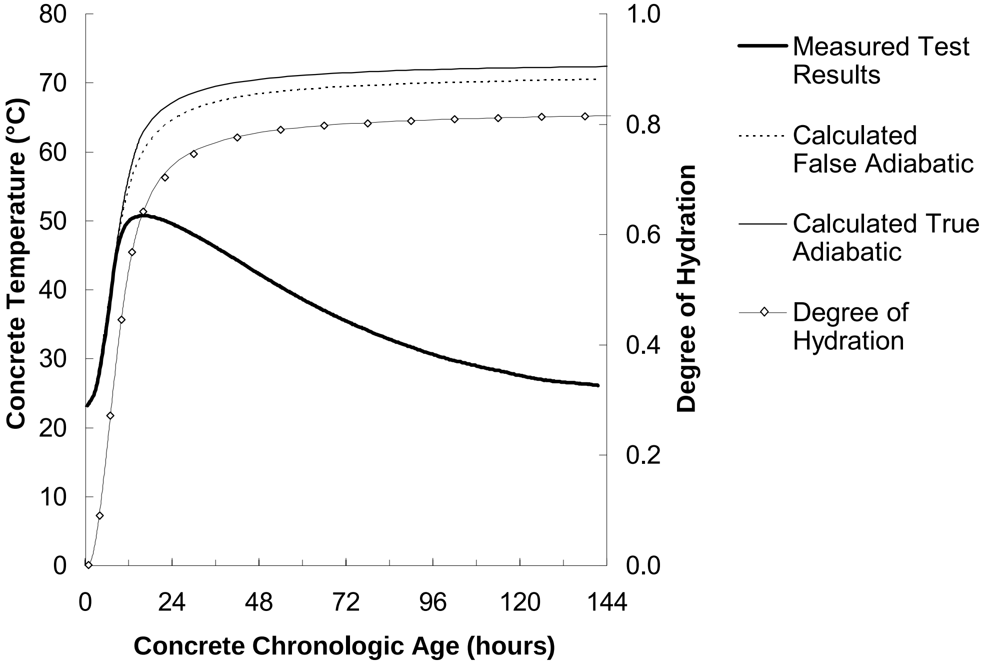

Figure 4-33: Differences in calculated adiabatic results obtained from semi-adiabatic testing (Type III cement, 5.0 sacks)

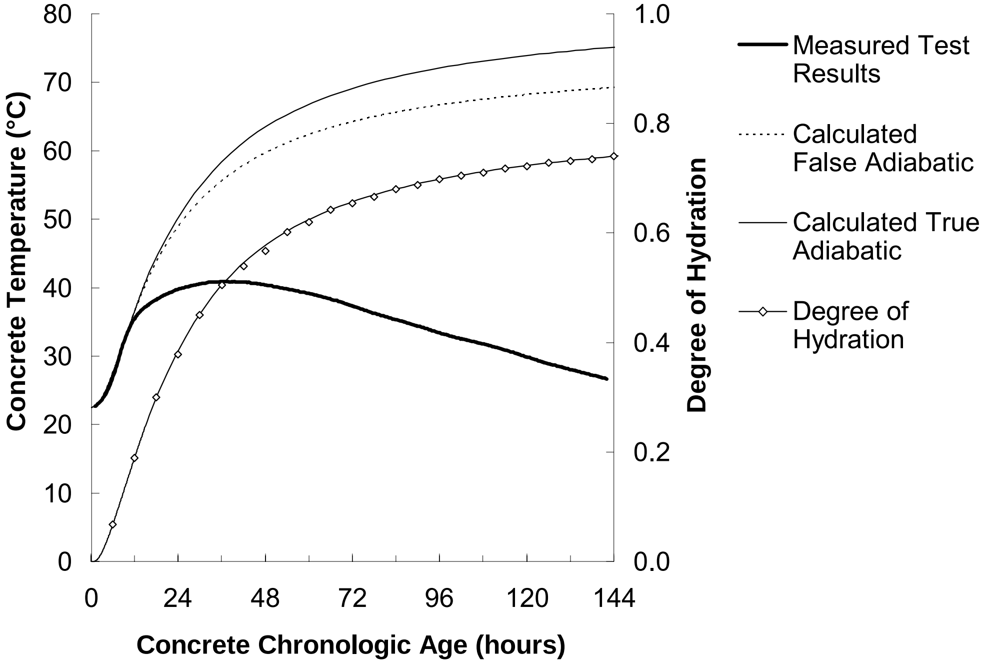

Figure 4-34: Differences in calculated adiabatic results obtained from semi-adiabatic testing (Type I/II cement + 35% Class C fly ash, 6.0 sacks)

The difference between the back-calculated true and false adiabatic temperature will become greater in mixtures in which the degree of hydration development occurs over a longer period, such as with Type F fly ashes and especially GGBF slags. This can be seen by looking at the degree of hydration curves plotted in Figures 4-33 and 4-34. This is simply because at later stages, when the more losses from the semi-adiabatic test setup have occurred, a large part of the hydration still has to occur, which will under fully adiabatic conditions actually occur at a higher temperature. This may be noticed by looking at the degree of hydration curves plotted in Figures 4-33 and 4-34. It is recommended that this effect be incorporated in all cases, since this will ensure that the semi-adiabatic test produces results are comparable to those obtained from full adiabatic testing.

Small concrete batches (1.5 ft^3) were made in a 4 ft^3 concrete mixer, for the materials characterization phase. The compressive and flexural strength gains of the field materials were determined, and this required a larger volume of concrete. In this case a 6.0 ft^3 concrete batch was used. In most cases, the 6x12-inch sample was placed into the calorimeter within 30 minutes after water was added to the cementitious materials. The mixture proportions used for each concrete mixture are presented in Appendices A and B. The results obtained from the semi-adiabatic testing are presented in Section 4.2.3.2.

4.2.2.3 *Penetration Resistance: ASTM C 403*

The time of initial and final set was determined through ASTM C 403, “Time of Setting of Concrete Mixtures by Penetration Resistance.” The application of these tests results in terms of the overall program was discussed in Section 3.5. The concrete mixtures were sieved through a number four (4.75 mm) sieve to obtain a mortar sample of the fresh concrete. In this test, the maximum force required to penetrate needles of different sizes to a depth of 25 mm over a 10 second period is measured. As the concrete stiffens, the sizes of needles are progressively reduced. At a penetration resistance of 500 psi initial setting occurs, and at a penetration resistance of 4000 psi final setting occurs. Setting results obtained from the field mixtures, have been presented in Section 4.1.3.

Six or more penetrations were performed during each test. Due to the size of the larger needles, and the 6-inch diameter of the sample, this required that two specimens be used. A thermocouple was used to monitor the temperature development of the cement paste. During the data analysis, the best-fit power function, as recommended by ASTM C 403, was fitted through the data points. The laboratory tests were performed in a room at a controlled temperature of 21°C (70°F). The results obtained from this procedure are presented in Section 4.2.3.3.

4.2.3 Laboratory Testing Results

4.2.3.1 *Results of the Activation Energy Testing Program*

This section presents the results of the activation energy tests, in accordance to the method outlined in ASTM C 1074. These results include the activation energy computed with the exponential strength-maturity function. More than 1500 cubes were tested during this phase of the project. In Chapter 5, more analysis on the results of these tests is presented.

The data collected during laboratory testing of the mixtures described above are summarized, respectively, in Appendices A and B for the field and laboratory mixtures. Figure 4-35 presents the strength gain for some of the mixtures tested. (Similar plots for 26 different paving mixtures are presented in Appendices A and B).

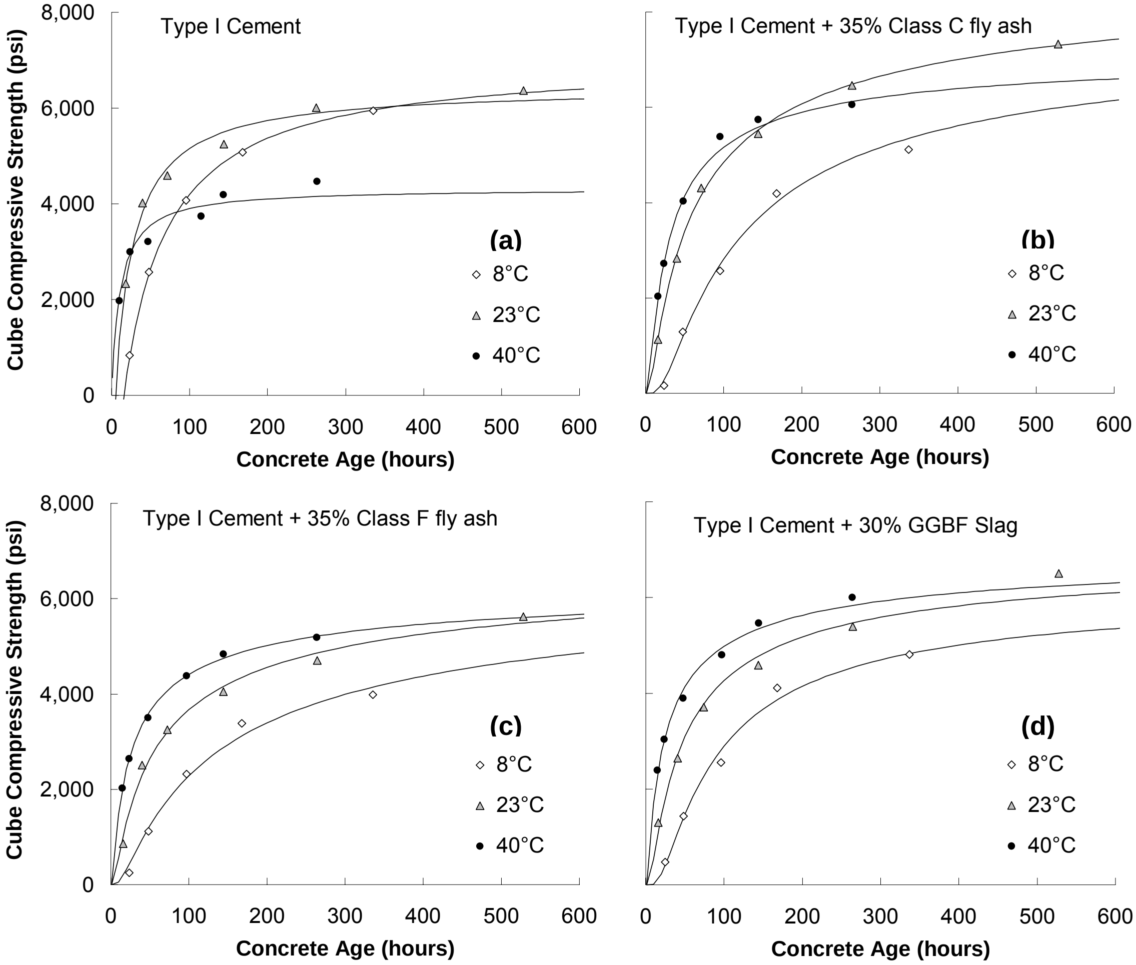

Figure 4-35: Compressive strength results for mortar cubes cured at different temperatures

From Figure 4-35, noteworthy behavior concerning the development of mechanical strength at different temperatures may be identified. In Figure 4-35(a), where only a Type I cement was used, it may be seen that the long-term concrete strength is reduced when it is made and cured at higher temperatures as compared to curing at lower temperatures. This mechanical behavior of concrete has been called the ***cross-over*** effect (Carino, 1991). In Figure 4-35 (a), the cross-over effect occurred early at a concrete age of 24 hours, and there is a 28% reduction in ultimate strength as compared to the mortar cured at 23°C. Whereas, the mortar cured at 8°C, shows a 4% increase in ultimate strength as compared to the mortar cured at 23°C.

In Figure 4-35(b), where Type I cement was replaced by 35% (by volume) Class C fly ash, the cross-over effect occurred at a concrete age of 160 hours. In Figure 4-35(c) where Type I cement was replaced by 35% (by volume) Class F fly ash, the cross-over effect was not as apparent, since the strength curves for the samples cured at 40°C was approaching the strength of the samples cured at 23°C after 600 hours, however they do not cross over. A similar effect may be seen in Figure 4-35(d) were Type I cement was replaced by 30% (by volume) GGBF Slag and no apparent converging can be identified.

From the discussion above, it may be concluded that the amount of strength loss due to curing at high temperatures as compared to curing at room temperature is influenced by the type and amount of mineral admixtures used in the concrete mixture. Chapter 5 provides a more detailed analysis on the strength gain behavior for all the mixtures.

The data were analyzed in accordance with the procedure (Section A1.1.8.1) outlined in Annex A, of ASTM C 1074. A Microsoft® Excel spreadsheet with its built-in solver routine was used to minimize the sum of the squares error during the regression analysis of both the hyperbolic and exponential strength-maturity functions. The regression parameters obtained at each curing temperature for each of the strength-maturity functions are shown in Appendices A and B. The activation energy of each of the mixtures was obtained based on the best-fit slope of the Arrhenius plot. The activation energy values obtained after the data analysis are listed in Table 4-16. Appendices A and B contain the calculations that were performed for each mixture. Table 4-16 indicates that different activation energy values are obtained when different strength-maturity functions are used. The strength-maturity function used to determine the activation energy should be used during the strength prediction. Similar discrepancies were obtained by Pinto (1999).

The datum temperature for use with the Nurse-Saul Maturity function (time-temperature factor) is shown in Table 4-16. In the original Nurse-Saul definition, the datum temperature was taken as -10°C. The ASTM recommends a datum temperature of 0°C for a Type I cement, and from Table 4-16 this is for most cases an adequate assumption. However, the datum temperature varies from -9.4°C to +5.2°C, which is a significant variation.

4.2.3.2 *Results of the Semi-Adiabatic Calorimetry Testing Program*

In order to investigate the hydration characteristics of typical Texas paving mixtures, 21 different concrete paving mixtures were tested by means semi-adiabatic calorimeter testing. The degree of hydration data collected during this project will be presented to provide a better understanding of the hydration of cementitious materials made from different mixture proportions, cements, and mineral admixtures.

Table 4-16: ASTM C 1074 activation energy values obtained from compressive strength data

Mix No.	Description	Datum Temperature [a] (°C)	Activation Energy (J/mol)	
			Hyperbolic	Exponential
1	Type I/II + 20% Class F fly ash	-1.0	31,062	38,359
2	Type I/II + 25% Class C fly ash	5.1	40,914	38,671
3	Type I	-0.9	31,486	42,081
4	Type I/II + 35% Class C fly ash	-1.3	32,370	35,121
5	Type I/II + 50% GGBF Slag	-3.4	29,597	38,400
6	Type I/II + 20% Class F fly ash	-1.0	30,565	40,790
7	Type I/II + 25% Class C fly ash	5.2	46,854	41,254
8	Type I + 30% Class C fly ash	-9.4	32,920	36,459
9	Type I Cement	2.6	38,985	42,330
10	Type I + 15% Class C Fly Ash	0.0	36,953	46,628
11	Type I + 25% Class C Fly Ash	-3.1	32,361	44,249
12	Type I + 35% Class C Fly Ash	0.3	34,976	41,283
14	Type I + 15% Class F Fly Ash	0.9	42,470	47,003
15	Type I + 25% Class F Fly Ash	2.0	39,731	49,378
16	Type I + 35% Class F Fly Ash	-0.6	32,556	45,017
18	Type I + 30% GGBF Slag	0.6	31,964	33,415
19	Type I + 50% GGBF Slag	0.9	39,415	43,374
20	Capitol Type I	1.4	34,938	38,147
21	Alamo Type I	-7.8	25,215	39,221

Note: [a] Determined in accordance with ASTM C 1074, and the Hyperbolic function

The data collected during the laboratory testing of the mixtures are summarized in graphs attached to Appendices A and B. The exponential formulation (3-21) was used, and Table 4-17 provides a summary of the best-fit hydration parameters that were obtained from the semi-adiabatic test data. The activation energy listed in Table 4-17 is determined through the use of the activation energy model developed in Chapter 5, and should not be compared to the activation energy values for strength listed in Table 4-16. The reference temperature for the definition of the degree of hydration calculation was selected to be 21.1°C (70°F), as this was the reference temperature used during the activation energy analysis.

Table 4-17: Best-fit hydration parameters obtained from semi-adiabatic testing (T_r = 21.1°C)

Mix No.	**Description**	**Activation Energy (J/mol)** [a]	**Hydration Parameters**			$\boldsymbol{H_u}$
			β	τ	α_u	**J/g**
1	Type I/II + 20% Class F fly ash	36,848	1.010	15.50	0.725	409
2	Type I/II + 25% Class C fly ash	36,636	0.818	31.05	0.841	476
3	Type I	45,712	0.935	13.39	0.729	489
4	Type I/II + 35% Class C fly ash	35,341	0.720	28.35	0.857	475
5	Type I/II + 50% GGBF Slag	50,600	0.562	40.58	0.800	486
6	Type I/II + 20% Class F fly ash	39,031	0.681	17.89	0.788	405
7	Type I/II + 25% Class C fly ash	38,375	0.573	35.95	0.850	480
8	Type I + 30% Class C fly ash	40,304	0.674	23.81	0.884	465
9	Type I Cement	45,991	0.905	13.69	0.689	477
10	Type I + 15% Class C Fly Ash	43,148	0.874	13.81	0.713	471
11	Type I + 25% Class C Fly Ash	41,252	0.772	23.28	0.793	468
12	Type I + 35% Class C Fly Ash	39,357	0.716	29.43	0.893	464
13	Type I + 45% Class C Fly Ash	37,461	0.724	36.66	0.849	460
14	Type I + 15% Class F Fly Ash	40,703	0.825	15.97	0.797	444
15	Type I + 25% Class F Fly Ash	37,178	0.786	18.30	0.831	421
16	Type I + 35% Class F Fly Ash	33,653	0.809	19.08	0.838	396
17	Type I + 45% Class F Fly Ash	30,127	0.774	21.73	0.894	370
18	Type I + 30% GGBF Slag	51,510	0.625	25.22	0.822	472
19	Type I + 50% GGBF Slag	55,189	0.554	38.22	0.854	469
20	Capitol Type I	41,977	0.719	16.88	0.887	513
21	Alamo Type I	46,269	0.727	16.32	0.882	492

Note: [a] Determined in accordance the formulation in Equation 5-34.

During the analysis of the results obtained from the semi-adiabatic tests, it was determined that the total heat of hydration (defined in Equation 3-14) can best be modeled by the following formulation:

$$H_u = H_{cem} \cdot p_{cem} + 461 \cdot p_{SLAG} + 1800 \cdot p_{FA-CaO} \cdot p_{FA} \qquad \textit{Equation 4-1}$$

where, H_u = total heat of hydration of cementitious materials at 100% hydration (J/g),
p_{SLAG} = slag mass ratio ito total cementitious content,
p_{FA} = fly ash mass ratio ito total cementitious content,
$p_{FA\text{-}CaO}$ = fly ash CaO mass ratio ito total fly ash content,
p_{cem} = cement mass ratio ito total cementitious content, and

H_{cem} = heat of hydration of the cement, defined in Equation 3-12.

The heat contribution of GGBF Slag in Equation 4-1 is the value recommended by Kishi and Maekawa (1995). The heat contribution of the fly ash was modeled in terms of its CaO content, since this provides an indication of its cementitious nature. The Class C fly ash used in this project had an CaO content of 24.3%, which according to Equation 4-1 will provide a heat contribution of 24.3×18 = 437 J/g. Similarly, for the Class F fly ash used in this project, it had an CaO content of 10.8%, which according to Equation will provide a heat contribution of 10.8×18 = 194 J/g. The value obtained for the Class F fly ash is in the order of magnitude use by Kishi and Maekawa, which recommended 209 J/g for a fly ash with a CaO content of 8.8%.

The validity of the contribution of fly ash in terms of its CaO content, as shown in Equation 4-1, should be evaluated based on long-term heat of hydration tests. The test results from semi-adiabatic testing alone cannot be used to evaluate the model's accuracy, since these values need to be known to back calculate the degree of hydration for the mixture.

Figure 4-36 presents the experimentally determined degree of hydration curves for different Class C fly ash replacement levels. It may be seen that at replacement levels of 15% and less no significant change in hydration behavior is noticeable. From this figure, the following trends may be associated with an increase in the amount of Class C fly ash used:

- the hydration of the total cementitious system is retarded,
- the ultimate degree of hydration is increased, and
- the rate (slope) of the hydration reaction is unaffected.

Figure 4-37 presents the experimentally determined degree of hydration curves for different Class F fly ash replacement levels. It appears that different replacement levels of Class F fly ash has little impact on the initial hydration process, and acts as an inert filler, since it contributes little to the early-age heat development. However, at later-ages the ultimate degree of hydration is increased as the amount of fly ash used in the mixture is increased. This increase in ultimate degree of hydration could be attributed to the pozzolanic reaction, which converts the calcium hydroxide into the denser C-S-H structure, which reduces the volume of the final hydration products. With the volume of the hydrated cement paste reduced, more of the original cementitious materials can react, and more complete hydration is obtained. This effect is similar to the results found by Mills (1966), who reported that cementitious systems with GGBF slag produce higher levels of ultimate degree of hydration. This effect was shown in Figure 3-13, where the ultimate degree of hydration is function of the water-cementitious ratio and the amount of GGBF slag used in the system.

More of the hydration characteristics that can be identified from the hydration results will be discussed after the model development stage, documented in detail in Chapter 5. In Section 5.3.3, the predicted results of the hydration model will be compared to the measured results and more analysis of the hydration behavior will be presented.

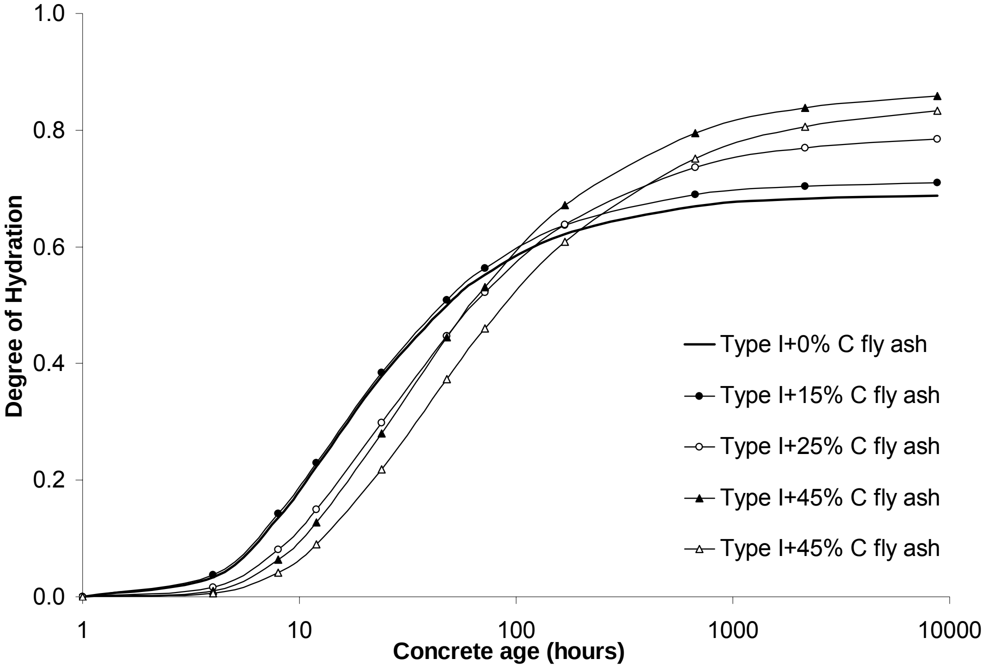

Figure 4-36: Degree of hydration development for different Class C fly ash dosages

4.2.3.3 *Results of the Concrete Setting Tests*

The results of the penetration resistance test, as per ASTM C 403, are presented in this section. This test was performed on the concrete mixtures obtained from the field sites, and on the two additional cement sources used during the materials characterization (Mix No. 20 and 21). The initial set and final set times as measured under field conditions were presented in Section 4.1. The graphs developed from the data obtained from this test are presented in Appendix A. The time to initial and final set are summarized in Table 4-18. Figures 4-38 and 4-39 provide a graphical summary of all the results obtained. The setting data collected in this section will be analyzed in Chapter 7.

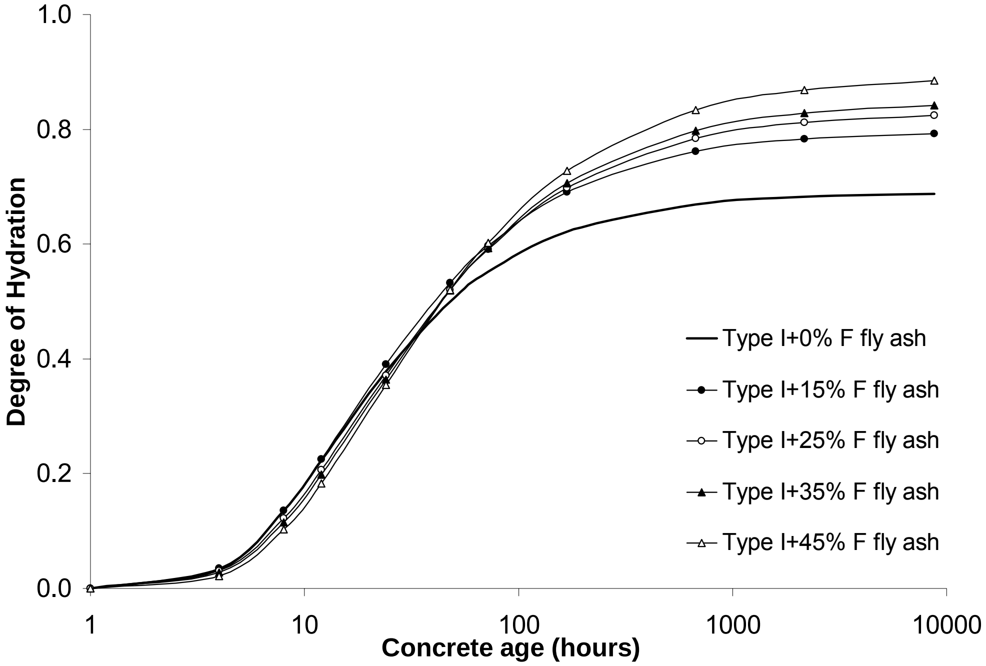

Figure 4-37: Degree of hydration development for different Class F fly ash dosages

Table 4-18: Summary of all initial and final set times as obtained by penetration resistance

Mix No.	**Description**	**Laboratory (hours)**		**Field Conditions (hours)**			
				Section No. 1		**Section No. 2**	
		Initial Set	**Final Set**	**Initial Set**	**Final Set**	**Initial Set**	**Final Set**
1	Dallas - May	4.9	6.5				
2	Houston - May	7.9	10.1				
3	Dallas - Aug	4.1	5.4	2.6	3.3		
4	Houston - Aug	5.8	8.7	4.4	5.4	3.3	4.7
5	El Paso - Aug	7.0	10.3	2.9	4.1	3.5	5.4
6	Dallas - Sept	7.2	9.1	3.3	4.2		
7	Houston - Oct	5.1	6.8	5.3	6.7		
20	Capitol Type I	3.8	5.3				
21	Alamo Type I	4.2	5.2				

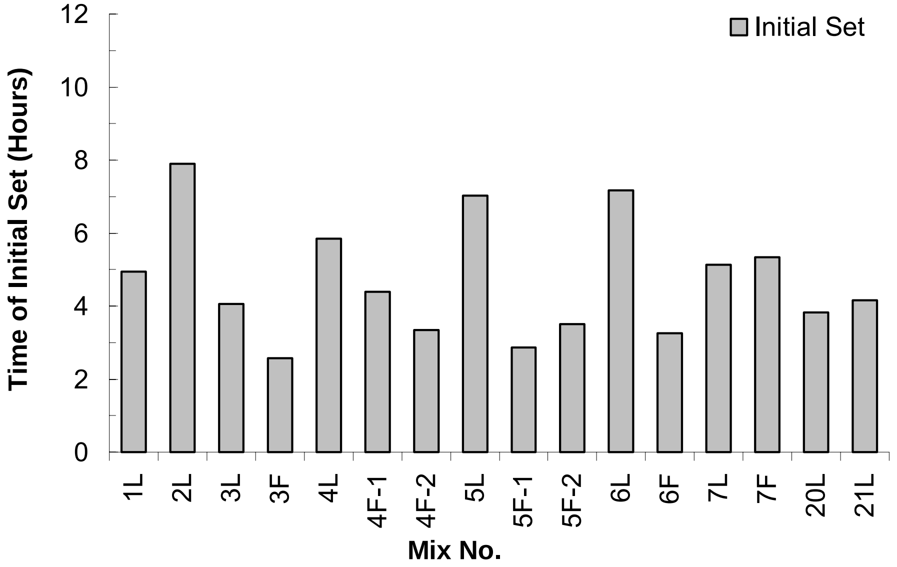

Figure 4-38: Time to **initial** set as defined by ASTM C 403

(*Note*: **L** = Laboratory conditions, **F**=Field conditions, **1**=Section No.1, **2**=Section No. 2)

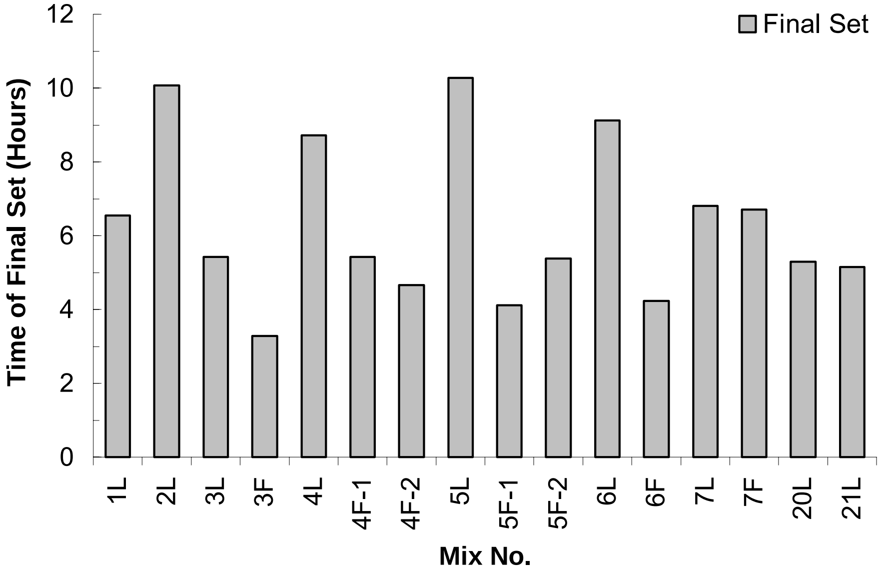

Figure 4-39: Time to **final** set as defined by ASTM C 403

(*Note*: **L** = Laboratory conditions, **F**=Field conditions, **1**=Section No.1, **2**=Section No. 2)

4.3 PHASE III: CONCRETE HYDRATION UNDER CONTROLLED CONDITIONS

During this phase, small insulated concrete slabs were cured under enclosed and controlled laboratory conditions. Environmental chambers were used to keep the air temperature around the specimens at predetermined levels. This process minimizes the impact climatic conditions such as fluctuating wind speeds, cloud cover, air temperatures, and fluctuating relative humidity. The objective of this phase was to gather data generated under controlled conditions for use during the calibration of the proposed temperature prediction program.

4.3.1 Small Concrete Specimens

Previous work performed at TxDOT has indicated that the use of small insulated slab specimens can be used for the direct measurement of the temperature development concrete pavements (McCullough, 1965). It was shown that 12 x 16 x 9.5-inch specimens would be sufficient in size to provide accurate temperature readings in the center of the specimen. The rectangular specimen was used due to the type of thermometers used in the 1960s. With the development of modern thermocouples, it is recommended that 13 x 13 x 10 inch specimens be used. The specimen layout used during this study can be seen in Figure 4-40. The specimen sides were insulated with one-inch of Styrofoam to minimize the potential heat transfer into or out of the small slab. The slab was based on a 1-inch thick layer of sand.

Three thermo-couples were placed in each specimen. The thermocouples were located at approximately, 0.5 inch from the top, mid-depth, and 0.5 inch from the bottom of the specimen. Figure 4-41 presents a picture of the actual specimens used.

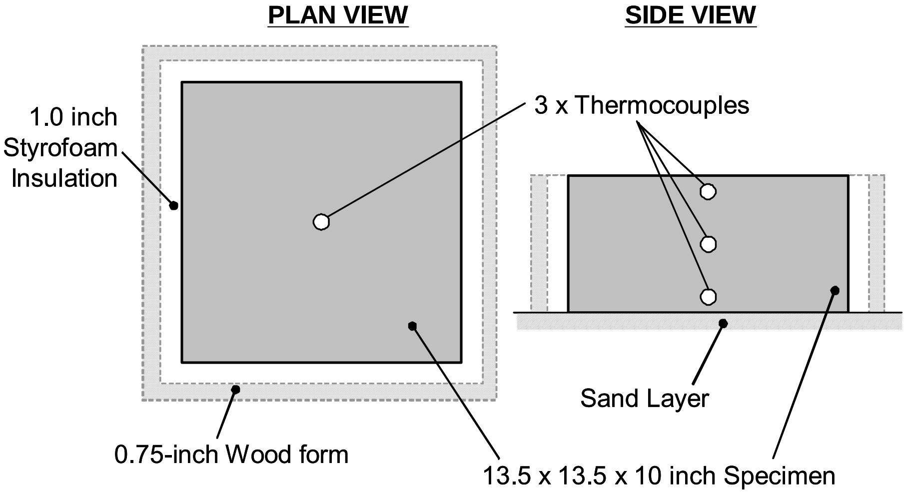

Figure 4-40: Specimen Layout

Figure 4-41: Small insulated concrete specimen in the environmental chamber

4.3.2 Materials, Mixing and Curing

The concrete mixture used for the test specimens was similar to the mixture proportions used during a paving project on U.S. 290 located in Hempstead (Mix No. 8). The mixture proportions are shown in Appendix A. Note that the mixture consisted of a Type I cement with 30% Class C fly ash, with a slump of 2 inches, which is representative of a typical Texas paving mixture.

Since proper control and uniformity of the mixture was important, all mixing was done in a temperature controlled mixing room. Each of the specimens were batched and cured at different temperatures ranging between 50°F and 105°F. The temperature ranges were chosen to obtain a wide range of mixing and curing temperatures. In some cases, duplicate specimens were made to evaluate the accuracy of the measured results. Since the fresh concrete temperature is one of the most important variables in this study, all mixing materials were brought to temperature equilibrium by leaving them for 24 hours at the intended mixing temperature before casting. After placement and vibrating, the small slab specimens were cured with a double layer of white curing compound.

The specimens were cured in environmental chambers, which can only increase the temperature. The system functions by monitoring the air temperature, and when it drops below the set lower limit, the temperature is regulated by adding heat to the environment until a set upper limit is reached. The chambers had the ability to keep the air temperature to within 6°F of the desired limit. For the low temperatures (50°F), a large refrigerating unit was used, which could keep the temperature within 4°F of the desired temperature.

4.3.3 Presentation of Results

The results obtained are summarized in Figure 4-42, which indicates the mid-slab temperature development. The results of duplicate specimens showed that repeatable results were obtainable with the experimental setup. Figure 4-43 present the result of two specimens mixed at 70°F and cured at around 105°F, and it may be seen that similar concrete temperatures were measured. All these tests were performed in an enclosed environment, and no solar radiation effects are present. Note that the highest concrete temperature reached is strongly influenced by the curing and placement temperature. The effect of more rapid hydration at higher temperatures, as shown in Figure 1-7, may be identified. The rate of hydration increases with an increase in concrete placement and curing temperature.

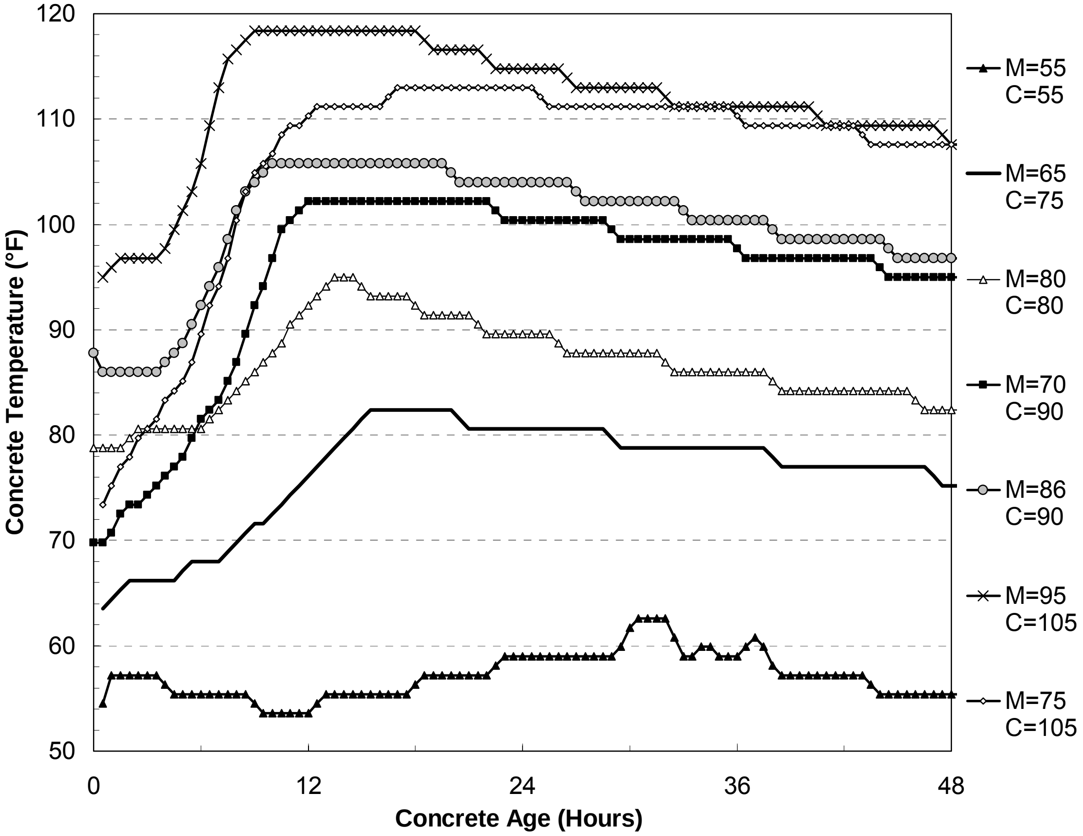

Figure 4-42: Temperature development for the small insulated concrete slabs

(*Note*: **M** = Approximate **Mixing** temperature, **C** = Approximate constant **Curing** temperature)

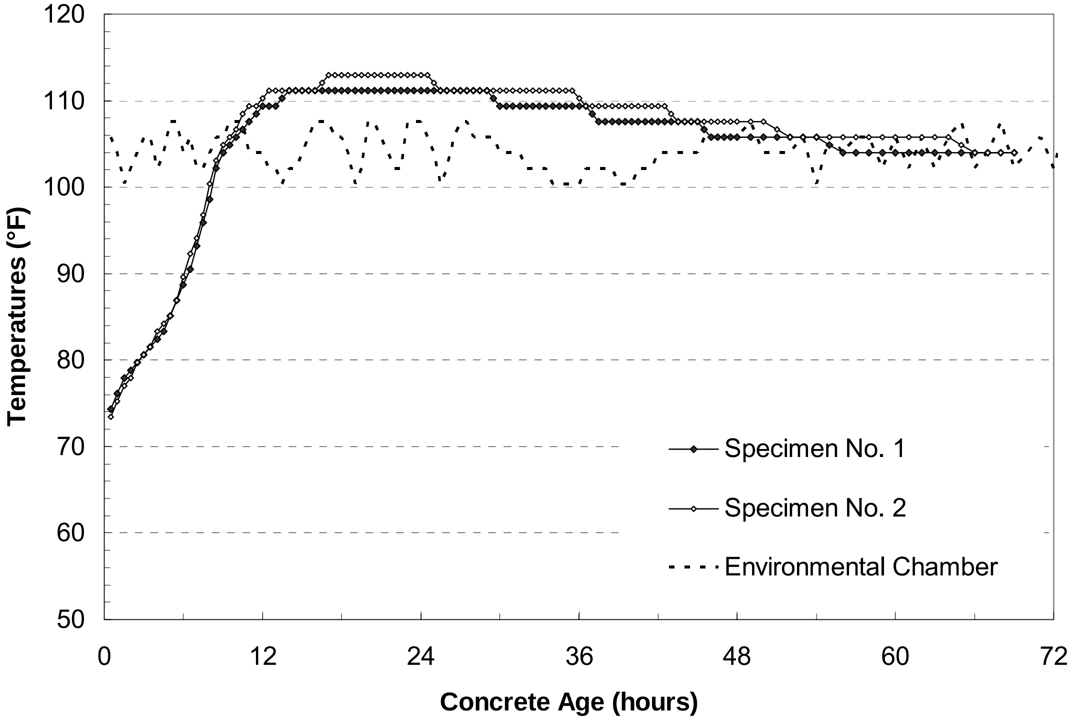

Figure 4-43: Comparison of results obtained from duplicate specimens

This information gathered under this laboratory exercise provides valuable data to characterize the effect of different placement and curing temperatures on the overall temperature development. The degree of hydration development of this concrete mixture was determined through semi-adiabatic testing, and this data will be used to calibrate the temperature prediction program. This data will fulfill an essential role, since it was collected under controlled conditions, which eliminates some of the uncertainties encountered during field instrumentation.

4.4 SUMMARY AND CONCLUDING REMARKS

This chapter presents the field and laboratory data collected during this project. The data will be used for the calibration of the models developed in Chapter 3. All the materials and concrete mixtures were selected to be representative of concrete paving mixtures in the state of Texas. Data were collected from the following three phases: (1) field work, (2) materials characterization, (3) concrete hydration under controlled conditions.

Seven field sites were instrumented in Texas: Dallas, Houston, and El Paso. At some field sites, two locations were instrumented. The variables that were collected include the mixture design properties, concrete properties, concrete temperature history, environmental conditions during placement, pavement thickness, subbase type, subbase temperature, and curing methods used. At each site, raw materials were collected for laboratory testing. The in place concrete temperatures are presented in this chapter. The highest concrete temperature of 144°F was measured in a section placed under summer conditions in Dallas. While on site, the adverse effects of placing concrete in hot weather conditions were clearly noticeable. Concrete setting occurred very quickly, and the window of opportunity for tining was very small and in some instances, the specified surface tining could not be achieved, since the concrete was already too hard. Portions of the pavement placed on this project showed significant plastic shrinkage cracking.

The time of setting with the penetration resistance method (ASTM C 403) was successfully determined on site. A portable vibration table was used to sieve the concrete mixture through the #4 sieve to obtain the mortar sample. Setting tests were performed on the same mixtures, under laboratory conditions, and a summary of the setting times are shown in Figures 4-38 and 4-39.

The activation energy for 21 different mixtures as per ASTM C 1074 was determined during this study. The results are summarized in Table 4-16. The activation energy of each of the mixtures was obtained based on the best-fit slope of the Arrhenius plot. As ASTM C 1074 only provides recommendations when Type I mixtures are used, the values in Table 4-16 may be a useful reference when activation energy values are required for mixtures with cements other than Type I. Table 4-16 provides the datum temperature for each mixture when the Nurse-Saul maturity method is to be implemented. Since this method is currently used by TxDOT, Table 4-16 might serve as a guide for the selection of an appropriate datum temperature value for the specific mixture under consideration.

In order to investigate the hydration characteristics of typical Texas paving mixtures, 21 different concrete paving mixtures were tested by semi-adiabatic calorimeter testing. A database of test results and all the known variables was developed for these mixtures. The degree of hydration data collected during this project will be useful to obtain a better understanding of the hydration of cementitious materials made from different mixture proportions, cement chemical composition, and mineral admixtures.

Small insulated concrete slabs were cured under enclosed and controlled laboratory conditions. This process minimizes the impact climatic conditions such as fluctuating wind speeds, cloud cover, air temperatures, and fluctuating relative humidity. The effect of solar radiation on the development of concrete temperatures is removed under these conditions. Using the data presented in Figure 4-42, the temperature prediction program can be calibrated to account for hydration and some heat transfer effects.

Chapter 5

General Hydration Model for Cementitious Materials

The activation energy defines the temperature sensitivity of a concrete mixture, and it is used in the equivalent age maturity method to determine the rate of hydration at any specific temperature relative to a reference temperature. The degree of hydration characterizes the formation of hydration products as hydration progresses over time, at the reference temperature, and is, therefore, a function of the equivalent age. Each concrete mixture exhibits a unique degree of hydration development over time. Figure 5-1 presents how knowledge of the temperature sensitivity (activation energy), the degree of hydration at the reference temperature, and the total heat of hydration available from the cementitious materials can be used to predict the heat of hydration development at any temperature.

In order to develop an accurate temperature prediction for concretes cured at temperatures other than a reference temperature, appropriate values for the activation energy has to be selected. Section 3.2.2.1 showed that there is currently great disparity in the literature concerning the selection of the appropriate activation energy. The following points of disparity will be investigated and addressed in this chapter:

1. ***Should the same activation energy be used for the prediction of mechanical properties and the development of hydration?***
2. ***Does the activation energy change as a function of temperature or degree of hydration?***
3. ***Should the same activation energy be used irrespective of the type of cementitious materials?***

During the hydration of cementitious materials, numerous factors and interaction are involved, some of which are currently not fully understood. Pure mechanistic models that account for all the possible interactions are not available. Many semi-adiabatic calorimeter tests were performed during this study, which provides a convenient indirect means to characterize the formation of hydration products by measuring the heat released during hydration.

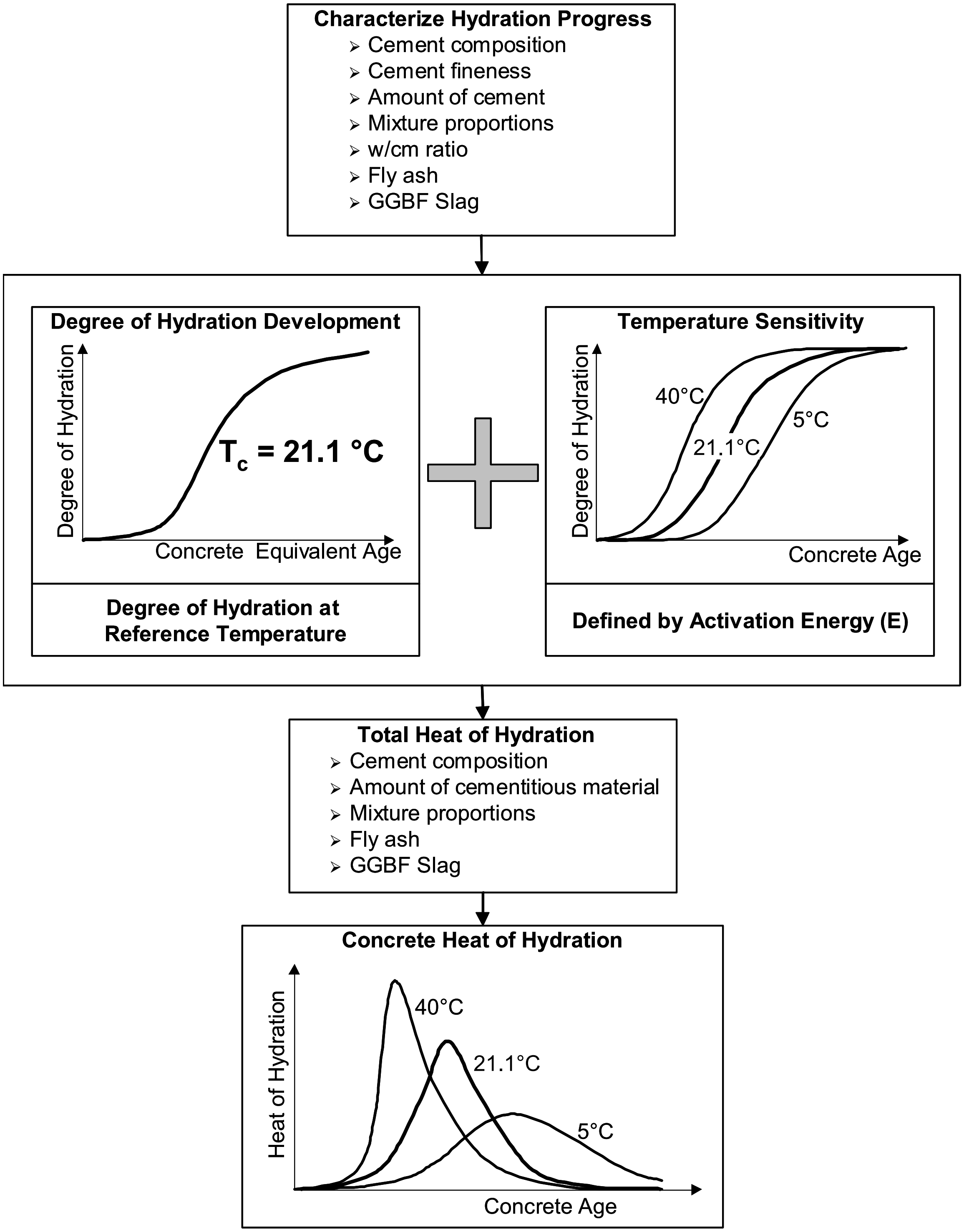

Figure 5-1: The hydration model concept, presenting the use of the degree of hydration and temperature sensitivity to predict the progress of hydration at any temperature

This chapter presents the formulation of a general hydration mechanistic model. The model will be calibrated with a multivariate nonlinear regression analysis. Thus, a mechanistic-empirical model is presented to characterize the heat of hydration of concrete at an isothermal curing temperature of 21.1°C. The model considers the effect of the following variables:

- Cement chemical composition: C_3A, C_3S, C_2S, C_4AF, SO_3, MgO, and Free Lime
- Cement fineness: specific surface area (Blaine Index)
- Mineral admixtures: Class F fly ash, Class C fly ash, and GGBF slag
- Mixture proportions: cement content, water-cementitious ratio, mineral admixture replacement level, coarse aggregate content, and fine aggregate content
- Concrete properties: density, thermal conductivity, specific heat

This chapter is structured to cover the model development approach (Section 5.1.) and then the primary components of the general hydration model as shown in Figure 5-1 are covered as follows:

- Quantify the temperature sensitivity of cementitious materials (Section 5.2); and
- Develop general hydration models for the degree of hydration development (Section 5.3).

5.1 MODEL DEVELOPMENT APPROACH

The model development approach is schematically indicated in Figure 5-2, and four main steps can be identified. In Figure 5-2, the approach is shown for the degree of hydration model, and the same approach will be used during the development of the temperature sensitivity model.

In the first step, models are developed based on mechanistic and theoretical principles. During this step, the most appropriate mathematic formulations are developed, but assumptions and simplifications are made to facilitate the development of a model. The development of appropriate models to predict the development of concrete temperatures was presented previously in Chapter 3. The shape of the degree of hydration model was chosen to capture the hydration of development of cementitious materials. The second step is to obtain test data that can be used to calibrate the model. The more detailed and comprehensive this data set, the higher the confidence in the calibrated model. In step three, the models developed under step one, should be evaluated against the test data. The models are now calibrated and adjusted to provide an accurate prediction of the measured results. These are now considered mechanistic-empirical models which contain calibrated adjustments for unforeseen occurrences that where not accounted for in the original mechanistic model. In the fourth and final step, the accuracy of the model is evaluated against a data set not used during model calibration. The accuracy of the model against the new test data will provide an indication of the validity of the model to other cases.

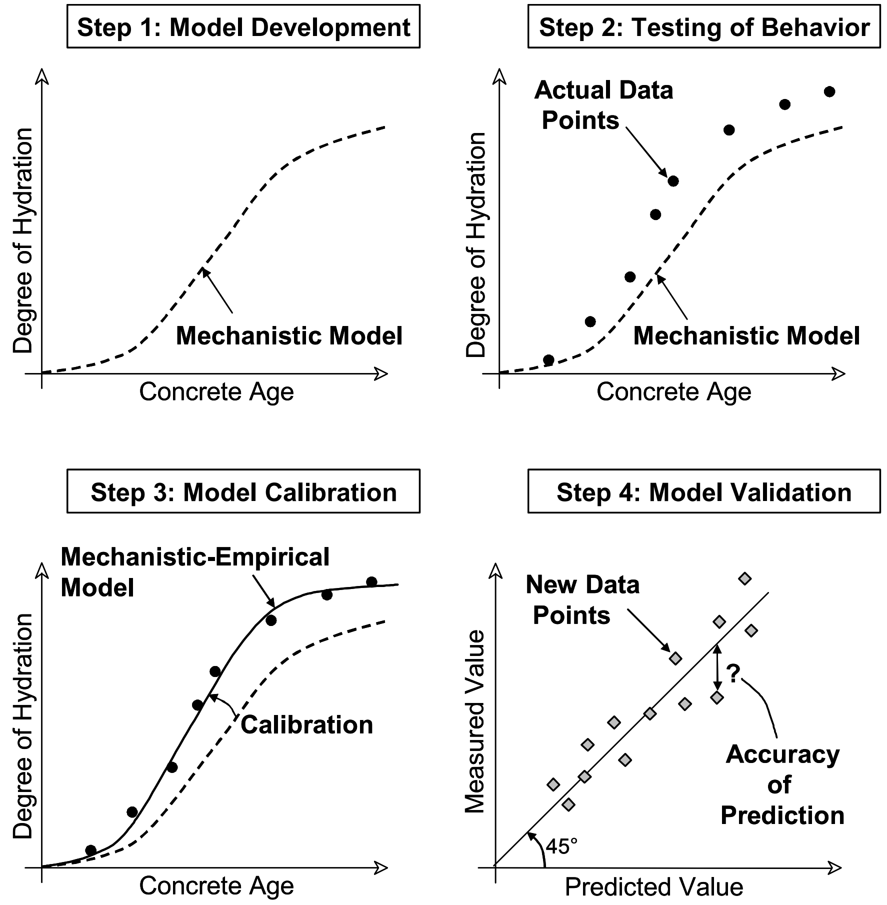

Figure 5-2: Model development approach

5.2 THE TEMPERATURE SENSITIVITY OF CEMENTITIOUS MATERIALS

This section presents a critical review of the meaning and definition of the activation energy for use in both hydration modeling and strength prediction. The activation energy defines the temperature sensitivity of a concrete mixture, and it is used in the equivalent age maturity method to determine the rate of hydration at any specific temperature relative to a reference temperature.

The maturity method (Section 3.2.1) is an approach to account for the combined effect of temperature and time on the development of concrete mechanical properties and the development of hydration. In the equivalent age maturity method as defined in Equation 3-3, an equivalent curing age relative to a reference temperature is calculated, with the Arrhenius rate concept.

Key to understanding the concept behind traditional maturity methods is to realize that the effect of temperature only adjusts the time of occurrence of the property being estimated. Figure 5-3 contains strength test data for cylinders moist cured at the isothermal temperature of 23°C. The best fit strength-maturity curve at the reference temperature (23°C) is shown to provide a good fit of the data. Based on this strength-maturity relationship, the maturity method (ASTM C 1074) was used to predict the strength at isothermal curing temperatures of 5°C and 40°C, and these curves are shown in Figure 5-3. From Figure 5-3, it is **evident that the maturity method only produces a translation with respect to time**. At curing temperature higher than the reference temperature the maturity (equivalent age) will elapse quicker, and visa versa.

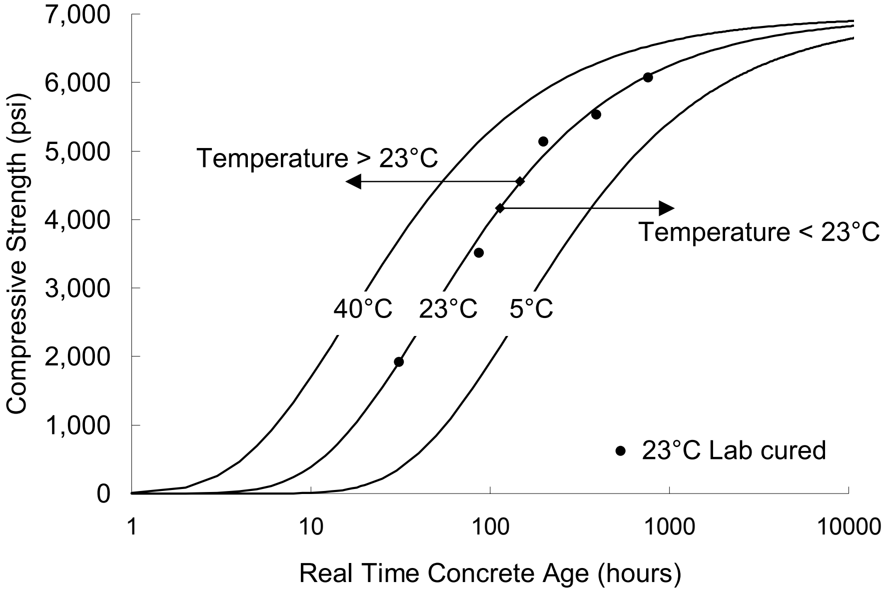

Figure 5-3: The effect of the traditional maturity method

The traditional maturity method assumes that the long-term strength of the concrete mixture is unaffected by the curing temperature magnitude. In section 1.1.2, it was demonstrated that in some concrete mixtures, high initial temperatures may cause decreased long-term strengths as compared to mixtures cured at low temperatures. This is referred to as the **cross-over effect**, which cannot be accounted for in the formulation of the traditional maturity method, and this will be discussed in more detail in this chapter.

5.2.1 Relationships between Concrete Properties and Maturity

In Section 3.2.1.2, it was explained how to determine the maturity of concrete in terms of the equivalent curing age. In order to apply the maturity method, one has to define the unique relationship between the maturity and the property that is to be predicted. This is an empirical relationship, which has to be determined at the reference temperature, which is the temperature at which the age conversion factor is unity. In the case of strength prediction, this relationship is termed the **strength-maturity relationship** (ASTM C 1074). In this work the objective will be to predict the hydration (degree of hydration) at different levels, and the relationship will be termed: **hydration-maturity relationship**. The mathematical formulation of the hydration-maturity relationship was previously presented in Section 3.2.5.1. The definition and behavior of strength-maturity and hydration-maturity relationships will be evaluated in the next section.

5.2.1.1 *Strength-Maturity Relationship*

Many mathematical forms of the strength-maturity and hydration-maturity relationships have been proposed in past publications. Carino (1991) provides an evaluation of some of these proposed strength-maturity functions, and based on the conclusions reached the ASTM recommends the use of three functions. Two of the recommended strength-maturity formulations are the **exponential** and **hyperbolic** functions. TxDOT recommends a third mathematical form (not recommended by ASTM), which is a **logarithmic** function. Table 5-1 defines the mathematical formulation of each of these three strength-maturity formulations. The **exponential** function was used by Freiesleben Hansen and Pedersen (1985).

Table 5-1: Different strength-maturity relationships

Strength-Maturity Relationship	Numbering
Exponential function: $S(t_e) = S_u \cdot \exp\left(-\left[\frac{\tau_s}{t_e}\right]^{\beta_s}\right)$ Where, S(t_e) = strength at equivalent age, t_e, (psi), t_e = maturity ito of equivalent age at reference temperature (hrs), τ_s = time constant for strength prediction (hours), β_s = shape constant for strength (unit less), and S_u = ultimate strength (psi).	*Equation 5-1*
Hyperbolic function: $S(t_e) = S_u \cdot \frac{K \cdot (t_e - t_{e0})}{1 + K \cdot (t_e - t_{e0})}$ Where, the parameters are as defined in Equation 5-1, except for: t_{e0} = maturity ito equivalent age when strength development begins (hours), and K = curve fit constant for strength prediction. *Note:* $K \cdot S_u$ provides the initial slope of the strength-maturity curve.	*Equation 5-2*
Logarithmic function: $S(t_e) = A \cdot \ln(t_e) + B$ Where, the parameters are as defined in Equation 10, except for: A = curve fit slope constant for strength prediction (psi/hours), and B = curve fit intercept constant for strength prediction (psi).	*Equation 5-3*

Figure 5-4 presents the compressive strength results for 6x12-inch cylinders moist cured at 23°C. The best-fit parameters were determined for each of the three strength-maturity formulations presented above, and the curves on Figure 5-4 indicate the results obtained. The scale on the horizontal axis is the equivalent age, however since the reference temperature is 23°C and the tests were performed at this temperature this axis could have been defined as the real time concrete age. The conclusion reached by Carino (1991), was that the logarithmic formulation provides the poorest fit ($r^2 = 0.96$) and the exponential and hyperbolic an equally accurate fit ($r^2 = 0.99$) of the compressive strength data. The results shown in Figure 5-4 are commonly plotted with the concrete age on a log scale, and this is shown in Figure 5-5. Note that the logarithmic function plots as a straight line on Figure 5-5, and this highlights its limitation. The logarithmic function does not reach an asymptotic value (or ultimate strength, S_u) which is the case with both the exponential and hyperbolic expressions. In this study, the exponential expression is chosen to define the strength-maturity relationship, as it will be shown in the next section that this relationship is also suited to define the hydration-maturity relationship.

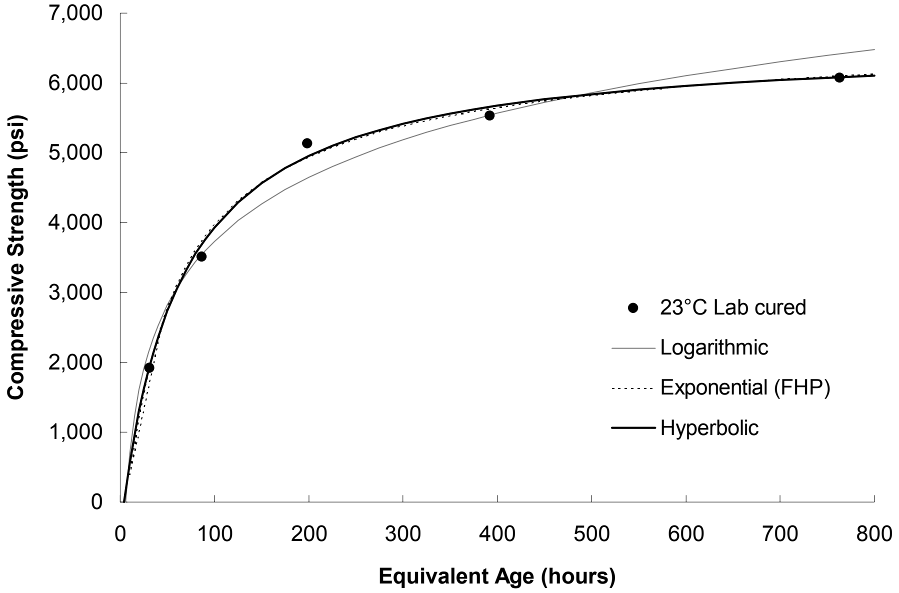

Figure 5-4: Comparison of different strength-maturity relationships

To illustrate the use of the maturity method, the strength at temperatures of 5°C and 40°C were predicted with the hyperbolic and logarithmic strength-maturity functions determined above. Figures 5-6 and 5-7 indicate the results obtained, and as mentioned in the introduction section, the current maturity method can **only** adjust the time of strength development, ***and the strength curves***

are thus translated with respect to time. The disadvantage of using the logarithmic function can be seen in this example, since the predicted strength reaches no limiting value.

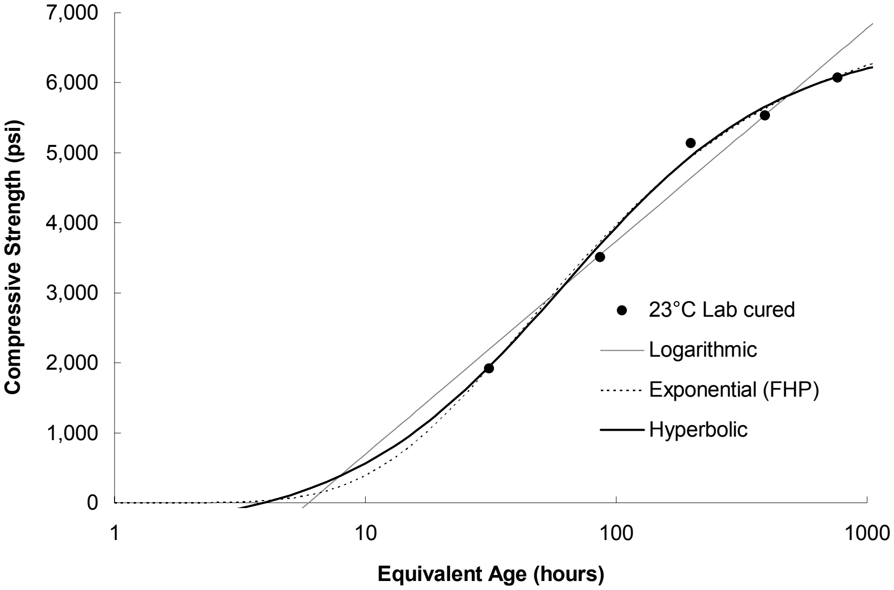

Figure 5-5: Different strength-maturity relationships with the equivalent age on a log scale

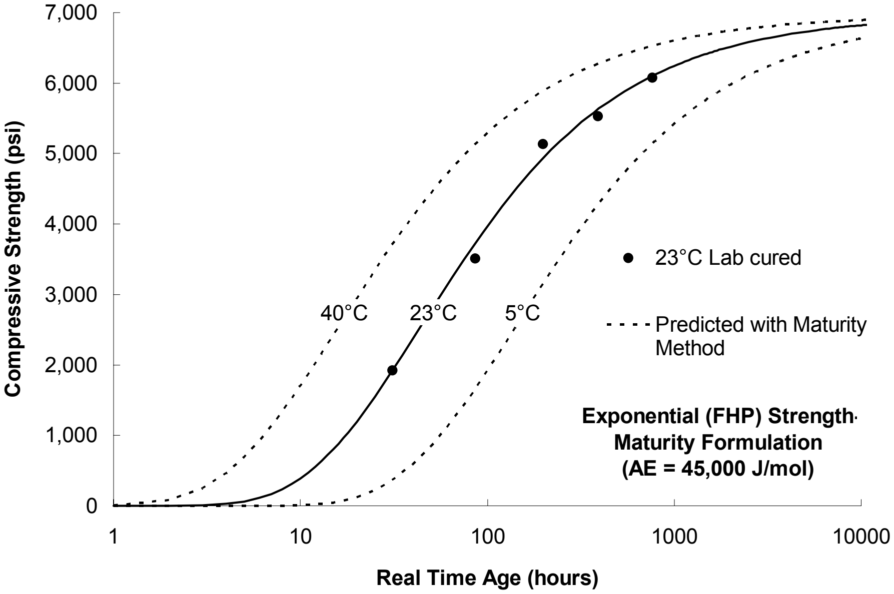

Figure 5-6: Predicted strength with the **exponential** strength-maturity relationship

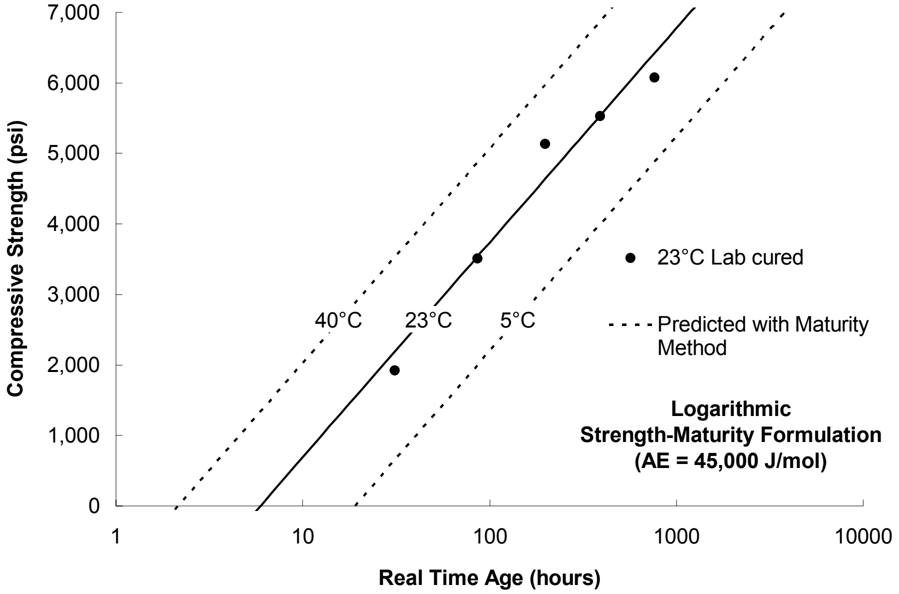

Figure 5-7: Predicted strength using the **logarithmic** strength-maturity relationship

5.2.1.2 *Hydration-Maturity Relationship*

In section 3.2.4, it was discussed that the degree of hydration for a concrete mixture can experimentally be determined by a number of techniques, some direct and others indirect. In this study, the more practical method of estimating the degree of hydration based the heat development that occurs during hydration is taken. It has been shown that the heat released divided by the total heat available provides a good measure of the degree of hydration (van Breugel, 1991; RILEM 119-TCE, 1981; Radjy et al., 1994), and this is mathematically express as follows:

$$\alpha(t) = \frac{H(t)}{H_u}$$

Previously Equation 3-16

where, $\alpha(t)$ = degree of hydration at time, *t*,

$H(t)$ = total heat development at time, *t*, (J/g), and

H_u = maximum heat development (at 100% complete hydration) (J/g).

During the hydration of cementitious materials, several stages of hydration can be identified, and they have been discussed in Section 2.1.3. These stages explain the characteristic s-shape of the degree of hydration curve. Figure 5-8 presents the s-shape of the heat development over time as measured by calorimeter testing. Once test data of the degree of hydration development with equivalent age has experimentally been determined, the best-fit mathematical model needs to be determined to represent the data. In Section 3.2.5.1, the many mathematical forms proposed to represent the hydration-maturity relationship were presented in Table 3-5. It was further shown that the exponential formulation (Equation 3-17) could be used to represent the s-shape of the hydration development. The use of the exponential function was selected for strength prediction, and the degree of hydration over time.

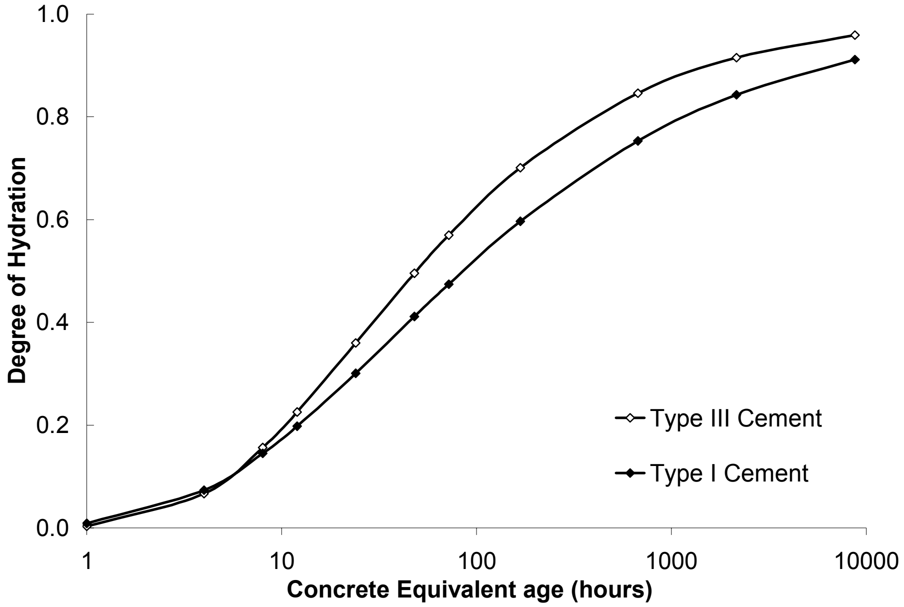

Figure 5-8: Characteristic s-shape of the degree of hydration curve

5.2.2 Effect of Temperature on Long-Term Strength Development

Concretes mixed, placed, and cured at elevated temperatures normally develop higher early strengths than concrete produced and cured at lower temperatures, but strengths are generally lower at 28 days and later ages (Neville, 1996; Emborg, 1989; USBR, 1975; Carino, 1981; Kjellsen and Detwiler, 1993; Verbeck and Helmuth, 1968).

Figure 5-9 presents test data for the development of compressive strength at isothermal curing temperatures of 20°C and 40°C (Chanvillard and D'Aloia, 1997). The best fit exponential strength gain curve was fitted through each of the data points. From these curves, it may be seen that the long-term concrete strength is reduced when it is made and cured at higher temperatures as compared to curing at lower temperatures. In Figure 5-9, the cross-over effect occurred when the concrete age was approximately 31 hours.

Figure 5-10 presents compressive strength test data for mortar specimens cast and cured at various different isothermal temperatures (Carino, 1981). The best fit exponential strength gain curve was fitted through each of the data points of a specific curing temperature. This figure illustrates the impact of the cross-over effect, and further indicates that the long-term strength is increased when the concrete is cured at low temperatures. In this instance, the cross-over effect is noticeable after 200 hours. In Section 1.1.2, reasons for the reduced long-term strength for concretes cured at high temperatures were presented.

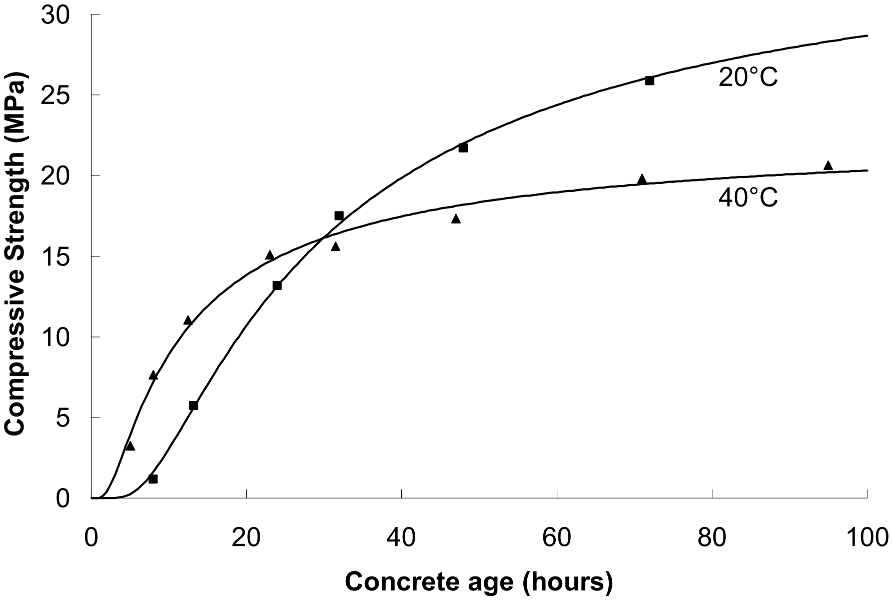

Figure 5-9: Compressive strength results for concrete, 0.45 w/c, Type I cement (Chanvillard and D'Aloia, 1997)

In this study, the compressive strength development for mortar samples cured at different temperatures was determined. Figure 4-35 showed some results for different cementitious materials, it was discussed that the magnitude of the cross-over effect is influenced by the cementitious materials used. The strength development curves for the 21 mixtures tested during this study are presented in Appendix A and B.

From the above discussion, it may be concluded that the amount of strength loss due to curing at high temperatures as compared to curing at room temperature is influenced by the type and amount of mineral admixtures used in the concrete mixture. However, data presented in later sections will show that few trends may be identified with regard to the use of different mineral admixtures.

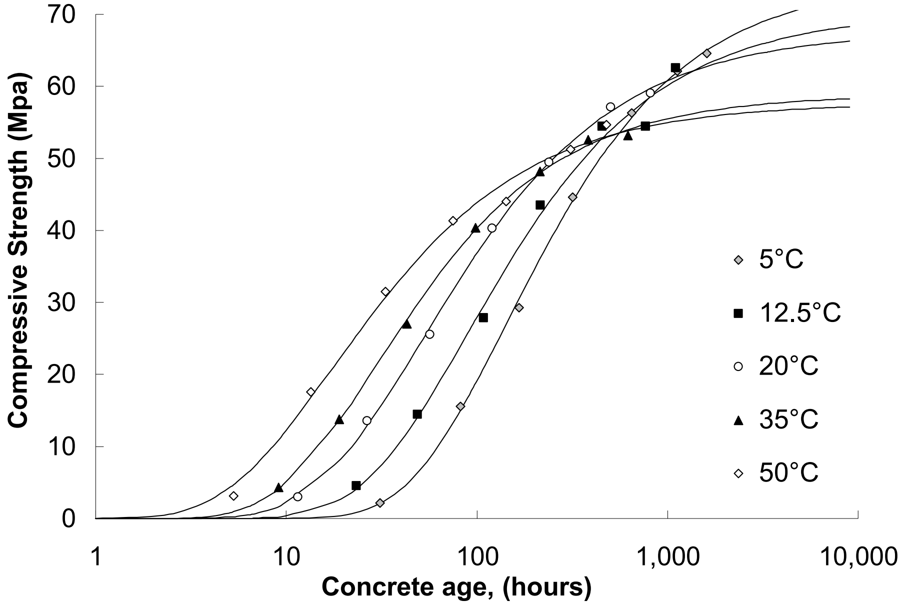

Figure 5-10: Compressive strength results for mortar, 0.43 w/c, Type I cement (Carino, 1981)

The purpose of the traditional maturity method was illustrated in Figure 5-3, and it was shown that it can only account for effect of temperature by causing the property being estimated to be translated with respect to time. Figures 1-9, 4-35, 5-9, and 5-10 have shown evidence that the development of the mechanical properties of concrete is not only dependent on the concrete age, since the long-term strength is reduced at higher curing temperatures. This effect cannot be accounted for with the traditional maturity method. Other authors have come to a similar conclusion and Byfors (1980) states that:

> …if strength growth for different constant temperatures is plotted in a chart with a logarithmic time axis, the developments should be displaced laterally not congruent. The following must consequently apply if a maturity function is to be able to take the influence of temperature on strength gain into consideration: the same strength must have been reached independently of the temperature at one and the same maturity (degree of hydration). This is not, however, always the case, curing at higher temperatures, 30-40°C, can entail losses in the final strength. Maturity functions cannot take effects of this type into consideration.

After comparing the intent of the maturity method shown in Figure 5-3 with the behavior of concrete shown in Figures 1-9, 4-35, 5-9, and 5-10, one may conclude that there is a “window of application” (before strength losses start to occur) during which the principles of the maturity method may work appropriately. This “window of application” occurs prior to the occurrence of the cross-over effect. This may be the reason why the data presented by the developers of the original Arrhenius maturity equation (see Figure 3-4) only applied it to early-age results (concrete equivalent age less than 4 days), since this would be the range in which the cross-over effect did not occur for the materials they were using. In the data shown in Figure 5-9, the cross-over effect occurred as early as 31 hours. European authors have documented some limitations to the application of the traditional maturity method. Some of the recommendations are as follows:

- Jonasson (1985) found that the maturity method worked satisfactorily up to about 50% of the 28-day strength reached after curing at the reference temperature.
- Byfors (1980) mentions that since the maturity function cannot take into considerations the reduced ultimate strength at higher curing temperatures, the maturity concept can only be applied at lower maturities.
- Kjellsen et al. (1993) states that, "... at maturities beyond that corresponding to approximately 40 percent of the normal 28-day strength, the estimation may be erroneous."
- "It seems that the expressions for equivalent age and compressive strength work satisfactory for up to 50% of the 28-day strength (about 2 days equivalent age). After the 50% level in strength have been reached the strength is influenced so that higher temperatures lead to lower strength and visa versa," Emborg (1989).

5.2.3 Effect of Temperature on Hydration Development

Section 5.2.3 showed that the cross-over effect occurred in the development of mechanical properties (strength). This section will evaluate if this phenomenon additionally manifests itself in degree of hydration data, i.e. structure formation.

Figure 5-11 presents the development of ***compressive strengths*** for mortar specimens cured at the isothermal temperatures of 5, 12.5, 20, 35, and 50°C (Kjellsen and Detwiler, 1993). This figure is very similar in nature to Figure 5-10, and the loss of strength due to curing at high temperatures is noticeable early on. The strength of the sample cured at 50°C started to cross-over the strength of the sample cured at 35°C after only 40 hours. The long-term strength loss at 50°C was about 17% as compared to the specimens cured at room temperature.

Figure 5-12 presents the degree of hydration development for mortar specimens cured at the isothermal temperatures of 5, 12.5, 20, 35, and 50°C (Kjellsen and Detwiler, 1992). This data were obtained from the same materials that were used to determine the strength data shown in Figure 5-11. The data in Figure 5-12 were determined based on the non-evaporatable water content as a means of estimating the degree of hydration. Note that this figure is very similar in nature to Figure 5-3 in that the curves at different temperatures are translated in time and convergence of the curves only tend to occur after 600 hours of hydration. In this analysis, the maximum degree of hydration is slightly higher for the lower cured samples, but the difference in maximum temperature is minimal.

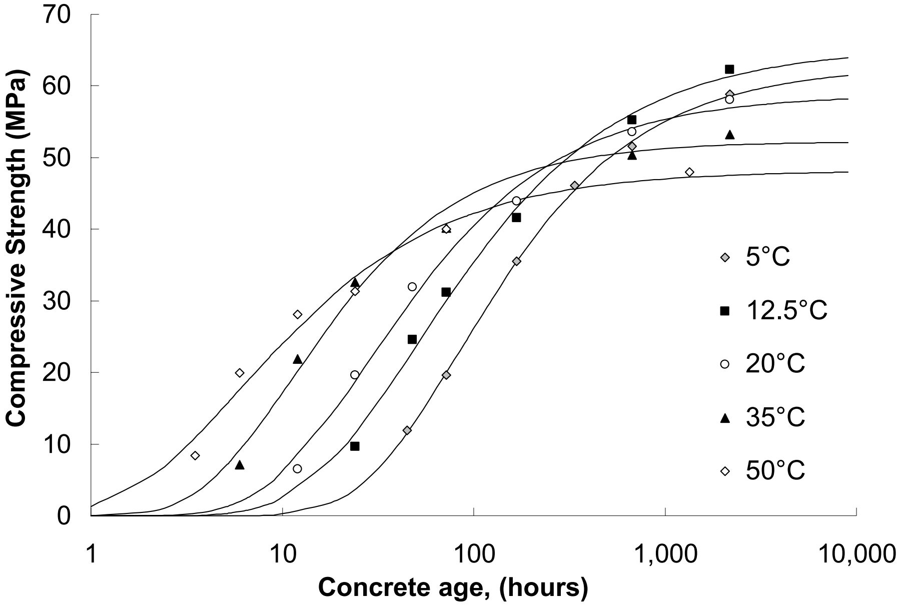

Figure 5-11: Kjellsen and Detwiler (1993) compressive strength results for mortar, 0.5 w/c, Type I/III cement

It may be concluded from Figures 5-11 and 5-12 that there is little or no reduction in maximum heat of hydration due to curing at high temperatures. Cervera and Prato (1999) came to a similar conclusion since they state that the final degree of hydration is the same for samples cured at any temperature, and that the final degree of hydration basically depends on the initial water content of the mixture. Chanvillard and D'Aloia (1997) mention that:

> By defining the hydration degree in terms of relative quantity of heat already generated, it can be noted that the relative quantity of generated heat versus age curves are affine, what ever the isothermal curing temperature of the concrete is, and that the affinity ratio follows the Arrhenius law.

From the data evaluated in Sections 5.2.2 and 5.2.3, it may be concluded that the cross-over effect develops only when mechanical properties are considered and not when the degree of hydration development is considered. This infers that the maturity method will be applicable over most of the hydration period when the degree of hydration is to be predicted at temperatures other than the reference temperature.

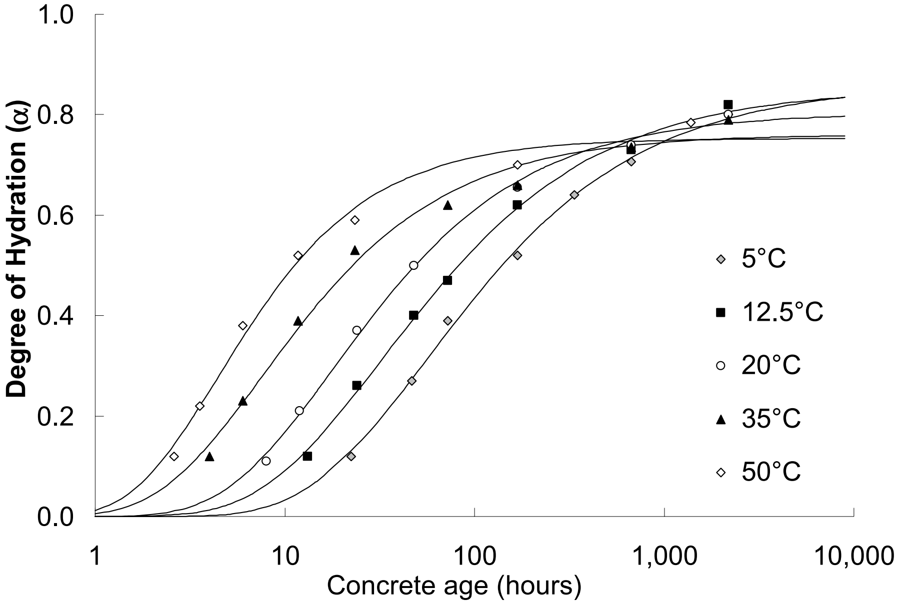

Figure 5-12: Degree of hydration development for mortar, 0.5 w/c, Type I/III cement (Kjellsen and Detwiler, 1992)

5.2.4 Activation Energy for Strength versus Hydration Prediction

In the previous section, it was shown that the curing temperature has an influence on the long-term strength development but not on the maximum degree of hydration reached. It was further shown that much controversy exist in the literature about the most appropriate activation energy values to use. Some researchers have used activation energy values as determined from heat of hydration tests, and used them for strength prediction. Kada-Benamure et al. (2000) commented that:

> ... the mechanical strength, unlike the heat of hydration, does not reflect a purely chemical mechanism and cannot, therefore, fully abide by the Arrhenius law.

The ASTM C 1074 procedure is based on strength tests, and the question becomes whether or not these test results are valid for use during hydration prediction. To investigate this apparent contradiction, this section will determine the activation energy for test results for both heat of hydration and compressive strength tests. This section discusses some of the contradictions, and then recommendations are made to implement the activation energy for use in the temperature prediction model.

5.2.4.1 *Determining the Activation Energy*

This section will indicate how the activation energy for use in the equivalent age maturity method can be determined based on basic principles. In order to determine the activation energy for use in the equivalent age definition of the maturity method, the slope of the Arrhenius plot at a specific temperature has to be determined relative to slope at the reference temperature. With this method, an age conversion factor can be determined relative to curing at the reference temperature. From the traditional maturity formulation shown in Equations 3-3 and 3-6, the age conversion factor, $f(T_c)$, can be defined as follows:

$$f(T_c) = \frac{k(T_c)}{k(T_r)} \qquad \textit{Equation 5-4}$$

where, $k(T_c)$ = rate constant at concrete temperature, T_c, and
$k(T_r)$ = rate constant at the isothermal reference temperature, T_r.

The age conversion factor defined in Equation 5-4, enables the conversion of the chronological concrete age into the equivalent age. The relation between the chronological concrete age and the equivalent age is as follows:

$$t_e = f(T_c) \cdot t \qquad \textit{Equation 5-5}$$

where, t_e = equivalent age at the reference temperature (hours),
t = chronological concrete age (hours).

The exponential formulations for both the development of mechanical properties and the degree of hydration can be used to determine the best fit curves to represent the experimental data points. The exponential functions used are as follows:

Strength-Maturity Relationship:

$$S(t_e) = S_u \cdot \exp\left(-\left[\frac{\tau_s}{t_e}\right]^{\beta_s}\right) \qquad \textit{Previously Equation 5-1}$$

where, $S(t_e)$ = strength at equivalent age, t_e, (psi),
t_e = maturity ito of equivalent age at reference temperature (hrs),
τ_s = time constant for strength prediction (hours),
β_s = shape constant for strength (unit less), and
S_u = ultimate strength (psi).

Hydration-Maturity Relationship: $$\alpha(t_e) = \alpha_u \cdot \exp\left(-\left[\frac{\tau}{t_e}\right]^{\beta}\right)$$ *Previously Equation 5-1*

where, $\alpha(t_e)$ = the degree of hydration at equivalent age, t_e,

τ = hydration time parameter (hrs),

β = hydration shape parameter, and

α_u = ultimate degree of hydration.

If the age conversion factor is known, Equation 3-21 can be defined in terms of the chronological age as shown in Equation 5-6. If experimental data are available at temperatures other than the reference temperature, the best fit hydration time parameters (τ_T) at each of the temperatures can be determined. Note that only the hydration time parameter is adjusted by the maturity method, and only the time parameter should therefore be altered. When the exponential equation is used, it is assumed that the slope parameter, β, is independent from the curing temperature. From Equation 5-6, it may be shown that the relationship between the hydration time parameter at the reference temperature (τ) and at any other temperature (τ_T) is similar to that shown in Equation 5-5. The age conversion factor may thus alternatively be determined as shown in Equation 5-7. From Equation 5-7, it may be seen that the age conversion factor may be obtained from the best fit hydration time parameters obtained at different temperatures.

$$\alpha(t) = \alpha_u \cdot \exp\left(-\left[\frac{\tau}{f(T_c)\cdot t}\right]^{\beta}\right)$$ *Equation 5-6*

where, $\alpha(t)$= the degree of hydration at chronological age, *t*.

$$\tau_T = \frac{\tau}{f(T_c)} \quad \Rightarrow \quad f(T_c) = \frac{k(T_c)}{k(T_r)} = \frac{\tau}{\tau_T}$$ *Equation 5-7*

where, τ_T = the hydration time parameter obtained for curing at temperature, *T*, (hrs),

From the fundamental definition of the activation energy as shown in Equation 3-2 and Figure 3-2, it was shown that the activation energy could be obtained from the slope of the plot of the natural the logarithm of the rate constant against the inverse of the absolute temperature. This can mathematically be defined as shown in Equation 5-8, which can be simplified to develop an expression for the activation energy in terms of the hydration time parameters. Equation 5-9 indicates that the activation energy can be determined from the plot of the natural logarithm of the hydration time parameter against the inverse of the absolute temperature. This procedure will now be applied to experimental data to evaluate the activation energy for use in the **hydration-maturity** relationship.

$$-\frac{E}{R}=\frac{\Delta \ln k(T)}{\Delta(1/T)} \qquad \textit{Equation 5-8}$$

$$=\frac{\ln k(T_r)-\ln k(T_c)}{(1/T_r-1/T_c)}$$

$$=\frac{\ln\left(k(T_r)/k(T_c)\right)}{(1/T_r-1/T_c)}$$

$$=\frac{\ln\left(\tau_T/\tau\right)}{(1/T_r-1/T_c)} \qquad \textit{Equation 5-9}$$

5.2.4.2 *Activation Energy for Hydration Development*

In order to evaluate the nature of the activation energy for the chemical processes involved during the reaction of portland cement, experimental data of two different sources will be evaluated. These sources are the data from Kjellsen and Detwiler (1992) as previously shown in Figure 5-12 and the data presented by Lerch and Ford (1948). The two data sets will be analyzed in the following two sections.

Tests of Kjellsen and Detwiler (1992)

The experimental data from Kjellsen and Detwiler (1992), as previously shown in Figure 5-12, will be used to determine the hydration activation energy. The following procedure was followed:

1. The best-fit degree of hydration curve for the experimental data obtained at the reference temperature was determined. From this, values for the following parameters as shown in Equation 3-21 are obtained:

   τ = hydration time parameter at the reference temperature (hrs),
   β = hydration shape parameter, and
   α_u = ultimate degree of hydration.

2. The hydration shape (β) parameter and the ultimate degree of hydration (α_u) determined at the reference temperature, is used as constants in the degree of hydration curves at the other test temperatures. This process is followed, since in the implementation of the maturity method, only the degree of hydration at the reference temperature is known. Furthermore, the maturity method cannot modify the hydration slope parameter (β) and β, thus has to remain the same at all temperatures.

3. Determine the best-fit hydration time parameters (τ_T) at all test temperatures, *T*, other that the reference temperature. Figure 3-1 presents the results obtained from these curve fits. The lowest r^2 obtained was 0.979 for the test performed at 35°C. Note that the difference between Figures 5-12 and 5-13 is that the ultimate degree of hydration as determined at the reference temperature was used for all the curves in Figure 5-13.
4. The Arrhenius plot can now be constructed, by plotting the natural logarithm of the hydration time parameters (τ, and τ_T) versus the inverse of the corresponding absolute curing temperature. Figure 5-14 presents the Arrhenius plot obtained for this data set.
5. The Arrhenius plot reveals that there is a strong linear trend (r^2 = 0.994) in the data. The slope of the best fit straight line is determined to be -4692.3, from which an experimental E value of **39,014** J/mol is determined.

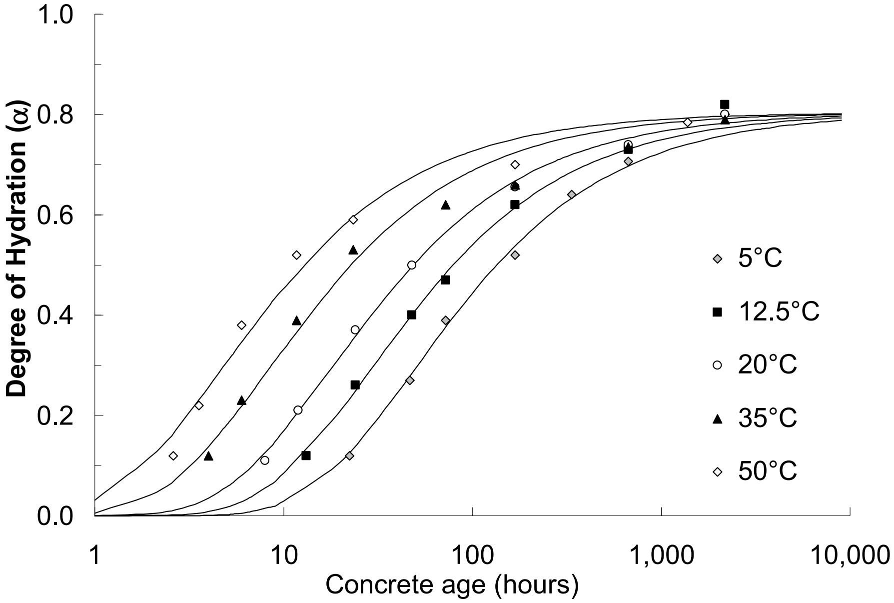

Figure 5-13: Best fit degree of hydration curves with equal ultimate degree of hydration

The procedure above can be validated by simply using the maturity method with the hydration-maturity relationship determined at the reference temperature (20°C). The test times are all converted into equivalent age by the experimentally determined activation energy and with Equation 3-3. By plotting the data in terms of equivalent age, all the data points should fall on a single curve: the hydration-maturity curve obtained at the reference temperature. Figure 5-15 indicates the results of this validation excise and it may be seen that all the test data approximately converge onto a single curve.

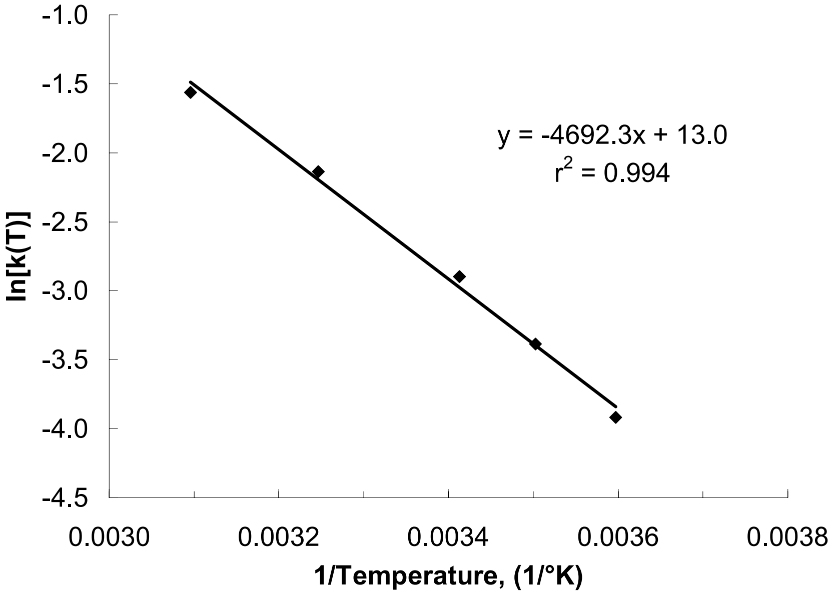

Figure 5-14: Arrhenius plot for degree of hydration test data of Kjellsen and Detwiler (1993)

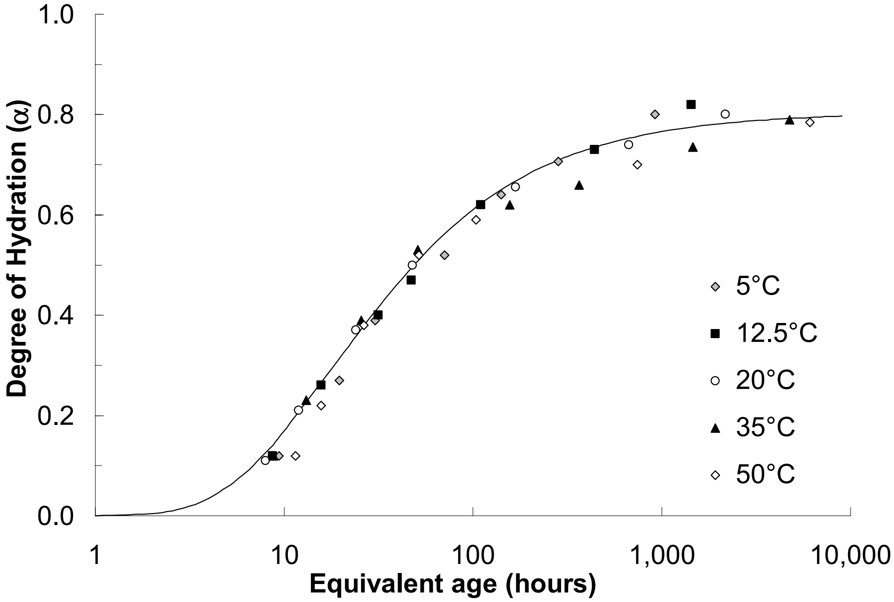

Figure 5-15: Results of the application of the maturity methods to hydration

Figure 5-16 presents a scatter plot of the measured versus predicted degree of hydration obtained for this exercise. The plot only includes the points predicted at temperatures other than the reference temperature. The r^2 obtained for the analysis is 0.980, which indicates that the constant activation energy provides an accurate technique to predict the experimental hydration results at different temperatures.

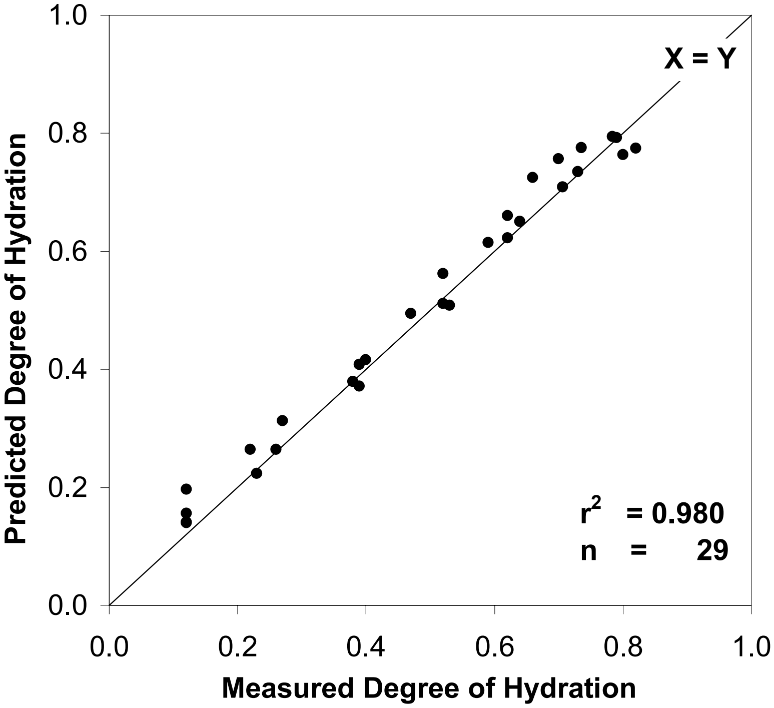

Figure 5-16: Measured versus predicted degree of hydration for data of Kjellsen and Detwiler

Tests of Lerch and Ford (1948)

One of the largest data sets available on the development of heat of hydration was generated by the Portland Cement Association (PCA) in a study to evaluate the long-term behavior of local U.S. cements (Lerch and Ford, 1948). Section 5.2.6.1 will present more background on the data analyses performed on the Lerch and Ford data set. The degree of hydration formation for each curing temperature is available for a period up to 72 hours. In the previous sections, it was shown that the ultimate degree of hydration is not affected by the curing temperature and the curves are only translated with respect to time. The accuracy of the equivalent age method as applied to the development of degree of hydration can be evaluated from this data set. A reference temperature of 21.1°C (70°F) was used during the analysis of this data set.

Figure 5-17 presents the results obtained after applying the equivalent age maturity method with the activation energy as formulated by FHP to a Type I and Type III cement. From the results of the Type I cement shown in Figure 5-17, is may be seen that the age adjustment factor calculated with the FHP activation energy is too high at the low temperatures, and too low at the high temperature. The results for the Type III cement indicate that the age conversion factor provides an accurate prediction at low temperatures, but is too low for the higher temperatures.

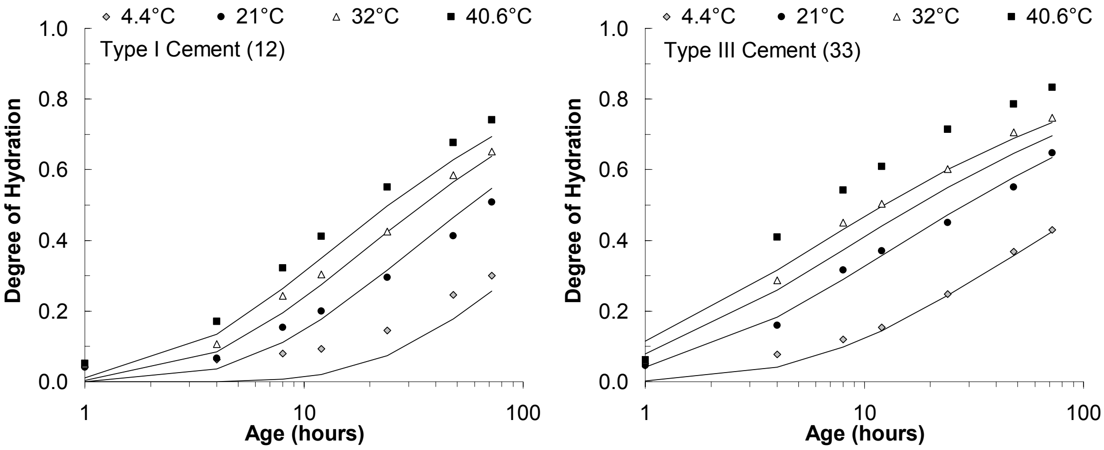

Figure 5-17: Results after applying FHP activation energy to Lerch and Ford data set

The Arrhenius plot was constructed for the heat of hydration of these cements. Figure 5-18 indicates the results obtained for a Type I (12) and Type III (33) cement. Figure 5-18 indicates that a linear curve is sufficient ($r^2 > 0.99$) to represent the rate of hydration, and that the activation energy is independent from the curing temperature. The Arrhenius rate theory for chemical reactions therefore applies to the hydration mechanism of these portland cements. On Figure 5-18, the slope of the Arrhenius plot is different for the two cements, which indicates that the activation energy is influenced by the composition of the cement. From the slopes shown in Figure 5-18, the activation energy is **42,171 J/mol** and **54,467 J/mol**, respectively, for the Type I and Type III cement.

The constant activation energy obtained from the Arrhenius plot in Figure 5-18 was used to evaluate the accuracy of the equivalent age maturity concept with regards to the prediction of the degree of hydration at different temperatures. Figure 5-19 presents the results obtained for the Type I and Type III cement, and these results should be compared to the results obtained with the variable FHP activation energy shown in Figure 5-17. Figure 5-19 indicates that an accurate estimate of the degree of hydration at high and low temperatures can be obtained through the use of a constant activation energy that is ***independent of the curing temperature***. The results further indicate that the activation energy is affected by the chemical composition the cement.

Figure 5-16 presents a scatter plot of the measured versus predicted degree of hydration obtained for this exercise. The plot only includes the points predicted at temperatures other than the reference temperature. The r^2 obtained for the analysis is 0.980, which indicates that the constant activation energy provides an accurate technique to predict the experimental hydration results at different temperatures.

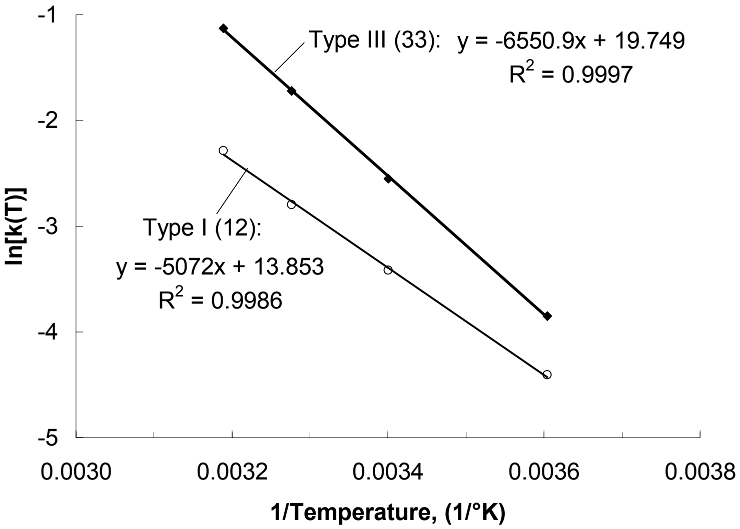

Figure 5-18: Arrhenius plot for degree of hydration of Lerch and Ford data set

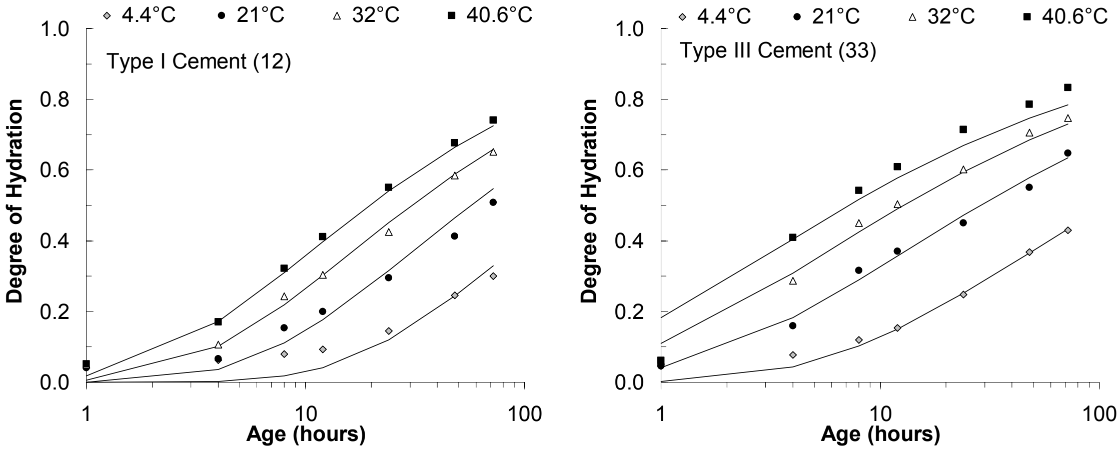

Figure 5-19: Results after applying **constant** activation energy to Lerch and Ford data set

5.2.4.3 *Activation Energy for Strength Development*

The experimental data from Kjellsen and Detwiler (1993), as previously shown in Figure 5-11, will be used to determine and evaluate the activation energy for strength prediction. The strength activation energy can then be compared to that obtained from the degree of hydration data evaluated in the section above. Due to the loss in long-term strength, the procedure above will have to be adjusted. The current maturity method will not produce accurate results, since the best-fit **strength-maturity curve at the reference temperature** has to be used to predict the strength at high temperatures such as 50°C. However, at these temperature levels, the cross-over effect occurs and strength losses are present.

If the FHP activation energy is used, the results of applying the traditional maturity method to the data shown in Figure 5-11, are as presented in Figure 5-20. The curve in Figure 5-20 is the predicted strength at the reference temperature, and all the data points should fall on this line for the traditional maturity method to produce an accurate prediction. All data points **under** the curve on Figure 5-20 are **over predicted**, and visa versa. Figure 5-20 indicates that the strengths at the higher temperatures are over predicted at an equivalent age over 85 hours. At early-age, strengths at low curing temperatures are over predicted. The r^2 for strength tests at 50°C is only 0.754. It should be mentioned, that the original FHP activation energy was developed for early-age strength prediction, and at equivalent ages less that 72 hours reasonable accurate results can be obtained.

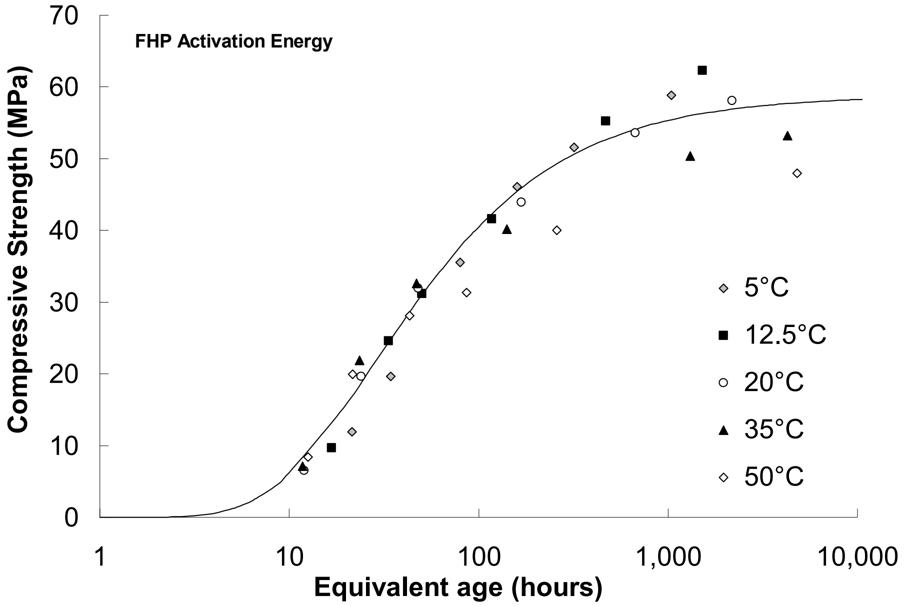

Figure 5-20: Application of the maturity method with the FHP activation energy definition on the data of Kjellsen and Detwiler (1993)

ASTM C 1074, “Standard practice for estimating concrete strength by the maturity method,” a procedure is outlined in Annex A to determine the activation energy based on mortar strength tests. This procedure recommends the use of the hyperbolic strength-maturity relationship as shown in

Equation 5-2, to determine the best-fit values of t_{e0}, K, and S_u. With this method, an average experimental activation energy value can be obtained from the Arrhenius plot. This value is, therefore, constant for a specific mixture and independent of the curing temperature. This procedure was followed with the experimental data from Kjellsen and Detwiler (1993), and an activation energy value of 45,219 J/mol was obtained. Table 5-2 provides a summary of all the curve-fit parameters obtained. Note that the ultimate strength (S_u) is different for each curing temperature, due to the loss of long-term strength at high curing temperatures.

Table 5-2: Curve-fit parameters and activation energy for hyperbolic equation

Curve-fit Parameter	**Curing Temperature (°C)**				
	5.0	12.5	20.0	35.0	50.0
S_u (psi) =	61	62	57	51	46
K	0.009	0.015	0.028	0.080	0.125
t_o (hours)	19.0	9.9	6.9	3.7	1.2
Activation Energy	45,219 J/mol				

If this activation energy value is reused in the traditional maturity method to predict the strength at all temperatures other than the reference temperature, the results shown in Figure 5-21 are obtained. These results are similar to those shown in Figure 5-20, in that the strength at high temperatures are over predicted as early as an equivalent age of 68 hours. The r^2 value for strength tests at 50°C is only 0.459. The results for curing at 35°C are over predicted.

The procedure above can be repeated by using the exponential strength-maturity relationship as shown in Equation 5-1. A different activation energy value of 44,778 J/mol was obtained and Table 5-3 provides a summary of all the curve-fit parameters obtained.

Table 5-3: Curve-fit parameters and activation energy for exponential equation

Curve-fit Parameter	**Curing Temperature (°C)**				
	5.0	12.5	20.0	35.0	50.0
S_u (psi)	64	64	59	53	47
β	0.785	0.785	0.785	0.785	0.785
τ (hours)	86.60	49.63	28.46	11.47	5.94
Activation Energy	44,778 J/mol				

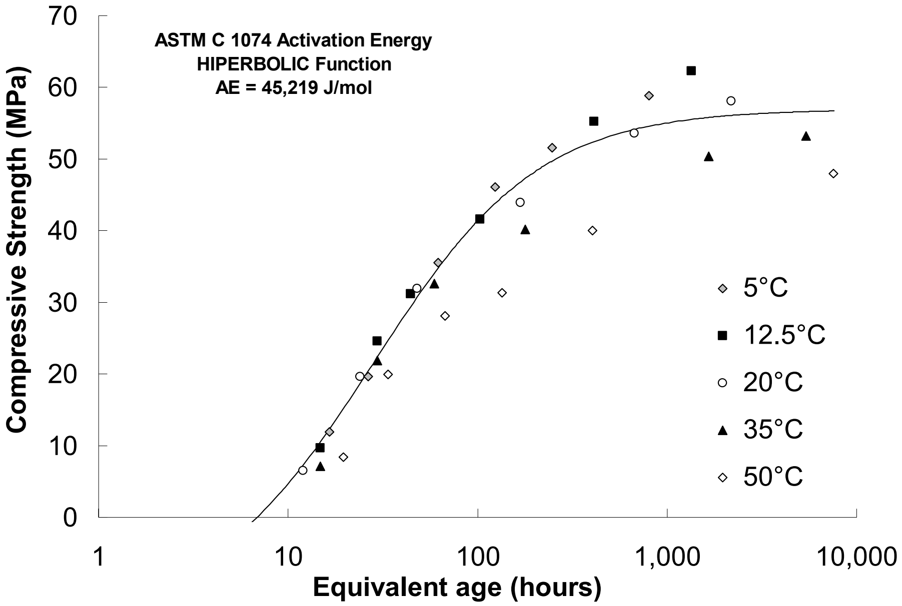

Figure 5-21: Application of the maturity method with the hyperbolic strength-maturity function

The activation energy value, as shown in Table 5-3, is further reused in the traditional maturity method to determine the accuracy of the predicted strengths at all temperatures other than the reference temperature. The results shown in Figure 5-22 were obtained. These results are similar to those shown in Figure 5-21, and the strength values at high temperatures are over predicted at an equivalent age of 66 hours.

The results above indicate that the choice of strength-maturity relationship influences the experimental activation energy value. This was observed by Pinto (1997) who determined different activation energy values for different strength-maturity functions as shown in Table 5-4. This is contrary to the recommendation in ASTM, which determines the activation energy based on the hyperbolic formulation, but recommends that either of the exponential or hyperbolic formulations could be used to develop the strength-maturity relationship. **The strength-maturity equation used during the calculation of the activation energy should be used during the development of the strength-maturity relationship.**

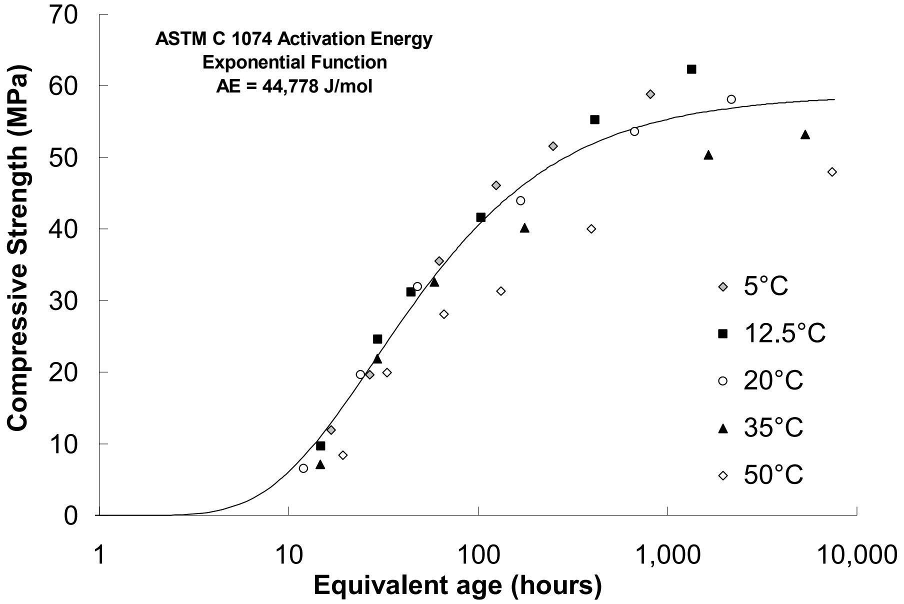

Figure 5-22: Results of the maturity method with the exponential strength-maturity function

Table 5-4: Curve-fit parameters and activation energy for exponential equation

Strength-Maturity Function	Activation Energy (J/mol)
Hyperbolic	33,900
Exponential	26,100

Carino's Modified Maturity Rule

In the ASTM procedure above, different ultimate strength values are used to provide the best-fit curve at each temperature (see S_u values in Tables 5-2 and 5-3). The modified maturity rule, as introduced by Carino (1991), works on a relative strength gain basis. This process recognized that the long-term strength is affected by high curing temperatures, and Carino proposed the following ***modified maturity rule***:

> Samples of a given concrete mixture which have the same equivalent age and which have had a sufficient supply of moisture for hydration will have developed equal fractions of their limiting strength irrespective of their actual temperature histories.

The modified maturity rule was implemented on the data from Kjellsen and Detwiler (1993) using both the hyperbolic and exponential functions. All the measured and predicted strengths were normalized to the ultimate strength measured at each specific curing temperature. Figure 5-23 and 5-24 indicate the results obtained and all the data points align on the relative strength curve obtained at the reference temperature. From this, it may be concluded that the modified maturity method provides an accurate estimate of the measured relative strength.

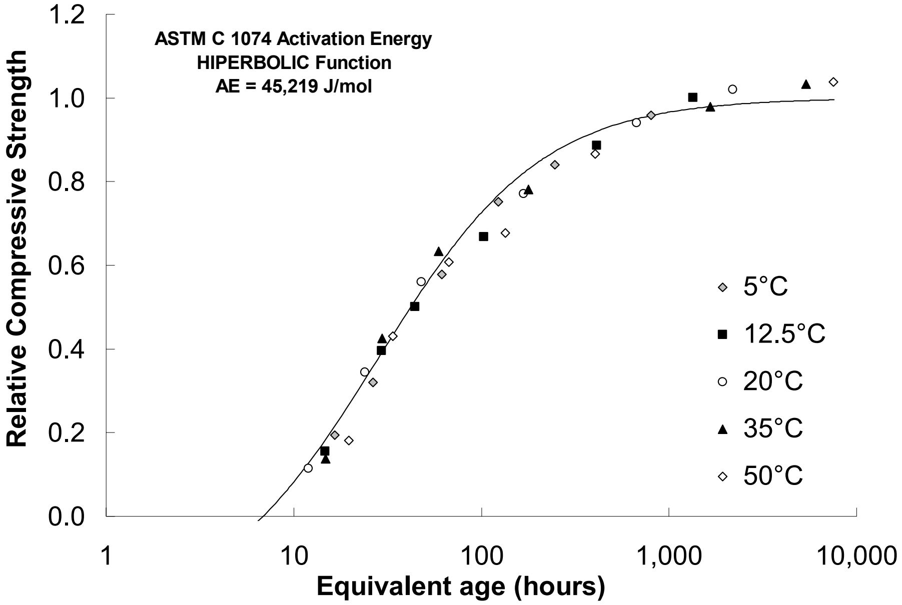

Figure 5-23: Use of the modified maturity method (Hyperbolic strength-maturity function)

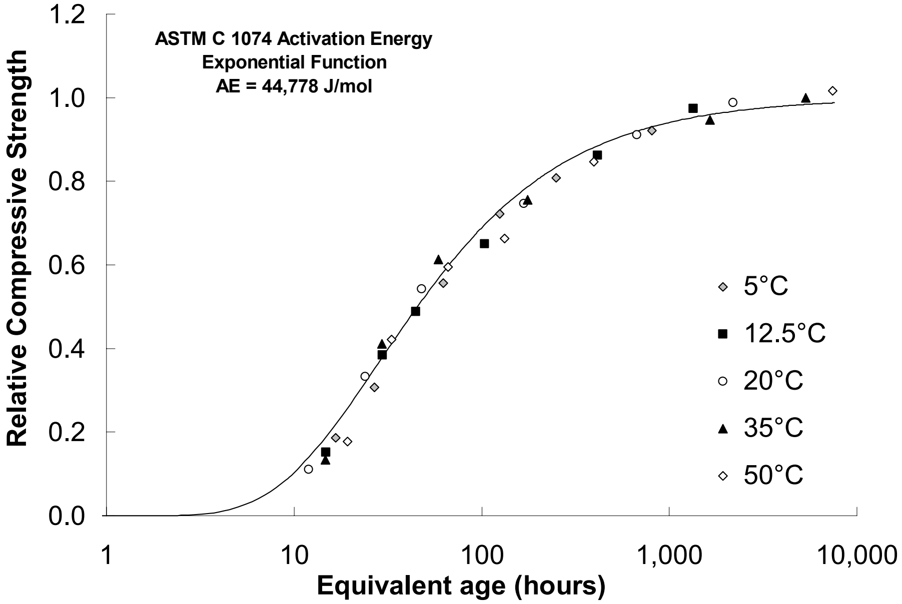

Figure 5-24: Use of the modified maturity method (exponential strength-maturity function)

However, concerning the ***modified maturity rule*** Carino (1991) provides the following comments that directly affect the practical implementation of this method to predict strengths:

> The significance of this modified maturity rule is that if one measures only the temperature of concrete while it is curing, only the relative strength gain can be estimated. Additional information is needed to estimate absolute strength values.

From the statement above, one may conclude that the modified maturity method requires knowledge of the ultimate strength at the temperature that the strength is to be predicted. This is not possible when one has to predict the strength, since the ultimate strength at high curing temperatures is unknown and insufficient information is available. This method is, therefore, only appropriate for use when other means of measuring the in place strength of concrete, such as the pullout method, is available. Carino's modified maturity method is, therefore, not appropriate for the application under evaluation.

This aspect is realized by Chanvillard and D'Aloia (1997) and Kjellsen and Detwiler (1993), which defined the relative strength gain in terms of the **28-day strength reached through an isothermal curing at the reference temperature**. In a later publication, Carino (1997) recommends this approach to estimate the relative strength. However, this definition of relative strength does not use the modified maturity rule, since the cross-over effect will cause the relative ultimate strength at high curing temperatures to be less than one. For the data shown in Table 5-2, the relative ultimate strength gain at a temperature of 50°C will be 0.81 (46/57). This would imply that results similar to that shown in Figures 5-21 and 5-22 are obtained, but with the vertical axis normalized with respect to the 28-day strength reached when the specimens are cured at the reference temperature.

Modifications to the Traditional Maturity Approach

In order to obtain accurate prediction of compressive strengths at all temperatures, Kjellsen and Detwiler (1993), Chanvillard and D'Aloia (1997), and Cervera et al. (1999) provide methods to modify the classic maturity method. The methods will briefly be described, however, the implementation of these methods are beyond the scope of this report, since they address strength prediction and not the development of hydration.

1. Kjellsen and Detwiler (1993):

Kjellsen and Detwiler (1993) modified the fundamental principle of the activation energy, by defining it in terms of the hydration temperature and relative strength development. Their motivation is based on the results shown in Figure 5-25, which clearly indicates that the activation energy varies as a function of the curing temperature and relative strength. This figure was obtained by determining the best-fit exponential strength-maturity curves, and then determining the instantaneous rate of reaction at different temperatures and equal relative strengths. From this, the activation energy values as shown in Figure 5-25 were obtained. The relative strength is defined in terms of the compressive strength at 28-day strength reached through isothermal curing at the reference temperature.

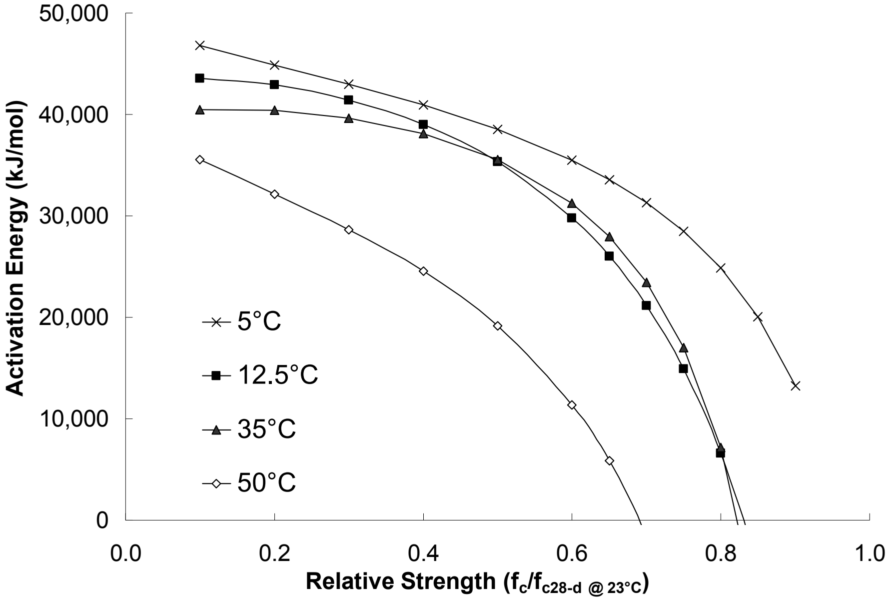

Figure 5-25: Activation energy values in terms of relative strength and temperature (Kjellsen and Detwiler, 1993)

This method provides an accurate estimate of the strengths at all curing temperatures. However, the method requires an iterative solution to the predicted strength, since the value of the relative strength is unknown when the current strength is to be estimated. This problem can be overcome when the maturity is calculated over small time intervals, and the error made by using the relative strength from the previous time step is reasonably small. This method defines the activation energy as a function of the concrete temperature, which is not consistent from the original Arrhenius definition point of view. However, the authors provide a detailed discussion why this effect is possible when the development of mechanical properties are considered.

Figure 5-25 presents some important aspects concerning the nature of the activation energy for strength prediction purposes. Since the curing temperature affects the long-term strength, the rate of strength development at equal relative strengths is decreased at later ages, irrespective of the curing temperature. It further indicates that the activation energy for strength determination is lower at higher curing temperatures. This conclusion is similar to the activation energy formulation developed by Freiesleben Hansen and Petersen (1977) and Jonasson (1984), which produces higher activation energies at lower curing temperatures (see Figure 3-5).

2. Chanvillard and D'Aloia (1997):

Chanvillard and D'Aloia (1997) introduce a strength adjustment factor, which modifies the long-term strength as a function of curing temperature. The 28-day strength is defined as a linear decreasing function of the isothermal curing temperature as shown in Equation 5-10.

$$f_{c28}(T_c) = f_{c28}(T_{ref}) \cdot \left(1 - S_f \cdot (T_c - 20)\right) \qquad \textit{Equation 5-10}$$

where, T_c = the isothermal curing temperature (°C),
T_{ref} = the reference isothermal curing temperature (°C),
$f_{c28}(T_c)$ = the 28-day compressive strength under curing at T_c (psi),
$f_{c28}(T_{ref})$ = the 28-day compressive strength under curing at T_{ref} (psi), and
S_f = strength reduction factor.

In this formulation, it is assumed that concrete mixture proportions are taken into account in $f_{c28}(T_{ref})$, and that the mixture proportions do not affect the strength loss factor (S_f). By taking the strength loss factor equal to zero, the original maturity function can be obtained. Equation 5-10 is now used to determine the relative strength as proposed in the modified maturity method (Carino, 1991). After calibration of the model to experimental data, a strength loss factor of 0.01 was recommended, which corresponds to a 20% strength loss at 40°C as compared to a reference temperature of 20°C.

3. Cervera et al. (1999):

In this method Cervera et al. (1997) introduce a concept of an aging function to predict the development of compressive strengths at different temperatures. The model is formulated in terms of the degree of hydration development and the curing temperature. It can, therefore, not be implemented without knowing the degree of hydration development for the specific mixture under investigation. Their aging factor, which has similarities to a strength reduction factor, is defined as follows:

$$\lambda(T_c) = \left(\frac{100 - T_c}{100 - T_{ref}}\right)^{n_T} \qquad \textit{Equation 5-11}$$

where, $\lambda(T_c)$ = the strength reduction factor when cured at T_c, and
n_T = a material property determined from experimental results.

Cervera et al. determined the degree of hydration from adiabatic test results and calibrated their aging factor for the experimentally determined cross-over effect. They obtained an n_T of 0.40 for the data of Kjellsen and Detwiler (1993). Figure 5-26 compares the strength reduction factors as formulated in Equations 5-10 and 5-11. The strength reduction should not directly be compared to each other, since they are applied in different ways, but one can notice that at an isothermal curing temperature of 50°C the maximum 28-day strength reduction is, respectively, 0.7 and 0.83 by Equations 25 and 26.

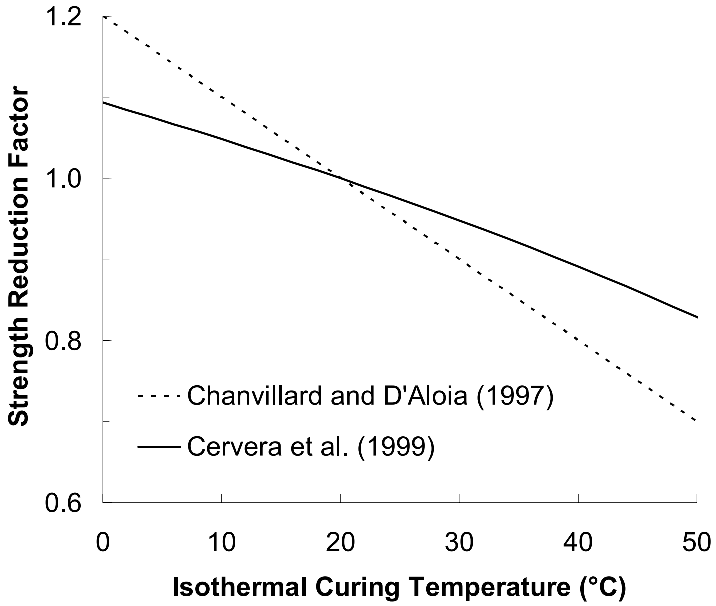

Figure 5-26: Comparison of strength reduction factors

5.2.5 Activation Energy: Conclusions and Recommendations

After all the above factors are considered, it may be observed that there is disparity in the literature concerning the selection of the appropriate activation energy. The primary points of disparity can be summarized by the following questions, which will be addressed:

1. Should the same activation energy be used for the prediction of mechanical properties and the development of hydration?

From the information presented, it may be concluded that different activation energies should be used when mechanical properties and the development of hydration is considered. In Section 5.2.4, hydration and strength activation energy values of 39,014 J/mol and 44,778 J/mol, respectively, were calculated for the same materials. From Figures 5-14 and 5-18, it may be concluded that the Arrhenius rate theory for chemical reactions applies to the hydration of portland cement. From the data evaluated in Section 5.2.2 and 5.2.3, it was concluded that the cross-over effect develops only when mechanical properties are considered and not when the degree of hydration development is considered. The Freiesleben Hansen and Pedersen activation energy formulation is developed for strength prediction, and still many authors recommended it for the prediction of the hydration development (RILEM Technical Committee 119-TCE, 1981; Radjy et al., 1994).

> ***Recommendations:*** For the prediction of the degree of hydration at temperatures other than the reference temperature, the appropriate activation energies should be determined based on heat of hydration tests, as discussed in Section 3.2.4. The use of an activation energy determined from strength test is not recommended for the use of predicting hydration development.
>
> In this study, the activation energy to predict the degree of hydration at different temperatures will be based on the results from hydration test results. Many compressive strength tests according to the ASTM C 1074 procedure have been conducted for this study, and these data are not appropriate for use of hydration prediction. However, the data will still be analyzed to present activation energy values to use for strength prediction purposes.

2. Does the activation energy change as a function of temperature or degree of hydration?

Tables 3-1, 3-2, and 3-3, presented in Section 3.2.2, presented numerous activation energy values that are constant and independent of temperature. All these activation energies are consistent with the original Arrhenius definition of rate processes since they are independent of the concrete temperature. It was further shown that some researchers have defined the activation energy as a function of the curing temperature (Equations 3-4, 3-8, and 3-10). In Section 5.2.4.2, degree of hydration data from Kjellsen and Detwiler (1993) was analyzed. It was shown in Figure 5-16 that a good prediction ($r^2 = 0.980$) of the degree of hydration at different temperatures can be predicted by using a **constant activation energy**.

Ma et al. (1994) performed isothermal calorimeter tests at a wide range of curing temperatures, and the Arrhenius plot from the data showed no temperature dependency. After the analysis on the Lerch and Ford (1948) data set, it was shown that the Arrhenius rate theory for chemical reactions applies to the hydration of portland cement. The activation energy for hydration prediction may be modeled independent from the curing temperature.

The calculation of activation energy (temperature sensitivity) values for strength prediction is complicated by the loss of strength due to curing at high temperatures. Long-term mechanical properties are affected by high curing temperatures, but the development of structure and hydration remains unaffected. Kada-Benameur et al. (2000) stated that the activation energy for hydration reflects the chemical mechanism of the Arrhenius theory for rate processes, but not the development of mechanical strength.

The evidence is not conclusive, however the origin of the disparity may be attributed to the difference in behavior when mechanical properties and degree of hydration data are analyzed. The activation energy formulation proposed by Freiesleben Hansen and Pedersen (1977) was developed to predict strength results at different temperatures. The fact that the cross-over effect occurs at high curing temperatures, lead to a reduced rate of strength gain, and this may the reason why the activation energy for strength prediction is lower at high temperatures and visa versa.

> ***Recommendations:*** In this study, the activation energy to predict the ***degree of hydration*** at different temperatures will be assumed to be constant and independent of the curing temperature. This is in accordance with the Arrhenius definition of rate processes in chemical reactions. This assumption will be reevaluated during the data analysis process.
>
> In order to calculate the activation energy for ***strength development***, the data analyzed indicate that the activation energy should be determined as a function of temperature, and relative strength. When constant activation energy values (ASTM C 1074) are used with the traditional maturity method, strength limits should be determined for the period over which accurate predictions are expected. Alternatively, the temperature range over which the maturity method is applied should be made smaller, by developing the strength-maturity relationship at a temperature closer to the anticipated temperatures under field conditions.

3. ***Should the same activation energy be used irrespective of the type of cementitious materials?***

Some authors presented different activation energy values for different cementitious materials, and others recommend the use of the same values for all cementitious systems. RILEM Technical Committee 119-TCE recommends the Freiesleben Hansen and Pedersen formulation for use with all cements. Due to the difference in mechanical behavior of different cementitious materials, it may be expected that more variation in activation energies for strength prediction may be present. The results obtained from the analysis of the Lerch and Ford (1948) data set showed that different activation energy values were obtained for the Type I and Type III cement. Figure 5-18 clearly indicates that the slope of the Arrhenius plot is different for different cements.

> ***Recommendations:*** It is recommended to determine the appropriate activation energy value based on the chemical composition of the cement. The data set of Lerch and Ford will be analyzed to determine the activation energy values for different cements.

4. Should the classic maturity method be used to predict long-term concrete strength?

From the data presented in Sections 5.2.2 and 5.2.4.3, it may be concluded that the traditional maturity method may over predict the long-term concrete strength at high curing temperatures when a concrete mixture is used that exhibits a loss of strength at such temperatures. The period over which the traditional maturity method provides accurate results should be determined for the specific mixture. In some of the data analyzed, the cross-over effect occurred as early as an equivalent age of 68 hours.

> ***Recommendations:*** The cross-over effects limits the accuracy of the test results under high temperature conditions. From the compressive strength tests results performed according to the ASTM C 1074 procedure, limits should be developed for which the traditional maturity method will produce acceptable results.

5.2.6 Development of a General Hydration Activation Energy Model

During this study, laboratory tests were performed in accordance with the recommendation of ASTM C 1074, which is based on the results obtained from **compressive strength tests**. When the lab testing was undertaken, it was reasoned that the activation energy could be determined from the results of strength test, which was the approach adopted by other researchers. **However, due to the cross-over effect seen in strength test results, which is not observed in heat of hydration test results, the activation energy results obtained from mechanical data are not applicable for use to predict the degree of hydration development at different temperatures.**

It is for these reasons that the activation energy, for the prediction of hydration development, will be based on heat of hydration test results obtained from past literature. The data set published by Lerch and Ford (1948) will be used for this purpose.

5.2.6.1 *Lerch and Ford Data Set*

The data set of Lerch and Ford (1948) represents one of the largest data sets available on the development of heat of hydration for different U.S. cements. The study included 27 different cements, ground from clinker produced at 14 different plants. All five portland cements currently specified in ASTM C 150 were tested and heat of hydration values were determined. These results for the non-air-entraining cements will be analyzed, which include eight Type I cements, five Type II cements, three Type III and IV cements, and one Type V cement. The chemical composition and physical properties of each of the cements are summarized in Table 5-5. The reader is referred to this publication if more information is required about the properties of the cement.

Lerch and Ford (1948) performed heat of hydration tests on pastes, with the following two techniques as previously discussed in Section 3.2.4:

1. ***Conduction calorimetry:*** Pastes were cured for up to 72 hours, at isothermal temperatures of 4.4°C, 23.9°C, 32.2°C, and 40.6°C. In US customary units the curing temperatures were 40°F, 75°F, 90°F, and 105°F.

2. ***Heat of solution method:*** Pastes with a water-cement ratio of 0.4 by weight were cured at 21.1°C (70°F) for up to a one year period. The test is performed at selected intervals and produces results that are comparable to that obtained with condition calorimetry. This test is typically suited to estimate the heat of hydration over extended periods of time (months).

Table 5-5: Chemical and physical properties of the cements tested by Lerch and Ford (1948)

ID	**Bogue Compounds**				**Chemical Composition**					**Blaine**
	C_3S	**C_2S**	**C_3A**	**C_4AF**	**SO_3**	**Free CaO**	**MgO**	**Na_2O**	**K_2O**	**m^2/kg**
	TYPE I CEMENTS									
11	50.0	22.0	12.1	7.2	1.6	0.40	3.70	0.21	0.51	343.6
12	45.0	28.0	12.6	7.3	1.6	0.10	3.10	0.28	0.40	327.6
13	50.0	26.0	10.1	6.5	1.6	1.60	1.10	0.04	0.19	342.8
14	42.5	32.0	8.2	9.2	1.7	0.20	2.50	0.06	1.30	342.4
15	64.5	10.0	12.1	7.5	1.9	0.40	0.80	0.08	0.23	322.9
16	53.5	21.0	7.5	10.7	1.7	0.70	2.10	0.23	0.46	326.1
17	52.0	23.0	10.4	9.3	1.7	0.40	1.10	0.08	0.43	398.5
18	44.5	28.0	13.2	6.8	1.8	0.30	2.60	0.12	0.13	326.8
Av.	*50.3*	*23.8*	*10.8*	*8.1*	*1.7*	*0.51*	*2.13*	*0.14*	*0.46*	*341.3*
	TYPE II CEMENTS									
21	40.0	41.0	6.4	9.7	1.2	0.70	1.30	0.22	0.40	289.1
22	41.5	33.5	6.6	11.7	1.4	0.10	3.20	0.24	0.37	306.5
23	51.0	24.0	3.7	16.6	1.5	0.40	0.90	0.59	0.14	310.9
24	41.0	29.0	5.4	14.8	1.8	0.90	3.10	0.06	1.30	369.7
25	34.0	39.0	4.7	14.9	1.9	0.20	2.20	0.21	0.54	328.7
Av.	*41.5*	*33.3*	*5.4*	*13.5*	*1.6*	*0.46*	*2.14*	*0.26*	*0.55*	*321.0*
	TYPE III CEMENTS									
31	56.0	17.0	10.8	6.4	2.2	1.50	3.30	0.23	0.22	579.5
33	60.0	13.0	10.4	7.7	2.3	1.80	1.50	0.21	0.44	527.2
34	64.0	10.5	5.7	10.1	1.7	2.30	2.50	0.28	0.28	496.9
Av.	*60.0*	*13.5*	*9.0*	*8.1*	*2.1*	*1.87*	*2.43*	*0.24*	*0.31*	*534.5*
	TYPE IV CEMENTS									
41	20.0	51.0	4.5	15.2	2.0	0.40	3.00	0.06	1.19	367.9
42	27.0	55.0	3.5	8.2	1.5	0.20	1.80	0.16	0.26	350.1
43	25.0	48.0	6.2	13.8	2.1	0.10	1.60	1.00	0.08	384.6
Av.	*24.0*	*51.3*	*4.7*	*12.4*	*1.9*	*0.23*	*2.13*	*0.41*	*0.51*	*367.5*
	TYPE V CEMENT									
51	41.0	39.0	3.7	10.0	1.4	0.50	1.70	0.08	0.22	348.3

The data was analyzed by Equation 3-12 to determine the maximum heat of hydration for each of the cements tested by Lerch and Ford. The temperature at which the heat of solution tests was performed, i.e. 21.1°C, was used as the reference temperature for this analysis. The degree of hydration at the reference temperature was determined by using the first 72 hours as tested by conduction calorimeter and the heat of solution tests thereafter. The heat of solution and the condition calorimetry tests has been shown to produce comparable results (Bogue, 1947; van Breugel, 1991). Since the conduction calorimeter test were performed at 23.9°C, this test data were converted into equivalent results at 21.1°C through the maturity concept. Since the activation energy was not known, an iterative procedure was followed throughout the analysis, until the assumed and final calculate activation energy values converged.

For the data produced by Lerch and Ford, the conduction calorimeter test results obtained after 3 days were on average five percent lower as compared to the heat of solution method, and the conduction calorimeter data were corrected for this inconsistency. Test results for the conduction calorimeter were reported from ages as early as 5, 10, 30, and 60 minutes. As the test results under an hour generally stayed constant, these points were not included in the analysis as this is still part of the dormant period. In this study, the heat developed after the dormant stage is of importance.

5.2.6.2 *Evaluation of the Arrhenius Formulation for Lerch and Ford Data set*

In this section, the Arrhenius principle for rate process will be evaluated based on the heat of hydration data from Lerch and Ford (1948). In order to evaluate the Arrhenius principle, the linearity of Arrhenius plot will be statistically reviewed. If the heat of hydration data are found to obey the Arrhenius principle, then a constant activation energy that is independent of the hydration temperature may be used.

In Section 5.2.4.2, the procedure to develop the Arrhenius plot was presented in a stepwise format. It was found that the heat of hydration data from Kjellsen et al. (1992) followed the Arrhenius principle. In this section, some of the data of Lerch and Ford were analyzed, and the Arrhenius plot for Cement 12 and 33 was evaluated and presented. It was shown that the data for both Cement 12 and 33 followed the Arrhenius principle during hydration at different temperatures. In the rest of this section, all the non-air entrained cements presented by Lerch and Ford will be evaluated by the procedure outlined in Section 5.2.4.2.

The best-fit degree of hydration curve for the experimental data obtained at the **reference temperature of 21.1°C** was determined. The degree of hydration was defined with the exponential function as shown in Equation 3-21. The best fit parameters for this equation obtained for all the cements are shown in Table 5-6. The coefficient of determination (r^2) is displayed to quantify the goodness of fit obtained with the model. Note that all the r^2 are either 0.99 or higher, showing that the exponential function provides a good representation of the degree of hydration data at the reference temperature.

Table 5-6: Hydration parameters for exponential degree of hydration model (Equation 3-21)

ID	**Isothermal Curing Temperature**									**H_u [a] (J/g)**
	21.1°C			**4.4°C**		**32.2°C**		**40.6°C**		
	β	τ (hours)	r^2	$\tau_{4.4}$ (hours)	r^2	$\tau_{32.2}$ (hours)	r^2	$\tau_{40.6}$ (hours)	r^2	
	TYPE I CEMENTS									
11	0.479	25.9	1.00	87.4	0.96	10.3	0.98	7.1	0.99	488
12	0.588	30.5	0.99	83.3	0.77	16.8	0.99	10.1	1.00	475
13	0.394	33.5	0.99	87.8	0.98	17.8	0.99	12.6	0.97	471
14	0.482	17.8	1.00	53.3	0.97	8.1	1.00	6.5	0.98	440
15	0.537	18.5	0.99	64.5	0.96	8.0	0.97	6.1	1.00	508
16	0.462	23.2	0.99	62.9	0.97	11.8	0.98	4.9	0.92	469
17	0.515	23.0	0.99	68.3	0.82	11.2	0.99	7.1	0.99	474
18	0.533	24.3	0.99	85.5	0.94	12.7	0.99	8.8	0.99	475
	TYPE II CEMENTS									
21	0.440	38.7	1.00	133.8	0.81	21.6	1.00	14.3	1.00	430
22	0.500	41.8	0.99	101.6	0.76	22.7	0.98	13.2	1.00	438
23	0.427	38.7	0.99	110.1	0.95	21.4	0.98	16.3	1.00	441
24	0.379	27.8	1.00	92.0	0.97	13.6	1.00	10.1	0.99	437
25	0.405	30.3	1.00	66.7	0.96	15.5	0.99	9.1	0.99	407
	TYPE III CEMENTS									
31	0.485	11.1	0.99	33.0	0.97	4.1	0.97	2.5	0.93	504
33	0.451	11.6	1.00	44.9	0.98	5.1	0.98	2.8	0.93	504
34	0.397	15.4	0.99	47.6	0.96	7.0	0.98	4.9	0.95	498
	TYPE IV CEMENTS									
41	0.369	30.2	1.00	93.3	0.94	16.4	0.99	10.5	0.99	378
42	0.370	48.2	0.99	128.3	0.96	30.4	0.97	20.9	0.97	370
43	0.409	30.3	0.99	83.0	0.75	12.7	0.99	8.2	0.99	389
	TYPE V CEMENT									
51	0.401	34.7	0.99	98.2	0.96	23.2	0.99	14.7	0.99	410

Note: [a] Calculated with Equation 3-12

Next, the hydration shape (β) parameters, determined at the reference temperature, were used as constants in the degree of hydration curves at the other test temperatures. This is necessary, since this parameter remains unchanged at all temperatures when the maturity method is used. Next, the best-fit hydration time parameters (τ_T) at all the other test temperatures are determined. Table 5-6 presents the hydration time parameter and r^2 values obtained. Figures 5-27 and 5-28 present typical results obtained form the regression analysis. The regression analysis for the temperature of 32.2°C and 40.6°C produced a good fit of the data, since the r^2 values ranged between 0.92 and 1.00.

The lowest r^2 values were obtained for the degree of hydration at the low curing temperature (4.4°C), and they ranged between 0.75 and 0.98. The reason for the apparent less accurate fit may be identified on Figure 5-27. This figure indicates that the degree of hydration before 12 hours remains constant, due to the low amounts of heat being released. The model assumes these early-age values will start from zero, however, this does not occur in the experimental results. This phenomenon may be attributed to the accuracy of the conduction calorimeter when low amounts of heat are being developed. These points will, however, be used in the analysis since r^2 values of 0.75 and higher are still acceptable.

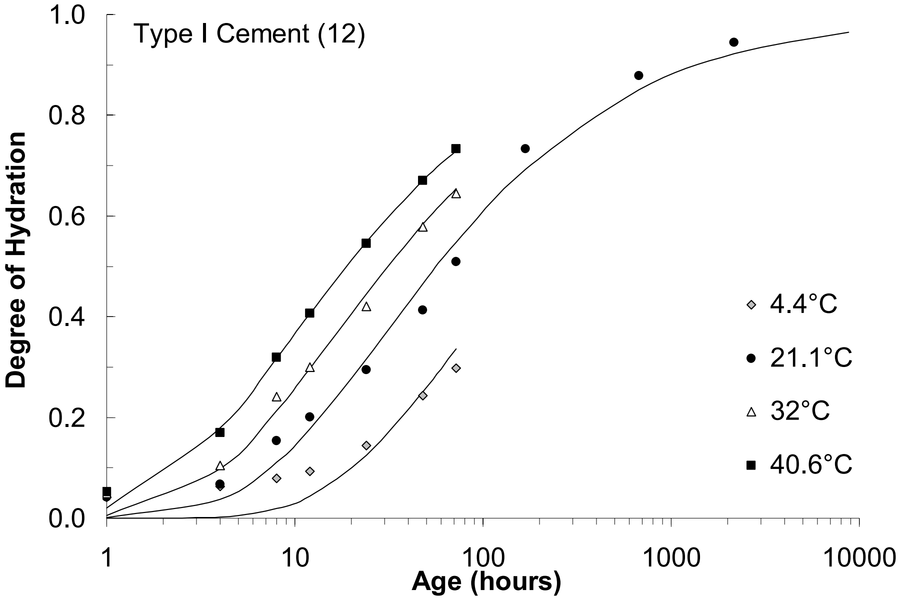

Figure 5-27: Best fit degree of hydration curves for Type I cement (12) of Lerch and Ford (1948)

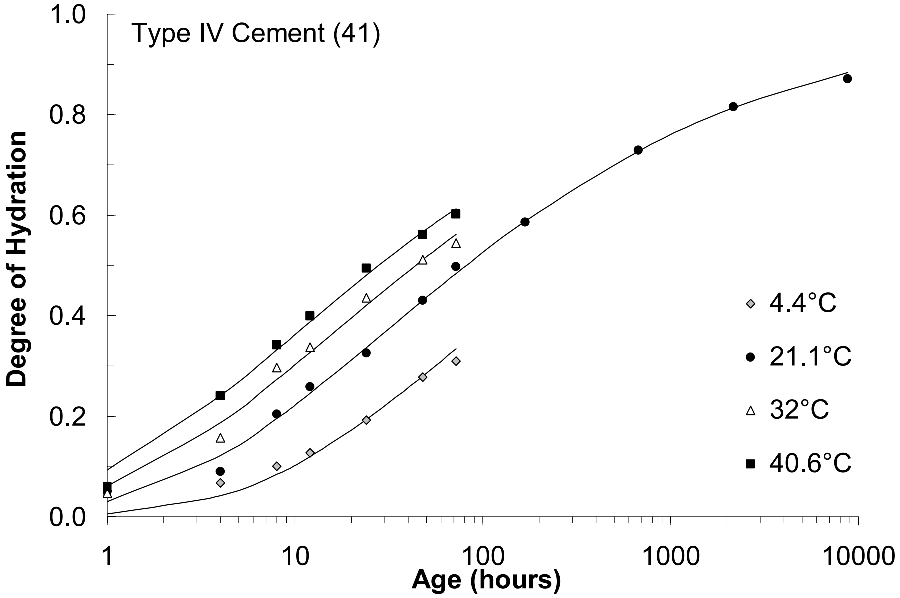

Figure 5-28: Best fit degree of hydration curves for Type IV cement (41) of Lerch and Ford (1948)

The data in Table 5-6 contain some valuable information, when the results of the regression analysis for different cements are compared. In Section 3.2.6, it was shown that the due to the formulation of the exponential model, the earlier the hydration time parameter, the more rapid the hydration. This parameter should, therefore, decrease with an increase in curing temperature, and this can be seen in Table 5-6. The time parameters for the Type III cements (high early strength) are the smallest, indicating that these cements will hydrate the fastest. The next smallest hydration time parameters can be associated with the Type I cements, while the largest time parameters can be associated with the Type IV (low heat of hydration) and V cements. By considering the hydration time parameter, the type of cement can by identified. It should be noted that the value of the hydration slope parameter (β) plays a role on the shape of the hydration curve, but its value is less informative.

With the data shown in Table 5-6, the Arrhenius plot can now be constructed for each of the cements. The Arrhenius plot can be obtained by plotting the natural logarithm of the hydration time parameters versus the inverse of the corresponding absolute curing temperature. This concept was previously shown to be true for the exponential function, and was derived in Equation 5-9. Earlier Figure 5-18 presented the Arrhenius plot for a Type I cement (12) and Type III cement (33). Figures 5-29 and 5-30 present the Arrhenius plot obtained for four more cements of this data set. All six the cements shown on these plot exhibit a strong linear trend on the Arrhenius plot.

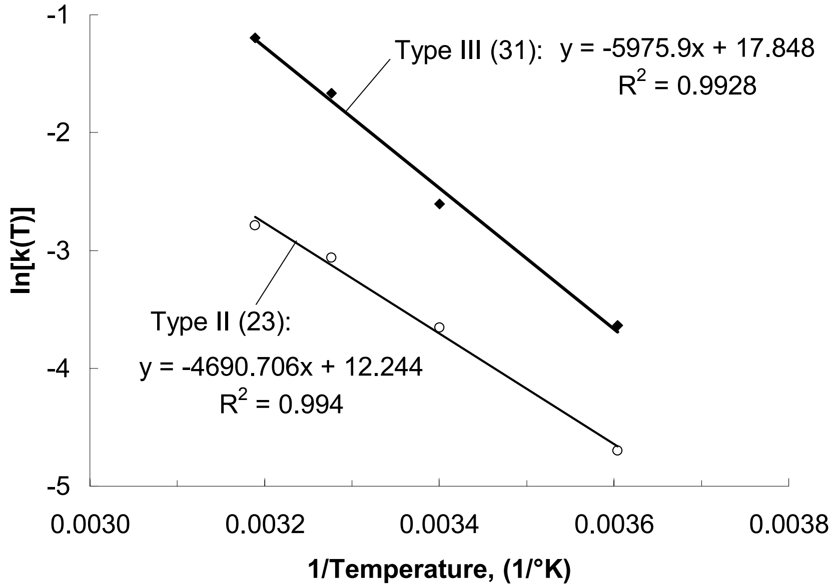

Figure 5-29: Arrhenius plot for Type II cement (23) and Type III cement (13) of Lerch and Ford (1948) data set

Table 5-7 presents the activation energy obtained for each of the cements tested, the r^2 value obtained for the linear regression line, and the average activation energy for each cement type. The activation energy values range from 36,132 J/mol to 54,467 J/mol, which is within the range reported by previous authors.

Table 5-7 indicates that the activation energy values are influenced by the chemical composition of each cement type. The order of the average activation energy per cement type, arranged from high to low, is as follows: Type III, Type I, Type II, Type V, and Type IV. This is significant since this order is similar that one would assign the rate of early-age hydration development. This provides a firm answer to one of the question posed from the disparity identified in the literature. The fact that the Type III cement has the highest activation energy is from a performance standpoint noteworthy, since it already has the highest rate of hydration and at higher temperatures, this will be exacerbated even further.

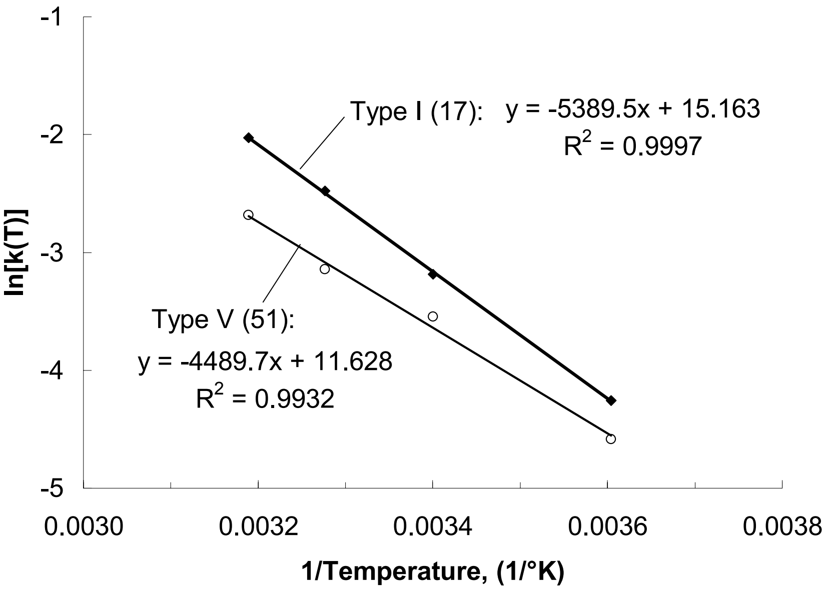

Figure 5-30: Arrhenius plot for Type I (17) and Type V (51) cement of Lerch and Ford (1948)

Table 5-7 further presents the r^2 values obtained for the linear fit of the Arrhenius plot. The lowest r^2 value obtained for the 20 cements was 0.976, for cement 16. From the high r^2 values shown in Table 5-7, and the strong linear trend shown by the data in Figures 5-4, 5-29 and 5-30, it may be concluded that the Arrhenius rate theory for chemical reactions additionally applies to the hydration of portland cement. **During hydration modeling, the activation energy for application in the maturity method may, therefore, be modeled independent from the curing temperature.** Chanvillard and D'Aloia (1997) come to a similar conclusion, as they mention:

> By defining the hydration degree in terms of relative quantity of heat already generated, it can be noted that the relative quantity of generated heat versus age curves are affine, what ever the isothermal curing temperature of the concrete is, and that the affinity ratio follows the Arrhenius law.

Table 5-7 indicates that the activation energy is affected by the chemical composition, and in the following section a general activation energy model will be developed based on statistical methods.

5.2.6.3 *Multivariate Regression Analysis*

The data set was prepared for analysis with the SAS program (Release 8.2), which is distributed by the SAS Institute Inc., Cary, NC, USA. The multivariate regression analysis was performed in the following three stages:

Table 5-7: Activation energy for cements tested by Lerch and Ford (1948)

ID	r^2 value	Activation Energy (J/mol)	Average Activation Energy (J/mol)
	TYPE I CEMENTS		
11	0.994	51,861	45,271
12	0.999	42,171	
13	0.999	38,926	
14	0.989	44,039	
15	0.990	47,315	
16	0.976	46,795	
17	1.000	44,810	
18	0.995	46,256	
	TYPE II CEMENTS		
21	0.995	44,899	41,788
22	0.994	40,369	
23	0.994	39,000	
24	0.993	45,185	
25	0.988	39,487	
	TYPE III CEMENTS		
31	0.993	49,686	49,955
33	1.000	54,467	
34	0.997	45,711	
	TYPE IV CEMENTS		
41	1.000	43,824	39,978
42	0.997	36,132	
43	0.994	46,676	
	TYPE V CEMENT		
51	0.993	37,329	37,329

1. Identify most significant variables:

For this analysis of variance analysis (ANOVA), the chemical and physical properties of the cements were taken as explanatory variables, and the activation energy determined for the cements shown in Table 5-7 was taken as the response variable. Since not all the chemical properties of the cements are independent of each other, their dependence was tested for simultaneous use in the model, by constructing and inspecting the correlation matrix of variables. In this stage, the relative contribution of each explanatory variable towards the overall regression model was assessed. This step enabled the selection of the explanatory variables that should be used in the model. Initial estimates of the nonlinear regression model were determined.

2. Develop Activation Energy model:

For this multivariate regression analysis, the chemical and physical properties of the cements were taken as independent variables, and the degree of hydration values at all temperatures other than the reference temperature were used as response variables. Based on the independent variables selected and initial values selected in stage 1, the nonlinear analysis was developed to determine the best-fit statistical values of each of the independent variables.

3. Evaluate Goodness of Fit:

The goodness of fit will be evaluated by means of the coefficient of determination (r^2), the mean square of the error (s^2), and tendencies from the residual plots (Barnes, 1994). A high r^2, a low s^2, and a random distribution of the unexplained error are desired. Residual plots are commonly used to diagnose nonlinearity or non-constant error variance.

After some initial analysis, it was determined that the data could best be modeled through the use of a nonlinear relationship. The data set was transformed into a linear relationship by taking the natural logarithm of both the independent and response variables. After the logarithmic transformation, the transformed data set can be analyzed by means of a multivariate linear regression analysis. This allows the regression analysis to fit a power function to the response variables. This can be shown to be valid when we consider the case of two independent parameters x_1, and x_2 that have a nonlinear relationship with regards to the response variable, y, as shown in Equation 5-12. By taking the natural logarithm on both sides of Equation 5-13, this equation is transformed into the two parameter multivariate linear model as shown in Equation 5-13. After comparison of equation 5-12 and 5-13, it may be seen that the linear model is obtained by taking the natural logarithm of the response and independent variables: $Y=\ln(y)$, $X_1 = \ln(x_1)$, and $X_2 = \ln(x_2)$.

$$y=(x_1)^{c_1} \cdot (x_2)^{c_2} \cdot e^{c_3} \qquad \textit{Equation 5-12}$$

where, y = the response variable,

x_i = independent variables, and

c_i = regression constants.

Take the natural logarithm of Equation 5-12:

$$\begin{aligned} \ln(y) &= \ln\left((x_1)^{c_1} \cdot (x_2)^{c_2} \cdot e^{c_3}\right) \\ &= \ln(x_1)^{c_1} + \ln(x_2)^{c_2} + \ln e^{c_3} \\ &= c_1 \cdot \ln(x_1) + c_2 \cdot \ln(x_2) + c_3 \\ Y &= c_1 \cdot X_1 + c_2 \cdot X_2 + c_3 \end{aligned}$$

Equation 5-13

The transformation above adds other statistical advantages to the regression analysis since it ensures that some of the underlying assumptions (homogeneity of variance) of the linear regression analysis are met. The only caution is with regards to the error structure of the transformed model, since the error structure is modified and this should be evaluated after the analysis is completed (Barnes, 1994). This will be verified by evaluating tendencies of the residuals, by means of scatter plots of the residuals. A plot of the residuals versus the predicted values is a useful diagnostic tool used in regression analysis and will identify poorly specified models or heterogeneity of variance. In the following section, the results of the statistical analysis will be presented.

5.2.6.4 *Activation Energy Model Development*

The statistical process outlined above was used to analyze the Lerch and Ford data set (1948). The analysis results from the SAS program are presented in Appendix A and only the final results will be presented herein.

The explanatory variables used in nonlinear analysis were selected by developing a regression model to predict the activation energy for each cement type. This allows the development of a linear relationship, but with only 20 data points. The form of this model will then be used to develop the final nonlinear model based on 420 data points. With the r^2 selection method, the significance of individual and combinations of explanatory variables was evaluated. It was found that with the use of three parameters in the regression model, an r^2 of 0.69 could be achieved. This coefficient of determination was considered appropriate only to identify the most significant parameters. After some iterative analysis, the three parameter model chosen was determined to be a function of the following variables:

$$E = f(p_{C3A}, p_{C4AF}, \text{Blaine},)$$

where, p_{C3A} = weight ratio of C_3A ito total cement content,
p_{C4AF} = weight ratio of C_4AF ito total cement content, and
Blaine = Blaine value, specific surface area of cement (m^2/kg).

Based on engineering judgment, it may be reasoned that two of the three parameters shown in the equation above are intuitively appropriate. Both high C_3A and Blaine value are associated with cements with high early-age strength gains such as Type III cements. ASTM C 150 limits the amount of C_3A in the low heat cements, such as Type II and IV cements. However, the role of the C_4AF compound is unexpected. The one parameter results obtained from the r^2 selection method (see Appendix C) reveals that with regards to the activation energy, the single most significant parameters were statistically ranked as follows: C_3A, C_2S, $S0_3$, Blaine, C_3S, free lime content, C_4AF, equivalent alkalies (Na_2O + $0.658K_2O$), and MgO. This indicates that the C_4AF content, as an individual parameter, does not provide a good estimate of the activation energy. However when its interaction with the other two parameters are incorporated it produces an accurate fit of the activation energy response.

With the three independent variables selected, initial values for the regression model were determined with a multivariate linear regression analysis. In Appendix C the output of the SAS GLM (General Linear Model) analysis is provided, which contains the summary of fit table, which provides the mean square of the error (s^2, Root MSE) and r^2. The analysis of variance (ANOVA) table provides a summary regarding the sources of variation in the data. From the small p-value (0.0003), the null hypothesis can confidently be rejected, and it is determined that there is a statistically significant relationship between all the independent variables (C_3A, Blaine, and C_4AF) and the activation energy (Barnes, 1994). The ANOVA results further present the Type I Sum of Squares error (Type I SS), which is the incremental error sum of squares for the model as each explanatory variable is added. From the F-statistic for this test, it may be concluded that the model is incrementally improved as each explanatory variable is added.

The Type III Tests table presents sums of squares error (Type III SS) associated with the estimated regression coefficients of the model. The Type III error provides an indication of the increase in the model sum of squares due to adding the variable to a model that already contains all the other variables in the model (SAS, 2001). The Type III error evaluates the assumption that the explanatory variables are uncorrelated. From the values of the F-statistic it may be concluded that the explanatory variables are uncorrelated and the use of all three are statistically significant. Based on the statistical results, the multivariate regression model shown in Equation 5-14 was developed. The r^2 for this model was 0.678. The scatter plot of the experimentally determined values listed in Table 5-7, versus the predicted activation energy values are shown in Figure 5-31. Figure 5-31 indicates that the model captures the trend in activation energy values.

$$E = {p_{C_3A}}^{0.28} \cdot {p_{C_4AF}}^{0.25} \cdot Blaine^{0.34} \cdot e^{10.037} \qquad \textit{Equation 5-14}$$

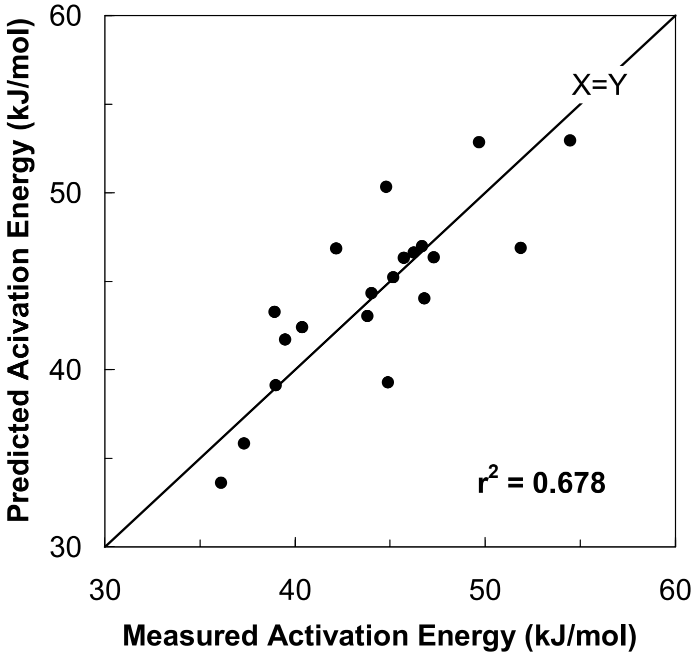

Figure 5-31: Experimentally determined versus the predicted activation energy values

In order to develop the best-fit activation energy model that applies to all the data collected by Lerch and Ford, the degree of hydration test data had to be included in the statistical model. The response variables of the data set comprised of the degree of hydration values versus concrete age, for each cement type, at the three isothermal curing temperatures of 4.4°C, 32.2°C, and 40.6°C. For example, for cement Type I (12) the response variables are the test points shown in Figure 5-27 at the three curing temperatures just mentioned. There are seven test points at each reference temperature, 20 different cements, and three temperatures, which yields a data set with 7 x 20 x 3 = 420 degree of hydration response variables.

Since the Arrhenius maturity function is a nonlinear function, the final nonlinear regression analysis was performed with the NLIN procedure in the SAS program. The NLIN procedure is an iterative method that requires that the nonlinear regression model be defined, and that initial estimates of the regression coefficients be provided. Therefore, Equation 5-14 was used as the initial nonlinear regression model.

Appendix C presents the results obtained from the NLIN procedure, and it may be seen that convergence was achieved, and that all 420-response variables were used. Based on the nonlinear model shown in Equation 5-14, the best-fit multivariate regression model is shown in Equation 5-15. An r^2 of 0.981 was achieved for this model. Note that the regression parameters shown in Equation 5-15 were rounded to obtain a usable form. The scatter plot of the experimentally determined versus the predicted degree of hydration values, with the activation energy as modeled with Equation 5-15, are shown in Figure 5-32. This figure indicates that the activation energy formulation in Equation 5-15 accurately accounts for the change in degree of hydration due to curing at different temperatures. In Section 5.2.6.5, the goodness of fit obtained from the proposed model will be evaluated.

$$E = 22{,}100 \cdot {p_{C_3A}}^{0.30} \cdot {p_{C_4AF}}^{0.25} \cdot Blaine^{0.35} \qquad \textit{Equation 5-15}$$

where, p_{C3A} = weight ratio of C_3A ito total cement content,
p_{C4AF} = weight ratio of C_4AF ito total cement content, and
Blaine = Blaine value, specific surface area of cement (m^2/kg).

5.2.6.5 *Evaluate Goodness of Fit of the Proposed Activation Energy Model*

The goodness of fit of the activation energy model presented in Equation 5-15 will be evaluated by means of the coefficient of determination (r^2), the mean square of the error (s^2), and tendencies from the residual plots (Barnes, 1994). In section 5.2.6.4, it was shown that an r^2 value of 0.981 was obtained for this model, which indicates that 98.1% of the experimental variation of the response variable variation is explained by the model. The mean square of the error provides an unbiased estimate of the standard deviation of the error as it is corrected for the degrees of freedom in the model. From the SAS output file, s^2 = 0.00095, which is a very small number (0.095%) as desired.

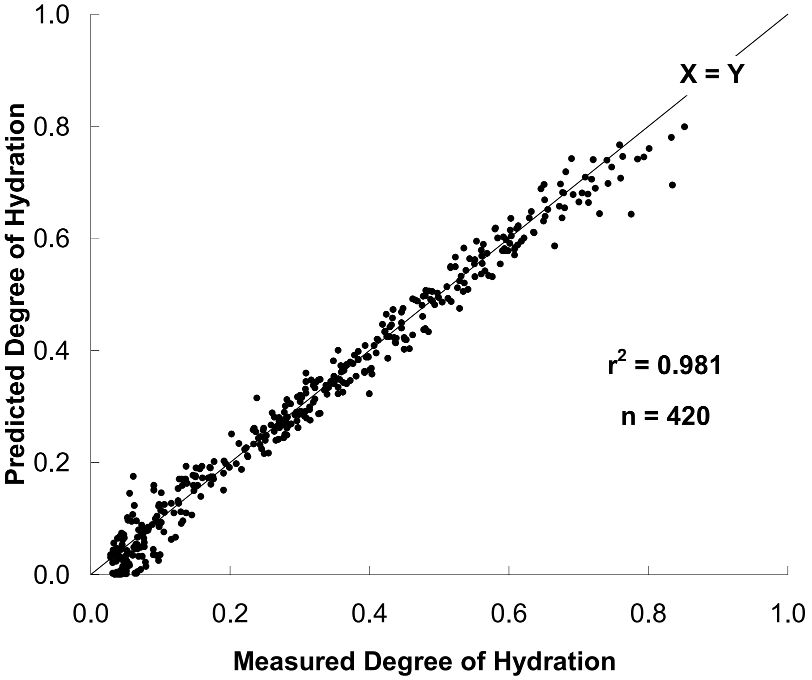

Figure 5-32: Plot of the measured versus the predicted degree of hydration

Since a random distribution of the unexplained error is desired, residual plots were used to evaluate the homogeneity of variance. Figures 5-33 and 5-34 provide the scatter plot of the residuals against the predicted and measured degree of hydration. These figures indicate that the error appears random for all degrees of hydration. Three possible outliers, outside the error range of 0.10 may be identified; however, since these were actual test results, and the fit of the model remains good, there appears to be no reason to remove them from the analysis. Figure 5-35 presents the cumulative distribution of the error, and it may be seen that 95% of the error is within a degree of hydration of ±0.055. It may be seen that 99% of the error is within a degree of hydration range of ±0.085.

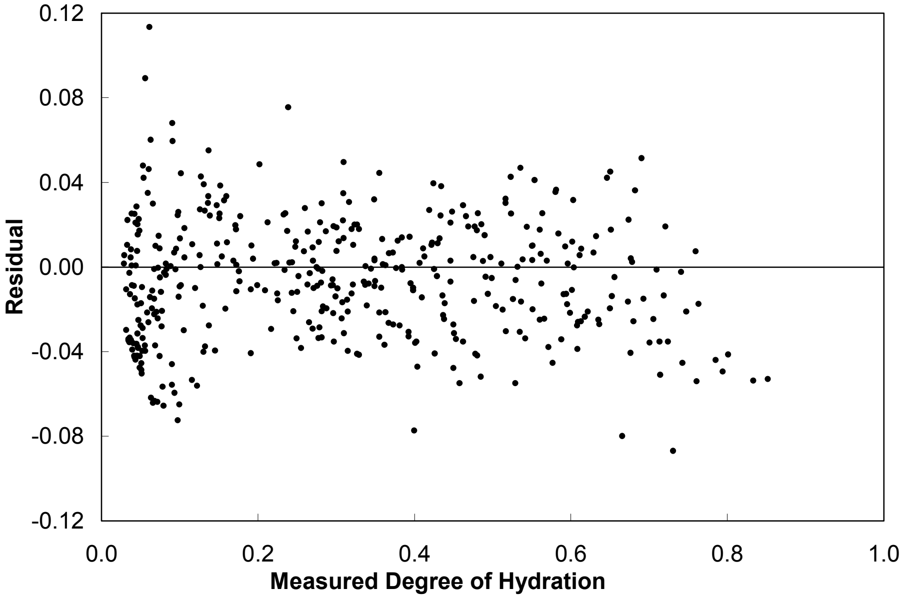

Figure 5-33: Plot of the residuals against the measured degree of hydration

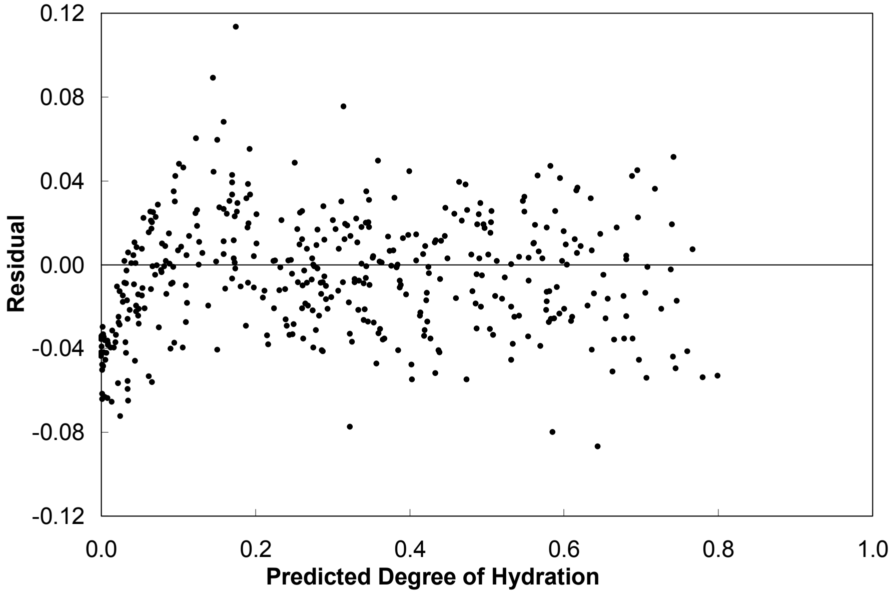

Figure 5-34: Plot of the residuals against the predicted degree of hydration

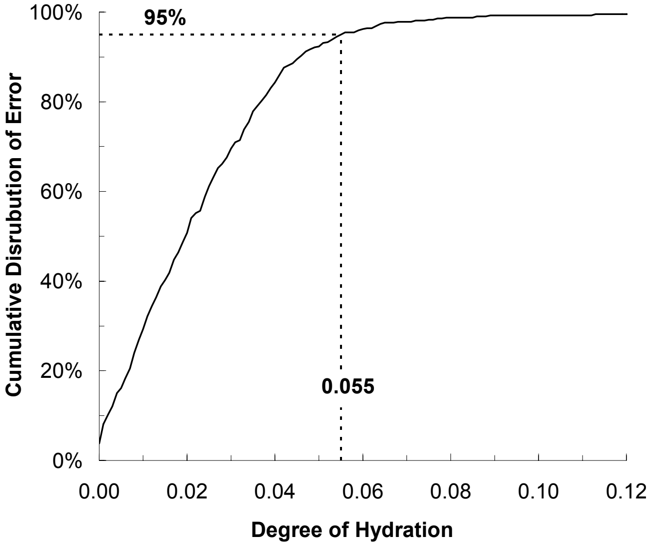

Figure 5-35: Cumulative distribution of the error of the degree of hydration

In multivariate analysis, it is considered good practice to evaluate the plot of the residuals plotted against all the explanatory variables of the model. The residual plots for the three explanatory variables of the activation energy are shown in Figures 5-36 to 5-38. In all cases, the distribution of error appears random, since no trends can be associated with a change in any of the explanatory variable.

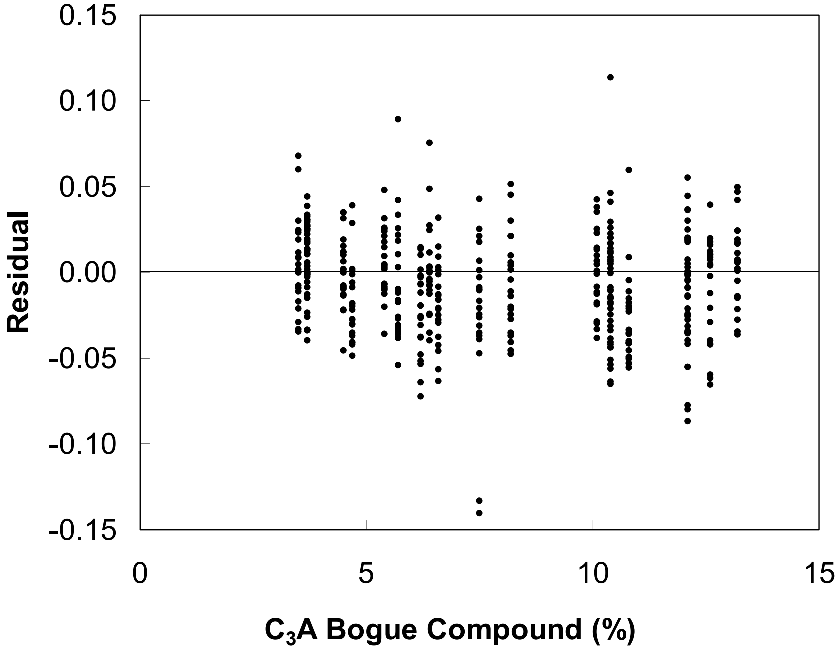

Figure 5-36: Plot of the residuals against the C_3A content

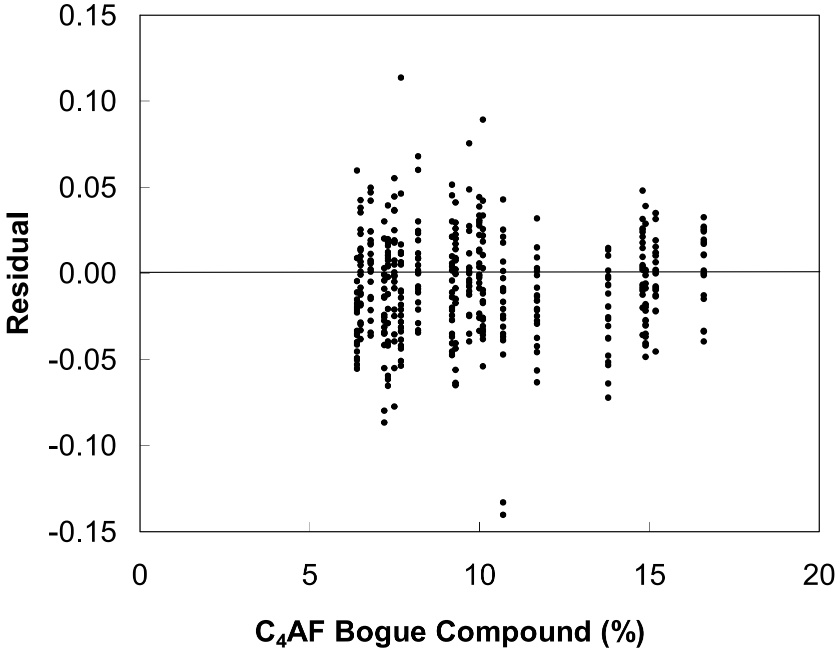

Figure 5-37: Plot of the residuals against the C_4AF content

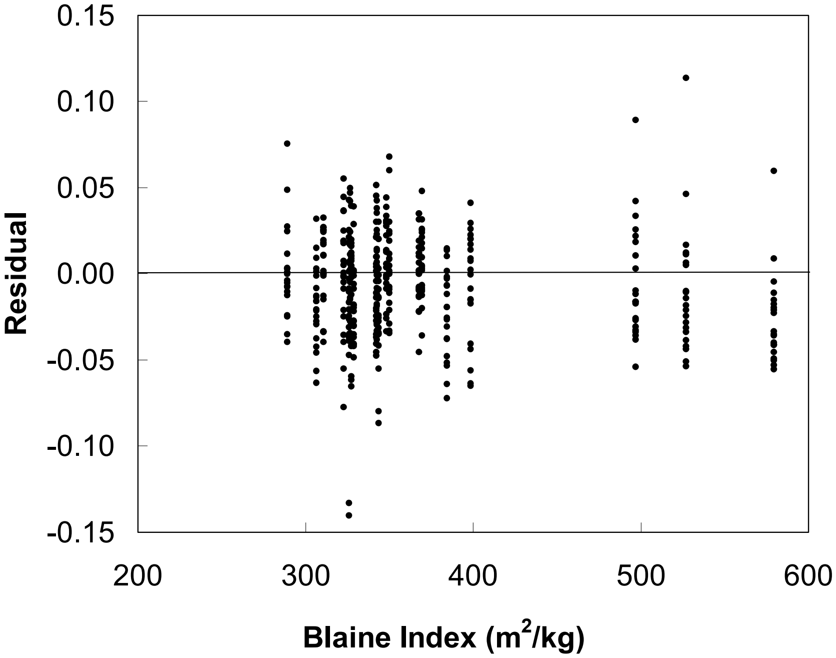

Figure 5-38: Plot of the residuals against the Blaine Index

In this section, the objective was to evaluate the goodness of fit, since the goodness of fit cannot solely be based on a large value of r^2. It was shown that the model meets all the requirements for a multivariate linear regression analysis, and that 95% of the error is within a degree of hydration of ±0.055. Therefore, it may be concluded that the model provides an accurate prediction of the measured degree of hydration at different curing temperatures.

5.2.6.6 *Effect of Mineral and Chemical Admixtures*

Mineral admixtures have been shown to affect the rate of hydration at different temperatures, which would thus impact the activation energy value for a specific concrete mixture. However, little heat of hydration test data performed at various temperatures is available to use for the development of an appropriate model. Few references even consider the effect of mineral admixtures on the activation energy. RILEM Technical Committee 119-TCE recommends the use of the FHP activation energy model for all cements, and that a higher value should be used for GGBF slag cements. However, a constant activation energy value (E = 48,804 J/mol) is recommended irrespective of the amount of GGBF slag used.

Ma et al. (1994) calculated the activation energy for different cementitious materials based on isothermal calorimeter test results. Test were performed at isothermal curing temperatures of 10°C, 15°C, 20°C, 25°C, 30°C, 35°C, 40°C, 45°C, 50°C, and 55°C. Ma et al. used the same cement type, and then produce different blended cements by either adding Class F fly ash or GGBF slag. In order to determine the best fit activation energy, the Arrhenius plot was constructed, which showed no temperature dependency for any of the cementitious systems tested. Their results are tabulated in Table 3-3, which can be summarized as follows:

Type I Cement:	39,000 J/mol
Type I+17% F Fly ash:	26,700 J/mol
Type 1+65% GGBF Slag:	49,300 J/mol

Ma et al. further mentioned that GGBF slag exhibits relatively low reactivity at room temperature, but is thermally activated at higher temperatures, which is reflected by the high activation energy value.

Based on the informative data produce by Ma et al., it is clear that the use of mineral admixtures will affect the activation energy. It is thus necessary to account for this effect when such materials are used in the mixture. Since no other data are currently available, the change in activation energy obtained by Ma et al. will be used together with engineering judgment to quantify the effect of fly ash and GGBF slag on the activation energy. This model should be considered as preliminary and this area requires more experimental work.

The Class F fly ash used by Ma et al., had a CaO content of 3.57%, which is typical for East Coast Class F fly ashes. The CaO content will be used to differentiate between the different fly ash types. According to their results, the use of 17% fly ash reduces the activation energy by 32%, and when 65% of GGBF slag is used, the activation energy is increased by 26%. The following assumptions will be made to develop the model:

- The change in activation energy value is directly proportional to amount of mineral admixtures used, and
- The change in activation energy is identical for all combinations of cements and mineral admixtures.

The activation energy for each cement will be determined based on the formulation provided in Equation 5-15, and then the activation energy modification factor (f_E) as shown in Equation 5-16 will be multiply with the value calculated for the cement. The impact of different replacement levels of fly ash and slag is shown in Figure 5-39.

$$f_E = 1 - 1.05 \cdot p_{FA} \cdot \left(1 - \frac{p_{FACaO}}{0.40}\right) + 0.40 \cdot p_{SLAG} \qquad \textit{Equation 5-16}$$

where, f_E = Activation energy modification factor,

p_{FA} = Mass ratio replacement of the fly ash,

p_{FACaO} = Mass ratio of the CaO content in the fly ash, and

p_{SLAG} = Mass ratio replacement of the GGBF Slag.

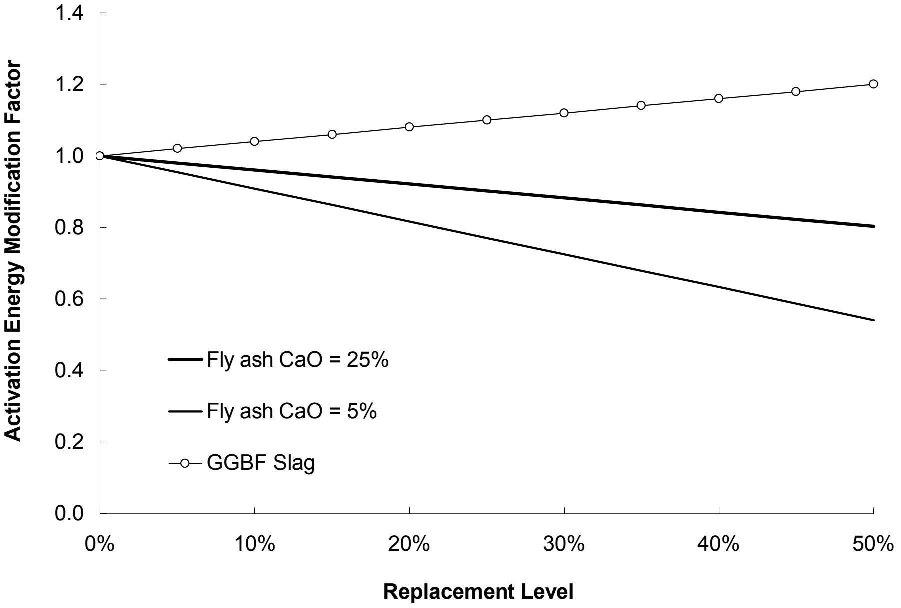

Figure 5-39: The activation energy modification factor for fly ash and GGBF slag

Due to limited data available, no effect on the activation energy due to the use of **chemical admixtures** will be assumed. However, the degree of hydration curve at the reference temperature will be affected, but the rate of hydration relative to this curve remains unchanged as compared to the rate for the cementitious system without any chemical admixtures. This is an area in which more development and research is required.

5.2.6.7 *Sensitivity Analysis of Proposed Activation Energy Model for Hydration Development*

This section will provide a sensitivity analysis of the activation energy model developed in this section. The proposed model can be summarized as follows:

$$E = 22{,}100 \cdot f_E \cdot {p_{C_3A}}^{0.30} \cdot {p_{C_4AF}}^{0.25} \cdot Blaine^{0.35} \qquad \textit{Equation 5-17}$$

where, p_{C3A} = weight ratio of C_3A ito total cement content,

p_{C4AF} = weight ratio of C_4AF ito total cement content,

Blaine = Blaine value, specific surface area of cement (m^2/kg), and

f_E = Activation energy modification factor, defined as:

$$f_E = 1 - 1.05 \cdot p_{FA} \cdot \left(1 - \frac{p_{FACaO}}{0.40}\right) + 0.40 \cdot p_{SLAG}$$

Previously Equation 5-16

where, p_{FA} = Mass ratio replacement of the fly ash,

p_{FACaO} = Mass ratio of the CaO content in the fly ash, and

p_{SLAG} = Mass ratio replacement of the GGBF Slag.

A sensitivity analysis is performed by choosing a baseline condition and, thereafter, only one of the parameters is varied at a time. This does not necessarily reflect what would happen for actual cements. For example: a change in C_3A would also require a change in C_4AF. However, in order to evaluate the effect of a change in each parameter this is considered appropriate. The ranges of variables were determined based on what is typically found in the state of Texas. Figure 5-40 presents the results obtained from the sensitivity analysis.

5.3 GENERAL HYDRATION MODELS TO CHARACTERIZE THE DEGREE OF HYDRATION DEVELOPMENT

Verbeck (1960) stated that the " ...heat evolution depends in part and in a rather complicated way upon the mutual effects of C_3A content, fineness, alkali content, and gypsum content of the cement." In order to investigate the hydration characteristics of typical Texas paving mixtures, different concrete paving mixtures were tested by semi-adiabatic calorimeter testing. A data base of test results and all the known variables was developed for these mixtures.

The degree of hydration development plays a key role in the overall temperature prediction scheme, and the overall use of the degree of hydration is illustrated in Figure 5-41. The degree of hydration curve is used to characterize the hydration behavior of a specific concrete mixture at the reference temperature. The total heat of hydration is next determined by the composition and amount of cementitious materials. The total heat of hydration is then multiplied by the degree of hydration to quantify the heat of hydration development of a mixture over time, at the reference temperature. Together with the activation energy, as shown in Figure 5-1, the heat of hydration development can now be estimated at any temperature. The degree of hydration test data collected during this study were previously presented in Section 4.2.3.2. These test results are all representative of typical concrete paving mixtures used in Texas.

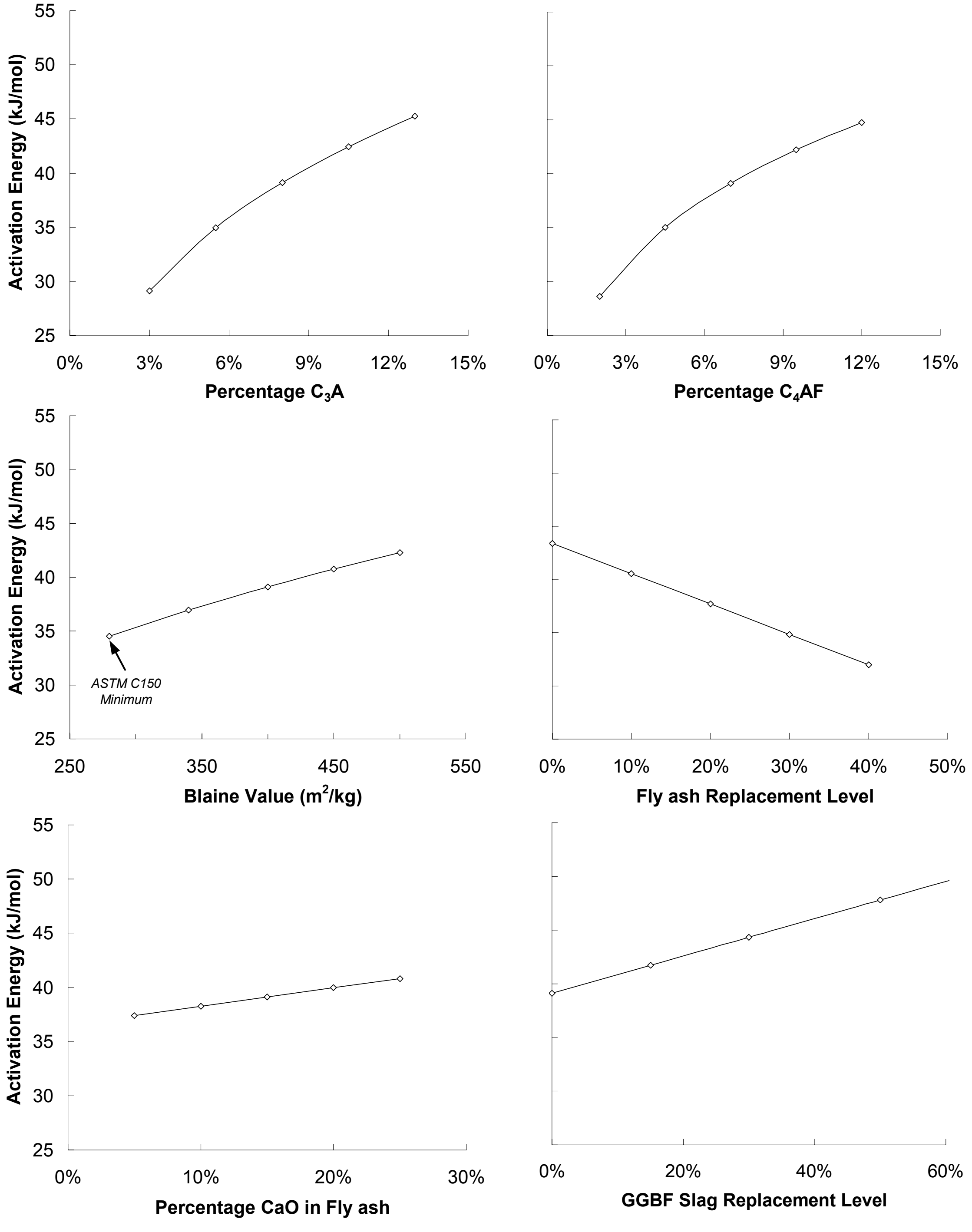

Figure 5-40: Sensitivity analysis of the proposed activation energy model (*Baseline parameters:* C_3A=8%,C_4AF=7%,Blaine=400 m^2/kg,p_{FA}=15%,p_{FACaO}=15%,p_{SLAG}=0%)

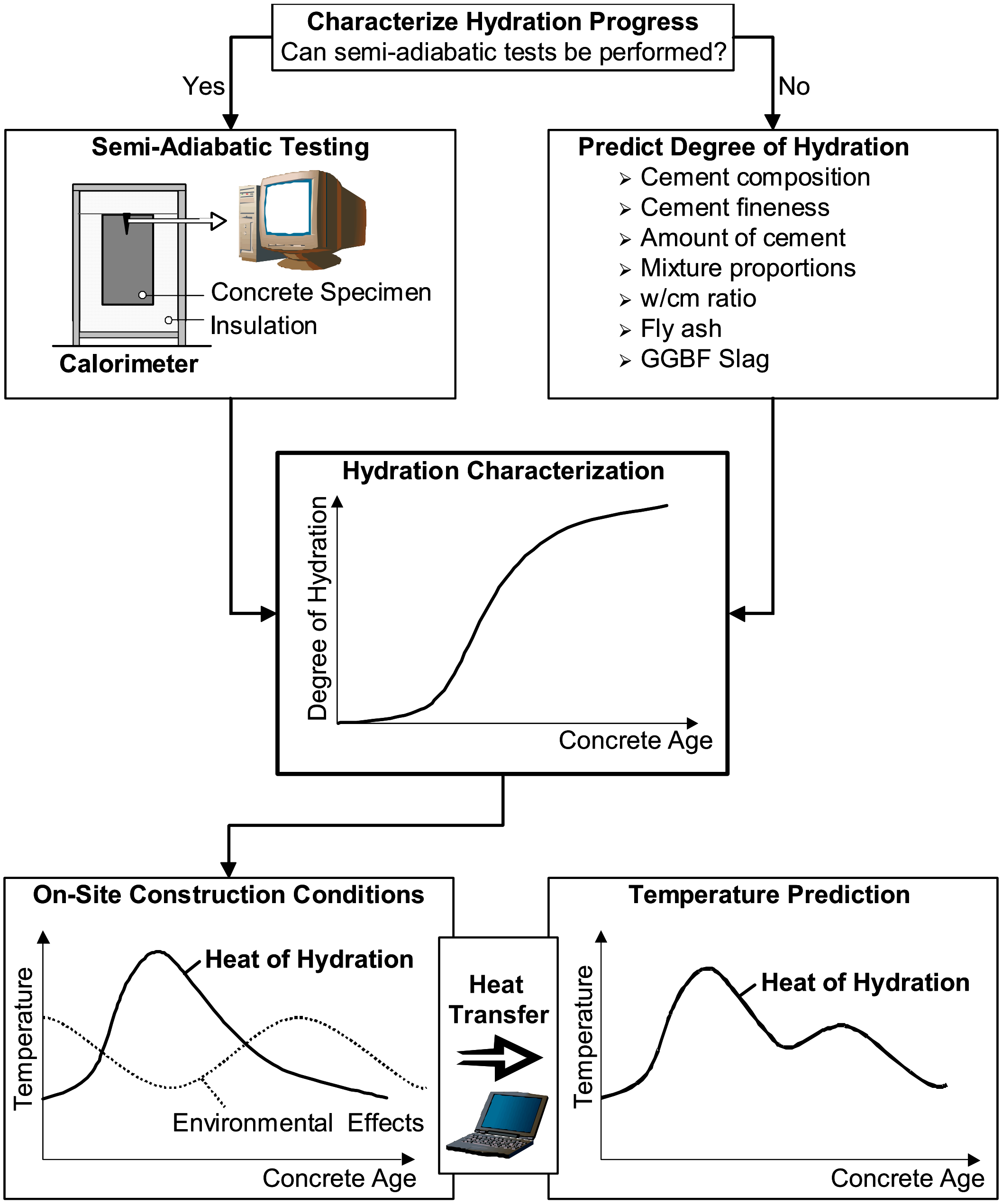

Figure 5-41: Schematic to emphasize the key function of the degree of hydration concept

The objectives of this phase of the work are to develop and document a general model to characterize the heat of hydration of concrete that will be used to predict the concrete temperature development. The models should be generic in nature and consider the effect of:

- mixture proportions,
- cement chemical composition,

- cement fineness, and
- mineral admixtures.

In the remainder of this section, the models developed and introduced in Chapter 3 will be calibrated to represent the best fit hydration curves. In terms of the model development approach presented in Section 5.1, the different sources of data used for the model development will be outlined. Next, the multivariate regression analysis used during this study will be reviewed. Models to predict the maximum degree of hydration and degree of hydration will then be presented. The goodness of the fit obtained from the model will be evaluated, and a sensitivity analysis of the proposed hydration model will be evaluated.

5.3.1 Model Development Data Sources and Approach

The model development approach is schematically shown in Figure 5-1, and both calibration and validation will be performed for the general hydration model developed during this study. The model development phase was previously presented in Section 3.2.5.

An essential part of the model calibration phase is to obtain sufficient test data that can be used to calibrate the model. The more detailed and comprehensive this data set, the higher the confidence in the calibrated mechanistic-empirical model becomes. Finally, the accuracy of the model can be evaluated against a data set not used during calibration of the model. The accuracy of the model against the new test data will provide an indication of the validity of the model to predict the degree of hydration development for different concrete mixtures.

In order to investigate the hydration characteristics of typical Texas paving mixtures, 21 different concrete paving mixtures were tested by means semi-adiabatic calorimeter testing. A data base of test results and all the known variables was developed for these mixtures. The result of tests performed by the PCA on 20 different cements (Lerch and Ford, 1948) was incorporated to expand the data base. These tests include heat of solution and conduction calorimeter tests data.

The different data sources and their use in the development of the hydration model are shown in Table 5-8. The test data used for the initial calibration of the model should be as large as possible. It was, thus decided to include all the test results obtained from the materials characterization phase and those presented by Lerch and Ford (1948) for the initial model calibration. The reader is referred to Section 5.2.6.1 for more background on the data developed by Lerch and Ford (1948).

Table 5-8: Different data sources and their use in the development of the hydration model

CALIBRATION Data Sources	**PCA (Lerch & Ford, 1948)**	**Current Study: Materials Characterization Phase**
	• U.S. cements sources • 8 Type I 5 Type II 3 Type III 3 Type IV 1 Type V • All cement properties known • Well know and recognized data source • Conduction calorimeter heat of solution tests	• Texas materials • 3 different cement sources • Different fineness • Class C and F fly ash • GGBF Slag • All cement properties known • Semi-adiabatic testing
VALIDATION Data Sources	**Kjellsen and Detwiler, 1991**	**Current Study: Field work phase**
	• Swedish cements source • All cement properties known • Type I Cement • Non-evaporatable water calculations	• Texas materials • Typical paving mixtures • Different cements • All cement properties known • Field data collected • Mixed usage of Class C and F fly ash, and GGBF Slag • Semi-adiabatic testing

The data collected from the field work phase will only be used to validate the model. Limited other data sources are available, as all the cement and mineral admixture properties need to the defined, and the degree of hydration test results need to be available for use in the analysis. Kjellsen and Detwiler (1991) presented sufficient material properties to include their hydration results for use during the validation of the model. More test results are thus used to calibrate the model as compare to those used for validation purposes.

Some Final Comments on Modeling Approach:

On the approach outlined above, it should be mentioned that the development is probably the first of many model to be developed following this approach. As more tests are performed and additional data become available, the data base can be expanded and improved models can be developed. The hydration of cementitious material is a very complicated process that has been researched and disputed for more than a century. A statistical analysis performed on 34 mixtures can hardly be expected to cover all the combinations and interactions experienced in present and future practice.

5.3.2 Multivariate Regression Analysis

The statistical process followed is similar to that presented previously in Section 5.2.6.3, during the development of the activation energy model. The data obtained from the semi-adiabatic tests, were discretized to correspond to the heat of solution test intervals adopted by Lerch and Ford (1948). This is necessary to ensure all tests set contribute equally to the overall statistical analysis. The data set was prepared for analysis with the SAS program (Release 8.2), distributed by the SAS Institute Inc., Cary, NC, USA. The multivariate regression analysis was performed in the following three stages: (1) identify most significant variables, (2) develop regression model, and (3) evaluate goodness of fit.

The goodness of fit will be evaluated by means of the coefficient of determination (r^2), the mean square of the error (s^2), and tendencies from the residual plots (Barnes, 1994). A high r^2, a low s^2, and a random distribution of the unexplained error are desired. Residual plots will be used to diagnose nonlinearity or non-constant error variance. As was the case during the development to the activation energy model, it was determined that the data could best be modeled through the use of a nonlinear relationship. The data set was transformed into a linear relationship by taking the natural logarithm of both the independent and response variables.

5.3.3 Calibration of the General Degree of Hydration Model

The statistical process outlined above was used to analyze the calibration data set. The analysis results from the SAS program is presented in Appendix C (Part II), and only the final results will be presented herein.

The explanatory variables to be used in the nonlinear analysis were selected by developing a regression model to predict the degree of hydration parameters for each mixture. This allows the development of a linear relationship, but with only 34 data points for each parameter. The model developed from this exercise will then be used to develop the final nonlinear model based on 352 degree of hydration data points. With the r^2 selection method, the significance of individual and combinations of explanatory variables were evaluated. The following variables were found to provide the best statistical fit:

Hydration time parameter (τ): (7 parameters, r^2= 0.863)

$$\tau = f(C_3A, C_3S, \text{Blaine}, SO_3, p_{SLAG}, p_{FA}, p_{FA\text{-}CaO})$$

Hydration slope parameter (β): (5 parameters, r^2= 0.900)

$$\beta = f(C_3A, C_3S, \text{Blaine}, SO_3, p_{SLAG})$$

where, p_{C3A} = weight ratio of tricalcium aluminate ito total cement content,
p_{C3S} = weight ratio of tricalcium silicate ito total cement content,
p_{SO3} = sulfate weight ratio ito total cement content,
p_{FA} = fly ash weight ratio ito total cementitious content,

$p_{FA\text{-}CaO}$ = fly ash CaO weight ratio ito total fly ash content,
p_{SLAG} = slag mass ratio ito total cementitious content, and
Blaine = Blaine value, specific surface area of cement (m^2/kg).

The ultimate degree of hydration model developed by Mills (1966) and presented in Section 3.2.7 was based on sound principles and numerous test results. Therefore, this model was used as basis to incorporate this effect into the generic hydration model. Figure 3-13 indicated that the ultimate degree of hydration is not only influenced by the water-cement ratio, but it is additionally influenced when GGBF slag is used. The formulation in Equation 3-35 was used, and the effect of using mineral admixtures was incorporated based on the test results. The increase beyond that determined by Equation 3-35 was thus incorporated as follows:

$$\alpha_u = \frac{1.031 \cdot w/cm}{0.194 + w/cm} + \Delta\alpha_u \qquad \textit{Equation 5-18}$$

where, p_{FA} = Mass ratio replacement of the fly ash, and
w/cm = the water-cementitious material ratio.

The increase in ultimate degree of hydration was found to be a function of the following variables:

Ultimate degree of hydration increase ($\Delta\alpha_u$): (2 parameters, r^2= 0.702)

$$\Delta\alpha_u = f(p_{SLAG}, p_{FA})$$

Based on engineering judgment, it may be reasoned that the parameters shown in the previous equations are intuitively appropriate. Both high C_3A and Blaine values are associated with cements with high early-age strength gains such as Type III cements. As discussed in Section 2.2.1.1, cements consist of 50-70% of C_3S, after which C_3A provides the largest contribution to the early-age heat development. Mindess and Young (1981) provide the following relevant comments:

> Since C_3S and C_3A are responsible for most of the early liberation of heat, reduction in the amounts of these compounds substantially reduces the amount of heat produced.

Therefore, the inclusion of the C_3S parameter to quantify the hydration parameters is in accordance with engineering judgment. This can be seen in Figure 2-1, where C_3A and C_3S are the most reactive compounds, whereas C_2S reacts much more slowly. Figure 2-1 further indicates that the presence of sulfates (gypsum, $C\overline{S}H_2$) slows the early hydration of C_3A, and this prevents flash setting. Gypsum added to the clinker during the grinding process is one source of sulfates, which is used to regulate the rheology of the hydration rate of the cement (Frigione, 1983). Gypsum was first used to retard the setting rate of cement, in order to allow proper placing of the concrete. Therefore, the presence of sulfates as a variable that predict both the hydration time and slope parameter is expected.

The results obtained from the r^2 selection method (see Appendix C) reveals with regards to the degree of hydration, that the ***single*** most significant parameters were statistically ranked as follows:

Hydration time parameter (τ):

C_2S, Blaine, C_3S, C_3A, $S0_3$, C_4AF, p_{SLAG}, Equivalent alkalies, p_{FA}, and MgO.

Hydration slope parameter (β):

$S0_3$, C_2S, p_{FA}, C_3A, C_3S, C_4AF, MgO, equivalent alkalies, Blaine, and p_{SLAG}.

The above results indicate that many other parameters other than those selected for use in the final model provide an indication of the hydration process. Literature indicates that alkalies could affect the hydration process, and from the results, they do seem to have an effect. However, when the contributions of many variables are considered, the statistical best-fit regression model does not necessarily include these parameters.

With the independent variables selected for the three hydration parameters, initial values for the regression model were determined with a multivariate linear regression analysis. From the analysis of variance (ANOVA) table for the development of the regression model the follow conclusions can be made regarding the sources of variation:

Hydration time parameter (τ):

The small p-value (0.001) indicates that there is a statistically significant relationship between all the independent variables (C_3A, C_3S, Blaine, SO_3, p_{SLAG}, p_{FA}, $p_{FA\text{-}CaO}$) and the degree of hydration.

Hydration slope parameter (β):

The small p-value (0.001) indicates that there is a statistically significant relationship between all the independent ϖαριαβλεσ (C_3A, C_3S, Blaine, SO_3, p_{SLAG}) and the degree of hydration.

The ANOVA results contained in Appendix C, presents the Type I Sum of Squares error (Type I SS), and from this, it may be seen that the F-statistic indicates that these models are all incrementally improved as each explanatory variable is added. From the values of the F-statistic for the Type III error, it may be concluded that the explanatory variables are uncorrelated and the use of all three are statistically significant. Based on the statistical results, the multivariate regression models shown in Equations 5-19 to 5-21 were developed. The r^2 was, respectively, 0.863 and 0.900 for the hydration time and slope parameters.

$$\tau = {p_{C_3A}}^{-0.149} \cdot {p_{C_3S}}^{-0.404} \cdot Blaine^{-0.8132} \cdot {p_{SO_3}}^{-0.757} \cdot \exp(2.17 \cdot p_{SLAG} + 9.32 \cdot p_{FA} \cdot p_{FA-CaO} + 4.27)$$

Equation 5-19

$$\beta = {p_{C_3A}}^{0.151} \cdot {p_{C_3S}}^{0.228} \cdot Blaine^{-0.561} \cdot {p_{SO_3}}^{0.583} \cdot \exp(-0.704 \cdot p_{SLAG} + 5.47) \qquad \textit{Equation 5-20}$$

$$\alpha_u = \frac{1.031 \cdot w/cm}{0.194 + w/cm} + 0.39 \cdot p_{FA} + 0.22 \cdot p_{SLAG} \ \leq \ 1.0 \qquad \textit{Equation 5-21}$$

In order to develop the best-fit activation energy model that applies to the degree of hydration development data, all the degree of hydration data was now used to develop the final model. The response variables of the data set comprised of the degree of hydration values versus concrete age, for each cement type. Since the degree of hydration development is a nonlinear function, the final nonlinear regression analysis was performed with the SAS NLIN procedure. The NLIN procedure is an iterative method that requires that the nonlinear regression model be defined, and that initial estimates of the regression coefficients be provided. Therefore, Equations 5-19 to 5-21 were used as the initial nonlinear regression models.

Appendix C presents the results obtained from the NLIN procedure, and it may be seen that convergence was achieved, and that all 352-response variables were used. The best-fit multivariate regression models are shown in Equations 5-22 to 5-24. An r^2 of 0.988 was achieved with this model.

$$\tau = 66.78 \cdot {p_{C_3A}}^{-0.154} \cdot {p_{C_3S}}^{-0.401} \cdot Blaine^{-0.804} \cdot {p_{SO_3}}^{-0.758} \cdot \exp(2.187 \cdot p_{SLAG} + 9.50 \cdot p_{FA} \cdot p_{FA-CaO}$$

Equation 5-22

$$\beta = 181.4 \cdot {p_{C_3A}}^{0.146} \cdot {p_{C_3S}}^{0.227} \cdot Blaine^{-0.535} \cdot {p_{SO_3}}^{0.558} \cdot \exp(-0.647 \cdot p_{SLAG}) \qquad \textit{Equation 5-23}$$

$$\alpha_u = \frac{1.031 \cdot w/cm}{0.194 + w/cm} + 0.50 \cdot p_{FA} + 0.30 \cdot p_{SLAG} \ \leq \ 1.0 \qquad \textit{Equation 5-24}$$

where, p_{C3A} = weight ratio of tricalcium aluminate ito total cement content,
p_{C3S} = weight ratio of tricalcium silicate ito total cement content,
p_{SO3} = sulfate weight ratio ito total cement content,
p_{FA} = fly ash weight ratio ito total cementitious content,
$p_{FA\text{-}CaO}$ = fly ash CaO weight ratio ito total fly ash content,
p_{SLAG} = slag mass ratio ito total cementitious content,
Blaine = Blaine value, specific surface area of cement (m^2/kg), and
w/cm = the water-cementitious material ratio.

The scatter plot of the experimentally determined versus the predicted degree of hydration values using the models shown in Equations 5-22 to 5-24 are shown in Figure 5-42. This figure indicates that the proposed models accurately account for effect of cement chemical composition, cement fineness, the use of mineral admixtures, and water-cementitious ratio on the degree of hydration development. In the following section, the goodness of fit obtained from the proposed model will be evaluated.

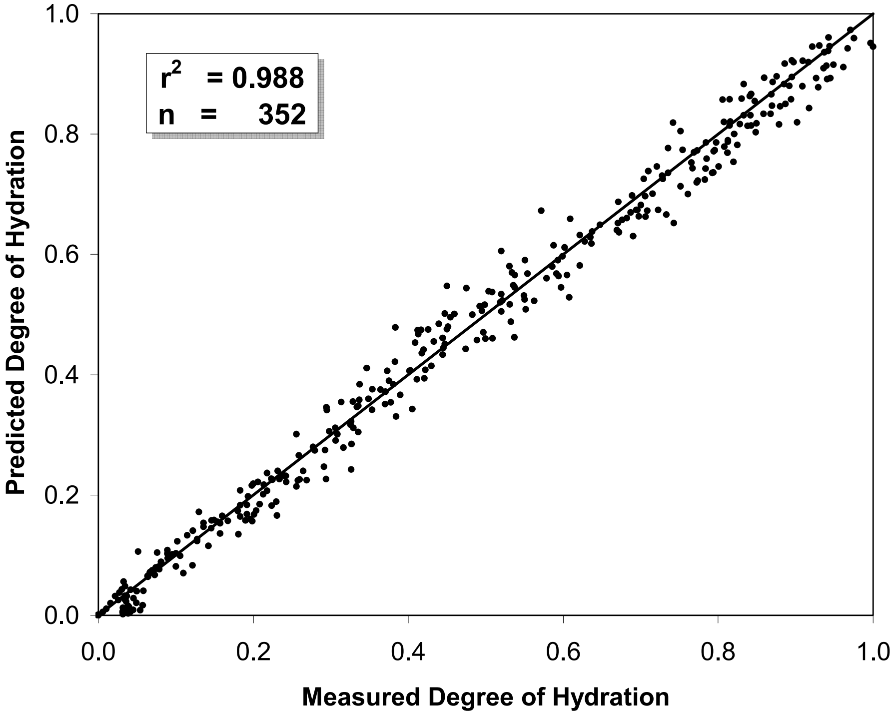

Figure 5-42: Plot of the measured versus the predicted degree of hydration

The manner in which the predicted degree of hydration (DOH) values characterize the measured data are graphically shown in Appendix D for every mixture. In the remainder of this section, some examples of the results will be shown.

Figure 5-43 indicates the degree of hydration behavior for typical Type I and II cements as tested by Lerch and Ford (1948). Note that the predicted DOH is very similar to the measured results. The DOH for the Type I cement starts to develop earlier, which can be attributed to its higher C_3A content, SO_3 content, C_3S content, and higher fineness.

Figure 5-44 presents a comparison of the DOH development for typical Type II and III cements as tested by Lerch and Ford (1948). As was the case in Figure 5-43, the predicted results accurately account for the difference in hydration behavior.

Figure 5-45 presents the measured and modeled DOH for different ASTM C 618 Class C fly ash replacement levels. As previously mentioned, the following trends may be associated with an increase in the amount of Class C fly ash used: the hydration of the total cementitious system is retarded, the ultimate degree of hydration is increased, and the rate (slope) of the hydration reaction is unaffected. The DOH model effectively predicts this behavior for the Class C fly ash.

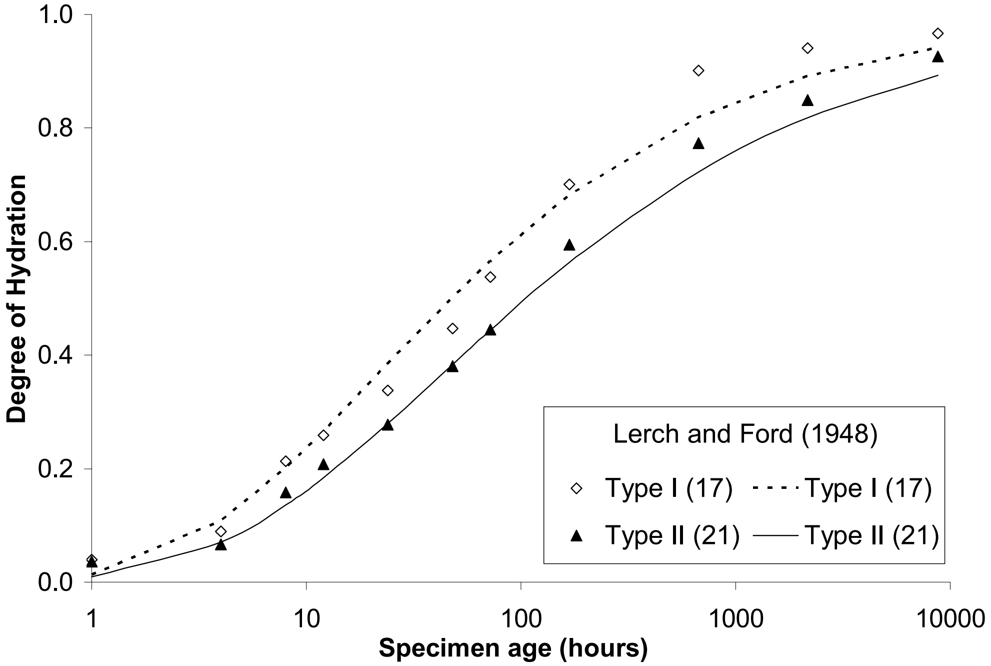

Figure 5-43: Predicted and measured degree of hydration for Lerch and Ford (1948) Type I and II mixtures

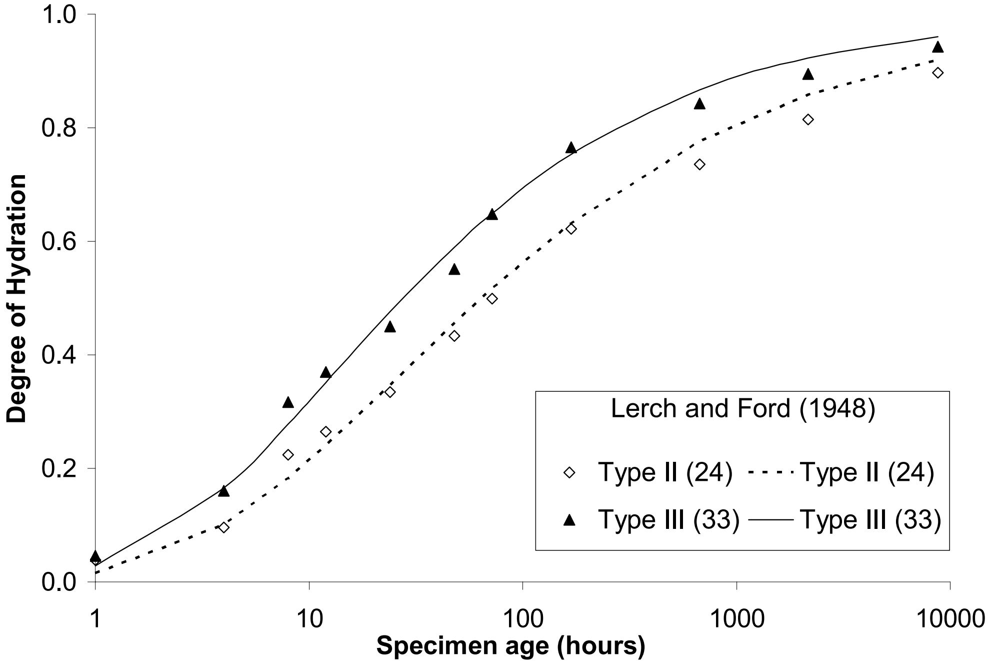

Figure 5-44: Predicted and measured degree of hydration for Lerch and Ford (1948) Type II and III mixtures

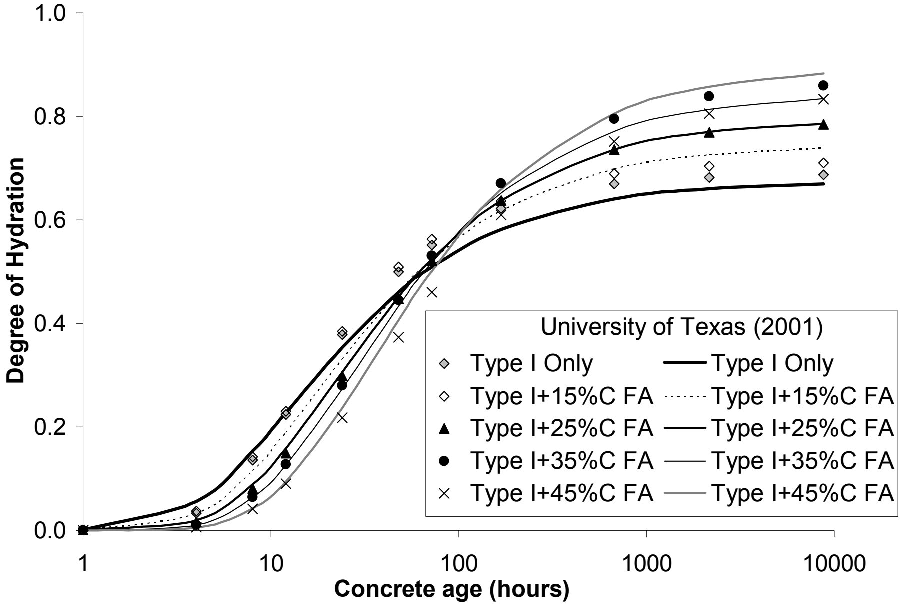

Figure 5-45: Predicted and measured degree of hydration for Class C fly ash mixtures

Figure 5-46 presents the experimentally determined degree of hydration curves for different Class F fly ash replacement levels. It appears that Class F fly ash has little impact on the initial hydration process. It may be concluded that it acts as inert filler, since it contributes little to the early-age heat development. However, at later-ages the ultimate degree of hydration is increased since the amount of fly ash used in the mixture is increased. The proposed model accurately predicts the hydration behavior when Class F fly ash is used.

Figure 5-47 presents the DOH results when GGBF slag is used to replace the Type I cement. The use of slag significantly retards the cement hydration, and it reduces the rate of hydration once it reaches the acceleration stage. It may further be seen that the ultimate degree of hydration is increased with higher GGBF slag dosage levels. The predicted degree of hydration behavior is in accordance with that measured from the test results.

Figure 5-48 presents the effect of the proposed ultimate degree of hydration model. When only cement is used, the model is as recommended by Mills (1966). Since the ultimate degree of hydration is influenced by the use of mineral admixtures, the model was modified as shown in Equation 5-24. Figure 5-48 evaluate the results of this model as compared to other models proposed by literature, as previously discussed in Section 3.2.7.

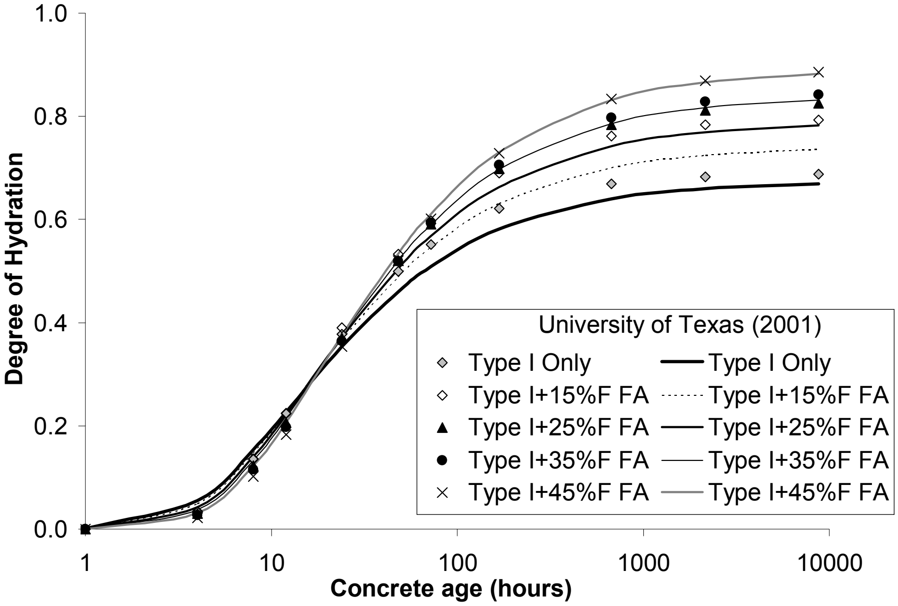

Figure 5-46: Predicted and measured degree of hydration for Class F fly ash mixtures

The curve for only cement, as proposed by Mills (1966), is the one used in the proposed model. From Figure 5-48 it may be conclude that the proposed models provides results within range of that previously found by other research studies. As the amount of mineral admixtures is increased, the ultimate degree of hydration is predicted to increase.

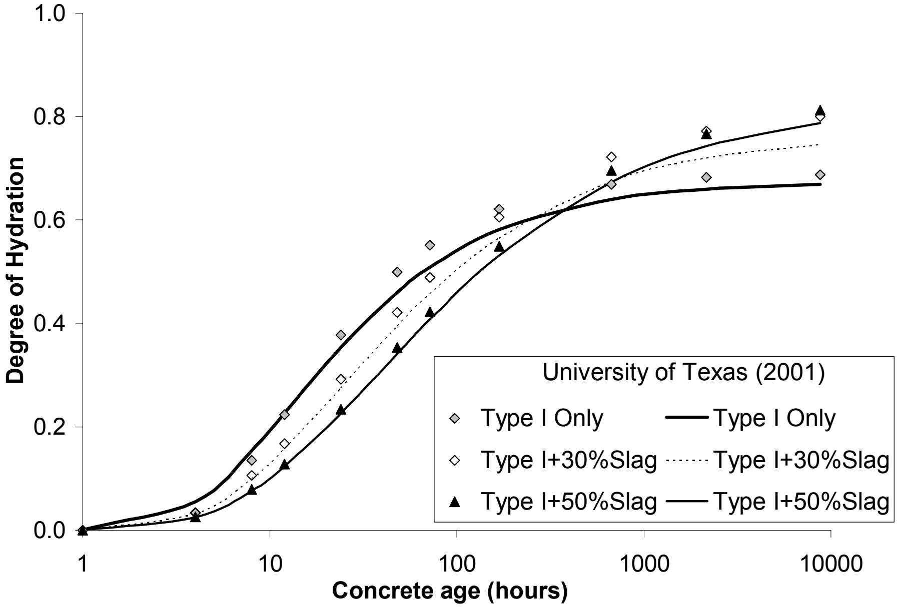

Figure 5-47: Predicted and measured degree of hydration for GGBF Slag mixtures

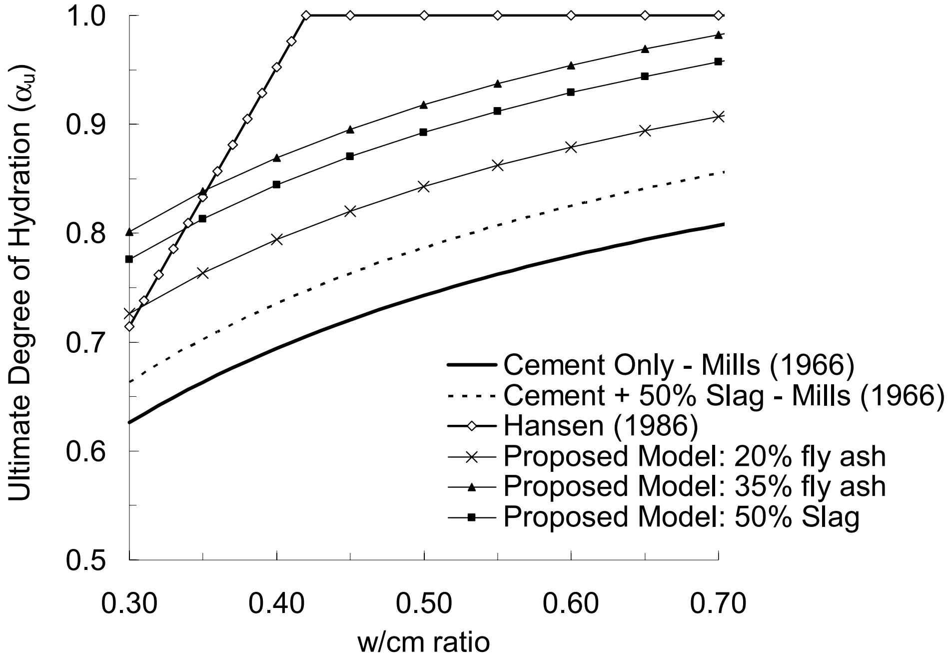

Figure 5-48: The effect of water-cementitious ratio on the ultimate degree of hydration

5.3.4 Goodness of Fit of the Proposed Degree of Hydration Model

The goodness of fit of the degree of hydration models, as shown in Equations 5-22 to 25, will be evaluated by means of the coefficient of determination (r^2), the mean square of the error (s^2), and tendencies from the residual plots (Barnes, 1994). In Section 5.3.3, it was shown that an r^2 of 0.988 was obtained for this model, which indicates that 98.8% of the experimental data are explained by the model. The mean square of the error provides an unbiased estimate of the standard deviation of the error since it is corrected for the degrees of freedom in the model. From the SAS output file s^2 = 0.0010, which is as desired, a very small number (0.01%).

Since a random distribution of the unexplained error is desired, residual plots were used to evaluate the homogeneity of variance. Figure 5-49 and 5-50 provide scatter plots of the residuals against the predicted and measured degree of hydration. Figure 5-49 indicates that the error appears random for all degrees of hydration. The largest error in the predicted degree of hydration was 0.1005, and Figure 5-51 presents the cumulative distribution of the error. From this figure, it may be seen that 95% of the error is within a degree of hydration of ±0.0490. It may further be seen that 99% of the error is within a degree of hydration range of ±0.0850.

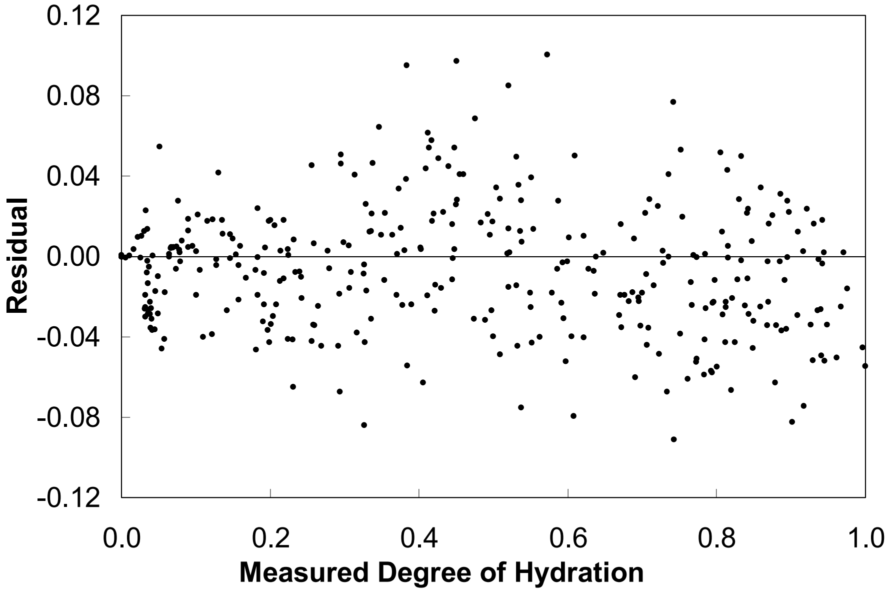

Figure 5-49: Plot of the residuals against the measured degree of hydration at 21.1°C

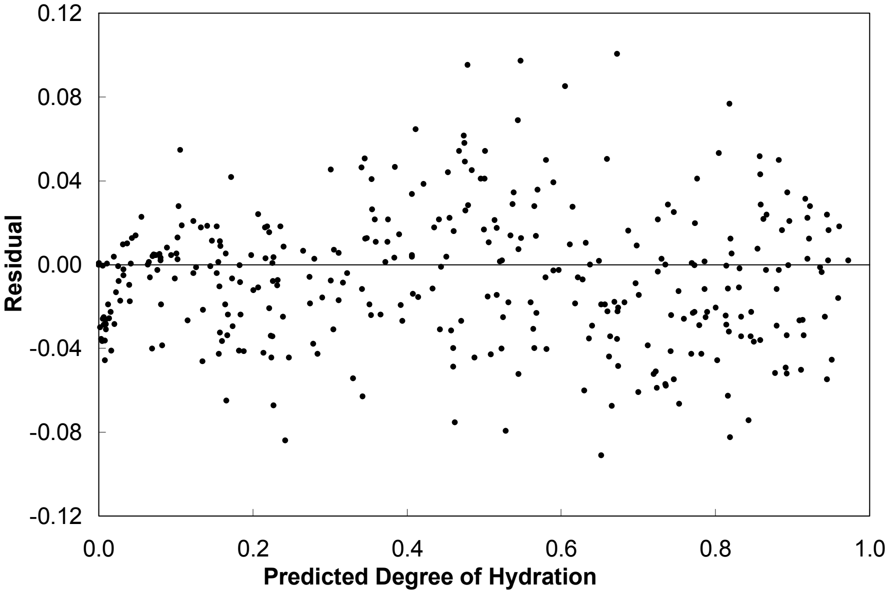

Figure 5-50: Plot of the residuals against the predicted degree of hydration at 21.1°C

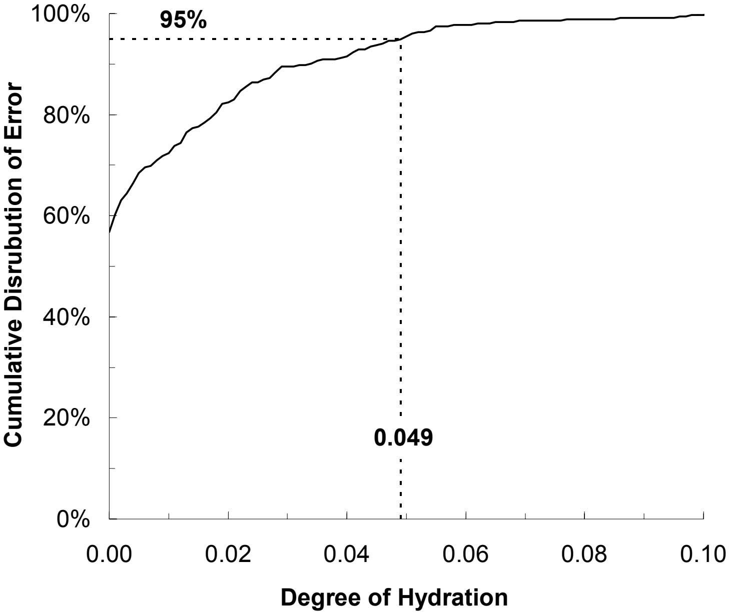

Figure 5-51: Cumulative distribution of the error of the degree of hydration

In multivariate analysis, it is good practice to evaluate the plot of the residuals plotted against all the explanatory variables of the model. The residual plots for all explanatory variables of the degree of hydration model are shown in Figures C-1 to C-7 (Appendix C). In all cases except with respect to the use of Slag, the distribution of error appears random, since no trends can be associated with a change in any of the explanatory variables. In Figure C-7, it may be seen that the proposed model under predict the hydration when GGBF Slag is used, however the maximum error is only 0.0548. The primary reason for this is related to the ultimate degree of hydration model, since the hydration time and slope parameters are accurately predicted. Figure 5-47 presents the predicted degree of hydration when GGBF Slag is used, and it may be concluded that the model provides an accurate fit of the measured values.

In this section, the objective was to evaluate the goodness of fit, since the goodness of fit cannot only be based on a large value of r^2. It was shown that the model meets all the requirements for a multivariate linear regression analysis, and that 95% of the error is within a degree of hydration of ±0.049. Therefore, it may be concluded that the model provides an accurate prediction of the measured degree of hydration for different cements, and combinations of mineral admixtures.

5.3.5 Model Assumptions and Calibration Ranges

Inherent in the development of the generic hydration model is the method of calibration, which determines the range of variables over which it should provide an accurate prediction. The assumptions and limitations associated with the use of this model are as follows:

- A mechanistic-empirical model is only valid within the range for which it was calibrated. The model should not be used to predict hydration outside of the range of parameters listed in Tables 5-9 and 5-10. It is not recommended to extrapolate beyond these ranges. Table 5-9 presents the range of chemical and physical properties of the cements. Table 5-10 presents the range of the range of mixture proportions and mineral admixtures properties used for the calibration of the hydration model
- The effects of chemical admixtures are currently not considered in the hydration models. (Note: Means to adjust the degree of hydration curve to account for the effect of mineral mixtures will be incorporated into the computer program. However, these means will be based on additional tests performed by the user).
- The model assumes that the interaction between the mineral admixtures and the base cement source applies to all combinations of cement and mineral admixtures. This model provides a prediction of the degree of hydration development. Due to the vast amount of interactions between different cementitious materials, it is anticipated that this model will provide limited accuracy for all results. For projects where higher confidence levels for temperature prediction is deemed necessary, it is recommended to test the proposed concrete mixture by means of adiabatic calorimeter tests as presented in Figure 5-41. This test data will characterize the degree of hydration, which can be used in the remainder of the temperature prediction program. With these test data, the prediction of the degree of hydration is no longer required, and the accuracy of the model irrelevant.

Table 5-9: Range of cement properties used for the calibration of the hydration model

	C_3S (%)	**C_2S** (%)	**C_3A** (%)	**C_4AF** (%)	**SO_3** (%)	**Free CaO**(%)	**MgO** (%)	**Alkalies**[a] (%)	**Blaine** (m^2/kg)
Average	52.5	20.8	8.4	9.3	2.6	1.4	1.8	0.6	373.7
Min	20.0	9.3	3.5	5.5	1.2	0.1	0.6	0.2	289.1
Max	64.5	55.0	13.2	16.6	4.4	2.9	4.0	1.1	579.5

Note: [a] Equivalent alkalies as per ASTM C 150 = $Na_2O + 0.658K_2O$

Table 5-10: Range of mixture proportions and mineral admixtures properties used for the calibration of the hydration model

	w/cm	Fly ash CaO (%)	Fly ash SiO_2 (%)	Fly ash Alkalies (%)	Fly ash Dosage (%)	GGBFS Dosage (%)
Average	0.42	-	-	-	-	-
Min	0.36	10.8	35.8	0.3	0.0	0.0
Max	0.54	24.3	54.1	1.4	45.0	50.0

5.3.6 Validation of the Proposed General Hydration Model

In Table 5-8, it was shown that the data collected from the field work, and the degree of hydration data presented by Kjellsen and Detwiler (1991), will be used to evaluate the accuracy of the proposed model. Limited data sources could be identified that presented all the necessary cement chemical and physical properties, mineral admixture properties, and degree of hydration data as measured by either heat of hydration or amount of chemically bound water tests. More data to validate the model against would be preferred, but only these two are presented in this section.

Table 4-1 provided a summary of concrete mixtures used during the **materials characterization phase**. These mixtures were obtained from continuously reinforced concrete paving projects, and in all cases a slip form concrete paver was used to place the concrete.

Table 4-17 presented the hydration parameters obtained from the semi-adiabatic tests performed on the mixtures listed in Table 4-1. The generic hydration model developed in Section 5.5.3 was used predict the degree of hydration development for these mixtures, and the results obtained are shown in Table 5-11. The degree of hydration development for the Type I cement tested by Kjellsen and Detwiler (1991) was predicted and the results are summarized in Table 5-11. The graphs showing the measured and predicted degree of hydration is shown in Appendix D. The smallest r^2 obtained was 0.955, which was obtained for Mix No. 4, and this mixture also had the largest residual of 0.111. The reason for the less accurate prediction could be related to the fact that chemical admixtures were used in all the field mixtures. Mix No. 4 contained more than 16.5 oz/yd^3 of retarder, since this was the amount used during construction. Figure 5-52 presents a plot of the predicted versus measured degree of hydration for all the field mixtures.

Table 5-11: Results after evaluating the proposed hydration model to independent test data

Mix No.	Cementitious Materials	r^2	Maximum Residual
1	Type I/II + 20% Class F fly ash	0.964	0.089
2	Type I/II+ 25% Class C fly ash	0.965	0.102
3	Type I	0.979	0.063
4	Type I/II + 35% Class C fly ash	0.955	0.111
5	Type I/II + 50% GGBF Slag	0.991	0.061
6	Type I/II + 20% Class F fly ash	0.972	0.064
7	Type I/II + 25% Class C fly ash	0.994	0.043
8	Type I + 30% Class C fly ash	0.990	0.046
Kjellsen [a]	Type I/III Cement (w/c=0.50)	0.937	0.087

Note: [a] Data presented by Kjellsen and Detwiler (1991)

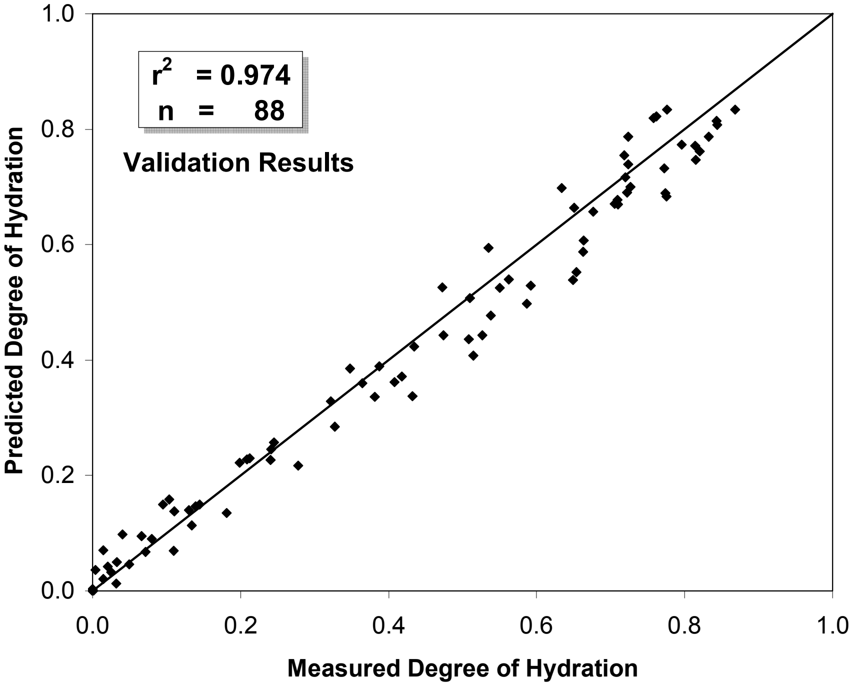

Figure 5-52: Plot of measured versus the predicted degree of hydration for all field site mixtures used in validation

Figures 5-53 and 5-54 are examples of the accuracy achieved after comparing the predicted versus the measured degree of hydration results for some of the field site mixtures. Note that the hydration model is able to characterize the differences in degree of hydration development.

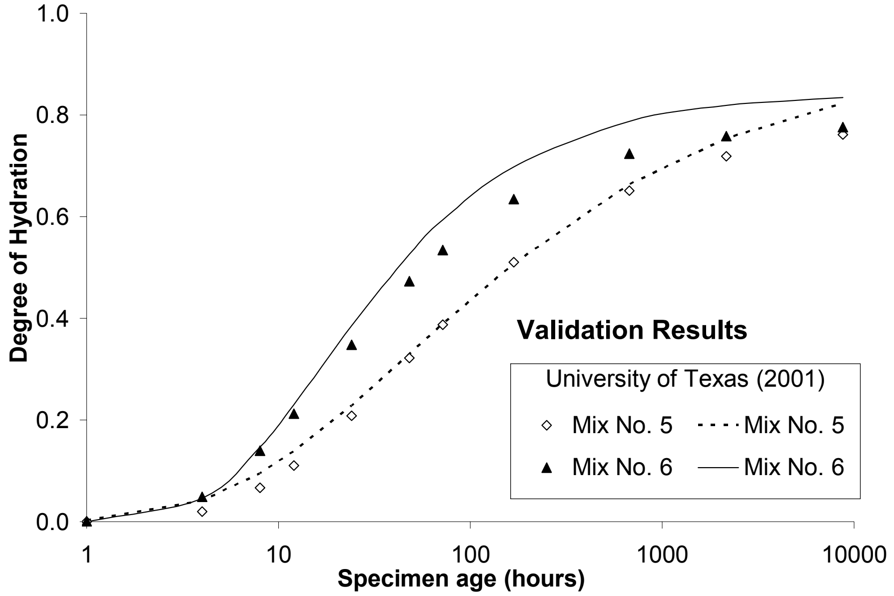

Figure 5-53: Predicted and measured degree of hydration for **field mixtures** test for this study (Mix No. 18 = Type I/II + 50% GGBF Slag, Mix No. 19 = Type I + 20% F fly ash)

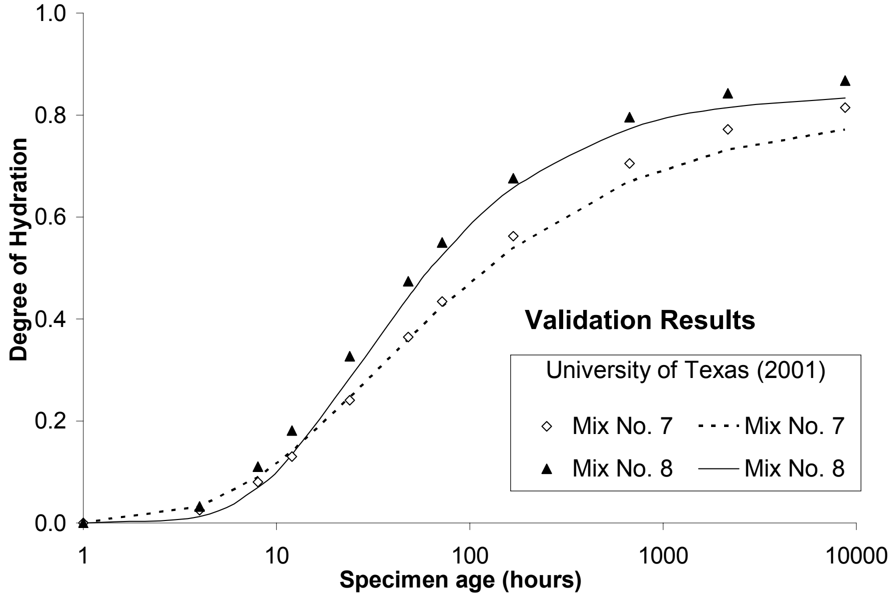

Figure 5-54: Predicted and measured degree of hydration for **field mixtures** test for this study (Mix No. 20 = Type I + 25% C fly ash, Mix No. 21 = Type I + 30% C fly ash)

After comparing the measured versus the predicted degree of hydration for the test results reported by Kjellsen and Detwiler (1991) an r^2 of 0.937 was obtained for the data. The comparison of the predicted and measured degree of hydration at 20°C is shown in Figure 5-55.

The largest difference in the predicted degree of hydration for the data collected by Kjellsen and Detwiler can be attributed in the difference in the ultimate degree of hydration. In order to evaluate the goodness of the prediction provided by the hydration time and slope parameters, the ultimate degree of hydration as test was used. This result is shown in Figure 5-56, and the accuracy of the prediction is much improved as an r^2 of 0.978 is now obtained.

In this section, the results predicted by a general use degree of hydration model was compared to that obtained from test other than those used during the initial calibration of the model. This validation exercise revealed that the recommended hydration model is able to accurately predict the degree of hydration development for different concrete mixtures.

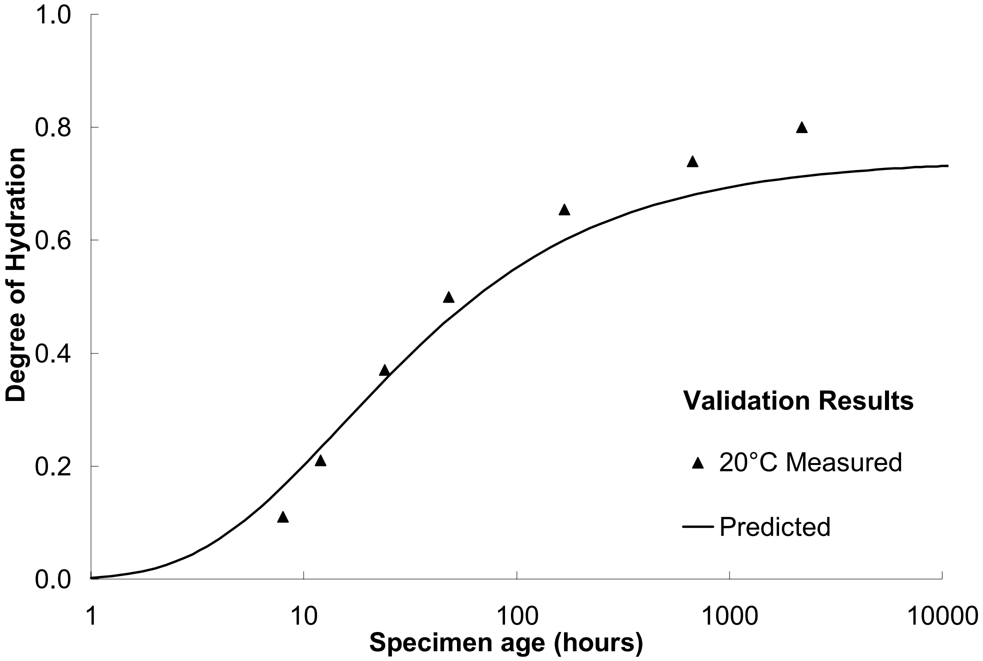

Figure 5-55: Measured versus predicted degree of hydration for Kjellsen and Detwiler (1991) data

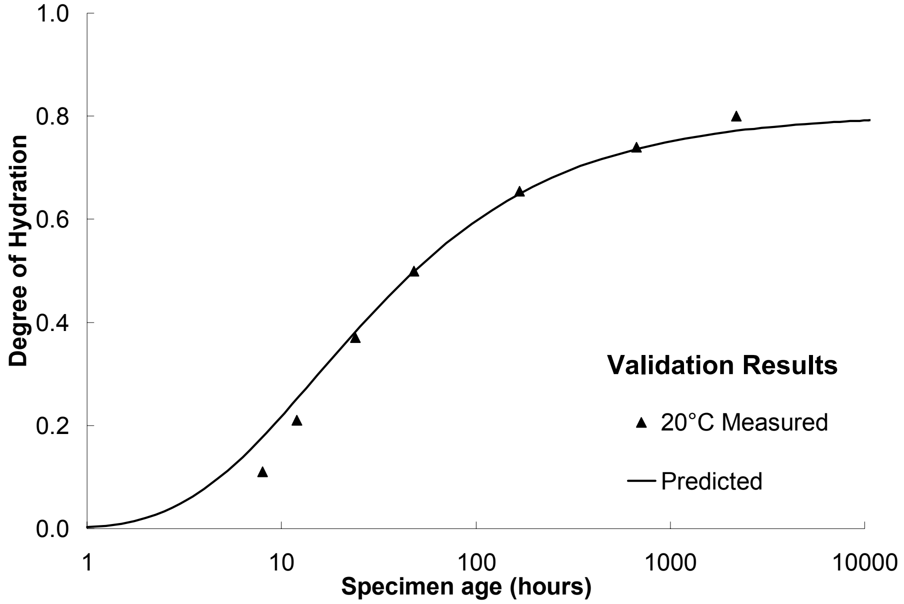

Figure 5-56: Prediction results with a modified ultimate degree of hydration for Kjellsen and Detwiler (1991) data

5.3.7 Sensitivity Analysis of the Recommended General Hydration Model

This section will provide a sensitivity analysis of the general hydration model developed during this study. The sensitivity analysis was performed by choosing a baseline condition and, thereafter, only one of the parameters is modified at a time. As stated previously, this does not necessarily reflect what would happen for actual cements. For example: a change in C_3A would necessitate a change in C_3S to keep the total compound percentage under 100%. However, in order to evaluate the effect of a change in each parameter, this approach is considered appropriate. The ranges of variables were determined based on what is typically found in the state of Texas. Figures 5-57 through 5-65 presents the results obtained from the sensitivity analysis. These results provide insight to the contribution of each of the parameters to the overall hydration process.

Since a change in fineness is generally accompanied by a change in gypsum to control the rate of setting the amount of sulfates were adjusted according to the formulation presented by Frigione (1981). The optimum gypsum content can be determined from Frigione (1981):

$$p_{SO_3} = 0.556 \cdot p_{Alkalies} + 0.00177 \cdot Blaine - 0.1072 \cdot P_{Fe2O3} - 0.00360 \qquad \textit{Equation 5-25}$$

where, p_{SO3} = weight ratio of optimum gypsum content,

$p_{Alkalies}$ = weight ratio of equivalent alkalies,

p_{Fe2O3} = weight ratio of ferric oxide, and

Blaine = Blaine value, specific surface area of cement (m^2/kg).

Equation 5-25 was used to incorporate the accompanying effect a change in fineness will have on a change in sulfate content. Figures 5-57 and 5-58 present what effect of change in cement fineness has on the degree of hydration development. The higher the cement fineness, the earlier the acceleration phase of the cement will initiate. This is due to the larger surface area of the cement grains that are exposed to water. This is in accordance with other research findings (Bentz et. al, 1999). When finer ground cement is used, the rate of hydration is higher and it occurs much earlier, compared to when coarse cement is used.

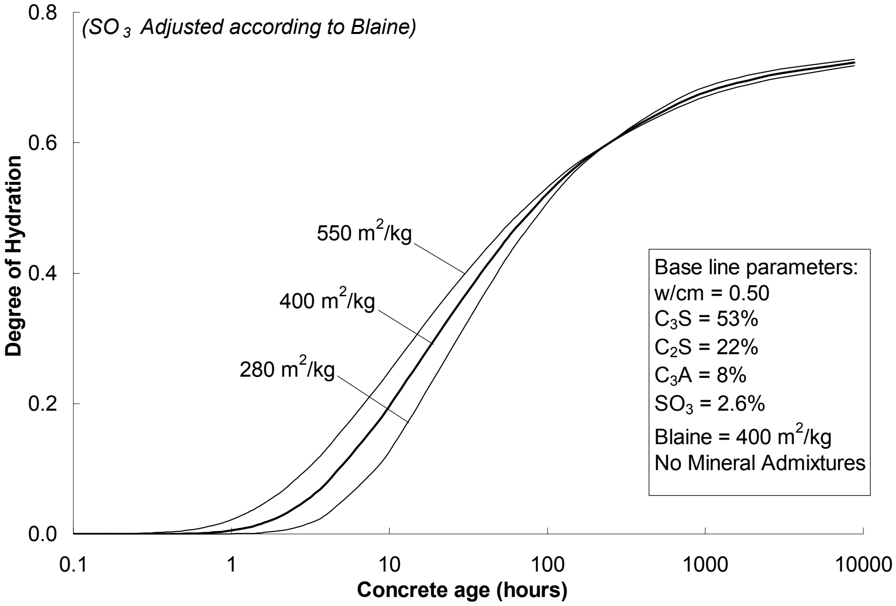

Figure 5-57: Sensitivity analysis of the degree of hydration model: Effect of Blaine Value

Figure 5-59 presents the predicted effect of change in C_3S content. The change in C_3S does not seem to have a significant impact on the degree of hydration development. However, it should be remembered that in the contents of this sensitivity analysis all other parameters were kept unchanged. This is very unlikely when the C_3S content changes by 35%. The analysis results indicate that the higher the C_3S content, the higher the slope of the degree of hydration curve, which was also found by previous researchers (Neville, 1995).

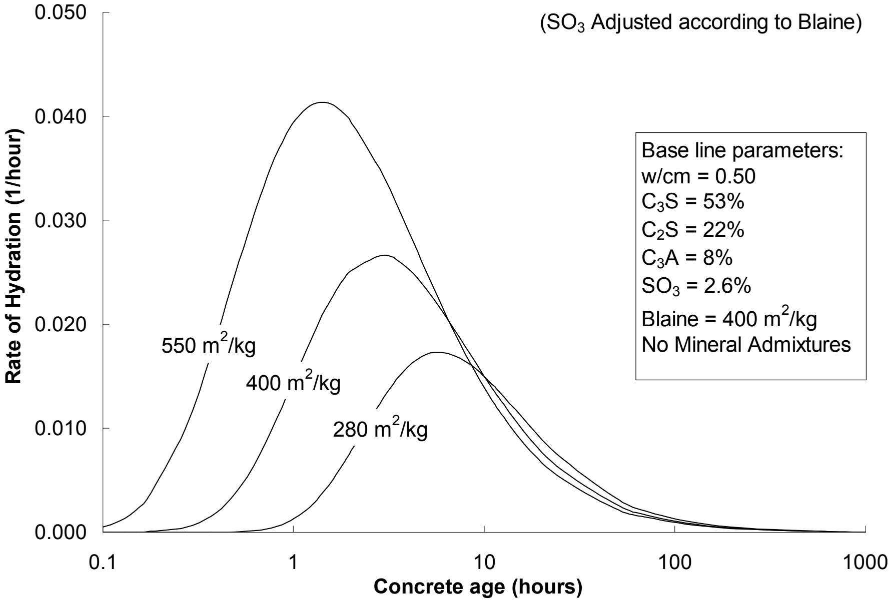

Figure 5-58: Sensitivity analysis of the rate of hydration: Effect of Blaine value

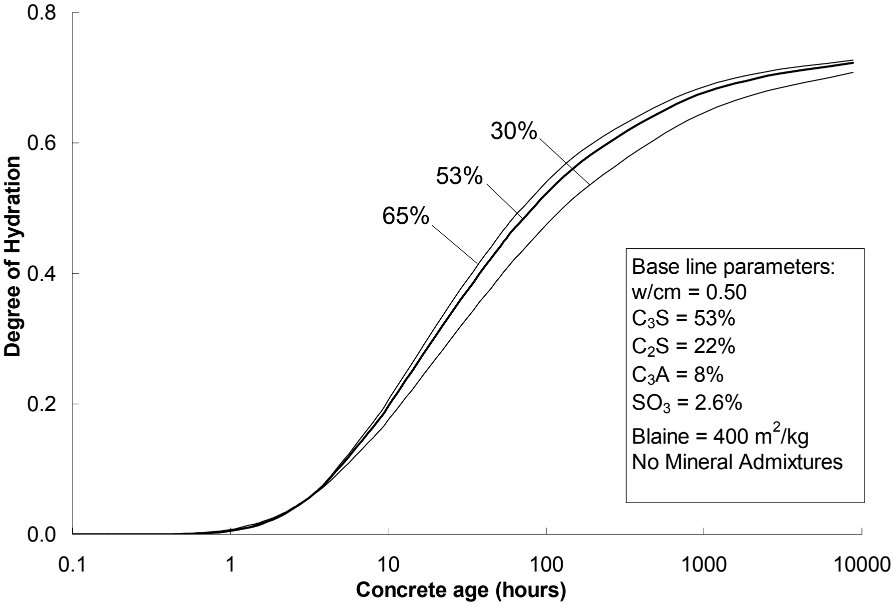

Figure 5-59: Sensitivity analysis of the rate of hydration: Effect of C$_3$S

Figure 5-60 presents the predicted effect of change in C$_3$A content, and the higher the C$_3$A content, the higher the slope of the degree of hydration curve. This effect is in accordance with past published results (Neville, 1995). Type III cements typically have higher C$_3$A contents, which is one reason why they exhibit rapid early-age strength gains.

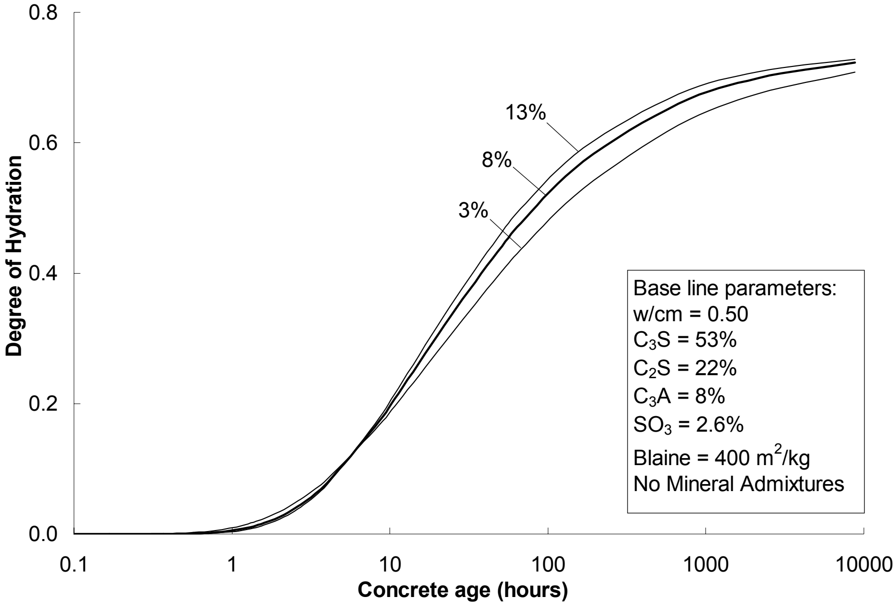

Figure 5-60: Sensitivity analysis of the rate of hydration: Effect of C_3A

Figure 5-61 presents the significant effect a change in SO_3 content has on the degree of hydration development. This figure indicates that the amount of sulfates in the cement have the most significant effect of all the parameters used in the model. The higher the sulfate content, the faster the early-age rate of hydration. These findings are in accordance with published results (Frigione, 1983). It is worth noting that parts of the sulfates are already in the clinker, and then calcium sulfate (gypsum ($CaSO_4 \cdot 2H_20$), hemihydrate ($CaSO_4 \cdot ½H_20$), or anhydrate ($CaSO_4$)) is further added during the grind process to obtain the final cement with the desired sulfate content.

The effect of sulfate on hydration can be explained by keeping the production of cement in the context of Equation 5-25 in mind. During the manufacture of cement, most of its chemical composition is balanced, in order to provide cement with the required rate of setting and appropriate rheology. Equation 5-28 indicates that when a higher fineness is desired (longer grinding) more sulfates (gypsum) are required to help with the grindability during production (Frigione, 1983). Sulfates are used to retard the hydration of C_3A to avoid flash set, and a high amount of sulfates indicate that a higher reactive amount of C_3A is present which needs to be controlled. The system is balanced, since having excess sulfates is undesirable as this could cause future durability problems. Excess gypsum may lead to expansion.

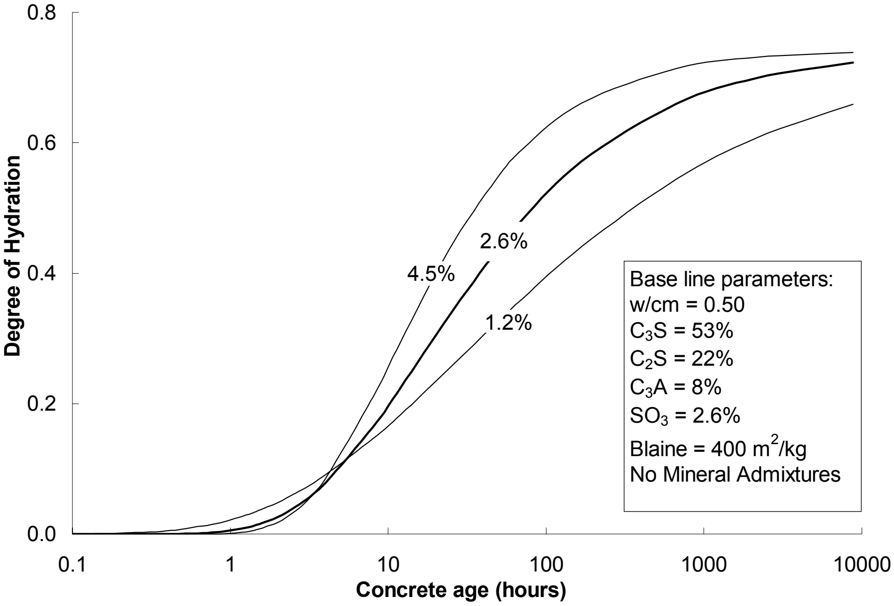

Figure 5-61: Sensitivity analysis of the degree of hydration model: Effect of SO_3

Figure 5-62 presents the effect of a change in water-cementitious ratio on the degree of hydration. As discussed in Section 2.2.2, the water-cementitious ratio affects the ultimate degree of hydration. Figure 5-62 is similar to the trends shown in Figure 2-8 and 2-9.

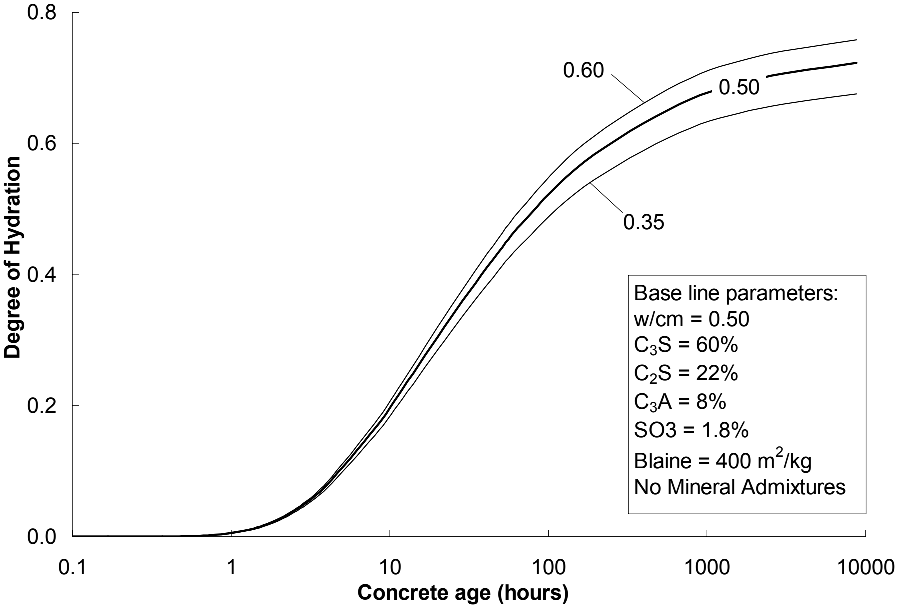

Figure 5-62: Sensitivity analysis of the degree of hydration model: Effect of w/cm ratio

Figures 5-63 through 5-65 present the effect of mineral admixtures on the degree of hydration development. The effect of fly ash and GGBF slag are as discussed in previous section. It is worth noting from Figures 5-63 and 5-64, that the fly ash CaO content appears to provide an effective means to differentiate between the cementitious nature of different fly ash sources.

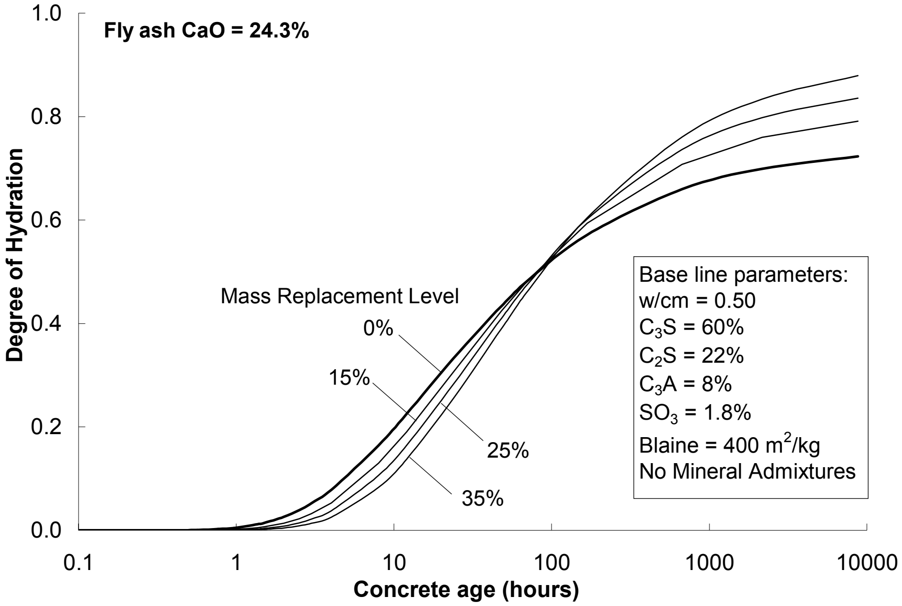

Figure 5-63: Sensitivity analysis of the degree of hydration model: Effect of Class C fly ash

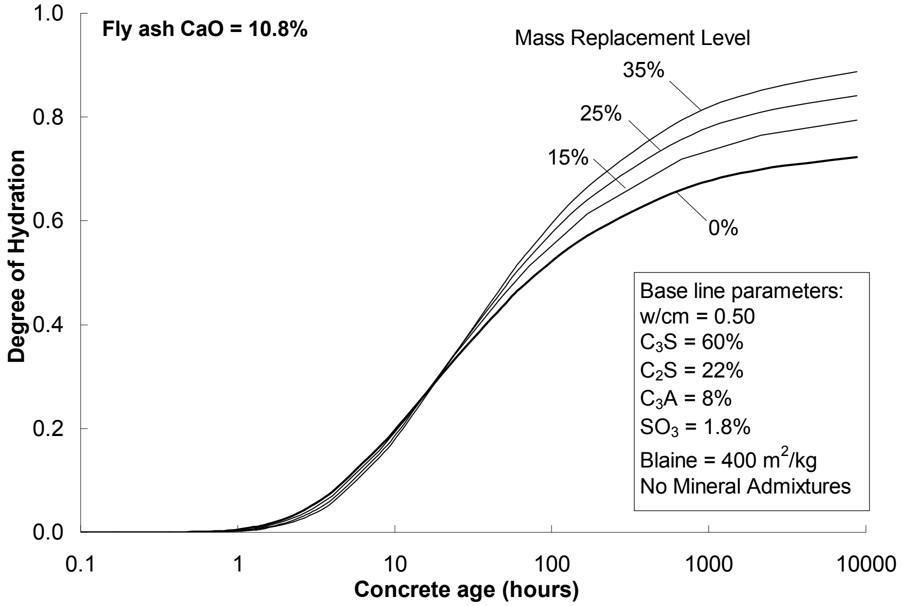

Figure 5-64: Sensitivity analysis of the degree of hydration model: Effect of Class F fly ash

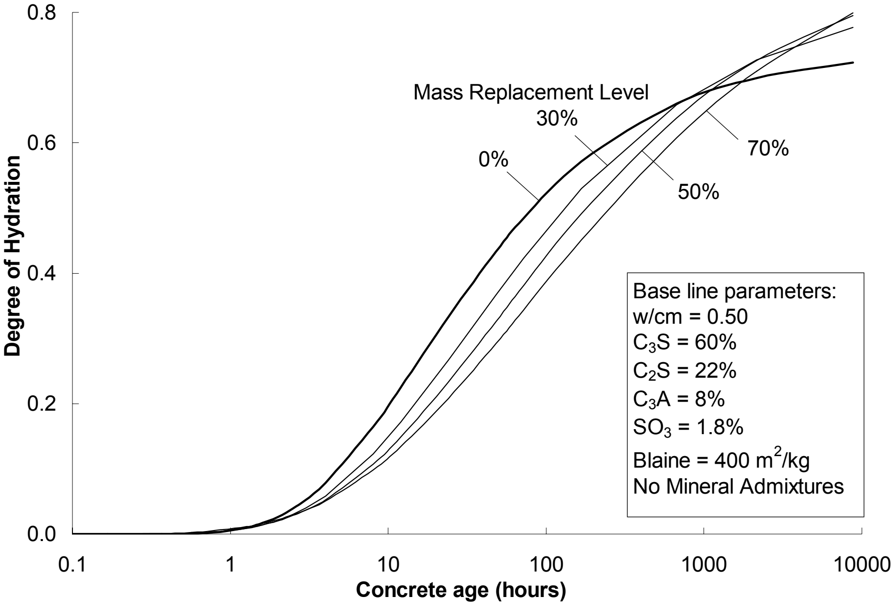

Figure 5-65: Sensitivity analysis of the degree of hydration model: Effect of GGBF Slag

5.3.7.1 *Comments of the Effect of Alkalies*

The effect of alkalies is not directly considered in the proposed model, since alkalies is not one of the predictor variables of the hydration model. The effects of alkalies can indirectly be considered, since the optimum amount of sulfates is strongly influenced by the amount of alkalies present. Neville (1995) states that, "...the amount of gypsum required increases with the C_3A content and also with the alkali content of the cement." In this section, it is proposed to evaluate the effect of an increase in alkali content, with Equation 5-25. This formulation indicates that an increase in alkalies will produce an increase in sulfate content, which will influence the degree of hydration development.

Figure 5-66 presents the indirect effect of equivalent alkalies on the degree of hydration development. More alkalies in the cement require more sulfates to produce optimum cement, which increases the slope of the degree of hydration development.

The equivalent alkali content of all the cements obtained from the field sites ranged from 0.53% to 0.63%. All these cements were, therefore, close to fulfilling the requirements of being low-alkali cements. ASTM C 150 limits the amount of equivalent alkalies to no more that 0.6% in low-alkali cements.

A

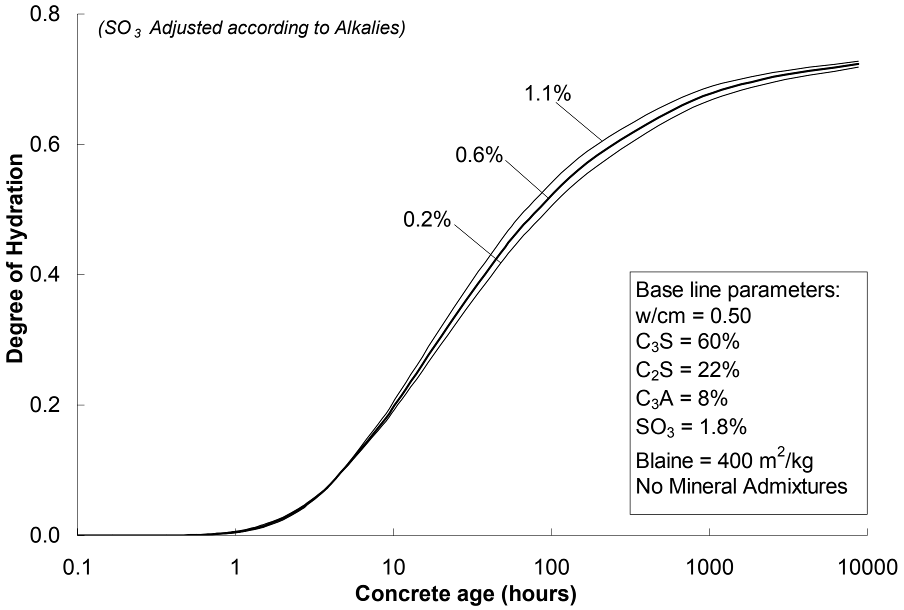

Figure 5-66: Sensitivity analysis of the degree of hydration model: Effect of Cement Alkalies

5.4 SUMMARY AND CONCLUSIONS

This chapter presented the development of a general hydration model for cementitious materials. In this section, conclusions and recommendation regarding the temperature sensitivity and degree of hydration model will separately be discussed.

5.4.1 Remarks Regarding the Temperature Sensitivity (Activation Energy)

This chapter presents a critical review of the meaning and definition of the activation energy for use in both hydration modeling and strength prediction. The activation energy defines the temperature sensitivity of a mixture. Key to understanding the concept behind the traditional maturity methods is to realize that the effect of temperature **only affects the time of occurrence** of the property being estimated.

This document presents evidence from various sources that different activation energy values should be used when mechanical properties and the development of hydration (chemical effects) are considered. The cross-over effect develops only when mechanical properties are considered and not when the degree of hydration development is considered. The activation energy determined with the ASTM C 1074 should not be used to define the temperature sensitivity of the cement hydration process. Conclusions, recommendations, and need for future research on the activation energy for use during hydration are as follows:

5.4.1.1 *Conclusions regarding the Activation Energy for Hydration Prediction*

In all cases investigated, the data indicated that the heat of hydration data obeys the Arrhenius principle, since the activation energy was determined to be independent of the hydration temperature. The Arrhenius plot was constructed for the 20 different cements tested by Lerch and Ford (1948). The lowest r^2 value obtained after fitting a straight line to the data on the Arrhenius plot was 0.978. Ma et al. (1994) performed isothermal calorimeter tests at a wide range of curing temperatures, and the Arrhenius plot obtained from their data showed no temperature dependency.

The Freiesleben Hansen Pedersen (1977) activation energy formulation is a function of the curing temperature, and it did not provide an accurate prediction for hydration development at different temperatures. The Freiesleben Hansen Pedersen (1977) formulation is more appropriate for use during the strength prediction.

The slope of the Arrhenius plot varied depending on the chemical composition of the cement. The highest activation energy was obtained for Type III cements and the lowest values for Type IV and V cements. The activation energy for different cements ranged from 36,132 J/mol to 54,467 J/mol. A multivariate nonlinear statistical analysis indicated that the change in activation energy can accurately be modeled in terms of the Blaine value, the C_3A content, and the C_4AF content of the cement. The goodness of fit was evaluated for this model, and it was shown to fulfill all the requirements of a valid regression analysis. The final model is shown under the recommendations contained in this section.

The **hydration** at different temperatures can accurately be predicted through the equivalent age maturity method and the use of an experimentally determined **constant** activation energy.

The maximum degree of hydration is unaffected by the curing temperature. Cervera and Prato (1999) came to a similar conclusion as they state that the final degree of hydration is the same for samples cured at any temperature, and that the final degree of hydration basically depends on the initial water content of the mixture.

5.4.1.2 *Recommendations*

In Chapter 4, Table 4-16, it is shown that different activation energy values are obtained when different strength-maturity functions are used. This was also found by Pinto (1997) as shown in Table 5-4, and the difference in activation energy values is significant. ASTM C 1074 does not account for this inconsistency, and it is recommended that it should be mentioned that the same strength-maturity function used to determine the activation energy should be used during the strength prediction.

It is recommended that the data obtained from the ASTM C 1074 test procedure be evaluated to determine the limits over which the traditional maturity method provides sufficient estimates of the measured strength. For mixtures where poor predictions with the maturity methods are obtained, it is recommended that the strength-maturity relationship be developed from specimens cured as close as possible, to the temperature range the in place concrete would be experience during early-ages. The temperature range over which the strength is to be predicted should be limited to a range wherein an accurate prediction can be reached.

An activation energy model is developed that accounts for differences in cement chemical composition, and the use of mineral admixtures. It was shown that the activation energy model for cements meets all the requirements for a multivariate linear regression analysis, and that 95% of the error is within a degree of hydration of ±0.055. The recommended activation energy is shown in Equations 5-16 and 5-17, and will be presented together with the general hydration model in Section 5.4.2.3.

The model above was developed based on an extensive data base of cement hydration characteristics. However, the activation energy modification factor to account for the effect of mineral admixtures was based on limited data and engineering judgment. Additional experimental work is required to determine the effect of both mineral and chemical admixtures on the activation energy.

5.4.1.3 *Recommendations for Future Research regarding the Activation Energy*

Based on the material covered in this document, the following aspects that required more development and research were identified:

- The temperature sensitivity of a cementitious system can best be evaluated by means of isothermal calorimeter testing, conducted at different temperatures. Isothermal conduction calorimeter tests at different temperatures are recommended to determine the activation energy for hydration purposes. Limited tests of this nature have been performed on cementitious materials used in Texas. It is recommended to test various cements, and cementitious systems to develop improved activation energy models for hydration and temperature prediction.
- The effect that mineral admixtures such as fly ash and GGBF Slag have on the activation energy should be determined. The model developed in this study is based on the limited information presented by Ma et al (1994).
- The effect that chemical admixtures have on the activation energy for hydration prediction is uncertain. Currently, little information is available on this subject. Isothermal calorimeter testing on mixtures with different chemical admixtures will provide valuable insight as to their effect on the temperature sensitivity of the hydration process.
- It is recommended that a statistical analysis be performed on the strength data collected during this study. A statistical analysis could provide useful insight to the factors that influence the strength development at different curing temperatures.

5.4.2 Concluding Remarks on the Degree of Hydration Model

In order to investigate the hydration characteristics of typical Texas paving mixtures, 21 different concrete paving mixtures were tested by semi-adiabatic calorimeter testing. A data base of test results and all the known variables was developed for these mixtures. Additionally, to expand the data base for cements, the result of tests performed by the PCA on 20 different cements was incorporated. These tests include heat of solution and conduction calorimeter tests data. After the formulation of a general hydration model, the model was calibrated to this data set by a multivariate nonlinear regression analysis. The data base consisted of 34 different mixtures, made from 23 different cements. It is shown that the explanatory variables are statistical significant, and that the model provides a reasonable accurate representation of the test data. A sensitivity analysis of the proposed degree of hydration model is provided, from which the effect and role of each variable in the model was evaluated.

A mechanistic-empirical model is proposed to characterize the heat of hydration of concrete at an isothermal curing temperature of 21.1°C. The model considers the effect of:

- Cement chemical composition: C_3A, C_3S, C_2S, C_4AF, SO_3, MgO, and Free Lime
- Cement Fineness: specific surface area (Blaine Index)
- Mineral admixtures: Class F fly ash, Class C fly ash, and GGBF slag
- Mixture proportions: cement content, water-cementitious ratio, mineral admixture replacement level, coarse aggregate content, and fine aggregate content
- Concrete properties: density, thermal conductivity, specific heat

5.4.2.1 *Conclusions regarding Concrete Hydration*

Based on the data reviewed and analyzed in this document the following conclusions can be made:

- Semi-adiabatic testing provides a convenient indirect means to characterize the formation of hydration products by measuring the heat released during hydration.
  - The temperature sensitivity (activation energy) of the mixture is required in order to back-calculate the true adiabatic temperature rise of the mixture.
  - During the back-calculation of the true adiabatic temperature rise, it is not sufficient to account for only the loss in temperature associated with the semi-adiabatic curing conditions. The additional concrete hydration, if the sample was at the higher adiabatic temperature, needs to be included to obtain the true adiabatic temperature.
- The degree of hydration development can effectively be modeled with the exponential expression shown in Equation 3-21.
- The development of the degree of hydration is influenced by the cement chemical composition, the cement fineness, the use of mineral admixtures, and the mixture proportions

used in the concrete mixture. The effect of each parameter can be summarized as shown in Table 5-12.

Table 5-12: The effect of different parameters on the proposed hydration model

Parameter	Value	See Figure	Effect on Degree of Hydration		
			Start of Acceleration Phase	Rate (Slope)	Ultimate Value
C_3A	↑	5-60	-	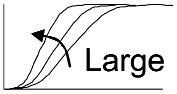	-
C_3S	↑	5-59	-	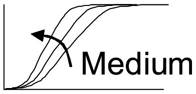	-
SO_3	↑	5-61	-	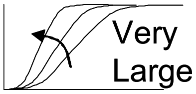	-
Cement Fineness: (Blaine Value)	↑	5-57 and 5-58	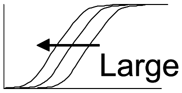	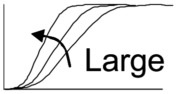	-
Class F fly ash dosage	↑	5-63	-	-	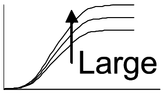
Class C fly ash dosage	↑	5-64	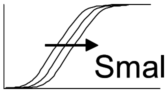	-	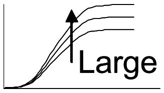
GGBF slag dosage	↑	5-65	-	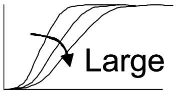	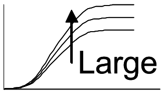
w/cm ratio	↑	5-62	-	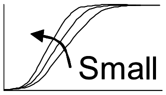	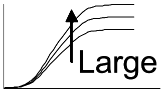
Alkalies [a]	↑	5-66	-	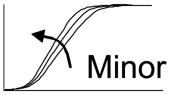	-

Note: [a] Alkalies are indirectly considered through the SO_3 content

- Results from semi-adiabatic tests revealed that complete hydration does not occur in any of the concretes tested. This directly affected the total amount of heat released during hydration. Past literature sources were reviewed that provides plausible explanations for this phenomenon. The ultimate degree of hydration is unaffected by the curing temperature.

- Class C fly ash retarded the hydration of cement, and increased the ultimate degree of hydration.
- The use of Class F fly ash reduces the amount of heat generated, since it acts as inert filler and contributes much less to the heat of hydration than the cement it replaced.
- The use of GGBF Slag is very effective to reduce the rate of hydration, however the total heat of hydration of GGBF appears to be similar to that of cement.

5.4.2.2 *Recommendations*

After the analysis performed in this document, the following recommendations may be made:

- A generic hydration model for cementitious materials was developed, calibrated and validated in this document. This model is recommended for use in the temperature prediction program in order to characterize the effect of different cements and mineral admixture on the hydration. The recommended model is summarized in Section 5.4.2.3:
    - In projects were higher confidence levels for temperature prediction is required, it is recommended to subject the proposed concrete mixture to adiabatic calorimeter tests. With this test data, the prediction of the degree of hydration is no longer required, and the accuracy of the model irrelevant.
    - As additional test data are collected, these should be centrally assembled in a data base. It is recommended to re-evaluate and modify the proposed models in this document based on this expanded data base.
    - The effects of chemical admixtures are currently not considered in the hydration models. It is recommended to incorporate means to adjust the degree of hydration curve to account for the effect of mineral mixtures. However, these means will be based on additional tests performed by the user.
- It is recommended to evaluate the ultimate degree of hydration based on the amount of non-evaporatable water. These tests could be performed for different mineral admixtures, and curing temperatures.
- The validity of the contribution of fly ash in terms of its CaO content, as shown in Equation 4-1, should be evaluated based on long-term heat of hydration tests. The test results from semi-adiabatic testing cannot be used to evaluate the models accuracy, since these value need to be known to back calculate the degree of hydration for the mixture.
- Cement fineness has a major impact on the degree of hydration development. Some literature reports greater accuracy by using the particle size distribution. This approach should be evaluated to determine if it provides increased prediction accuracy. In this work, the Blaine value was used, simply because it leans it self to implementation, since it can readily be obtained from the cement certificate.

5.4.2.3 *Recommended General Hydration Model for Cementitious Materials*

Over the course of this Chapter, the component necessary to predict the hydration of a cementitious mixture is presented. In this section, all the recommended components are presented in a concise format. The degree of hydration is expressed with the following exponential function:

$$\alpha(t_e) = \alpha_u \cdot \exp\left(-\left[\frac{\tau}{t_e}\right]^{\beta}\right)$$

Previously Equation 3-21

where, $\alpha(t_e)$ = the degree of hydration at equivalent age, t_e,

τ = hydration time parameter (hrs),

β = hydration shape parameter, and

α_u = ultimate degree of hydration.

The rate of heat liberation is defined as follows:

$$Q_h(t) = H_u \cdot C_c \cdot \left(\frac{\tau}{t_e}\right)^{\beta} \cdot \left(\frac{\beta}{t_e}\right) \cdot \alpha(t_e) \cdot \frac{E}{R}\left(\frac{1}{273+T_r} - \frac{1}{273+T_c}\right)$$

Previously Equation 3-39

where, $Q_h(t_e)$ = rate of heat liberation at equivalent age, t_e, (W/m^3),

C_c = cementitious materials content (g/m^3), and

H_u = total heat of hydration of cementitious materials at 100% hydration (J/g), defined as:

$$H_u = H_{cem} \cdot p_{cem} + 461 \cdot p_{SLAG} + 1800 \cdot p_{FA-CaO} \cdot p_{FA}$$

Previously Equation 4-1

where, p_{SLAG} = slag mass ratio ito total cementitious content,

p_{FA} = fly ash mass ratio ito total cementitious content,

p_{FA-CaO} = fly ash CaO mass ratio ito total fly ash content,

p_{cem} = cement mass ratio ito total cementitious content, and

H_{cem} = heat of hydration of the cement, defined by (Bogue, 1947) as:

$$H_{cem} = 500 \cdot p_{C_3S} + 260 \cdot p_{C_2S} + 866 \cdot p_{C_3A} + 420 \cdot p_{C_4AF} + 624 \cdot p_{SO_3} + 1186 \cdot p_{FreeCa} + 850 p_{MgO}$$

Previously Equation 3-12

where, p_i = mass ratio of i-th component ito total cement content.

A multivariate nonlinear regression model was developed based on heat of solution, conduction calorimeter, and semi-adiabatic calorimeter test data. An r^2 of 0.988 was achieved with this model. At the isothermal curing temperature of 21.1°C, the recommended model is as follows:

$$\tau = 66.78 \cdot p_{C_3A}{}^{-0.154} \cdot p_{C_3S}{}^{-0.401} \cdot Blaine^{-0.804} \cdot p_{SO_3}{}^{-0.758} \cdot \exp(2.187 \cdot p_{SLAG} + 9.50 \cdot p_{FA} \cdot p_{FA-CaO})$$

Previously Equation 5-22

$$\beta = 181.4 \cdot p_{C_3A}{}^{0.146} \cdot p_{C_3S}{}^{0.227} \cdot Blaine^{-0.535} \cdot p_{SO_3}{}^{0.558} \cdot \exp(-0.647 \cdot p_{SLAG})$$

Previously Equation 5-23

$$\alpha_u = \frac{1.031 \cdot w/cm}{0.194 + w/cm} + 0.50 \cdot p_{FA} + 0.30 \cdot p_{SLAG} \ \leq \ 1.0$$

Previously Equation 5-24

where, p_{C3A} = weight ratio of tricalcium aluminate ito total cement content,
p_{C3S} = weight ratio of tricalcium silicate ito total cement content,
p_{SO3} = sulfate weight ratio ito total cement content,
Blaine = Blaine value, specific surface area of cement (m^2/kg), and
w/cm = the water-cementitious material ratio.

The temperature sensitivity of the hydration process was evaluated based on heat of solution and conduction calorimeter tests data. The tests were performed over a temperature range of 4.4°C to 40.6°C. The best fit activation energy (*E*) model was developed and found to be **independent** of curing temperature. This is in agreement with the Arrhenius theory for rate processes in chemical reactions. The recommended activation energy model is defined as follows:

$$E = 22{,}100 \cdot f_E \cdot p_{C_3A}{}^{0.30} \cdot p_{C_4AF}{}^{0.25} \cdot Blaine^{0.35}$$

Previously Equation 5-17

where, p_{C3A} = weight ratio of tricalcium aluminate Bogue compound,
p_{C4AF} = weight ratio of tetracalcium aluminoferrite Bogue compound,
Blaine = Blaine value, specific surface area of cement (m^2/kg), and
f_E = Activation energy modification factor, defined as:

$$f_E = 1 - 1.05 \cdot p_{FA} \cdot \left(1 - \frac{p_{FACaO}}{0.40}\right) + 0.40 \cdot p_{SLAG}$$

Previously Equation 5-16

where, p_{FA} = Mass ratio replacement of the fly ash,
p_{FACaO} = Mass ratio of the CaO content in the fly ash, and
p_{SLAG} = Mass ratio replacement of the GGBF Slag.

5.4.2.4 *Assumptions/Limitations:*

There are inherent limitations and assumptions to the proposed model. The calibration approach taken during the model development imposes some limits of which the user should take account off. The assumptions and limitations associated with the proposed hydration model are as follows:

- A mechanistic-empirical model is only valid with the range it was calibrated for. The model should not be used to predict hydration outside of the range of parameters listed in Tables 5-9 and 5-10. It is not recommended to extrapolate beyond these ranges. Table 5-9 presents the range of chemical and physical properties of the cements. Table 5-10 presents the range of the range of mixture proportions and mineral admixtures properties used for the calibration of the hydration model
- The effects of chemical admixtures are currently not considered in the hydration models.
- The model assumes that the interaction between the mineral admixtures and the base cement source applies to all combinations of cement and mineral admixtures.

Chapter 6

Temperature Model Calibration

The hydration of a concrete mixture is a process that liberates heat, and the rate of heat generation is accelerated with an increase in concrete temperature. Concrete is a poor conductor of heat, and at high temperatures, the rate of heat evolution due to the hydration process is, therefore, much greater than the rate of heat dissipation. The temperature development in the concrete structure is determined by the balance between heat generated in the hardening concrete and heat exchange with the environment.

In Chapter 3, different models were selected to facilitate the prediction of in place concrete temperatures. All the model components and the primary variables considered are schematically summarized in Figure 3-1. The overall model includes:

- the heat of hydration of the cementitious materials,
- environmental effects, and
- a heat transfer model that incorporates the heat transfer mechanisms of thermal conduction, convection (including evaporative cooling), solar radiation, and irradiation.

In Chapter 5, the major components of the heat of hydration model were calibrated based on calorimeter data collected under laboratory conditions. These models were also validated with additional test data. Numerous factors influence the concrete temperatures that develop during early-ages, and the interactions of these factors are very complex. It is essential with any mechanistic empirical model that local materials are tested and that the models are calibrated for local conditions. The temperature prediction model will be calibrated based on data collected from actual construction projects across the state of Texas.

In this Chapter, the overall temperature prediction model is calibrated to produce accurate predictions of early-age concrete temperatures measured for the seven construction projects visited during this research effort. Table 6-1 provides a summary of the seven different CRC construction sites visited during this study, and it may be seen that a wide range of paving conditions was encountered that is representative of normal and hot weather paving conditions. Additionally, small insulated concrete specimens were made under controlled laboratory conditions to facilitate the calibration of the temperature prediction model. The model will be calibrated by comparing the concrete temperatures measured in the field to the concrete temperatures predicted with the temperature model. Based on the available data, the model will be calibrated in two phases:

- temperature prediction of small thermal slabs, and

- temperature prediction of field instrumentation sites.

Table 6-1: Different CRC construction sites visited during this study

Construction Site	Date	Description	Temperature Ranges (°C)	
			Air [a]	Concrete
Dallas, IH 45	May 5-7	13¼-inch	19 - 26	23 - 39
Houston, US 59 South	May 11-13	13-inch	26 - 29	28 - 44
Dallas, SH 190	Aug 4-6	12-inch	27 - 38	32 - 62
Houston, FM 529	Aug 25-27	10-inch	23 - 39	32 - 51
El Paso, Loop 375	Aug 17-19	11-inch	19 - 33	30 - 43
Dallas, IH 30	Sept 29-Oct 1	13¼-inch	14 - 30	23 - 40
Houston, US 59 North	Oct 19-21	15-inch	16 - 28	26 - 40

Note: [a] Air temperature range during day of paving

6.1 TEMPERATURE MODEL CALIBRATION WITH DATA COLLECTED FROM SMALL THERMAL SLABS

The third phase of the laboratory test (Section 4.3) involved the measurement of the temperature development in small insulated concrete specimens cured in environmental chambers. The test setup and configuration of the slabs are shown in Figures 4-40 and 4-41. The test results from this phase of the experimental work were presented in Figure 4-42. The hydration parameters were determined by semi-adiabatic calorimeter testing and were previously presented in Table 4-17. For convenience, the specific parameters used for this mixture (Mix No. 8) are summarized in Table 6-2. Other parameters used for the temperature perdition are summarized in Table 6-3.

Table 6-2: Hydration parameters for Mix No. 8

Mix No.	Description	Activation Energy (J/mol) [a]	Hydration Parameters			H_u J/g
			β	τ	α_u	
8	Type I + 30% Class C fly ash	40,304	0.674	23.81	0.884	465

Note: [a] Determined in accordance with the formulation in Equation 5-34.

Table 6-3: Summary of variables for small insulated slabs cured under laboratory conditions

Parameters	Values		
Pavement design and materials			
Measured specimen thickness	10.0 inch (255 mm)		
Coarse aggregate type	0.75-inch Crushed limestone		
Coarse aggregate specific heat [a]	910 J/(kg°C)		
PCC density [a]	2330 kg/m^3		
Thermal conductivity of hardened PCC [a]	2.70 W/m/°C		
Subbase type	Dry sand		
Sand specific heat [a]	795 J/(kg°C)		
Sand thermal conductivity [a]	0.520 W/m/°C		
Sand layer density [a]	1760 kg/m^3		
Environmental conditions	***Day 1***	***Day 2***	***Day 3***
Relative humidity (%)			
Environmental Chamber	35	35	35
Refrigerator Unit	50	50	50
Wind speed (mph)			
Environmental Chamber [b]	5	5	5
Refrigerator Unit	0	0	0
Construction operations	May 5, 2000		
Initial sand temperature	Equal to curing temperature [c]		
Time of carpet drag texturing	Within 30 minutes		
Time of curing application	Within 45 minutes		
Curing method	Double layer white curing compound		

Note: [a] Values were based on published data, as documented in Chapter 3

[b] Air flow in environmental chamber due to use of fans to supply warm air.

[c] Forms and sand layer was left at the curing temperature for 48-hours prior to concrete placement.

6.1.1 Prediction of Temperature Development in Small Thermal Slabs

The temperature prediction model was calibrated by comparing the mid-depth concrete temperature of the small insulated specimens with the values predicted by the models developed in Chapter 3.

The goodness of the temperature prediction was calculated in terms of the coefficient of determination (r^2), and the maximum residual (Error) between the predicted and measured temperature. The calculation of the r^2 value was performed by comparing only two variables; measured versus predicted concrete temperature. This process was used to evaluate prediction accuracy, since the r^2 with this procedure takes into account possible systematic trends in over-prediction or under-prediction. The r^2 with this procedure is determined with only two variables. This allows the use of the simple linear regression model, which guarantees appropriate use of the r^2 value.

It was determined that some of the heat transfer models had to be adjusted to reflect the boundary conditions of the small slabs. Although these specimens were insulated, the fact that the edges were insulated affected the concrete temperatures. The small slabs lose heat in two directions; whereas actual pavements are wide enough so that heat losses primarily occur in one direction. This effect was verified by taking one of the small specimens to the construction project visited in Dallas, May 2000. The specimen was constructed on the actual asphalt surface, and the concrete as delivered to site was used. The small slab was cured similarly to the actual pavement. The pavement was 13.25 inches thick, whereas the small slab specimen was only 10-inches thick. Figure 6-1 presents the measured temperatures at mid-depth of a pavement and in the small insulated specimen from this field site. Note that the initial temperature rise in the small slab is very similar to that of the actual pavement. However, due to the effects described above, the maximum concrete temperature reached is less in the insulated specimen, and the amount of heat lost occurred more rapidly over time. The mid-slab temperature trends of the small slab closely followed the air temperatures, whereas the pavement dissipated the generated heat over a longer period.

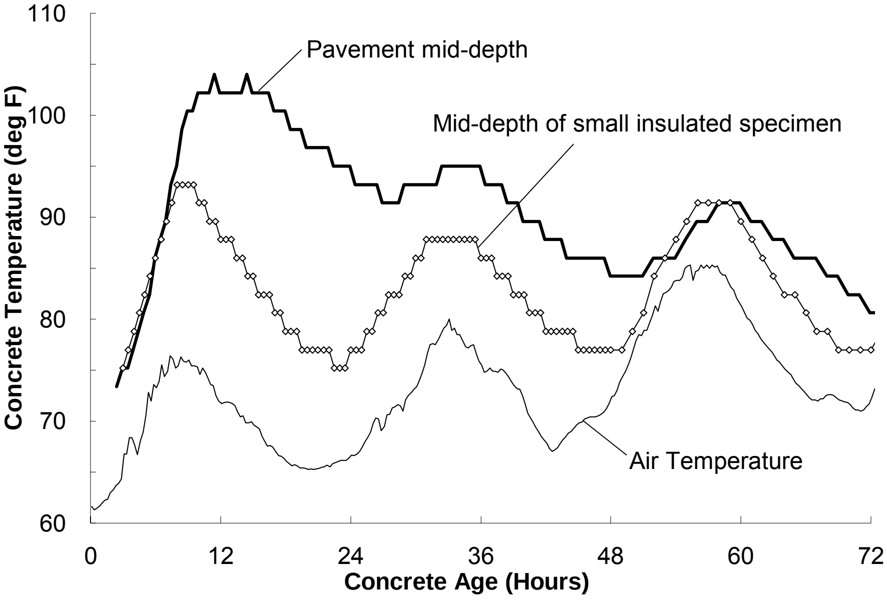

Figure 6-1: Measured temperatures at mid-depth of pavement and small insulated specimen for the field site instrumented in Dallas, May

The approach was taken to adjust the heat transfer models to account for this effect. However, these models will ***not*** be used to represent the actual pavement conditions. With the adjusted heat transfer model, only the effect of the early-age evaporative cooling model and heat of hydration model can be evaluated. The preliminary recommended adjustment to the original age evaporative cooling model and heat hydration model presented in Chapter 3 are discussed in Section 6.1.2. The results of the temperature prediction for all the slabs are presented in Appendix E and Figure 6-1 provides an example of the results obtained.

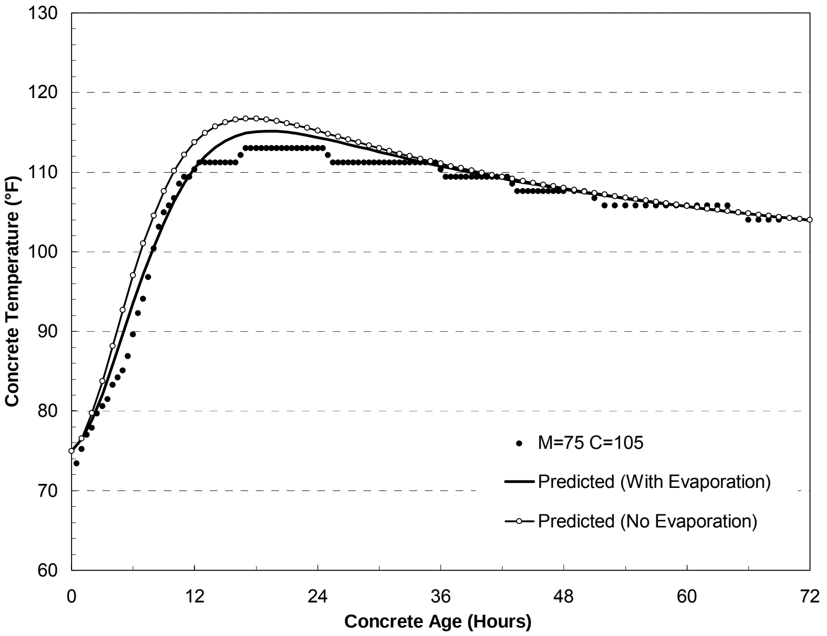

Figure 6-2: Predicted and measured concrete temperature at mid-depth (M=75, C=105)

Table 6-4 provides a summary of the r^2 values and the maximum error obtained from this calibration effort. The average r^2 values range between 0.65 and 0.99, and the error in the predicted maximum temperature ranged between 3.2 and 5.8°F. The lowest r^2 value was obtained for the slab placed and cured under the coldest conditions.

6.1.2 Concluding Remarks Based on Calibration on Small Insulated Slabs

It was determined that the heat transfer in an insulated 13.5x13.5x10-inch concrete slab does not provide an accurate simulation of the heat transfer in hydrating pavements. In retrospect, it was realized that the size of the small slab specimen were initially developed to track the long-term temperature of hardened concrete pavements. Larger small slabs are required to provide temperatures comparable those that develop during early-ages in hydrating pavements. Based on this finding, only preliminary recommendations are provided concerning the heat of hydration model and the effects of evaporative cooling. Based on the initial calibration, the following preliminary conclusions were reached:

- The hydration parameters obtained from the semi-adiabatic calorimeter tests provide an accurate estimate of the heat contribution due to the hydration of the cementitious materials.
- Temperature development in the small insulated slabs is not representative of actual pavement conditions. The use of larger specimens should be considered if this approach is pursued in the future.
- The effect of evaporative cooling of bleed water and free surface water should be accounted for in the heat transfer analysis. Section 6.1.2.1 provides more information on the preliminary model recommended for further calibration with the data collected from the field sites.

Table 6-4: Summary of prediction results obtained for small insulated slabs

Insulated Slab		**Appendix E**	**Prediction Results**	
Mixing Temperature	**Curing Temperature**	**Figure Number**	**r^2**	**Maximum Error (°F)**
55	55	E-1	0.65	4.0
65	75	E-2	0.85	3.2
80	80	E-3	0.94	4.6
70	90	E-4	0.99	5.8
86	90	E-5	0.99	4.5
75	105	E-6	0.97	4.6
95	105	E-7	0.90	5.6

6.1.2.1 *Evaporative cooling effects*

During this temperature prediction exercise, it was found that the effects of evaporative cooling affects the very early-age concrete temperatures. The effect of evaporative cooling may be identified from the temperature history of the thermocouples located close to the top of the pavement surface, as shown in Figures 6-3 and 6-4.

At placement, the fresh concrete temperature was assumed to be uniformly distributed, since it has been thoroughly mixed and vibrated into the wooden forms. The fresh concrete temperatures were respectively 86°F and 95°F in the cases shown in Figures 6-3 and 6-4. However, before 6 hours has elapsed, an apparent reduction in concrete surface temperature occurred immediately following placement. At this time the concrete is still plastic, since setting has not yet occurred and bleeding and the accumulation of surface water is expected. These specimens were cured with liquid curing compound, which will further add surface moisture that will evaporate over time.

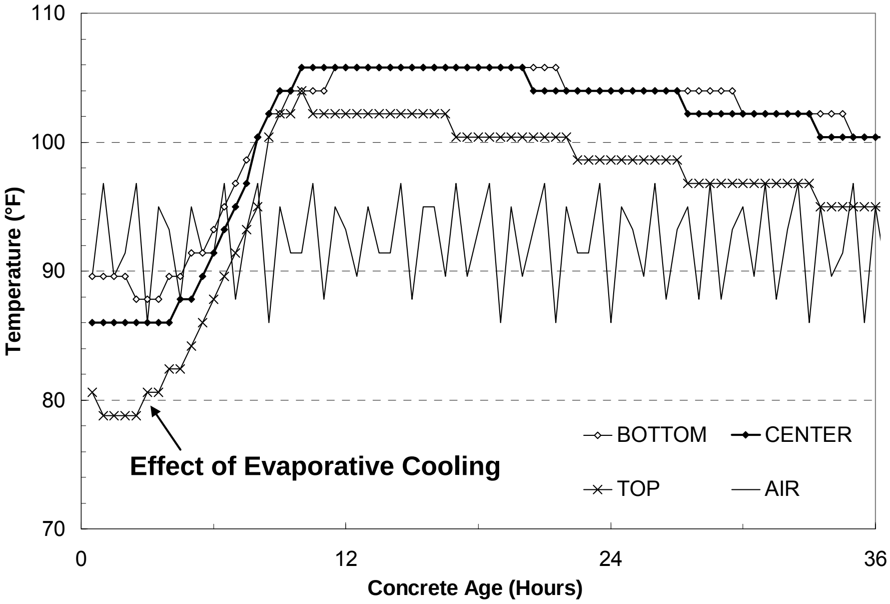

Figure 6-3: Measured top, mid-depth, and bottom temperatures in small specimen (M=86, C=90)

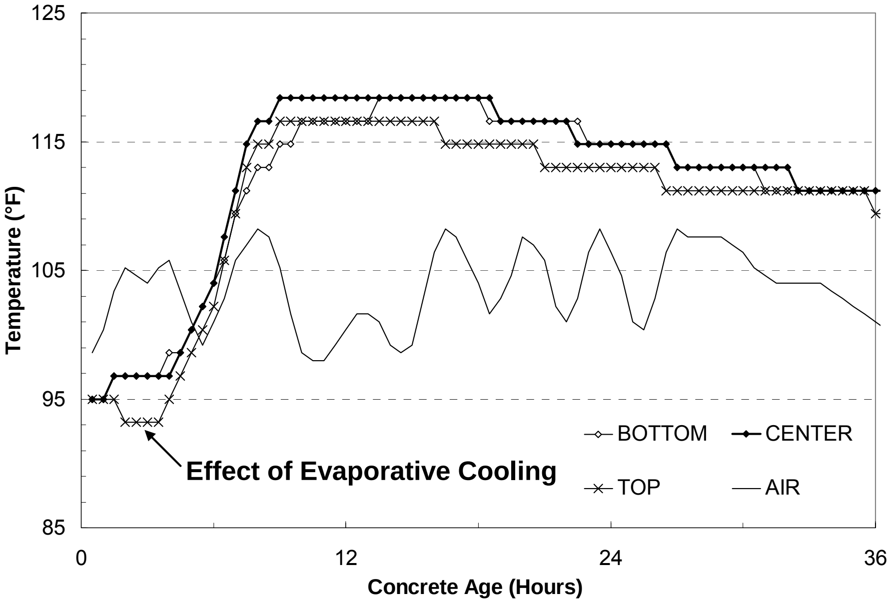

Figure 6-4: Measured top, mid-depth, and bottom temperatures in small specimen (M=95, C=105)

In both the cases shown in Figure 6-3, and 6-4, the air temperature is higher than the concrete temperature, and based on normal heat transfer principles (excluding evaporative cooling), it is expected that the concrete surface temperature should increase due to the presence of warmer air directly above it. However, this does not happen; instead the surface temperature decreases by 6°F and 2°F in the respective figures. It may be concluded that evaporative cooling occurred during early-ages and prevented an increase in concrete surface temperatures due to convection effects.

Heat transfer through evaporative cooling, as presented in Section 3.3.2.1, was included during the prediction of the measured concrete temperatures. The proposed model estimates the rate of evaporation from the concrete surface (E_c). The rate of evaporation from the concrete surface is a function of the concrete age and the evaporation rate of water from a free surface (E_w). Al-Fadhala and Hover (2001) presented the formulation in Equation 3-43 to determine the rate of water loss from a concrete surface as compared to the water loss from a free surface. The effect of this formulation is shown in Figure 6-5 and it may be seen that a rapid reduction in concrete and mortar evaporation rate occurs as the concrete hardens over time. Based on the formulation recommended by Al-Fadhala and Hover (2001), the best fit E_c/E_w model was determined for the small insulated slabs. Based on the heat transfer analysis, the formulation shown in Equation 6-1 is initially recommended for use. The effect of the equation is plotted with the original model in Figure 6-5

$$\frac{E_c}{E_w} = 0.7 \cdot \exp\left(-\left(\frac{t}{3.75} \right)^{1.5} \right) \qquad \textit{Equation 6-1}$$

where, E_c = evaporation rate from a concrete surface (kg/m^2/h),

E_w = evaporation rate from a free water surface (kg/m^2/h), and

t = concrete age (hours).

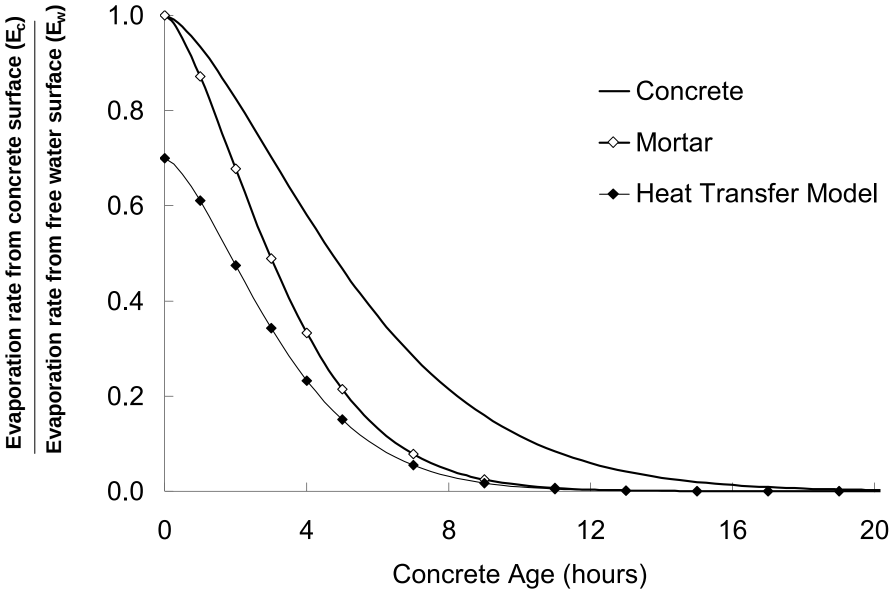

Figure 6-5: Recommended E_c/E_w development compared with published values

The formulation in Equation 6-1 is similar to that originally proposed by Al-Fadhala and Hover (2001) except that the overall effect is reduced by 30%. The reason for this reduction is not known, but it may be attributed to the fact that the tested slabs were covered with two layers of curing compound. In the test performed by Al-Fadhala and Hover, surface curing was not used, which could explain the higher rate of evaporation obtained from their tests.

The accuracy of this evaporative cooling model will be evaluated during the calibration of the temperature prediction model on the data collected from actual PCC construction sites.

6.2 TEMPERATURE MODEL CALIBRATION WITH DATA COLLECTED FROM FIELD SITES

The temperature prediction model was calibrated by comparing the concrete temperatures measured in the field to the simulated concrete temperatures predicted with the temperature model. The measured versus predicted temperatures one-inch from the top, at mid-depth, one-inch from the bottom, as well as the gradient between the top and bottom thermocouple locations were compared.

The approach documented for the small insulated slabs was followed, where the goodness of the temperature prediction is expressed in terms of the coefficient of determination (r^2) and the maximum residual (Error) between the predicted and measured temperatures. The calculation of the r^2 value is performed by comparing only two variables, measured versus predicted concrete temperatures, which guarantees appropriate use of the r^2 value.

Only minor calibration of the models presented in Chapter 3 were necessary to achieve accurate temperature predictions with the heat of hydration and finite difference model. The necessary adjustments are discussed in Section 6.2.1. The measured temperatures and the predicted temperatures for all the field sites are presented in Appendix E.

Figure 6-6 presents a typical example of the measured versus predicted mid-depth concrete temperatures for the afternoon placement in Houston in August. It should be emphasized, that these are sample results for a typical location, which represents neither the best nor worst of the temperature prediction results. Figure 6-7 presents the predicted versus measured temperature gradient for the same section. In both cases it may be seen that an accurate prediction of the in place temperatures is obtained.

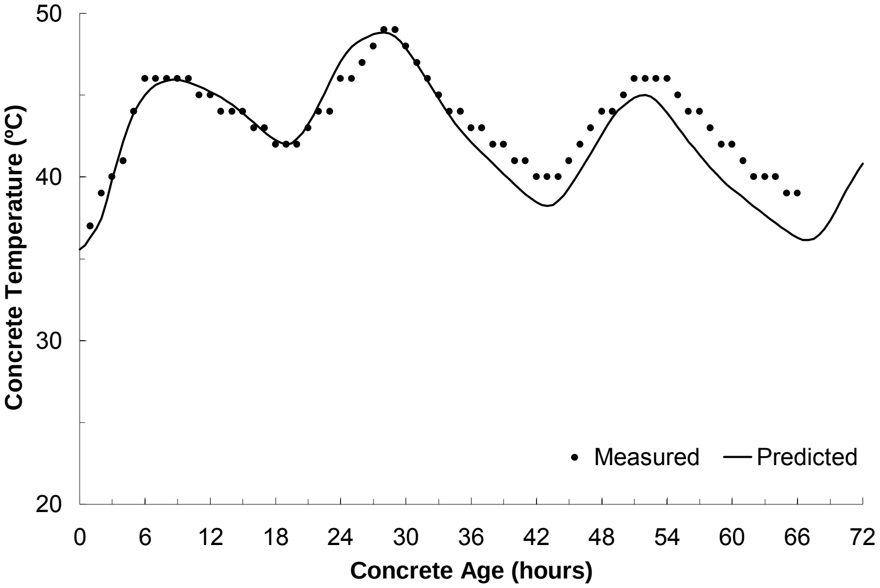

Figure 6-6: Calibration results: Concrete temperatures at mid-depth for Houston, August, 2:45pm placement

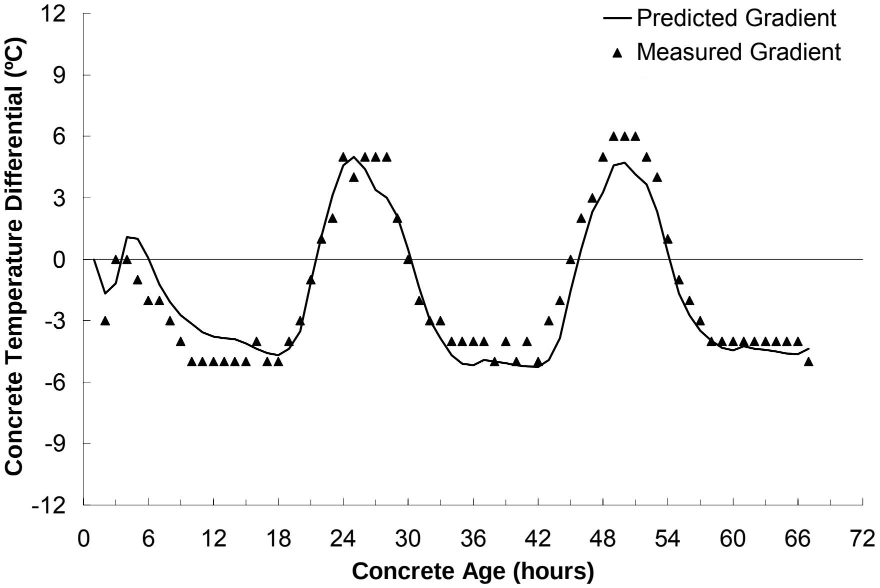

Figure 6-7: Calibration results: Concrete temperature gradient for Houston, August, 2:45pm placement

The r^2 values obtained for all the sites are summarized in Table 6-5. This table provides r^2 values for each of the three locations instrumented, the average r^2 value for all the measured temperatures, and the r^2 value obtained for the temperature gradient. Figure 6-8 provides the cumulative distribution plots of the r^2 values for each of the three locations instrumented and for the temperature gradient. Figure 6-9 provides the cumulative distribution plot of the average r^2 values obtained for the calibration of the temperature prediction model. From these Figures, the following comments may be made:

- **Top of Slab,** Figure 6-8 (a): In 36% of the cases, the r^2 value was equal to or less than 0.80.
- **Mid-depth,** Figure 6-8 (b): In 27% of the cases, the r^2 value was equal to or less than 0.80.
- **Bottom of Slab,** Figure 6-8 (c): In 27% of the cases, the r^2 value was equal to or less than 0.80.
- **Temperature Gradient,** Figure 6-8 (d): In 36% of the cases, the r^2 value was equal to or less than 0.78.
- **Average at all locations,** Figure 6-9: In 27% of the cases, the r^2 value was equal to or less than 0.78.

Table 6-5: Summary of results obtained during the calibration of the temperature model

Construction Site		**Coefficient of Determination (r^2)**				
		Top	**Mid-depth**	**Bottom**	**Average**	**Gradient**
Dallas	May, 8am	0.84	0.90	0.63	0.79	0.84
Houston	May, 8am	0.68	0.81	0.83	0.77	0.42
Houston	May, 3pm	0.84	0.89	0.87	0.85	0.68
Dallas	Aug, 7am	0.87	0.83	0.84	0.84	0.78
Houston	Aug, 9am	0.80	0.86	0.90	0.85	0.78
Houston	Aug, 3pm	0.87	0.76	0.84	0.82	0.92
El Paso	Aug, 10am	0.83	0.84	0.76	0.81	0.86
Dallas	Sept, Noon	0.71	0.83	0.88	0.80	0.78
Dallas	Sept, 3pm	0.88	0.93	0.91	0.91	0.88
Houston	Oct, 10am	0.56	0.71	0.80	0.69	0.65
Houston	Oct, 3pm	0.59	0.60	0.68	0.62	0.71

In general, the highest r^2 was obtained at the mid-depth and bottom locations, which is not surprising since these locations are least affected by heat transfer to the environment. These r^2 values are in general high for the prediction of in place behavior. This indicates that the majority of the experimental data are explained by the developed model. Based on the average r^2 values, it may be concluded that 78% of the measured in place concrete temperatures can be explained by the temperature prediction model.

Table 6-6 provides the maximum error between the measured and predicted maximum in place concrete temperature at any location and time. Figure 6-10 provides the cumulative distribution plots of the values presented in Table 6-6. From Figure 6-10(a), it may be concluded that in 82% of the sections, the error in predicted maximum temperature was equal to or less than 3.25°F. Figure 6-10(b) indicates that in 82% of the sections, the error in predicted maximum temperature was equal to or less than 4.25% of the actual maximum.

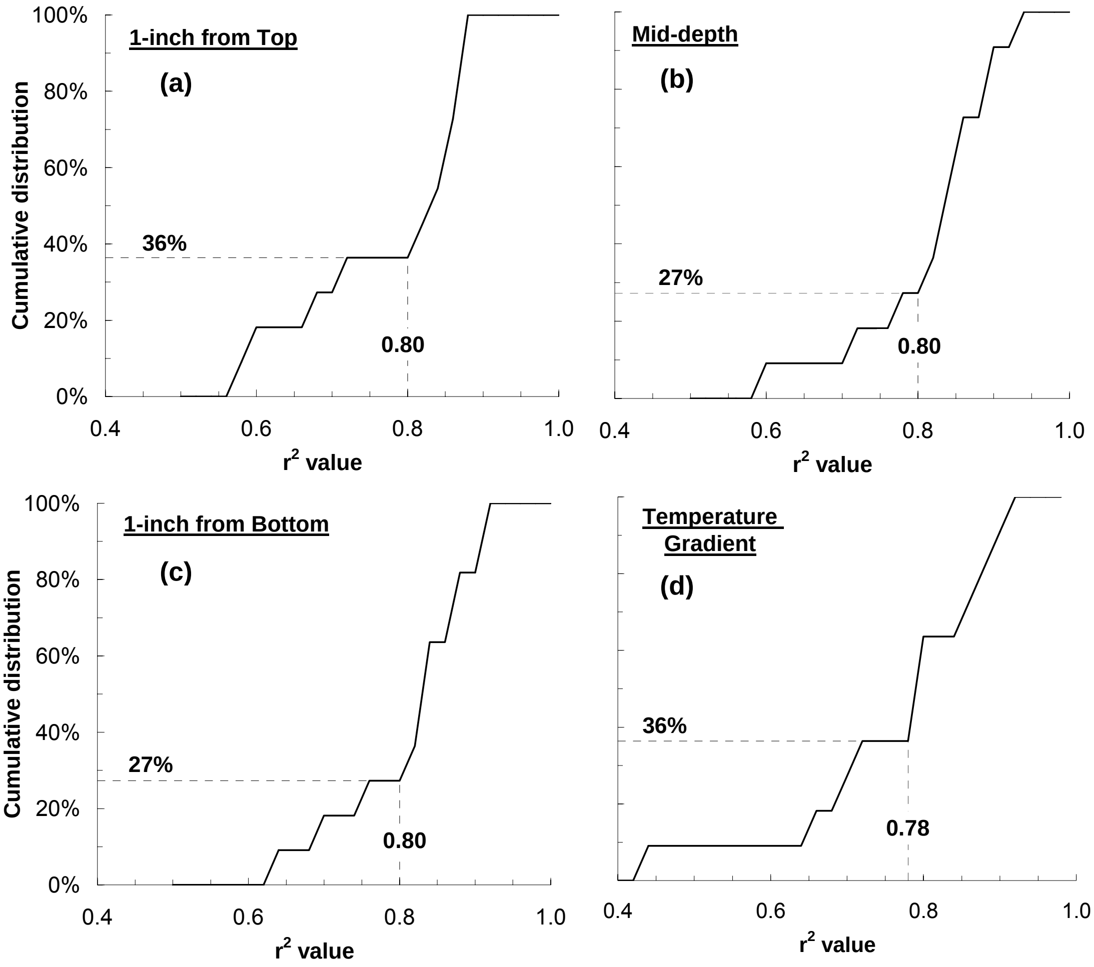

Figure 6-8: Cumulative distributions of the r^2 values obtained during the calibration of the temperature prediction model

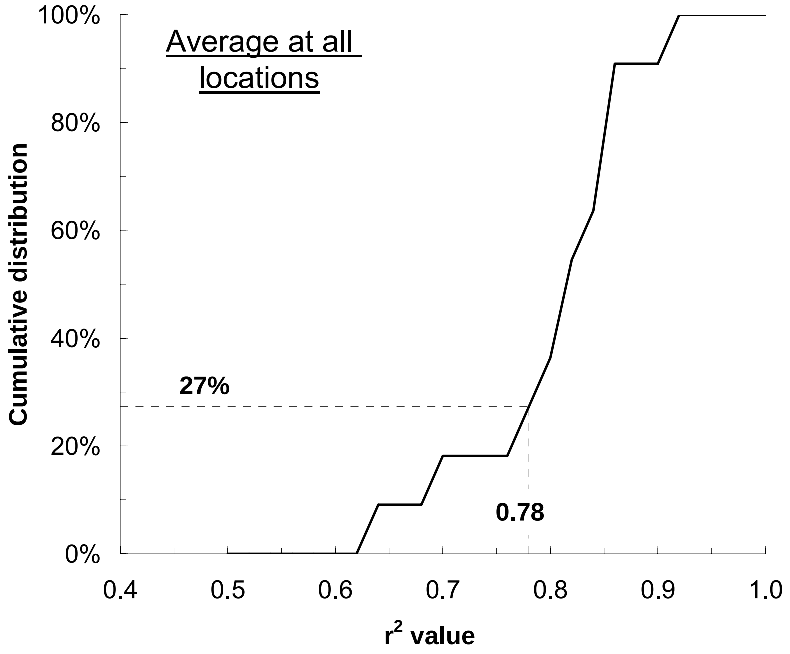

Figure 6-9: Cumulative distribution of the **average** r^2 values obtained during the calibration of the temperature prediction model

Table 6-6: Summary of predicted versus measured maximum in place concrete temperature

Construction Site		Maximum Concrete Temperature [a]	
		Error (°F)	**Error (%)**
Dallas	May, 8am	1.3	1.8%
Houston	May, 8am	-0.3	-0.4%
Houston	May, 3pm	-3.5	-4.6%
Dallas	Aug, 7am	-5.1	-4.6%
Houston	Aug, 9am	3.0	3.4%
Houston	Aug, 3pm	-1.4	-1.5%
El Paso	Aug, 10am	2.6	3.3%
Dallas	Sept, Noon	-0.5	-0.8%
Dallas	Sept, 3pm	-1.8	-2.5%
Houston	Oct, 10am	-3.1	-4.3%
Houston	Oct, 3pm	0.1	0.2%

Note: [a] Maximum error between the measured and predicted maximum in place concrete temperature.

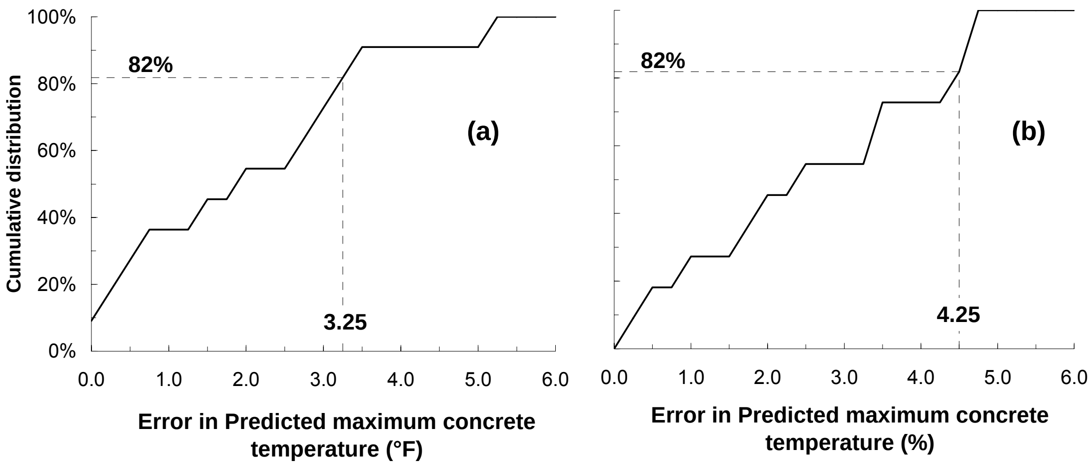

Figure 6-10: Cumulative distributions of predicted versus measured maximum in place concrete temperature

From the r^2 values and range of errors obtained during this analysis, it may be concluded that the proposed temperature prediction model is calibrated for the conditions considered. It is recommended that the model be validated to determine the accuracy of the temperature prediction model for portland cement concrete paving applications.

6.2.1 Recommendations regarding the Temperature Prediction Model

During the calibration of the temperature model, it was determined that the prediction accuracy could be improved by modifying some aspects of the models. These adjustments are necessary, since the overall model consists of many components that were not necessarily based on the same underlying assumptions during their initial development. These adjustments calibrate the unforeseen field occurrences that could not be accounted for in the original mechanistic model.

After all the concrete temperatures from all the sites were evaluated against the predicted values, the following recommendations are made:

- **Portland Cement Concrete Hydration Model:** The hydration model developed in Section 3.2.6 provides a good prediction of the in place heat generation of the concrete mixture. The use of the ultimate degree of hydration parameter introduced in Section 3.2.7, together with the ultimate heat of hydration defined in Section 3.2.3, provides an accurate estimate of the heat of hydration available during the hydration process. The results obtained from semi-adiabatic calorimeter testing provide a means of characterizing concrete hydration with time. With the parameters determined through this test, the effects of different mixture proportions and constituents can be incorporated into the temperature prediction model.

- **Temperature Sensitivity:** The activation energy determines the temperature sensitivity of the concrete hydration process relative to that at the reference temperature. The activation energy model developed in Section 5.2.6.4 provided temperature sensitivity to the heat of hydration model, which accurately reflected the measured concrete temperatures. This model is recommended for use and the sensitivity of the predicted temperatures to a change in the activation energy is investigated in Chapter 8.
- **Heat Transfer due to Evaporative Cooling:** When evaporation of the water from a surface occurs, the energy associated with the phase change is the latent heat of vaporization, which causes evaporative cooling. Based on the initial calibration of the temperature model on the results obtained from the small insulated slabs, the formulation shown in Equation 6-1 was recommended for use. This model was used on all the field sites and in general, accurate predictions of initial concrete temperature development were obtained. However, the temperature history of the surface temperature in the sections instrumented in Houston (October 2000) indicates that the effect of evaporative cooling was larger than what can be accounted for with the proposed model. This can be seen in Figures E-44 and E-48 (see Appendix E), as the temperature gain during the first few hours is much less than predicted by the model. This is an area where further research is required to model the interaction between moisture movement, bleeding, concrete materials, curing compound effectiveness, and evaporation.
- **Solar Radiation/Cloud Cover:** The amount of heat gain due to solar radiation varies with longitude, latitude, altitude, time of day, day of year, cloud cover, and prevailing atmospheric conditions. After the heat of hydration, the solar radiation is the most important heat source for the pavement system and needs to be accurately accounted for in the heat transfer model. During field validation exercises, it is recommended to use an on-site solar radiation meter to obtain site specific solar radiation values.

  During daytime hours, cloud cover affects the intensity of the direct and diffuse solar radiation that reaches the pavement surface. During nighttime hours, the extent of cloud cover determines the amount of re-radiation and influences the magnitude of irradiation from an exposed surface. In order to achieve accurate temperature predictions, the amount of cloud cover should be defined as accurately as possible by the user. During field validation exercises, it is recommended that the atmospheric cloud cover conditions be documented on an hourly basis.
- **Solar Absorptivity Constant:** The solar absorptivity of portland cement concrete is a function of the surface color, with typical values ranging from 0.5 to 0.6. A solar absorptivity constant of 0.50 was found most appropriate for concrete pavements cured with white curing

compound. Before any curing takes place, a solar absorptivity of 0.65 was found to account for the darker surface color of fresh concrete.

- **Heat Transfer by Convection/Conduction:** The heat transfer model outlined in Section 3.3.2 provides an accurate means to model the heat loss on the pavement surface. The effect of the plastic sheets used during the construction of the Dallas (May 2000) section was accurately modeled by the proposed model.
- **Initial Temperature Profile:** The calculation of the initial temperature profile with Barbers model (Section 3.3.5.5) provided an effective means to obtain an initial temperature profile for the finite difference model. No in place subgrade temperatures were collected during this study and it is recommended that this temperature profile be obtained in future field work.

6.3 LIMITATIONS, ASSUMPTIONS, AND RANGE OF VARIABLES CONSIDERED

Based on the data collected for these paving projects, the ranges of values covered during the calibration of the temperature prediction model are as follows:

- Pavement thickness: 10 to 15-inch (255 to 380 millimeters),
- Subbase type: asphalt concrete was used in all cases
- Cement Type: I, and I/II. The ranges of chemical composition of the cements used are presented in Table 6-7.
- Cement factor: 5.0 to 6.5 sacks of cement (See Table 4-1).
- Water-cementitious materials ratio: 0.39 to 0.54 (See Table 4-1),
- Mineral admixtures: Class C and F fly ash was used on the projects. GGBF slag was used in the El Paso project. The range of replacement levels and the chemical composition of the fly ashes are summarized in Table 6-8.
- The air temperature during construction varied between 14 and 39°C.
- Time of placement: Varied between 7:05am and 3:10pm
- Surface texturing: Tining was applied to all projects.
- Curing method: White liquid curing compound was used at all of the sites. In some instances, one layer of curing compound was used and in other cases, a double layer of curing compound was used. However, due to rain, black plastic sheets were used in Dallas (May 2000).

Table 6-7: Range of cement properties used for the temperature prediction model calibration

	C_3S (%)	**C_2S** (%)	**C_3A** (%)	**C_4AF** (%)	**SO_3** (%)	**Free CaO**(%)	**MgO** (%)	**Alkalies**^{a} (%)	**Blaine** (m^2/kg)
Average	58.1	16.1	6.6	9.8	2.8	1.2	2.3	0.531	360
Min	52.9	13.6	5.0	7.1	2.3	0.7	1.0	0.46	342
Max	60.4	23.4	11.4	11.6	3.8	2.3	4.0	0.63	374

Note: ^{a} Equivalent alkalies as per ASTM C 150 = $Na_2O + 0.658K_2O$

Table 6-8: Range of mineral admixtures properties used for the temperature prediction model calibration

	Fly ash CaO (%)	**Fly ash SiO_2** (%)	**Fly ash Alkalies** (%)	**Fly ash Dosage** (%)	**GGBFS Dosage** (%)
Average	-	-	-	-	-
Min	10.6	32.4	0.3	20	50
Max	25.4	58.2	1.61	35	50

The basis for the development of all the different components of the temperature prediction model was presented along with the initial model development. Based on the assumptions made and the models currently incorporated the following conditions are not considered:

- **Silica Fume:** Silica fume is rarely used in concrete paving applications, and its effect on the hydration development was beyond the scope of this study. The effect of silica fume is not modeled by the current hydration models incorporated into the temperature prediction program. However, the heat of hydration of a mixture containing silica fume can be characterized by semi-adiabatic calorimeter tests, and with these results, the effect of silica fume can be investigated.
- **Rainfall (precipitation):** Any precipitation will have a significant effect on the heat transfer mechanisms and their interaction with the hydrating concrete. The effect of rainfall, frost, snow, or any other forms of precipitation is not considered in the model.
- **Freezing Conditions:** When freezing of the pavement structure occurs, the thermal properties of the materials are changed, and this effect is not accounted for in the current model. In Texas, these conditions rarely occur, and the primary focus of this study is to predict concrete temperatures under hot weather conditions.

6.4 SUMMARY AND CONCLUSIONS

This Chapter covered the calibration of the temperature prediction model developed during this study. The model was calibrated based on field data collected from seven CRC construction sites visited during this study. Concrete temperatures measured in the field were compared to the temperatures predicted with the temperature model. The r^2 values obtained for all the sites are summarized in Table 6-5. Based on the average r^2 values, it may be concluded that in 27% of the cases, the r^2 value was equal to or less than 0.78. This indicates that 78% of the measured in place concrete temperatures can be explainable by the temperature prediction model. The error obtained between the measured and predicted maximum in place concrete temperature ranged between -4.6% and 3.4%. From Figure 6-10(a), it may be concluded that in 82% of the sections, the error in predicted maximum temperature was equal to or less than 3.25°F.

The obtained r^2 values are in general high for the prediction of in place behavior. This indicates that the majority of the experimental data are explained by the developed model. Based on this calibration effort, and the temperature predictions shown in Appendices E, it may be concluded that the temperature prediction model is able to produce accurate predictions of early-age concrete temperatures in concrete paving applications.

The program was successfully calibrated for the variables that may have a significant impact on the in place concrete temperature. It may be concluded that the proposed temperature prediction model could be used as a tool (design aid) to evaluate the effect of different cement contents, cement composition, water-cement ratio, cement fineness, mineral admixtures, initial concrete temperature at placement, environmental conditions, curing method, subbase temperature, pavement thickness, and time of placement. This model will allow the designer/contractor to evaluate, in a short time frame, the effect of the different options on the predicted in place concrete temperature development.

6.4.1 Recommendations

During the calibration of the temperature model, it was determined that the prediction accuracy could be improved by modifying some aspects of the models developed in Chapter 3. Section 6.2.1 provides recommendations on the models to use during the final development of the temperature prediction program. It is recommended that the model be validated to determine the accuracy of the temperature prediction model for general use in portland cement concrete paving applications. During the selection of field sites for validation of the temperature prediction model, it is recommended that the ranges used for calibration of the temperature prediction model be expanded. The ranges of variables considered are listed in Section 6.3.

6.4.2 Recommendations on Data Collection on Future Field Sites

Many parameters influence the development of in place concrete temperatures, and most of these parameters were collected at the field sites. However, based on the calibration exercise performed in this Chapter, it was determined additional information would have provided more accurate means to calibrate the models. The following recommendations can be made concerning data collection at future field sites:

- **Solar Radiation/Cloud Cover:** It is recommended to use an on-site solar radiation meter to obtain site specific solar radiation values. Commercial solar radiation gauges are available to use with the weather station. The use of the solar gauge will indirectly account for the effect of cloud cover during daytime hours. Alternatively, the atmospheric cloud cover could be documented on an hourly basis.
- **Pavement Structure Temperature Profile:** The temperature of the subbase impacts the temperature development in the concrete slab. It is recommended to install temperature probes at various depths into the subbase and to monitor the development of these temperatures prior to construction and during curing of the concrete.
- **Small Insulated Specimens:** Should it be desired to use small insulated specimens for future work, it is recommended to determine the size of the specimen required to provide temperature comparable to an actual concrete pavement. In the field, specimens of various sizes and different insulation methods can be cured alongside the pavement to determine the geometry best suited for this purpose.

Chapter 7

Initial and Final Set of Concrete

Final setting of concrete relates to the point where stresses and stiffness start to develop in freshly placed concrete. The point at which initial set occurs is of importance, since it provides an estimate of when the concrete has reached the point where it has stiffened to such an extent that it can no longer be vibrated without damage occurring in the concrete. Under hot weather conditions, the time to initial set will be shorter than under normal temperatures, which will affect the construction crew's ability to consolidate and finish the in place concrete. With knowledge of the time to initial set, contractors will be able plan measures to finish and texture the concrete pavement in time to prevent setting occurring before these activities. In this study, experimental work was performed under laboratory and field conditions to determine the effect of temperature, different cements, and mineral admixtures on the initial and final times. This Chapter will evaluate and calibrate the setting model presented in Section 3.5 based on the data collected during this study.

7.1 BACKGROUND AND APPROACH

Pinto and Hover (1999) stated that: "Although the setting process is influenced by the rheology effects of the water-cement ratio (*w/c*), aggregates, air voids, bleeding, and evaporation, setting is primarily influenced by hydration of the cement." Pinto and Hover correlated the degree of hydration at initial (α_i) and final (α_f) set to the corresponding times of set, and found the best fit activation energy to account for the effect of temperature on setting. Their finding are shown in Figure 7-1. Although the final set times varied considerably when tested at different temperatures, they concluded that the computed equivalent age at setting was much more uniform.

One of the primary purposes of this study's laboratory test program was to characterize the development of concrete hydration over time (degree of hydration). Numerous adiabatic tests were performed on local concretes and concretes mixed with different admixtures. In Section 3.2.4, it was shown that the amount of heat released during hydration provides a means to quantify indirectly the formation of hydration products over time.

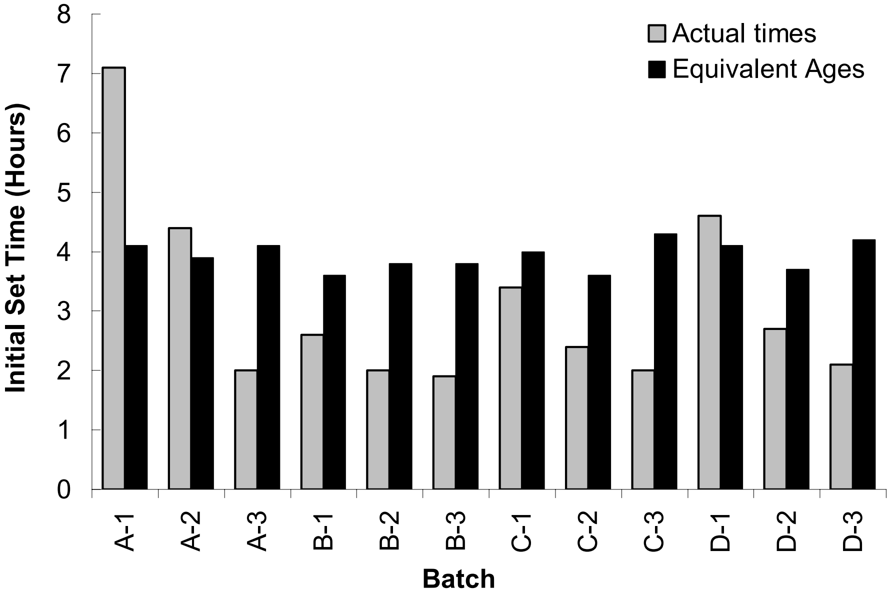

Figure 7-1: Comparison of initial set times and equivalent age (Pinto and Hover, 1999)

In Figure 3-8, it was shown that the degree of hydration provides a method to quantify the progress of hydration for a specific concrete mixture. Figure 3-8 illustrates the interaction between the formation of structure and the development of the degree of hydration, which explains why initial and final set is correlated to the degree of hydration.

In Section 3.5, it was discussed that Byfors (1980) defined the “critical degree of hydration” (α_{cr}) as the amount of hydration that has to be reached before any strength gain will occur. Byfors concluded that the critical degree of hydration is dependent on the water-cement ratio and presented the following expression:

$$\alpha_{cr} = k_s \cdot (w/c)$$

Previously Equation 3-63

Where, k_s = constant that varies between 0.4 and 0.46, and
w/c = water-cement ratio

Byfors’s definition of the critical degree of hydration is very similar to the point at which final setting occurs; however, the value was obtained by extrapolating the degree of hydration versus strength development data until the time of zero strength is reached.

Chen and Odler (1992) found that “...the setting time extended as the amount of mixing water increased.” Setting of concrete is often associated with the formation of ettringite. However, Chen and Odler (1992) found that “... for setting to occur a certain amount of hydrated material has to be formed, however, it appears to be of little relevancy whether the primary hydration products is C-S-H-phase or ettringite."

In this Section, initial and final set times of concrete will be evaluated in terms of the degree of hydration development. The effect of the water-cement ratio will be incorporated, since it has been shown to influence the degree of hydration at setting.

7.2 CALIBRATION OF THE INITIAL AND FINAL SETTING MODEL

The convention introduced by Pinto and Hover (1999) will be adopted, and the degree of hydration corresponding to initial (α_i) and final (α_f) set will be determined for all the mixtures. Time of setting tests were performed under laboratory and field conditions. These results were previously shown in Table 4-16 and Figures 4-38 and 4-39. These figures indicated a wide range of initial and final set times. During testing, temperature of the pastes were monitored under both laboratory and field conditions. Figure 7-2 presents a typical example of the temperature development in the mortar sample. It may be seen that there is a rise in temperature as the concrete continues to hydrate.

The measured concrete temperatures were used to determine the equivalent ages at initial and final set. The hydration parameters and activation energy as listed in Table 4-17 were used to determine the degree of hydration that correspond to the respective setting times. The results are summarized in Tables 7-1 and 7-2. In general, it was found that setting occurred at around the same equivalent ages in the field and laboratory mixtures, which is in agreement with the findings reported by Pinto and Hover (1999). As the degree of hydration is a function of the equivalent age, this is in agreement with the formulation of Byfors, who stated that setting occurs at a specific degree of hydration. Figures 7-3 and 7-4 provide examples of setting as compared to the equivalent age and degree of hydration at set. In these figures, it may be seen that setting occurs at around the same degree of hydration for a particular mixture.

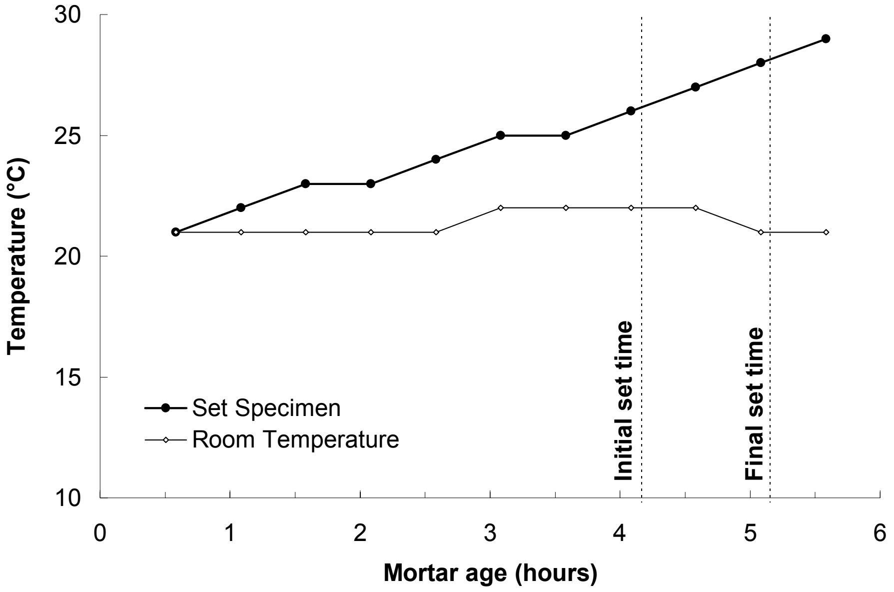

Figure 7-2: Temperature of mortar specimen used during setting test (Mix No. 21)

Table 7-1: Summary of **initial** set actual times and equivalent ages

Mix No.	Description	Laboratory			Field Conditions		
		Actual Time (hrs)	**Equiv. Age (hrs)**	α_I^a	**Actual Time (hrs)**	**Equiv. Age (hrs)**	α_I^a
1	Dallas - May	4.9	5.9	0.052			
2	Houston - May	7.9	9.9	0.066			
3	Dallas - Aug	4.1	5.7	0.080	2.6	5.0	0.060
4	Houston - Aug (Section No. 2)	5.8	7.0	0.055	4.4	7.8	0.069
					3.3	7.3	0.061
5	El Paso - Aug (Section No. 2)	7.0	6.9	0.054	2.9	6.6	0.050
					3.5	7.5	0.060
6	Dallas - Sept	7.2	5.9	0.094	3.3	5.4	0.082
7	Houston - Oct	5.1	6.4	0.059	5.3	7.1	0.067
20	Capitol Type I	3.8	4.4	0.065			
21	Alamo Type I	4.2	4.9	0.081			

Note: α_I = degree of hydration at **initial** set

Table 7-2: Summary of **final** set actual times and equivalent ages

Mix No.	Description	Laboratory			Field Conditions		
		Actual Time (hrs)	Equiv. Age (hrs)	$\alpha_f{}^a$	Actual Time (hrs)	Equiv. Age (hrs)	$\alpha_f{}^a$
1	Dallas - May	6.5	8.06	0.10			
2	Houston - May	10.1	12.70	0.11			
3	Dallas - Aug	5.4	7.78	0.14	3.3	7.8	0.137
4	Houston - Aug	8.7	10.36	0.11	5.4	10.3	0.108
	(Section No. 2)				4.7	10.8	0.116
5	El Paso - Aug	10.3	12.18	0.11	4.1	10.6	0.096
	(Section No. 2)				5.4	11.7	0.107
6	Dallas - Sept	9.1	7.67	0.13	4.2	7.9	0.136
7	Houston - Oct	6.8	8.99	0.09	6.7	9.3	0.097
20	Capitol Type I	5.3	6.53	0.12			
21	Alamo Type I	5.2	6.41	0.12			

Note: α_f = degree of hydration at **final** set

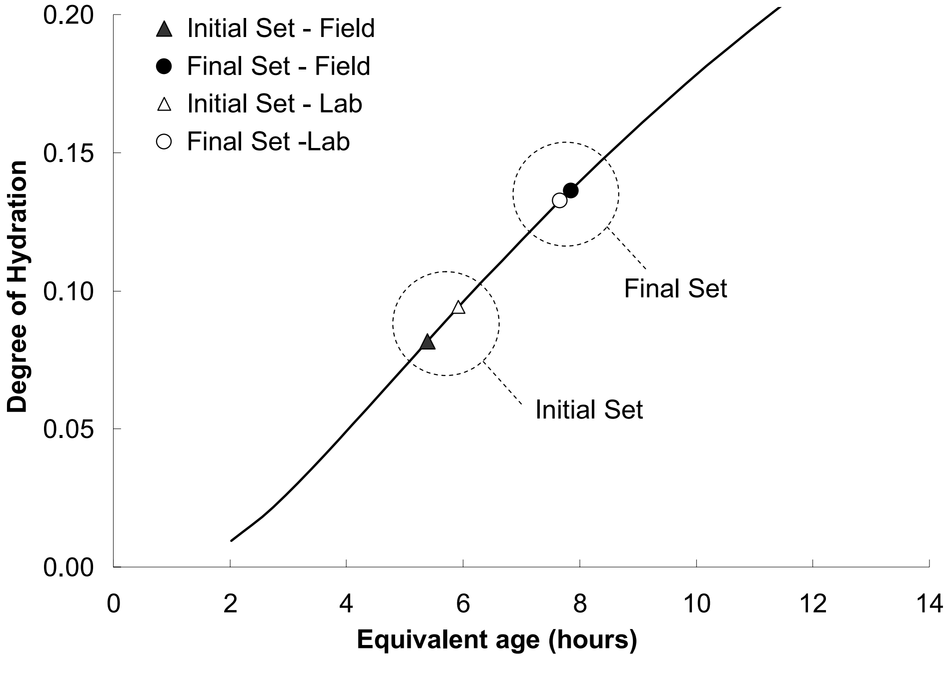

Figure 7-3: Degree of hydration at initial and final set for Dallas, September

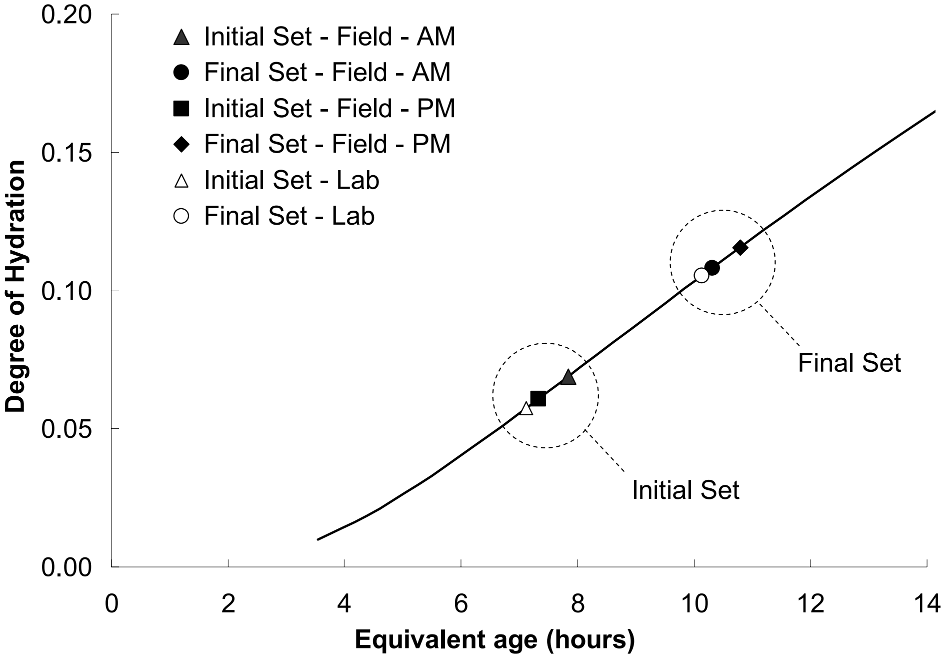

Figure 7-4: Degree of hydration at initial and final set for Houston, August

The formulation shown in Equation 3-63 was used to incorporate the effect of the water-cementitious materials ratio into the degree of hydration at initial and final set. The ratio between the critical degree of hydration at setting and the water-cementitious materials ratio for initial and final set is shown in Figures 7-5 and 7-6. It may be seen that for most of the mixtures the ratio appears constant; however, when GGBF slag is used, setting occurs at an earlier degree of hydration. This effect is present in all three cases where the setting of GGBF slag was tested. The reason for this effect is not clear at this point in time, and based on the limited data set available, no attempt will be made to modify the setting effect when GGBF slag is used. It is however recommended that the interaction between setting and hydration of GGBF slag be further investigated.

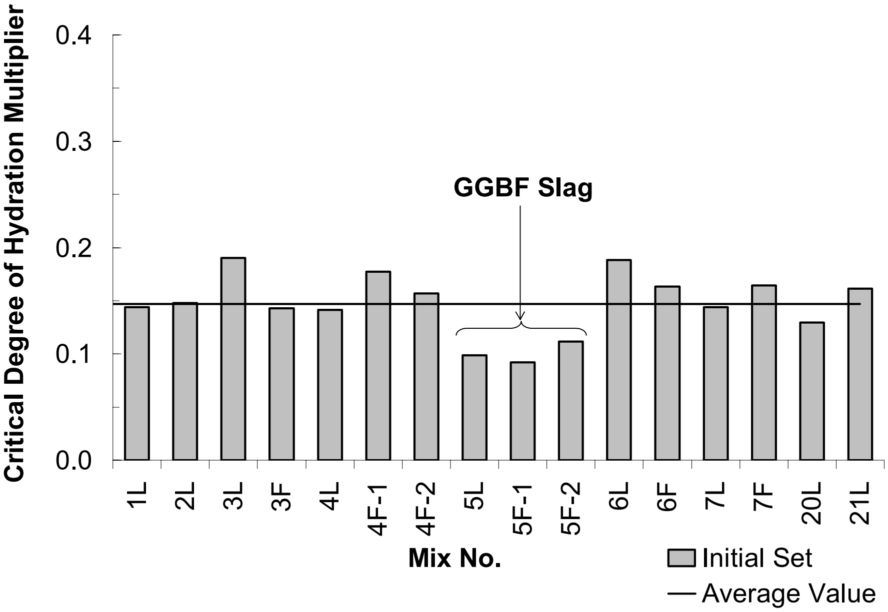

Figure 7-5: Multiplier (k_s) to the w/cm ratio to determine the degree of hydration at **initial** set

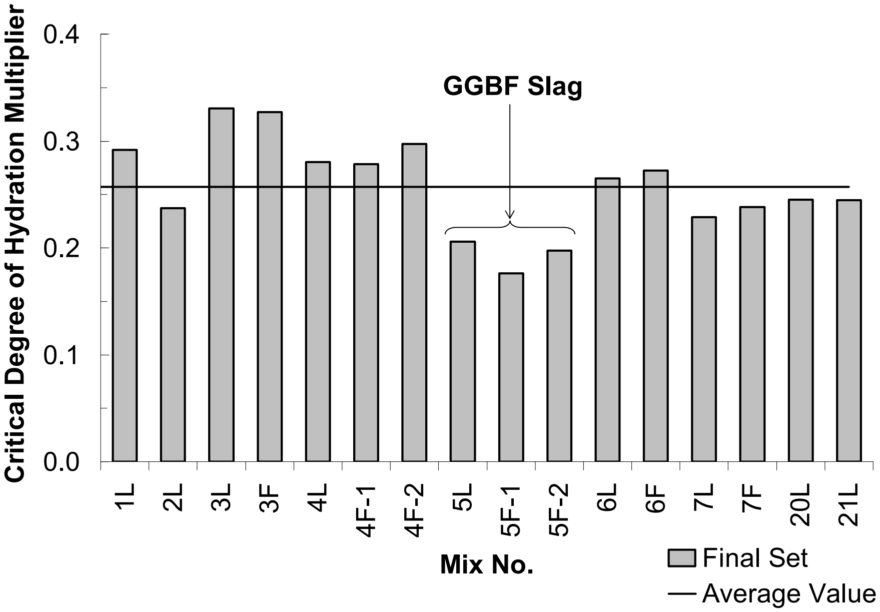

Figure 7-6: Multiplier (k_s) to the w/cm ratio to determine the degree of hydration at **final** se

Based on the results shown in Figures 7-5 and 7-6, the average k_s values were determined and the following formulation is recommended for use:

ASTM C 403 Initial set: $\alpha_i = 0.15 \cdot (w/cm)$ *Equation 7-1*

ASTM C 403 Final set: $\alpha_f = 0.26 \cdot (w/cm)$ *Equation 7-2*

where, α_i = degree of hydration at initial set,

α_f = degree of hydration at final set, and

w/cm = water-cementitious materials ratio.

The degree of hydration computed with formulations shown in Equations 7-1 and 7-2 are evaluated for different water-cementitious materials ratios in Table 7-3. With at w/cm of 0.50, it may be seen that initial and final set are predicted to occur after, respectively, 7.5% and 13% of hydration products have been developed. Table 7-3 indicates that for setting to occur, more hydration products have developed at higher w/cm ratios, and visa versa, which is in accordance with past findings in the literature (Chen and Odler, 1992).

Table 7-3: Sample degree of hydration values at different w/cm ratios

ASTM C 403	**Degree of Hydration**		
	w/cm 0.40	**w/cm 0.50**	**w/cm 0.60**
Initial Set	0.060	0.075	0.090
Final Set	0.104	0.130	0.156

Figures 7-7 and 7-8 provide a comparison of the back-calculated equivalent age versus the measured equivalent age at setting. These figures indicate that an accurate estimate of the equivalent age at setting can be obtained. However, the equivalent age at initial and final set for mixtures that contain GGBF slag is over predicted. The r^2 values for the predicted setting times were 0.735 and 0.766, respectively, for initial and final setting.

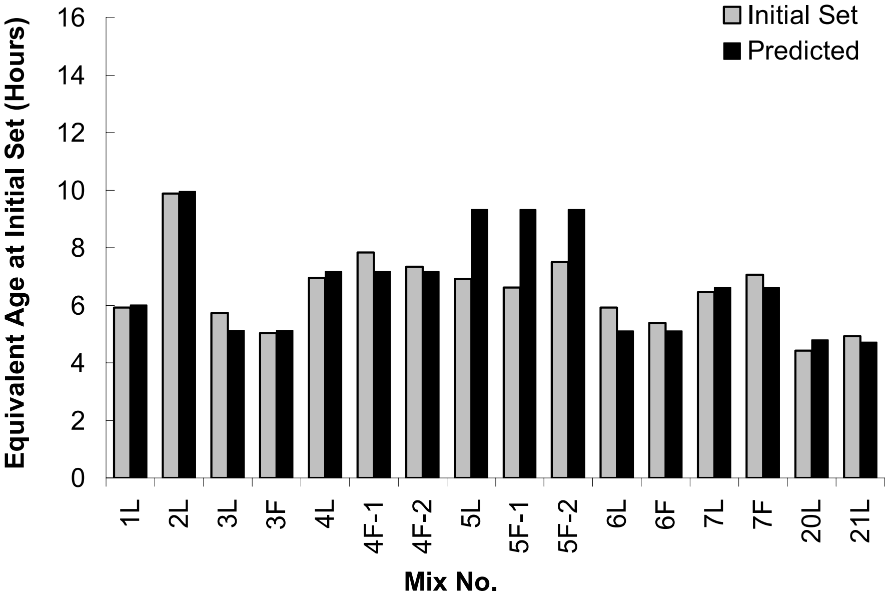

Figure 7-7: Comparison of measured and predicted equivalent ages to reach **initial set** (*Note*: **L** = Laboratory conditions, **F**=Field conditions, **1**=Section No.1, **2**=Section No. 2)

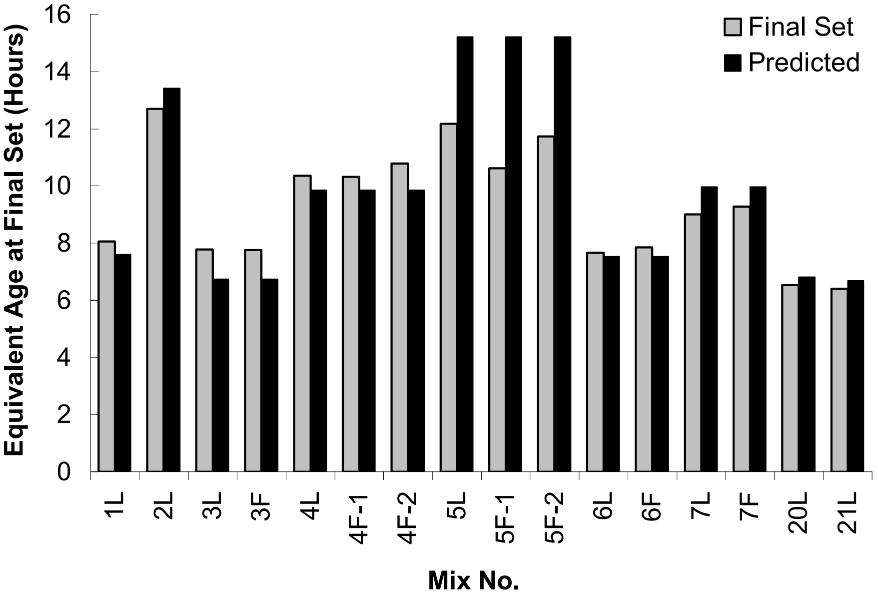

Figure 7-8: Comparison of measured and predicted equivalent ages to reach **final set** (*Note*: **L** = Laboratory conditions, **F**=Field conditions, **1**=Section No.1, **2**=Section No. 2)

7.2.1 Closed-form Mathematical Formulation of Concrete Setting Times

In Section 3.2.5.1, the use of the exponential formulation to characterize the degree of hydration development was recommended. The exponential function documented in Equation 3-21 was recommended to characterize the degree of hydration development. The formulation was defined as follows:

$$\alpha(t_e) = \alpha_u \cdot \exp\left(-\left[\frac{\tau}{t_e}\right]^{\beta}\right)$$

Previously Equation 3-21

where, $\alpha(t_e)$ = the degree of hydration at equivalent age, t_e,

τ = hydration time parameter (hrs),

β = hydration shape parameter, and

α_u = ultimate degree of hydration.

With the formulations recommended in Equations 7-1 and 7-2, the equivalent age at setting can directly be determined from the hydration parameters. The closed-form formulation is shown in Equations 7-3 and 7-4. This formulation can be very useful, since the setting times at the reference temperature can now be obtained.

ASTM C 403 Initial set: $$t_{ei} = \tau \cdot \left(-\ln\left[\frac{0.14 \cdot w/cm}{\alpha_u}\right]\right)^{\frac{-1}{\beta}}$$

Equation 7-3

ASTM C 403 Final set: $$t_{ef} = \tau \cdot \left(-\ln\left[\frac{0.26 \cdot w/cm}{\alpha_u}\right]\right)^{\frac{-1}{\beta}}$$

Equation 7-4

where, t_{ei} = equivalent age at initial set (hours),

t_{ef} = equivalent age at final set (hours), and

w/cm = water-cementitious materials ratio.

7.2.1.1 *Modification of Hydration Parameters to Include Effect of Chemical Admixtures*

It is customary to express the effect of chemical admixtures such as retarders and accelerators in terms of their effect on initial set at different temperatures. With the formulation presented in Equation 7-3, the initial set time for the cement without any chemical admixtures can be estimated. Next, the effect recommend by the supplier of the chemical admixture can be added to the calculated initial set time. In the case of retarders, the initial set time will be increased, and when accelerators are used the initial set time will be reduced. With this approach, the assumption is made that only the hydration time parameter is affected by the use of chemical admixtures. The following is an example of the guidelines contained in manufactures data sheet for different chemical admixtures:

- **Retarder:** ASTM 494 Type B and Type D (Grace, 2002):

  Daratard 17 retards the initial and final set of concrete. At the usual addition rate of 195 mL/ 100 kg (3 fl oz/100 lb) cement it will extend the initial setting time of portland cement concrete by 2 to 3 hours at 21°C (70°F).

- **Accelerator:** ASTM 494 Type E (Grace, 2002):

  Daraccel is used at an addition rate of 520 to 2600 mL/100 kg (8 to 40 fl oz/100 lb) of cement. The amount used will depend upon the setting time of the non-admixtured concrete and the temperature at placement. In most instances, the addition of 780 to 1040 mL of Daraccel/100 kg (12 to 16 fl oz/100 lb) of cement will reduce the setting time of a typical Type I cement concrete at 10°C (50°F) by 2 to 3 hours and increase the 3 day compressive strength by 25 to 50%.

With the above information the new hydration time parameter can be determined, which includes the use of chemical admixtures. The new hydration time parameter can be determined as follows:

ASTM C 403 Initial set:

$$\tau_{chem} = (t_{ei} + \Delta_{chem}) \cdot \left(-\ln\left[\frac{0.14 \cdot w/cm}{\alpha_u} \right] \right)^{\frac{1}{\beta}} \qquad \textit{Equation 7-5}$$

where, τ_{chem} = adjusted hydration time parameter to include the effect of retarder or accelerators (hours),

t_{ei} = equivalent age at initial set of the cement without chemical admixtures determined from Equation 7-3 (hours), and

Δ_{chem} = effect of mineral admixture on the time at initial set at the reference temperature (21.1°C), where positive retards and negative accelerates.

The use of the approach outlined above is best explained by an example. The hydration parameters used for this exercise are listed in Table 7-4.

Table 7-4: Hydration parameters for Mix No. 20

Cement	Hydration Parameters			w/c
	β	τ (hrs)	α_u	
Type I Cement	0.70	15.0	0.750	0.50

Concrete without Chemical Admixtures:

From Equation 7.3, it may be found that initial setting at 70°F is expected to occur at the following time:

$$t_{ei} = 15.0 \cdot \left(-\ln\left[\frac{0.14 \cdot 0.50}{0.75} \right] \right)^{\frac{-1}{0.70}} \quad = 4.37 \text{ hours}$$

Concrete with Retarder:

The effect of the retarder listed above, will extend the initial setting time of portland cement concrete by 2 hours at 21°C (70°F).

Δ_{chem} = + 2 hours

From Equation 7.5 it may be found that:

$$\tau_{chem} = (4.37 + 2.0) \cdot \left(-\ln\left[\frac{0.14 \cdot 0.50}{0.75} \right] \right)^{\frac{1}{0.70}} \quad = 21.9 \text{ hours}$$

Concrete with Accelerator:

The effect of the accelerator retarder listed above, will reduce the initial setting time of portland cement concrete by 3 hours at 10°C (50°F).

Δ_{chem} = - 3 hours × f(T_c), where f(T_c) the age conversion factor defined in Equation 3-5,

= - 3 hours × 0.509 = - 1.527 hours

From Equation 7.5 it may be found that:

τ_{chem} = 9.8 hours

This example indicates that the retarder extended the hydration time parameter from 15.0 hrs to 21.9 hours. The accelerator reduced the hydration time parameter from 15.0 hrs to 9.8 hours. The effect of using a retarder and accelerator as compared to the original cement is shown in Figures 7-9 and 7-10. These figures indicate that the retarder would significantly reduce the amount of early-age heat development and increase the setting times.

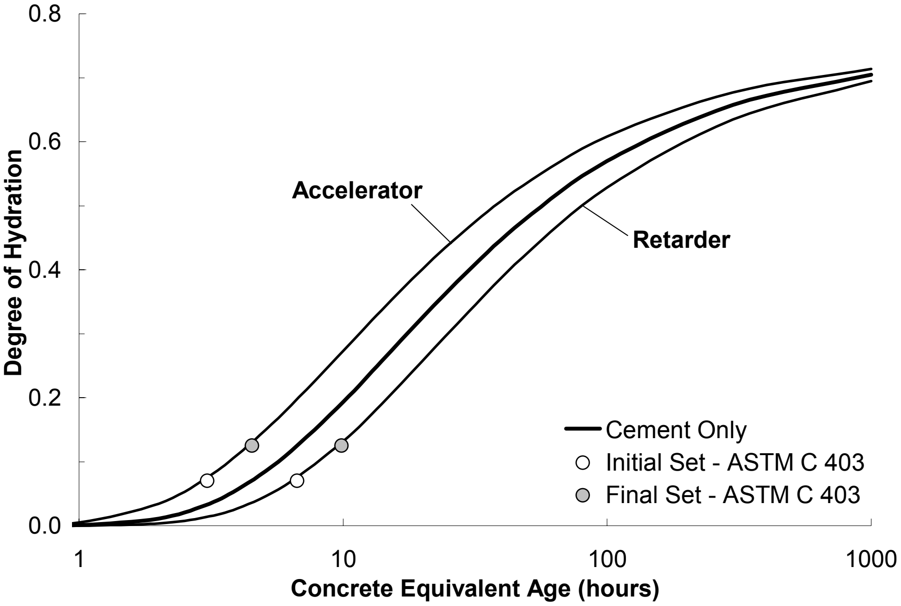

Figure 7-9: Hypothesis on differences in setting degree of hydration

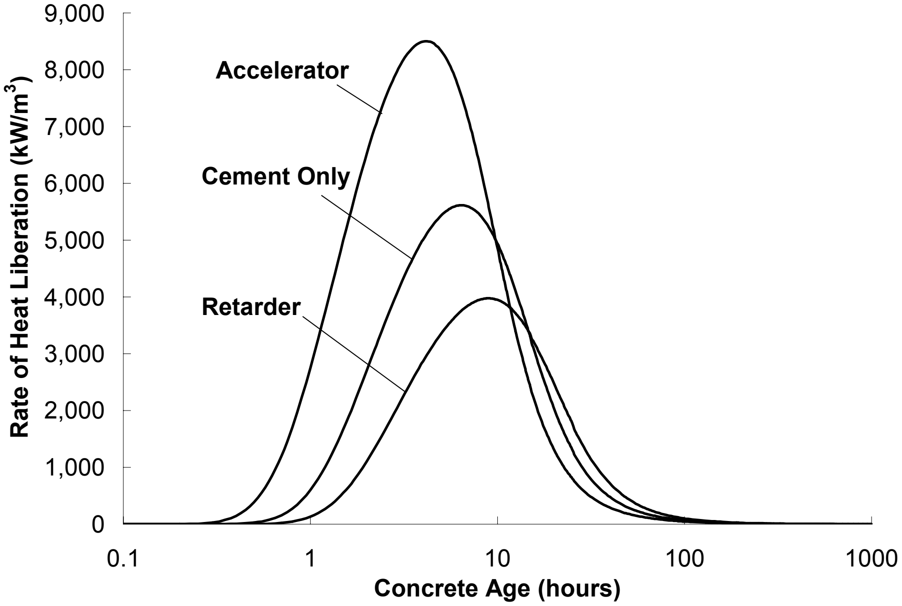

Figure 7-10: Hypothesis on differences in setting degree of hydration

7.2.2 Additional Remarks on Concrete Setting

In Section 3.5, it was shown that Byfors (1980) recommended a k_s value between 0.4 and 0.46 to multiply with the water-cement ratio to obtain the critical degree of hydration where strength development starts. However, based on the calibration of the ASTM C 403 test data, a k_s value of 0.26 is recommended to determine the final set, which has been defined as the point at which strength development starts. These values appear to contradict one another.

The transition from liquid to solid is a gradual process, and the definition of any point at which the paste is considered set is somewhat arbitrary (Neville, 1996). ASTM C 403 defines the setting of the concrete in terms of penetration resistance of 500 psi and 4000 psi respectively for initial and final set.

The "arbitrary" definition of set used by ASTM C 403 and that used by Byfors originate from different requirements. Byfors determined the start of strength development by extrapolating a linear line from degree of hydration versus strength graphs, as shown in Figure 7-11. The horizontal axis in Figure 7-11 provides an indication of the degree of hydration (See Section 3.2.4.1) and the vertical axis reflects the compressive strength. Figure 7-11 clearly indicates an increase in the start of the initial strength gain with an increase in the water-cement ratio.

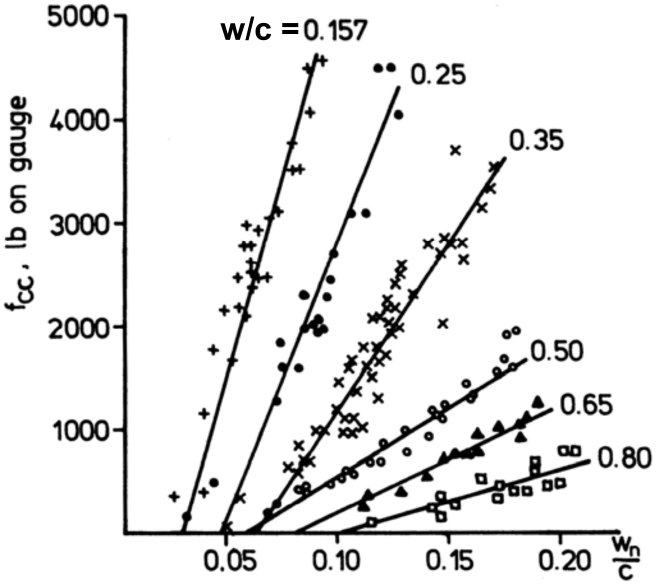

Figure 7-11: Relation between compressive strength and amount of chemically bound water, i.e. degree of hydration (Byfors, 1980, original source Taplin, 1959)

The hard copy version received shows this figure as 7-1 and it should be 7-11 as shown here.

The difference between the ASTM C 403 approach and that taken by Byfors (1980) is schematically shown in Figure 7-12. The "arbitrary" points of zero strength do not occur at the same times. By extrapolating a linear line from the later age strength, the slow initial gain in strength is not considered. Concerning this issue, Byfors remarks that, "...the relation between strength and the degree of hydration is, however, exponential at a very early stage, from the setting phase and a few hours after." This exponential gain in initial strength is captured by the ASTM C 403 procedure and a typical example of the test results obtained from this test is shown in Figure 7-13. The exponential gain in strength at the very early-ages may be identified in Figure 7-13.

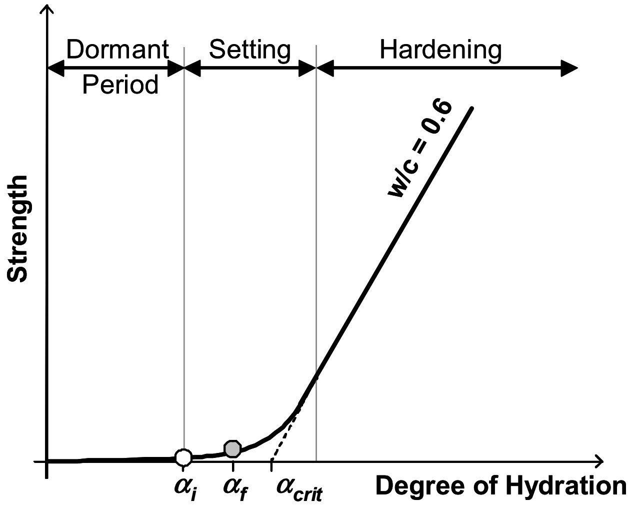

Figure 7-12: Hypothesis on differences in setting degree of hydration

Based on the discussion above, it may be concluded that a difference between the degree of hydration at final set as proposed by the author and Byfors (1980) is not surprising. The difference arises from the use of different definitions of the time of final set.

The use of either of the two approaches may be adopted; however, compatibility concerning strength and stiffness gain should be maintained. If the strength gain is defined in terms of Equation 7-2, then this should be the time used to determine the strength-maturity relationship, and visa versa if Equation 3-63 is used. It is recommended to determine the degree of hydration at initial set in terms of the formulation shown in Equation 3-63.

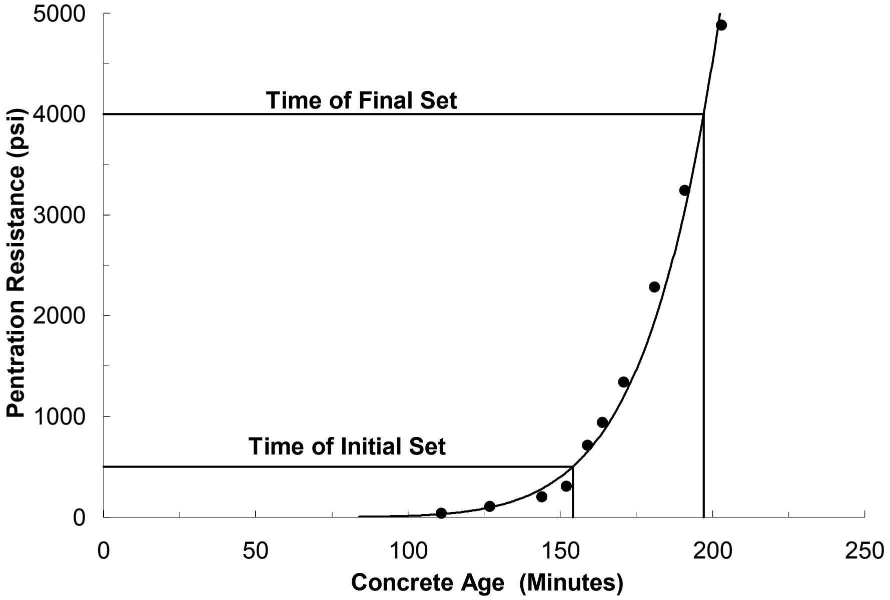

Figure 7-13: Time of setting by penetration resistance (Dallas, August 2000)

7.3 SUMMARY AND CONCLUSIONS

ASTM C 403 (1998) setting data were collected under field and laboratory conditions for concrete mixtures containing different cements, fly ash types, and GGBF slag. The water-cementitious materials ratio of the mixtures varied between 0.39 and 0.54, and the cement factor varied between 5.0 and 6.5 sacks of cement. This Chapter showed that the setting of concrete in general occurs when a specific amount of hydration products have been formed. These findings are in agreement with those reported by Byfors (1980), Chen and Odler (1992), and more recently Pinto and Hover (1999).

The formulation shown in Equation 3-63 was used to incorporate the effect of the water-cementitious materials ratio into the degree of hydration at initial and final set. This is necessary since a higher water-cement ratio indicates a greater distance between cement particles, which will in turn require a higher degree of hydration before stiffening of the mixture occurs. The ratio between the critical degree of hydration at setting and the water-cementitious materials ratio for initial and final set is shown in Figures 7-5 and 7-6. These figures reveal that for most mixtures, the ratio appears constant. However, when GGBF slag is used setting occurs at an earlier degree of hydration. It is for this reason recommended that the interaction between setting and hydration of GGBF slag be further investigated.

It is recommended to use the following formulations to estimate the degree of hydration at initial and final set:

ASTM C 403 Initial set: $\alpha_i = 0.15 \cdot (w/cm)$ *Previously Equation 7-1*

ASTM C 403 Final set: $\alpha_f = 0.26 \cdot (w/cm)$ *Previously Equation 7-2*

where, α_i = degree of hydration at initial set,
α_f = degree of hydration at final set, and
w/cm = water-cementitious materials ratio.

The test results obtained through penetration resistance testing (ASTM C 403) provide useful data that can be used to characterize the setting of concrete at early-ages. It is recommended to compare set times in terms of equivalent ages. For this reason, it is further recommended to measure the temperature development in the mortar specimens used in the ASTM C 403 test.

With the formulation recommended in Equations 7-1 and 7-2, the equivalent age at setting can directly be determined from the hydration parameters. The closed-form formulation is as shown in Equations 7-3 and 7-4. This formulation can be very useful, since setting times at the reference temperature can now be obtained. Based on the assumption that only the hydration time parameter (τ) is affected by the use of retarders and accelerators, the effect of chemical admixtures can be incorporated into the general hydration models developed in Chapter 5.

It is customary to express the effect of chemical admixtures such as retarders and accelerators in terms of their effect on initial set at different temperatures. With the formulation presented in Equation 7-3, the initial set time for the cement without any chemical admixtures can be estimated, and a new hydration time parameter can be determined that includes the effect of the retarder or accelerator. Since limited data are available to characterize the effect of chemical admixtures on the heat of hydration development, the method outlined above is recommended for preliminary implementation.

7.3.1.1 *Recommendations for Additional Research*

Based on the material covered in this document, the following aspect that required more development and research was identified:

- A more detailed experimental program, designed specifically to evaluate the influence of water-cementitious ratio, GGBF slag, and chemical admixtures (retarders and accelerators) on setting is recommended. The testing should include calorimetry testing to characterize the degree of hydration development over time.

With knowledge of the time to initial set, contractors will be able to plan measures to finish and texture the concrete pavement in time to prevent setting occurring before these activities. With the results presented in this Chapter, the effect of temperature, different cements, and mineral admixtures on the initial and final times may be evaluated.

Chapter 8

Sensitivity Analysis of Models

After the development of a mechanistic-empirical model, it is important to establish which input variables cause the largest changes in the predicted results. These variables must be known or measured to achieve accurate predictions with the model. The variables that have little impact on the predicted results can be assigned a representative value and be removed as a model input. This may be done, if it were established that the confidence in the error with these variables assigned a representative value have little impact on the final result.

Four primary models were developed in this study: (1) general hydration model, (2) temperature prediction, (3) concrete setting, and (4) the development of thermal stresses. The sensitivity of the hydration model was evaluated and presented in Section 5.3.7. The three remaining models are analyzed in this chapter to determine their sensitivity to the input variables. Based on the results of the sensitivity analysis, the variables that have the largest effect on the predicted results are identified.

8.1 SENSITIVITY ANALYSIS APPROACH

Numerous variables affect the development of concrete temperatures, concrete setting, and the zero-stress temperature. The impact of some of the variables are nonlinear, as they might have little impact under one set of conditions, while under a different set of conditions it might have a significant effect. It is well established that the development of in place concrete temperatures is affected by the curing temperature. For this reason, the sensitivity analysis was performed under three environmental conditions: Hot, normal, and cold paving conditions. The overall analysis approach is shown in Figure 8-1, which provides the process followed to determine the effect of the time of concrete placement. Under each three paving environments, the paving time of paving was varied while keeping all other inputs constant. The parameters directly affected by the paving time were additionally modified, since this reflects actual on-site conditions. The result of the different analysis will then be compared to criteria to determine the sensitivity of the results based on a change in paving time.

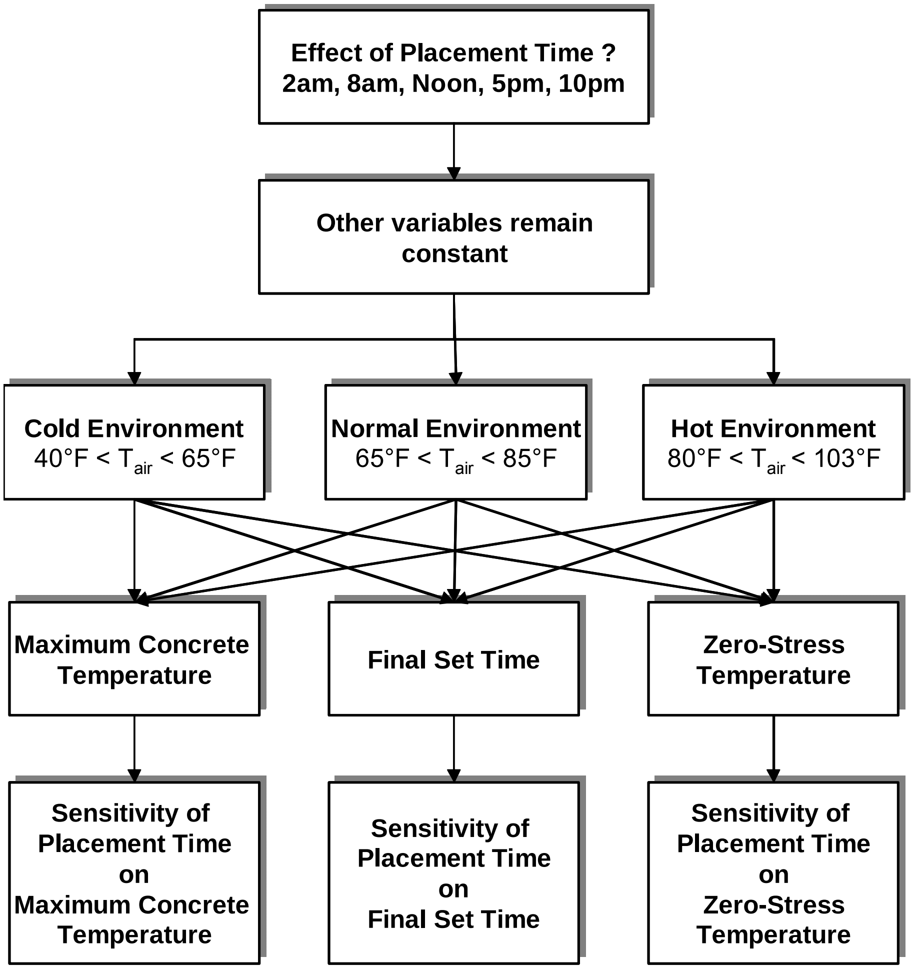

Figure 8-1: Sensitivity analysis approach

This sensitivity analysis was conducted to evaluate the effect of the different model parameters on the following three model output results:

- maximum concrete temperature ($\mathbf{T_{max}}$),
- final set time ($\mathbf{t_{fs}}$), and
- the zero-stress temperature ($\mathbf{T_{zs}}$).

The main parameters that were used to define the three paving environments are shown in Table 8-1.

Table 8-1: Environmental conditions assigned to the three sensitivity environments

Constant Variables	**Paving Environment**		
	Cold	**Normal**	**Hot**
Minimum Air Temperature, °F	40	65	80
Maximum Air Temperature, °F	65	85	103
Maximum Solar Radiation, W/m^2	650	900	1150

8.1.1 Selection of Variable Ranges

A systematic approach is required to evaluate the effect of the proposed models. A baseline set of inputs were created for each of the three paving climates. These inputs will be chosen to be representative of typical Texas paving conditions. The data collected during the field work exercise were evaluated to ensure that appropriate standard inputs were chosen. The variables and their ranges are presented under the following main categories:

1. **General variables**, presented in Table 8-2,
2. **Mixture proportion variables**, presented in Table 8-3,
3. **Materials characterization variables**, presented in Table 8-4,
4. **Environmental variables**, presented in Table 8-5, and
5. **Construction variables**, presented in Table 8-6.

Table 8-2: General variables and their ranges

Variable	**Unit**	**Range of Values**				
PCC Thickness	in	7	10	**12**	18	
Subbase Thickness	in	4	**8**	12	24	
Subbase Type	-	**Asphalt Concrete**	Cement Stabilized	Asphalt Stabilized	Granular	Existing PCCP
Subgrade Thickness	in	24	**40**	60		
Time of Placement	hr	2am	**8am**	Noon	5pm	10pm

Note: Bold values denote the baseline condition

Table 8-3: Mixture proportion variables and their ranges

Variable	Unit	Range of Values			
Cement Factor	Sacks	5.0	5.0	**6.0**	7.5
w/cm ratio	-	0.35	0.35	**0.45**	0.55
Class C Ash Content (CaO = 29%)	%	**0**	**0**	20	35
Class F Ash Content (CaO = 14%)	%	**0**	**0**	20	35
Class F Ash Content (CaO = 5%)	%	**0**	**0**	20	35
GGBF Slag Content	%	**0**	**0**	30	50

Note: Bold values denote the baseline condition

Table 8-4: Materials characterization variables and their ranges

Variable	Unit	Range of Values			
Cement Type	-	**Type I**	Type II	Type III	
Blaine Value	m^2/kg	280	**350**	550	
Activation Energy	J/mol	30,000	**40,000**	55,000	
Hydration time parameter, τ	hours	10	**13.7**	35	55
Hydration slope parameter, β	-	0.365	**0.7636**	1.2	
Ultimate degree of hydration, α_u	-	0.65	**0.72**	1	
Aggregate Type	-	**Limestone**		River Gravel	
Coefficient of Thermal Expansion	εμ/°F	4	**6**	8.5	

Note: Bold values denote the baseline condition

Table 8-5: Environmental variables and their ranges

Variable	Unit	Range of Values			
Relative Humidity [a]	%	30	**60**	100	
Wind Speed [a]	mph	**5**	10	25	
Solar Radiation [b]	W/m^2	650	900	1250	
Cloud Cover	%	0	**30**	60	100
Deep ground temperature	°C	16	**21**	26	

Note: Bold values denote the baseline condition

[a] Constant values were assumed

[b] This value was varied along with the three paving environments

Table 8-6: Construction variables and their ranges

Variable	Unit	Range of Values			
Concrete Placement Temperature	°F	Ambient - 10°F	**At Ambient**	Ambient + 10°F	
Base temperature	°F	Ambient - 10°F	**At Ambient**	Ambient + 10°F	
White wash base	-	**No**	Yes		
Curing method	-	None	Single Coat CC [a]	**Double Coat CC** [a]	
Color of plastic sheet	-	**None**	White	Yellow	Black
Curing Blanket thickness	-	**None**	0.75	1.5	

Note: Bold values denote the baseline condition

[a] CC = Liquid Curing Compound

8.1.2 Sensitivity Rating

Overall, the models showed a wide range of sensitivity to changes in the paving environment and the input variables listed in Tables 8-2 through 8-6. Overall, the models were stable, and reasonable results were obtained. The results of the sensitivity analysis are presented in Appendix F, and are summarized and discussed in Section 8.2.

The model sensitivity to changes in the input variables is summarized by assigning a sensitivity rating to the input parameters for each of the three models. The sensitivity definitions were selected by keeping the overall study objectives in mind, and by engineering judgment. The criteria for the sensitivity rating are based on the **change** in the predicted result, relative to the baseline case and are as presented in Table 8-7. Based on the variable's relative effect on the predicted behavior, one of the following sensitivity definitions were assigned to each variable:

- **High** = These variables are primarily responsible for the predicted results, and large differences in the predicted response may be seen with a modest change is these variables. These inputs should be defined as accurately as possible.
- **Moderate** = A significant change in the output occurs with a change in this variable.
- **Low** = The impact of the input variable is small. By using approximate values for these variables, only small changes in the results are obtained.
- **None** = These variables have little or negligible effect on the output results. Default values of these variables may be used throughout the model.

Table 8-7: Criteria for sensitivity rating

Sensitivity Rating	Model Output Results		
	Maximum concrete temperature (T_{max})	**Final set time (t_{fs})**	**Zero-stress temperature (T_{zs})**
High	$\Delta T_{max} > 8°F$	$\Delta t_{fs} > 1.5$ hrs	$\Delta T_{zs} > 8°F$
Moderate	$4 < \Delta T_{max} \leq 8°F$	$1.0 < \Delta t_{fs} \leq 1.5$ hrs	$4 < \Delta T_{zs} \leq 8°F$
Low	$2 < \Delta T_{max} \leq 4°F$	$0.5 < \Delta t_{fs} \leq 1$ hrs	$2 < \Delta T_{zs} \leq 4°F$
None	$\Delta T_{max} \leq 2°F$	$\Delta t_{fs} \leq 0.5$ hrs	$\Delta T_{zs} \leq 2°F$

8.2 RESULTS OF SENSITIVITY ANALYSIS

The sensitivity analysis was performed with the range of input variables listed in Tables 8-2 through 8-6. The results obtained from the baseline variables under the three paving environments are summarized in Table 8-8. The detailed results of the sensitivity analysis are presented in Appendix F. The sensitivity rating was assigned based on the worst case from the three paving environments analyzed. Based on the criteria defined in Table 8-7, the sensitivity ratings for the variables are summarized in Table 8-9.

Table 8-8: Results obtained for the baseline conditions under the three paving environments

Paving Environment	Results for the Baseline Condition		
	Maximum concrete temperature (T_{max})	**Final set time (t_{fs})**	**Zero-stress temperature (T_{zs})**
Cold	80°F	7.9 hours	75°F
Normal	114°F	4.2 hours	107°F
Hot	139°F	2.6 hours	128°F

When reviewing the results in Table 8-9, it should be kept in mind that the sensitivity rating reflects the change that is obtained by changing the input variable ***relative*** to the results obtained with the baseline condition shown in Table 8-8. For example, the cement factor's sensitivity to the maximum concrete temperature is rated as "moderate"; in other words, by changing the cement factor from 6.0 to 7.5 sacks, the maximum concrete temperature will be affected by 4 to 8°F. It may be seen from the result in Appendix F that the actual effect of this parameter was around 7°F.

The results in Table 8-9 reveal that the maximum concrete temperature and the zero-stress temperature appear to be similarly impacted by a change in the input variables. This indicates that an underlying correlation might exist between these two output results and this aspect is further investigated in Section 9.1.3.1.

In Section 6.2.1, it was concluded that the activation energy model developed in this study should be implemented. However, the sensitivity of the results to changes in activation energy should first be evaluated. The results in Table 8-9 indicate that the activation energy has a moderate effect on the maximum concrete temperature development. This warrants the use of the activation energy model recommended in Section 6.2.1.

Based on the results shown in Table 8-9, it may be recommended that default values be assigned to the following variables with a low sensitivity rating:

- subgrade thickness (assign default value of 40-inches),
- deep ground temperature (assign default value of 20°C), and
- relative humidity (assign default value of 50%).

The coefficient of thermal expansion (CTE) appears to have little impact as compared to the baseline conditions. However, it has a significant effect on the magnitude of the computed thermal stress, which was not one of the parameters considered during this sensitivity analysis. It is for this reason that it is not recommended to assign a default value to this parameter.

It is worth commenting that the sensitivity analysis performed in this study only reflects the effect when **one** of the parameters is changed. If some parameters could change the maximum concrete temperature by more that 8°F, the combined effect of modifying many of these high sensitivity parameter could become very significant. The scenarios that may occur with this condition will be presented in Section 8.3.

Table 8-9: Summary of the sensitivity rating obtained for each variable

	Variable	**Sensitivity Rating**		
		Maximum Concrete Temperature	**Final Set Time**	**Zero-Stress Temperature**
	Paving Environment	**High**	**High**	**High**
General Variables	PCC Thickness	Moderate	None	Low
	Subbase Thickness	Low	None	Low
	Subbase Type	Low	None	Low
	Subgrade Thickness	None	None	None
	Time of Placement	**High**	**High**	**High**
Mixture Proportion	Cement Factor	Moderate	None	Moderate
	w/cm ratio	Low	Low	Low
	Class C Ash Content (CaO= 29%)	**High**	**High**	**High**
	Class F Ash Content (CaO= 14%)	**High**	**High**	Moderate
	Class F Ash Content (CaO= 5%)	**High**	**High**	**High**
	GGBF Slag Content	Moderate	**High**	High
Materials Characterization	Cement Type	**High**	**High**	**High**
	Blaine Value	Moderate	**High**	Low
	Activation Energy	Moderate	Low	Low
	Hydration time parameter, τ	**High**	**High**	**High**
	Hydration slope parameter, β	**High**	**High**	Moderate
	Ultimate degree of hydration, α_u	**High**	Moderate	High
	Aggregate Type	Low	None	Low
	Coefficient of Thermal Expansion	None	None	None
Environmental Variables	Relative Humidity	None	None	None
	Wind Speed	Moderate	None	Moderate
	Solar Radiation	Moderate	Low	Moderate
	Cloud Cover	**High**	Low	Moderate
	Deep ground temperature	None	None	None
Construction Variables	Concrete Placement Temperature	**High**	**High**	**High**
	Base temperature	Moderate	None	Moderate
	White wash base	Low	None	Low
	Curing method	Low	None	Low
	Color of plastic sheet	**High**	None	**High**
	Curing Blanket thickness	**High**	None	**High**

8.2.1 Identification of the Most Critical Variables

The sensitivity of the input variables was established in Section 8.2 and with this information available; the most critical variables may be identified. The maximum concrete temperature and zero-stress temperatures are significantly impacted by numerous variables from all five input categories. Variables with high to moderate impact on the maximum in place concrete temperature can be summarized as follows:

• color of plastic sheet,	effect ± 19°F,
• cement type,	effect ± 14°F,
• hydration parameters,	effect ± 13°F,
• time of placement,	effect ± 12°F,
• curing blankets,	effect ± 12°F.
• concrete placement temperature,	effect ± 11°F,
• cloud cover,	effect ± 11°F,
• use of mineral admixtures,	effect ± 10°F,
• cement factor,	effect ± 7°F,
• wind speed,	effect ± 7°F,
• base temperature,	effect ± 7°F,
• activation energy,	effect ± 6°F,
• PCC thickness,	effect ± 6°F,
• cement fineness,	effect ± 5°F, and
• solar radiation,	effect ± 5°F.

Most of the variables listed above were found to have a moderate to high impact on the zero-stress temperature. The only variable of those listed above that did not have a moderate to high impact was the PCC thickness.

The final set time was affected differently as compared to the maximum and zero-stress temperatures. Variables with high to moderate impact on the time to final set can be summarized as follows:

• hydration parameters,	effect ± 12.5 hours,
• use of mineral admixtures,	effect ± 9.5 hours,
• time of placement,	effect ± 5.5 hours,
• cement fineness,	effect ± 3.5 hours,
• cement type,	effect ± 2.5 hours, and
• concrete placement temperature,	effect ± 2.0 hours.

8.3 ADDITIONAL RESPONSE ANALYSIS RESULTS TO EVALUATE THE EFFECT OF MOST SIGNIFICANT VARIABLES

This section presents the predicted development of mid-depth concrete temperatures over the first 48-hours for some of the variables with a high sensitivity rating. These results are shown to facilitate an understanding of the sensitivity analysis and the reasons for the effect of these parameters. Figure 8-2 presents the effect of paving time on the development of mid-depth concrete temperatures, and these results may be compared to the results as shown in Figure 8-3, as obtained by the Michigan Engineering Experiment Station (MEES) (1948). If one considers that the materials used in the MEES project and environmental conditions (cloud cover, etc.) are different from that used to obtain the results shown in Figure 8-2, then it may be concluded that the trends in the behavior are very similar. The responses of the remaining variables are shown in Figures 8-4 through 8-14. The figures illustrate the effect of a change in the most significant variables.

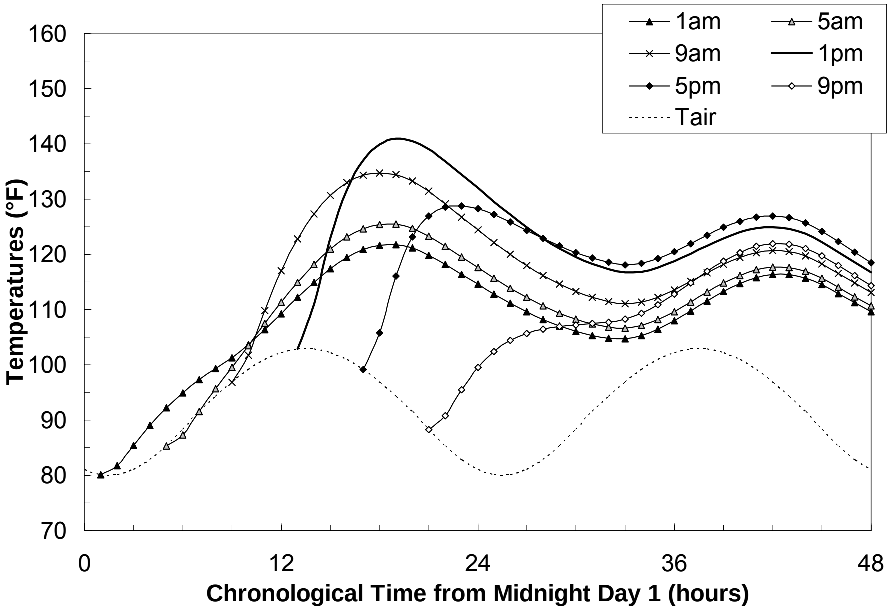

Figure 8-2: Effect of paving time on the development of mid-depth concrete temperatures

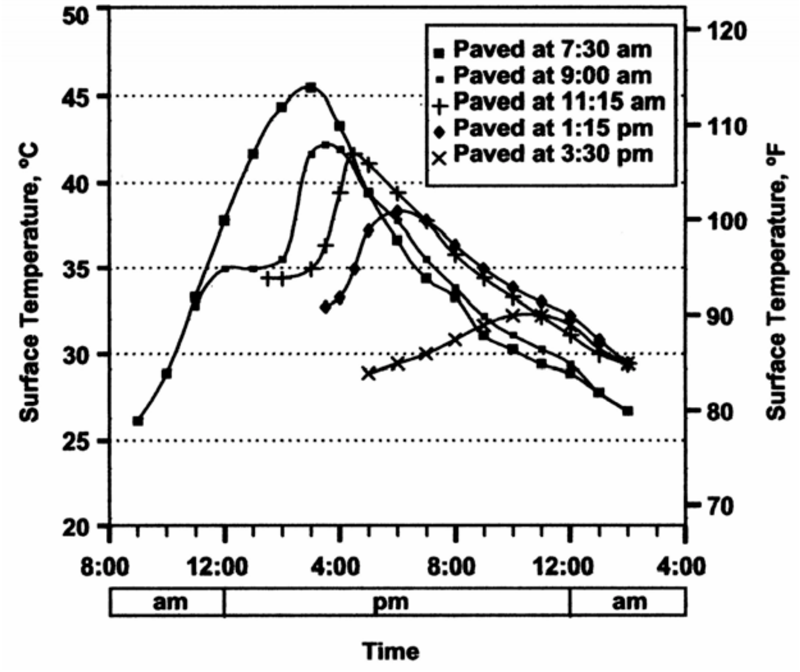

Figure 8-3: Surface temperatures of pavement slabs paved at different times of the day (MEES, 1948)

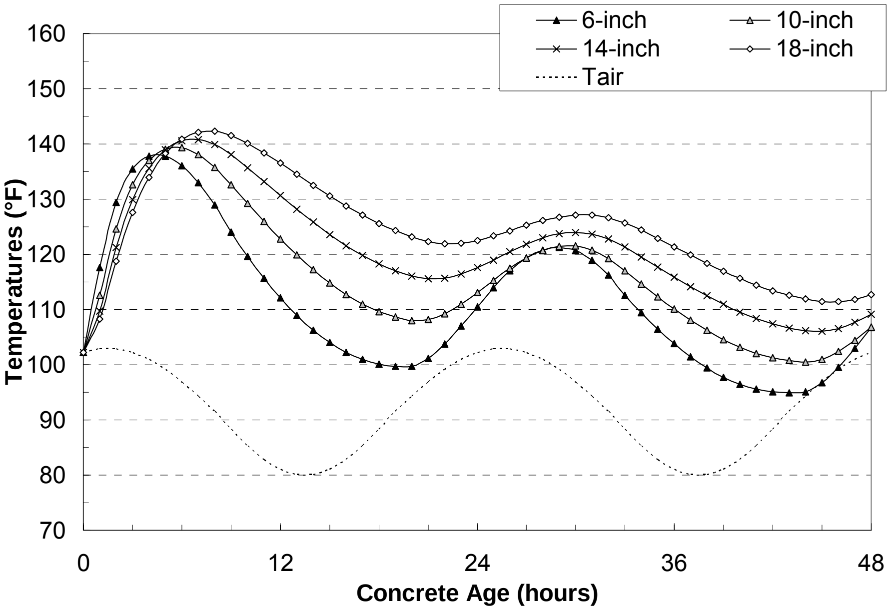

Figure 8-4: Effect of PCC thickness on the development of mid-depth concrete temperatures

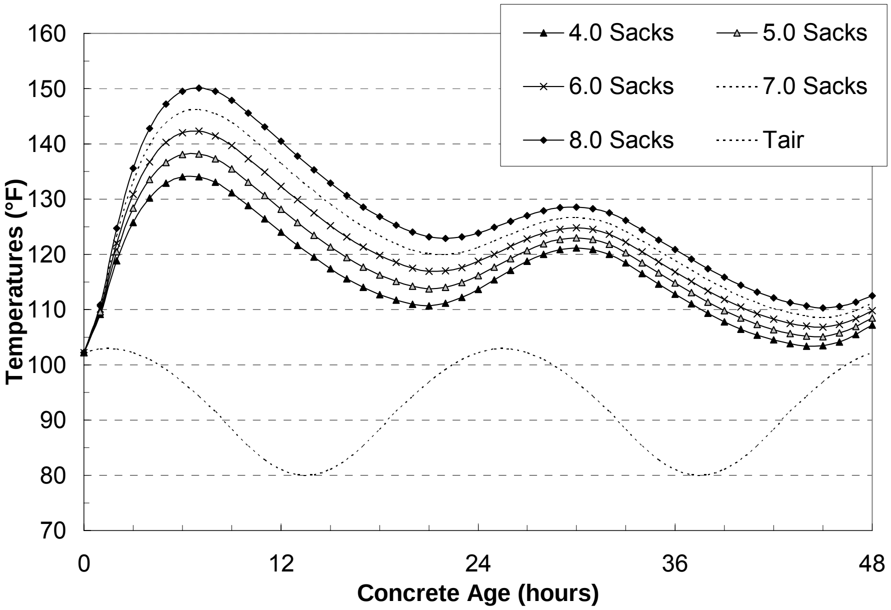

Figure 8-5: Effect of cement factor on the development of mid-depth concrete temperatures

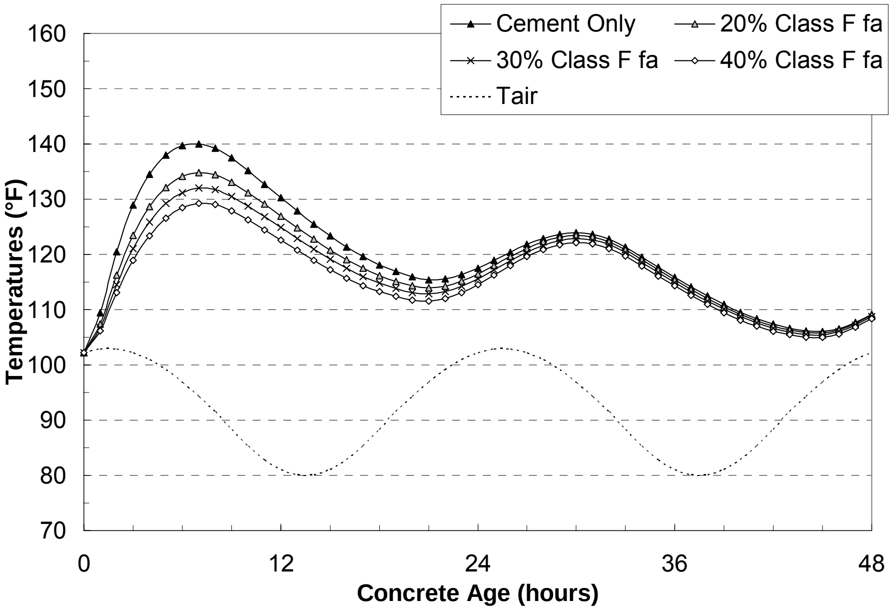

Figure 8-6: Effect of different class F fly ash dosages on the development of mid-depth concrete temperatures

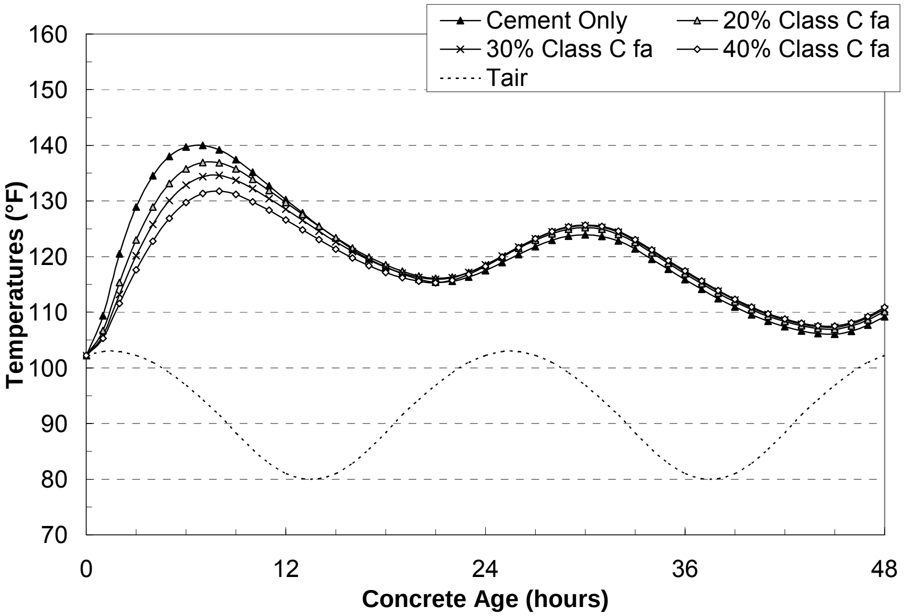

Figure 8-7: Effect of different class C fly ash dosages on the development of mid-depth concrete temperatures

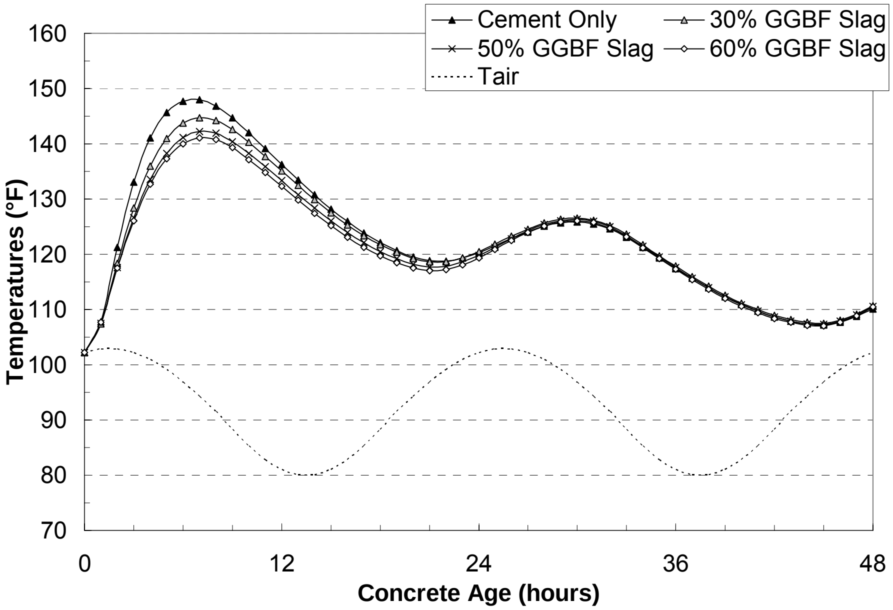

Figure 8-8: Effect of different GGBF slag dosages on the development of mid-depth concrete temperatures

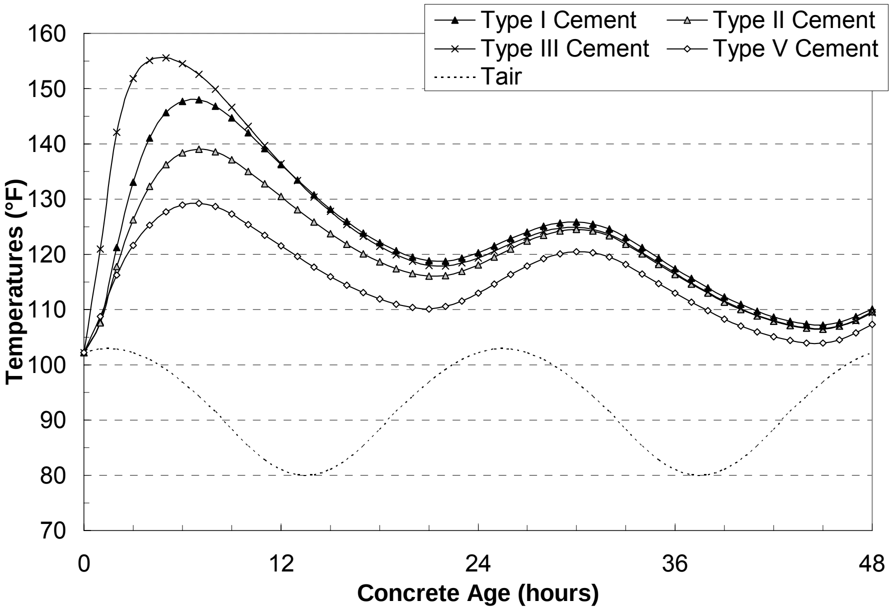

Figure 8-9: Effect of different types of cement on the development of mid-depth concrete temperatures

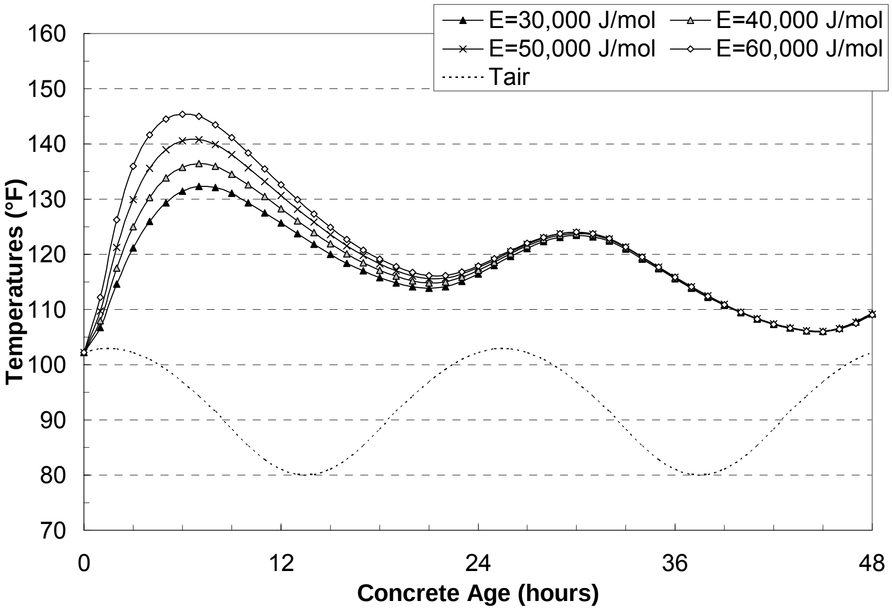

Figure 8-10: Effect of activation energy on the development of mid-depth concrete temperatures

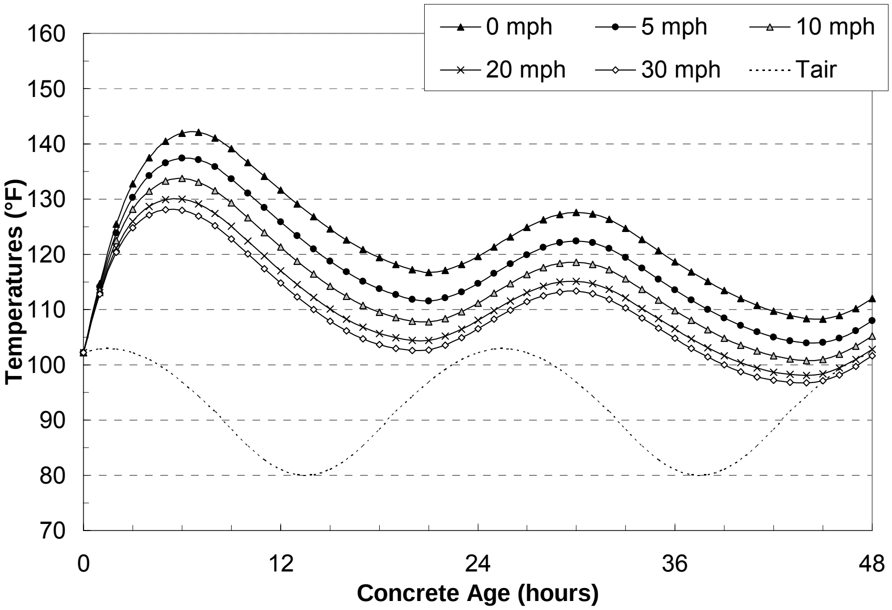

Figure 8-11: Effect of wind speed on the development of mid-depth concrete temperatures

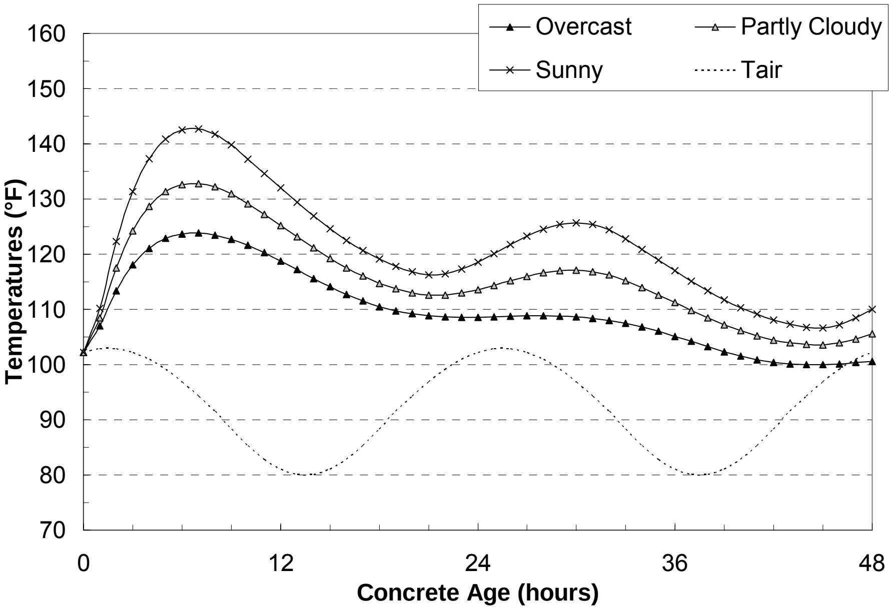

Figure 8-12: Effect of cloud cover on the development of mid-depth concrete temperatures

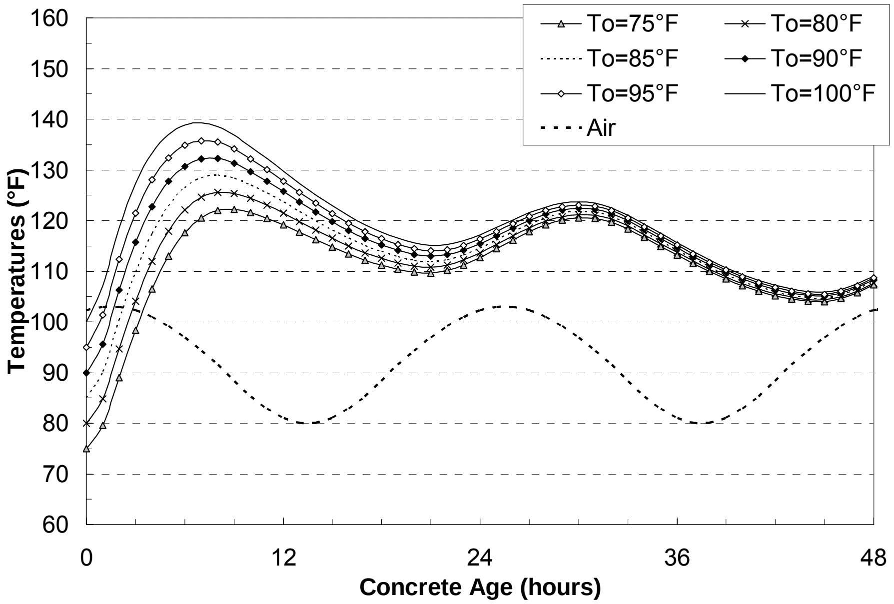

Figure 8-13: Effect of paving time on the development of mid-depth concrete temperatures

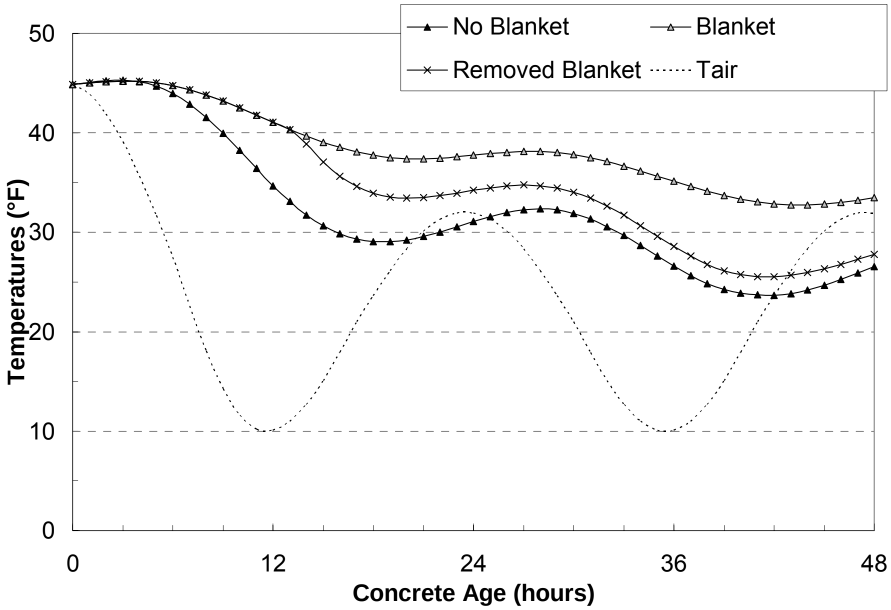

Figure 8-14: Effect of paving time on the development of mid-depth concrete temperatures
(*Note:* Cold paving conditions were used for this analysis, since blankets are generally used under these conditions)

8.4 CONCLUDING REMARKS

This chapter represented the results obtained from a sensitivity analysis performed on the temperature prediction, concrete setting, and time to zero-stress prediction models. All the input variables were grouped into the following categories:

1. **General variables**,
2. **Mixture proportion variables**,
3. **Materials characterization variables**,
4. **Environmental variables**, and
5. **Construction variables.**

This sensitivity analysis was conducted to evaluate the effect of the different model parameters on: (1) the maximum concrete temperature, (2) final set time, and (3) zero-stress temperature. The sensitivity rating presented in Table 8-7 was used to evaluate the effect of changing the input variable ***relative*** to the results obtained when the baseline condition was analyzed. The results of the sensitivity are summarized in Table 8-9. The following variables were found to have a moderate to high impact on the different responses:

1. **Maximum in place concrete temperature:**
   PCC thickness, time of placement, cement factor, use of mineral admixtures, cement type, cement fineness, activation energy, hydration parameters, wind speed, solar radiation, cloud cover, concrete placement temperature, base temperature, color of plastic sheet, and the use of curing blankets.
2. **Final set time:**
   Time of placement, use of mineral admixtures, cement type, cement fineness, hydration parameters, and the concrete placement temperature.
3. **Zero-stress temperature:**
   All the variables listed for the maximum in place concrete temperature, except the pavement thickness.

The variables listed above are the input variables, which will cause the largest change in the predicted results. During use of the prediction model and in implementation of the finding of this work, these variables must be known or measured to achieve accurate predictions. The most sensitive controllable variables should be identified and targeted in any method-based specification to ensure excessive concrete temperatures do not develop under in place conditions.

Chapter 9

Mitigation and Implementation Measures

High concrete temperatures affect fresh concrete properties, which may produce in place concrete properties that reduce long-term pavement performance. Section 1.1.2 demonstrated that high early-age concrete temperatures may lead to reduced long-term pavement life since it causes increased thermal stress, and lower long-term strengths, which result in closer crack spacings in continuously reinforced concrete pavements. This may also casuse uncontrolled cracking in jointed concrete pavements.

One possible measure to minimize the potential problems associated with hot weather concreting can be to control the concrete mixture temperature (Samarai et al., 1975; Komonen et al., 1997; McCullough et al., 1998; and ACI 305, 2000). An effort should be made to keep the concrete temperature as low as economically feasible. By controlling the temperature of the ingredients, the temperature of the fresh concrete can be regulated (ACI 305, 2000). This is currently the approach adopted by most states, since they specify a maximum concrete temperature at placement to mitigate the detrimental effects of hot weather placement.

The specification of a limiting concrete temperature at placement might be applicable to some conditions, but unnecessary in others. The limits selected by most states were based on mixture proportions (1970s) that contain no mineral or chemical admixtures, which have been shown to be effective in reducing the rate of heat evolution. As the same limit applies to all cases, it does not account for the effect of mineral admixtures, different concrete placement times, and/or different aggregates. For example, the maximum placement limit remains unchanged in all of the following cases, although they may reduce the development of in place concrete temperatures and/or stresses:

- Type III cement versus a Type II cement with 35 Class F fly ash is used,
- Concrete paving at 10am versus 5pm, and/or
- Concrete with a coefficient of thermal expansion of 6 or 10 microstrain/°F is used.

On a national level, ACI 305 (2000) states that for general types of construction in hot weather, a "...maximum ambient or concrete temperature that will serve a specific case may be unrealistic in others." The ACI committee advises on this subject that:

> …at some temperature between approximately 75 F and 100 F (24 and 38 C) there is a limit that will be found to be most favorable for best results in each hot weather operation, and such a limit should be determined for the work.

In this study, a temperature prediction program was developed that will directly serve the purpose to enable the Designer and Contractor to select the materials, construction practices, and/or maximum concrete placement temperature most favorable for the paving conditions.

The content of this Chapter is outlined in Figure 9-1. In Section 9.1, design and behavior principles of PCC are discussed. Next, current construction and design practices are presented in Section 9.2. In Section 9.3, an approach different from specifying a maximum placement temperature is offered. The approach will emphasize the selection of improved materials, and the most appropriate construction practices for the specific placement conditions. The approach is specifically applicable to all PCC pavement types, since they are subjected to long-term thermal stresses, which may affect the mechanism in which the load is carried and distributed. The proposed mitigation approach is discussed and presented in detail in Section 9.3. The computer-based temperature prediction program for used during the proposed mitigation approach is discussed in Section 9.4. In Section 9.5, a concept to develop site specific reinforcement standards for use throughout Texas is presented. To facilitate the implementation of the proposed temperature control specification, an interim temperature control specification is developed that is based on the current Texas reinforcement standards. Section 9.6 provides a discussion on the proposed interim temperature control specification.

9.1 PORTLAND CEMENT CONCRETE PAVEMENT DESIGN AND BEHAVIOR PRINCIPLES

Thermal stresses affect the performance of both continuously reinforced concrete (CRC) pavements and jointed concrete pavements. These effects will be discussed in this Section. This Section will define the long term temperature change for use during pavement design (Section 9.1.3) and will also introduce the concept of the maximum stress index (Section 9.1.4).

9.1.1 CRC Pavement Reinforcement Design Process

Continuously reinforced concrete (CRC) pavements are designed without transverse contraction joints, and transverse cracks are allowed to occur naturally. The long-term temperature changes the pavement is subjected to largely determines the long-term stabilized crack distribution. This stabilized cracking spacing is then exposed to traffic over the remaining life of the pavement. The design of CRC pavements consists of two main phases: thickness design and reinforcement design. The thickness design is based on the fatigue of the PCC under repeated wheel loading; the procedure in the AASHTO 1993 Design Guide is generally used for this phase.

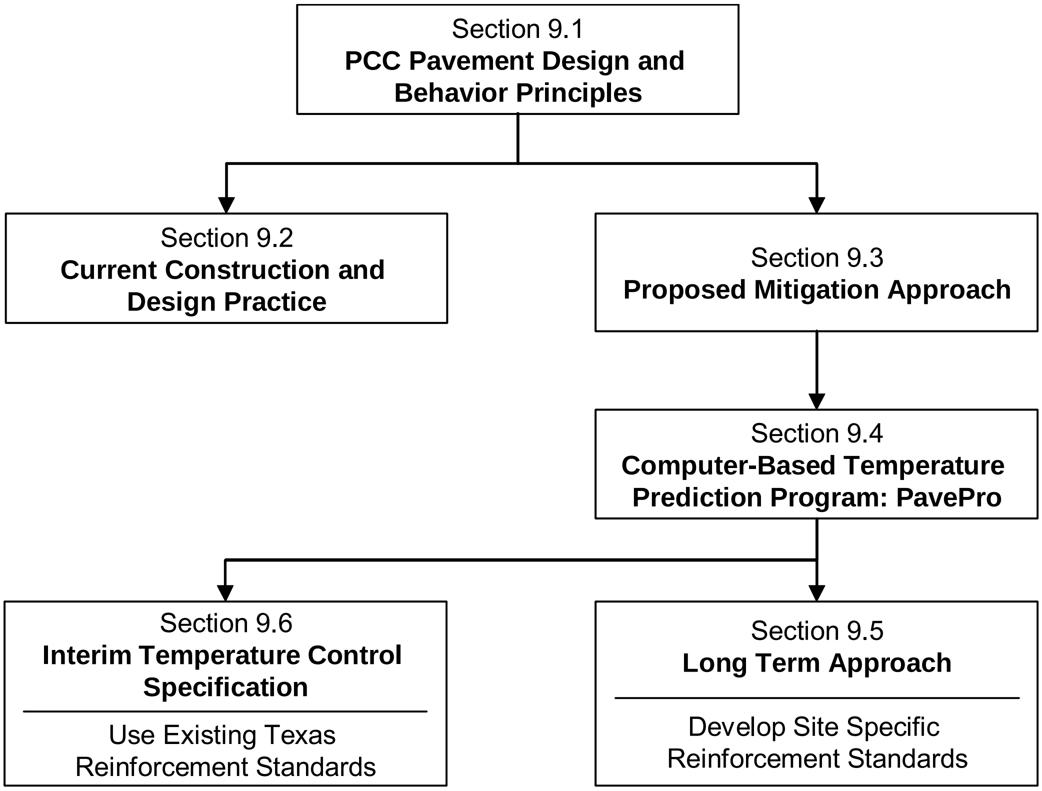

Figure 9-1: Layout and structure of the contents of Chapter 9

The reinforcement design is primarily based on the thermal and moisture induced stresses the pavement is subjected to. In Texas, the CRCP-8 computer program (Won et al., 1991) is used to determine the optimum amount of reinforcement. The reinforcement design phase is directly affected by early-age and long-term temperature effects, and this phase will be discussed in more detail.

The amount of reinforcement affects the stabilized crack distribution in the CRC pavements. The distribution of these transverse cracks are of utmost importance, since research has shown that cracks spaced close to each other could lead to punchouts, the most detrimental continuously reinforced concrete (CRC) pavement distress (McCullough et al., 1998). During the longitudinal reinforcement design, three main design requirements have to be considered to ensure good pavement performance. These three main design requirements are (McCullough, 1993):

1. Maximum allowable crack width at freezing temperature,
2. Maximum allowable steel stress at the minimum temperature expected to occur during the design life of the pavement, and
3. Cumulative percentage of transverse cracks spaced at less than three feet.

With the CRCP-8 program, current CRC pavement reinforcement design practice involves the selection of a long-term temperature change to obtain the reinforcement amount best suited for the pavement thickness under design. Based on the thermal stress design equation shown in Equation 1-1, the long-term temperature gradient is determined by the difference between the **zero-stress temperature** and the **minimum concrete temperature** the pavement will be exposed to during its service life. This concept is illustrated in Figure 9-2.

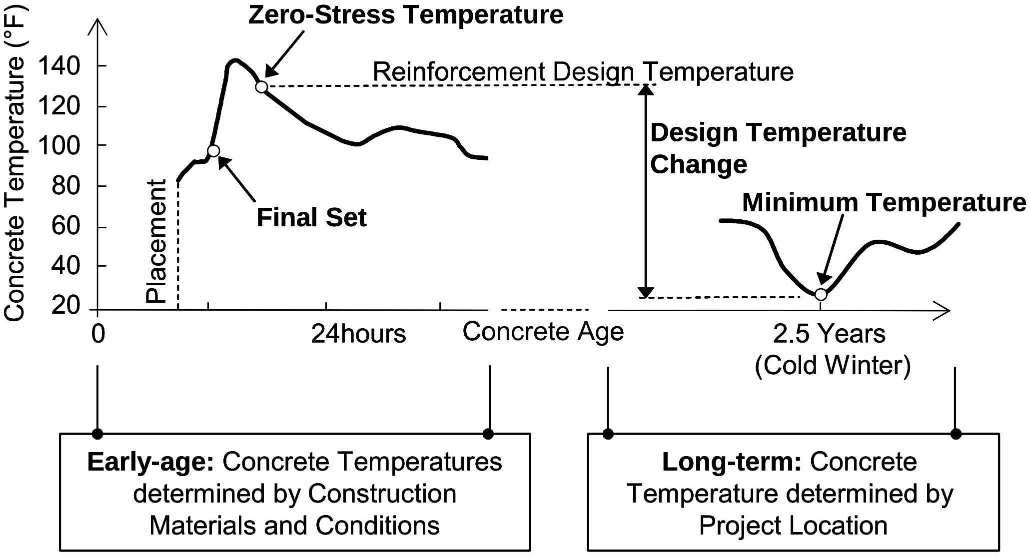

Figure 9-2: CRC pavement design temperature change principles

Figure 9-2 indicates that the zero-stress temperature is influenced by the development of early-age temperatures and stresses, i.e. by the construction operations. The higher the concrete temperature at early-ages, the higher the long-term thermal stress becomes, which will be revealed in the pavement by closer crack spacings. The minimum temperature the pavement is subjected to is determined by the prevailing winter conditions that occur at the project location. This value is determined by the effects of nature, and cannot be controlled; however, this effect can be incorporated into the design process by developing site specific reinforcement standards. These site specific reinforcement standards should be based on the minimum concrete temperature expected to occur with the design confidence levels at the project location.

Physical evidence of the impact of the effect of early-age concrete temperatures can be seen from two test projects in the Houston District, located on State Highway 6 (Hankins et al., 1991). These two projects encompassed eight test sections, constructed in distinctly different environmental conditions, namely winter and summer. These sections are ideal to evaluate the effect of early-age concrete temperatures on the behavior of CRC pavements. The stabilized crack spacing distributions

(2800-days) of the sections are shown in Figures 9-3 and 9-4. These figures indicate that the sections constructed under winter conditions exhibit a much lower percentage of cracks that form at spacings of 3 feet or less. This phenomenon is due to the development of lower zero-stress temperatures for a section constructed under winter conditions. From this physical evidence, it may be concluded that the stabilized crack spacing is influenced by the season of placement and the type of coarse aggregates used in the project.

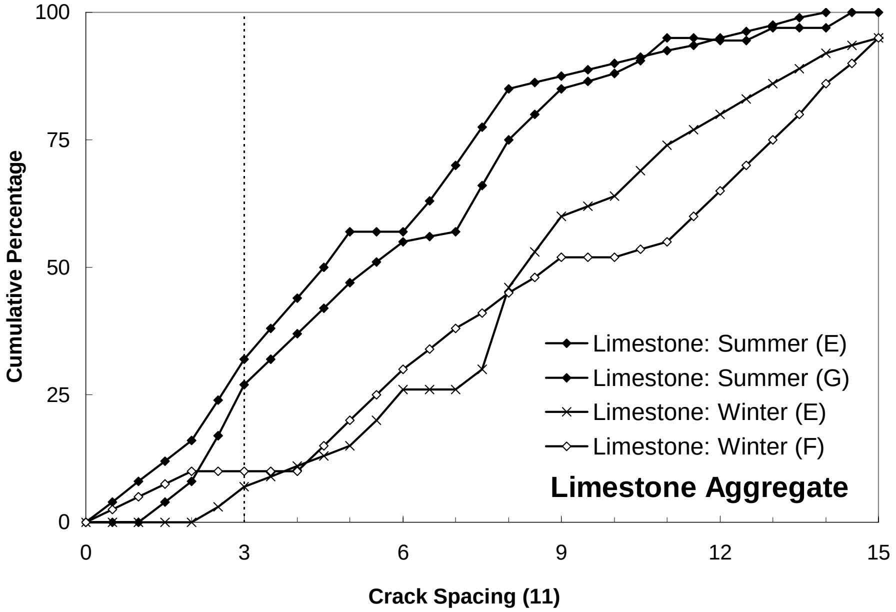

Figure 9-3: Long term crack distribution for **limestone** summer and winter placements on SH6, Houston

The impact of close crack spacings on long term PCC pavement performance is schematically indicated in Figure 9-5; a condition with a high probability of punchouts is established when transverse cracks are spaced very close to each other (McCullough et al. 1998). It may thus be concluded that the sections constructed under winter conditions with the use of limestone coarse aggregates will generally provide the best performance.

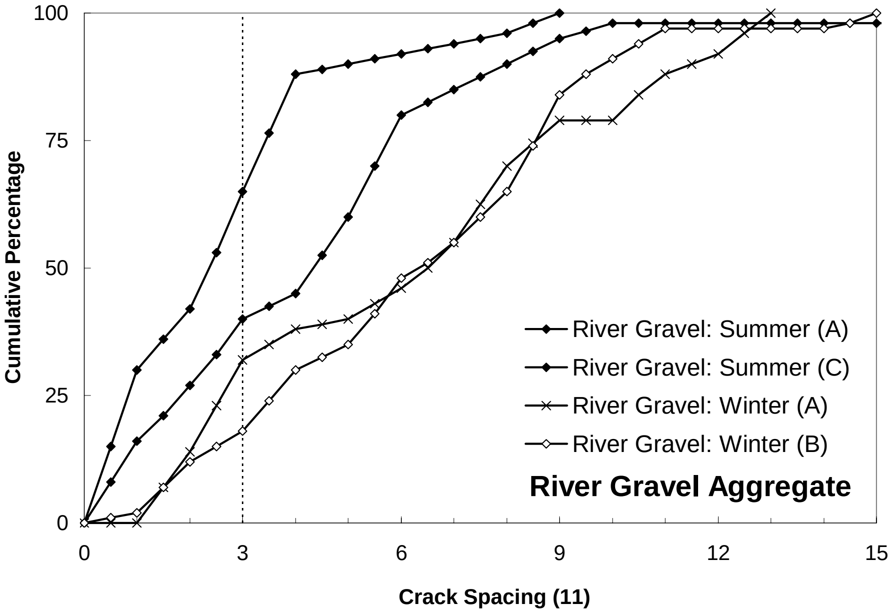

Figure 9-4: Long term crack distribution for river gravel summer and winter placements on SH6, Houston

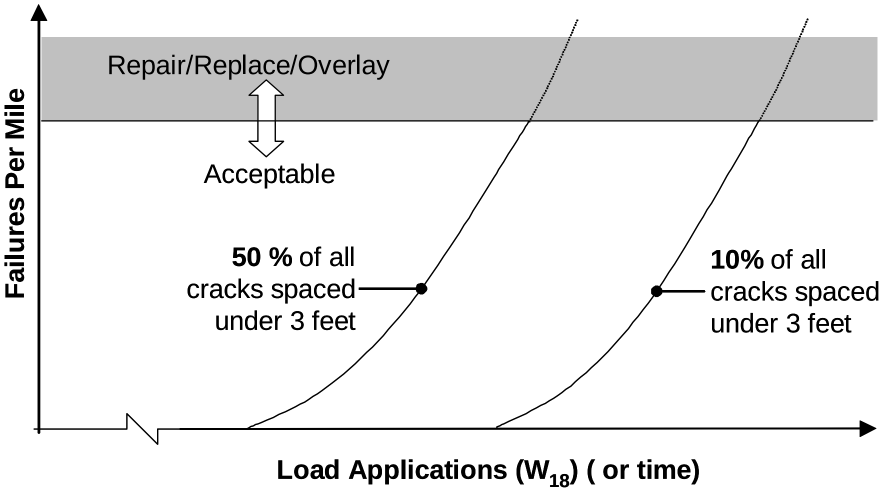

Figure 9-5: The impact of close crack spacing on long-term pavement performance

9.1.2 Jointed Concrete Pavement Behavior

The magnitude of thermal stress a jointed concrete pavement is subjected to during its design life has a significant impact on its long-term performance. The design temperature change shown in Figure 9-2 is used during the design of jointed concrete pavements to determine the amount of reinforcement required for an optimal design.Misstatement because we don't use temp differential for design of steel in JRCP. The magnitude of the as constructed temperature change will determine the magnitude of the joint widths and mid-slab thermal stresses. The higher the concrete temperature at early-ages, the higher the long-term thermal stress becomes, which may cause increased joint widths in the pavement, and an increased probability for the occurrence of mid-slab cracks. Therefore, it is recommended to control the development of in place concrete temperatures to acceptable limits in the as constructed jointed concrete pavement.

9.1.3 Long Term Temperature Change for Reinforcement Design

In Section 9.1.1, it was discussed that the long-term temperature change is determined by the difference between the **zero-stress temperature** and the **minimum concrete temperature** the pavement will be exposed to during its service life. This concept is shown in Figure 9-2. This Section will provide recommendations to determine both of the temperatures required to define the temperature change for reinforcement design purposes.

9.1.3.1 Approximation of the Zero-Stress Temperature

In this study, models were developed to characterize the development of in place concrete temperatures and early-age thermal stresses. The early-age stress model was used to determine the zero-stress temperature. During the sensitivity analysis (Chapter 8) of the maximum in place (**T_{max}**) and the zero-stress temperatures (**T_{zs}**), it was found that these responses were similarly affected by the variables, which implies that they may be correlated. In this Section, the correlation between these two variables is investigated for use to integrate design procedures with construction practices.

Figures 1-4 and 3-35 presented that the zero-stress temperature is related to the point at which the concrete is at zero stress after the initial compression. Initial compression in a slab is caused by continued hydration and rapid heat development after initial set has occurred and due to a restraint of movement. The more rapid the hydration temperature, the higher the initial compression, which at the same time increases T_{zs}.

The correlation between **T_{max}** and **T_{zs}** was evaluated though the data generated during the sensitivity analysis of the models. Since the reinforcement design will be performed for high concrete temperature conditions, this analysis was only performed at the normal and hot paving environments defined in Table 8-1. Based on the results shown in Appendix F, it was found that on average, the difference between **T_{zs}** and **T_{max}** remained a constant function of **T_{max}**. In order to analyze this effect, the following variable (R_d) was defined:

$$R_d = \frac{T_{\max} - T_{zs}}{T_{\max}} \qquad \textit{Equation 9-1}$$

where, R_d = T_{max} reduction ratio to obtain T_{zs}.

The results obtained by comparing R_d for the main categories of variables are contained in Appendix F, and are summarized in Table 9-1. Average R_d values of six and eight percent were found, respectively, for the normal and hot weather paving environments. The two percent difference in R_d value may be attributed to the rapid initial temperature build-up and higher early-age compressive stresses that develop in the hot weather paving environment, which lead to increased early-age stress relaxation.

Table 9-1: Summary of R_d values expressed as percentages for each variable category

Variable Category	**Average R_d (%)**	
	Paving Environment	
	Normal	**Hot**
General variables	6%	8%
Mixture proportion variables	5%	7%
Materials characterization variables	7%	8%
Environmental variables	6%	7%
Construction variables	6%	8%
Average of all categories	**6%**	**8%**

The average ratios of 6% and 8% were selected and used to back-calculate T_{zs} from the T_{max} values. Figures 9-6 and 9-7 present the results, and it may be seen that the use of the simplified R_d ratio provides an accurate estimate of T_{zs} as modeled by the early-age relaxation theory.

An experimental procedure was developed in Research Project 1244-3 (Suh et al., 1992) to determine the zero-stress temperature on site. It was determined that the setting temperature was about 93% of the maximum concrete temperature, which corresponded to a R_d of 7%, which is in agreement with the results obtained.

The validity of using the R_d value to approximate the zero-stress temperature from the maximum concrete temperature will be evaluated. This approach will be evaluated with the restrained thermal cracking tests data from Springenschmid and Breitenbücher (1991). Their published results consisted of 17 different cements, and the T_{max} and T_{zs} values for all the concretes were documented. These tests were performed under semi-adiabatic conditions, after the concrete is mixed at 20°C (68°F). Due to the concrete temperature development, these test conditions correspond to the normal paving conditions defined in this study.

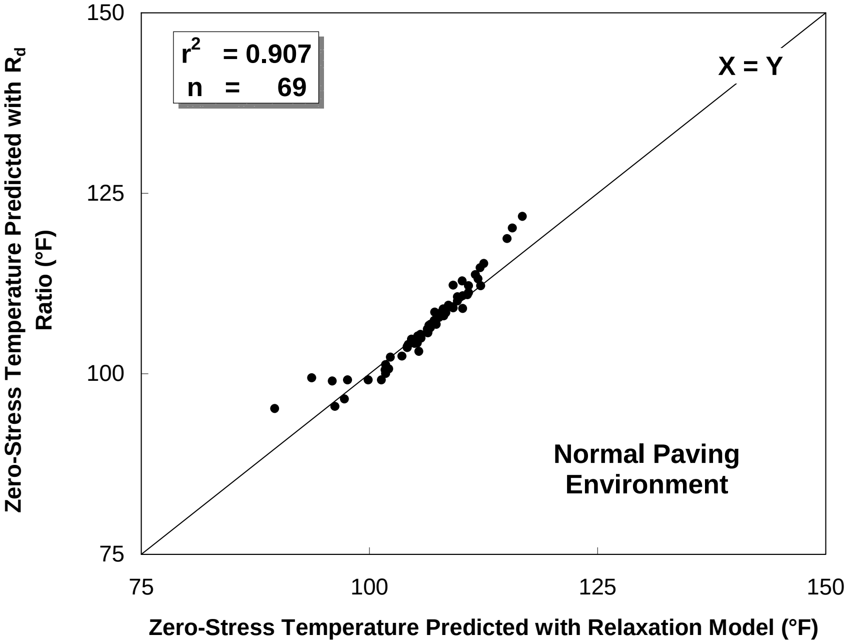

Figure 9-6: T_{zs} predicted with relaxation model versus predicted with ΔT_{max} ratio under a normal paving environment

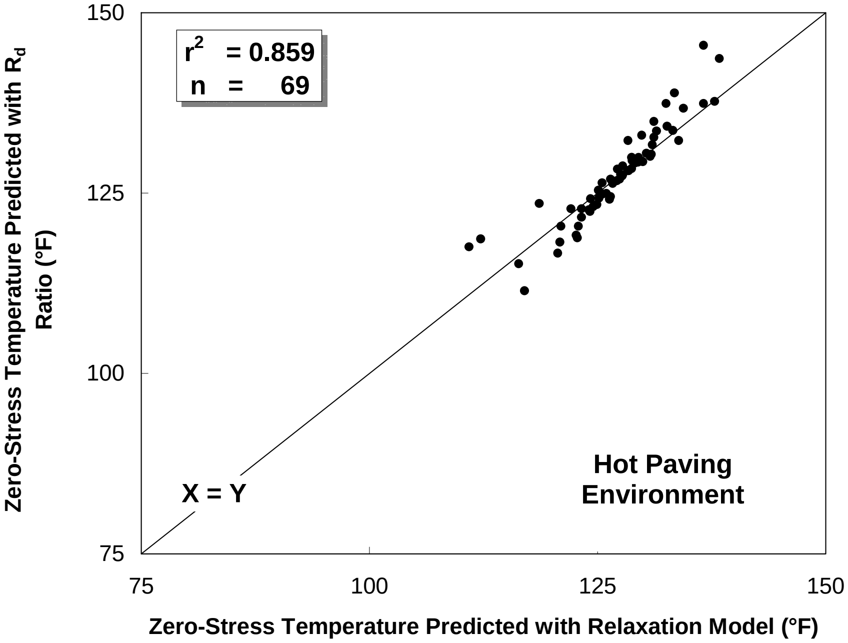

Figure 9-7: T_{zs} predicted with relaxation model versus predicted with ΔT_{max} ratio under a hot paving environment

Based on the data from Springenschmid and Breitenbücher, R_d was calculated for all the cements, and the results are shown in Figure 9-8. This figure indicates that the R_d ratio remains approximately constant, with the exception of cement S. The average R_d from these data is 4.50. These results are similar to the R_d of 6% obtained from the mathematical model at normal paving conditions.

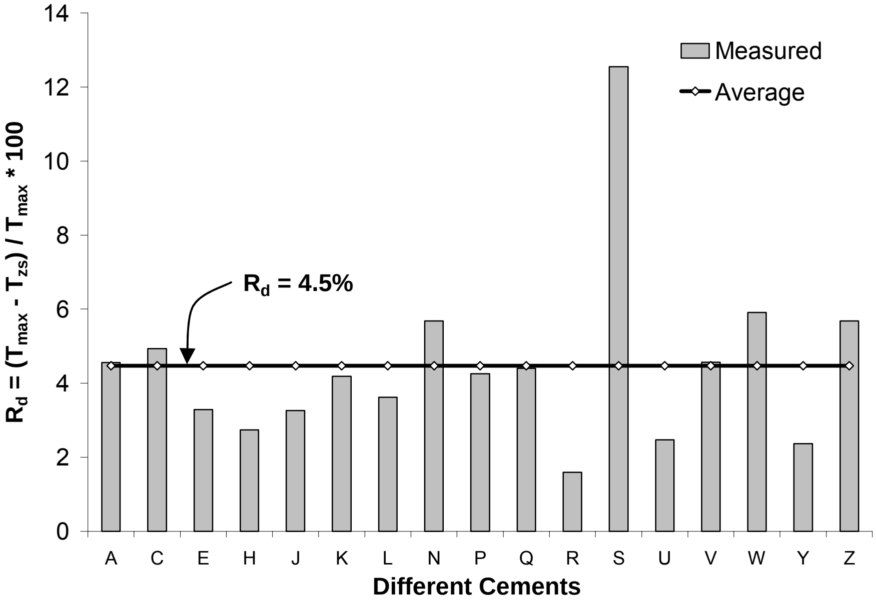

Figure 9-8: ΔT_{max} computed from tests results obtained by Springenschmid and Breitenbücher. (1991)

These results provide confirmation that the R_d factor can be used for **implementation** purposes to link the design temperature (T_{zs}) to the maximum in place temperature (T_{max}). This will enable the integration of design and construction practices, since reinforcement can now be designed at T_{zs} and quality control can be performed at T_{max}, and these two values are correlated to R_d. The integration of design and specifications maybe achieved by transforming Equation 9-1 to a specification format by solving for the maximum temperature as a function of the zero-stress temperature as follows:

$$T_{\max} = \frac{T_{zs}}{1 - R_d} \qquad \textit{Equation 9-2}$$

By using the R_d values listed in Table 9-1, Equation 9-2 may be expressed as follows:

with $R_d = 0.06$, $$T_{\max} = 1.064 \times T_{zs}$$ *Equation 9-3*

with $R_d = 0.08$, $$T_{\max} = 1.087 \times T_{zs}$$ *Equation 9-4*

It should be emphasized that the R_d value will be influenced by the development of temperatures versus the development of concrete stiffness. The R_d values presented in this Section are representative of temperature losses and rate of heat transfer for flat slabs that dissipate the internal temperatures over a relatively short period.

9.1.3.2 Minimum Concrete Temperature for Design

The minimum concrete temperature can be estimated based on the minimum air temperature that is expected to occur at a given location. However, there is a difference in heat transfer properties of the ambient air and the concrete pavement. The pavement does not cool down as much under cold conditions as the ambient temperature. Under Project 1244-4, a relationship was determined between the measured US weather bureau air temperature and the measured hardened PCC pavement temperatures in the Houston District (Otero-Jimenez, 1992). The regression analysis provided the following relationship:

$$T_c = 20.2 + 0.758 \cdot T_{air}$$ *Equation 9-5*

where, T_c = hardened concrete temperature (°F), and
T_{air} = ambient air temperature (°F).

Historical climatic data from Texas were obtained to determine the minimum air temperatures for different locations. The mean 30-year hourly average temperature and its standard deviation were used to determine the fifth percentile of the minimum air temperatures. The fifth percentile minimum air temperature coincides to the minimum hourly air temperature that had a 5% probability of occurrence over the past 30-years. Next, the minimum of all the hourly fifth percentiles were determined, and these values are presented in Table 9-2 for different cities in Texas.

Equation 9-5 was used to estimate the corresponding concrete temperature. This concrete temperature is listed in Table 9-2. The fifth percentile minimum **concrete** temperatures are the values recommended for use to determine the long-term temperature change for the reinforcement design of CRC pavements.

Table 9-2: Summary of the fifth percentile minimum air and concrete temperatures for different cities in Texas

Location	Fifth Percentile Minimum Air Temperature (°F)	Fifth Percentile Concrete Temperature (°F) [a]
Dallas / Fort Worth	13	30
Brownsville	28	42
San Antonio	18	34
Corpus Christi	24	39
Houston	17	33
Austin	18	34
Waco	14	31
Abilene	10	28
Wichita Falls	7	26
Midland	11	28
San Angelo	12	29
Lubbock	6	25
El Paso	12	29
Amarillo	2	22
Lufkin	12	29

Note: [a] Computed with Equation 9-5.

9.1.4 Maximum Stress Index (MSI)

In this study, it has been shown that the magnitude of thermal stresses in PCC pavements are influenced by the use of different coarse aggregate types in the concrete mixture, the development of early-age concrete temperatures, the minimum temperature the pavement will be subjected to (project location), and the creep adjusted modulus of elasticity of the concrete mixture. A new index is introduced to assist with the evaluation of the magnitude of the thermal stress due to these variables. The new index is termed the Maximum Stress Index (MSI), and is based on the thermal stress design equation presented in Equation 1-1. The Maximum Stress Index is defined as shown in Equation 9-6, and in order to account for early-age relaxation of stresses, the temperature change is determined by the difference between the zero stress temperature and the minimum concrete temperature. This formulation determines the magnitude of the maximum thermal stress in a fully restrained, uncracked specimen. However, since this value is significantly higher than the tensile strength of concrete, the value is termed an index, rather than a stress.

$$\begin{aligned} Maximum\ Stress\ Index\,(MSI) &= \Delta T \cdot CTE \cdot E_c \\ &= \left(T_{zs} - T_{\min}\right) \cdot CTE \cdot E_c \end{aligned}$$

Equation 9-6

where, ΔT = temperature change = $T_{zs} - T_{min}$, (°C),
CTE = concrete coefficient of thermal expansion (strain/°C),
E_c = creep adjusted Modulus of Elasticity (Pa),
T_{zs} = concrete zero-stress temperature (°C), and
T_{min} = minimum concrete temperature on a coldest winter night (°C).

Through the use of the MSI concept, the combined effect of some of the factors used to develop the state-wide reinforcement design can be quantified into a single index. It should be emphasized that this is a simplified approach, introduced to assist with implementation and is not intended for use during the initial design process. The implementation of the MSI concept is best explained by illustrating its usefulness to evaluate current construction and design practices, which is presented in Section 9.2.

9.2 CURRENT CONSTRUCTION AND DESIGN PRACTICES

In the previous Section, it was both discussed and shown in Figure 9-2, that the current CRC pavement reinforcement design practice involves the selection of a long-term temperature change to obtain the reinforcement amount best suited for the pavement thickness under design. **However, no attempt is made during the construction of the pavement to ensure that the design long-term temperature change is not exceeded under field conditions.**

This is analogous to not having weight limits on bridges to guard against overloading which would exceed the initial design loads. Longer lasting concrete pavements will be produced if the assumptions made during design are not exceeded in the field.

In this study, it was shown that numerous variables affect the development of in place concrete temperatures. Any combination of these factors may contribute to produce in place temperature conditions that exceed the design temperature limit. If the design temperature limit is exceeded, the pavement will be subjected to higher thermal stresses, which would reduce the long-term concrete pavement performance.

In Chapter 8, it was shown that the time of paving has a significant impact on the development of in place concrete temperatures. A scenario is illustrated in Figure 9-9 where the development of in place concrete temperatures is influenced by the time of paving. The temperature rise in the section paved early in the morning and late in the afternoon is such that the reinforcement design temperature is not exceeded. However, due to the effect of solar radiation and hydration, the section paved around noon exhibits a rapid rise in early-age temperature and the design conditions are exceeded. This is an example of where changes on a daily basis may affect the temperature development in such a manner that the design conditions are exceeded.

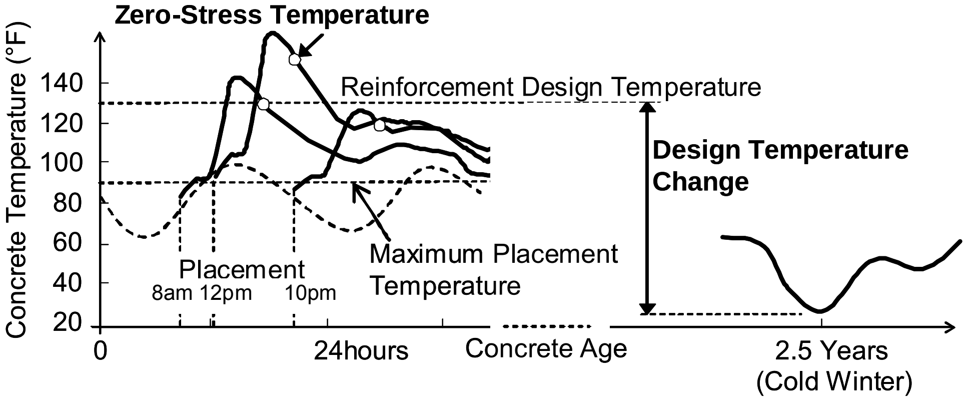

Figure 9-9: Effect of uncontrolled maximum concrete temperature

Figure 9-9 further presents that even though a maximum concrete placement temperature limit is used, the problem of excessive thermal stress will not be addressed. In this scenario, reduced long-term performance will occur due to the development of excessive in place concrete temperatures.

The maximum stress index (MSI) introduced in Section 9.1.4, can be used to incorporate the effect of the variables that have the most significant effect on long term PCC pavement performance. The impact of current design and construction practices on long-term PCC pavement performance is schematically presented in Figure 9-10, and the pavement performance can be expressed by the failures per mile versus load applications curve. During the design process, the reinforcement design is selected to provide acceptable crack spacings, crack widths, and steel stresses. Thus, the failures per mile versus load applications curve reaches an unacceptable level of failures per mile at or after the design loadings indicated by the highlighted curve. Any curve to the left is unacceptable and any curve to the right is acceptable.

Based on these design condition, a MSI value can be determined that reflects the coefficient of thermal expansion of the concrete, the long-term temperature change, and the modulus of elasticity used during the design process. Figure 9-10 indicates that the intended pavement life is achieved when the as constructed MSI is equal to the design MSI. However, there is currently no control over the variables affecting performance such as the type of aggregate used. By using an aggregate type that will produce a concrete with a higher CTE, the pavement will be subjected to higher thermal stresses. This is captured with the MSI, since it will indicate that the maximum thermal stresses are increased, which may lead to reduced pavement life.

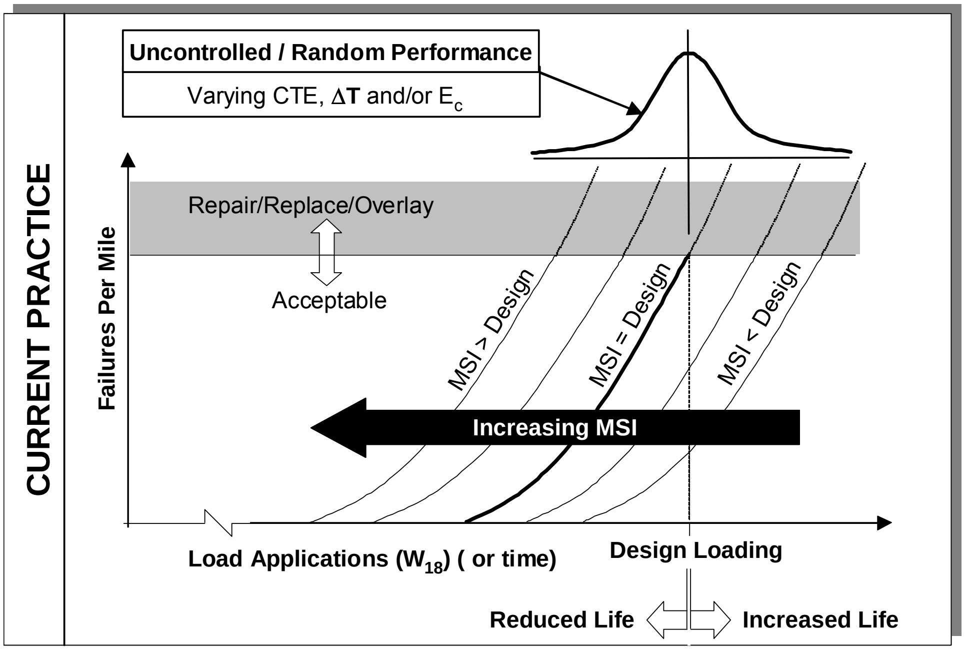

Figure 9-10: The impact of current practices on pavement performance

This concept applies similarly to changes in the ΔT, and E_c. Figure 9-10 illustrates that the long-term pavement performance will be decreased when the MSI is increased. In other words, the long-term performance will be decreased when: an aggregate type with a higher CTE is used, a greater ΔT occurs, and/or a higher E_c is achieved on-site. The function of the MSI can be summarized as follows: **The MSI provides a means to evaluate the site specific trade-offs between in place CTE, ΔT, and E_c, since these three parameters have a significant effect on the long-term pavement performance.**

9.2.1 Current TxDOT Reinforcement Standard

The current TxDOT longitudinal reinforcement requirements are shown in Table 9-3. These requirements are the same irrespective of the PCC pavement location, coarse aggregates used, and actual in place concrete temperatures that develop in the pavement.

Table 9-1: State-wide longitudinal reinforcement details for CRC pavement (TxDOT, 2003)

LONGITUDINAL STEEL (STEEL BAR PLACEMENT)							
Slab Thickness and Bar Size			Regular Steel Bars	First Spacing at Edge or Joint	Second Spacing from Edge or Joint	Additional Steel Bars at Transverse Const. Joint	
T (in.)		Bar Size	Spacing C (in.)	Spacing C (in.)	Spacing B (in.)	Spacing 2 x C (in.)	Length L (in.)
One Layer	8	#6	9	3 to 4	3 to 9	18	42
	9	#6	8	3 to 4	3 to 8	16	42
	10	#6	7	3 to 4	3 to 7	14	42
	11	#6	6.5	3 to 4	3 to 6.5	13	42
	12	#6	6	3 to 4	3 to 6	12	42
	13	#6	5.5	3 to 4	3 to 5.5	11	42
Two Layer	14	#6	9.5	3 to 4	3 to 9.5	9.5	42
	15	#6	8.5	3 to 4	3 to 8.5	8.5	42

9.1.1 Advances in Texas towards Site Specific Reinforcement Standards

In recent years, advances have been made towards site specific reinforcement standards. In Houston, reinforcement standards were developed based on (McCullough and Schindler, 1998):

- historical environmental conditions in Houston, Texas,
- the use of limestone and? siliceous river gravel (SRG) aggregates (during summer months, the use of SRG is only permitted if concrete is placed at night.), and
- the season of placement.

During the design of a 355-mm (14-inch) CRC pavement located on Interstate 35 in the Waco District, site specific reinforcement standards were developed for (Schindler, McCullough, and Krauss, 1999):

- historical environmental conditions in Waco, Texas,
- the temperature condition at placement, and
- the concrete coefficient of thermal expansion.

On the Waco project, the selection of the coefficient of thermal expansion (CTE) for the reinforcement design purpose was based on chemical analysis of the likely coarse aggregate sources from the Waco District. Based on the oxide contents, the CHEM2 computer program (Dossey et al., 1994) was used to predict the coefficient of thermal expansion of the concrete made with these aggregates.

9.3 PROPOSED MITIGATION APPROACH

Longer lasting concrete pavements will be constructed if the assumptions made during design are not exceeded under field conditions. In Section 9.3.1, the principles that would lead to improved long term pavement performance is presented. In Section 9.3.2, a method to integrate the design assumptions to the construction process by means of an end-result temperature control specification is introduced and discussed.

9.3.1 Principles to Improve Pavement Performance under Hot Weather Construction Conditions

In Figure 9-10, it was shown that current practices do not control or limit the CTE, ΔT, or E_c and the actual values achieved on-site are random. These values may be favorable for good performance in some instances; however, in other cases, it may produce conditions that compound each other and a pavement with a 15-year life rather than a 30-year life is obtained. Scenarios might develop where the compound effect of these variables never appears on some projects; however, it could manifest itself on a heavily trafficked Interstate, and the consequences could be costly.

Figure 9-11 presents the desired practice, which forms part of the long-term objectives envisioned for concrete construction practices. PCC pavement construction specifications are recommended that control the **in place properties**, which significantly affect the long-term performance. It is recommended that the values of CTE, ΔT, and E_c be controlled to ensure that the design conditions (MSI) are achieved on-site. This practice will ensure improved long-term performance under most construction conditions. Contrary to the practice shown in Figure 9-10, Figure 9-11 indicates that the likelihood of good performance will be decreased if the in place CTE, ΔT, and E_c combine to produce a MSI greater than the value used during design. The focus of this study is to address temperature effects, and the approach documented in this study will address controlling the in place ΔT. The effect of varying CTE will be incorporated into the reinforcement used in the pavement.

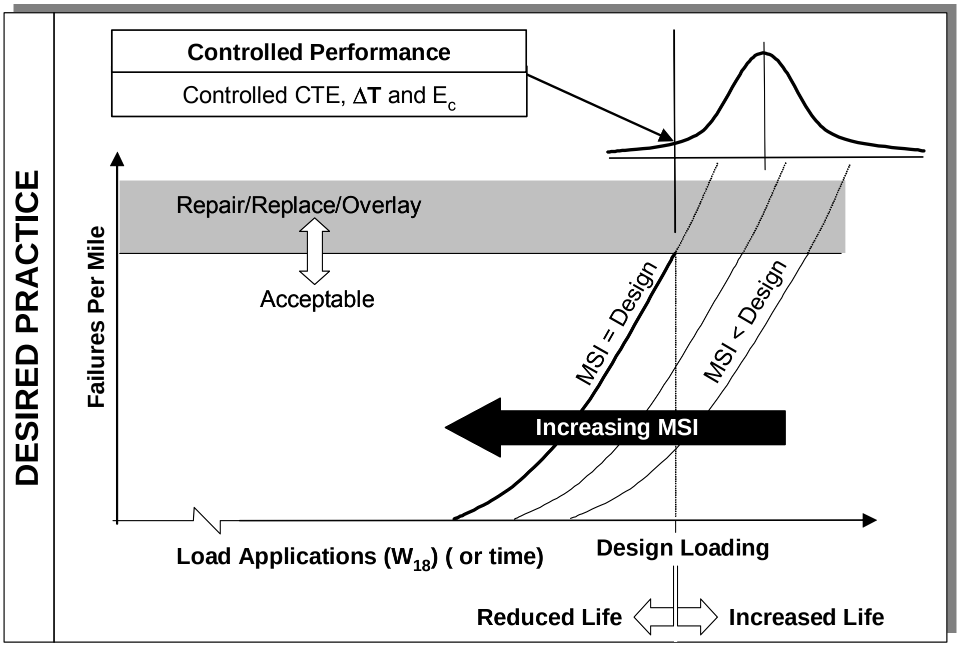

Figure 9-11: Effect of controlled Maximum Stress Index (MSI) on pavement performance

9.3.2 Implementation Approach

The development of high zero-stress temperatures will increase the thermal stresses the pavement is subjected to over its intended life. In order to ensure improved long-term performance, temperature control in pavements is, therefore, related to the control and minimization of excessive zero-stress temperatures, which is not achieved by controlling the maximum concrete placement temperature.

The effect of the proposed approach is illustrated with the example shown in Figure 9-12. In Chapters 5 and 8, it was concluded that the rate and amount of heat released during hydration could significantly be reduced by the type of cement used and by the use of mineral admixtures. Figure 9-12 indicates that when only a Type I cement is used, the initial reinforcement design temperature is exceeded, which may lead to reduced long-term performance. However, by selecting the most appropriate cementitious materials the in place temperature can be controlled to be within the temperature assumed during design. With this approach, any of the parameters found in Section 8.2.2 to have a significant impact on the development of in-place temperatures could be targeted and controlled. For example these parameters could include: time of day of placement, placement temperature, low heat cements, coarser ground cement, mineral admixtures, chemical admixtures, reduced cement contents, and/or placement environment (season).

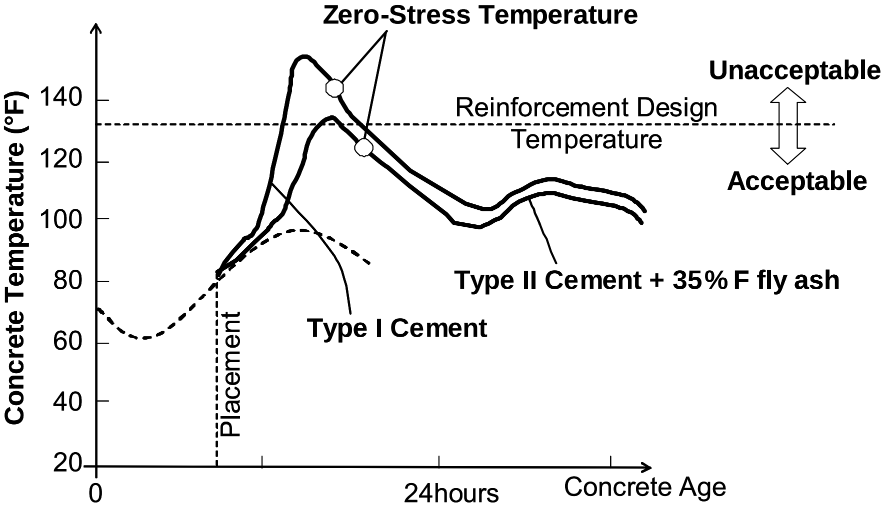

Figure 9-12: Impact of controlled maximum concrete temperature

This approach will allow contractor innovation during the selection of the mixture constituents and their proportions. The contractor will now be able to consider and optimize the cost of cooling the mixture versus the use of mineral and/or chemical admixtures during hot weather placement conditions. The contractor is in the position to schedule the paving activity at different times of the day, or even different times of the year, since this has been shown to significantly impact the maximum in place concrete temperature development.

The zero-stress temperature, however, cannot currently be measured in a cost-effective and efficient manner. Due to the advances in modern technology, inexpensive devices (Thermachron® i-Buttons) are currently available to monitor the temperature of in place concrete. In Section 9.1.3.1, a simplified method was developed to obtain the zero-stress temperature (**T_{zs}**) from the maximum in place temperature. The existence of such a correlation integrates the design conditions (zero-stress temperature) with the construction specification, since temperature control can be specified to limit the maximum in place concrete temperature.

The overall implementation approach is schematically outlined in Figure 9-13. The approach will involve the development of an end-result type specification, which limits the maximum in place concrete temperature of the hydrating concrete. The specified values should be based on the amount of reinforcement provided in the section, project location, and type of coarse aggregate used in the concrete mixture. The optimum reinforcement design temperature should be determined for each location, since this value could change significantly from one location in the state to another. A conceptual approach to determine the optimum reinforcement design temperature is provided in Section 9.5. The recommended approach will link the design conditions to the actual construction conditions experienced on site. The use of inexpensive temperature probes is recommended for quality assurance purposes to monitor the development of in place concrete temperatures.

The temperature prediction model developed in this study will be further developed into a tool that can be used by contractors and designers to evaluate the effect of the many variables that influence the in place concrete temperature. This program is recommended to assist with the implementation of the proposed temperature control provision. The program can be used to evaluate the in place temperature development during pre-construction planning and the actual construction operations.

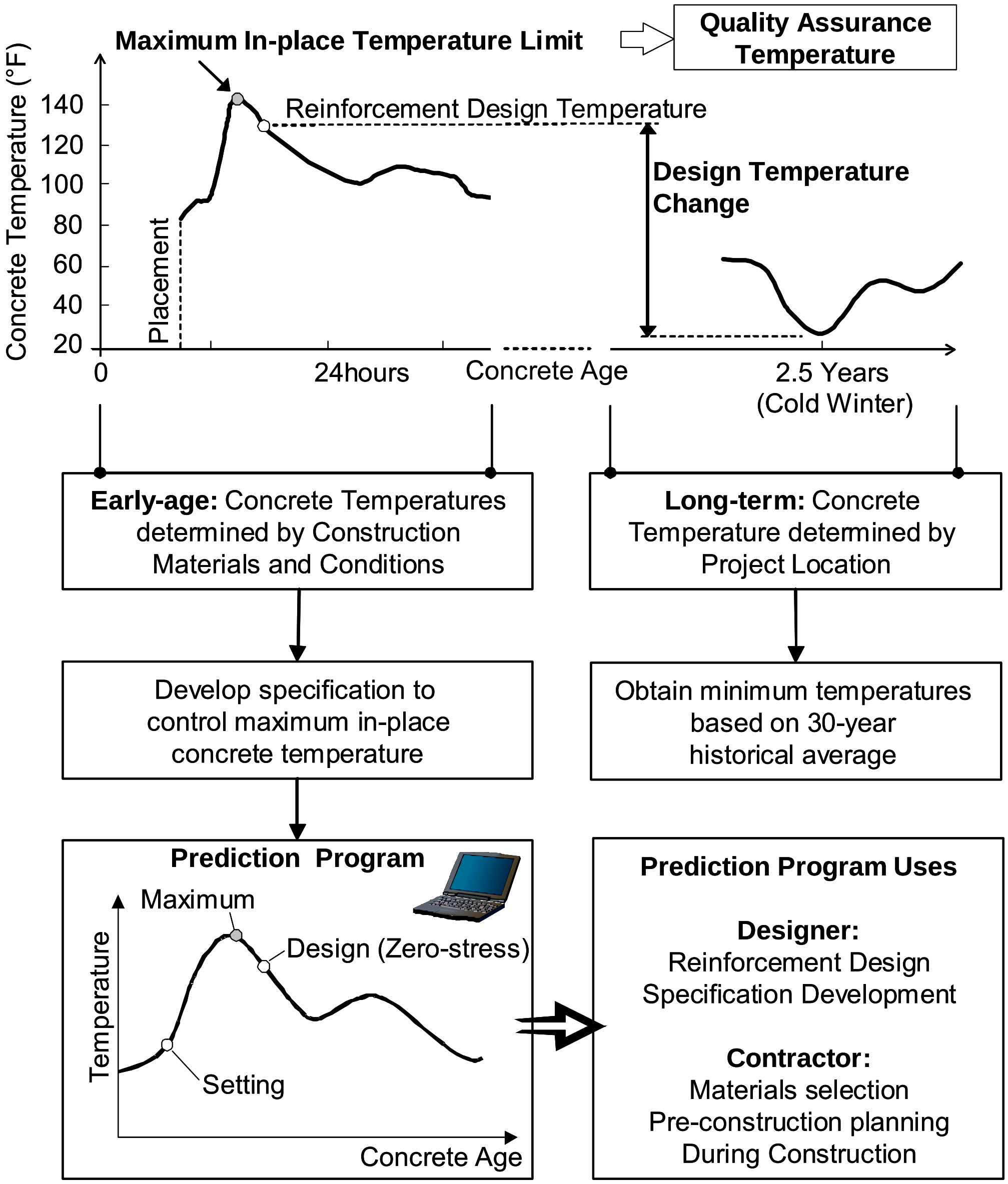

Figure 9-13: Overview of research strategy

9.4 COMPUTER-BASED TEMPERATURE PREDICTION PROGRAM: PAVEPRO

The temperature and setting prediction models were further developed into a computer program. The overall system is termed **PavePro**, an acronym for “The Paving Program”. PavePro was developed as an easy-to-use Excel spreadsheet. The spreadsheet serves as a method to gather user inputs and to display the analysis results. The program layout is presented in Appendix G. The program inputs, grouped into the categories used during the sensitivity analysis, are as follows:

1. **General variables,**
2. **Mixture proportion variables,**
3. **Materials characterization variables**,
4. **Environmental variables, and**
5. **Construction variables.**

PavePro was developed to be a useful tool to evaluate the in place temperature development under different environmental conditions. In Figure 5-41, the concept was presented where the hydration development (degree of hydration) of the concrete mixture could either be estimated by the hydration model or be obtained from semi-adiabatic calorimeter testing. With these results available, PavePro can easily be used during the following stages:

1. **Pre-construction planning:**
   PavePro was developed to contain average historical data of environmental conditions that can be used to evaluate the temperature development at a specific location in the state. The effect of paving in the winter versus spring or fall can be determined. The appropriate combination of concrete mixture proportions, cement types, mineral admixtures, and aggregates can be optimized. The use of alternatives such as nighttime paving and cooling of the mixture can be considered during the pre-construction planning phase. It is envisioned that PavePro will be used during both the bidding of the project and during planning and scheduling of the construction activities.
2. **During construction:**
   During actual construction, PavePro can be used to determine the appropriate actions to ensure that the in place concrete temperature does not exceed the specification limit. The forecasted 5-day or 3-day climatic conditions can be obtained and entered into PavePro to evaluate the temperature development. The output of PavePro was developed to indicate “Pave” and “No-Pave” times of the day, based on whether or not the maximum in place temperature is exceeded or not. If “No-Pave” times occur during times the contractor has scheduled placement, mitigation techniques can be investigated to ensure that the maximum in place concrete temperature is not exceeded.
3. **During pavement design:**

During the pavement design phase, the magnitude of the thermal stresses the pavement is subjected to needs to be estimated. Currently little guidelines are available to assist with this process. PavePro can be used to determine the appropriate thermal stresses to use for design, based on the anticipated cementitious materials, and site specific environmental conditions.

The temperature prediction model developed during this study will enable the development of performance-based specifications to guard against premature concrete failures. This model will provide the designer, contractor, and specification developer with the means to evaluate and quantify the effect of all the various complex interactions that affect the concrete temperature development during early-ages.

9.5 CONCEPT TO DEVELOP SITE SPECIFIC REINFORCEMENT STANDARDS

The specific design of the site specific reinforcement is not covered in this report; however, a conceptual approach will be provided. It is recommended to develop reinforcement standards, which are optimized for the environmental conditions at the **specific location** under investigation. These standards should provide more economic reinforcement contents, since the minimum temperature across the state varies significantly from the gulf coast to high plains regions. The development of these site specific reinforcement standards should be based on the expected maximum in place temperature as determined by PavePro, the coefficient of thermal expansion of the concrete, and the minimum concrete temperature expected in the location.

Using the PavePro program and the latest CRC pavement design program developed at the Center for Transportation Research, the optimum design temperature change may be determined. Based on either different cities or regions within Texas, environmental conditions can be generated that is representative of the design condition for that location. For example, the minimum concrete temperature for design can be obtained from Table 9-2. Now the effect of different concrete zero-stress temperatures may be evaluated with the CRC pavement design program, to determine the critical design temperature for that specific location.

The proposed concept is schematically illustrated in Figure 9-14, where the optimum concrete zero-stress may be determined from the graph of the predicted pavement performance versus different concrete zero-stress temperatures. In order to determine the critical concrete zero-stress temperature, two cases are shown that might be encountered. In Case A, the critical zero-stress temperature corresponds to the temperature at which there is a sudden decrease in performance. In this case, the critical concrete zero-stress temperature may be identified from the inflection point of the graph. In Case B, there is no specific concrete zero-stress temperature where a marked increase in pavement failures occurs. In this case, the critical concrete zero-stress temperature may be obtained from the point at which the limit of distresses is reached. In Figure 9-14 a distress limit of 10 failures per mile is shown, from which the critical concrete zero-stress temperature is obtained.

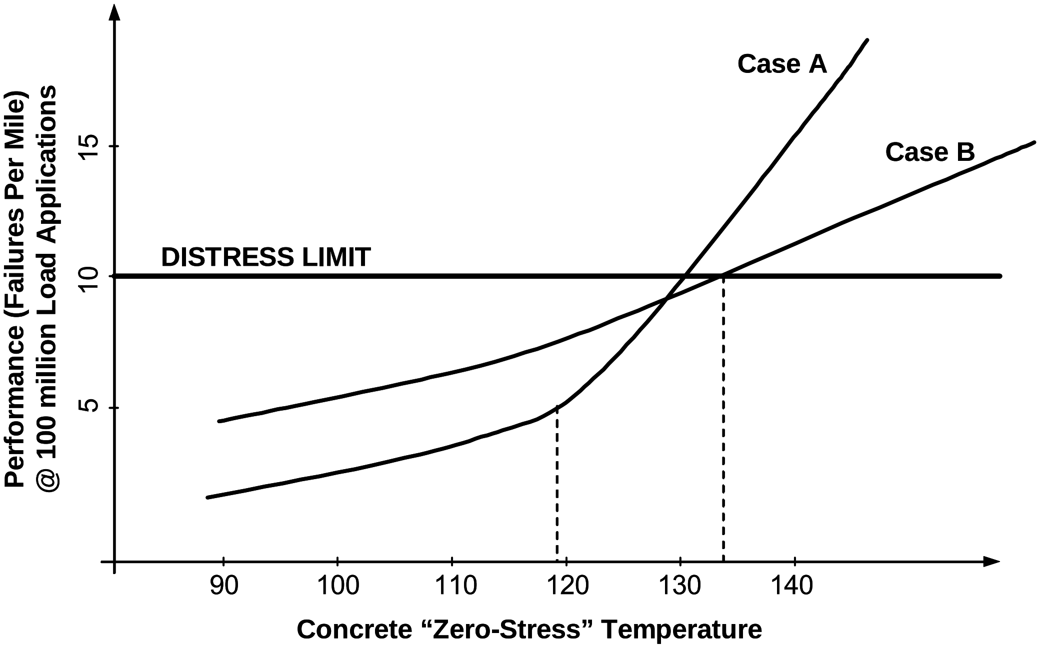

Figure 9-14: Conceptual method to determine the critical concrete "zero-stress" temperature for use during the site specific reinforcement design

9.6 SUMMARY, CONCLUSIONS AND RECOMMENDATIONS

This Chapter documented the development of a procedure to produce long-life pavements even when constructed under hot weather conditions. A temperature control specification is proposed, which encourages contractor innovation along with the use of improved materials. The proposed specification requires that attention be paid to scheduling concrete placement times relative to the time of day as well as the season of construction. The implementation approach involves the use of an end-result type specification, which limits the maximum in place concrete temperature of the hydrating concrete. This method ensures that the maximum in place concrete does not exceed the maximum concrete temperature used during the reinforcement design. This proposed specification integrates construction operations and design procedures, and should produce concrete pavements with the necessary in place characteristics to produce a pavement with the performance intended during the initial design. The following sections contain conclusions and recommendations based on the work documented in this Chapter.

9.6.1 Conclusions

This approach will account for the impact of modern paving materials and other mitigation methods that lower the in place concrete temperature and will ensure improved PCC pavement performance under all placement conditions. The mitigation methods could include: time of day of placement, placement temperature, low heat cements, coarser ground cement, mineral admixtures, chemical admixtures, reduced cement contents, and placement environment (season). To provide improved performance for a pavement constructed under hot weather conditions, it is further proposed that the CRC pavement reinforcement standards be re-designed to provide steel quantities for specific use during hot weather conditions, and that an end-result specification that limits the maximum in place concrete temperature during hydration be implemented.

Inexpensive devices are currently available to monitor the temperature of the in place concrete. It is recommended that the use of such devices, installed at specified intervals, be considered for quality assurance purposes in the concrete temperature control specification.

A simplified method is developed in this Chapter to obtain the design temperature for thermal stresses. This method is based on early-age relaxation concepts, and provides an estimate of the zero-stress condition after the initial compression stage. Finally, interim special provisions to Item 360 are proposed that contain the proposed concept.

9.6.2 Recommendations for Future Work

It is recommended to develop reinforcement standards, which are optimized for the environmental conditions at the **specific location** under investigation. These standards should provide more economic reinforcement contents, since the minimum temperature across the state varies significantly from the gulf coast to high plains regions. The development of these site specific reinforcement standards should be based on the expected maximum in place temperature as determined by PavePro, the coefficient of thermal expansion of the concrete, and the minimum concrete temperature expected in the location. With the PavePro program and the latest CRC pavement design program developed at the Center for Transportation Research, the optimum design temperature change can be determined.

In Section 9.1.3.2, it was recommended to use Equation 9-5 to determine the minimum concrete temperature once the minimum air temperature has been selected for design purposes. It is recommended that this formulation be re-evaluated during the validation of the temperature prediction program. This is considered necessary, as this formulation significantly influences the magnitude of the thermal stress used during design of the longitudinal reinforcement. The effect of aggregate type on the formulation in Equation 9-5 should specifically be evaluated.

Early-age thermal cracking will affect the long-term performance of concrete pavements. Early-age cracking can be controlled by procedures that asses the risk of cracking by comparing the early-age strength gain and stress development (McCullough and Rasmussen, 1998; Bernander, 1998). The scope of the current study was limited to the control of long-term thermal stresses, which can be achieved by ensuring that the design temperature change is not exceeded. It is recommended that the use of the HIPERPAV program (McCullough and Rasmussen, 1998) be considered to minimize the occurrence of early-age distresses.

Chapter 10

Summary, Conclusions, and Recommendations

This chapter provides a summary of the work undertaken over the course this study. Conclusions regarding the significant findings are offered, and recommendations are provided. Finally, items that were identified for future research and development are provided.

10.1 SUMMARY

High concrete temperatures increase the rate of hydration, thermal stresses, the tendency for drying shrinkage cracking, permeability, and decrease long-term concrete strength, and durability because of cracking. Findings from past research efforts have demonstrated that the concrete temperature development during the first 24 to 72 hours has a major impact on long-term pavement performance (Hankins et al., 1991; Dossey et al., 1994; and McCullough et al., 1998). Excessive portland cement concrete (PCC) temperature development may result in reduced pavement performance. All these factors emphasize that concrete temperature control during construction in hot weather conditions is essential to assure the improvement of the durability of PCC pavements.

The long-term temperature change the pavement is subjected to and the aggregate type used during construction, largely determines the long-term stabilized crack distribution in continuously reinforced concrete (CRC) pavements. Current CRC pavement reinforcement design practice involves the selection of a long-term temperature change to obtain the reinforcement amount best suited for the pavement under design. However, no attempt is made during construction to ensure that the design long-term temperature change is not exceeded under field conditions. This is analogous to not having weight limits on bridges to guard against overloading. Longer lasting concrete pavements will be produced if the assumptions made during design are not exceeded in the field.

Most states specify a maximum concrete temperature at placement, and the limit remains the same irrespective of the type of mineral or chemical admixtures used. In modern paving operations, the use of mineral admixtures has become common practice, and under certain conditions, these admixtures could mitigate some of the problems associated with hot weather placement. Furthermore, the use of a maximum concrete placement temperature does not address long-term performance issues, since the maximum in place concrete temperature remains uncontrolled. Through the appropriate selection of construction materials and construction practices, the detrimental effects of hot weather concreting can be countered. However, in order to control the in place temperature, the variables that influence it most need to be identified and their effect quantified.

The key element of this study involved the development of a temperature prediction program to characterize and quantify the early-age temperature development in hardening concrete. As part of this effort, general hydration models were developed to characterize the heat of hydration of concrete for different cementitious materials and mixture proportions. The model was developed from 34 different mixtures, made from 23 different cements. The model considers the effect of cement chemical composition, cement fineness, mineral admixtures (fly ash, and GGBF slag), mixture proportions, and concrete properties.

Next, the concrete temperature prediction model was calibrated for field conditions with data collected from seven different concrete paving projects located across the state of Texas. Data were collected from three different locations in Texas: Dallas, Houston, and El Paso. The highest concrete temperature of 144°F was measured in a section placed under summer conditions in Dallas. While on site, the adverse effects of placing concrete in hot weather conditions were clearly noticeable. Portions of the pavement placed on this project showed significant plastic shrinkage cracking (see Figure 4-18), thus emphasizing the need for concrete temperature control and improved materials selection under hot weather construction conditions.

The temperature program was successfully calibrated with the data collected from the field sites. Based on the average r^2 values, it may be concluded that in 27% of the cases, the r^2 value was equal to or less than 0.78. This indicates that 78% of the measured in place concrete temperatures can be explainable by the temperature prediction model. The error obtained between the measured and predicted maximum in place concrete temperature ranged between -4.6% and 3.4%. In 82% of the sections, the error in predicted maximum temperature was equal to or less than 3.25°F. A sensitivity analysis was also conducted to determine which model parameters significantly affected the predicted results.

ASTM C 403 (1998) setting data were collected under field and laboratory conditions, for concrete mixtures containing different cements, fly ash types, and GGBF slag. A model was developed that makes use of the hydration parameters and the water-cementitious materials ratio to estimate the time to initial and final set. Based on the initial set model, a formulation was developed to allow the user to quantify the effect of chemical admixtures on the hydration development.

Use of the temperature prediction model developed in this study, will enable the development of performance based specifications to guard against premature concrete failures. This model will further provide the designer, contractor, and specification developer with the means to evaluate and quantify the effect of most of the various complex interactions that affect the concrete temperature development during early-ages.

This study proposes an innovative temperature control specification, which encourages contractor innovation and the use of improved materials. This approach will account for the impact of modern paving materials and will ensure improved concrete performance under all placement conditions.

10.2 CONCLUSIONS

The primary objective of this study was fulfilled through the development of the temperature prediction program and an innovative temperature control specification. This program provides the means to quantify the effect of time of day of placement, placement temperature, cement content, cement chemical composition, cement fineness, mineral admixtures, chemical admixtures, pavement thickness, different curing methods, and placement environment (season) on the development of early-age concrete temperatures. The proposed temperature control specification encourages contractor innovation and focuses on material selection for the particular location and environmental conditions. This approach links pavement design with the in place pavement properties and will ensure improved concrete performance under hot weather placement conditions.

The study addressed many aspects of concrete hydration, laboratory testing, field work and the development of mitigation measures. Based on the work documented in this report, conclusions are made regarding the following areas:

1. Hydration of cement based materials,
2. Temperature prediction of in place concrete, and
3. Concrete setting.

10.2.1 Hydration of cement based materials

The hydration of different cementitious systems can be characterized by the mechanistic-empirical models developed during this study. It is shown that the explanatory variables are statistically significant. The model provides a reasonable and accurate representation of the in place temperature development of concrete pavements.

The hydration model uses the activation energy with the equivalent age maturity method to define the temperature sensitivity of the hydration process. The degree of hydration characterizes the formation of hydration products as hydration progresses over time, and each concrete mixture has a unique degree of hydration development. Based on the temperature sensitivity (activation energy), the degree of hydration at the reference temperature, and the total heat of hydration, the heat of hydration of a concrete mixture can accurately be characterized. Conclusions regarding the temperature sensitivity and degree of hydration model will be discussed separately.

10.2.1.1 *Temperature Sensitivity (Activation Energy)*

This document presents evidence from various sources that different activation energy values should be used when mechanical properties and the development of hydration (chemical effects) are considered. The cross-over effect develops only when mechanical properties are considered and not when the degree of hydration development is considered. The activation energy determined with the ASTM C 1074 should not be used to define the temperature sensitivity of the cement hydration process.

In all the cases investigated, the data indicated that the heat of hydration data obeys the Arrhenius principle, since the activation energy was determined to be independent of the hydration temperature.

The slope of the Arrhenius plot is influenced by the chemical composition of the cement and the use of mineral admixtures. The activation energy for different cements ranged from 36,132 J/mol to 54,467 J/mol. A multivariate nonlinear statistical analysis indicated that the change in activation energy may be modeled in terms of the Blaine value, the C_3A content, and the C_4AF content of the cement. The hydration at different temperatures can accurately be predicted through the equivalent age maturity method and the use of an experimentally determined constant activation energy.

10.2.1.2 *Concrete Hydration Development*

A mechanistic-empirical model is proposed to characterize the heat of hydration of concrete at an isothermal curing temperature of 21.1°C. The model considers the effect of:

- Cement chemical composition: C_3A, C_3S, C_2S, C_4AF, SO_3, MgO, and Free Lime
- Cement fineness: specific surface area (Blaine Index)
- Mineral admixtures: Class F fly ash, Class C fly ash, and GGBF slag
- Mixture proportions: cement content, water-cementitious ratio, mineral admixture replacement level, coarse aggregate content, and fine aggregate content
- Concrete properties: density, thermal conductivity, specific heat

Based on the data reviewed and analyzed in this study the following conclusions can be made:

- Semi-adiabatic testing provides a convenient indirect means to characterize the formation of hydration products by measuring the heat released during hydration.
- The development of the degree of hydration is influenced by the cement chemical composition, the cement fineness, the use of mineral admixtures, and the mixture proportions used in the concrete mixture. The effect of each parameter is summarized in Table 10-1.
- Results from semi-adiabatic tests revealed that complete hydration does not occur in any of the concretes tested. This is attributed to the low water-cement ratios used in the concretes tested. This directly affected the total amount of heat released during hydration.

- The ultimate degree of hydration is unaffected by the curing temperature. The ultimate degree of hydration appears to be increased when fly ash or GGBF slag is used.

Table 10-1: The effect of different parameters on the general hydration model

Parameter	**Value**	**See Figure**	**Effect on Degree of Hydration**		
			Start of Acceleration Phase	Rate (Slope)	Ultimate Value
C_3A	↑	5-60	-	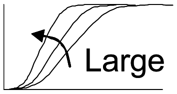	-
C_3S	↑	5-59	-	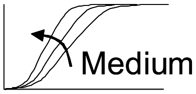	-
SO_3	↑	5-61	-	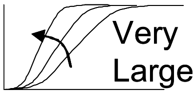	-
Cement Fineness: (Blaine Value)	↑	5-57 and 5-58	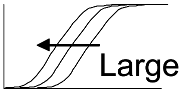	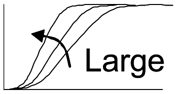	-
Class F fly ash dosage	↑	5-63	-	-	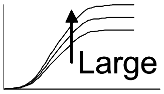
Class C fly ash dosage	↑	5-64	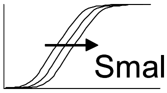	-	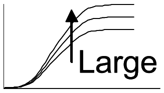
GGBF slag dosage	↑	5-65	-	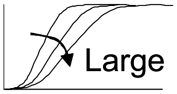	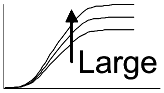
w/cm ratio	↑	5-62	-	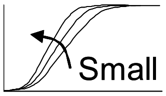	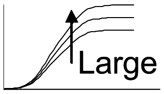
Alkalies [a]	↑	5-66	-	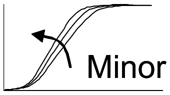	-

Note: [a] Alkalies are indirectly considered through the SO_3 content

10.2.2 Temperature Prediction Program (PavePro)

One of the key objectives of this study was to quantify the effect of different materials and construction practices on the development of concrete temperatures. A temperature prediction program was developed. The program was successfully calibrated for the variables that may have a significant impact on the in place concrete temperature. It may be concluded that the proposed temperature prediction model could be used as a tool (design aid) to evaluate the following parameters:

- different cement contents,
- cement composition,
- water-cement ratio,
- cement fineness,
- the use of Class F and C fly ash,
- the use of GGBF slag,
- initial concrete temperature at placement,
- environmental conditions,
- curing methods,
- subbase temperature,
- pavement thickness, and
- time of placement.

The temperature prediction model will enable the designer and contractor to evaluate, in a short time frame, the effect of the different options on the predicted in place concrete temperature development. The temperature prediction model enables the development of performance based specifications to guard against premature concrete failures. The model can be used to determine the most effective combination of materials and construction operations to ensure that the reinforcement design temperature is not exceeded under field conditions.

10.2.3 Concrete Setting

ASTM C 403 (1998) setting data were collected under field and laboratory conditions for concrete mixtures containing different cements, fly ash types, and GGBF slag. It was found that setting of concrete in general occurs when a specific amount of hydration products have formed, and that the effect of temperature on setting can be accounted for with the equivalent age maturity method. The amount of hydration product that has to form for setting is influenced by the water-cement ratio. The recommended model uses the degree of hydration data obtained from the calorimeter tests to estimate the initial and final setting times.

With knowledge of the time to initial set, contractors will be able to plan measures to finish and texture the concrete pavement in time to prevent setting occurring before these activities. This may assist contractors in hot weather conditions to prevent concrete problems in the fresh state from occurring.

10.3 RECOMMENDATIONS

The recommendation and models from this study will be directly applicable to help the concrete industry to construct longer lasting concrete pavements under hot weather conditions. Based on the work undertaken during the course of this study, the following recommendations can be made:

10.3.1 PavePro Validation

The temperature prediction program was developed based on inherent assumptions and experimental work that cannot cover all the conditions encountered under field conditions. It is recommended to pursue the validation of PavePro during actual construction projects. During this effort, the following goals may be accomplished:

- Establish the accuracy of the temperature prediction model for general use in portland cement concrete paving applications,
- Determine the variability associated with the development of concrete temperatures between different concrete batches and over the course of the construction day,
- Expose Contractors and TxDOT personnel to the program, and
- Provide increased awareness to contractors and TxDOT personnel regarding the importance of concrete temperature control in PCC pavements.

An essential component of the successful implementation of the temperature prediction program is the understanding and careful definition of the program inputs. In order to improve acceptance and aid implementation, it is recommended to develop user-friendly guidelines that document the use of the temperature prediction model. Training of TxDOT and contractors is recommended. This will ensure appropriate use of the program and that the output of the program is correctly interpreted.

10.3.1.1 *Capabilities of the Temperature and Setting Prediction Models*

The use of the temperature prediction should be explored for uses in other applications. These could include:

- strength prediction with the maturity method,
- temperature control in mass concrete structures,
- temperature control in bridge deck applications, and

- optimal time for surface texturing based on initial setting predictions.

10.3.2 Temperature Control Specification

The use of an end-result type specification that limits the maximum in place concrete temperature is recommended for implementation. The overall concept is summarized in Figure 10-1. This approach ensures that the maximum in place concrete does not exceed the maximum concrete temperature used during the reinforcement design process. The recommended approach integrates construction operations and design procedures and will produce concrete pavements with the necessary in place characteristics to reach the performance intended during design. The proposed temperature control specification will only be effective during the warmest time of the year, which is defined as the period of April 1st until October 31st.

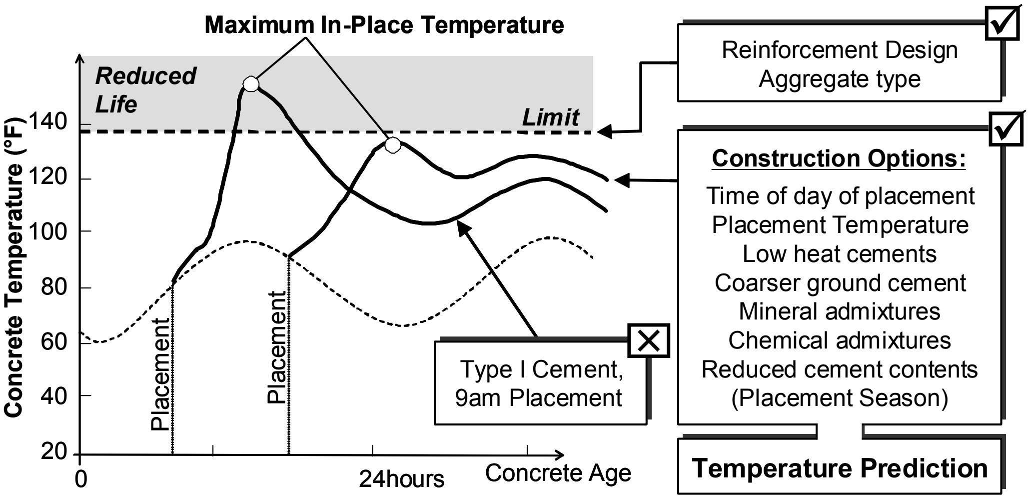

Figure 10-1: Summary of the temperature control approach recommended for implementation

The use of inexpensive temperature probes (Thermachron® i-Buttons) is recommended for quality assurance purposes to monitor the development of in place concrete temperatures. The use of these probes enables other uses, such as for strength prediction with the maturity method or, in the long-term, even to indicate freezing of the concrete surface.

The recommended maximum in place temperatures were selected based on the project location, the type of coarse aggregate used in the concrete mixture, and the amount of reinforcement provided in the section. It is recommended to divide the state of Texas into four paving zones. These paving zones account for the differences in winters experienced across the state. The lower the thermal coefficient of expansion of the concrete used on the project, the higher the specified maximum in place concrete temperature becomes.

The temperature prediction program developed from this study is recommended for use to assist with the implementation of the proposed temperature control provision. The program can be used to evaluate the in place temperature development during pre-construction planning and actual construction operation.

This approach will allow contractor innovation during the selection of the mixture constituents and their proportions. The contractor will now be able to consider and optimize the cost of cooling the mixture versus the use of mineral chemical admixtures or the importing of different coarse aggregates during hot weather placement conditions. The contractor is in the position to schedule the paving activity at different times of the day, which has been shown to have a significant impact on the concrete temperature development. The use of different cementitious materials can be evaluated for use in different seasons.

10.3.3 Concrete Hydration Prediction

A general hydration model for cementitious materials was developed, calibrated, and validated during this study. The recommended model is summarized in Section 5.4.2.3. This model is recommended for use in the temperature prediction program in order to characterize the effect of different cements and mineral admixture on the hydration. The following specific recommendation can be made concerning the characterization of hydration:

- In projects where higher confidence levels for temperature prediction are required, it is recommended to subject the proposed concrete mixture to adiabatic calorimeter tests. With these test data, the prediction of the degree of hydration is no longer required, and the accuracy of the model irrelevant.
    - The use of adiabatic testing is recommended for use at the Materials and Test Division of TxDOT. These test results will provide a means to characterize the heat development in the concrete. This test method provides useful information that may be used to address temperature development issues in other applications, such as bridge decks and mass concrete elements.
- As additional test data are collected, these should be centrally assembled in a database. It is recommended to re-evaluate and modify the proposed models in this document, based on this expanded database.
- A means to allow the user to modify the hydration model for the effect of chemical admixtures was developed. However, this method is temporarily recommend for use until additional test

data become available to modify the hydration models with mechanistic models to account for the effect of chemical admixtures.

10.4 IMPROVING AND REFINING PCC DESIGN MODELS

The temperature prediction program predicts the development of early-age concrete temperatures, gradients, and the occurrence of the zero-stress. All these parameters affect the early-age and long-term performance of CRC pavements, and are required inputs to the latest CRCP design program, CRCP-10. It is recommended to integrate the temperature prediction program with the current CRCP design program. This will enable the use of more representative concrete temperatures during the design and analysis of CRC pavements.

The magnitude of the built-in temperature gradient has been shown to have a major effect on the long-term performance of *jointed concrete pavements* (Yu et al., 1998). The amount of built-in curl can be determined from the thermal gradients at final set, which is estimated by the program developed in this study. This variable will be an input parameter to the AASHTO 2002 mechanistic design procedure, and should be calibrated for local conditions. It is recommended to use the temperature prediction program to determine the built-in curl most appropriate for Texas paving materials and conditions. The variables that affect the built-in curl can be identified and measures can be evaluated to control the amount of built-in curl, or the design can be based on the gradient that may develop under different paving conditions.

10.5 RECOMMENDATIONS FOR FUTURE WORK

Based on the material covered in this document, the following aspects that require more development and research were identified:

10.5.1 Variability of the early-age in place concrete temperatures

The variability associated with the development of early-age concrete temperature is unknown and needs to be established to aid with the development of construction specifications. It is recommended to collect detailed early-age concrete temperature histories for different paving conditions throughout the year. The variability associated with the development of concrete temperature during the paving day should be determined. This data can further be used to validate and improve the temperature prediction program developed during this study.

10.5.1.1 *Pay-Factor for In Place Maximum Concrete Temperature*

After the variability associated with the development of in place temperatures has been established, a pay-factor for the maximum in place temperature should be pursued. This process will provide an incentive to the contractor to place emphasis on the selection of appropriate materials and the scheduling of concrete paving under hot weather conditions. The pay-factor should be developed to capture the effect of maximum concrete temperature on long-term concrete pavement performance.

10.5.2 Further Investigation of Concrete Hydration

Further development work is required to evaluate the ultimate degree of hydration of concrete consisting of different mineral admixtures. These tests should be performed for different water-cementitious materials ratios, mineral admixtures, and curing temperatures. The validity of the heat of hydration contribution of fly ash in terms of its CaO content should be evaluated based on long-term heat of hydration tests. Cement fineness has a major impact on the degree of hydration development. Some literature reports greater accuracy when fineness is characterized by means of the cement particle size distribution. This approach should be evaluated to determine if it provides increased prediction accuracy. In this study, the Blaine value was used to characterize the cement fineness, since it can readily be obtained from the cement certificate. This also allows easier implementation of the program, as the Blaine values are immediately available for use.

10.5.2.1 *Temperature Sensitivity*

Based on the material covered in this document, the following aspects that required more development and research were identified:

- The temperature sensitivity of a cementitious system can best be evaluated by means of isothermal calorimeter testing, conducted at different temperatures. Isothermal conduction calorimeter tests at different temperatures are recommended to determine the activation energy for hydration purposes. Limited tests of this nature have been performed on cementitious materials used in Texas. It is recommended to test various cements and cementitious systems to develop improved activation energy models for hydration and temperature prediction.
- The effect of mineral admixtures on the activation energy should be established. The model developed in this study is based on limited information available on the effect of mineral admixtures on the activation energy.
- The effect that the use of chemical admixtures has on the activation energy for hydration prediction is currently uncertain. Currently, little information is available to address this subject. Isothermal calorimeter testing on mixtures with different chemical admixtures will provide valuable insight as to their effect on the temperature sensitivity of the hydration process.

10.5.2.2 *Expansion of the Hydration Data Set*

An essential part of the model calibration phase is to obtain sufficient test data that can be used to calibrate the model. The more detailed and comprehensive this data set, the higher the confidence in the calibrated mechanistic-empirical model becomes. It is recommended to expand the hydration database used during the calibration of the general hydration model developed in this study. Specifically, the effect of GGBF slag should be evaluated with a more comprehensive experimental program. Furthermore, the effect of chemical admixtures commonly used in concrete paving projects should be investigated. The semi-adiabatic calorimeter test provides very useful information; however, a standardized test procedure does not exist for this test. The development of a standardized test procedure and method to analyze the test results are recommended.

10.5.3 Characterization of Concrete Setting

A more detail experimental program designed specifically to evaluate the influence of water-cementitious ratio, GGBF slag, and chemical admixtures (retarders and accelerators) on setting is recommended. The testing should include calorimetry testing to characterize the degree of hydration development over time.

10.5.4 Development of Early-Age Thermal Stresses

The development of early-age stresses have a significant impact on the early-age and long-term behavior of concrete pavements. The magnitude of early-age stresses determines the magnitude of the zero-stress temperature, which determine the magnitude of the early-age and long-term thermal gradient. Little data are currently available to characterize the development of early-age stresses, and further research and testing on this subject is recommended. The use of restrained thermal cracking tests should be evaluated for this purpose.

REFERENCES

AASTHO, "AASHTO Guide for Design of Pavement Structures", American Association of State Highway and Transportation Officials, Washington D.C., 1993.

AASTHO TP60, "Standard test method for the Coefficient of Thermal Expansion of Hydraulic Cement Concrete", American Association of State Highway and Transportation Officials, Washington D.C., 2000.

ACI 207.2R, “Effect of restraint, volume change, and reinforcement on cracking in massive concrete,” American Concrete Institute, Farmington Hills, Michigan, 1995.

ACI 209, “Prediction of Creep, Shrinkage, and Temperature Effects in Concrete Structures,” American Concrete Institute, Farmington Hills, Michigan, 1992.

ACI 232.2R, “Use of Fly Ash in Concrete,” American Concrete Institute, Farmington Hills, Michigan, 1996.

ACI 233R, “Ground Granulated Blast-Furnace Slag as a Cementitious Constituent in Concrete,” American Concrete Institute, Farmington Hills, Michigan, 1995.

ACI 305R, “Hot Weather Concreting – Reported by ACI Committee 305,” American Concrete Institute, Farmington Hills, Michigan, 2000.

ACPA, “Database of State DOT Concrete Pavement Practices,” www.pavement.com/practices/sap.asp, Skokie, Illinois American Concrete Pavement Association, Accessed April 5, 2000, 1998.

Al-Fadhala, M., and Hover, K.C., “Rapid Evaporation from Freshly Cast Concrete and the Gulf Environment,” Construction and Building Materials, Vol. 15, pp. 1-7, 2001.

Almusallam, A.A., Maslehuddin, M., Abdul-Waris, M., and Khan, M.M.,”Effect of Mix Proportions on Plastic Shrinkage Cracking of Concrete in Hot Environments,” Construction and Building Materials, Vol. 12, pp. 353-58, 1998.

ASHRAE, “1993-ASHRAE Handbook,” American Society of Heating, Refrigerating and Air-Conditioning Engineers, Incorporated, Atlanta, 1993.

ASTM C 1074, “Standard practice for estimating concrete strength by the maturity method,” American Society for Testing and Materials, Pennsylvania, 1998.

ASTM C 150, “Standard Specification for Portland Cement,” American Society for Testing and Materials, Pennsylvania, 1998.

ASTM C 209, “Prediction of Creep, Shrinkage, and Temperature Effects in Concrete Structures,” American Society for Testing and Materials, Pennsylvania, 1997.

ASTM C 309, “Standard Specification for Liquid Membrane-Forming Compounds for Curing Concrete,” American Society for Testing and Materials, Pennsylvania, 1998.

ASTM C 403, “Standard Test Method for Time of Setting of Concrete Mixtures by Penetration Resistance,” ASTM C 403-95, Annual Book of ASTM Standards, American Society for Testing and Materials, Pennsylvania, 1998.

ASTM C 494, “Specification for Chemical Admixtures for Concrete,” Annual Book of ASTM Standards, American Standards for Testing and Materials, Pennsylvania, 1984.

ASTM C 618, “Standard Specification for fly ash and raw or calcined natural pozzolan for us as a mineral admixture in Portland cement concrete,” Annual Book of ASTM Standards, American Standards for Testing and Materials, 1994.

Barber, E.S., “Calculation of Maximum Pavement Temperatures From Weather Reports,” Bulletin 168, Highway Research Board, Washington, D.C., 1-8 pp., 1957.

Barnes, J.W., “Statistical Analysis for Engineers and Scientists: A Computer-Based Approach,” Second Edition, McGraw-Hill, Inc., New York, pp. 396, 1994.

Barrow, R.S., and Carrasquillo, R.L., "The effect of fly ash on the temperature rise in concrete," Research Report 481-2, Center for Transportation Research, The University of Texas at Austin, February 1988.

Baźant, Z., P., “Numerical Determination of Long-Range Stress History From Strain History in Concrete,” Materials and Structures, (RILEM Paris), Vol. 5, No. 27, pp. 135-141, 1972.

Baźant, Z., P., and Najjar, L.J., “Nonlinear Water Diffusion in Nonsaturated Concrete,” Materials and Structures, (RILEM Paris), Vol. 5, No. 25, pp. 3-20, 1972.

Baźant, Z.P., and Panula, L., “Practical predictions of time-dependent deformations of concrete,” Materials and Structures, Third RILEM, Vol. 11, 1978.

Baźant, Z.P., and Chern, J.C., “Strain softening with creep and exponential algorithm,” Journal of Engineering Mechanics Division, ASCE, Vol. 111, No. 3, 1985.

Bensted, J., “Hydration of Portland Cement,” in, “Advances in Cement Technology”, Edited by S.N. Ghosh, Pergamon Press, New York, Press, pp. 307-347, 1981.

Bentz, D.P., Garboczi, E.J., Haecker, C.J., and Jensen, O.M., “Effects of Cement Particle Size Distribution on Performance Properties of Portland Cement-Based Materials,” Cement and Concrete Research, 1999.

Bernander, S., "Parcical Measures to Avoid Early- Age Thermal Cracking in Concrete Structures," RILEM Report 15, Prevention of Thermal Cracking in Concrete at Early Ages, Edited by R. Springenschmid, E & FN Spon, London, pp 255-314, 1998.

Biernacki, J.J., Williams, P.J., and Stutzman, P.E., “Kinetics of the Reaction of Calcium Hydroxide and Fly Ash,” ACI Materials Journal, Vol. 98, No. 4, pp. 340-349, 2001.

Blanks, R.F., Meissner, H.S., and Rawhouser, C., "Cracking in Mass Concrete," Proceedings of the American Concrete Institute, Vol. 34, No. 3, pp. 477-515, 1938.

Bliss, R.W., “Atmospheric Radiation Near the Surface of the Ground: Summary for Engineers,” Solar Energy, Vol. 5, No. 3, pp. 103-120, 1961.

Bogue, R.H., “The Chemistry of Portland Cement,” Reinhold Publishing Corporation, New Yrk, pp. 572, 1947.

Byfors, J. “Plain Concrete at Early Ages,” Research 3:80, Swedish Cement and Concrete Research Institute, Stockholm, Sweden, 1980.

Carino, N.J., “Nondestructive Test Methods – Chapter 19,” Concrete Construction Engineering Handbook, Edited by Nawy, E.G., CRC Press, Florida, pp.19-1 to 19-68, 1997.

Carino, N.J., “Temperature Effects on the Strength-Maturity Relationship of Mortar,” Report No. NBSIR 81-2244, National Bureau of Standards, Washington, D.C., 90 pp., 1981.

Carino, N.J., “The maturity method,” In: “CRC Handbook on nondestructive testing of concrete”, Chapter 5, Edited by: Malhorta, V.M., and Carino, N.J., CRC Press, Florida, 1991.

Cervera, M., Oliver, J., and Prato, T., “Thermo-chemo-mechanical model for concrete. II: damage and creep,” Journal of Engineering Mechanics, Vol. 125, No. 9, pp. 1028-1039, 1999.

Cervera, M., Oliver, J., and Prato, T., “Thermo-Chemo-Mechanical Model for Concrete. Part I: Hydration and Aging,” Journal of Engineering Mechanics, Vol. 125, No. 9, pp. 1018-1027, 1999.

Chanvillard, G., and D’Aloia, L., Concrete Strength Estimation at Early Ages: Modification of the Method of Equivalent Age,” ACI Materials Journal, Vol. 91, No. 6, 1997, pp. 520-530.

Chapra, S., and Canale, R.P., “Numerical Methods for Engineers, With Programming and Software Applications,” Third Edition, McGraw-Hill, New York, 924 pp., 1998.

Chen, Y., and Odler, I., “On the Origin of Portland Cement Setting,” Cement and Concrete Research, Vol. 22, No. 6, pp. 1130-1140, 1992.

CEB-FIP, “Model Code for Concrete Structures,” Comité Europeén du Béton, CEB Bulletin No. 124/125-E, Paris, 348 pp., 1978.

De Schutter, G., and Taerwe, L., “Degree of Hydration-Based Description of Mechanical Properties of Early-Age Concrete,” Materials and Structures, Vol. 29, No. 7, pp. 335-344, 1996.

De Schutter, G., and Taerwe, L., “General Hydration Model for Portland Cement and Blast Furnace Slag Cement,” Cement and Concrete Research, Vol. 25, No. 3, pp. 593-604., 1995.

Digital Site Systems Inc., “CIMS, Computer Active Maturity System,” Software and Hardware Manual, October 1988.

Dossey, T., McCullough, B.F. and Dumas, A., "Effects of Aggregate Blends on the Properties of Portland Cement Concrete Pavements," Research Report 1224-8, Center for Transportation Research, The University of Texas at Austin, August 1994.

Emborg, M., "Thermal Stress in Concrete Structures at Early Ages," Doctoral Thesis, Luleå University of Technology, Division of Structural Engineering, 285 pp., 1989.

FHWA SP 201, “Accelerated Rigid Paving Techniques: State-of-the-Art Report (Special Project 201),” FHWA-SA-94-080, Federal Highway Administration, Washington, D.C., 255 pp., December 1994.

Freiesleben Hansen, P., and Pedersen, E.J., “Curing of Concrete Structures,” Draft DEB-Guide to Durable Concrete Structures, Appendix 1, Comité Euro-International du Béton, Lausanne, Switzerland, 1985.

Freiesleben Hansen, P., and Pedersen, E.J., “Maturity computer for controlling curing and hardening of concrete,” Nordisk Betong, Vol. 1, No. 19, pp. 21-25, 1977.

Frigione, G., “Gypsum in Cement,” in, “Advances in Cement Technology”, Edited by S.N. Ghosh, Pergamon Press, New York, Press, pp. 485-535, 1981.

Gebhardt, R.F., “Survey of North American Portland Cements,” Cement, Concrete, and Aggregates, pp. 145-189, 1995.

Germann Instruments, “4C-Temp & Stress – Temperature and Stress Simulation during Hardening,” User Manual, Evanston, Illinois, 1998.

Glasstone, S., Laidler, K.J., and Eyring, H., ‘The Theory of Rate Processes,” McGraw-Hill Book Company, Inc., New York, 611 pp., 1941.

Grace, “Concrete Production Information, Daratard® 17 Initial Set Retarder ASTM C 494, Type B and Type D”, http://www.grace.com, Grace Construction Products, Accessed February 2002.

Grace, “Concrete Production Information, Daraccel®, Water-Reducing Admixture ASTM C 494, Type E”, http://www.grace.com, Grace Construction Products, Columbia, Accessed February 2002.

Hankins, K., Suh, Y.C., and McCullough, B.F., "Field Evaluation of Coarse Aggregate Types: Criteria for Test Sections," Research Report 422/1244-1, Center for Transportation Research, The University of Texas at Austin, January 1991.

Hansen, T.C., “Physical structure of hardened cement paste. A classical approach,” Materials and Structures, Vol. 19, No. 114, Nov-Dec 1986, pp. 423-436.

Heilman, R.H., “Surface Heat Transmission,” Transactions of the Society of Mechanical Engineers, Vol. 51, Part 1, pp. 287-302, 1929.

Hellund, S., “Curing Control by Micro Computer,” Nordisk Beton, Vol 1-2, pp. 63-70, 1986.

Hewlett, P.C., “Lea’s Chemistry of Cement and Concrete,” John Wiley and Sons Inc., New York, 1053, 1998.

Hottel, H.C., and Egbert, R.B., “Radiant Heat Transmission from Water Vapor,” Transactions of the American Institute of Chemical Engineers, New York, Vol. 38, pp. 531-568, 1942.

Incorpera, F.P, and DeWitt, D., “Fundamentals of Heat and Mass Transfer,” Third Edition, Jon Wiley & Sons, New York, 919 pp, 1990.

Janna, W.S., “Engineering Heat Transfer,” Second Edition, CRC Press, Florida, 683 pp., 2000.

Jonasson, J.E., “Hett – A computer program for the calculation of strength, equivalent hydration period and temperature,” (In Swedish), Swedish Cement and Concrete Research Institute, Stockholm, 53 pp., 1988.

Jonasson, J.E., Groth, P., and Hedlund, H., "Modeling of temperature and moisture field in concrete to study early age movements as a basis for stress analysis," Proceedings of the International RILEM Symposium on Thermal Cracking in Concrete at Early Ages, Edited by R. Springenschmid, E & EF Spon, London, pp 45-52, 1995.

Kada-Benameur, H., Wirquin, E., and Duthoit, B., "Determination of Apparent Activation Energy of Concrete by Isothermal Calorimetry," Cement and Concrete Research, Vol. 30, pp. 301-305., 2000.

Khan, A.A., Cook, W.D., and Mitchell, D., "Thermal Properties and Transient Analysis of Structural Members during Hydration," ACI Materials Journal, pp. 293-302, May-June 1998.

Kishi, T., and Maekawa, K., "Thermal and mechanical modeling of young concrete based on hydration process of multi-component cement minerals," Proceedings of the International RILEM Symposium on Thermal Cracking in Concrete at Early Ages, Edited by R. Springenschmid, E & EF Spon, London, pp 11-18, 1995.

Kjellsen, K.O., and Detwiler, R.J., "Later-Age Strength Prediction by a Modified Maturity Model," ACI Materials Journal, Vol. 90, No. 3, pp. 220-227, 1993.

Kjellsen, K.O., and Detwiler, R.J., "Pore Structure of Plain Cement Paste Hydrated at Different Temperatures," Cement and Concrete Research, Vol. 20, No. 6, pp. 927-933, 1990.

Kjellsen, K.O., and Detwiler, R.J., "Reaction Kinetics of Portland Cement Mortars Hydrated at Different Temperatures," Cement and Concrete Research, Vol. 22, No. 1, pp. 112-120, 1992.

Kjellsen, K.O., and Detwiler, R.J., and, Gjørv, O.E., "Development of Microstructure in Plain Cement Pastes Hydrated at Different Temperatures," Cement and Concrete Research, Vol. 21, No. 1, pp. 179-189, 1991.

Knudsen, T., "Modeling Hydration of Portland Cement - The Effect of Particle Size Distribution," Conference Proceedings, "Characterization and Performance Prediction of Cement and Concrete, Edited by Young, J.F., United Engineering Trustees, Inc., New Hampshire, pp. 125-150, 1982.

Komonen, J., and Penttala, V., "Influence of Admixture Type and Concrete Temperature on Strength and Heat of Hydration of Concrete," Proceedings of the 10th International Congress on the Chemistry of Cement, Gothenburg, Sweden, Edited by H. Justnes, Published by Amarkai AB and Congrex Goteborg AB, Vol. 3, pp. 1-8., 1997.

Larson, G., and Dempsey, B.J., "Enhanced Integrated Climatic Model," Final Report DTFA MnDOT 72114, 99 pp., October, 1997.

Lerch, W., and Bogue, R.H., "Heat of Hydration of Portland Cement Pastes," Journal of Research, National Bureau of Standards, Vol. 12, No. 5, pp. 645-64, 1934.

Lerch, W., Ford, C.L., "Long-Term Study of Cement Performance in Concrete: Chaper 3. Chemical and Physical Tests of the Cements," ACI Journal, Vol. 19, No. 8, pp. 745-795, 1948.

Lundgren, B.W. and McElrath, G.W., "Introduction to probability and statistics," The MacMillan Company, New York, 1966.

Lytton, R.L., Pufahl, D.E., Michalak, C.H., Liang, H.S., and Dempsey, B.J., “An Integrated Model of the Climatic Effects on Pavements,” Report Number FHWA-RD-90-033, Federal Highway Administration, 285 pp., November 1989.

Ma, W., Sample, D., Martin, R., and Brown, P.W., “Calorimetric Study of Cements Blends Containing Fly Ash, Silica Fume, and Slag at Elevated Temperatures,” Cement, Concrete, and Aggregates, Vol. 16, No. 2, pp. 93-99, 1994.

Mather, B., “The Warmer the Concrete the Faster the Cement Hydrates,” in Practitioner’s Guide to Hot Weather Concreting, PP-1, American Concrete Institute, pp. 71-75, 1996.

McAdams, W.H., “Heat Transmission,” McGraw Hill Series in Chemical Engineering, McGraw Book Company, New York, pp. 532, 1954.

McCullough, B.F., “Development of Equipment and Techniques for a Statewide Rigid Pavement Deflection Study,” Research Report 46-1, Highway Design Division, Texas Highway Department, January 1965.

McCullough, B.F., “CRC-Highway Pave, Design of Continuously Reinforced Concrete Pavements,” Concrete Reinforcing Steel Institute, Schaumburg, Illinois, June 1993.

McCullough, B.F., and Rasmussen, R.O., “Fast track paving: Concrete temperature control and traffic opening criteria for bonded concrete overlays,” Task G, Final Report, FHWA, U.S. Department of Transportation, 1999.

McCullough, B.F., Zollinger, D. and Dossey, T., "Evaluation of the performance of Texas pavements made with different coarse aggregates ", Research Report 3925-1F, The Center for Transportation Research, The University of Texas at Austin, 1998.

McCullough, B.F., and Schindler, A.K., "Longitudinal Reinforcement Design of CRC Pavements in the Houston District", Technical Memorandum 98-0142-05, The Center for Transportation Research, The University of Texas at Austin, 1998.

Medina Chavez, C.I, and McCullough, B.F. Updated Status of the Continuously Reinforced Concrete Pavement Database in Texas: Improvements and Trends. Research Report 1778-2, Center for Transportation Research, The University of Texas at Austin, 2000.

MEES, “An appraisal of the Membrane Method of Curing Concrete Pavements,” Bulletin 108, Michigan Engineering Experiment Station, 1948.

Menzel, C.A., “Causes and Prevention of Crack Development in Plastic Concrete,” Proceedings of the Portland Cement Association, pp. 130-136, 1954.

Metha P.K., and Monteiro, P.J.M., “Concrete Microstructure, Properties, and Materials,” Second Edition, The McGraw-Hill Companies, Incorporated, New York, 1993.

Mills, R.H., “Factors Influencing Cessation of Hydration in Water-Cured Cement Pastes,” Special Report No. 90, Proceedings of the Symposium on the Structure of Portland Cement Paste and Concrete, Highway Research Board, Washington, D.C., pp. 406-424, 1966.

Mindess, S., and, Young, J.F., “Concrete,” Prentice-Hall Inc., New Jersey, 671 pp., 1981.

Morabito, P., "Methods to Determine the Heat of Hydration of Concrete," RILEM Report 15, Prevention of Thermal Cracking in Concrete at Early Ages, Edited by R. Springenschmid, E & FN Spon, London, pp 1-25, 1998.

Morimoto, H., and Koyanagi W., “Estimation of Stress Relaxation in Concrete at Early Ages,” Proceedings of the International RILEM Symposium on Thermal Cracking in Concrete at Early Ages, Edited by R. Springenschmid, E & EF Spon, London, pp ?-?, 1995.

NAE, “Greatest Engineering Achievements of the 20th Century”, www.greatachievements.org/greatachievements/ga_11_2.html, National Academy of Engineering, Accessed February 2002, 2000.

Naik, T.R., “Maturity Functions Concrete Cured During Winter Conditions,” in Temperature Effects on Concrete, Edited by T.R. Naik, ASTM special technical publication 858, 1985.

Nakamura, H., Hamada, S., Tanimoto, T., and Miyamoto, A., “Estimation of Thermal Cracking Resistance for Mass Concrete Structures with Uncertain Material Properties,” ACI Structural Journal, Vol. 96, No. 4, 1999, pp. 509-518.

NCDC, “Solar and Meteorological Surface Observational Network, CD-ROM,” National Climatic Data Center, North Carolina, 1996.

Neville, A.M., "Properties of Concrete," Fourth Edition, John Wiley and Sons, Incorporated, New York, 1996.

Onken, P., and Rostásy, F.S., "A Practical Planning Tool for the Simulation of Thermal Stresses and for the Prediction on Early Thermal Cracks in Massive Concrete Structures," Proceedings of the International RILEM Symposium on Thermal Cracking in Concrete at Early Ages, Edited by R. Springenschmid, E & EF Spon, London, pp 289-296, 1995.

Otero-Jimenez, M., McCullough, B.F., and Hankins, K. "Monitoring of Siliceous River Gravel and Limestone Continuously Reinforced Concrete Pavement Test Sections in Houston 2 Years After Placement, and Development of a Crack Width Model for the CRCP-7 Program," Research Report 1244-4, Center for Transportation Research, The University of Texas at Austin, March 1992.

PCA, “Pavements,” www.portcement.org/pv/pavements_highways.asp, Portland Cement Association, Skokie, Illinois, Accessed February 2002.

Pinto, R., C., A., and Hover, K., C., “Application of Maturity Approach to Setting Times,” ACI Materials Journal, Volume 96, Number 6, pp. 686-691, 1999.

Powers, T.C., and Brownyard, T.L., “Studies of the Physical Properties of Hardened Portland Cement Paste,” Portland Cement Association, Bulletin, Vol. 22, 992 p., 1948.

Price, P.H., and Slack, M.R., “Stability and Accuracy of Numerical Solutions of the Heat Flow Equation,” British Journal of Applied Physics, Vol. 3, No. 12, pp. 379-384, 1952.

Radjy, F.F., and Vunic, D.W., “Heat Signature Testing of Concrete,” Proceedings of Structural Materials Technology, an NDT Conference, Atlantic City, Feb. 1994.

Ramachandran, V.S., “Waste and Recycled Materials in Concrete Technology”, Edited by S.N. Ghosh, Pergamon Press, New York, Press, pp. 649-671, 1981.

RILEM 42-CEA, “Properties of Set Concrete at Early Ages: State of the Art Report,” Materials and Structures, Vol.14, No. 84, pp. 399-450, 1981.

RILEM Technical Committee 119-TCE, “Adiabatic and Semi-Adiabatic Calorimetry to Determine the Temperature Increase in Concrete due to Hydration Heat of Cement,” RILEM Report 15, Prevention of Thermal Cracking in Concrete at Early Ages, Edited by R. Springenschmid, E & FN Spon, London, pp 315-330, 1998.

Rochefort J.L., McCullough, B.F., Dossey, T., and Fowler, D.W., “Evaluation of the Effects of the Tining Operation on the Performance of Portland Cement Concrete Pavements,” Research Report 4978-1, The Center for Transportation Research, Austin, Texas, 2000.

Roy, D.,M., Luke, K., and Diamond, S., “Characterization of Fly Ash and Its Reactions in Concrete, “ Fly Ash and Coal Conversion By-Products: Characterization, Utilization, and Disposal I, Materials Research Society Symposia Proceedings, Vo. 43, pp. 3-20., 1989.

Ruiz, J.M., Schindler, A.K., Rasmussen, R.O., Kim, P.J., and Chang, G.K. “Concrete Temperature Modeling and Strength Prediction Using Maturity Concepts in the FHWA HIPERPAV Software,” Proceedings of the seventh international conference on concrete pavements, Orlando, Florida, September 2001.

Samarai, M., Popovics, S., and Malhotra, V.M., "Effect of High Temperatures on the Properties of Fresh Concrete," Transportation Research Record, 924 pp. 42-50, 1975.

SAS, “SAS System help documentation,” Software Release 8.2, SAS Institute Inc., Cary, North Carolina, 2001.

Scanlon, J.M., and, McDonald, J.E., “Thermal Properties, Significance of Tests and Properties of Concrete and Concrete-Making Materials,” Edited by Klieger, P., and Lamonds, J.F., ASTM Special Technical Publication No. 169C, Philadelphia, pp. 229-239, August 1994.

Schindler, A.K., McCullough, B.F., and Krauss, T.S., “The Design of a High Performance Concrete Pavement in the Waco District, Texas”, Research Report 0215-1F, The Center for Transportation Research, The University of Texas at Austin, 1999.

Shahin, M.Y., and McCullough, B.F., “Prediction of Low-Temperature and Thermal-Fatigue Cracking in Flexible Pavements,” Research Report 123-14, Texas Highway Department, 225 pp., August 1972.

SHRP-C-321, “A Guide to Evaluating Thermal Effects in Concrete Pavements,“ Strategic Highway Research Program, National Research Council, Washington, D.C., 1993.

Soroka, I. “Concrete in Hot Environments,” E & FN Spon, London, UK, 251 pp, 1993.

Springenschmid, R., and Breitenbücher, R., “Cement with Low-Crack-Susceptibility”, Proceedings of the Conference on Advances in Cementitious Materials, Edited by: Mindess, Ceramic Transactions, Vol. 16, pp. 701-713, 1991.

Springenschmid, R., and Fleischer, W., “Recent Development in Design and Construction of Concrete Pavements at German Expressways (Autobahns)”, Proceedings from the Seventh International Conference on Concrete Pavements, September 9-13, 2001, Orlando, Florida, pp. 437-450, 2001.

Springenschmid, R., Breitenbücher, R., and Mangold, M., "Development of the Cracking Frame and the Temperature-Stress Testing Machine," Proceedings of the International RILEM Symposium on Thermal Cracking in Concrete at Early Ages, Edited by R. Springenschmid, E & EF Spon, London, pp 137-144, 1995.

Suh, Y.C., Hankins, K., and McCullough, B.F., "Early-Age Behavior of Continuously Reinforced Concrete Pavement and Calibration of the Failure Prediction Model in the CRCP-7 Program," Research Report 1244-3, Center for Transportation Research, The University of Texas at Austin, March 1992.

Tank, C.J., and Carino, N.J., “Rate Constant Functions for Strength Development of Concrete,” ACI Materials Journal, Vol. 88, No. 1, pp. 74-83, Jan-Feb 1991.

Tank, R.C., “The rate constant model for strength development of concrete,” Ph.D. dissertation, Polytechnic University, Brooklyn, New York, June 1988.

Taplin, J.H., “A Method for Following the Hydration Reaction in Portland Cement Paste,” Australian Journal of Applied Science, Vol. 10, No. 3, pp. 329-345,1959.

Taylor, H.F.W., “Modification of Bogue Calculation,” Advances in Cement Research, Vol. 2, No. 6, pp. 73-79, 1989.

Texas Department of Transportation (TxDOT), “Standard Specifications for Construction of Highways, Streets and Bridges”, Austin, Texas, 1993.

Tompson, M.R., Dempsey, B.J., Hill, H., and Vogel, J., “Characterizing Temperature Effects for Pavement Analysis and Design,” Transportation Research Record 1121, pp. 14-22, 1998.

Tritsch, S.L., "Temperature management of slabs," SP 201, Federal Highway Administration, 23 pp., 1994.

Turner, W.C., and Malloy, J.F., “Thermal Insulation Properties,” McGraw-Hill Book Company, New York, 629 pp., 1981.

Tuthill, L.H., and Cordon, W.A., “Properties and Uses of Initially Retarded Concrete,” Proceedings of the American Concrete Institute, Vol. 52, Part 2, pp. 273-286, 1955.

TxDOT, “Standard Specifications for Construction of Highways, Streets and Bridges”, Texas Department of Transportation, Austin, Texas, 1995.

TxDOT, “Concrete Pavement Details, Continuously Reinforced Steel Bars, CPCR (1) and (2)”, Texas Department of Transportation, Austin, Texas, 1994.

TxDOT SP 360-035, “1993 English Special Provisions to Item 360 - Concrete Pavement, SP 360-035,” Texas Department of Transportation, Austin, Texas, 2000.

USBR, “Concrete Manual,” Eight Edition, Water Resources Technical Publication, U.S. Department of the Interior, Bureau of Reclamation, 1975.

Van Breugel, K., “Simulation of hydration and formation of structure in hardening cement based materials,” Ph.D. Thesis, Second Edition, Delft University Press, Netherlands, 1997.

Van Breugel, K., "Prediction of Temperature Development in Hardening Concrete," RILEM Report 15, Prevention of Thermal Cracking in Concrete at Early Ages, Edited by R. Springenschmid, E & FN Spon, London, pp 51-75, 1998.

Verbeck, G.J., and Helmuth, R.H., “Structure and Physical Properties of Cement Pastes,” Proceedings of the Fifth International Symposium on the Chemistry of Cement, Tokoyo, Vol. III, pp. 1-32, 1968.

Westman, G., "Concrete Creep and Thermal Stresses," Doctoral Thesis, Luleå University of Technology, Division of Structural Engineering, 301 pp., 1999.

Wilde, W.J., Waalkes, S., and Harrison, R., “Life Cycle Cost Analysis of Portland Cement Concrete Pavements,” Research Report 1739-1, Center for Transportation Research, The University of Texas at Austin, September 1999.

Won, M., McCullough, B.F., and Hudson, W.R., "Evaluation of Proposed Texas SDHPT Design Standards for CRCP," Research Report 472-1, Center for Transportation Research, The University of Texas at Austin, April 1988.

Won, M., Hankins, K., and McCullough, B.F., "Mechanistic analysis of continuously reinforced concrete pavements considering material characteristics, variability, and fatigue," Research Report 1169-2, Center for Transportation Research, The University of Texas at Austin, March 1991.

Yang, S., "A Temperature Prediction Model in New concrete Pavement and a New Method for Concrete Fracture Parameters," Ph.D. Dissertation, Texas A&M University, pp. 176, May 1996.

Yu, H.T., Khazanovich, L., Darter, M.I., and Ardani, A., “Analysis of Concrete Pavement Responses to Temperature and Wheel Loads Measured from Instrumented Slabs,” Transportation Research Record No. 1639, p. 94-101, 1998.

APPENDIX A

Data from Field Site Concrete Mixtures

Mixture No. 1

Description: Dallas – May, Type I/II Cement + 20% Class F fly ash

Table A-1: Mixture proportions

Component	Concrete	Mortar *
Cement (lbs/yd^3) Sunbelt (New Braunfels)	414	634
Class F fly ash (lbs/yd^3) Big Brown, Boral Materials	80	133
Water (lbs/yd^3) City of Wilmer	193	276
Coarse Aggregate (lbs/yd^3) Limestone, Hanson (Perch Hill)	2,099	-
Fine Aggregate (lbs/yd^3) Hanson, Cobb Seagoville, TX	1,239	2,860
W/R Retarder (oz/yd^3) Plastimix 100-R	11.0	10.8
Air Entraining Agent (oz/yd^3) Proair VR	6.0	5.9
Field slump (inch)	0.75“	-
Field measured Air Content	3.5%	-
Field 7-day flexural strength (psi)	687 psi	-

Table A-2: Activation energy cube compressive strength results

Test Data - 8°C		Test Data - 23°C		Test Data - 40°C	
Age (hours)	**Strength (psi)**	**Age (hours)**	**Strength (psi)**	**Age (hours)**	**Strength (psi)**
31.3	820	18.0	1583	15.5	2504
47.4	1521	39.6	2813	24.1	3261
96.3	2754	72.1	3610	47.9	4309
167.7	3652	143.9	4473	95.0	4728
335.5	4593	263.2	5121	142.7	5074
671.9	5185	528.0	5676	265.3	6096

Table A-3: Summary of Activation Energy analysis results

HYPERBOLIC STRENGTH GAIN			
Mix No:	1		
Description:	Dallas - May		
E =	**31,062**	J/mol	
T, (°K) =	281.0	295.8	313.0
1/T =	0.00356	0.00338	0.00319
ln(K) =	-4.52	-3.92	-3.16
Slope =	-3736.0		

EXPONENTIAL STRENGTH GAIN			
Mix No:	1		
Description:	Dallas - May		
E =	**38,359**	J/mol	
T, (°K) =	281.0	295.8	313.0
1/T =	0.00356	0.00338	0.00319
ln(K) =	-4.43	-3.40	-2.75
Slope =	-4613.5		

Curve Fit Parameters			
T, (°F) =	46.4	73.0	104.0
Su, psi =	5,907	6,141	6,284
K =	0.0109	0.0199	0.0422
to, hrs =	16.1	0.0	0.0

Curve Fit Parameters			
T, (°F) =	46.4	73.0	104.0
Su, psi =	6,135	6,350	6,452
τ, hrs =	84.09	29.82	15.64
β =	0.694	0.694	0.694

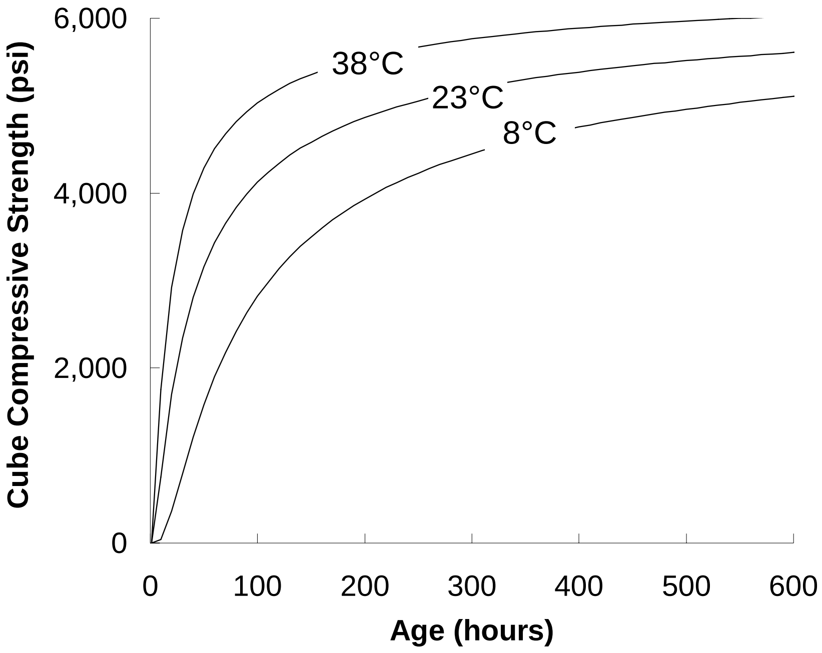

Figure A-1: Strength development over time at different curing temperatures

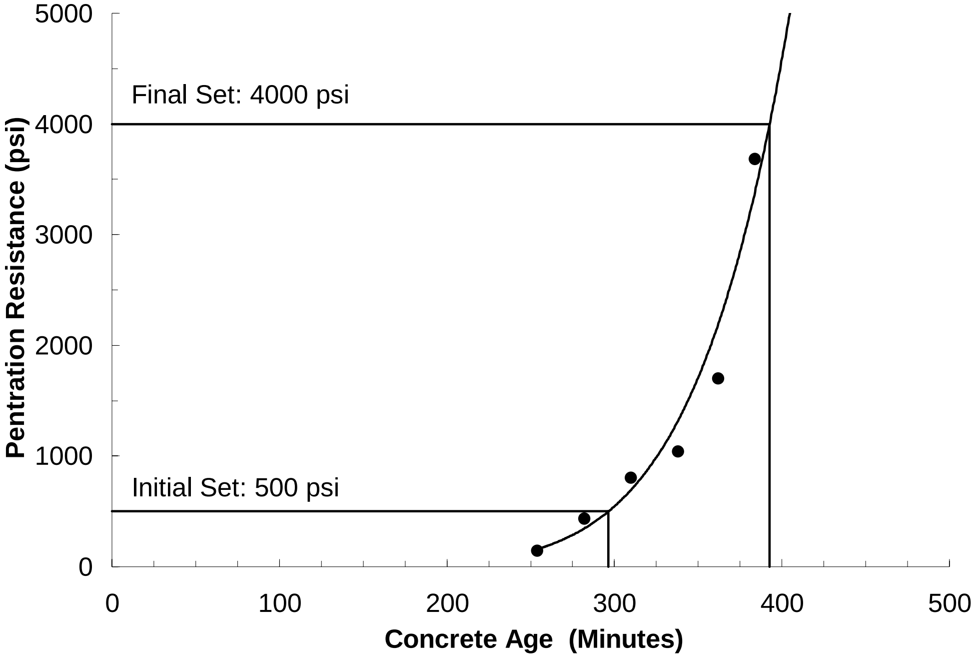

Figure A-2: ASTM C 403 setting times under **laboratory** conditions Dallas, May 2000

Mixture No. 2

Description: Houston – May, Type I/II Cement + 25% Class C fly ash

Table A-4: Mixture proportions

Component	Concrete	Mortar
Cement (lbs/yd^3) Cemex #16 (Tong Yang)	423	580
Class C fly ash (lbs/yd^3) W.A. Parish Unit #8	113	155
Water (lbs/yd^3) City of Houston	238	326
Coarse Aggregate (lbs/yd^3) 1.5” Crushed Limestone - Sunbelt	1,966	-
Fine Aggregate (lbs/yd^3) Sand Supply	1,112	2695
Retarder (oz/yd^3) WRDA / HYCOL	15.0	15.0
Air Entraining Agent (oz/yd^3) Daravair 1000	3.0	3.0
Field slump (inch)	2.25“	-
Field measured Air Content	4.1%	-
Field 7-day flexural strength (psi)	664 psi	-

Table A-5: Activation energy cube compressive strength results

Test Data - 8°C		Test Data - 23°C		Test Data - 40°C	
Age (hours)	Strength (psi)	Age (hours)	Strength (psi)	Age (hours)	Strength (psi)
39.5	366	16.9	465	15.9	1316
48.4	558	39.8	1529	24.9	2213
95.9	1657	72.3	2714	48.1	3735
167.9	3184	145.8	4337	95.9	4848
336.5	4183	264.1	5355	144.4	5590
672.1	5545	529.2	6262	264.4	5871

Table A-6: Summary of Activation Energy analysis results

HYPERBOLIC STRENGTH GAIN			
Mix No:	2		
Description:	Houston - May		
E =	**40,914**	J/mol	
T, (°K) =	281.0	295.8	313.0
1/T =	0.00356	0.00338	0.00319
ln(K) =	-5.26	-4.68	-3.47
Slope =	-4920.9		

EXPONENTIAL STRENGTH GAIN			
Mix No:	2		
Description:	Houston - May		
E =	**38,671**	J/mol	
T, (°K) =	281.0	295.8	313.0
1/T =	0.00356	0.00338	0.00319
ln(K) =	-5.17	-4.37	-3.48
Slope =	-4651.1		

Curve Fit Parameters			
T, (°F) =	46.4	73.0	104.0
Su, psi =	7,082	7,619	6,714
K =	0.0052	0.0093	0.0310
to, hrs =	30.7	10.8	8.3

Curve Fit Parameters			
T, (°F) =	46.4	73.0	104.0
Su, psi =	7,012	8,099	6,688
τ, hrs =	175.35	79.12	32.30
β =	0.725	0.725	0.725

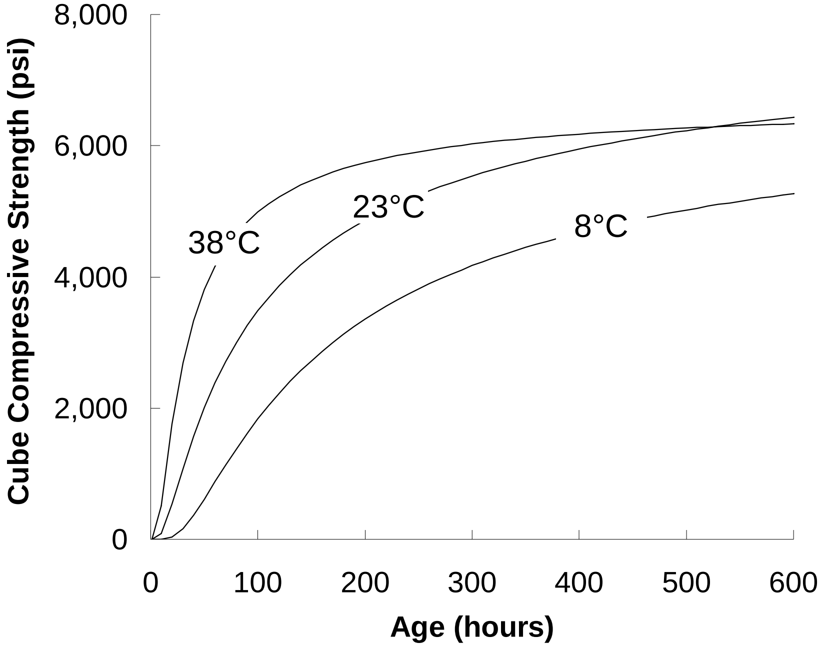

Figure A-3: Strength development over time at different curing temperatures

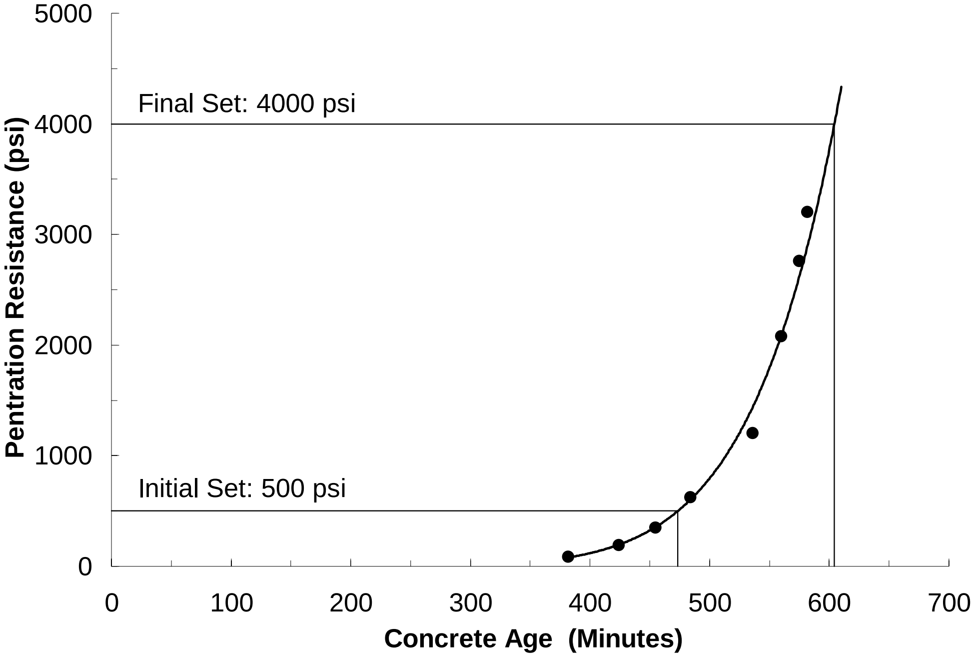

Figure A-4: ASTM C 403 setting times under **laboratory** conditions, Houston, May 2000

Mixture No. 3

Description: Dallas – August, Type I Cement (5.0 sacks)

Table A-7: Mixture proportions

Component	Concrete	Mortar
Cement (lbs/yd^3) Holnam (Texas)	470	683
Water (lbs/yd^3) City of Dallas	217	286
Coarse Aggregate (lbs/yd^3) Crushed Limestone - Bridgeport	1,941	-
Fine Aggregate (lbs/yd^3) Trinity Materials, Valley Farms 206	1,340	2844
Type A and F (oz/yd^3) Sikament 10 ESL	14.9	15.1
Air Entraining Agent (oz/yd^3) Sika AEA-15	2.0	2.0
Field slump (inch)	2.0“	-
Field measured Air Content	3.5%	-
Field 7-day flexural strength (psi)	610 psi	-

Table A-8: Activation energy cube compressive strength results

Test Data - 8°C		Test Data - 23°C		Test Data - 40°C	
Age (hours)	Strength (psi)	Age (hours)	Strength (psi)	Age (hours)	Strength (psi)
25.8	879	16.6	1691	15.1	1875
48.0	1985	39.6	2766	24.0	2319
96.2	3137	71.8	3448	49.0	2897
168.9	4065	144.2	4216	95.8	3677
336.8	4681	262.9	4686	142.8	3517
672.9	5525	528.5	5275	264.4	4007

Table A-9: Summary of Activation Energy analysis results

HYPERBOLIC STRENGTH GAIN			
Mix No:	3		
Description:	Dallas - August		
E =	**31,486**	J/mol	
T, (°K) =	281.0	295.8	313.0
1/T =	0.00356	0.00338	0.00319
ln(K) =	-4.36	-3.72	-2.98
Slope =	-3786.9		

EXPONENTIAL STRENGTH GAIN			
Mix No:	3		
Description:	Dallas - August		
E =	**42,081**	J/mol	
T, (°K) =	281.0	295.8	313.0
1/T =	0.00356	0.00338	0.00319
ln(K) =	-4.63	-3.46	-2.79
Slope =	-5061.2		

Curve Fit Parameters			
T, (°F) =	46.4	73.0	104.0
Su, psi =	6,038	5,538	4,219
K =	0.0128	0.0243	0.0507
to, hrs =	11.7	0.0	0.0

Curve Fit Parameters			
T, (°F) =	46.4	73.0	104.0
Su, psi =	6,431	6,750	4,690
τ, hrs =	103.02	31.97	16.27
β =	0.494	0.494	0.494

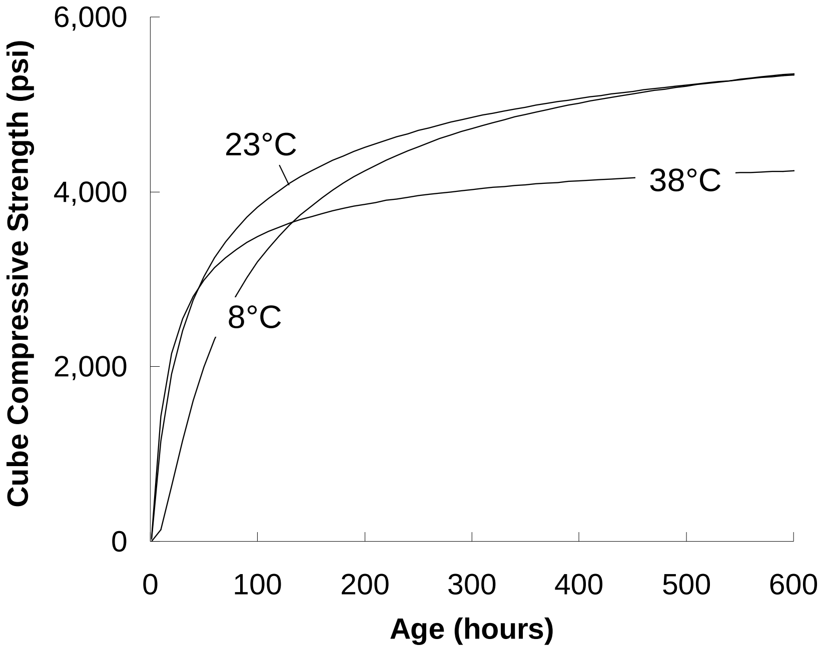

Figure A-5: Strength development over time at different curing temperatures

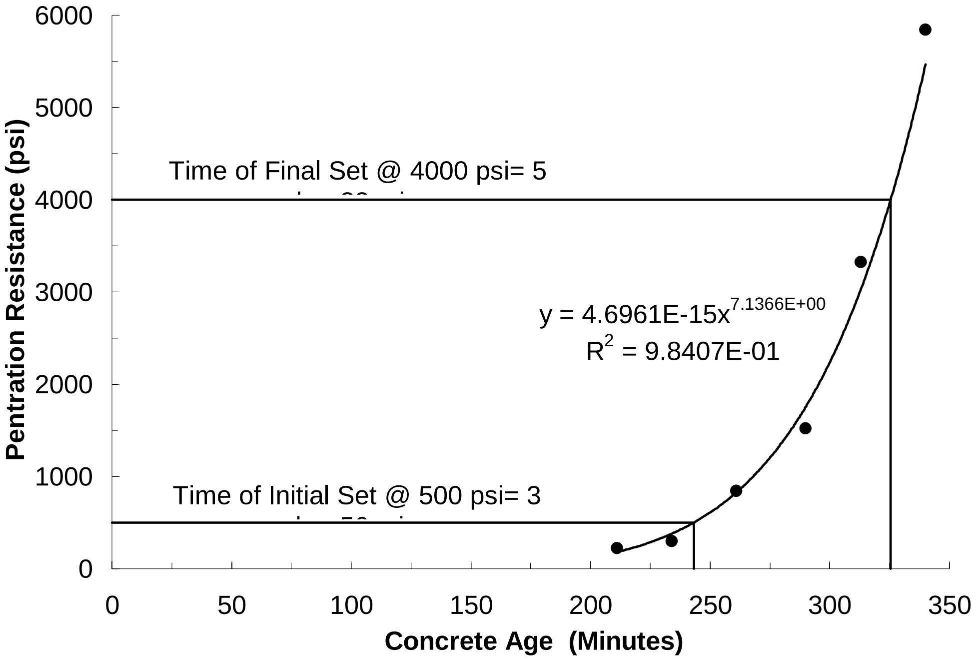

Figure A-6: ASTM C 403 setting times under **laboratory** conditions, Dallas, August

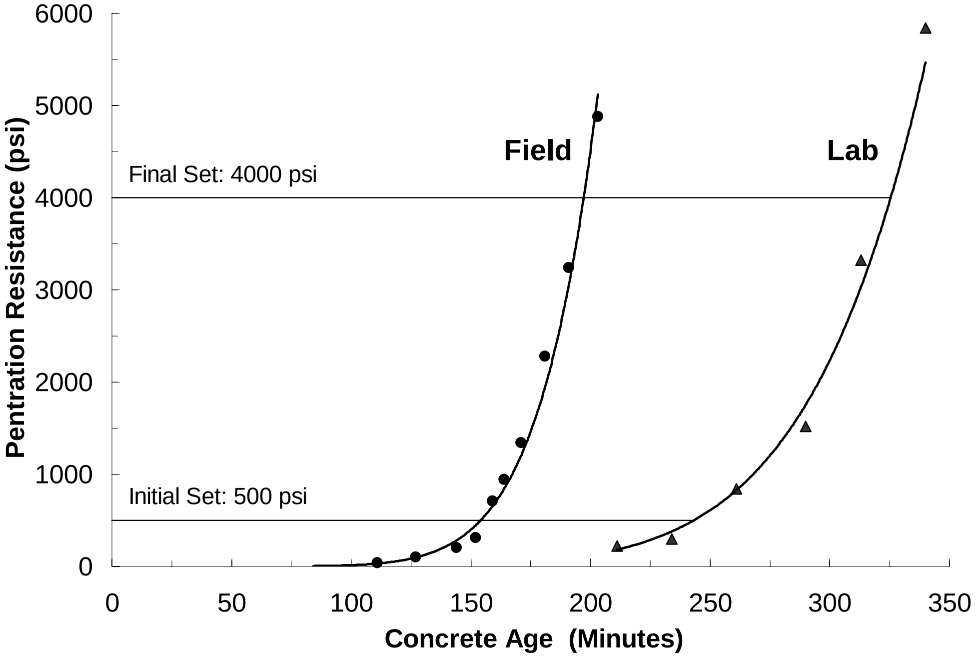

Figure A-7: ASTM C 403 setting times under **laboratory and field** conditions, Dallas, August

Mixture No. 4

Description: Houston – August, Type I/II Cement + 35% Class C fly ash

Table A-10: Mixture proportions

Component	Concrete	Mortar
Cement (lbs/yd^3) Cemex (Tong Yang)	367	534
Class C fly ash (lbs/yd^3) Lagrange, Boral Materials	172	253
Water (lbs/yd^3) Local well water	220	305
Coarse Aggregate (lbs/yd^3) Crushed limestone – Martin Marrietta	1,827	-
Fine Aggregate (lbs/yd^3) Sand Supply – Columbus Pit	1,282	2658
Retarder (oz/yd^3)	16.5	16.3
Air Entraining Agent Daravair (oz/yd^3)	4.0	4.5
Field slump (inch)	0.75“	-
Field measured Air Content	4.1%	-
Field 7-day flexural strength (psi)	680 psi	-

Table A-11: Activation energy cube compressive strength results

Test Data - 8°C		**Test Data - 23°C**		**Test Data - 40°C**	
Age (hours)	**Strength (psi)**	**Age (hours)**	**Strength (psi)**	**Age (hours)**	**Strength (psi)**
24.6	221	16.2	723	15.4	1289
48.1	898	39.3	2183	24.7	2113
96.5	2260	70.5	3749	46.8	3301
167.5	4155	144.5	5423	93.8	4203
336.4	5337	263.8	6645	143.4	4822
672.3	6671	527.6	7397	265.7	5594

Table A-12: Summary of Activation Energy analysis results

HYPERBOLIC STRENGTH GAIN			
Mix No:	4		
Description:	Houston - August		
E =	**32,370**	J/mol	
T, (°K) =	281.0	295.8	313.0
1/T =	0.00356	0.00338	0.00319
ln(K) =	-5.19	-4.40	-3.77
Slope =	-3893.3		

EXPONENTIAL STRENGTH GAIN			
Mix No:	4		
Description:	Houston - August		
E =	**35,121**	J/mol	
T, (°K) =	281.0	295.8	313.0
1/T =	0.00356	0.00338	0.00319
ln(K) =	-4.94	-4.09	-3.40
Slope =	-4224.1		

Curve Fit Parameters			
T, (°F) =	46.4	73.0	104.0
Su, psi =	8,535	8,648	6,416
K =	0.0056	0.0123	0.0230
to, hrs =	22.9	9.5	3.9

Curve Fit Parameters			
T, (°F) =	46.4	73.0	104.0
Su, psi =	8,274	9,039	7,203
τ, hrs =	139.60	59.74	29.98
β =	0.760	0.760	0.760

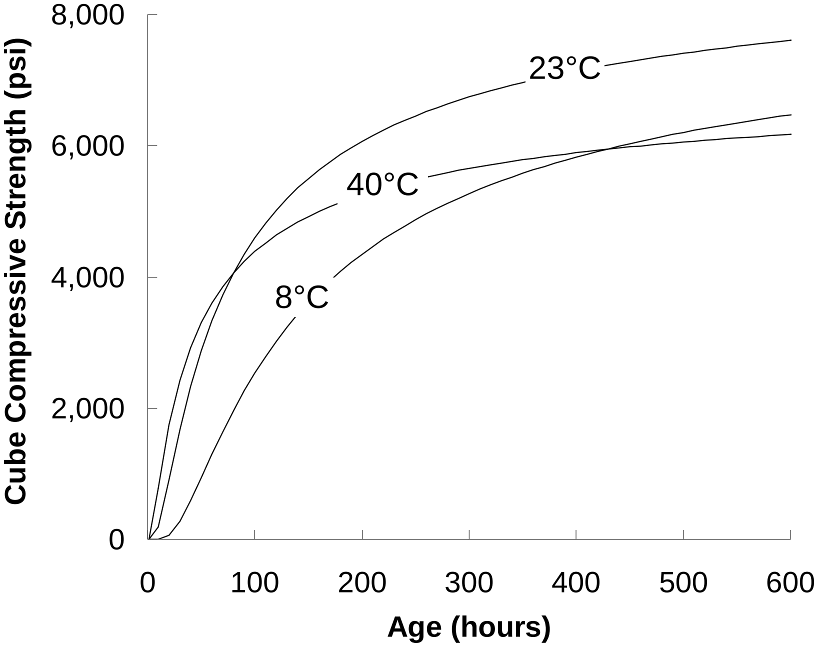

Figure A-8: Strength development over time at different curing temperatures

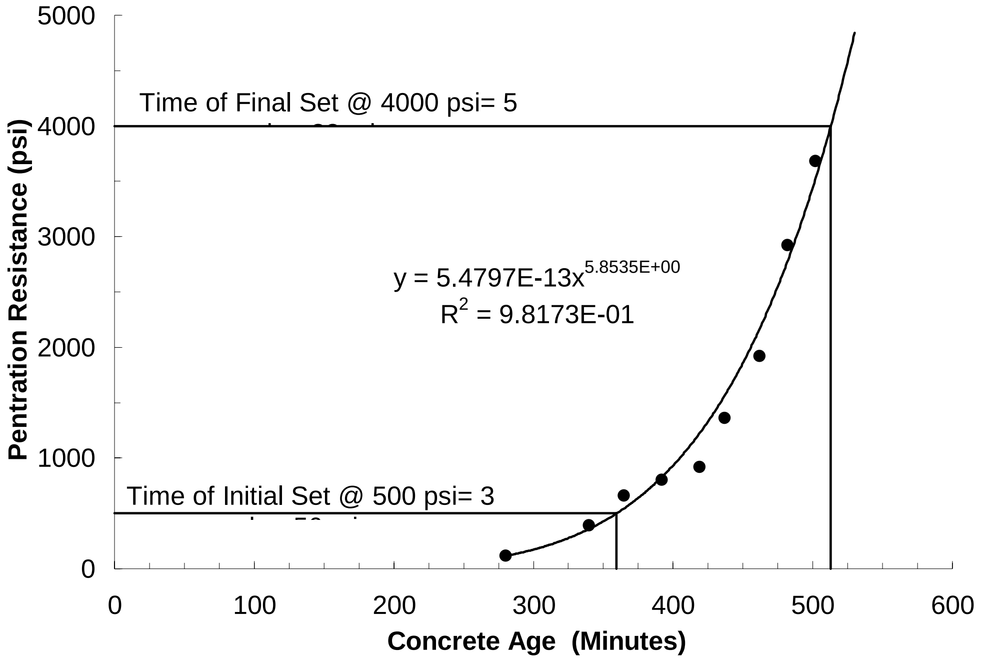

Figure A-9: ASTM C 403 setting times under **laboratory** conditions, Houston, August

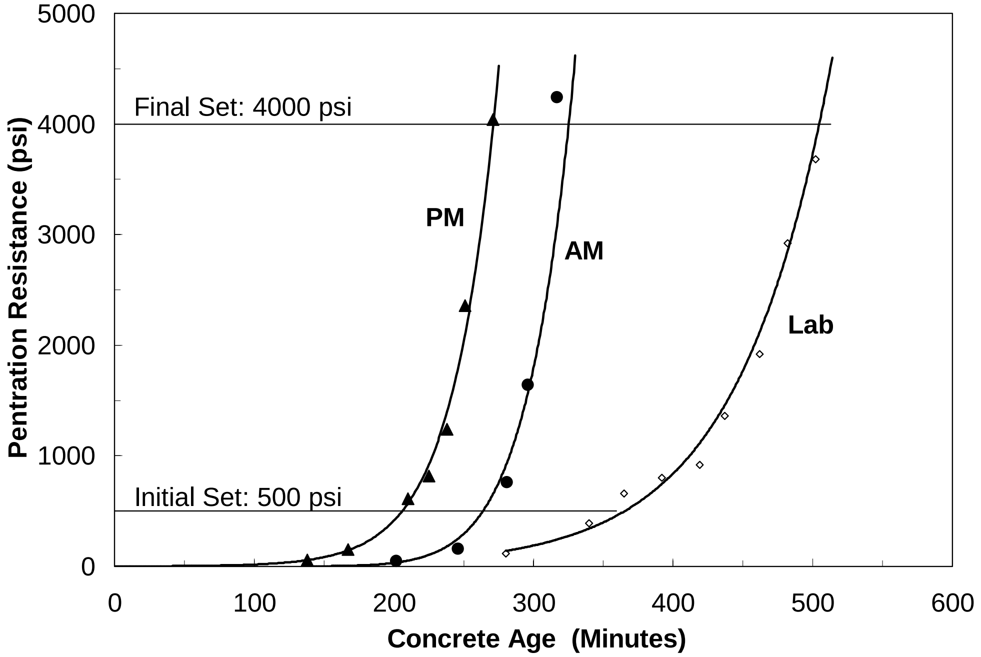

Figure A-10: ASTM C 403 setting times under **laboratory and field** conditions, Houston, Aug.

Mixture No. 5

Description: El Paso– August, Type I/II Cement + 50% GGBF Slag

Table A-13: Mixture proportions

Component	Concrete	Mortar
Cement (lbs/yd^3) Rio Grande (Samalaynca)	470	683
GGBF Slag (lbs/yd^3) Lone Star – Grade 120	0	0
Water (lbs/yd^3)	217	286
Coarse Aggregate (lbs/yd^3) S. Quarry #4, McKelligon #67	1,941	-
Fine Aggregate (lbs/yd^3)	1,340	2844
W/R for pozzolans (oz/yd^3) Monex X-15	14.9	15.1
Air Entraining Agent (oz/yd^3) Boral Monex Air-40	2.0	2.0
Field slump (inch)	1.5“	-
Field measured Air Content	4.3%	-
Field 7-day flexural strength (psi)	585 psi	-

Table A-14: Activation energy cube compressive strength results

Test Data - 8°C		Test Data - 23°C		Test Data - 40°C	
Age (hours)	Strength (psi)	Age (hours)	Strength (psi)	Age (hours)	Strength (psi)
24.5	113	16.5	257	15.7	890
47.9	283	39.6	889	24.7	1305
96.0	750	69.9	1519	48.1	2045
168.4	1484	142.4	2411	97.0	3164
335.7	2061	264.7	3104	143.5	3734
671.8	2973	527.8	4055	264.4	4513

Table A-15: Summary of Activation Energy analysis results

HYPERBOLIC STRENGTH GAIN			
Mix No:	5		
Description:	El Paso - August		
E =	**29,597**	J/mol	
T, (°K) =	281.0	295.8	313.0
1/T =	0.00356	0.00338	0.00319
ln(K) =	-5.82	-5.09	-4.52
Slope =	-3559.7		

EXPONENTIAL STRENGTH GAIN			
Mix No:	5		
Description:	El Paso - August		
E =	**38,400**	J/mol	
T, (°K) =	281.0	295.8	313.0
1/T =	0.00356	0.00338	0.00319
ln(K) =	-6.11	-5.15	-4.42
Slope =	-4618.5		

Curve Fit Parameters			
T, (°F) =	46.4	73.0	104.0
Su, psi =	4,473	5,237	6,106
K =	0.0030	0.0062	0.0109
to, hrs =	22.1	7.0	0.0

Curve Fit Parameters			
T, (°F) =	46.4	73.0	104.0
Su, psi =	5,426	7,146	8,855
τ, hrs =	448.39	172.89	83.37
β =	0.496	0.496	0.496

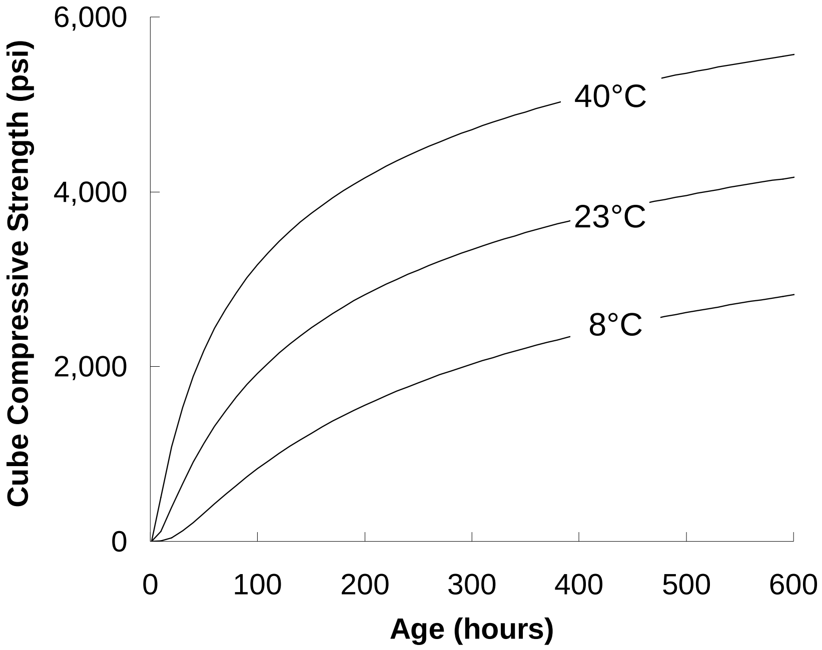

Figure A-11: Strength development over time at different curing temperatures

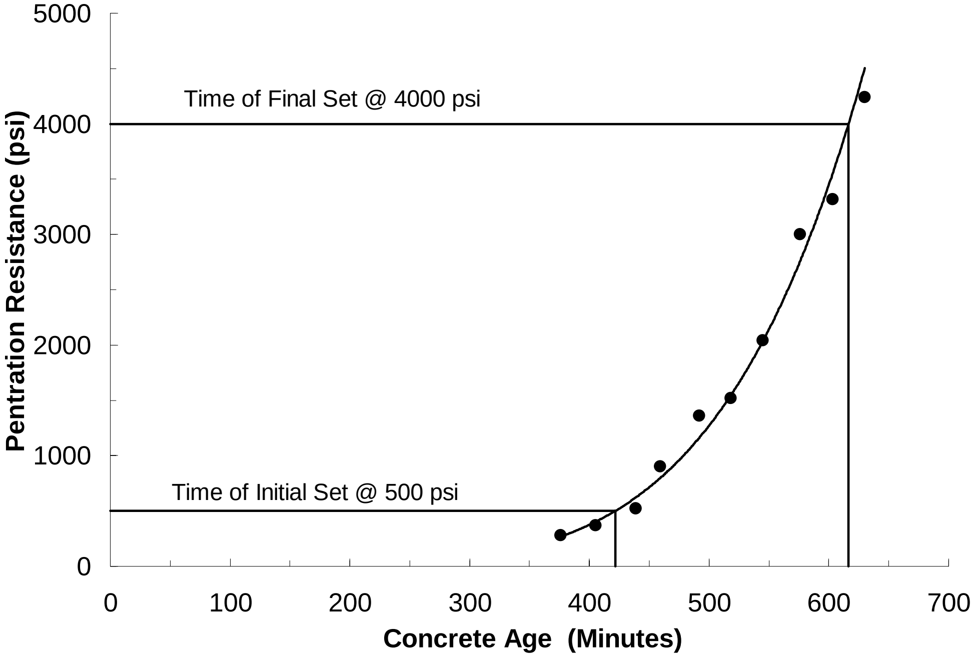

Figure A-12: ASTM C 403 setting times under **laboratory** conditions, El Paso, August 2000

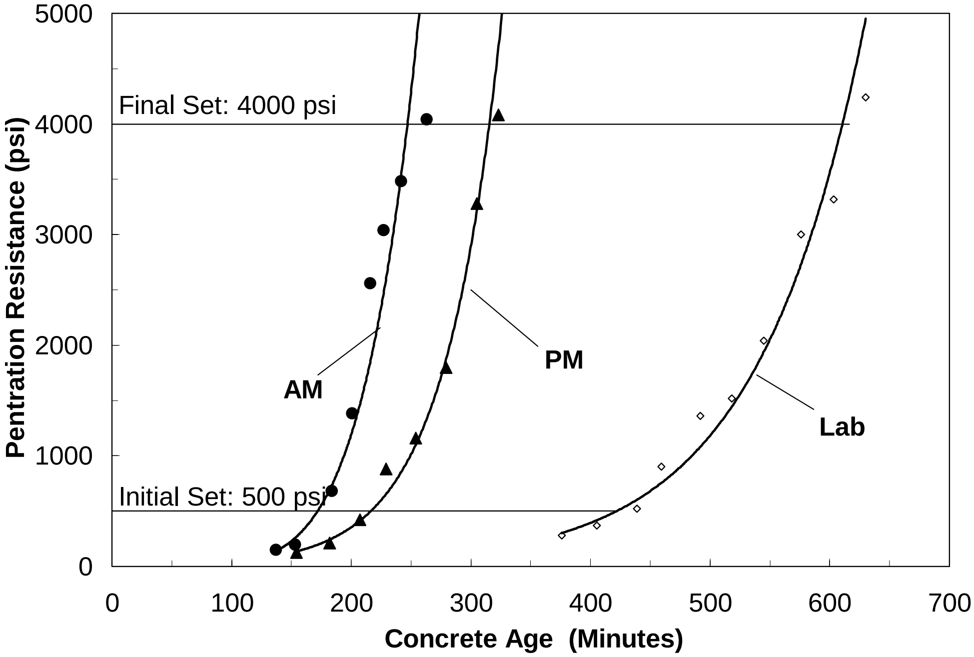

Figure A-13: ASTM C 403 setting times under **laboratory and field** conditions, El Paso

Mixture No. 6

Description: Dallas – September, Type I Cement + 20% Class F fly ash

Table A-16: Mixture proportions

Component	Concrete	Mortar
Cement (lbs/yd^3) TXI (Midlothian)	376	540
Class F fly ash (lbs/yd^3) Big Brown, Boral Materials	82	119
Water (lbs/yd^3) City	229	313
Coarse Aggregate (lbs/yd^3) TXI Bridgeport, 1.5” Limestone	1,978	-
Fine Aggregate (lbs/yd^3) TXI Paradise	1,269	2,824
Retarder (oz/yd^3) Hunt Process HPSR	20.6	21.0
Air Entraining Agent (oz/yd^3) Hunt Process Air-Inxt	2.7	5.5
Field slump (inch)	2.0“	-
Field measured Air Content	4.8%	-
Field 7-day flexural strength (psi)	577 psi	-

Table A-17: Activation energy cube compressive strength results

Test Data - 8°C		**Test Data - 23°C**		**Test Data - 40°C**	
Age (hours)	**Strength (psi)**	**Age (hours)**	**Strength (psi)**	**Age (hours)**	**Strength (psi)**
23.8	349	18.0	863	16.1	1545
48.0	1024	40.7	1944	24.3	1832
96.1	1982	74.6	2564	47.9	2562
168.1	2740	142.3	3222	95.9	3102
336.6	3387	265.2	3728	143.8	3448
672.2	4025	528.4	4548	264.2	3912

Table A-18: Summary of Activation Energy analysis results

HYPERBOLIC STRENGTH GAIN			
Mix No:	6		
Description:	Dallas - September		
E =	**30,565**	J/mol	
T, (°K) =	281.0	295.8	311.0
1/T =	0.00356	0.00338	0.00322
ln(K) =	-4.72	-4.27	-3.45
Slope =	-3676.2		

EXPONENTIAL STRENGTH GAIN			
Mix No:	6		
Description:	Dallas - September		
E =	**40,790**	J/mol	
T, (°K) =	281.0	295.8	311.0
1/T =	0.00356	0.00338	0.00322
ln(K) =	-4.81	-3.95	-3.13
Slope =	-4905.9		

Curve Fit Parameters			
T, (°F) =	46.4	73.0	100.4
Su, psi =	4,668	4,982	4,260
K =	0.0089	0.0139	0.0317
to, hrs =	15.1	0.9	0.0

Curve Fit Parameters			
T, (°F) =	46.4	73.0	100.4
Su, psi =	4,922	5,750	4,955
τ, hrs =	123.32	51.72	22.89
β =	0.569	0.569	0.569

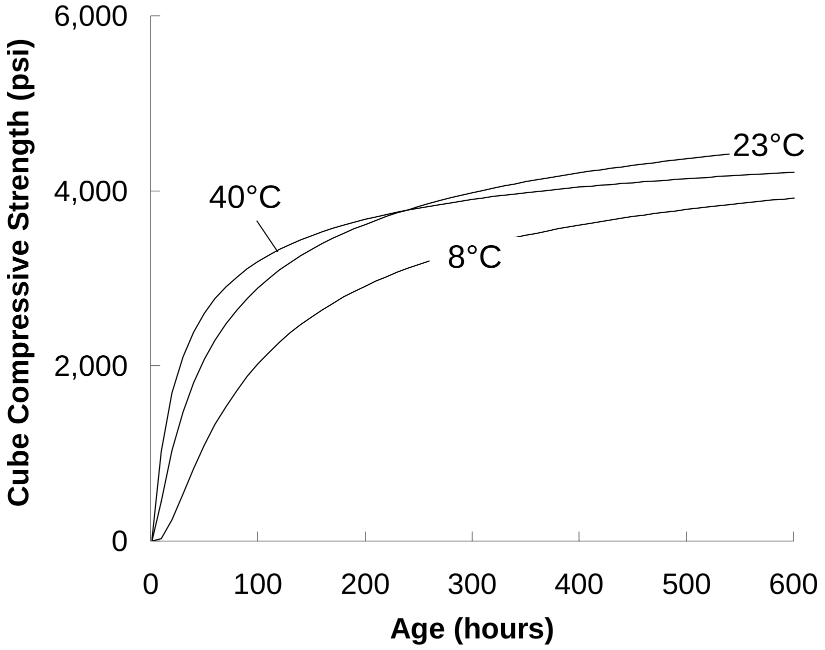

Figure A-14: Strength development over time at different curing temperatures

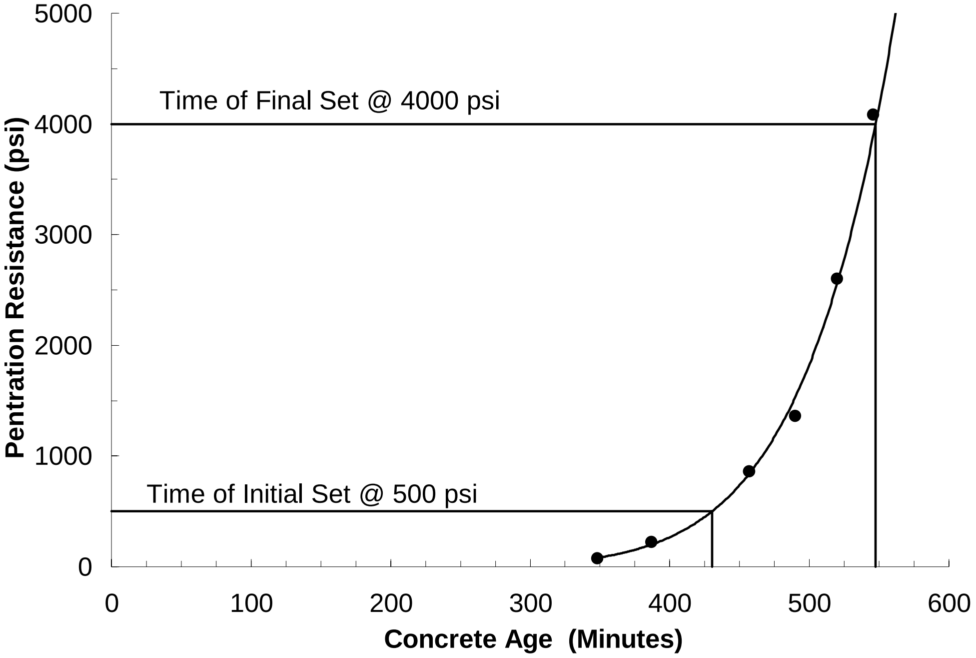

Figure A-15: ASTM C 403 setting times under **laboratory** conditions, Dallas, September

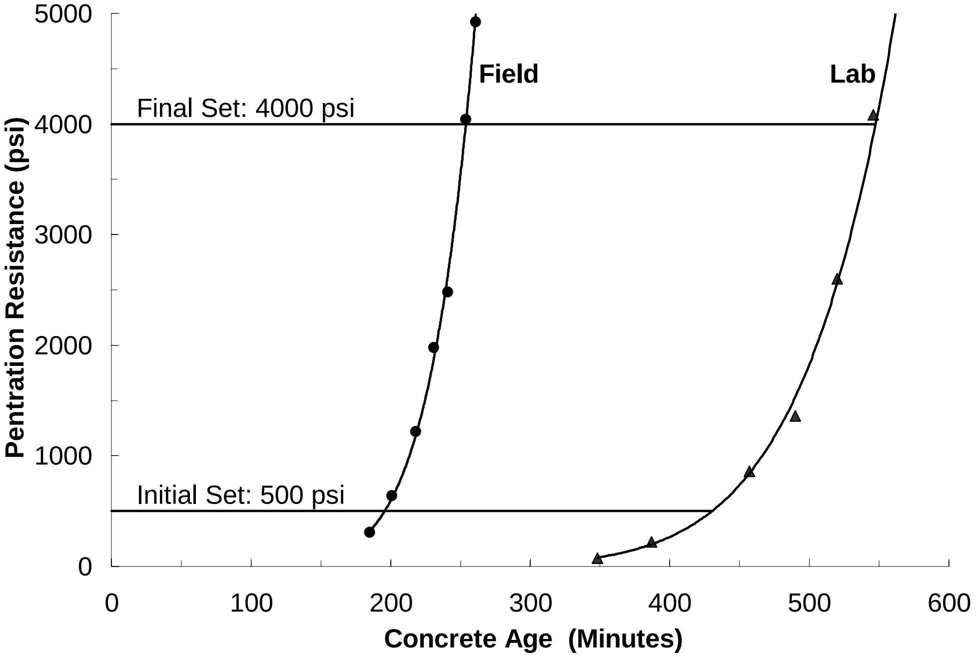

Figure A-16: ASTM C 403 setting times under **laboratory and field** conditions, Dallas, Sept.

Mixture No. 7

Description: Houston – October, Type I Cement + 25% Class C fly ash

Table A-19: Mixture proportions

Component	Concrete	Mortar
Cement (lbs/yd^3) Cemex (Tong Yang)	458	659
Class C fly ash (lbs/yd^3) W.A. Parish Unit #7	127	182
Water (lbs/yd^3) City Municiple	238	344
Coarse Aggregate (lbs/yd^3) 1.5” Redland Limestone Beckman	1,760	-
Fine Aggregate (lbs/yd^3) Cleveland Pit. DDS. Aggr. Inc.	1,259	2545
Retarder (oz/yd^3) Pozz. Master Builders 300R	14.0	13.8
Air Entraining Agent (oz/yd^3) Pave Air 90 MB	6.0	5.9
Field slump (inch)	1.0”“	-
Field measured Air Content	3.9%	-
Field 7-day flexural strength (psi)	660 psi	-

Table A-20: Activation energy cube compressive strength results

Test Data - 8°C		Test Data - 23°C		Test Data - 40°C	
Age (hours)	Strength (psi)	Age (hours)	Strength (psi)	Age (hours)	Strength (psi)
24.8	108	18.4	855	15.4	1468
48.1	569	39.7	1983	23.7	2229
96.6	1460	71.4	3190	47.5	3513
168.3	2726	143.9	4630	95.4	4692
335.8	3703	264.9	5706	143.4	5100
672.2	4880	527.2	6159	283.4	5481

Table A-21: Summary of Activation Energy analysis results

HYPERBOLIC STRENGTH GAIN			
Mix No:	7		
Description:	Houston - October		
E =	**46,854**	J/mol	
T, (°K) =	281.0	295.8	313.0
1/T =	0.00356	0.00338	0.00319
ln(K) =	-5.44	-4.34	-3.39
Slope =	-5635.2		

EXPONENTIAL STRENGTH GAIN			
Mix No:	7		
Description:	Houston - October		
E =	**41,254**	J/mol	
T, (°K) =	281.0	295.8	313.0
1/T =	0.00356	0.00338	0.00319
ln(K) =	-5.03	-3.96	-3.22
Slope =	-4961.8		

Curve Fit Parameters			
T, (°F) =	46.4	73.0	104.0
Su, psi =	6,594	7,214	6,145
K =	0.0043	0.0130	0.0337
to, hrs =	24.0	8.8	6.4

Curve Fit Parameters			
T, (°F) =	46.4	73.0	104.0
Su, psi =	6,998	7,200	6,207
τ, hrs =	152.20	52.45	24.96
β =	0.819	0.819	0.819

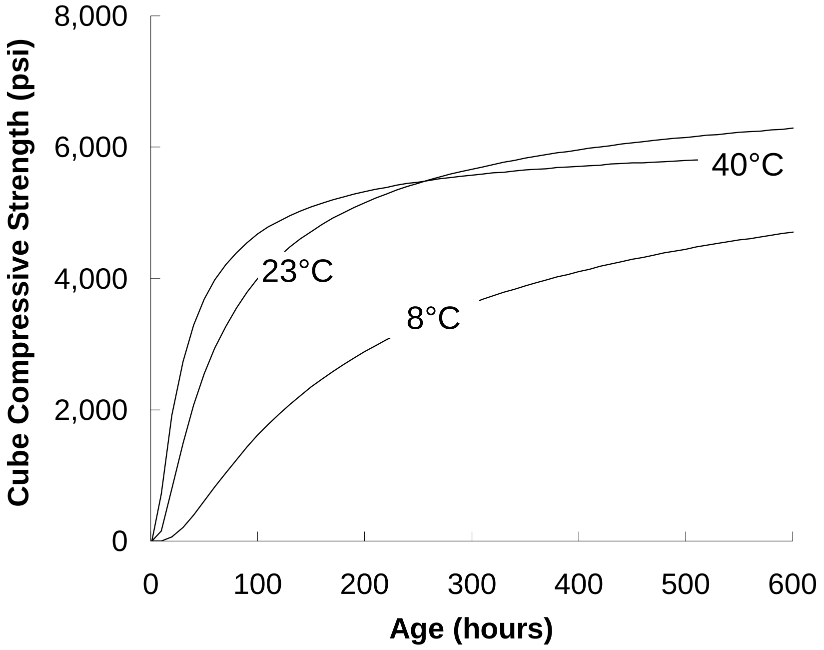

Figure A-17: Strength development over time at different curing temperatures

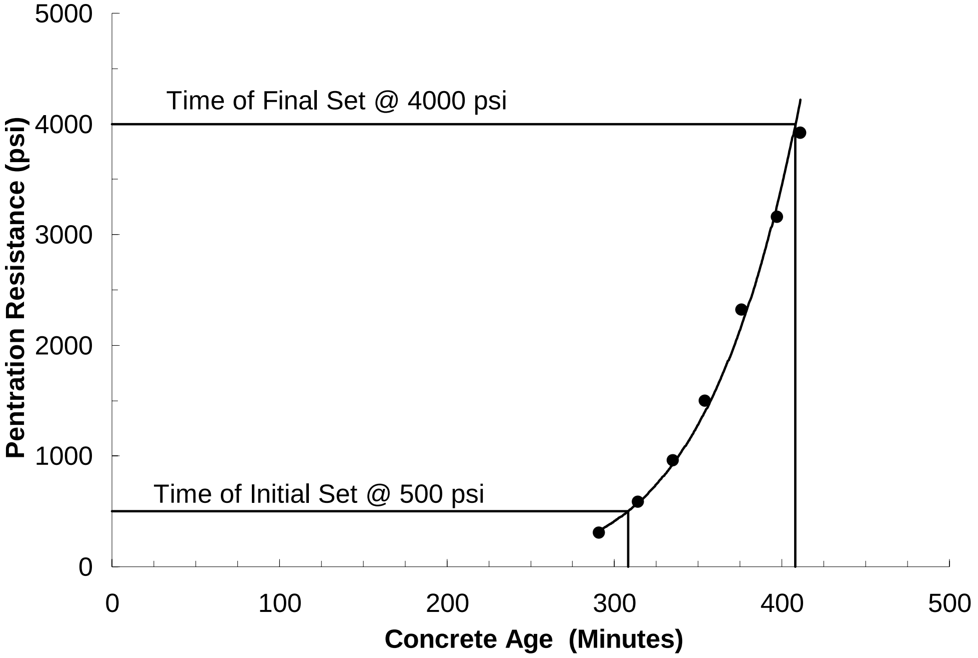

Figure A-18: ASTM C 403 setting times under **laboratory** conditions, Houston, October

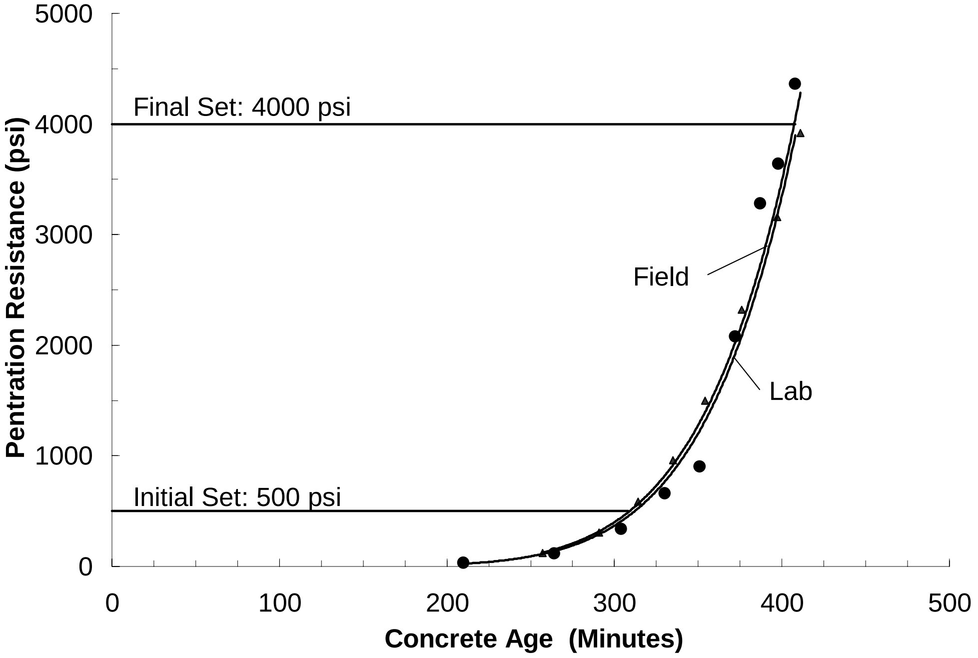

Figure A-19: ASTM C 403 setting times under **laboratory and field** conditions, Houston, Oct.

Mixture No. 8

Description: Hempstead, Type I Cement + 30% Class C fly ash

Table A-22: Mixture proportions

Component	Concrete	Mortar
Cement (lbs/yd^3) Texas Lehigh	362	546
Class C fly ash (lbs/yd^3) J.T. Deely, Boral Materials	155	234
Water (lbs/yd^3)	207	312
Coarse Aggregate (lbs/yd^3) Limstone - Capitol Aggregates	1,745	-
Fine Aggregate (lbs/yd^3) Capitol Aggregates	1,335	2,630
Retarder (oz/yd^3) Daratard 17	8	12
Air Entraining Agent (oz/yd^3) Daravair 1000 (oz/yd^3)	2	3
Field slump (inch)	2.0“	-
Field measured Air Content	5.0%	-
Field 7-day flexural strength (psi)	555 psi	-

Table A-23: Activation energy cube compressive strength results

Test Data - 8°C		Test Data - 23°C		Test Data - 40°C	
Age (hours)	**Strength (psi)**	**Age (hours)**	**Strength (psi)**	**Age (hours)**	**Strength (psi)**
23.2	115	22.7	1409	15.6	1875
48.2	885	47.8	2685	24.4	2536
96.4	1944	72.0	3935	49.0	3597
167.7	2833	143.8	4628	96.2	4536
336.9	3984	271.0	4856	144.5	5070
672.5	4783	528.6	5557	263.9	5589

Table A-24: Summary of Activation Energy analysis results

HYPERBOLIC STRENGTH GAIN			
Mix No:	8		
Description:	Hempstead - Limestone		
E =	**32,919**	J/mol	
T, (°K) =	281.0	295.8	313.0
1/T =	0.00356	0.00338	0.00319
ln(K) =	-5.08	-3.57	-3.63
	1.51		-0.06
Slope =	-3959.3		

EXPONENTIAL STRENGTH GAIN			
Mix No:	8		
Description:	Hempstead - Limestone		
E =	**36,459**	J/mol	
T, (°K) =	281.0	295.8	313.0
1/T =	0.00356	0.00338	0.00319
ln(K) =	-4.60	-3.48	-3.00
	1.11		0.49
Slope =	-4385.0		

Curve Fit Parameters			
T, (°F) =	46.4	73.0	104.0
Su, psi =	5,973	5,798	6,370
K =	0.0062	0.0282	0.0266
to, hrs =	20.1	11.7	0.0

Curve Fit Parameters			
T, (°F) =	46.4	73.0	104.0
Su, psi =	5,420	5,757	5,811
τ, hrs =	99.16	32.61	20.01
β =	1.001	1.001	1.001

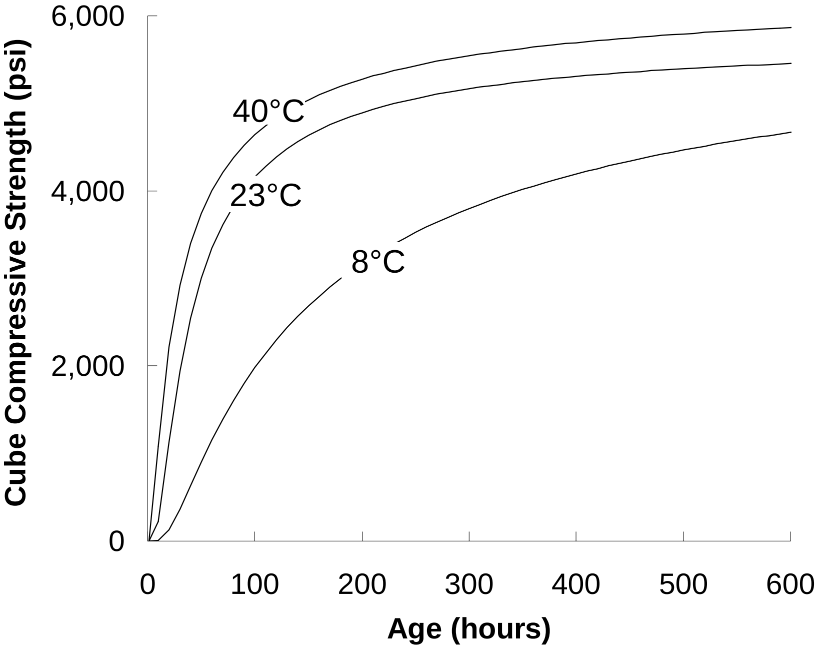

Figure A-20: Strength development over time at different curing temperatures

APPENDIX B

Data Collected During the Laboratory Testing Phase

Mixture No. 9

Description: Type I, Texas Lehigh Cement Company, Buda plant (April 2000)

Table B-1: Mixture proportions

Component	Concrete	Mortar
Cement (lbs/yd^3) Texas Lehigh	564	823
Water (lbs/yd^3)	207	302
Coarse Aggregate (lbs/yd^3) Limestone - Capitol Aggregates	1,825	-
Fine Aggregate (lbs/yd^3) Capitol Aggregates	1,250	2,664
Retarder (oz/yd^3) Daratard 17	8.0	8.2
Air Entraining Agent (oz/yd^3) Daravair 1000 (oz/yd^3)	2.0	2.0

Table B-2: Activation energy cube compressive strength results

Test Data - 8°C		Test Data - 23°C		Test Data - 40°C	
Age (hours)	Stress (psi)	Age (hours)	Stress (psi)	Age (hours)	Stress (psi)
23.3	832	18.3	2336	6.2	1038
47.9	2574	39.3	4018	23.6	2991
95.6	4075	71.1	4596	46.5	3210
167.7	5079	143.6	5244	115.0	3651
335.3	5947	264.4	6005	143.3	4187
671.8	6582	527.5	6370	263.5	4463

Table B-3: Summary of Activation Energy analysis results

HYPERBOLIC STRENGTH GAIN			
Mix ID:	1		
Description:	Cement Type I		
E =	**38,985**	J/mol	
T, (°K) =	281.0	295.8	311.0
1/T =	0.00356	0.00338	0.00322
ln(K) =	-4.09	-3.33	-2.48
Slope =	-4688.8		

EXPONENTIAL STRENGTH GAIN			
Mix ID:	1		
Description:	Cement Type I		
E =	**42,330**	J/mol	
T, (°K) =	281.0	295.8	311.0
1/T =	0.00356	0.00338	0.00322
ln(K) =	-4.11	-2.98	-2.37
Slope =	-5091.1		

Curve Fit Parameters			
T, (°F) =	46.4	73.0	100.4
Su, psi =	7,121	6,582	4,593
K =	0.0167	0.0359	0.0835
to, hrs =	15.1	2.1	2.6

Curve Fit Parameters			
T, (°F) =	46.4	73.0	100.4
Su, psi =	7,167	6,982	4,676
τ, hrs =	61.11	19.61	10.70
β =	0.700	0.700	0.700

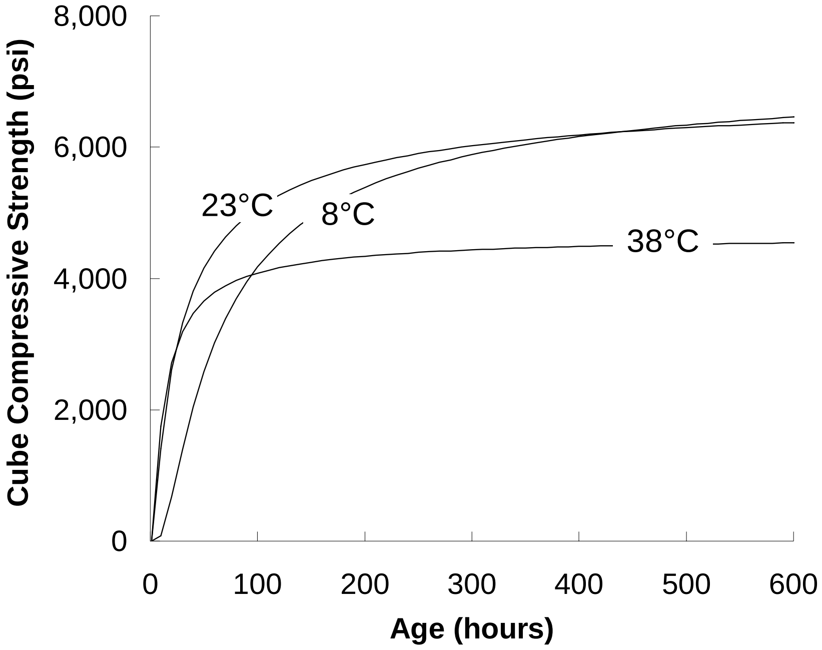

Figure B-1: Strength development over time at different curing temperatures

Mixture No. 10

Description: Type I + 15% Class C Fly Ash

Table B-4: Mixture proportions

Component	Concrete	Mortar
Cement (lbs/yd^3) Texas Lehigh	479	700
Class C fly ash (lbs/yd^3) J.T. Deely, Boral Materials	74	108
Water (lbs/yd^3)	207	302
Coarse Aggregate (lbs/yd^3) Limestone - Capitol Aggregates	1,825	-
Fine Aggregate (lbs/yd^3) Capitol Aggregates	1,250	2,664
Retarder (oz/yd^3) Daratard 17	8.0	8.2
Air Entraining Agent (oz/yd^3) Daravair 1000 (oz/yd^3)	2.0	2.0

Table B-5: Activation energy cube compressive strength results

Test Data - 8°C		Test Data - 23°C		Test Data - 40°C	
Age (hours)	Stress (psi)	Age (hours)	Stress (psi)	Age (hours)	Stress (psi)
24.1	520	16.6	2072	15.9	3188
51.8	2245	39.9	3902	43.2	4300
96.2	3268	72.0	4753	47.3	4524
167.8	4893	144.1	5515	94.4	5354
335.8	5785	264.0	6205	143.4	5648
672.6	6203	528.1	6514	263.4	5875

Table B-6: Summary of Activation Energy analysis results

HYPERBOLIC STRENGTH GAIN			
Mix ID:	2		
Description:	Type Class C FA - 15%		
E =	**36,953**	J/mol	
T, (°K) =	281.0	295.8	311.0
1/T =	0.00356	0.00338	0.00322
ln(K) =	-4.34	-3.37	-2.82
Slope =	-4444.4		

EXPONENTIAL STRENGTH GAIN			
Mix ID:	2		
Description:	Type Class C FA - 15%		
E =	**46,628**	J/mol	
T, (°K) =	281.0	295.8	311.0
1/T =	0.00356	0.00338	0.00322
ln(K) =	-4.31	-3.07	-2.39
Slope =	-5608.1		

Curve Fit Parameters			
T, (°F) =	46.4	73.0	100.4
Su, psi =	7,064	6,833	6,230
K =	0.0130	0.0343	0.0596
to, hrs =	18.0	3.6	0.0

Curve Fit Parameters			
T, (°F) =	46.4	73.0	100.4
Su, psi =	6,961	7,111	6,445
τ, hrs =	74.45	21.53	10.92
β =	0.760	0.760	0.760

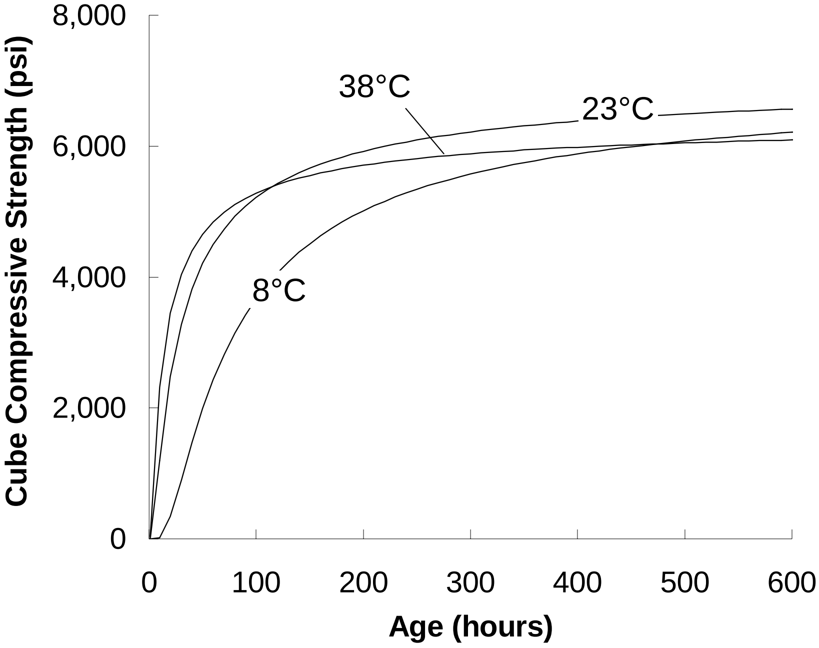

Figure B-2: Strength development over time at different curing temperatures

Mixture No.11

Description: Type I + 25% Class C Fly Ash

Table B-7: Mixture proportions

Component	Concrete	Mortar
Cement (lbs/yd^3) Texas Lehigh	423	617
Class C fly ash (lbs/yd^3) J.T. Deely, Boral Materials	123	180
Water (lbs/yd^3)	207	302
Coarse Aggregate (lbs/yd^3) Limestone - Capitol Aggregates	1,825	-
Fine Aggregate (lbs/yd^3) Capitol Aggregates	1,250	2,664
Retarder (oz/yd^3) Daratard 17	8.0	8.2
Air Entraining Agent (oz/yd^3) Daravair 1000 (oz/yd^3)	2.0	2.0

Table B-8: Activation energy cube compressive strength results

Test Data - 8°C		Test Data - 23°C		Test Data - 40°C	
Age (hours)	**Stress (psi)**	**Age (hours)**	**Stress (psi)**	**Age (hours)**	**Stress (psi)**
24.2	330	17.3	1830	15.6	2444
48.1	1760	40.0	3698	24.0	2947
96.0	3204	71.7	4974	47.9	4129
167.9	4932	144.5	5948	96.0	4801
336.4	5963	263.5	6812	144.6	5344
672.5	6891	528.3	7441	264.5	5913

Table B-9: Summary of Activation Energy analysis results

HYPERBOLIC STRENGTH GAIN			
Mix ID:	3		
Description:	Type Class C FA - 25%		
E =	**32,361**	J/mol	
T, (°K) =	281.0	295.8	311.0
1/T =	0.00356	0.00338	0.00322
ln(K) =	-4.63	-3.73	-3.30
Slope =	-3892.1		

EXPONENTIAL STRENGTH GAIN			
Mix ID:	3		
Description:	Type Class C FA - 25%		
E =	**44,249**	J/mol	
T, (°K) =	281.0	295.8	311.0
1/T =	0.00356	0.00338	0.00322
ln(K) =	-4.59	-3.43	-2.77
Slope =	-5322.0		

Curve Fit Parameters			
T, (°F) =	46.4	73.0	100.4
Su, psi =	7,988	7,937	6,307
K =	0.0097	0.0240	0.0368
to, hrs =	19.8	4.5	-1.6

Curve Fit Parameters			
T, (°F) =	46.4	73.0	100.4
Su, psi =	7,955	8,434	6,921
τ, hrs =	98.60	30.85	15.95
β =	0.718	0.718	0.718

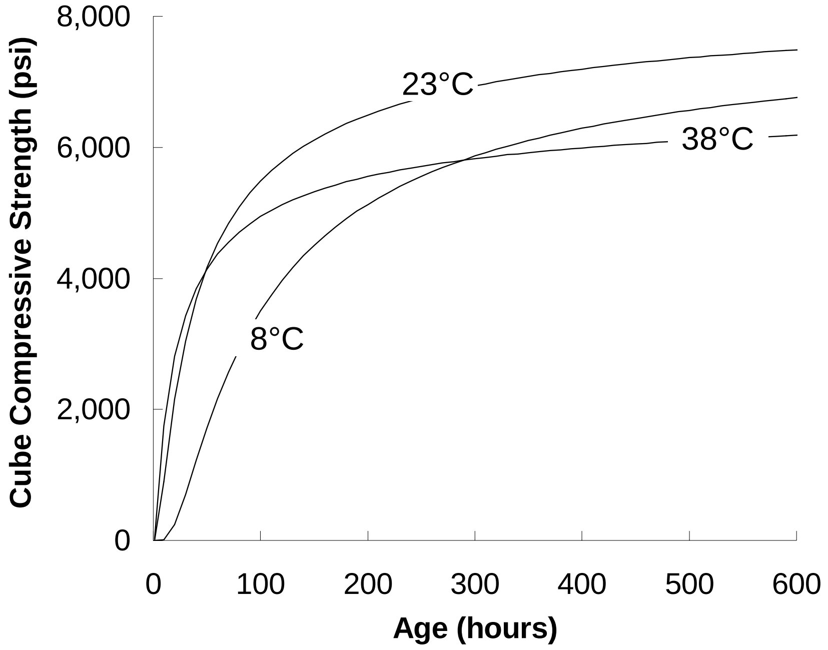

Figure B-3: **Strength development over time at different curing temperatures**

Mixture No. 12

Description: Type I + 35% Class C Fly Ash

Table B-10: Mixture proportions

Component	Concrete	Mortar
Cement (lbs/yd^3) Texas Lehigh	367	535
Class C fly ash (lbs/yd^3) J.T. Deely, Boral Materials	172	252
Water (lbs/yd^3)	207	302
Coarse Aggregate (lbs/yd^3) Limestone - Capitol Aggregates	1,825	-
Fine Aggregate (lbs/yd^3) Capitol Aggregates	1,250	2,664
Retarder (oz/yd^3) Daratard 17	8.0	8.2
Air Entraining Agent (oz/yd^3) Daravair 1000 (oz/yd^3)	2.0	2.0

Table B-11: Activation energy cube compressive strength results

Test Data - 8°C		Test Data - 23°C		Test Data - 40°C	
Age (hours)	Stress (psi)	Age (hours)	Stress (psi)	Age (hours)	Stress (psi)
23.6	161	15.7	1130	15.6	2036
47.8	1291	39.8	2831	23.9	2719
95.7	2575	71.5	4306	48.4	4035
168.0	4195	144.3	5448	95.7	5388
336.9	5113	264.4	6463	144.3	5741
672.0	6331	527.9	7330	264.2	6053

Table B-12: Summary of Activation Energy analysis results

HYPERBOLIC STRENGTH GAIN			
Mix ID:	4		
Description:	Type Class C FA - 35%		
E =	**34,976**	J/mol	
T, (°K) =	281.0	295.8	311.0
1/T =	0.00356	0.00338	0.00322
ln(K) =	-4.89	-4.15	-3.45
Slope =	-4206.6		

EXPONENTIAL STRENGTH GAIN			
Mix ID:	4		
Description:	Type Class C FA - 35%		
E =	**41,283**	J/mol	
T, (°K) =	281.0	295.8	311.0
1/T =	0.00356	0.00338	0.00322
ln(K) =	-4.89	-3.86	-3.18
Slope =	-4965.2		

Curve Fit Parameters			
T, (°F) =	46.4	73.0	100.4
Su, psi =	7,580	8,124	6,851
K =	0.0075	0.0158	0.0317
to, hrs =	20.9	5.4	2.6

Curve Fit Parameters			
T, (°F) =	46.4	73.0	100.4
Su, psi =	7,666	8,975	7,226
τ, hrs =	132.33	47.40	24.15
β =	0.654	0.654	0.654

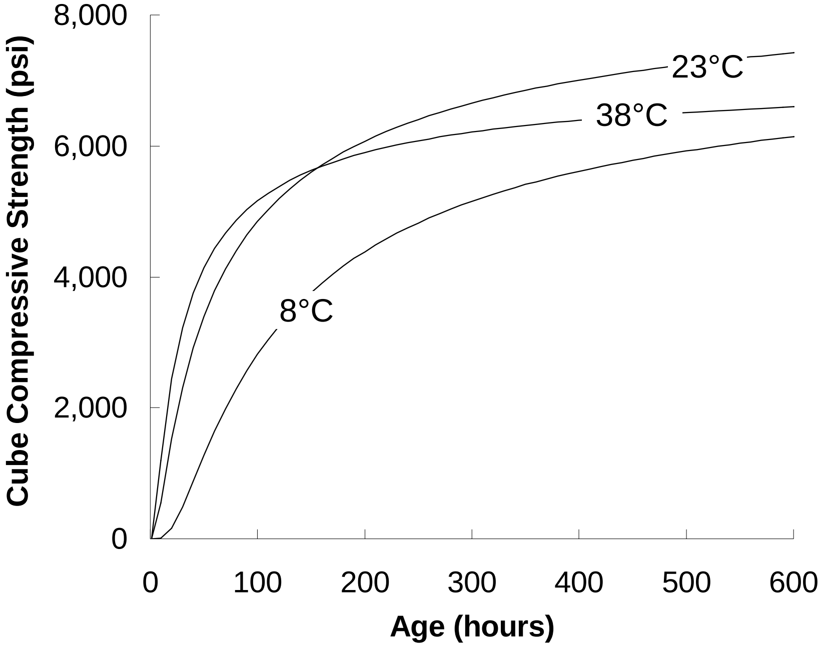

Figure B-4: **Strength development over time at different curing temperatures**

Mixture No. 13

Description: Type I + 45% Class C Fly Ash

Table B-13: Mixture proportions

Component	Concrete
Cement (lbs/yd^3) Texas Lehigh	310
Class C fly ash (lbs/yd^3) J.T. Deely, Boral Materials	222
Water (lbs/yd^3)	207
Coarse Aggregate (lbs/yd^3) Limestone - Capitol Aggregates	1,825
Fine Aggregate (lbs/yd^3) Capitol Aggregates	1,250
Retarder (oz/yd^3) Daratard 17	8.0
Air Entraining Agent (oz/yd^3) Daravair 1000 (oz/yd^3)	2.0

Mixture No. 14

Description: Type I + 15% Class F Fly Ash

Table B-14: Mixture proportions

Component	Concrete	Mortar
Cement (lbs/yd^3) Texas Lehigh	479	700
Class Ffly ash (lbs/yd^3) Rockdale, Materials	63	91
Water (lbs/yd^3)	207	302
Coarse Aggregate (lbs/yd^3) Limestone - Capitol Aggregates	1,825	-
Fine Aggregate (lbs/yd^3) Capitol Aggregates	1,250	2,664
Retarder (oz/yd^3) Daratard 17	8.0	8.2
Air Entraining Agent (oz/yd^3) Daravair 1000 (oz/yd^3)	2.0	2.0

Table B-15: Activation energy cube compressive strength results

Test Data - 8°C		**Test Data - 23°C**		**Test Data - 40°C**	
Age (hours)	**Stress (psi)**	**Age (hours)**	**Stress (psi)**	**Age (hours)**	**Stress (psi)**
23.5	510	16.0	1658	7.0	1255
47.6	1935	39.3	3372	23.4	2787
95.4	3434	72.3	3971	47.3	3440
167.5	4676	144.7	4416	96.0	3888
336.6	5253	264.6	4829	144.2	4225
671.9	6415	527.8	5172	272.8	4880

Table B-16: Summary of Activation Energy analysis results

HYPERBOLIC STRENGTH GAIN			
Mix ID:	5		
Description:	Type Class F FA - 15%		
E =	**42,470**	J/mol	
T, (°K) =	281.0	295.8	311.0
1/T =	0.00356	0.00338	0.00322
ln(K) =	-4.32	-3.02	-2.58
Slope =	-5108.0		

EXPONENTIAL STRENGTH GAIN			
Mix ID:	5		
Description:	Type Class F FA - 15%		
E =	**47,003**	J/mol	
T, (°K) =	281.0	295.8	311.0
1/T =	0.00356	0.00338	0.00322
ln(K) =	-4.16	-2.92	-2.22
Slope =	-5653.2		

Curve Fit Parameters			
T, (°F) =	46.4	73.0	100.4
Su, psi =	6,802	5,258	5,614
K =	0.0132	0.0489	0.0757
to, hrs =	17.4	6.4	0.0

Curve Fit Parameters			
T, (°F) =	46.4	73.0	100.4
Su, psi =	6,800	5,334	5,637
τ, hrs =	63.84	18.49	9.22
β =	0.904	0.904	0.904

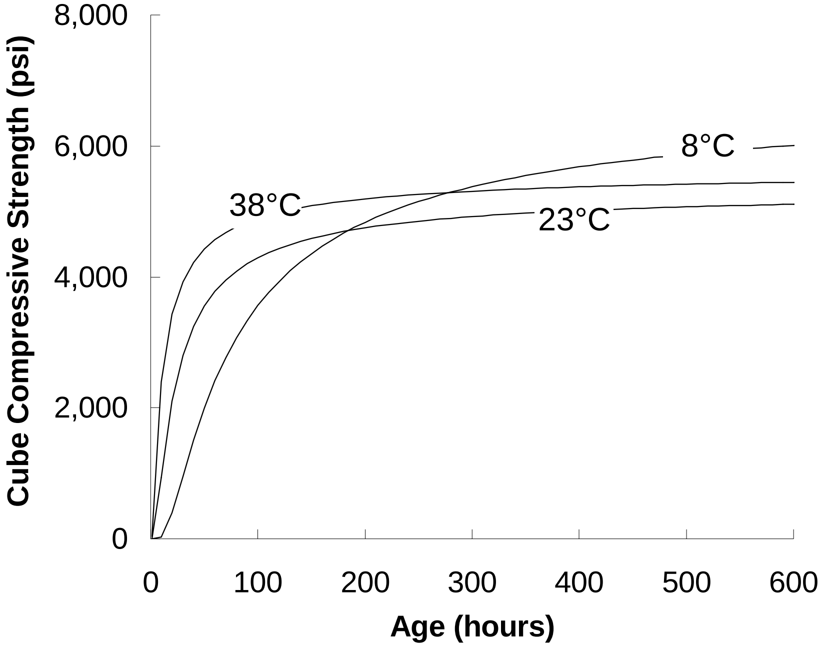

Figure B-5: **Strength development over time at different curing temperatures**

Mixture No. 15

Description: Type I + 25% Class F Fly Ash

Table B-17: Mixture proportions

Component	Concrete	Mortar
Cement (lbs/yd^3) Texas Lehigh	423	617
Class Ffly ash (lbs/yd^3) Rockdale, Materials	104	152
Water (lbs/yd^3)	207	302
Coarse Aggregate (lbs/yd^3) Limestone - Capitol Aggregates	1,825	-
Fine Aggregate (lbs/yd^3) Capitol Aggregates	1,250	2,664
Retarder (oz/yd^3) Daratard 17	8.0	8.2
Air Entraining Agent (oz/yd^3) Daravair 1000 (oz/yd^3)	2.0	2.0

Table B-18: Activation energy cube compressive strength results

Test Data - 8°C		Test Data - 23°C		Test Data - 40°C	
Age (hours)	Stress (psi)	Age (hours)	Stress (psi)	Age (hours)	Stress (psi)
23.8	323	15.6	1255	14.8	2764
47.4	1361	40.2	2995	22.7	3316
96.2	2713	73.9	3875	47.3	4061
168.0	3702	143.7	4555	97.1	5094
335.8	4675	264.7	5274	139.3	5516
671.5	5661	528.6	5983	264.3	6101

Table B-19: Summary of Activation Energy analysis results

HYPERBOLIC STRENGTH GAIN			
Mix ID:	7		
Description:	Type Class F FA - 25%		
E =	**39,731**	J/mol	
T, (°K) =	281.0	295.8	311.0
1/T =	0.00356	0.00338	0.00322
ln(K) =	-4.74	-3.81	-3.10
Slope =	-4778.5		

EXPONENTIAL STRENGTH GAIN			
Mix ID:	7		
Description:	Type Class F FA - 25%		
E =	**42,264**	J/mol	
T, (°K) =	281.0	295.8	311.0
1/T =	0.00356	0.00338	0.00322
ln(K) =	-4.45	-3.52	-2.71
Slope =	-5083.2		

Curve Fit Parameters			
T, (°F) =	46.4	73.0	100.4
Su, psi =	6,514	6,302	6,401
K =	0.0088	0.0222	0.0451
to, hrs =	17.5	3.6	0.0

Curve Fit Parameters			
T, (°F) =	46.4	73.0	100.4
Su, psi =	6,841	6,964	7,008
τ, hrs =	85.68	33.63	14.97
β =	0.645	0.645	0.645

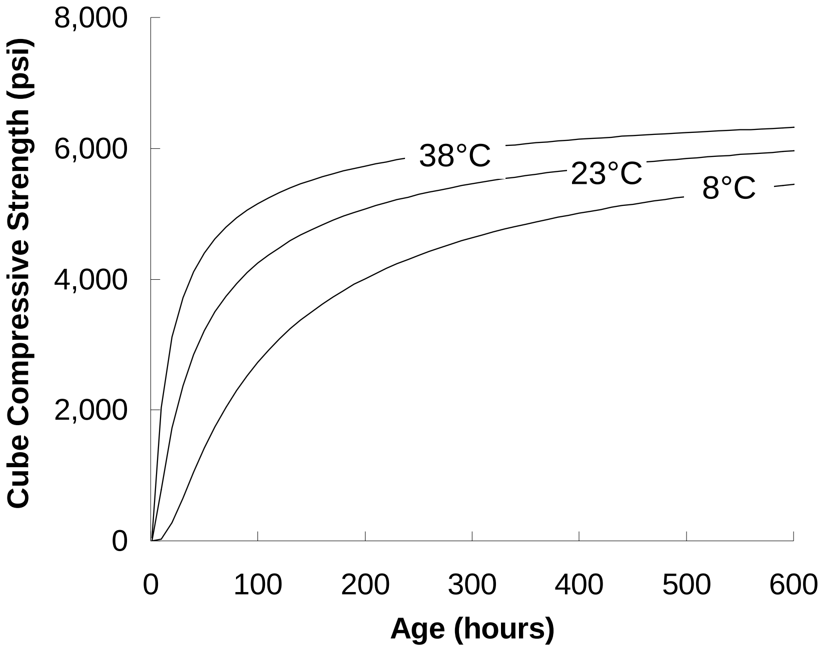

Figure B-6: **Strength development over time at different curing temperatures**

Mixture No. 16

Description: Type I + 35% Class F Fly Ash

Table B-20: Mixture proportions

Component	Concrete	Mortar
Cement (lbs/yd^3) Texas Lehigh	367	535
Class F fly ash (lbs/yd^3) Rockdale, Materials	146	213
Water (lbs/yd^3)	207	302
Coarse Aggregate (lbs/yd^3) Limestone - Capitol Aggregates	1,825	-
Fine Aggregate (lbs/yd^3) Capitol Aggregates	1,250	2,664
Retarder (oz/yd^3) Daratard 17	8.0	8.2
Air Entraining Agent (oz/yd^3) Daravair 1000 (oz/yd^3)	2.0	2.0

Table B-21: Activation energy cube compressive strength results

Test Data - 8°C		Test Data - 23°C		Test Data - 40°C	
Age (hours)	Stress (psi)	Age (hours)	Stress (psi)	Age (hours)	Stress (psi)
23.9	255	15.9	863	14.7	2020
48.4	1119	39.8	2506	23.5	2645
96.8	2317	72.6	3248	47.8	3500
167.7	3390	144.4	4053	96.9	4380
335.7	3990	264.4	4707	144.0	4835
671.4	4859	528.0	5630	263.8	5187

Table B-22: Summary of Activation Energy analysis results

HYPERBOLIC STRENGTH GAIN			
Mix ID:	8		
Description:	Type Class F FA - 35%		
E =	**32,556**	J/mol	
T, (°K) =	281.0	295.8	311.0
1/T =	0.00356	0.00338	0.00322
ln(K) =	-4.68	-4.07	-3.34
Slope =	-3915.6		

EXPONENTIAL STRENGTH GAIN			
Mix ID:	8		
Description:	Type Class F FA - 35%		
E =	**45,017**	J/mol	
T, (°K) =	281.0	295.8	311.0
1/T =	0.00356	0.00338	0.00322
ln(K) =	-4.83	-3.86	-2.97
Slope =	-5414.3		

Curve Fit Parameters			
T, (°F) =	46.4	73.0	100.4
Su, psi =	5,586	6,005	5,716
K =	0.0093	0.0171	0.0356
to, hrs =	19.3	4.5	0.0

Curve Fit Parameters			
T, (°F) =	46.4	73.0	100.4
Su, psi =	5,598	6,964	6,500
τ, hrs =	125.39	47.37	19.55
β =	0.596	0.596	0.596

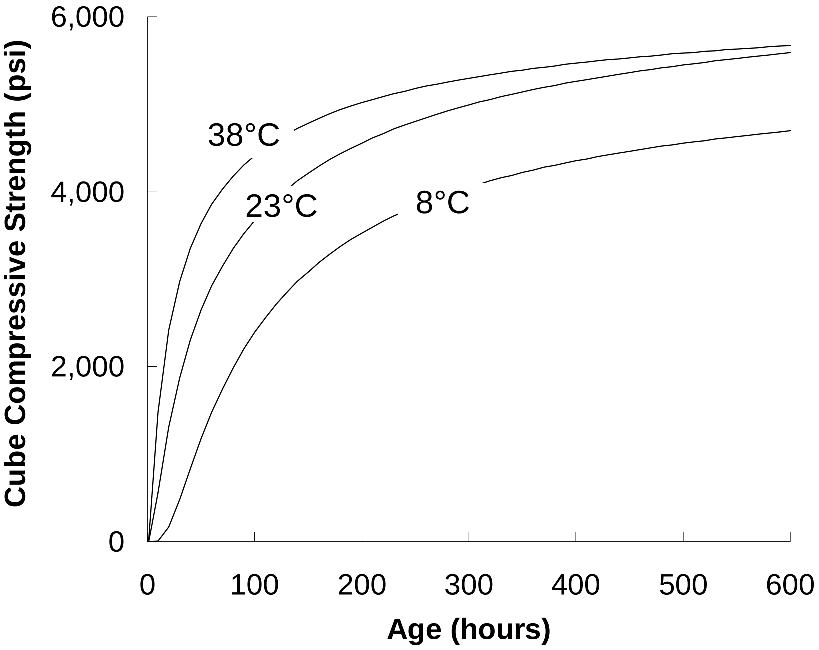

Figure B-7: **Strength development over time at different curing temperatures**

1.

Mixture No. 17

Description: Type I + 45% Class F Fly Ash

Table B-23: Mixture proportions

Component	Concrete
Cement (lbs/yd^3) Texas Lehigh	310
Class F fly ash (lbs/yd^3) Rockdale, Materials	188
Water (lbs/yd^3)	207
Coarse Aggregate (lbs/yd^3) Limestone - Capitol Aggregates	1,825
Fine Aggregate (lbs/yd^3) Capitol Aggregates	1,250
Retarder (oz/yd^3) Daratard 17	8.0
Air Entraining Agent (oz/yd^3) Daravair 1000 (oz/yd^3)	2.0

Mixture No. 18

Description: Type I + 30% GGBF Slag

Table B-24: Mixture proportions

Component	Concrete	Mortar
Cement (lbs/yd^3) Texas Lehigh	395	576
GGBF Slag (lbs/yd^3) Lone Star Industries	156	228
Water (lbs/yd^3)	207	302
Coarse Aggregate (lbs/yd^3) Limestone - Capitol Aggregates	1,825	-
Fine Aggregate (lbs/yd^3) Capitol Aggregates	1,250	2,664
Retarder (oz/yd^3) Daratard 17	8.0	8.2
Air Entraining Agent (oz/yd^3) Daravair 1000 (oz/yd^3)	2.0	2.0

Table B-25: Activation energy cube compressive strength results

Test Data - 8°C		Test Data - 23°C		Test Data - 40°C	
Age (hours)	**Stress (psi)**	**Age (hours)**	**Stress (psi)**	**Age (hours)**	**Stress (psi)**
24.7	473	16.0	1300	14.7	2392
48.1	1438	40.7	2640	23.5	3038
96.0	2556	73.9	3707	47.8	3899
167.7	4115	143.9	4590	96.9	4801
336.7	4813	264.2	5390	144.0	5468
672.0	5382	527.4	6500	263.8	6001

Table B-26: Summary of Activation Energy analysis results

HYPERBOLIC STRENGTH GAIN			
Mix ID:	10		
Description:	GGBF Slag - 30%		
E =	**31,964**	J/mol	
T, (°K) =	281.0	295.8	311.0
1/T =	0.00356	0.00338	0.00322
ln(K) =	-4.66	-4.29	-3.33
Slope =	-3844.4		

EXPONENTIAL STRENGTH GAIN			
Mix ID:	10		
Description:	GGBF Slag - 30%		
E =	**33,415**	J/mol	
T, (°K) =	281.0	295.8	311.0
1/T =	0.00356	0.00338	0.00322
ln(K) =	-4.42	-3.63	-3.04
Slope =	-4018.9		

Curve Fit Parameters			
T, (°F) =	46.4	73.0	100.4
Su, psi =	6,451	7,164	6,468
K =	0.0095	0.0136	0.0357
to, hrs =	17.1	0.0	0.0

Curve Fit Parameters			
T, (°F) =	46.4	73.0	100.4
Su, psi =	6,450	9,778	6,812
τ, hrs =	82.74	37.60	20.86
β =	1.003	1.003	1.003

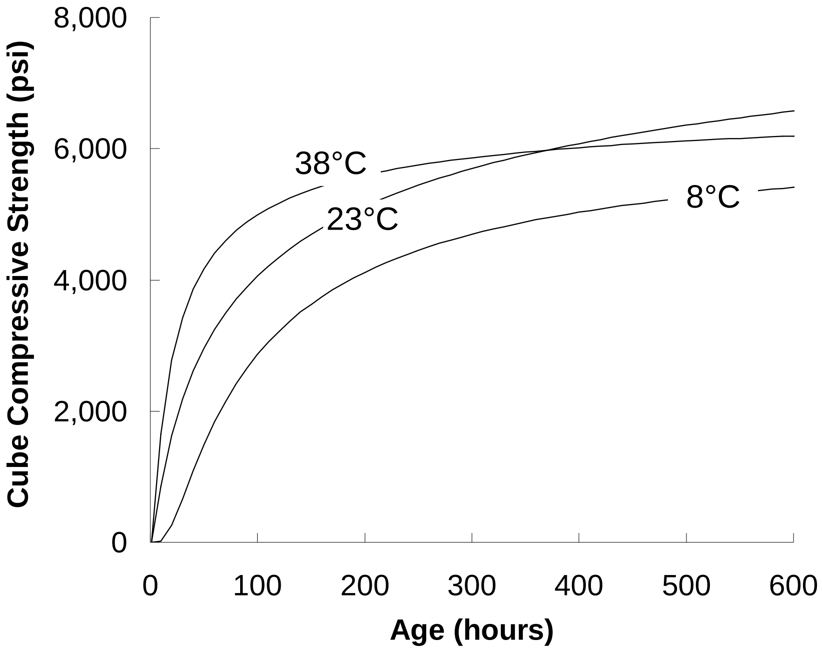

Figure B-8: **Strength development over time at different curing temperatures**

Mixture No. 19

Description: Type I + 50% GGBF Slag

Table B-27: Mixture proportions

Component	**Concrete**	**Mortar**
Cement (lbs/yd^3) Texas Lehigh	282	411
GGBF Slag (lbs/yd^3) Lone Star Industries	261	380
Water (lbs/yd^3)	207	302
Coarse Aggregate (lbs/yd^3) Limestone - Capitol Aggregates	1,825	-
Fine Aggregate (lbs/yd^3) Capitol Aggregates	1,250	2,664
Retarder (oz/yd^3) Daratard 17	8.0	8.2
Air Entraining Agent (oz/yd^3) Daravair 1000 (oz/yd^3)	2.0	2.0

Table B-28: Activation energy cube compressive strength results

Test Data - 8°C		**Test Data - 23°C**		**Test Data - 40°C**	
Age (hours)	**Stress (psi)**	**Age (hours)**	**Stress (psi)**	**Age (hours)**	**Stress (psi)**
23.2	351	15.4	789	14.4	1489
48.3	1095	39.8	1905	23.4	2117
95.3	1891	71.9	3013	47.9	3185
167.3	2476	143.4	4341	95.8	4017
335.3	3336	328.0	5656	142.6	4386
671.4	4466	528.6	6436	327.2	5180

Table B-29: Summary of Activation Energy analysis results

HYPERBOLIC STRENGTH GAIN			
Mix ID:	11		
Description:	GGBF Slag - 50%		
E =	**39,415**	J/mol	
T, (°K) =	281.0	295.8	310.2
1/T =	0.00356	0.00338	0.00322
ln(K) =	-5.30	-4.69	-3.70
Slope =	-4740.6		

EXPONENTIAL STRENGTH GAIN			
Mix ID:	11		
Description:	GGBF Slag - 50%		
E =	**43,374**	J/mol	
T, (°K) =	281.0	295.8	310.2
1/T =	0.00356	0.00338	0.00322
ln(K) =	-5.28	-4.62	-3.52
Slope =	-5216.8		

Curve Fit Parameters			
T, (°F) =	46.4	73.0	99.0
Su, psi =	5,692	7,692	5,750
K =	0.0050	0.0092	0.0247
to, hrs =	5.7	3.0	0.0

Curve Fit Parameters			
T, (°F) =	46.4	73.0	99.0
Su, psi =	8,682	9,915	6,555
τ, hrs =	196.41	101.71	33.83
β =	0.507	0.507	0.507

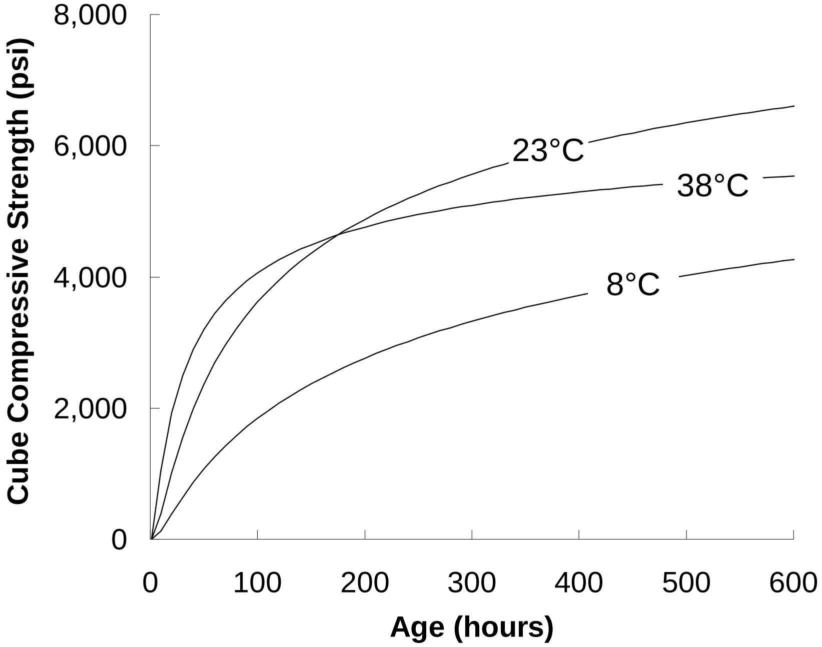

Figure B-9: **Strength development over time at different curing temperatures**

Mixture No. 20

Description: Capitol Type I Cement

Table B-30: Mixture proportions

Component	Concrete	Mortar
Cement (lbs/yd^3) Texas Lehigh	517	734
Water (lbs/yd^3)	259	367
Coarse Aggregate (lbs/yd^3) Limestone - Capitol Aggregates	1,809	-
Fine Aggregate (lbs/yd^3) Capitol Aggregates	1,250	2569
Retarder (oz/yd^3) Daratard 17	8.0	8.2
Air Entraining Agent (oz/yd^3) Daravair 1000 (oz/yd^3)	2.0	2.0

Table B-31: Activation energy cube compressive strength results

Test Data - 8°C		Test Data - 23°C		Test Data - 40°C	
Age (hours)	Stress (psi)	Age (hours)	Stress (psi)	Age (hours)	Stress (psi)
18.8	170	6.5	125	7.9	1244
48.0	1679	24.4	2060	23.5	3199
96.0	3162	73.4	4018	48.5	4024
167.9	4551	144.8	5261	94.3	5112
336.0	5333	264.3	5799	143.5	5280
671.3	6247	529.0	6318	263.6	5559

Table B-32: Summary of Activation Energy analysis results

HYPERBOLIC STRENGTH GAIN			
Mix ID:	13		
Description:	Capitol - Type I		
E =	**34,938**	J/mol	
T, (°K) =	281.0	295.8	313.0
1/T =	0.00356	0.00338	0.00319
ln(K) =	-4.49	-3.81	-2.97
Slope =	-4202.0		

EXPONENTIAL STRENGTH GAIN			
Mix ID:	13		
Description:	Capitol - Type I		
E =	**38,147**	J/mol	
T, (°K) =	281.0	295.8	313.0
1/T =	0.00356	0.00338	0.00319
ln(K) =	-4.36	-3.51	-2.69
Slope =	-4588.1		

Curve Fit Parameters			
T, (°F) =	46.4	73.0	104.0
Su, psi =	6,910	6,856	6,011
K =	0.0112	0.0221	0.0515
to, hrs =	17.2	5.6	2.8

Curve Fit Parameters			
T, (°F) =	46.4	73.0	104.0
Su, psi =	6,708	7,103	6,240
τ, hrs =	78.38	33.31	14.76
β =	0.778	0.778	0.778

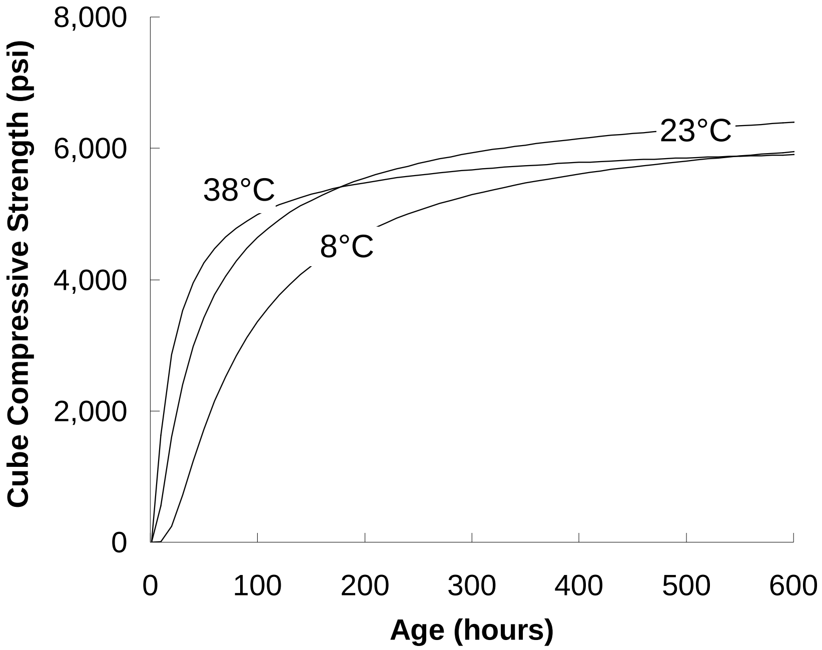

Figure B-10: **Strength development over time at different curing temperatures**

Mixture No. 21

Description: Alamo Type I Cement

Table B-33: Mixture proportions

Component	Concrete	Mortar
Cement (lbs/yd^3) Texas Lehigh	517	734
Water (lbs/yd^3)	259	367
Coarse Aggregate (lbs/yd^3) Limestone - Capitol Aggregates	1,809	-
Fine Aggregate (lbs/yd^3) Capitol Aggregates	1,250	2569
Retarder (oz/yd^3) Daratard 17	8.0	8.2
Air Entraining Agent (oz/yd^3) Daravair 1000 (oz/yd^3)	2.0	2.0

Table B-34: Activation energy cube compressive strength results

Test Data - 8°C		Test Data - 23°C		Test Data - 40°C	
Age (hours)	Stress (psi)	Age (hours)	Stress (psi)	Age (hours)	Stress (psi)
23.3	832	18.3	2336	6.2	1038
47.9	2574	39.3	4018	23.6	2991
95.6	4075	71.1	4596	46.5	3210
167.7	5079	143.6	5244	115.0	3651
335.3	5947	264.4	6005	143.3	4187
671.8	6582	527.5	6370	263.5	4463

Table B-35: Summary of Activation Energy analysis results

HYPERBOLIC STRENGTH GAIN

Mix ID:	16		
Description:	Alamo Type I		
E =	**25,215**	J/mol	
T, (°K) =	281.0	295.8	313.0
1/T =	0.00356	0.00338	0.00319
ln(K) =	-3.89	-3.23	-2.78
Slope =	-3032.7		

EXPONENTIAL STRENGTH GAIN

Mix ID:	16		
Description:	Alamo Type I		
E =	**39,221**	J/mol	
T, (°K) =	281.0	295.8	313.0
1/T =	0.00356	0.00338	0.00319
ln(K) =	-3.95	-3.06	-2.24
Slope =	-4717.2		

Curve Fit Parameters

T, (°F) =	46.4	73.0	104.0
Su, psi =	7,516	6,864	5,323
K =	0.0205	0.0394	0.0618
to, hrs =	18.6	5.9	0.2

Curve Fit Parameters

T, (°F) =	46.4	73.0	104.0
Su, psi =	7,283	6,972	5,743
τ, hrs =	52.08	21.42	9.35
β =	0.882	0.882	0.882

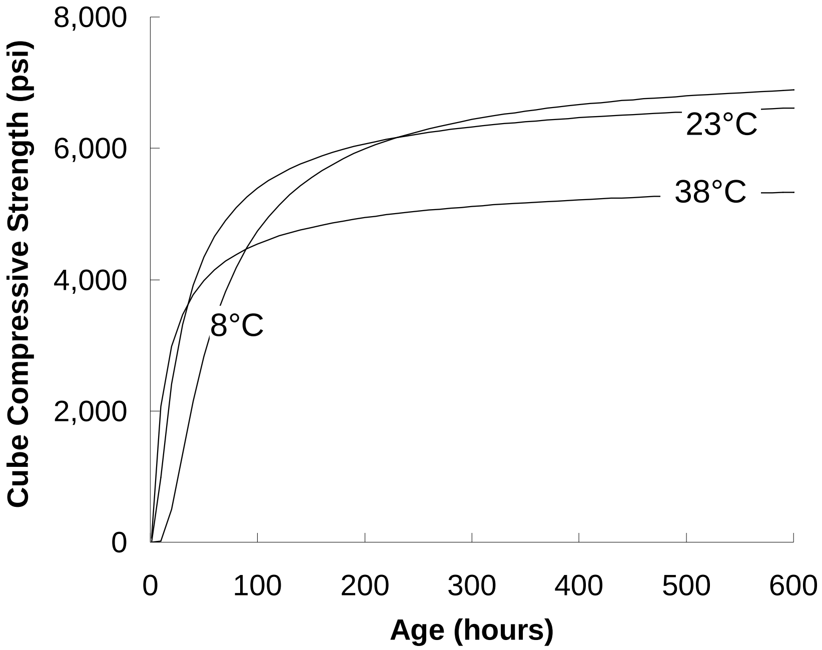

Figure B-11: **Strength development over time at different curing temperatures**

APPENDIX C

Statistical Analysis Results

APPENDIX C - PART I

SAS Inputs and Outputs for the Activation Energy Model

1. ANOVA analysis on Variables:

- **SAS Program:**

```
data transform; set lerch;
        lc3s=log(c3s); lc3a=log(c3a); lcao=log(cao); lc2s=log(c2s);
        lc4af=log(c4af); lso3=log(so3);  mgo=log(mgo); lnaequ=log(naequ);
        lblaine=log(blaine); lae=log(E);
run;
proc rsquare c;
        model lae = lc3s lc3a lcao lblaine lc2s lc4af lso3 lmgo lnaequ
        /select=6 stop=6;
run;
```

- **Analysis Results:**

The SAS System: The RSQUARE Procedure: R-Square Selection Method

```
  Dependent Variable: log(E)

 Number in Model      R^2     Variables in Model
               1   0.4084   lc3a
               1   0.3235   lc2s
               1   0.3127   lso3
               1   0.2514   lblaine
               1   0.1501   lc3s
               1   0.1271   lcao
               1   0.0868   lc4af
               1   0.0457   lnaequ
               1   0.0370   lmgo
          ------------------------------------------------------------------------
               2   0.5864   lc3a lnaequ
               2   0.5668   lc3a lblaine
               2   0.5583   lc3a lso3
               2   0.4953   lc3a lcao
               2   0.4827   lc3a lc2s
               2   0.4817   lc2s lso3
          ------------------------------------------------------------------------
               3   0.7631   lc3a lcao lnaequ
               3   0.7164   lc3a lblaine lnaequ
               3   0.6965   lc3a lc2s lnaequ
               3   0.6783   lc3a lblaine lc4af
               3   0.6622   lc3a lso3 lnaequ
               3   0.6256   lc2s lc4af lnaequ
          ------------------------------------------------------------------------
               4   0.7890   lc3a lcao lso3 lnaequ
               4   0.7796   lc3a lcao lblaine lnaequ
               4   0.7715   lc3a lcao lc2s lnaequ
               4   0.7657   lc3s lc3a lcao lnaequ
```

```
      4      0.7631    lc3a lcao lmgo lnaequ
      4      0.7631    lc3a lcao lc4af lnaequ
------------------------------------------------------------------------
      5      0.8099    lc3s lc3a lcao lc2s lnaequ
      5      0.7947    lc3a lcao lc2s lso3 lnaequ
      5      0.7899    lc3a lcao lblaine lso3 lnaequ
      5      0.7892    lc3a lcao lc4af lso3 lnaequ
      5      0.7890    lc3s lc3a lcao lso3 lnaequ
      5      0.7890    lc3a lcao lso3 lmgo lnaequ
------------------------------------------------------------------------
```

2. General Linear Model (GLM) Development

- **SAS Program:**

```
data transform; set lerch;
        lc3s=log(c3s); lc3a=log(c3a); lcao=log(cao); lc2s=log(c2s);
        lc4af=log(c4af); lso3=log(so3);  mgo=log(mgo); lnaequ=log(naequ);
        lblaine=log(blaine); lae=log(aemean);
run;
proc glm;
        model lae=lc3a lblaine lc4af /solution;
        output out=test p=pred r=resid stdr=eresid;
run;
proc gplot;
        plot pred*lae resid*pred eresid*pred;
run;
```

- **Analysis Results:**

The SAS System: The GLM Procedure

```
Number of observations    20
Dependent Variable: log(E)

Source              DF    Sum of Squares    Mean Square    F Value    Pr > F
Model                3      0.15035428       0.05011809    11.25      0.0003
Error               16      0.07129885       0.00445618
Corrected Total     19      0.22165313

R-Square      Coeff Var     Root MSE     log(E) Mean
0.678331      0.624341      0.066755     10.69201

Source          DF     Type I SS     Mean Square    F Value    Pr > F
lc3a             1    0.09052694    0.09052694     20.31     0.0004
lblaine          1    0.03509865    0.03509865      7.88     0.0127
lc4af            1    0.02472869    0.02472869      5.55     0.0316

Source          DF    Type III SS    Mean Square    F Value    Pr > F
lc3a             1    0.08761364    0.08761364     19.66      0.0004
lblaine          1    0.04498239    0.04498239     10.09      0.0059
lc4af            1    0.02472869    0.02472869      5.55      0.0316

 Parameter      Estimate          Standard Error    t Value        Pr > |t|
```

```
Intercept      10.08442359     0.55244299      18.25        <.0001
lc3a           0.22475318      0.05068754       4.43        0.0004
lblaine        0.27270382      0.08583239       3.18        0.0059
lc4af          0.17543114      0.07447103       2.36        0.0316
```

3. Final Lon-Linear Model (NLIN) Development

- **SAS Program:**

```
data temp; set lerchDOH;
        tc=(temp-32)/1.8;
run;
proc nlin;
        parms C1=0.30 C2=0.25 C3=0.35 C4=7.587;
        E=c3a**C1*c4af**c2*blaine**C3*exp(C4);
        /*parms C5=0.35;  */
        /*E=c3a**0.30*c4af**0.25*blaine**c5*(22100);*/
        model alpha =exp(-(tau/(exp(-(E)/8.3144*(1/(tc+273)-
        0.0034))*time))**beta);
        output out=good p=predict r=resid stdr=eresid;
run;
proc gplot;
        plot alpha*predicted resid*predicted resid*alpha
        resid*c3a resid*c4af resid*blaine;
run;
```

- **Analysis Results:**

The SAS System: The NLIN Procedure

Dependent Variable = alpha = degree of hydration
Method: Gauss-Newton

```
Iterative Phase
   Iter      C1         C2         C3         C4      Sum of Squares
     0     0.3000     0.2500     0.3500     7.5870      6.6441
     1     0.0661     0.1176     0.4201     8.7253      0.4385
     2     0.2596     0.2346     0.3369     9.9460      0.3966
     3     0.2802     0.2523     0.3365    10.0392      0.3963
     4     0.2800     0.2521     0.3366    10.0374      0.3963
   NOTE: Convergence criterion met.
```

```
             Estimation Summary
Method                  Gauss-Newton
Iterations                   4
Subiterations                2
Average Subiterations       0.5
R                            4.346E-6
PPC(C2)                      0.000011
RPC(C2)                      0.000696
Object                       5.125E-8
Objective                    0.396316
Observations Read             420
```

```
                 Observations Used         420
                 Observations Missing        0
Source            DF    Sum of Squares   Mean Square   F Value   Approx Pr>F
Regression         4           61.0818       15.2705   16028.9       <.0001
Residual         416            0.3963      0.000953
Uncorrected Total 420          61.4781
Corrected Total  419           20.0616
```

```
Parameter     Estimate   Approx Std Error    Approximate 95% Confidence Limits
         C1     0.2800     0.0506                      0.1806          0.3794
         C2     0.2521     0.0723                      0.1100          0.3942
         C3     0.3366     0.0610                      0.2167          0.4566
         C4    10.0374     0.4067                      9.2379         10.8368
```

APPENDIX C - PART II

SAS Inputs and Outputs for the Degree of Hydration Model

1. **ANOVA analysis on Hydration Variables (τ and β):**

- **SAS Program:**

```
data temp; set ctrall;
    lc3s=log(c3s); lc3a=log(c3a); lcao=log(cao);
    lc2s=log(c2s); lc4af=log(c4af); lso3=log(so3); lmgo=log(mgo);
    lnaequ=log(naequ); lblaine=log(blaine); lbeta=log(beta);
    ltau=log(tau);
    i1=c3s*c3a; i2=c3s*blaine; i3=c3s*so3; i4= c3s*naequ;
    i5=c3a*blaine; i6=c3a*so3; i7=c3a*naequ; i8=blaine*so3;
    i9=blaine*naequ; i10=c2s*c4af; i11=c2s*so3; i12=c2s*naequ;
    i13=c4af*so3; i14=so3*mgo; i15=so3*naequ; i16=mgo*naequ;
    i17=pfa*FACaO; i18=pfa*FASiO2; i19=pfa*Falk;
    i20=pfa*FACaO*FASiO2; i20=pfa*FACaO*FASiO2*Falk;
run;
proc rsquare c;
        model lbeta ltau = lc3s lc3a lblaine lc2s
        lc4af lso3 lmgo lnaequ ggbf pfa
        select=10 stop=10;
run;
```

- **Analysis Results:**

The SAS System: The RSQUARE Procedure: Correlation

```
Variable   lc3s       lc3a      lblaine     lc2s      lc4af      lso3
lc3s      1.0000     0.6307     0.2128   -0.9052   -0.5741    0.4477
lc3a      0.6307     1.0000     0.1348   -0.6359   -0.7752    0.4840
lblaine   0.2128     0.1348     1.0000   -0.3341   -0.2079    0.1782
lc2s     -0.9052    -0.6359    -0.3341    1.0000    0.5229   -0.6825
```

lc4af	-0.5741	-0.7752	-0.2079	0.5229	1.0000	-0.3655
lso3	0.4477	0.4840	0.1782	-0.6825	-0.3655	1.0000
lmgo	-0.4028	-0.1416	0.1857	0.4322	0.1674	-0.4270
lnaequ	-0.1112	-0.0636	0.0119	-0.0885	0.3985	0.4585
GGBF	0.1529	0.1348	-0.0156	-0.2050	-0.1189	0.3039
PFA	0.3511	0.3096	-0.0358	-0.4709	-0.2730	0.6980

Variable	**lmgo**	**lnaequ**	**GGBF**	**PFA**
lc3s	-0.4028	-0.1112	0.1529	0.3511
lc3a	-0.1416	-0.0636	0.1348	0.3096
lblaine	0.1857	0.0119	-0.0156	-0.0358
lc2s	0.4322	-0.0885	-0.2050	-0.4709
lc4af	0.1674	0.3985	-0.1189	-0.2730
lso3	-0.4270	0.4585	0.3039	0.6980
lmgo	1.0000	0.0676	-0.1562	-0.3587
lnaequ	0.0676	1.0000	0.1381	0.3171
GGBF	-0.1562	0.1381	1.0000	-0.1430
PFA	-0.3587	0.3171	-0.1430	1.0000

The SAS System: The RSQUARE Procedure: **R-Square Selection Method**

Dependent Variable: log(Beta)

Number in Model	R^2	Variables in Model
1	0.6938	lso3
1	0.4659	lc2s
1	0.4620	PFA
1	0.4091	lc3a
1	0.3504	lc3s
1	0.2596	lc4af
1	0.1704	lmgo
1	0.0932	lnaequ
1	0.0050	lblaine
1	0.0031	GGBF

2	0.7669	lc3a lso3
2	0.7538	lc3s lso3
2	0.7434	lblaine lso3
2	0.7424	lc4af lso3
2	0.7367	lso3 GGBF
2	0.7182	lc2s lso3
2	0.7127	lso3 PFA
2	0.7013	lso3 lnaequ
2	0.6978	lso3 lmgo
2	0.6657	lc3a PFA

3	0.8236	lc3a lblaine lso3
3	0.8228	lc3s lblaine lso3
3	0.8100	lblaine lc4af lso3
3	0.8081	lc3a lso3 GGBF
3	0.7987	lc3s lso3 GGBF
3	0.7973	lblaine lc2s lso3
3	0.7936	lblaine lso3 GGBF
3	0.7892	lc3a lso3 PFA
3	0.7860	lc4af lso3 GGBF

```
      3     0.7837    lc3s lc2s lso3
--------------------------------------------------------------------------------
      4     0.8772    lc3s lblaine lso3 GGBF
      4     0.8725    lc3a lblaine lso3 GGBF
      4     0.8627    lblaine lc4af lso3 GGBF
      4     0.8496    lblaine lc2s lso3 GGBF
      4     0.8479    lc3s lc3a lblaine lso3
      4     0.8424    lc3s lblaine lc4af lso3
      4     0.8354    lc3a lblaine lc2s lso3
      4     0.8333    lc3a lblaine lso3 PFA
      4     0.8328    lc3s lc2s lso3 GGBF
      4     0.8326    lc3s lblaine lso3 lmgo
--------------------------------------------------------------------------------
      5     0.9000    lc3s lc3a lblaine lso3 GGBF
      5     0.8971    lc3s lblaine lc4af lso3 GGBF
      5     0.8870    lc3s lblaine lso3 lmgo GGBF
      5     0.8857    lc3a lblaine lc2s lso3 GGBF
      5     0.8848    lblaine lc2s lc4af lso3 GGBF
      5     0.8841    lc3s lblaine lso3 GGBF PFA
      5     0.8836    lc3s lblaine lc2s lso3 GGBF
      5     0.8794    lc3a lblaine lc4af lso3 GGBF
      5     0.8772    lc3s lblaine lso3 lnaequ GGBF
      5     0.8734    lc3a lblaine lso3 GGBF PFA
--------------------------------------------------------------------------------
      6     0.9114    lc3s lblaine lc4af lso3 lnaequ GGBF
      6     0.9061    lc3s lc3a lblaine lc2s lso3 GGBF
      6     0.9048    lc3s lblaine lc4af lso3 GGBF PFA
      6     0.9042    lc3s lblaine lc4af lso3 lmgo GGBF
      6     0.9038    lc3s lc3a lblaine lso3 GGBF PFA
      6     0.9032    lc3s lc3a lblaine lc4af lso3 GGBF
      6     0.9032    lc3s lc3a lblaine lso3 lmgo GGBF
      6     0.9015    lc3s lc3a lblaine lso3 lnaequ GGBF
      6     0.8999    lc3s lblaine lc2s lc4af lso3 GGBF
      6     0.8989    lblaine lc2s lc4af lso3 lnaequ GGBF
--------------------------------------------------------------------------------
      7     0.9202    lc3s lblaine lc4af lso3 lnaequ GGBF PFA
      7     0.9134    lc3s lblaine lc2s lc4af lso3 lnaequ GGBF
      7     0.9132    lc3s lc3a lblaine lc4af lso3 lnaequ GGBF
      7     0.9127    lc3s lblaine lc4af lso3 lmgo lnaequ GGBF
      7     0.9119    lc3s lblaine lc4af lso3 lmgo GGBF PFA
      7     0.9112    lc3s lc3a lblaine lc2s lso3 GGBF PFA
      7     0.9087    lc3s lblaine lc2s lc4af lso3 GGBF PFA
      7     0.9087    lc3s lc3a lblaine lc2s lso3 lmgo GGBF
      7     0.9085    lc3s lc3a lblaine lc4af lso3 GGBF PFA
      7     0.9081    lc3s lc3a lblaine lc2s lso3 lnaequ GGBF
--------------------------------------------------------------------------------
```

The SAS System: The RSQUARE Procedure: **R-Square Selection Method**

Dependent Variable: log(tau)

```
Number in Model     R^2     Variables in Model
      1     0.3780    lc2s
      1     0.3360    lblaine
      1     0.2612    lc3s
```

```
     1     0.2458   lc3a
     1     0.1823   lso3
     1     0.1394   lc4af
     1     0.0373   GGBF
     1     0.0170   lnaequ
     1     0.0082   PFA
     1     0.0012   lmgo
------------------------------------------------------------------------------
     2     0.5357   lblaine lc2s
     2     0.5137   lc3a lblaine
     2     0.4935   lc3s lblaine
     2     0.4844   lc2s GGBF
     2     0.4442   lblaine lso3
     2     0.4441   lc2s lmgo
     2     0.4288   lc2s PFA
     2     0.4029   lblaine lc4af
     2     0.3965   lc3a lc2s
     2     0.3895   lc3s lc2s
------------------------------------------------------------------------------
     3     0.6205   lblaine lc2s GGBF
     3     0.5949   lso3 GGBF PFA
     3     0.5924   lc2s GGBF PFA
     3     0.5735   lc3a lblaine GGBF
     3     0.5678   lc3a lblaine lc2s
     3     0.5563   lc3s lblaine GGBF
     3     0.5545   lblaine lc2s PFA
     3     0.5482   lblaine lc2s lmgo
     3     0.5432   lc3s lc3a lblaine
     3     0.5428   lblaine lc2s lnaequ
------------------------------------------------------------------------------
     4     0.7829   lc2s lso3 GGBF PFA
     4     0.7639   lc3s lso3 GGBF PFA
     4     0.7065   lblaine lso3 GGBF PFA
     4     0.6803   lc3a lso3 GGBF PFA
     4     0.6772   lblaine lc2s GGBF PFA
     4     0.6608   lc4af lso3 GGBF PFA
     4     0.6573   lc2s lnaequ GGBF PFA
     4     0.6521   lc3a lblaine lc2s GGBF
     4     0.6388   lc3s lc2s GGBF PFA
------------------------------------------------------------------------------
     5     0.8320   lc3s lblaine lso3 GGBF PFA
     5     0.8275   lblaine lc2s lso3 GGBF PFA
     5     0.8163   lc2s lso3 lmgo GGBF PFA
     5     0.8019   lc3s lso3 lmgo GGBF PFA
     5     0.7922   lc3a lc2s lso3 GGBF PFA
     5     0.7909   lc2s lc4af lso3 GGBF PFA
     5     0.7888   lc2s lso3 lnaequ GGBF PFA
     5     0.7848   lc3a lblaine lso3 GGBF PFA
     5     0.7837   lc3s lc2s lso3 GGBF PFA
------------------------------------------------------------------------------
     6     0.8452   lc3s lblaine lso3 lmgo GGBF PFA
     6     0.8432   lc3a lblaine lc2s lso3 GGBF PFA
     6     0.8430   lc3s lc3a lblaine lso3 GGBF PFA
     6     0.8416   lc3s lblaine lso3 lnaequ GGBF PFA
```

```
       6       0.8405    lblaine lc2s lso3 lmgo GGBF PFA
       6       0.8349    lc3s lblaine lc2s lso3 GGBF PFA
       6       0.8334    lc3s lblaine lc4af lso3 GGBF PFA
       6       0.8334    lblaine lc2s lc4af lso3 GGBF PFA
       6       0.8328    lblaine lc2s lso3 lnaequ GGBF PFA
       6       0.8217    lc2s lc4af lso3 lmgo GGBF PFA
-------------------------------------------------------------------------------
       7       0.8583    lblaine lc2s lc4af lso3 lnaequ GGBF PFA
       7       0.8577    lc3s lc3a lblaine lso3 lnaequ GGBF PFA
       7       0.8566    lc3s lblaine lc4af lso3 lnaequ GGBF PFA
       7       0.8546    lc3a lblaine lc2s lso3 lnaequ GGBF PFA
       7       0.8506    lc3s lc3a lblaine lso3 lmgo GGBF PFA
       7       0.8501    lc3a lblaine lc2s lso3 lmgo GGBF PFA
       7       0.8499    lc3s lblaine lso3 lmgo lnaequ GGBF PFA
       7       0.8491    lc3s lblaine lc2s lso3 lmgo GGBF PFA
       7       0.8462    lc3s lc3a lblaine lc2s lso3 GGBF PFA
       7       0.8458    lc3s lblaine lc4af lso3 lmgo GGBF PFA
-------------------------------------------------------------------------------
```

4. **General Linear Model (GLM) Development**

- **SAS Program:**

```
data transform; set ctrall;
        lc3s=log(c3s); lc3a=log(c3a); lcao=log(cao);
        lc2s=log(c2s); lc4af=log(c4af); lso3=log(so3); lmgo=log(mgo);
        lnaequ=log(naequ); lblaine=log(blaine); lbeta=log(beta);
        ltau=log(tau);
        i1=c3a*so3; i2=blaine*naequ; i3=c3s*so3;
        i4=c3s*blaine; i5=c3a*naequ; i6=pfa*FAcao;
run;
proc glm;
        model ltau = lc3s lc3a lblaine lso3 ggbf i6 /solution ;
        output out=plotit p=pred; run;
        proc gplot; plot pred*ltau;
run;
proc glm;
        proc glm; model lbeta = lc3a lc3s lblaine lso3 ggbf /solution ;
        output out=plotit p=pred; run;
        proc gplot; plot pred*lbeta;
run;
```

- **Analysis Results:**

The SAS System: The GLM Procedure (β)

```
Number of observations    352
Dependent Variable: log(beta)

 Source              DF      Sum of Squares     Mean Square    F Value   Pr > F
Model                 5     24.89654051        4.97930810      622.58   <.0001
Error               346       2.76726614       0.00799788
Corrected Total     351     27.66380665
```

```
          R-Square       Coeff Var     Root MSE     log(E) Mean
          0.899968       -14.69696     0.089431    -0.608499

Source             DF      Type I SS      Mean Square    F Value    Pr > F
lc3a                1    11.31801546    11.31801546    1415.13    <.0001
lc3s                1     1.63292940     1.63292940     204.17    <.0001
lblaine             1     1.12201424     1.12201424     140.29    <.0001
lso3                1     9.38317036     9.38317036    1173.21    <.0001
GGBF                1     1.44041104     1.44041104     180.10    <.0001

Source             DF     Type III SS     Mean Square    F Value    Pr > F
lc3a                1    0.63088336      0.63088336      78.88    <.0001
lc3s                1    0.75968361      0.75968361      94.99    <.0001
lblaine             1    2.09702300      2.09702300     262.20    <.0001
lso3                1   10.71619596     10.71619596     339.88    <.0001
GGBF                1    1.44041104      1.44041104     180.10    <.0001

Parameter      Estimate            Standard Error    t Value        Pr > |t|
  Intercept    5.473033067           0.21970089        24.91     <.0001
  lc3a         0.150832641           0.01698276         8.88     <.0001
  lc3s         0.228098671           0.02340420         9.75     <.0001
  lblaine     -0.561129955           0.03465367       -16.19     <.0001
  lso3         0.582985693           0.01592667        36.60     <.0001
  GGBF        -0.704101446           0.05246618       -13.42     <.0001
```

The SAS System: The GLM Procedure (τ)

```
Number of observations    352
Dependent Variable: log(tau)

Source                  DF    Sum of Squares     Mean Square    F Value    Pr > F
Model                    6     38.72612166        6.45435361     362.39    <.0001
Error                  345      6.14459535        0.01781042
Corrected Total        351     44.87071701

                    R-Square     Coeff Var     Root MSE     log(E) Mean
                    0.863060     4.154141      0.133456     3.212594

            Source    DF      Type I SS     Mean Square    F Value    Pr > F
            lc3s                 1    11.71853237    11.71853237    657.96    <.0001
            lc3a                 1     2.24171380     2.24171380    125.87    <.0001
            lblaine              1    10.41553668    10.41553668    584.80    <.0001
            lso3                 1     0.60988185     0.60988185     34.24    <.0001
            GGBF                 1     4.17727026     4.17727026    234.54    <.0001
            i6                   1     9.56318668     9.56318668    536.94    <.0001

            Source    DF     Type III SS    Mean Square    F Value    Pr > F
            lc3s                 1     2.32854921     2.32854921    130.74    <.0001
            lc3a                 1     0.61083005     0.61083005     34.30    <.0001
            lblaine              1     4.08591104     4.08591104    229.41    <.0001
            lso3                 1     9.46937423     9.46937423    531.68    <.0001
            GGBF                 1    10.64051541    10.64051541    597.43    <.0001
            i6                   1     9.56318668     9.56318668    536.94    <.0001
```

```
Parameter        Estimate        Standard Error        t Value    Pr > |t|
 Intercept        4.274562468      0.37135061           11.51     <.0001
 lc3s            -0.404032512      0.03533546          -11.43      <.0001
 lc3a            -0.149358149      0.02550385           -5.86     <.0001
 lblaine         -0.813232025      0.05369170          -15.15      <.0001
 lso3            -0.756832848      0.03282286          -23.06      <.0001
 GGBF             2.171046522     0.08882289            24.44      <.0001
 i6               9.324928866     0.40242162            23.17      <.0001
```

5. **Final Lon-Linear Model (NLIN) Development for τ and β:**

- **SAS Program:**

```
          proc nlin;
                    parms c1=0.15 c2=0.228 c3=-0.5611 c4=0.583 c5=-0.704 c6=5.47
                    e1=-0.404 e2=-0.149 e3=-0.813 e4=-0.7567 e5=2.171 e6=9.324
e7=4.275;
                    beta1 = c3a**c1*c3s**c2*blaine**c3*so3**c4*exp(c5*ggbf+c6);
                    tau1=c3s**e1*c3a**e2*blaine**e3*so3**e4*exp(e5*ggbf+pfa*FACaO*
e6+e7);
                    model alpha =exp(-((tau1/time)**beta1))*amax;
                    output out=good p=predict r=resid stdr=eresid;
          run;

          proc gplot;
                    plot alpha*predicted resid*predicted resid*alpha
          run;
```

- **Analysis Results:**

The SAS System: The NLIN Procedure

Dependent Variable = alpha = degree of hydration
Method: Gauss-Newton

Iterative Phase

```
Iter c1       c2       c3      c4       c5       c6      e1       e2        e3       e4       e5
0   0.15    0.228   -0.561  0.583   -0.704  5.470   -0.4040  -0.149   -0.813   -0.757   2.1710
1  0.1456  0.2268 -0.5345 0.5578  -0.6465 5.1957 -0.4013  -0.1534  -0.8043  -0.7583  2.1868
2  0.1455  0.2271 -0.5349 0.5580  -0.6467 5.1986 -0.4011  -0.1539  -0.8042  -0.7581  2.1873
3  0.1455  0.2271 -0.5349 0.5580  -0.6467 5.1987 -0.4011  -0.1539  -0.8042  -0.7581  2.1873

Iter   e6          e7    Sum of Squares
0   9.3240      4.2750      0.3095
1   9.4923      4.2038      0.3082
2   9.4980      4.2023      0.3082
3   9.4980      4.2025      0.3082
```

NOTE: Convergence criterion met.

Estimation Summary

```
Method                   Gauss-Newton
```

```
                          Iterations                3
                          R                   4.072E-6
                          PPC(e2)                  0.000018
                          RPC(c1)                  0.000171
                          Object                4.255E-9
                          Objective              0.308224
                          Observations Read              352
                          Observations Used              352
                          Observations Missing             0
                          NOTE: An intercept was not specified for this model.

             Source            DF   Sum of Squares  Mean Square  F Value  Approx Pr>F
             Regression        13      103.7            7.9795   8776.25     <.0001
             Residual         339   0.3082             0.000909
             Uncorrected Total 352   104.0
             Corrected Total   351    32.4636

          Parameter     Estimate   Approx Std Error    Approximate 95% Confidence Limits
              c1          0.1455     0.0336                  0.0794          0.2116
              c2          0.2271     0.0460                  0.1366          0.3177
              c3         -0.5349     0.0701                 -0.6728         -0.3970
              c4          0.5580     0.0366                  0.4860          0.6300
              c5         -0.6467     0.1325                 -0.9074         -0.3860
              c6          5.1987     0.4608                 4.2922          6.1051
              e1         -0.4011      0.0709                -0.5406         -0.2616
              e2         -0.1539      0.0491                -0.2504         -0.0574
              e3         -0.8042      0.1040               -1.0088          -0.5995
              e4         -0.7581      0.0600                -0.8761         -0.6401
              e5          2.1873      0.1747                 1.8436          2.5309
              e6          9.4980      0.6888                 8.1431         10.8528
              e7          4.2025      0.7086                 2.8086          5.5964

      Approximate Correlation Matrix
             c1        c2          c3              c4              c5             c6             e1
      c1   1.000    -0.5295    0.0400958    -0.2942069    0.0426007     0.0184427    -0.0920438
      c2  -0.529     1.0000   -0.1559342    -0.0944974   -0.0597097     0.0894941     0.1689144
      c3   0.040    -0.1559    1.0000000    -0.1883975    0.1044326    -0.9592790    -0.0093210
      c4  -0.294    -0.0945   -0.1883975     1.0000000   -0.3108832     0.4168574    -0.0187741
      c5   0.042    -0.0597    0.1044326    -0.3108832    1.0000000    -0.1912082    -0.0093839
      c6   0.018     0.0895   -0.9592790     0.4168574   -0.1912082     1.0000000    -0.0013087
      e1  -0.092     0.1690   -0.0093210    -0.0187741   -0.0093839    -0.0013087     1.000000
      e2   0.1738  -0.0973    0.0071570    -0.0505965    0.0067728     0.0028987    -0.5297556
      e3   0.0124  -0.0124    0.2751948    -0.0653108    0.0179626    -0.2644622    -0.1557741
      e4  -0.0446  -0.0175   -0.0592343     0.1652883   -0.0488028     0.0946853    -0.077822
      e5   0.0073  -0.0112    0.0215084    -0.0628679    0.1426501    -0.0392363    -0.0814824
      e6   0.0008  -0.0021    0.0077986    -0.0214157    0.0083838    -0.0140555    -0.1241341
      e7  -0.0017   0.0010   -0.2560062     0.1006581   -0.0319668     0.2596303     0.0931383

            e2              e3             e4             e5             e6             e7
      c1    0.1737918     0.0124130     -0.0445646     0.0072827     0.0008676    -0.0016777
      c2   -0.0972615    -0.0123916     -0.0174659    -0.0111842    -0.0027315     0.0010472
      c3    0.0071570     0.2751948     -0.0592343     0.0215084     0.0077986    -0.2560062
      c4   -0.0505965    -0.0653108      0.1652883    -0.0628679    -0.0214157     0.1006581
      c5    0.0067728     0.0179626     -0.0488028     0.1426501     0.0083838    -0.0319668
```

```
c6    0.0028987    -0.2644622     0.0946853    -0.0392363    -0.0140555     0.2596303
e1   -0.5297556    -0.1557741    -0.0778229    -0.0814824    -0.1241341     0.0931383
e2    1.0000000     0.0596516    -0.2306292     0.0675119     0.1030963     0.0055150
e3    0.0596516     1.0000000    -0.2546590     0.1606375     0.2448542    -0.9508743
e4   -0.2306292    -0.2546590     1.0000000    -0.4574929    -0.6979173     0.5077060
e5    0.0675119     0.1606375    -0.4574929     1.0000000     0.4431966    -0.2911433
e6    0.1030963     0.2448542    -0.6979173     0.4431966     1.0000000    -0.4439241
e7    0.0055150    -0.9508743     0.5077060    -0.2911433    -0.4439241     1.0000000
```

6. Final Lon-Linear Model (NLIN) Development for ultimate degree of hydration:

- **SAS Program:**

```
                data temp1; set ctrall; if ID=1; amax1=1; run;
                data temp2; set ctrall; if ID=2; amax1=1.031*wcm/(0.194+wcm);
                data temp3; set temp2;  if amax1<=1;run;
                data temp4; set temp2;  if amax1>1; amax1=1; run;
                run;
                data all; set temp1 temp3 temp4; run;
                proc sort; by key; run;
                data temp; set all; if id2=1;run;
                proc print; run;
                proc nlin;
                    parms f1=0.533 f2=0.216;
                    c1=.146; c6=181.4; c2=0.227; c3=-0.535; c4=0.558; c5=-0.647;
                    e1=-.401; e7=66.78; e2=-0.154; e3=-0.804; e4=-0.758; e5=2.187;
                    e6=9.500;
                    beta1 = c6*c3a**c1*c3s**c2*blaine**c3*so3**c4*exp(c5*ggbf);

tau1=e7*c3s**e1*c3a**e2*blaine**e3*so3**e4*exp(e5*ggbf+pfa*FACaO*e6);
                    model alpha =exp(-((tau1/time)**beta1))*(amax1+f1*pfa+f2*ggbf);
                   output out=good p=predict r=resid stdr=eresid;
                run;

                proc gplot;
                       plot alpha*predicted resid*predicted resid*alpha
                run;
```

- **Analysis Results:**

The SAS System: The NLIN Procedure

Dependent Variable = alpha = degree of hydration
Method: Gauss-Newton

Iterative Phase

```
Iter     C1        C2      Sum of Squares
 0     0.5330    0.2160     0.3661
 1     0.5181    0.3292     0.3516
NOTE: Convergence criterion met.
```

```
        Estimation Summary
Method               Gauss-Newton
Iterations                1
```

```
                         R                          0
                         PPC                        0
                         RPC(f2)               0.524147
                         Object                0.039772
                         Objective             0.351586
                         Observations Read          352
                         Observations Used          352
                         Observations Missing         0
                    NOTE: An intercept was not specified for this model.

  Source              DF   Sum of Squares  Mean Square  F Value  Approx Pr>F
 Regression            2     103.7            51.8450     51611.2   <.0001
 Residual            350        0.3516          0.00100
 Uncorrected Total   352     104.0
 Corrected Total     351       32.4636

Parameter     Estimate   Approx Std Error   Approximate 95% Confidence Limits
      f1       0.5181     0.0182                  0.4824           0.5538
      f2       0.3292     0.0305                  0.2693           0.3891
```

The following figures present the residual plots for the all explanatory variables of the degree of hydration model as developed in Chapter 5.

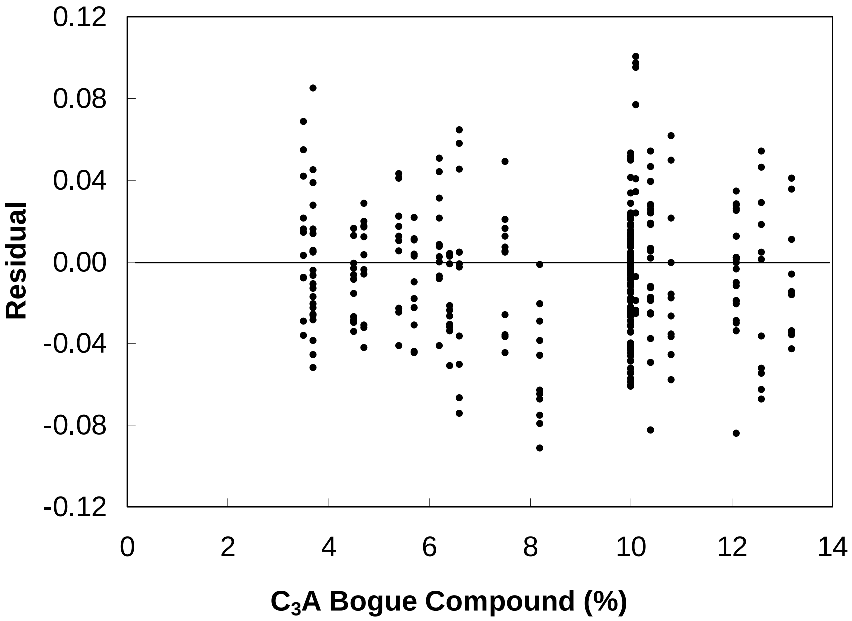

Figure C-1: Plot of the residuals against the C_3A content

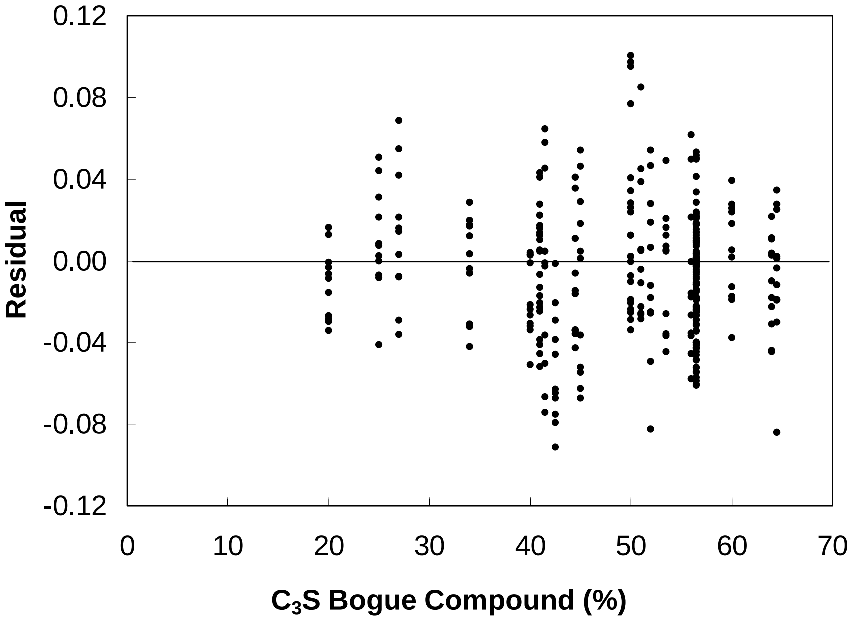

Figure C-2: Plot of the residuals against the C$_3$S content

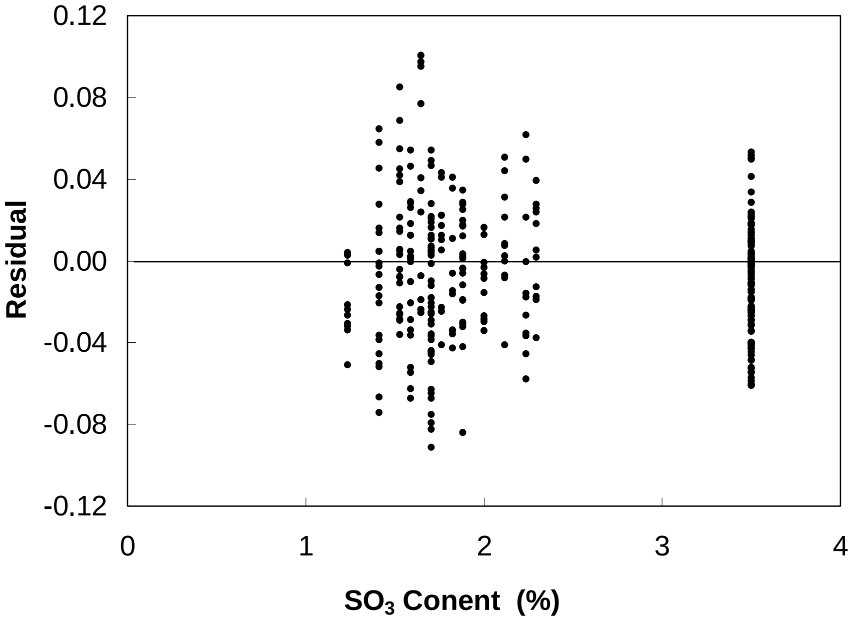

Figure C-3: Plot of the residuals against the SO$_3$ content

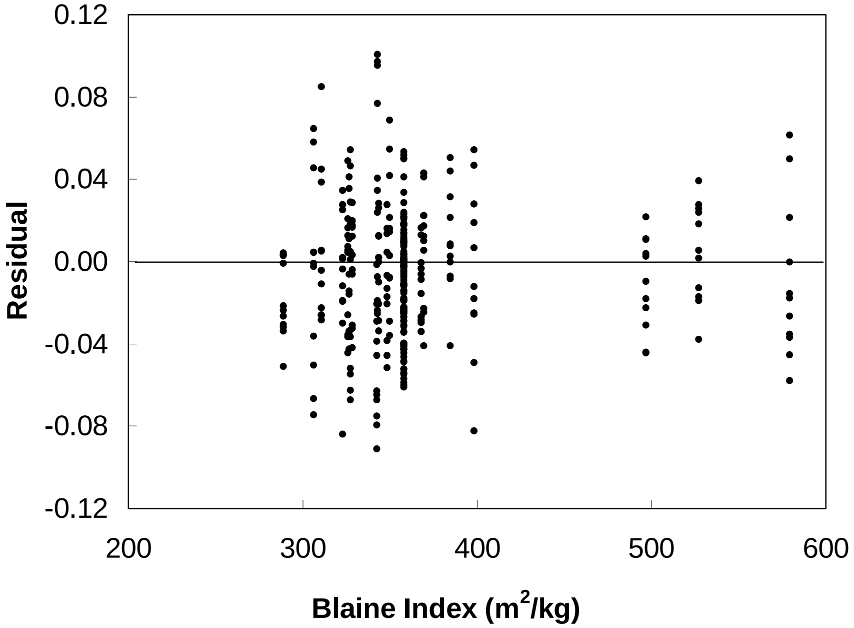

Figure C-4: Plot of the residuals against the Blaine index

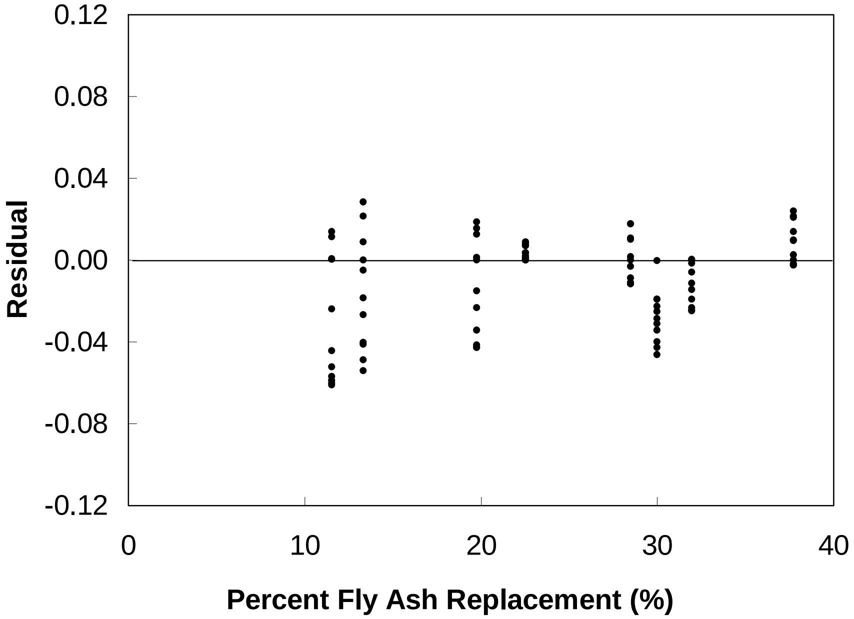

Figure C-5: Plot of the residuals against the fly ash content

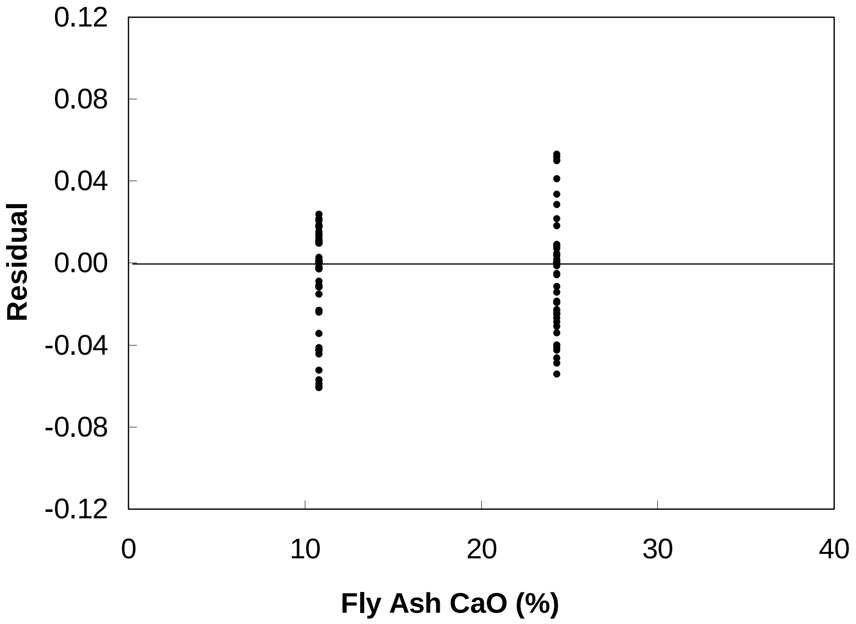

Figure C-6: Plot of the residuals against the fly ash CaO content

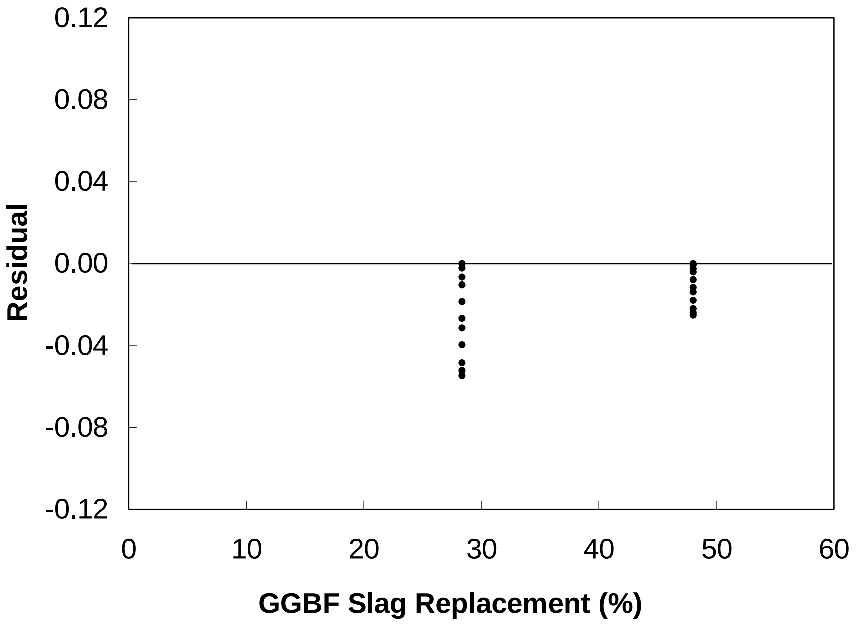

Figure C-7: Plot of the residuals against the GGBF replacement level

APPENDIX D

General Hydration Model Development Results

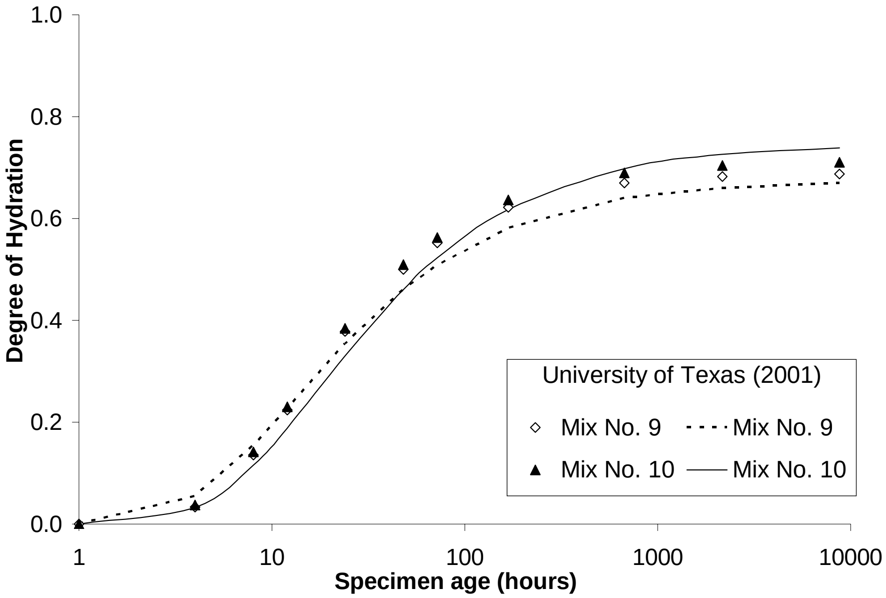

Figure D-1: Predicted and measured degree of hydration for mixtures test during this project (Mix No. 9 = Texas Lehigh (6 sacks), Mix No. 10 = Type I + 15% C fly ash)

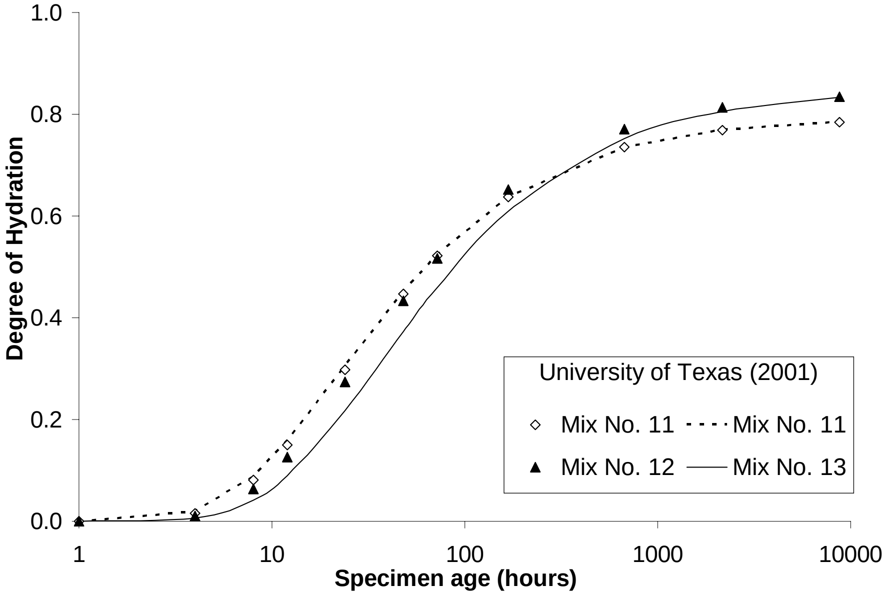

Figure D-2: Predicted and measured degree of hydration for mixtures test during this project (Mix No. 11 = Type I + 25% C fly ash, Mix No. 12 = Type I + 35% C fly ash)

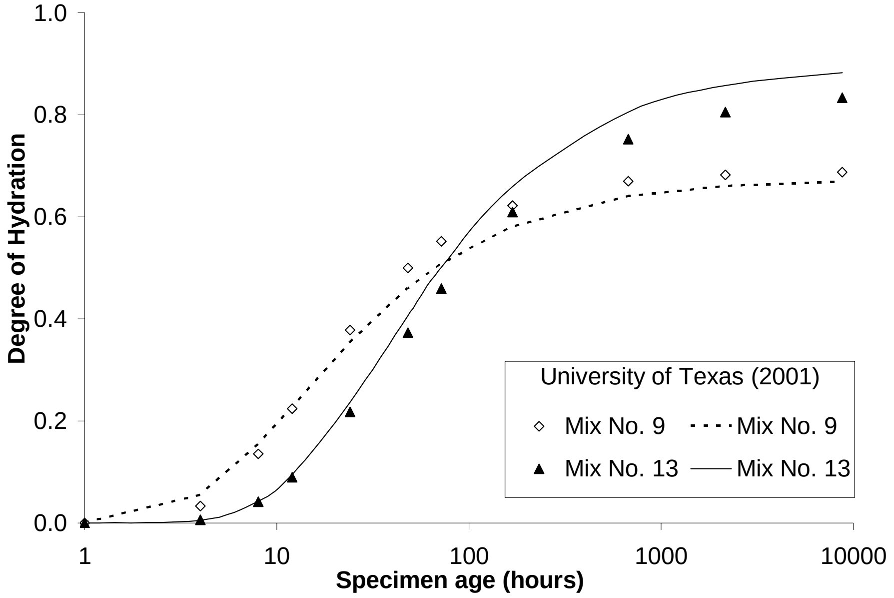

Figure D-3: Predicted and measured degree of hydration for mixtures test during this project (Mix No. 9 = Texas Lehigh (6 sacks), Mix No. 13 = Type I + 45% C fly ash)

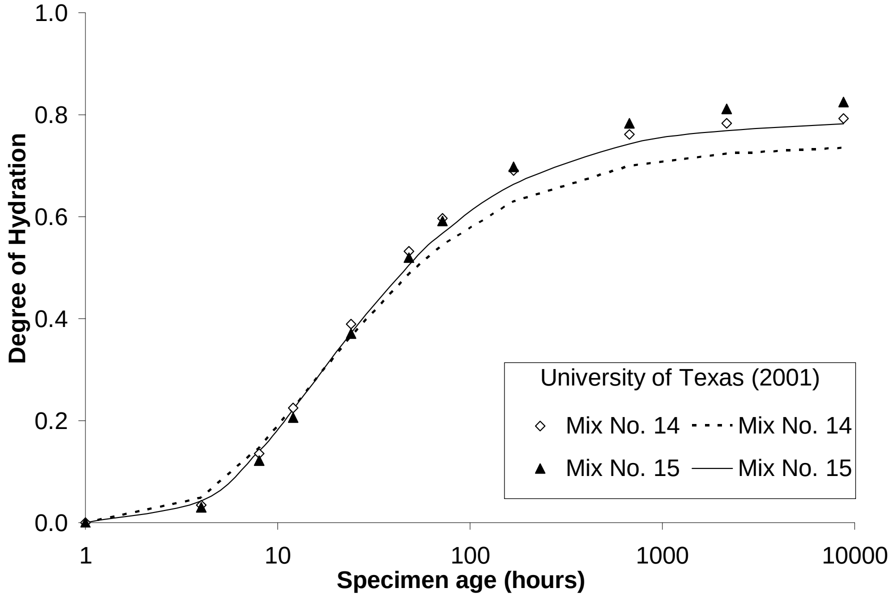

Figure D-4: Predicted and measured degree of hydration for mixtures test during this project (Mix No. 14 = Type I + 15% F fly ash, Mix No. 15 = Type I + 25% F fly ash)

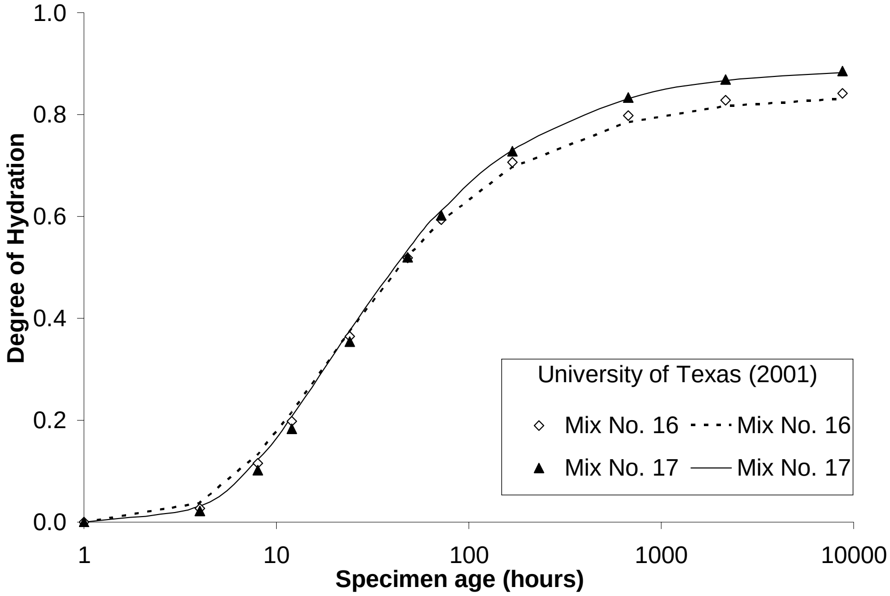

Figure D-5: Predicted and measured degree of hydration for mixtures test during this project (Mix No. 16 = Type I + 35% F fly ash, Mix No. 17 = Type I + 45% F fly ash)

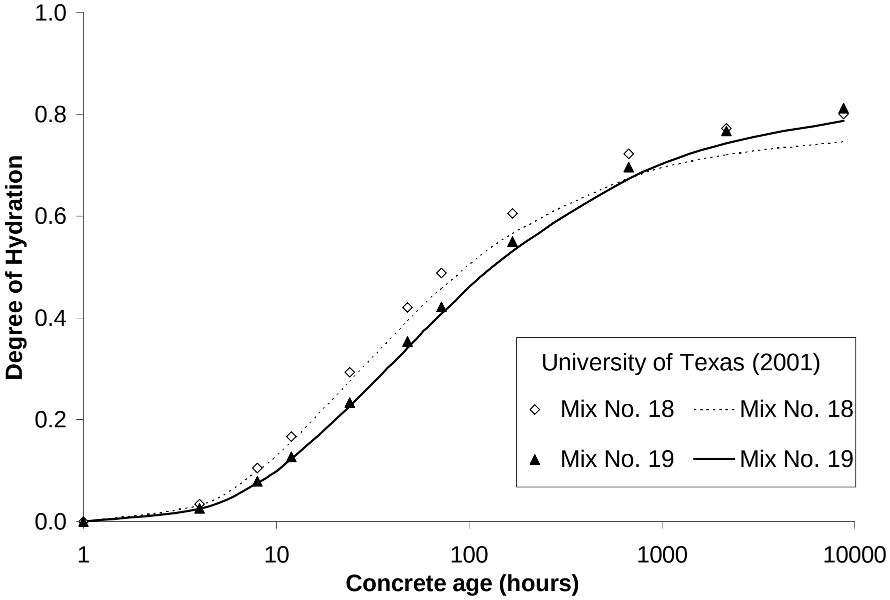

Figure D-6: Predicted and measured degree of hydration for mixtures test during this project (Mix No. 18 = Type I + 30% GGBF Slag, Mix No. 19 = Type I + 50% GGBF Slag)

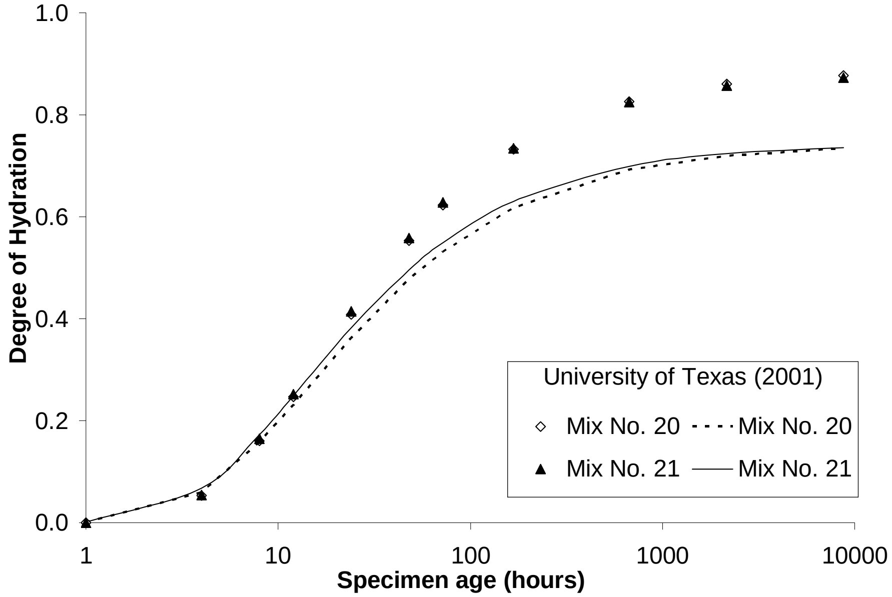

Figure D-7: Predicted and measured degree of hydration for mixtures test during this project (Mix No. 20 = Capitol Type I, Mix No. 21 = Alamo Type I)

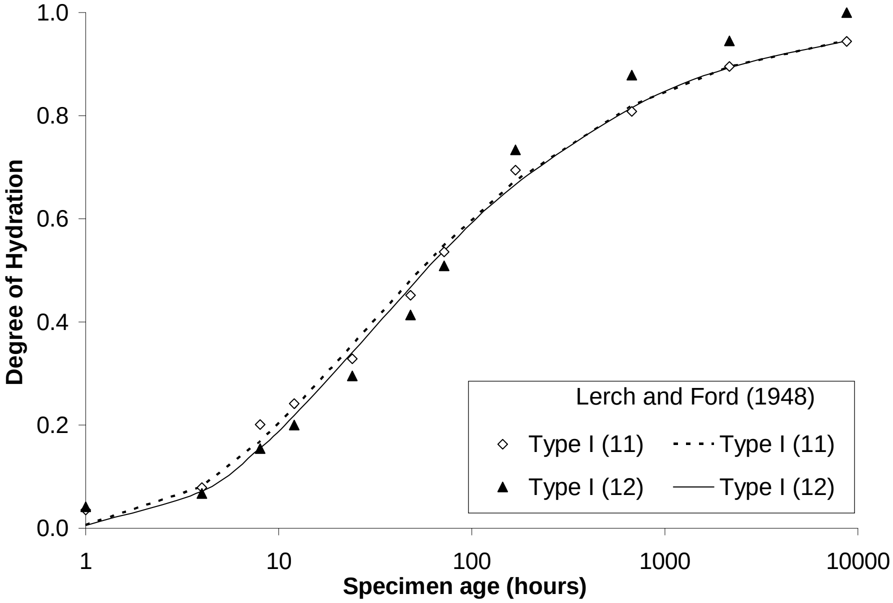

Figure D-8: Predicted and measured degree of hydration for Lerch and Ford (1948)

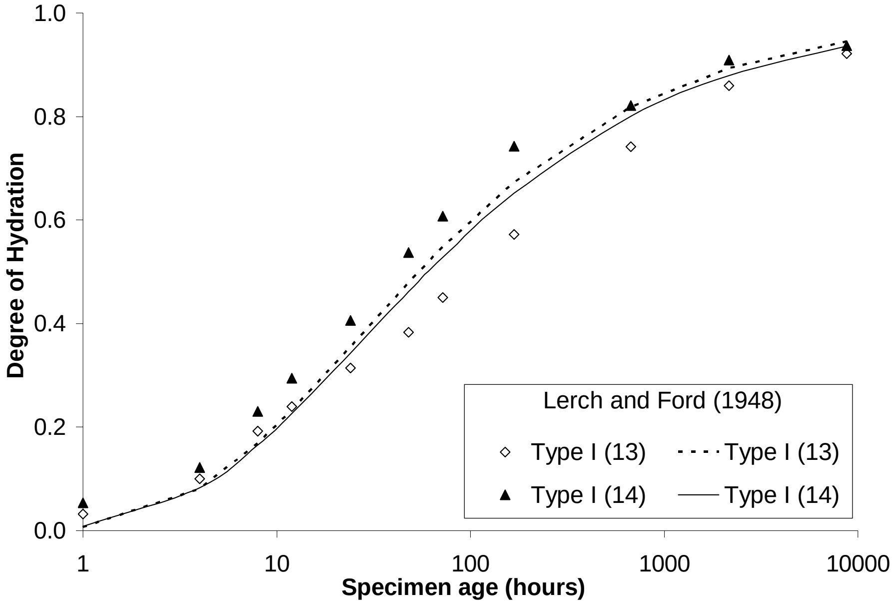

Figure D-9: Predicted and measured degree of hydration for Lerch and Ford (1948)

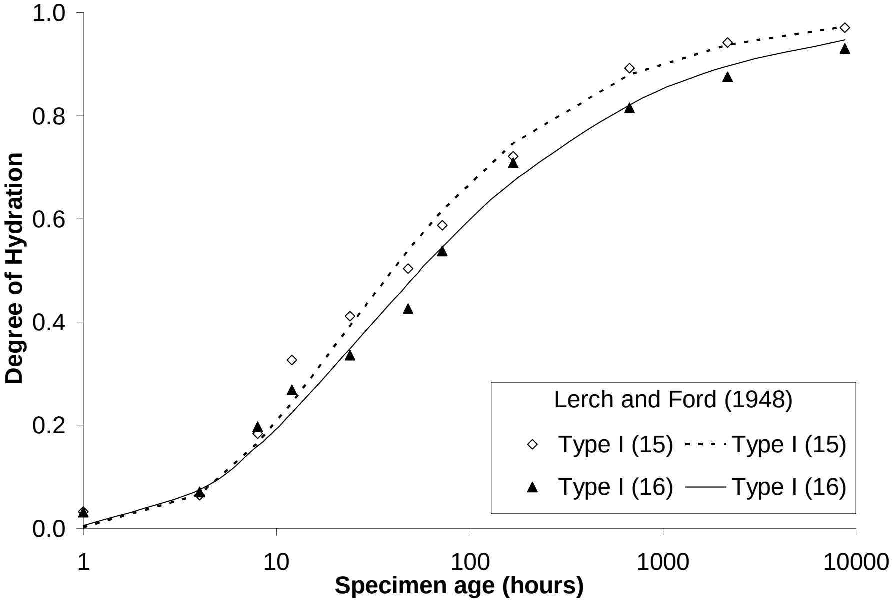

Figure D-10: Predicted and measured degree of hydration for Lerch and Ford (1948)

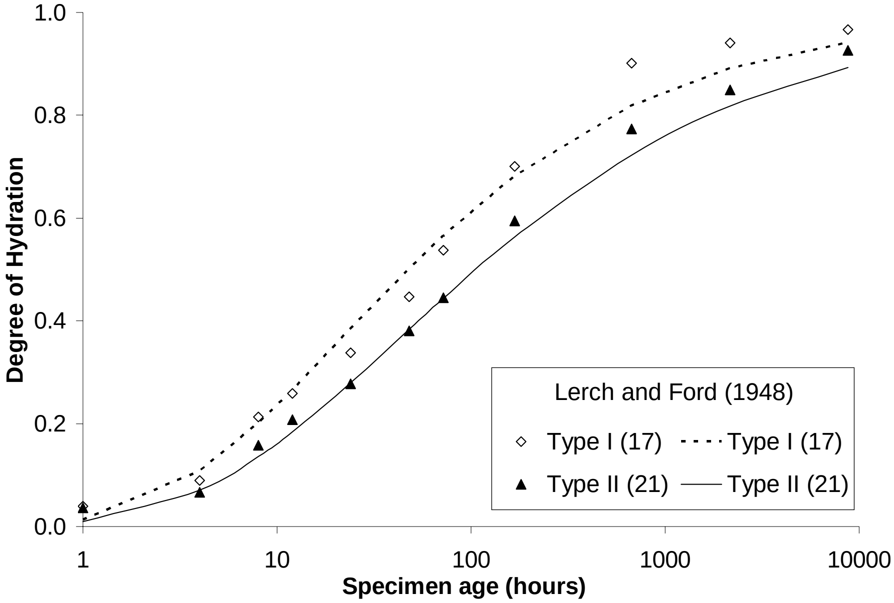

Figure D-11: Predicted and measured degree of hydration for Lerch and Ford (1948)

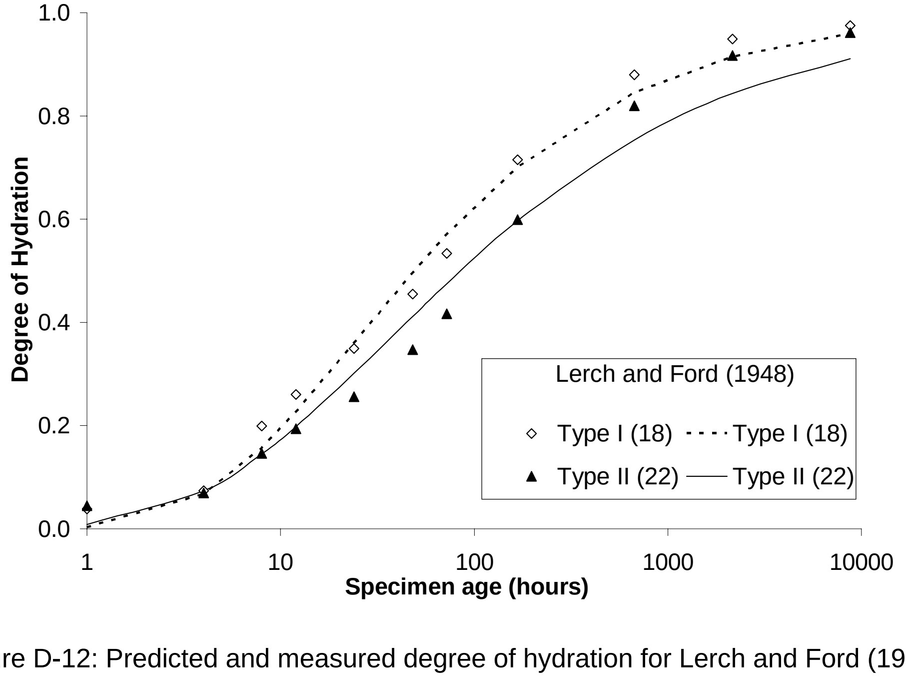

Figure D-12: Predicted and measured degree of hydration for Lerch and Ford (1948)

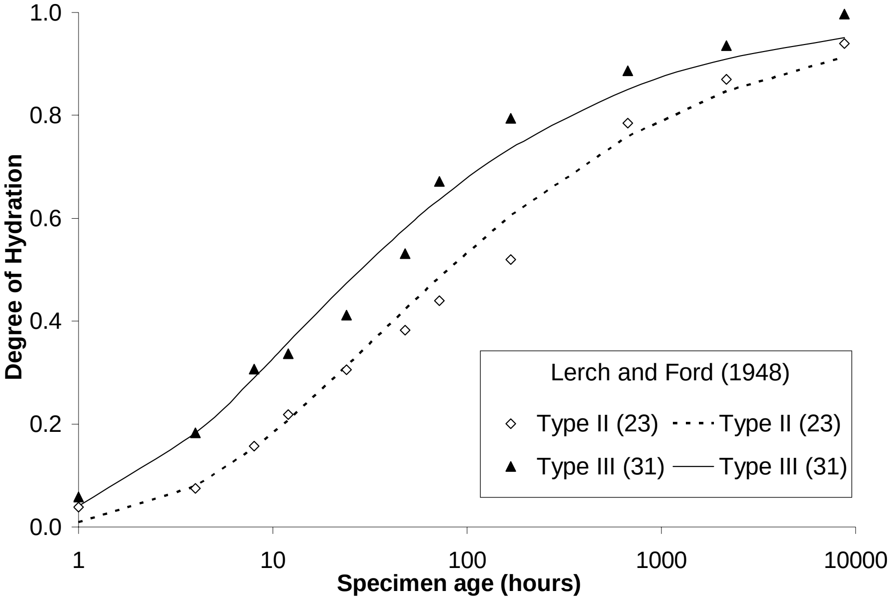

Figure D-13: Predicted and measured degree of hydration for Lerch and Ford (1948)

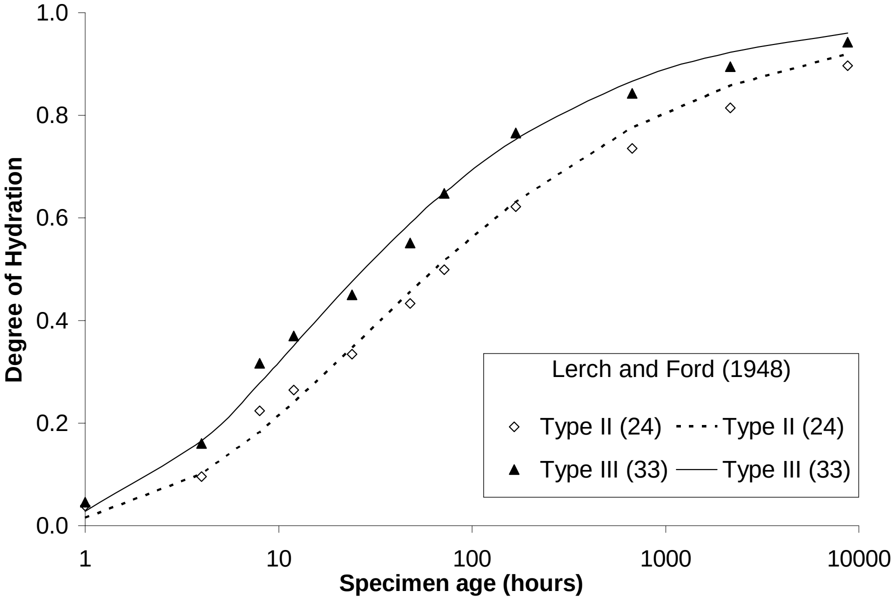

Figure D-14: Predicted and measured degree of hydration for Lerch and Ford (1948)

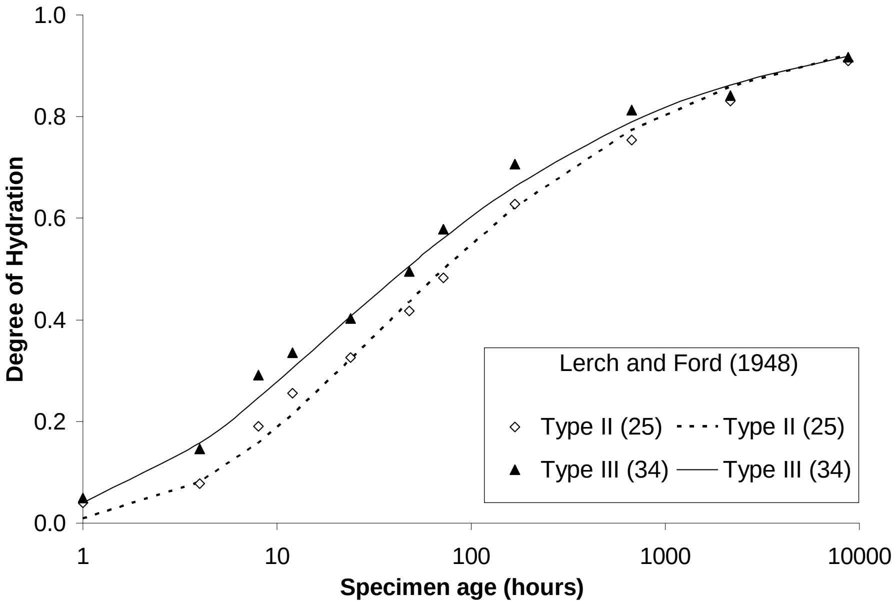

Figure D-15: Predicted and measured degree of hydration for Lerch and Ford (1948)

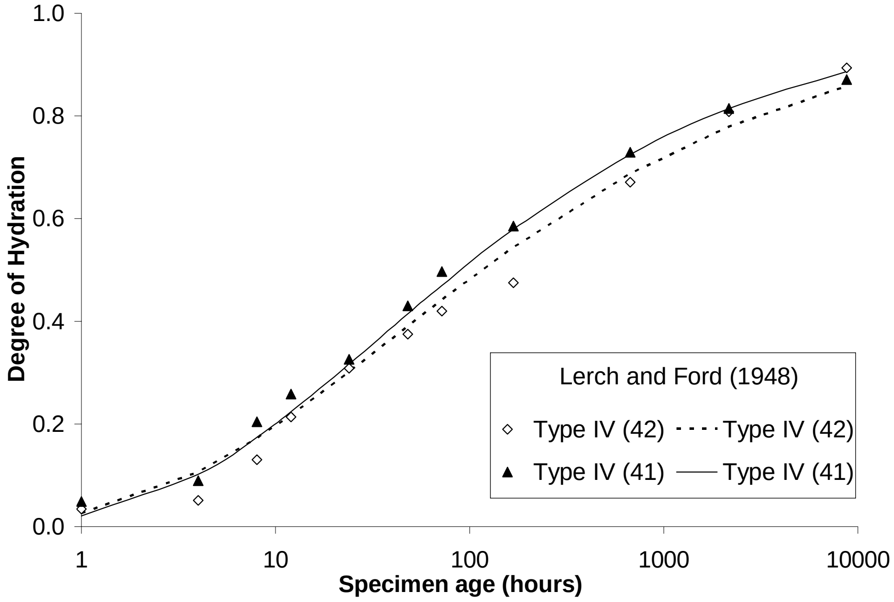

Figure D-16: Predicted and measured degree of hydration for Lerch and Ford (1948)

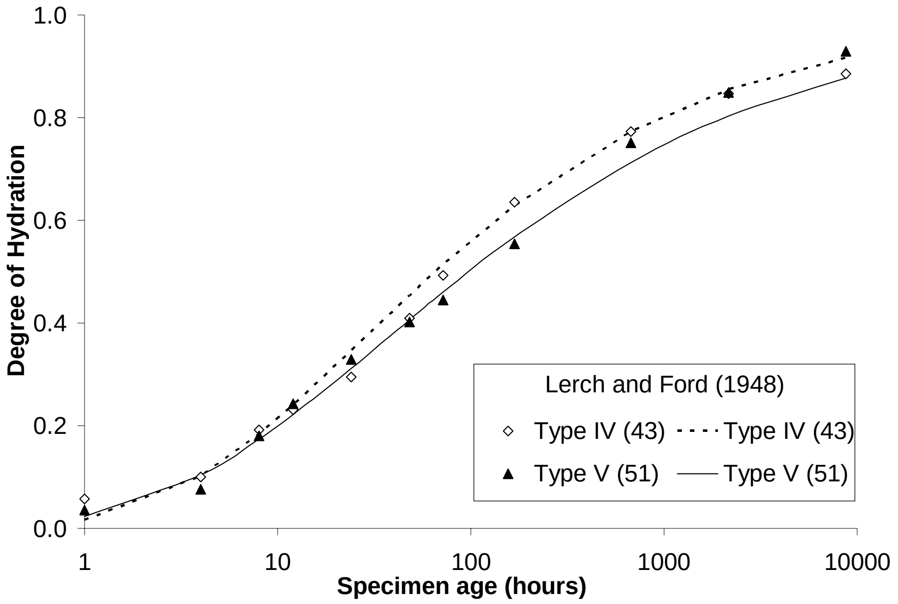

Figure D-17: Predicted and measured degree of hydration for Lerch and Ford (1948)

VALIDATION GRAPHS FOLLOW

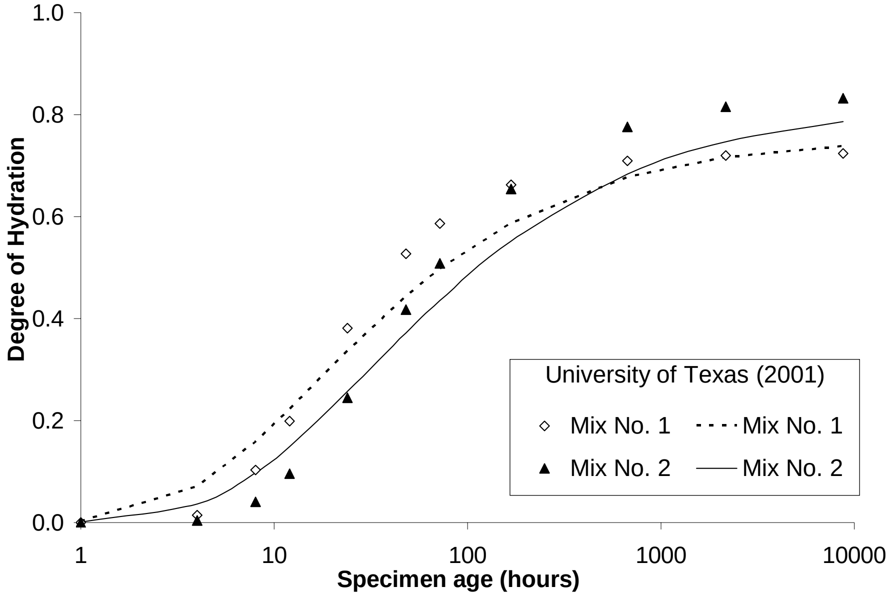

Figure D-18: Predicted and measured degree of hydration for field mixtures test in this project (Mix No. 1 = Type I/II + 20% F fly ash, Mix No. 2 = Type I/II + 25% C fly ash)

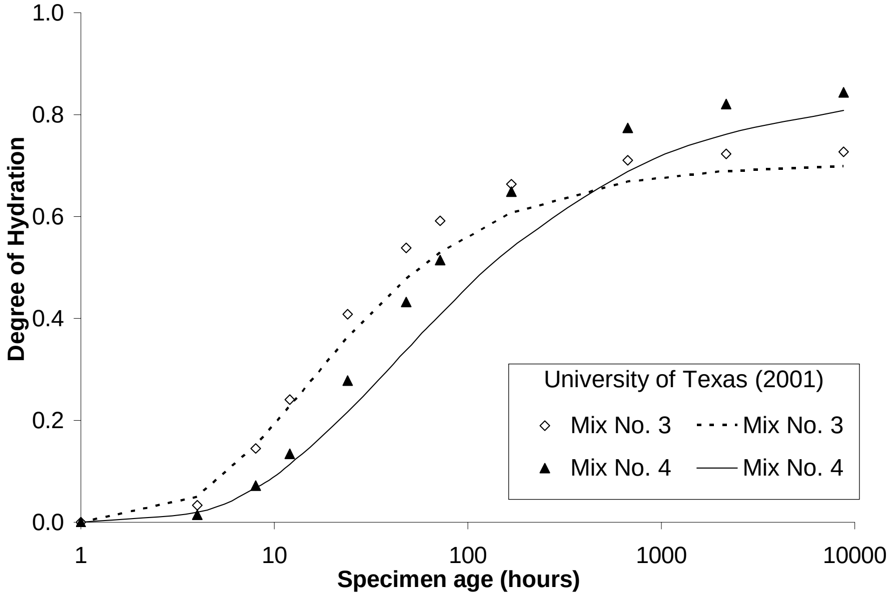

Figure D-19: Predicted and measured degree of hydration for field mixtures test in this project (Mix No. 3 = Type I cement only, Mix No. 4 = Type I/II + 35% C fly ash)

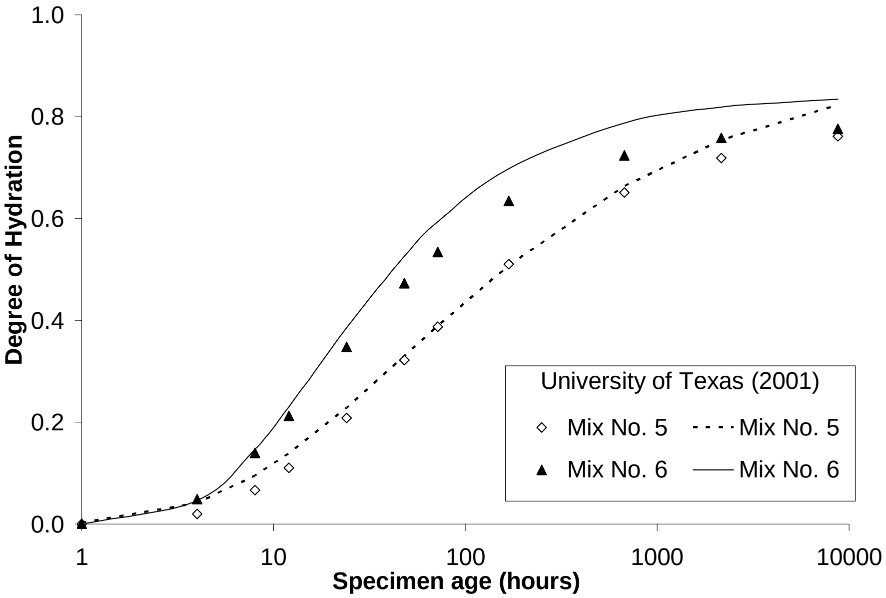

Figure D-20: Predicted and measured degree of hydration for field mixtures test in this project (Mix No. 5 = Type I/II + 50% GGBF Slag, Mix No. 6 = Type I + 20% F fly ash)

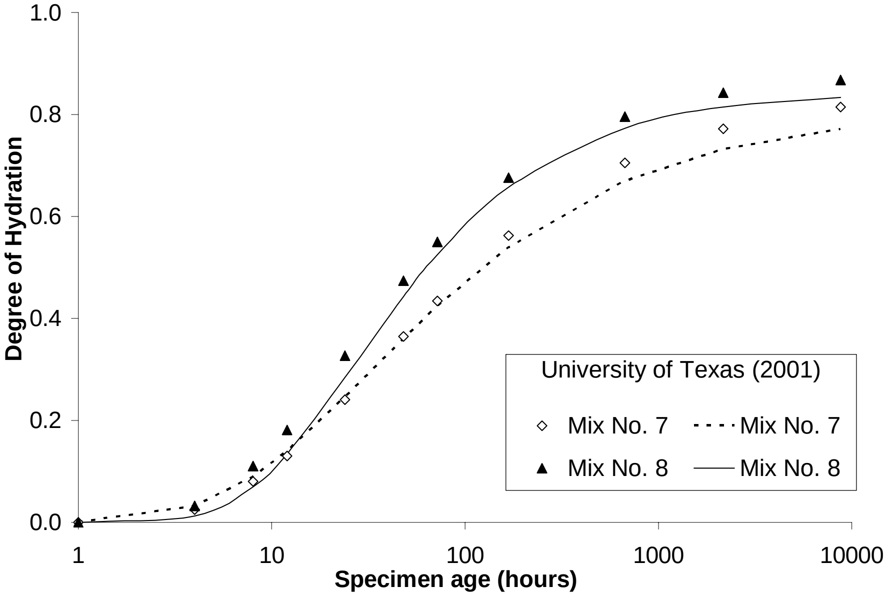

Figure D-21: Predicted and measured degree of hydration for field mixtures test in this project (Mix No. 7 = Type I + 25% C fly ash, Mix No. 8 = Type I + 30% C fly ash)

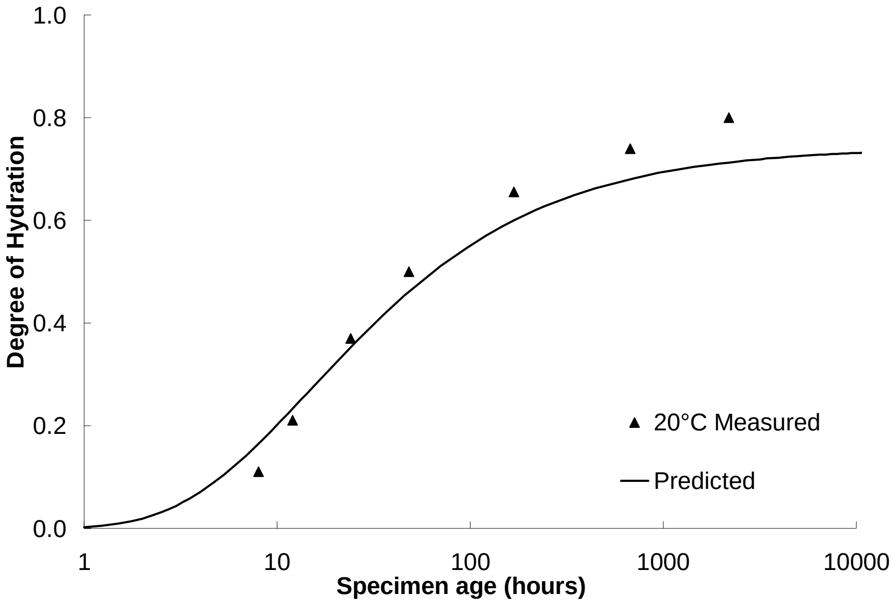

Figure D-22: Measured versus predicted degree of hydration for Kjellsen and Detwiler (1991)

APPENDIX E

Temperature Prediction Results

Part I: Small Insulated Slab Specimens

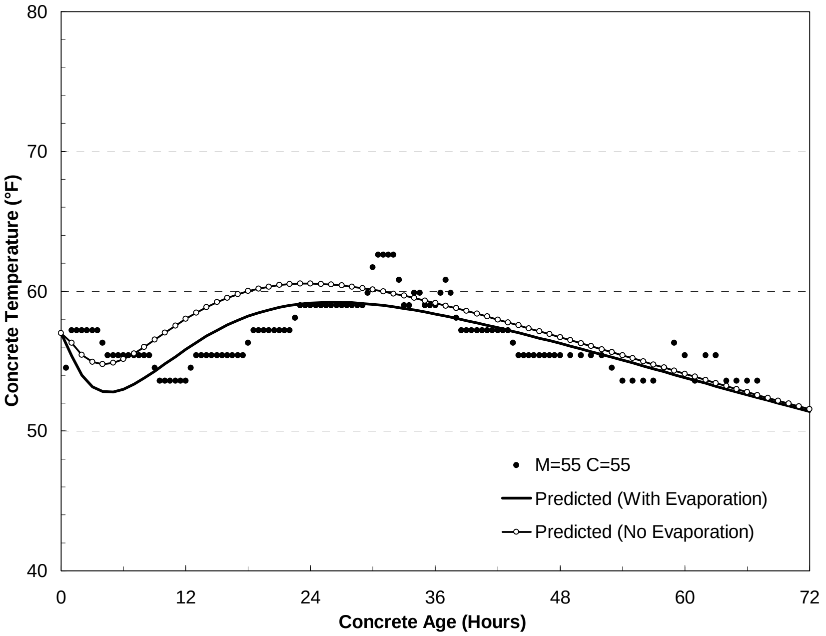

Figure E-1: Predicted and measured concrete temperature at mid-depth (M=55, C=55) (**M** = Approximate Mixing temperature, **C** = Approximate constant Curing temperature)

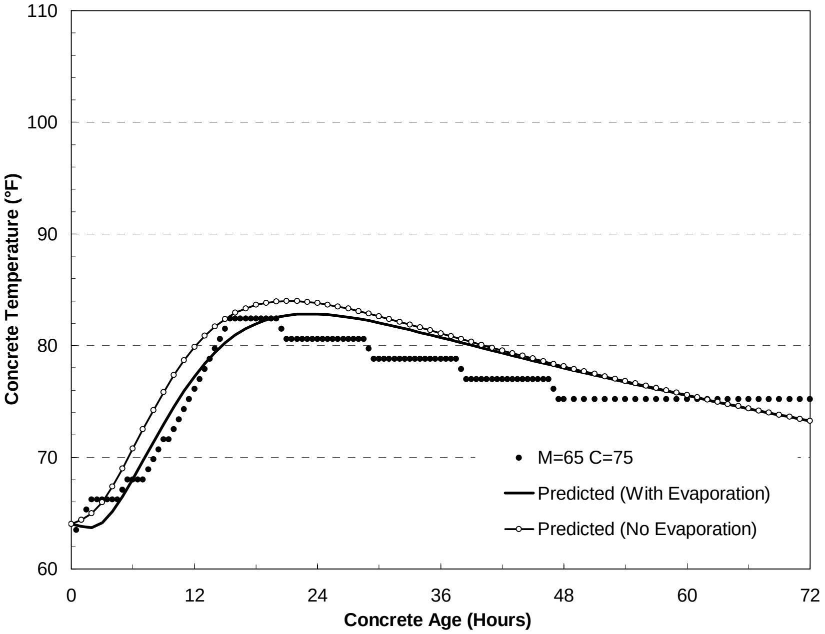

Figure E-2: Predicted and measured concrete temperature at mid-depth (M=65, C=75) (**M** = Approximate Mixing temperature, **C** = Approximate constant Curing temperature)

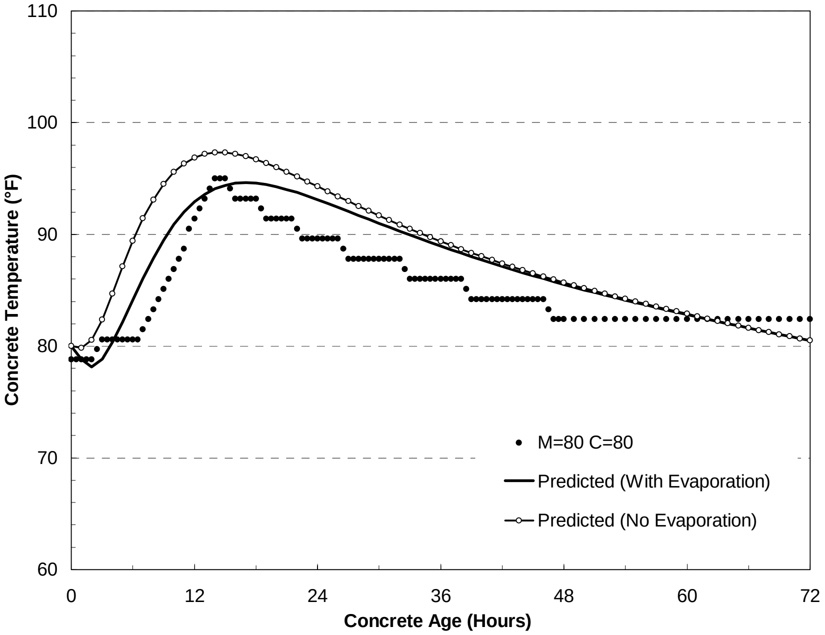

Figure E-3: Predicted and measured concrete temperature at mid-depth (M=80, C=80) (**M** = Approximate Mixing temperature, **C** = Approximate constant Curing temperature)

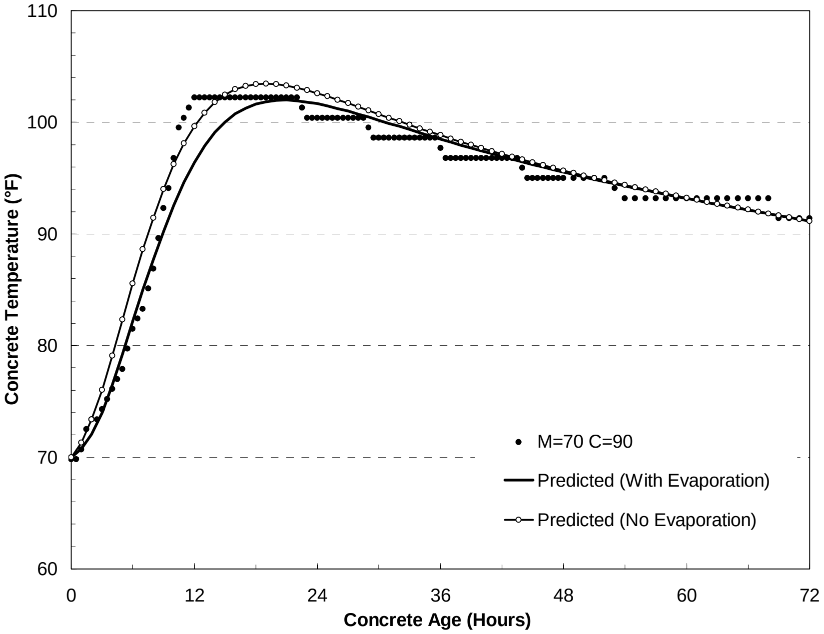

Figure E-4: Predicted and measured concrete temperature at mid-depth (M=70, C=90) (**M** = Approximate Mixing temperature, **C** = Approximate constant Curing temperature)

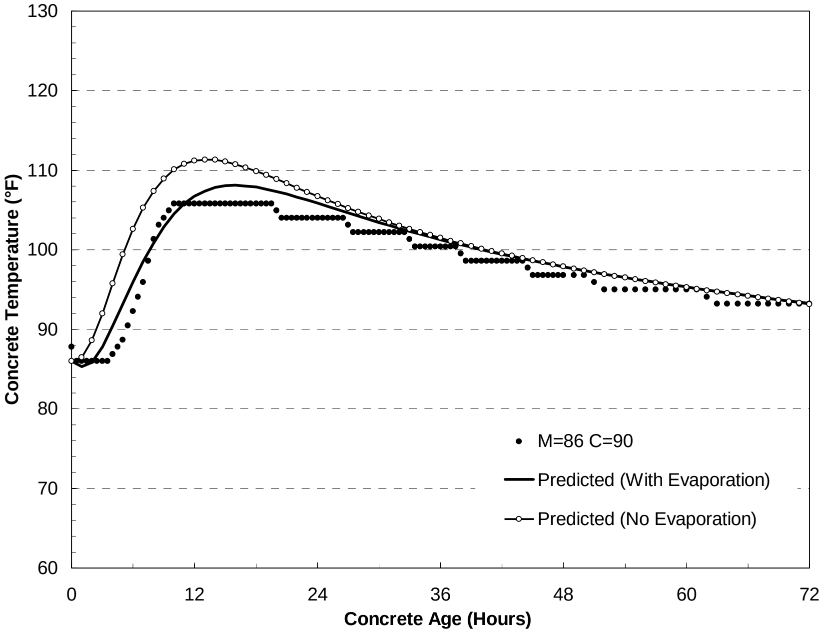

Figure E-5: Predicted and measured concrete temperature at mid-depth (M=86, C=90) (**M** = Approximate Mixing temperature, **C** = Approximate constant Curing temperature)

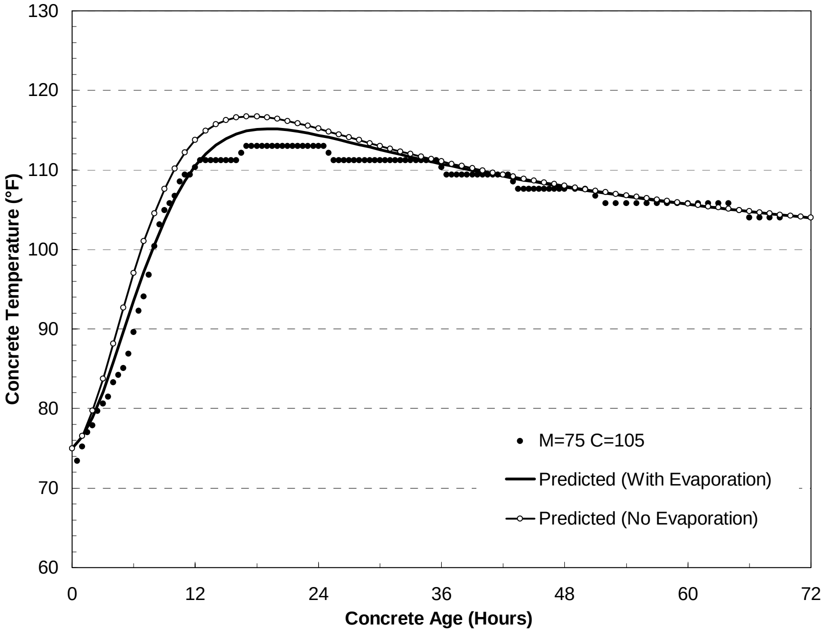

Figure E-6: Predicted and measured concrete temperature at mid-depth (M=75, C=105) (**M** = Approximate Mixing temperature, **C** = Approximate constant Curing temperature)

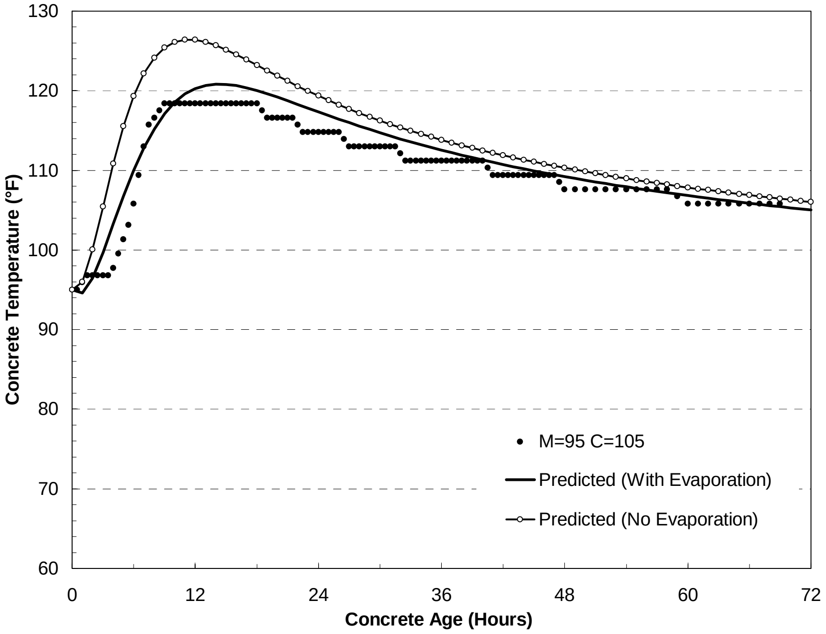

Figure E-7: Predicted and measured concrete temperature at mid-depth (M=95, C=105) (**M** = Approximate Mixing temperature, **C** = Approximate constant Curing temperature)

Part II: Field site calibration Results

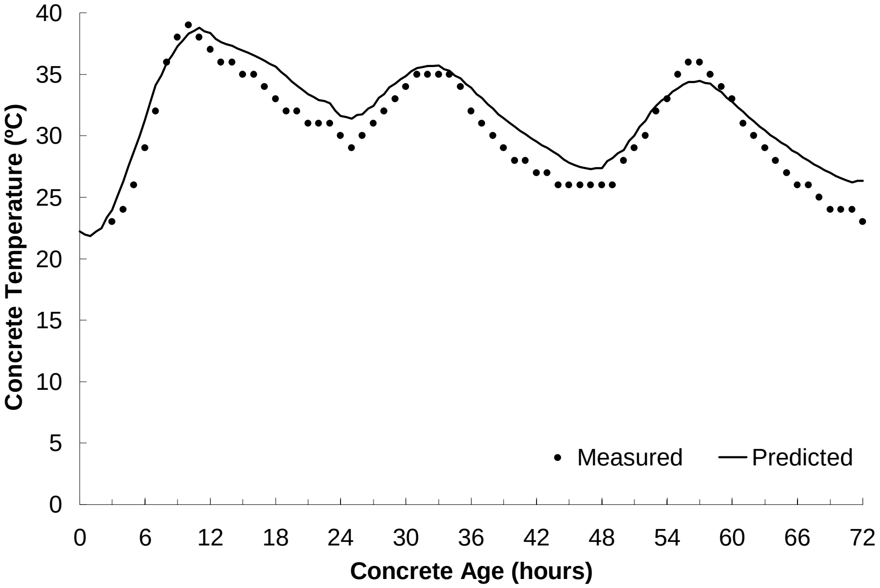

Figure E-8: Calibration results: Concrete temperatures 1” from top of slab for Dallas, May

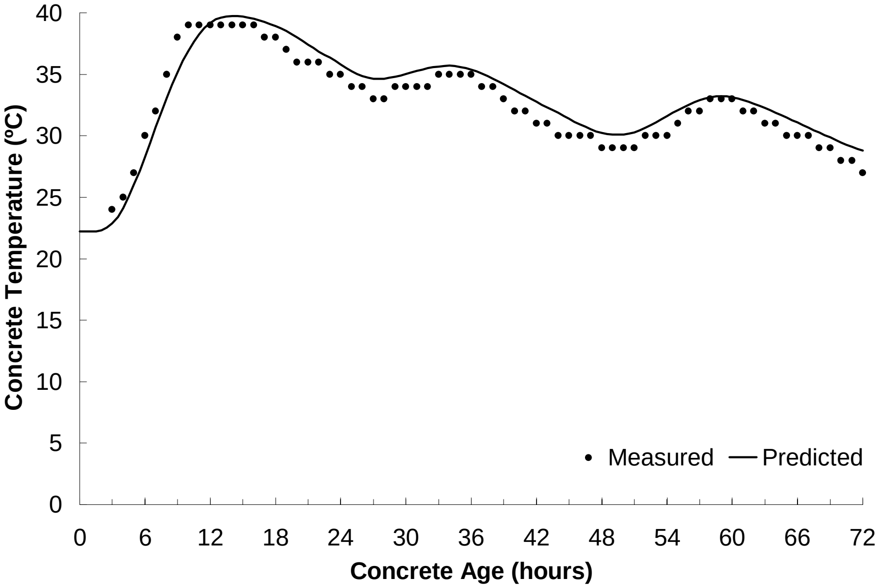

Figure E-9: Calibration results: Concrete temperatures at mid-depth for Dallas, May

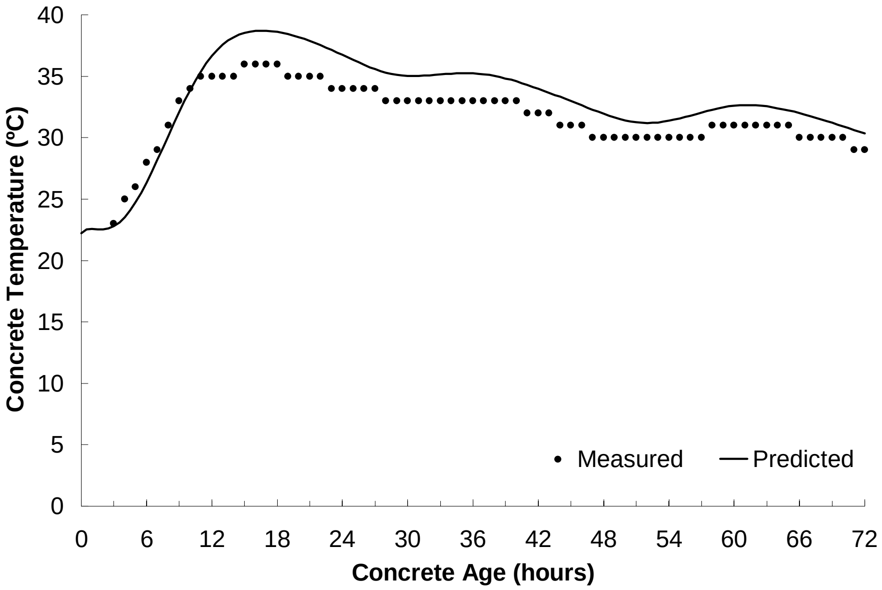

Figure E-10: Calibration results: Concrete temperature 1” from bottom of slab for Dallas, May

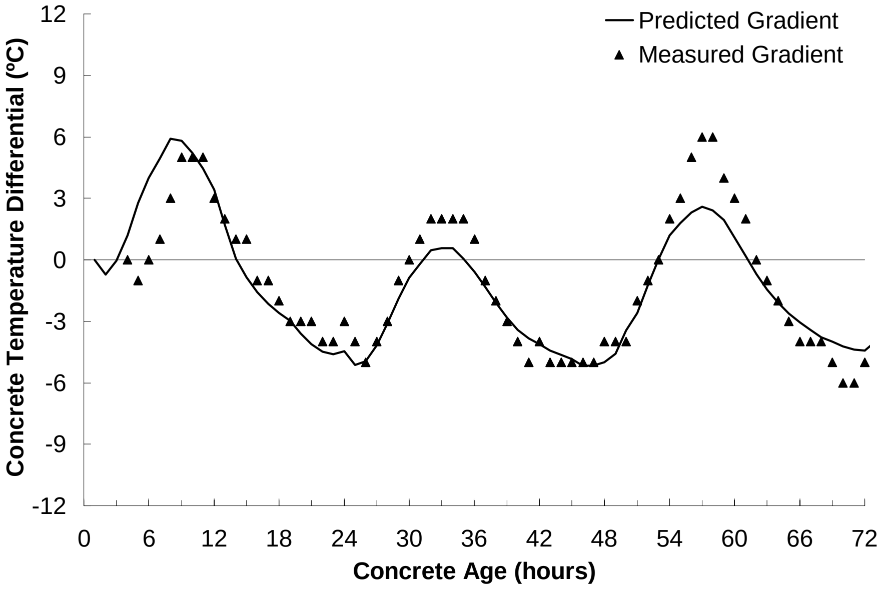

Figure E-11: Calibration results: Concrete temperature gradient for Dallas, May

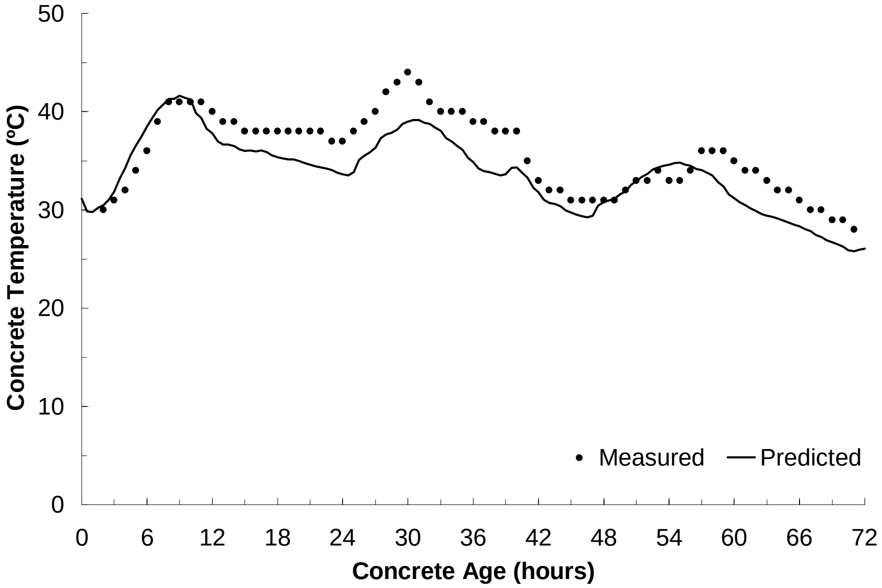

Figure E-12: Calibration results: Concrete temperatures 1" from top of slab for Houston, May, 8:45am placement

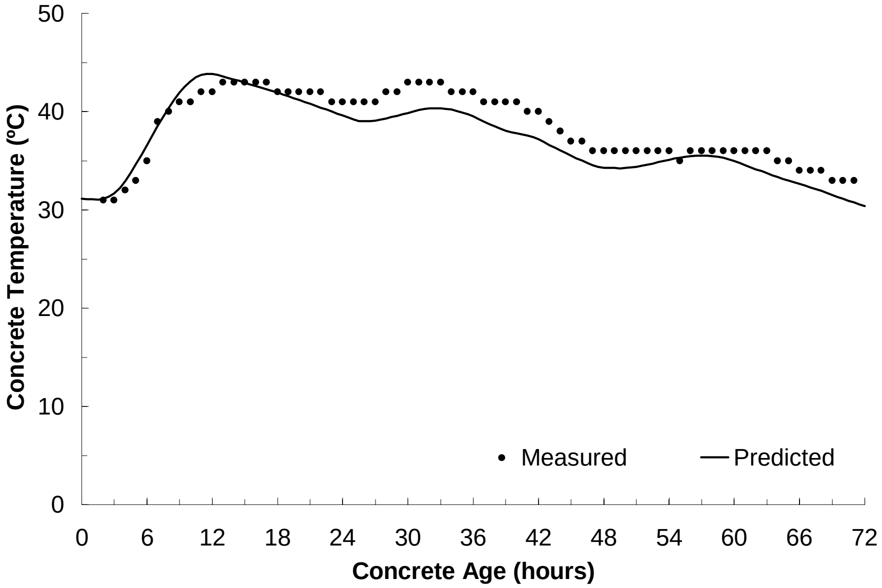

Figure E-13: Calibration results: Concrete temperatures at mid-depth for Houston, May, 8:45am placement

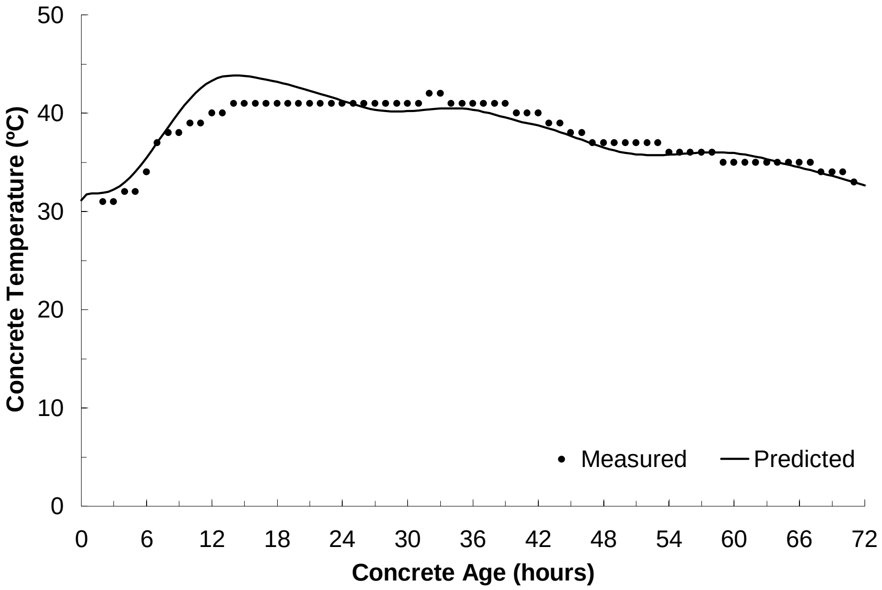

Figure E-14: Calibration results: Concrete temperature 1” from bottom for Houston, May, 8:45am placement

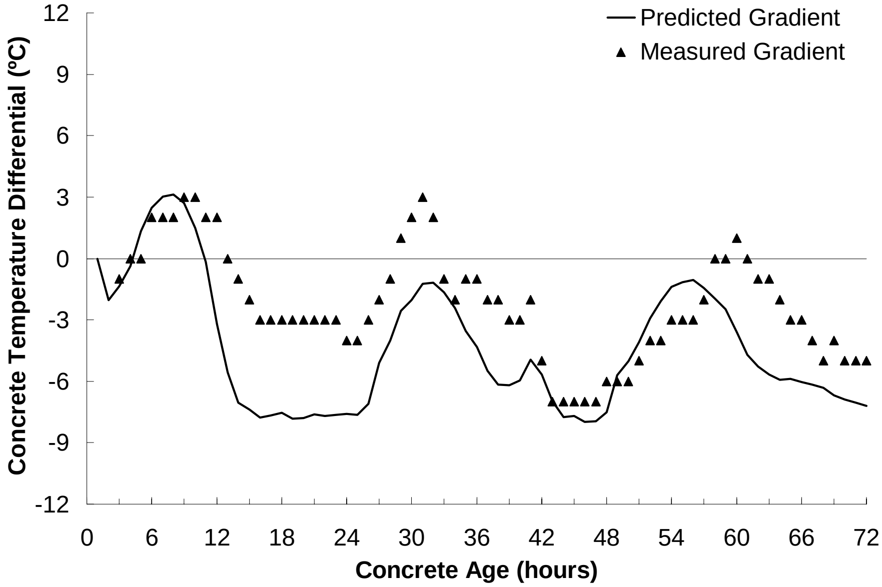

Figure E-15: Calibration results: Concrete temperature gradient for Houston, May, 8:45am placement

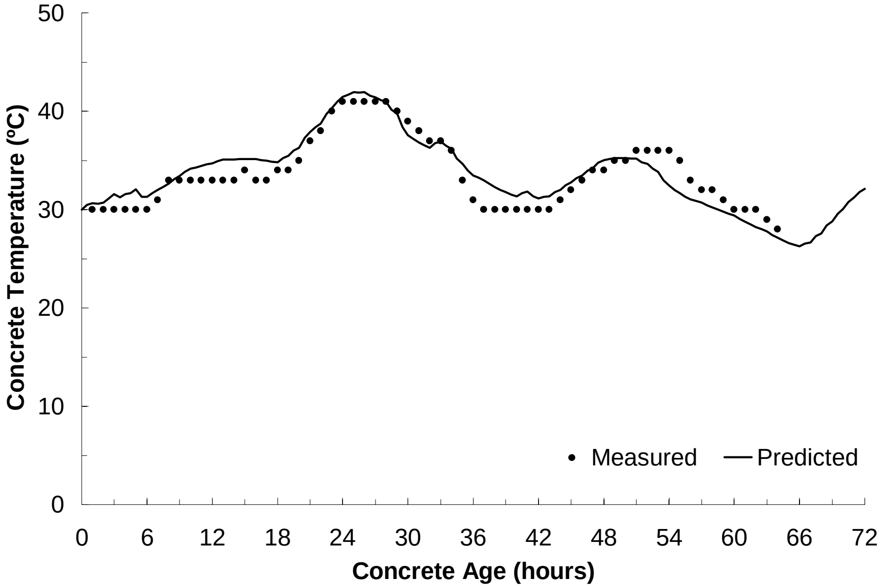

Figure E-16: Calibration results: Concrete temperatures 1" from top of slab for Houston, May, 3:10pm placement

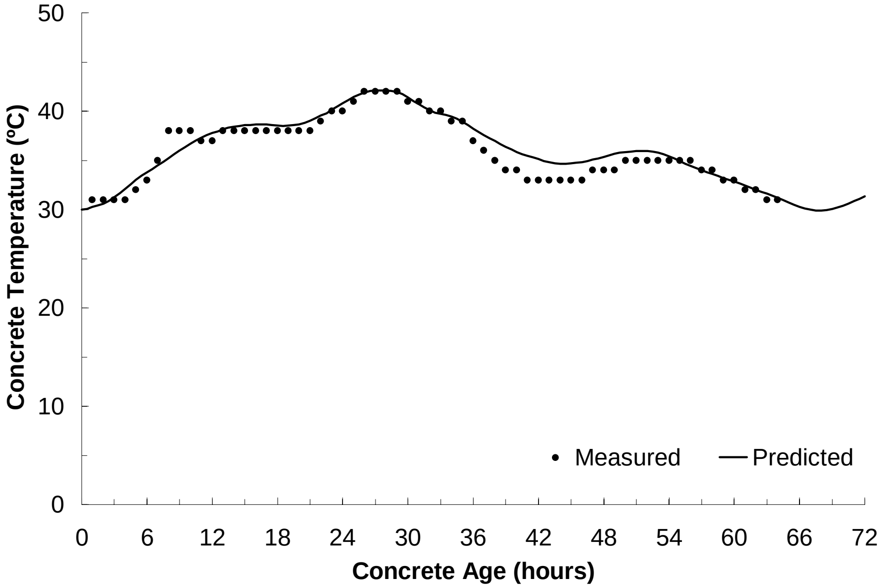

Figure E-17: Calibration results: Concrete temperatures at mid-depth for Houston, May, 3:10pm placement

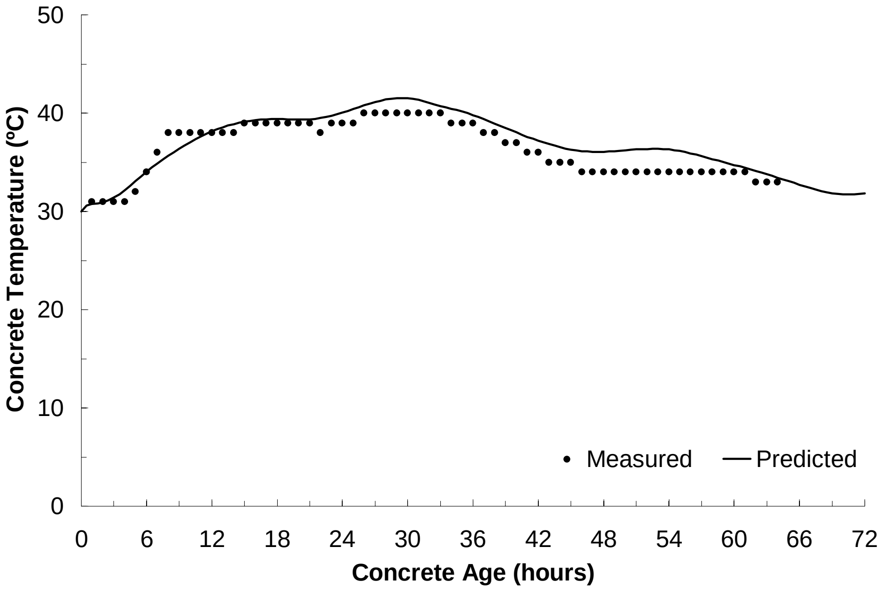

Figure E-18: Calibration results: Concrete temperature 1” from bottom for Houston, May, 3:10pm placement

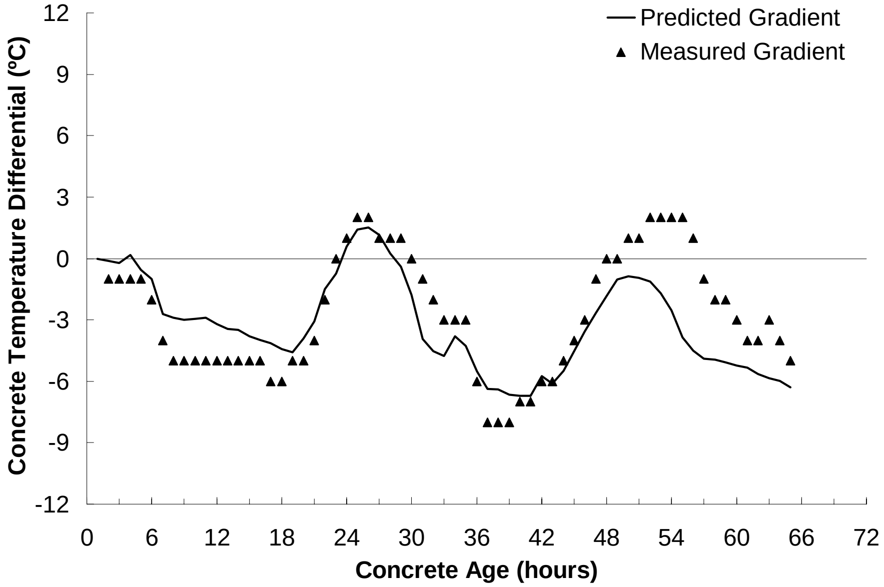

Figure E-19: Calibration results: Concrete temperature gradient for Houston, May, 3:10pm placement

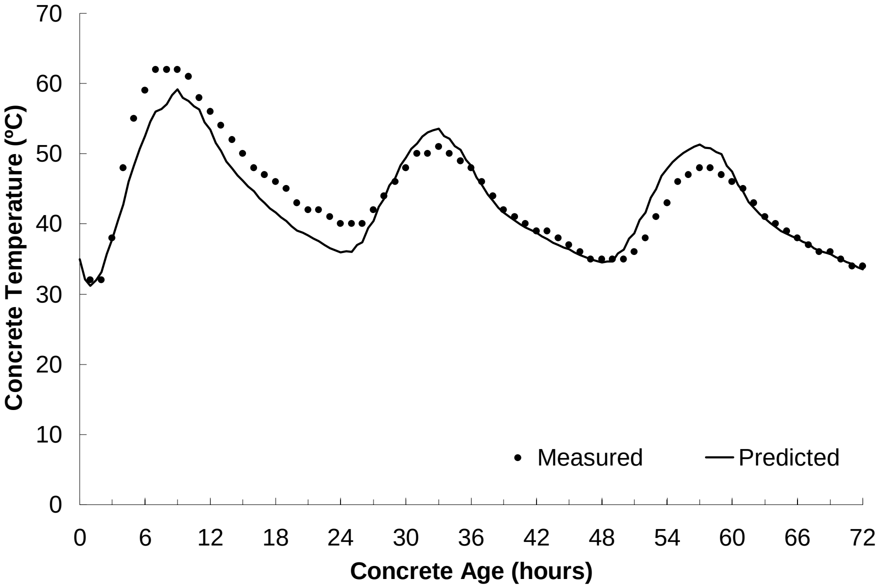

Figure E-20: Calibration results: Concrete temperatures 1” from top of slab for Dallas, August

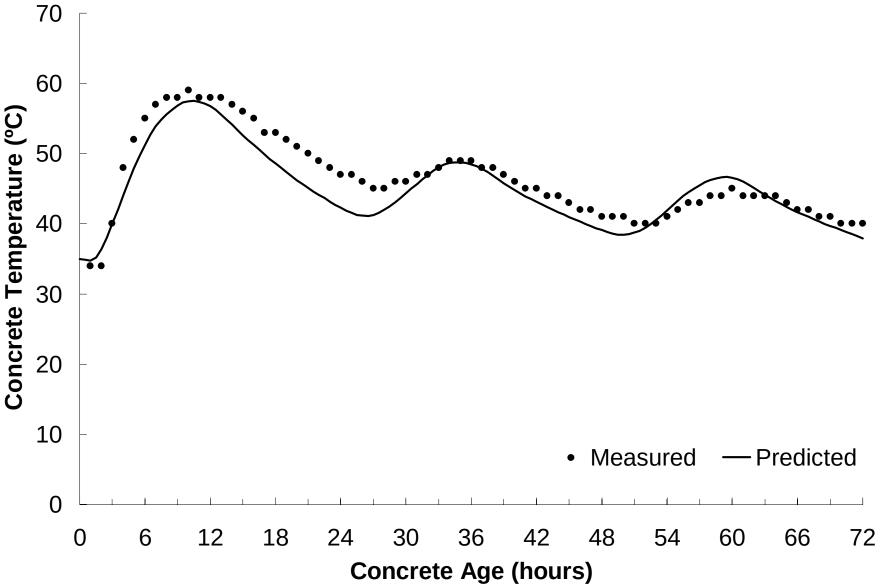

Figure E-21: Calibration results: Concrete temperatures at mid-depth for Dallas, August

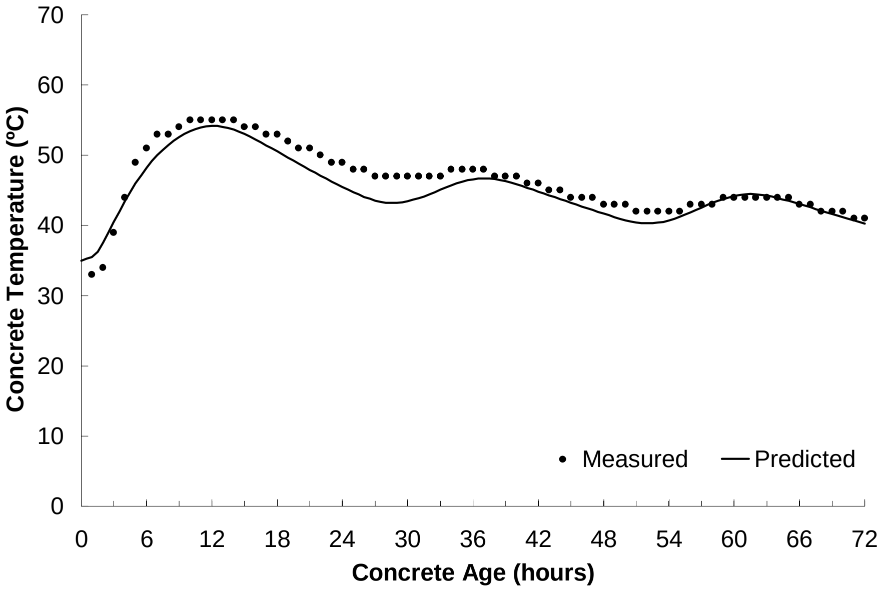

Figure E-22: Calibration results: Concrete temperature 1” from bottom of slab for Dallas, August

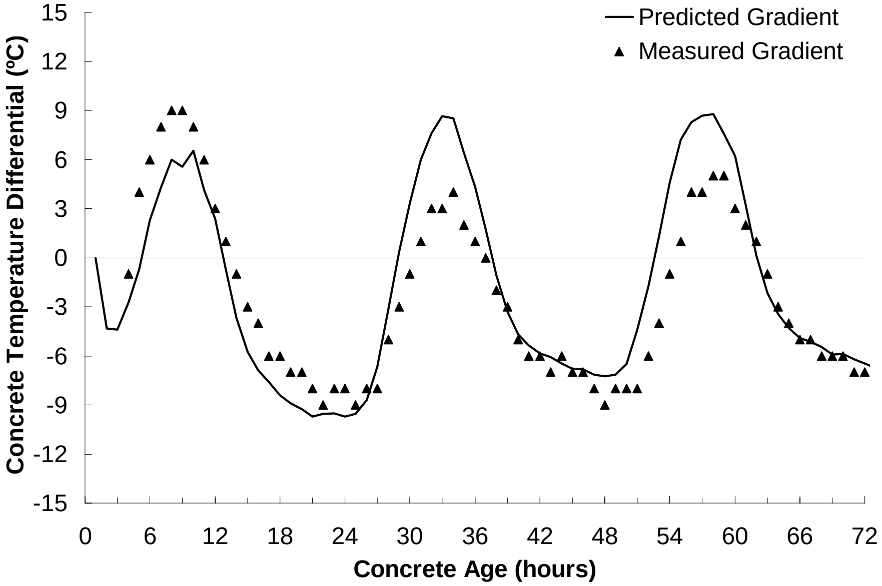

Figure E-23: Calibration results: Concrete temperature gradient for Dallas, August

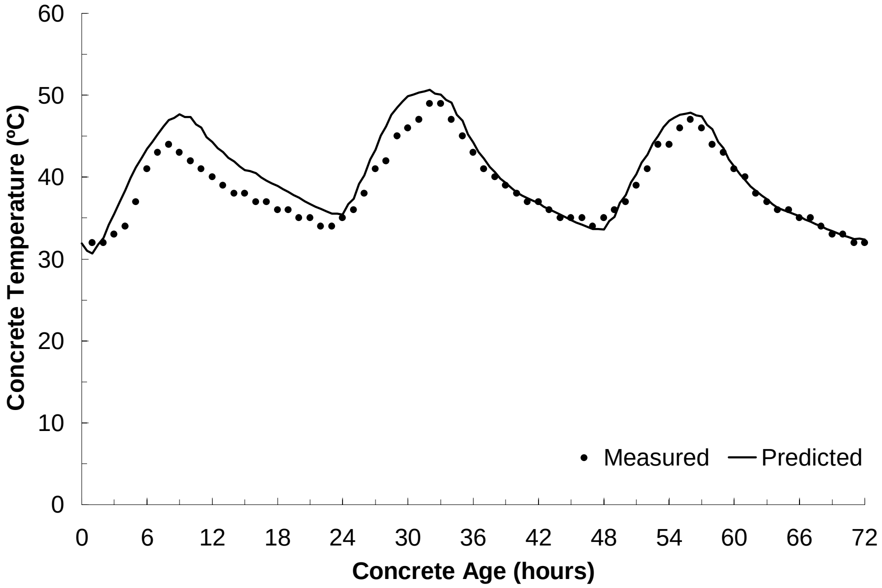

Figure E-24: Calibration results: Concrete temperatures 1” from top of slab for Houston, August, 9:30am placement

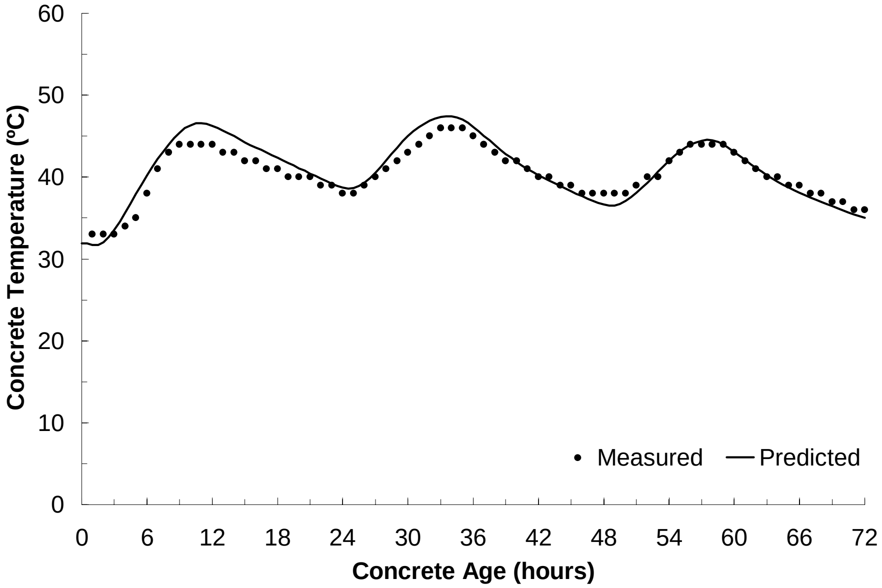

Figure E-25: Calibration results: Concrete temperatures at mid-depth for Houston, August, 9:30am placement

Figure E-26: Calibration results: Concrete temperature 1” from bottom for Houston, August, 9:30am placement

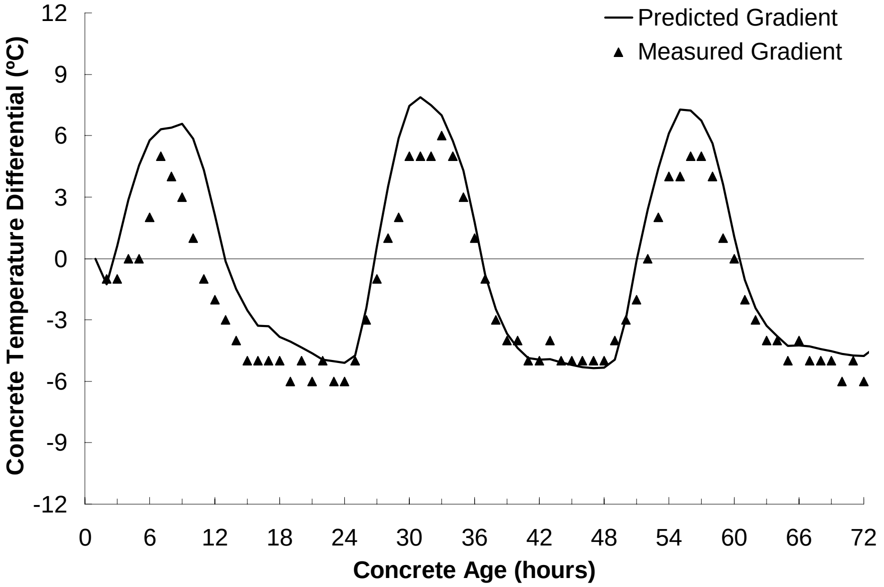

Figure E-27: Calibration results: Concrete temperature gradient for Houston, August, 9:30am placement

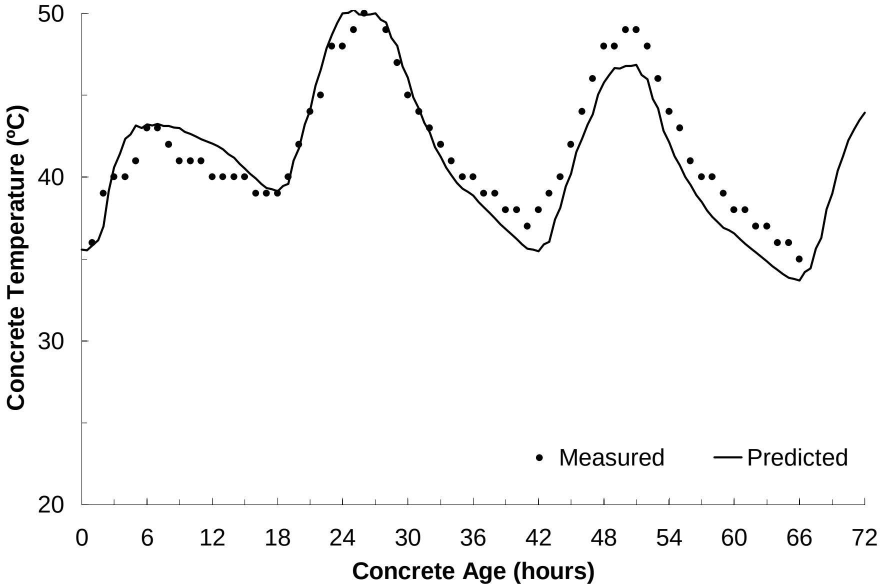

Figure E-28: Calibration results: Concrete temperatures 1" from top of slab for Houston, August, 2:45pm placement

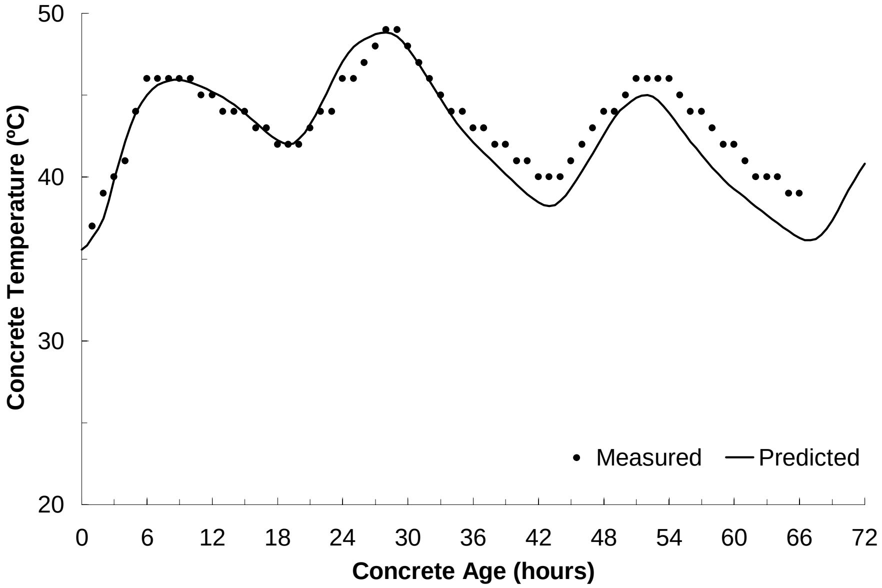

Figure E-29: Calibration results: Concrete temperatures at mid-depth for Houston, August, 2:45pm placement

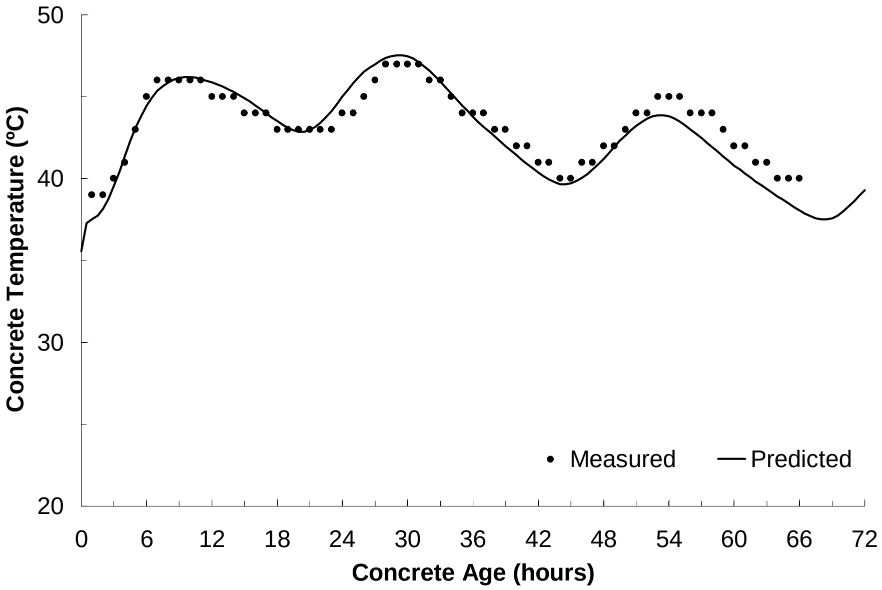

Figure E-30: Calibration results: Concrete temperature 1” from bottom for Houston, August, 2:45pm placement

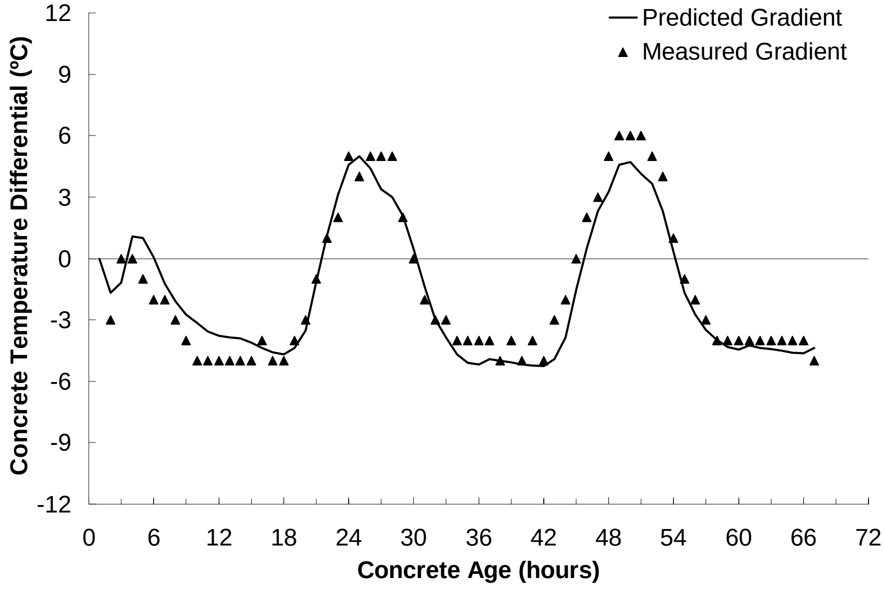

Figure E-31: Calibration results: Concrete temperature gradient for Houston, August, 2:45pm placement

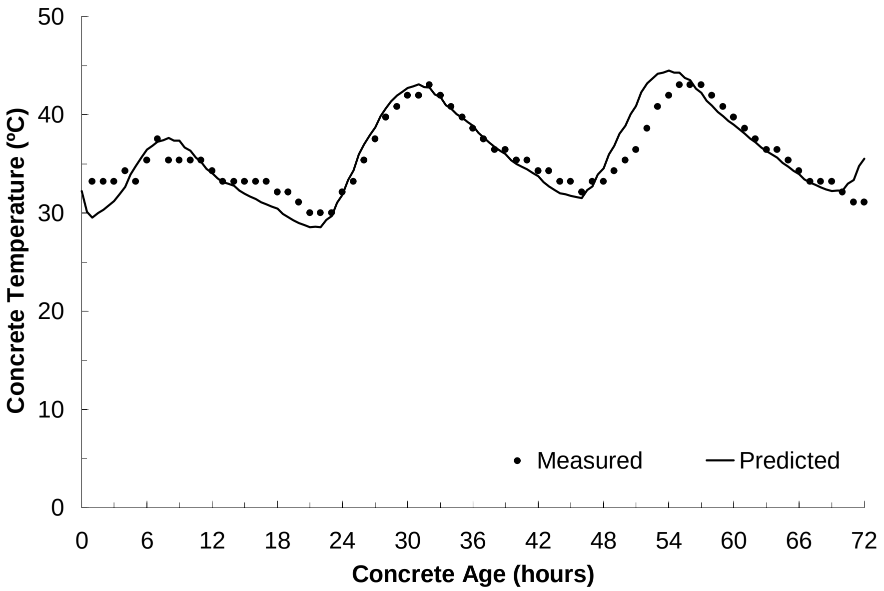

Figure E-32: Calibration results: Concrete temperatures 1” from top of slab for El Paso, August

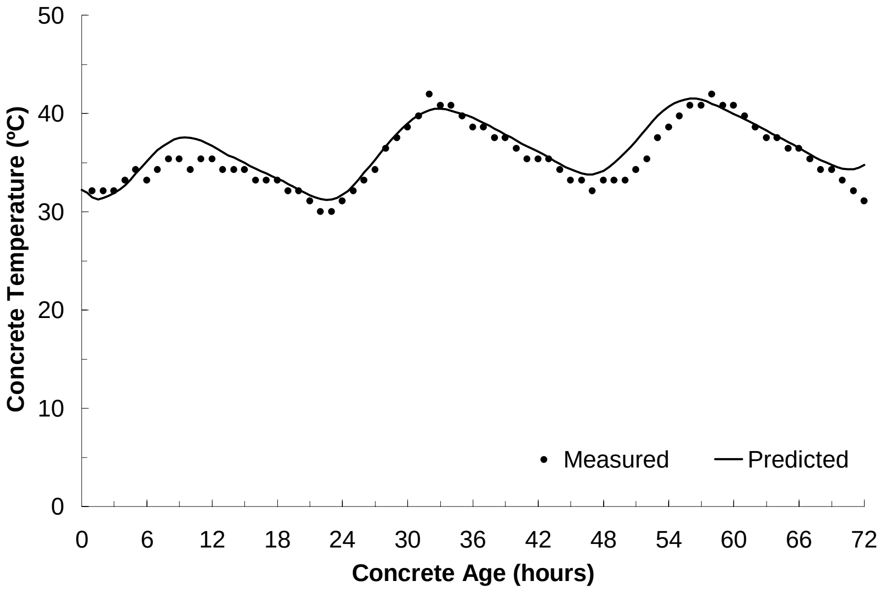

Figure E-33: Calibration results: Concrete temperatures at mid-depth for El Paso, August

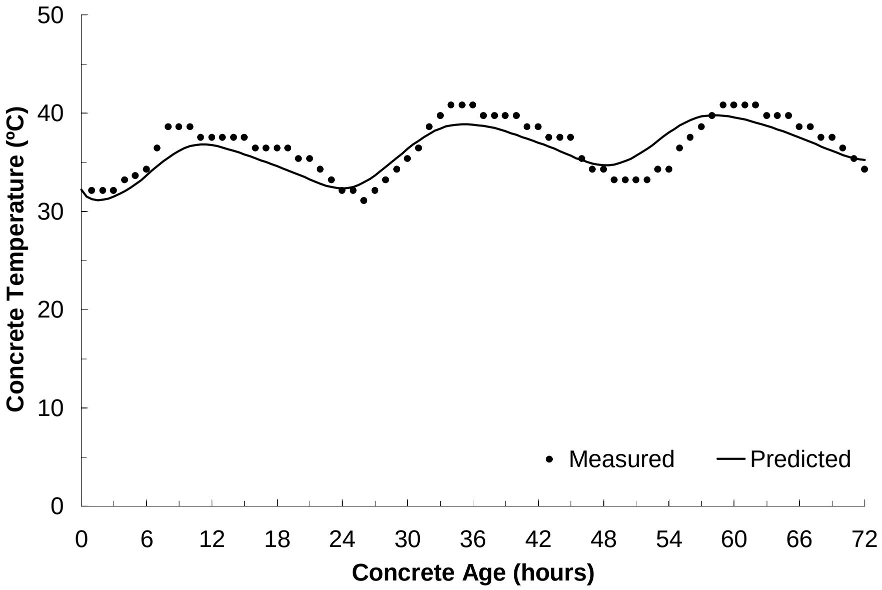

Figure E-34: Calibration results: Concrete temperature 1” from bottom of slab for El Paso, August

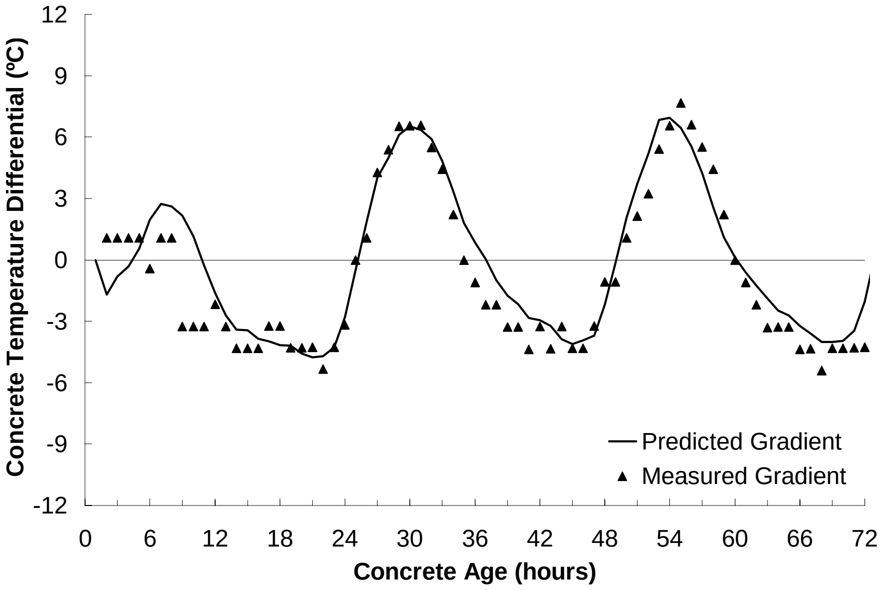

Figure E-35: Calibration results: Concrete temperature gradient for El Paso, August

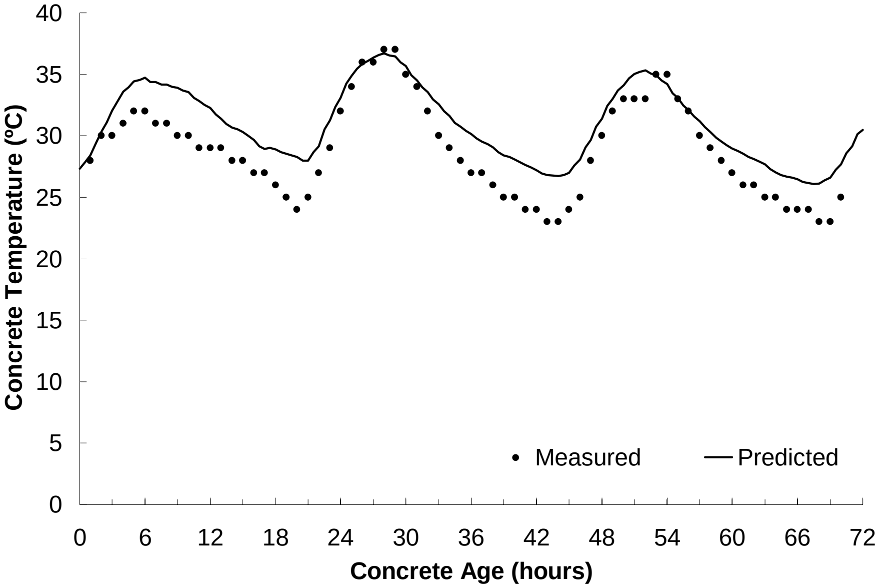

Figure E-36: Calibration results: Concrete temperatures 1” from top of slab for Dallas, September, 12:20pm placement

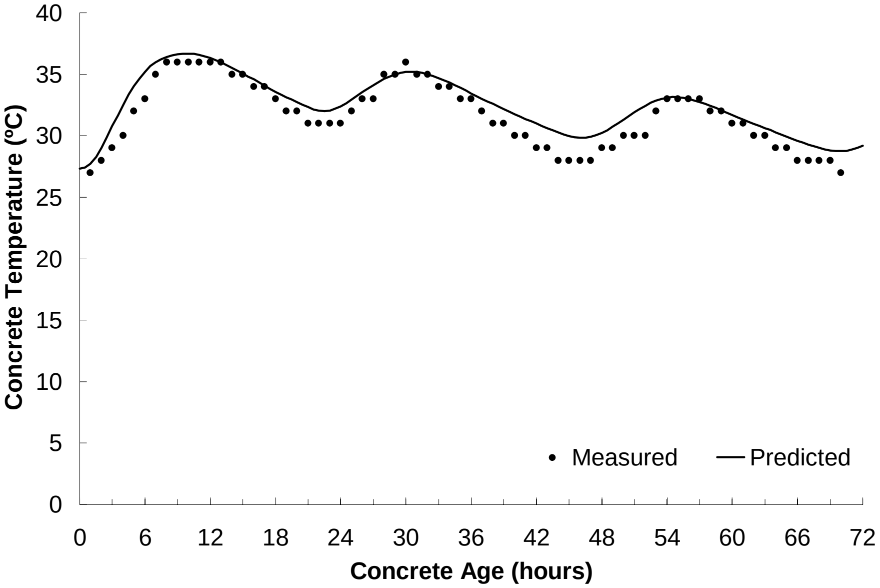

Figure E-37: Calibration results: Concrete temperatures at mid-depth for Dallas, September, 12:20pm placement

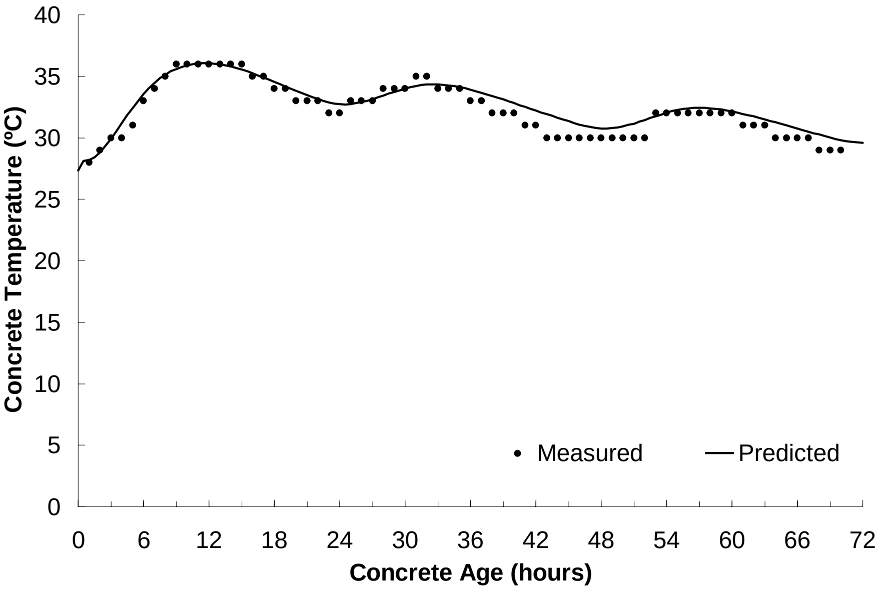

Figure E-38: Calibration results: Concrete temperature 1" from bottom for Dallas, September, 12:20pm placement

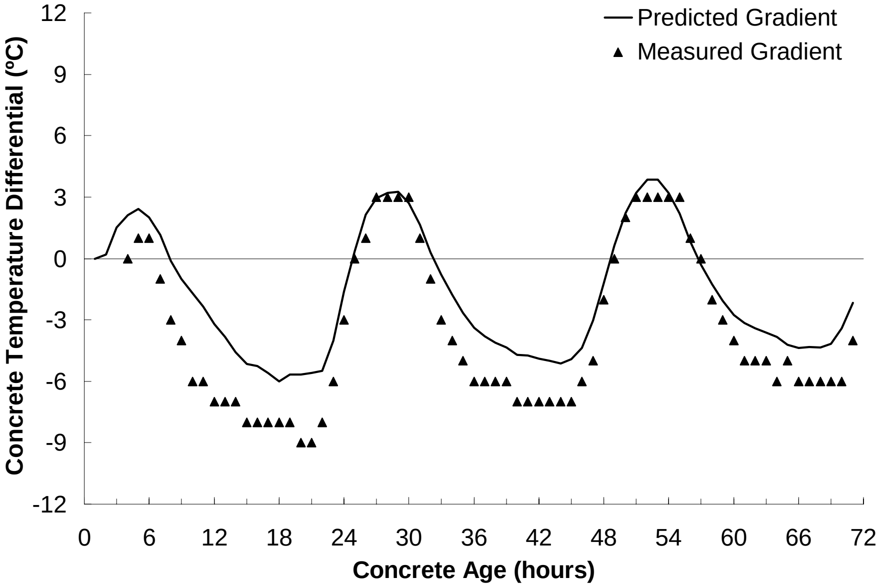

Figure E-39: Calibration results: Concrete temperature gradient for Dallas, September, 12:20pm placement

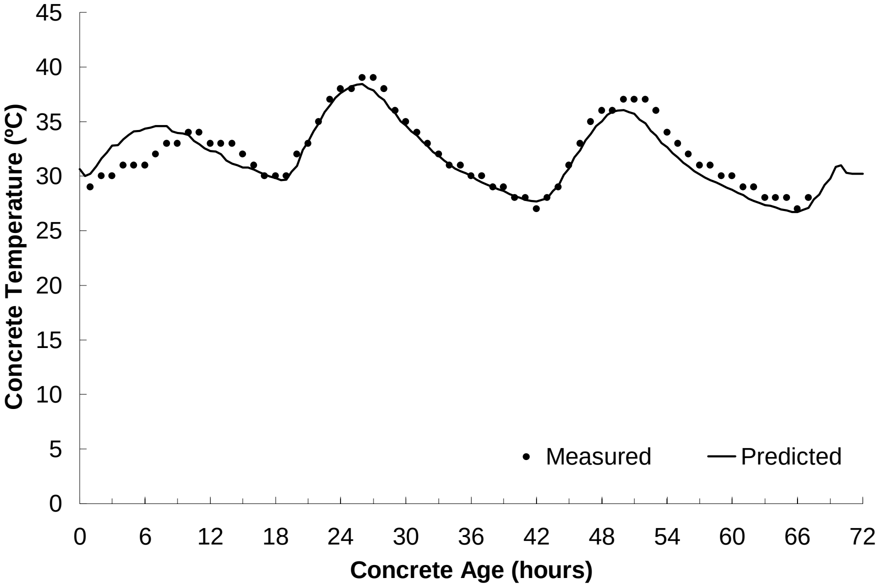

Figure E-40: Calibration results: Concrete temperatures 1" from top of slab for Dallas, September, 2:30pm placement

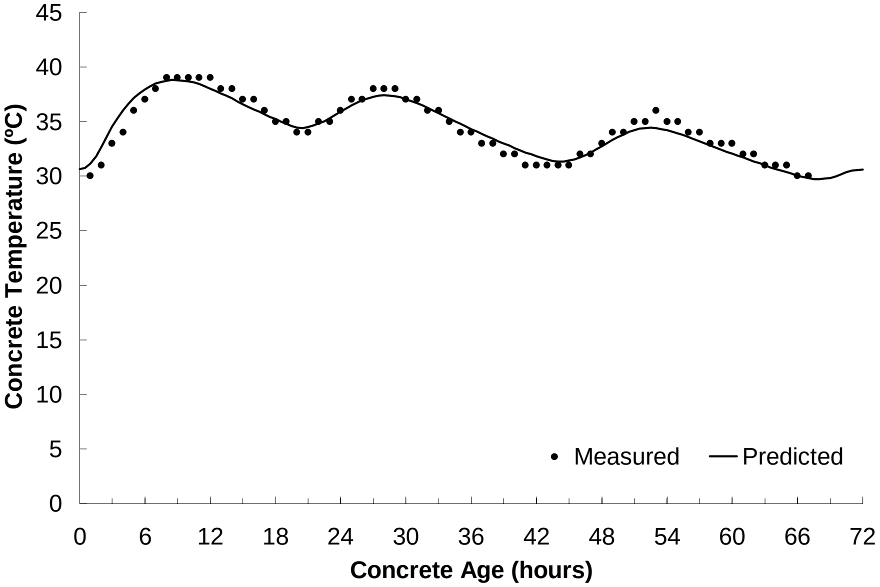

Figure E-41: Calibration results: Concrete temperatures at mid-depth for Dallas, September, 2:30pm placement

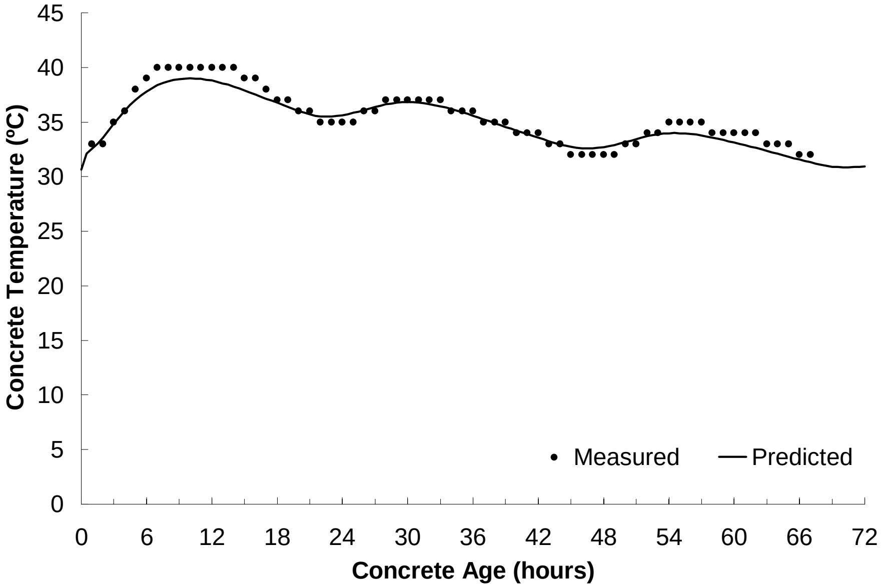

Figure E-42: Calibration results: Concrete temperature 1" from bottom for Dallas, September, 2:30pm placement

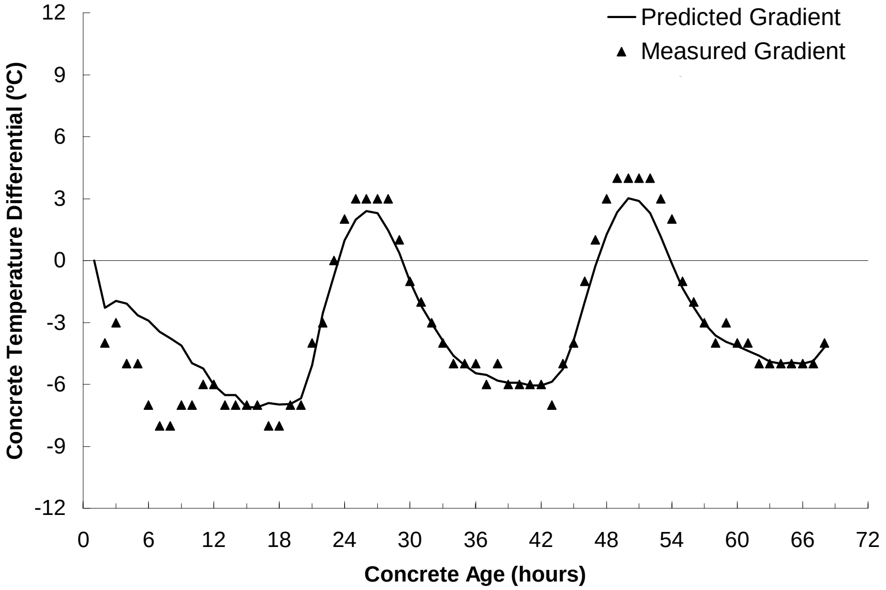

Figure E-43: Calibration results: Concrete temperature gradient for Dallas, September, 2:30pm placement

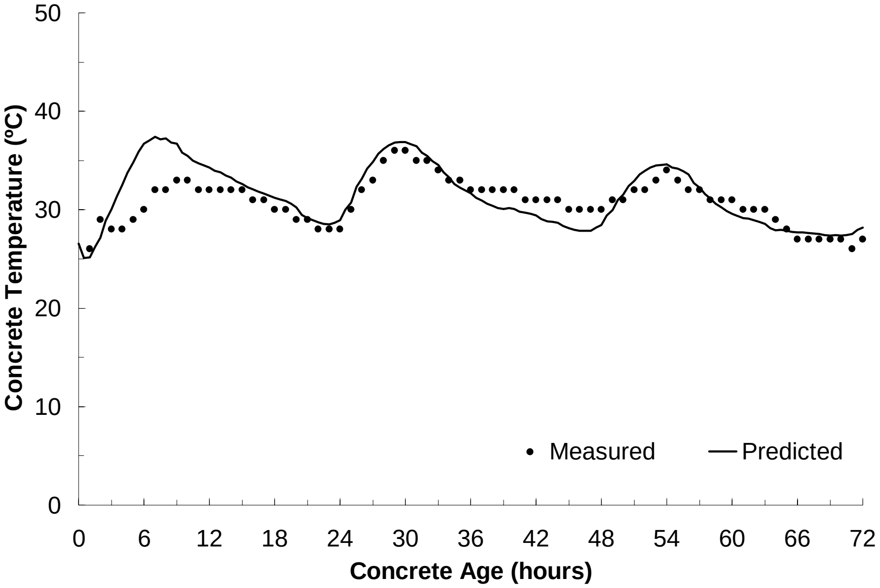

Figure E-44: Calibration results: Concrete temperatures 1” from top of slab for Houston, October, 10:00am placement

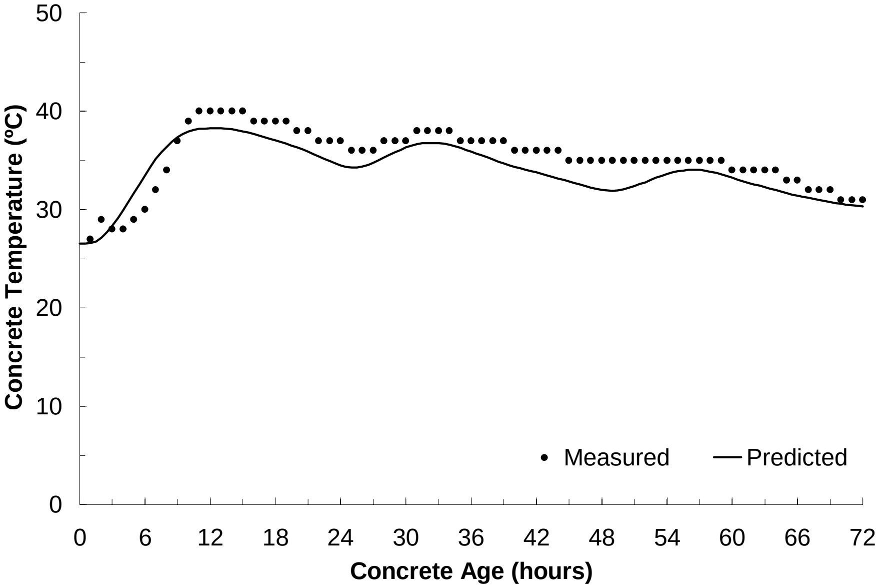

Figure E-45: Calibration results: Concrete temperatures at mid-depth for Houston, October, 10:00am placement

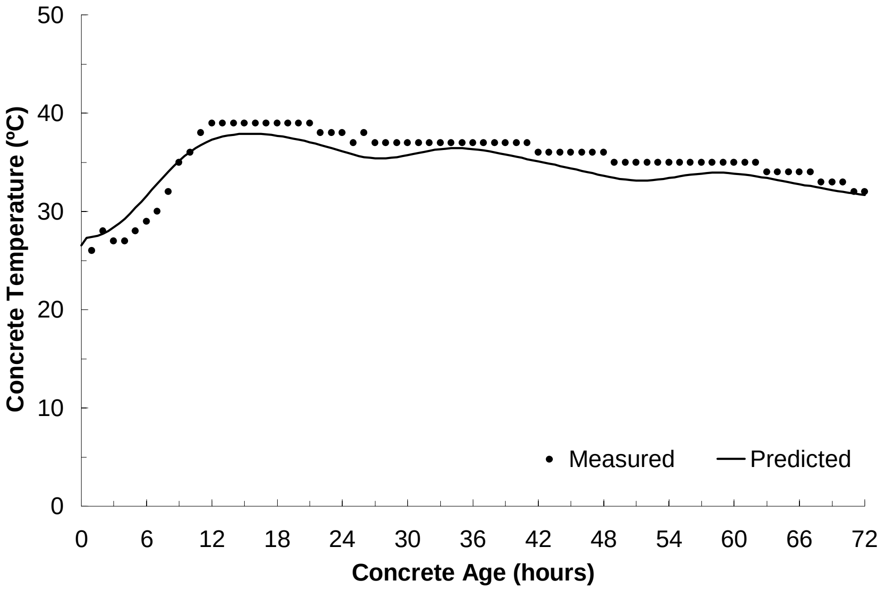

Figure E-46: Calibration results: Concrete temperature 1” from bottom for Houston, October, 10:00am placement

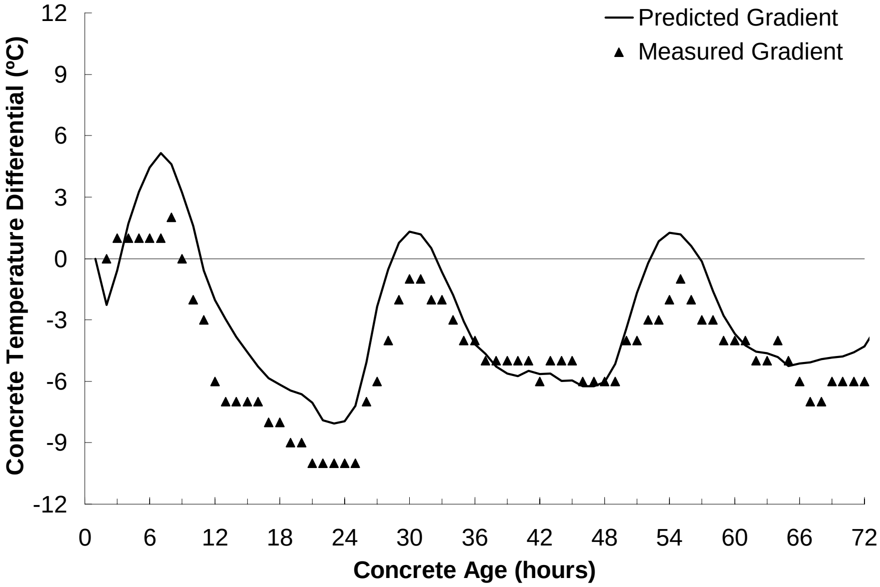

Figure E-47: Calibration results: Concrete temperature gradient for Houston, October, 10:00am placement

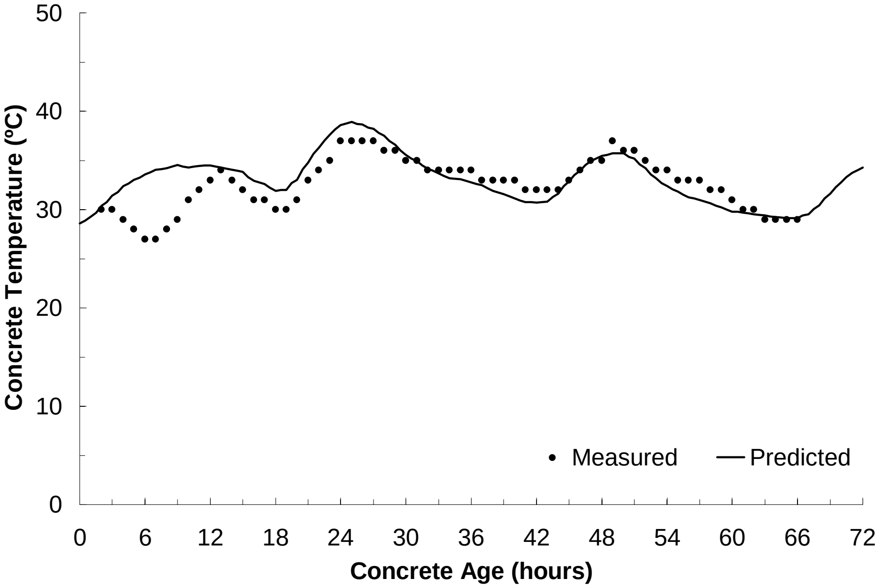

Figure E-48: Calibration results: Concrete temperatures 1” from top of slab for Houston, October, 2:45pm placement

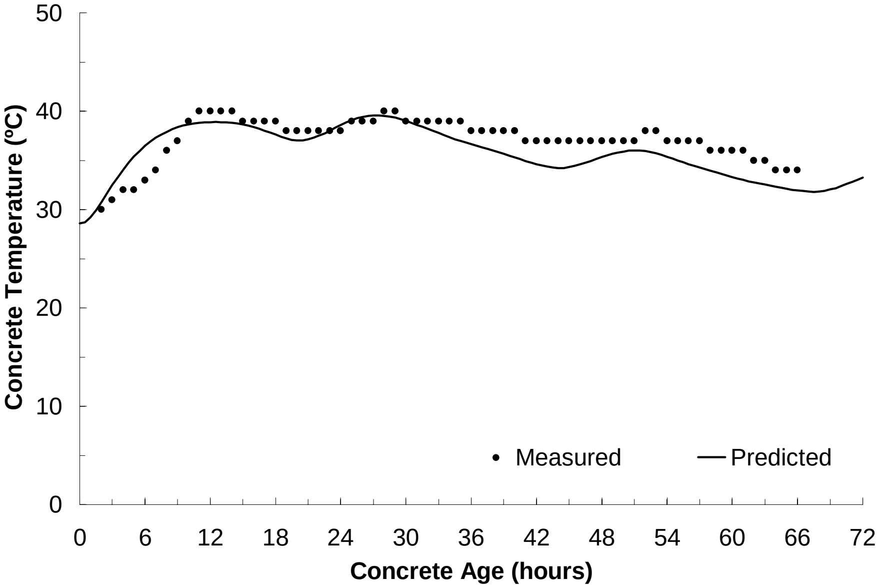

Figure E-49: Calibration results: Concrete temperatures at mid-depth for Houston, October, 2:45pm placement

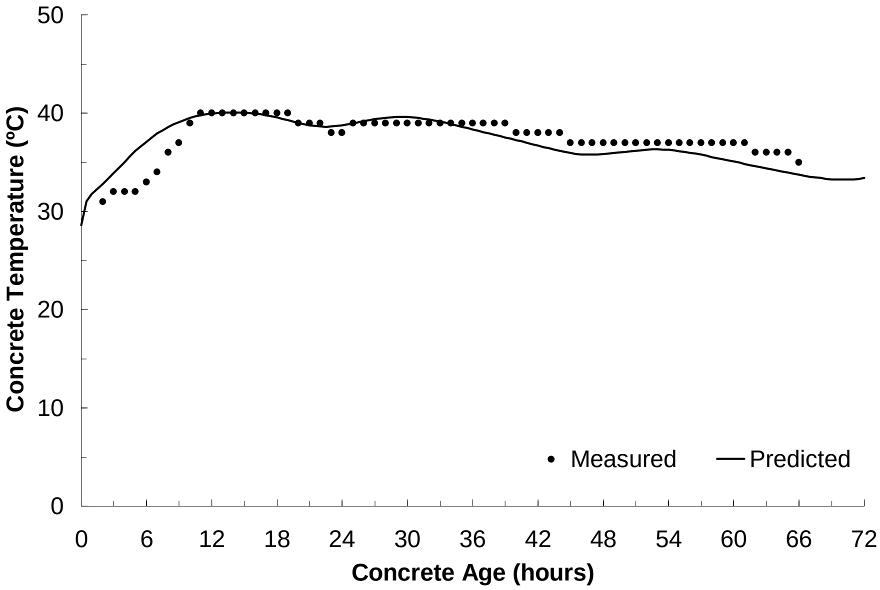

Figure E-50: Calibration results: Concrete temperature 1” from bottom for Houston, October, 2:45pm placement

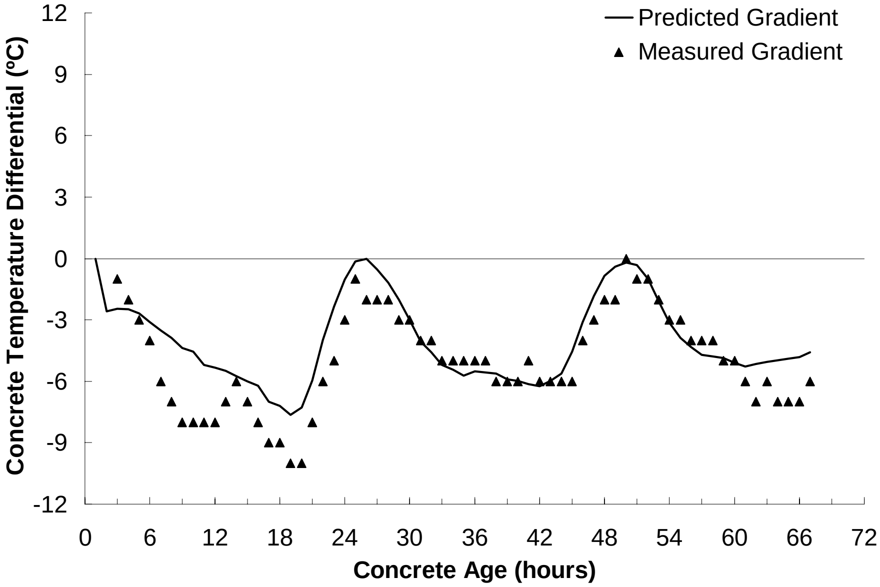

Figure E-51: Calibration results: Concrete temperature gradient for Houston, October, 2:45pm placement

APPENDIX F

Sensitivity Analysis Results

Table F-1: Sensitivity analysis results for the **maximum concrete temperature**

Variables	Units	Range	Change in Temperature, °F			% Change from Base Line			Sensitivity Rating
			Paving Climate			Paving Climate			
			Cold	Normal	Hot	Cold	Normal	Hot	
GENERAL INPUTS									
PCC Thickness	in	7	-2.3	-4.5	-5.1	-3%	-4%	-4%	Moderate
		10	-1.1	-1.8	-1.9	-1%	-2%	-1%	
		12	.	.	.	.	.	.	
		18	4.2	5.2	5.4	5%	5%	4%	
Subbase Thickness	in	4	-0.9	-1.2	-1.5	-1%	-1%	-1%	Low
		8	.	.	.	.	.	.	
		12	1.1	1.2	1.4	1%	1%	1%	
		24	3.2	3.5	3.9	4%	3%	3%	
Subbase Type	**Asphalt Concrete**		.	.	.	.	.	.	Low
	Cement Stabilized		1.4	1.7	1.6	2%	1%	1%	
	Asphalt Stabilized		1.9	2.3	2.0	2%	2%	1%	
	Granular		-0.5	-0.5	-0.5	-1%	0%	0%	
	Existing PCCP		-1.7	-2.0	-1.8	-2%	-2%	-1%	
Subgrade Thickness	in	24	0.0	0.0	0.0	0%	0%	0%	None
		40	.	.	.	.	.	.	
		60	0.0	0.0	0.0	0%	0%	0%	
Time of Placement	hr	2am	-5.4	-8.9	-10.2	-7%	-8%	-7%	High
		8am	.	.	.	.	.	.	
		Noon	2.4	1.8	4.6	3%	2%	3%	
		5pm	-0.4	-8.7	-9.7	0%	-8%	-7%	
		10pm	-5.1	-8.4	-11.4	-6%	-7%	-8%	

Note: Values in bold represent the baseline condition.

Table F-2: Sensitivity analysis results for the **maximum concrete temperature**

Variables	**Units**	**Range**	Change in Temperature, °F			% Change from Base Line			**Sensitivity Rating**
			Paving Climate			**Paving Climate**			
			Cold	Normal	Hot	Cold	Normal	Hot	
MIXTURE PROPORTION									
Cement Factor	Sacks	5.0	-2.7	-4.0	-4.2	-3%	-3%	-3%	Moderate
		6.0	·	·	·	·	·	·	
		7.5	4.3	6.2	6.7	5%	5%	5%	
Water/cementitious ratio	-	0.35	-1.0	-1.4	-1.5	-1%	-1%	-1%	Low
		0.45	·	·	·	·	·	·	
		0.55	0.4	0.7	0.7	1%	1%	1%	
Class C Ash Content	%	0	·	·	·	·	·	·	High
(CaO = 29%)		20	-1.9	-2.5	-1.3	-2%	-2%	-1%	
		35	-3.2	-8.7	-6.1	-4%	-8%	-4%	
Class F Ash Content	%	0	·	·	·	·	·	·	High
(CaO = 14%)		20	-2.2	-2.5	-3.8	-3%	-2%	-3%	
		35	-2.6	-7.1	-8.3	-3%	-6%	-6%	
Class F Ash Content	%	0	·	·	·	·	·	·	High
(CaO = 5%)		20	-2.2	-3.0	-5.4	-3%	-3%	-4%	
		35	-3.2	-7.2	-10.1	-4%	-6%	-7%	
GGBF Slag Content	%	0	·	·	·	·	·	·	Moderate
		30	-3.7	-3.8	-2.9	-5%	-3%	-2%	
		50	-5.1	-7.8	-5.7	-6%	-7%	-4%	

Note: Values in bold represent the baseline condition.

Table F-3: Sensitivity analysis results for the **maximum concrete temperature**

Variables	**Units**	**Range**	Change in Temperature, °F			% Change from Base Line			**Sensitivity Rating**
			Paving Climate			**Paving Climate**			
			Cold	Normal	Hot	Cold	Normal	Hot	
MATERIALS INPUTS									
Cement Type	-	**Type I**	·	·	·	·	·	·	High
		Type II	-6.5	-12.6	-14.0	-8%	-11%	-10%	
		Type III	11.5	12.1	10.2	14%	11%	7%	
Blaine Value	m^2/kg	280	-1.6	-1.0	0.2	-2%	-1%	0%	Moderate
		350	·	·	·	·	·	·	
		550	4.3	0.5	-1.2	5%	0%	-1%	
Activation Energy	J/mol	30,000	-0.2	-3.3	-4.3	0%	-3%	-3%	Moderate
		40,000	·	·	·	·	·	·	
		55,000	0.3	5.8	6.0	0%	5%	4%	
Hydration time parameter, t	hours	10	5.4	3.8	2.6	7%	3%	2%	High
		13.7	·	·	·	·	·	·	
		35	-5.4	-11.5	-12.4	-7%	-10%	-9%	
Hydration slope parameter, b	-	0.365	0.0	-6.5	-8.3	0%	-6%	-6%	High
		0.764	·	·	·	·	·	·	
		1.2	1.5	8.4	9.4	2%	7%	7%	
Ultimate degree of hydration. a_u	-	0.65	-2.2	-3.3	-3.5	-3%	-3%	-3%	High
		0.72	·	·	·	·	·	·	
		1.00	10.6	15.4	16.9	13%	13%	12%	
Aggregate Type		**Limestone**	·	·	·	·	·	·	Low
		River Gravel	1.4	2.1	2.2	2%	2%	2%	
CTE	eμ/°F	4.0	0.0	0.0	0.0	0%	0%	0%	None
		6.0	·	·	·	·	·	·	
		8.5	0.0	0.0	0.0	0%	0%	0%	

Note: Values in bold represent the baseline condition.

Table F-4: Sensitivity analysis results for the **maximum concrete temperature**

Variables	Units	Range	Change in Temperature, °F			% Change from Base Line			Sensitivity Rating
			Paving Climate			**Paving Climate**			
			Cold	Normal	Hot	Cold	Normal	Hot	
ENVIRONMENTAL									
Relative Humidity	%	30	-0.6	-0.7	-0.6	-1%	-1%	0%	None
(constant values)		**60**	·	·	·	·	·	·	
		100	0.5	0.4	0.4	1%	0%	0%	
Wind Speed	mph	**5**	·	·	·	·	·	·	Moderate
(constant values)		10	-1.4	-2.3	-3.4	-2%	-2%	-2%	
		25	-3.1	-5.2	-7.0	-4%	-5%	-5%	
Solar Radiation	W/m2	650	·	-2.9	-4.8	·	-3%	-4%	Moderate
		900	3.1	·	-2.0	4%	·	-2%	
		1250	7.8	4.2	1.1	10%	4%	1%	
Cloud Cover	%	0	2.5	3.7	5.1	3%	3%	4%	High
		30	·	·	·	·	·	·	
		60	-2.5	-3.5	-4.1	-3%	-3%	-3%	
		100	-5.8	-8.8	-10.7	-7%	-8%	-8%	
Deep ground temperature	°C	16	0.0	0.0	0.0	0%	0%	0%	None
		21	·	·	·	·	·	·	
		26	0.0	0.0	0.0	0%	0%	0.0	
CONSTRUCTION INPUTS									
Fresh Concrete Temperature	°F	Air- 10°F	-2.8	-5.4	-4.9	-4%	-5%	-4%	High
		At Air	·	·	·	-	-	-	
		Air+10°F	6.0	5.2	10.5	8%	5%	8%	
Base temperature	°F	Air- 10°F	-3.3	-2.8	-5.7	-4%	-2%	-4%	Moderate
		At Air	·	·	·	-	-	-	
		Air+10°F	3.5	2.9	6.1	4%	3%	4%	
White wash base	-	**No**	·	·	·	-	-	-	Low
		Yes	-1.4	-1.5	-1.9	-1.7%	-1.3%	-1.4%	
Curing method	-	None	1.4	1.8	2.5	2%	2%	2%	Low
		Single Coat CC	0.7	0.9	1.2	1%	1%	1%	
		Double Coat CC	·	·	·	-	-	-	
		Plastic Sheeting	3.0	1.2	2.0	4%	1%	1%	
Color of plastic sheet	-	**None**	·	·	·	-	-	-	High
		White	0.1	1.2	2.0	0%	1%	1%	
		Yellow	3.7	5.1	7.4	5%	4%	5%	
		Black	10.6	13.6	18.9	13%	12%	14%	
Blanket Thickness	inches	**None**	·	·	·	-	-	-	High
		0.75	8.3	6.8	10.2	10%	6%	7%	
		1.50	10.0	7.8	11.7	13%	7%	8%	

Note: Values in bold represent the baseline condition.

Table F-5: Sensitivity analysis results for the **time to final set**

Variables	**Units**	**Range**	Change in set time, hrs			% Change from Base Line			**Sensitivity Rating**
			Paving Climate			**Paving Climate**			
			Cold	Normal	Hot	Cold	Normal	Hot	
GENERAL INPUTS									
PCC Thickness	in	7	-0.2	-0.1	0.0	-3%	-2%	-1%	None
		10	-0.1	0.0	0.0	-1%	0%	0%	
		12	·	·	·	·	·	·	
		18	0.2	0.0	0.0	2%	1%	1%	
Subbase Thickness	in	4	0.1	0.0	0.0	1%	1%	1%	None
		8	·	·	·	·	·	·	
		12	-0.1	0.0	0.0	-1%	-1%	-1%	
		24	-0.2	-0.1	0.0	-2%	-2%	-2%	
Subbase Type	**Asphalt Concrete**		·	·	·	·	·	·	None
	Cement Stabilized		0.0	0.0	0.0	0%	0%	0%	
	Asphalt Stabilized		0.0	0.0	0.0	-1%	0%	0%	
	Granular		0.0	0.0	0.0	0%	0%	0%	
	Existing PCCP		0.1	0.0	0.0	1%	1%	1%	
Subgrade Thickness	in	24	0.0	0.0	0.0	0%	0%	0%	None
		40	·	·	·	·	·	·	
		60	0.0	0.0	0.0	0%	0%	0%	
Time of Placement	hr	2am	5.4	2.2	1.5	69%	54%	56%	High
		8am	·	·	·	·	·	·	
		Noon	-1.8	-0.9	-0.6	-23%	-21%	-22%	
		5pm	-0.3	-0.4	-0.3	-3%	-10%	-13%	
		10pm	4.7	1.5	0.9	60%	37%	35%	

Note: Values in bold represent the baseline condition.

Table F-6: Sensitivity analysis results for the **time to final set**

Variables	Units	Range	Change in set time, hrs			% Change from Base Line			Sensitivity Rating
			Paving Climate			**Paving Climate**			
			Cold	Normal	Hot	Cold	Normal	Hot	
MIXTURE PROPORTION									
Cement Factor	Sacks	5.0	0.1	0.0	0.0	1%	1%	1%	None
		6.0	·	·	·	·	·	·	
		7.5	-0.1	-0.1	0.0	-1%	-1%	-1%	
Water/cementitious ratio	-	0.35	-0.6	-0.3	-0.2	-8%	-8%	-8%	Low
		0.45	·	·	·	·	·	·	
		0.55	0.6	0.3	0.2	8%	8%	9%	
Class C Ash Content	%	0	·	·	·	·	·	·	High
(CaO = 29%)		20	4.1	2.0	2.0	52%	48%	78%	
		35	9.5	4.4	4.0	120%	106%	156%	
Class F Ash Content	%	0	·	·	·	·	·	·	High
(CaO = 14%)		20	1.4	0.8	1.2	18%	20%	48%	
		35	2.8	1.8	2.3	35%	43%	87%	
Class F Ash Content	%	0	·	·	·	·	·	·	High
(CaO = 5%)		20	0.2	0.2	0.8	2%	5%	32%	
		35	9.5	0.5	1.4	120%	13%	53%	
GGBF Slag Content	%	0	·	·	·	·	·	·	High
		30	3.1	1.1	1.0	40%	27%	38%	
		50	5.6	2.0	1.5	72%	48%	56%	

Note: Values in bold represent the baseline condition.

Table F-7: Sensitivity analysis results for the **time to final set**

Variables	**Units**	**Range**	Change in set time, hrs			% Change from Base Line			**Sensitivity Rating**
			Paving Climate			**Paving Climate**			
			Cold	Normal	Hot	Cold	Normal	Hot	
MATERIALS INPUTS									
Cement Type	-	**Type I**	·	·	·	·	·	·	High
		Type II	2.2	1.3	0.9	28%	31%	33%	
		Type III	-2.3	-1.9	-1.4	-29%	-45%	-54%	
Blaine Value	m^2/kg	280	2.2	1.2	1.3	28%	29%	49%	High
		350	·	·	·	·	·	·	
		550	-3.3	-1.8	-1.2	-43%	-44%	-45%	
Activation Energy	J/mol	30,000	-0.5	0.4	0.6	-6%	9%	23%	Low
		40,000	·	·	·	·	·	·	
		55,000	0.7	-0.5	-0.7	9%	-12%	-26%	
Hydration time parameter, t	hours	10	-1.9	-1.1	-0.7	-25%	-26%	-26%	High
		13.7	·	·	·	·	·	·	
		35	12.3	5.5	3.6	156%	132%	139%	
Hydration slope parameter, b	-	0.365	-4.6	-2.5	-1.6	-59%	-60%	-60%	High
		0.764	·	·	·	·	·	·	
		1.2	2.6	1.4	0.9	33%	35%	36%	
Ultimate degree of hydration. a_u	-	0.65	0.5	0.3	0.2	7%	7%	7%	Moderate
		0.72	·	·	·	·	·	·	
		1.00	-1.3	-0.7	-0.5	-17%	-17%	-18%	
Aggregate Type		**Limestone**	·	·	·	·	·	·	None
		River Gravel	-0.1	-0.1	0.0	-1%	-1%	-1%	
CTE	eμ/°F	4.0	0.0	0.0	0.0	0%	0%	0%	None
		6.0	·	·	·	·	·	·	
		8.5	0.0	0.0	0.0	0%	0%	0%	

Note: Values in bold represent the baseline condition.

Table F-8: Sensitivity analysis results for the **time to final set**

Variables	Units	Range	Change in set time, hrs			% Change from Base Line			Sensitivity Rating
			Paving Climate			**Paving Climate**			
			Cold	Normal	Hot	Cold	Normal	Hot	
ENVIRONMENTAL									
Relative Humidity	%	30	0.1	0.0	0.0	1%	1%	0%	None
(constant values)		**60**	·	·	·	·	·	·	
		100	0.0	0.0	0.0	0%	0%	0%	
Wind Speed	mph	**5**	·	·	·	·	·	·	None
(constant values)		10	0.0	0.0	0.0	1%	0%	1%	
		25	0.1	0.0	0.0	1%	1%	1%	
Solar Radiation	W/m2	650	·	0.1	0.0	-	1%	2%	Low
		900	-0.2	·	0.0	-3%	·	1%	
		1250	-0.5	-0.1	0.0	-7%	-2%	0%	
Cloud Cover	%	0	-0.2	-0.1	0.0	-2%	-1%	-1%	Low
		30	·	·	·	·	·	·	
		60	0.2	0.1	0.0	3%	1%	1%	
		100	0.6	0.2	0.1	8%	4%	3%	
Deep ground temperature	°C	16	0.0	0.0	0.0	0%	0%	0%	None
		21	·	·	·	·	·	·	
		26	0.0	0.0	0.0	0%	0%	0%	
CONSTRUCTION INPUTS									
Fresh Concrete Temperature	°F	Air- 10°F	1.6	1.0	0.5	21%	23%	21%	High
		At Air	·	·	·	·	·	·	
		Air+10°F	-1.4	-0.8	-0.5	-18%	-20%	-18%	
Base temperature	°F	Air- 10°F	0.4	0.1	0.1	5%	3%	5%	None
		At Air	·	·	·	·	·	·	
		Air+10°F	-0.3	-0.1	-0.1	-4%	-3%	-4%	
White wash base	-	**No**	·	·	·	·	·	·	None
		Yes	0.2	0.1	0.0	2%	2%	2%	
Curing method		None	-0.1	0.0	0.0	-2%	-1%	-2%	None
		Single Coat CC	-0.1	0.0	0.0	-1%	0%	-1%	
		Double Coat CC	·	·	·	·	·	·	
		Plastic Sheeting	0.2	0.0	0.0	2%	1%	1%	
Color of plastic sheet	-	**None**	·	·	·	·	·	·	None
		White	0.2	0.0	0.0	2%	1%	1%	
		Yellow	0.0	0.0	0.0	-1%	0%	0%	
		Black	-0.4	-0.1	0.0	-5%	-3%	-2%	
Blanket Thickness	inches	**None**	·	·	·	·	·	·	None
		0.75	0.2	0.0	0.0	2%	1%	1%	
		1.50	0.2	0.0	0.0	2%	1%	1%	

Note: Values in bold represent the baseline condition.

Table F-9: Sensitivity analysis results for the **zero-stress temperature**

Variables	**Units**	**Range**	Change in Zero-Stress T, °F			% Change from Base Line			**Sensitivity Rating**
			Paving Climate			**Paving Climate**			
			Cold	Normal	Hot	Cold	Normal	Hot	
GENERAL INPUTS									
PCC Thickness	in	7	-1.2	-1.7	-3.4	-2%	-2%	-3%	Low
		10	-0.6	-0.8	-1.7	-1%	-1%	-1%	
		12	.	.	.	.	.	.	
		18	1.9	2.0	1.5	3%	2%	1%	
Subbase Thickness	in	4	-0.7	-0.8	-1.2	-1%	-1%	-1%	Low
		8	.	.	.	.	.	.	
		12	1.0	1.2	1.6	1%	1%	1%	
		24	2.2	2.5	2.6	3%	2%	2%	
Subbase Type	**Asphalt Concrete**		.	.	.	.	.	.	Low
	Cement Stabilized		0.7	0.9	0.5	1%	1%	0%	
	Asphalt Stabilized		1.2	1.5	1.1	2%	1%	1%	
	Granular		-0.5	0.2	-0.8	-1%	0%	-1%	
	Existing PCCP		-1.3	-1.6	-2.8	-2%	-1%	-2%	
Subgrade Thickness	in	24	0.0	0.0	0.0	0%	0%	0%	None
		40	.	.	.	.	.	.	
		60	0.0	0.0	0.0	0%	0%	0%	
Time of Placement	hr	2am	-11.5	-11.2	-16.2	-15%	-10%	-13%	High
		8am	.	.	.	.	.	.	
		Noon	3.0	3.1	5.6	4%	3%	4%	
		5pm	-1.9	-9.5	-5.7	-3%	-9%	-4%	
		10pm	-8.0	-13.5	-17.4	-11%	-13%	-14%	

Note: Values in bold represent the baseline condition.

Table F-10: Sensitivity analysis results for the **zero-stress temperature**

Variables	**Units**	**Range**	Change in Zero-Stress T, °F			% Change from Base Line			**Sensitivity Rating**
			Paving Climate			**Paving Climate**			
			Cold	Normal	Hot	Cold	Normal	Hot	
MIXTURE PROPORTION									
Cement Factor	Sacks	5.0	-1.7	-3.0	-4.1	-2%	-3%	-3%	Moderate
		6.0	·	·	·	·	·	·	
		7.5	3.2	4.7	4.2	4%	4%	3%	
Water/cementitious ratio	-	0.35	-1.1	-0.7	-1.8	-2%	-1%	-1%	Low
		0.45	·	·	·	·	·	·	
		0.55	0.6	0.9	-0.6	1%	1%	0%	
Class C Ash Content	%	0	·	·	·	·	·	·	High
(CaO = 29%)		20	-4.5	-1.5	-1.9	-6%	-1%	-1%	
		35	-12.7	-5.9	-4.2	-17%	-5%	-3%	
Class F Ash Content	%	0	·	·	·	·	·	·	Moderate
(CaO = 14%)		20	-2.6	-2.0	-1.9	-3%	-2%	-2%	
		35	-4.3	-5.0	-5.5	-6%	-5%	-4%	
Class F Ash Content	%	0	·	·	·	·	·	·	High
(CaO = 5%)		20	-1.9	-2.2	-3.8	-3%	-2%	-3%	
		35	-12.7	-5.5	-5.6	-17%	-5%	-4%	
GGBF Slag Content	%	0	·	·	·	·	·	·	High
		30	-4.0	-3.0	-3.2	-5%	-3%	-3%	
		50	-8.5	-5.4	-6.3	-11%	-5%	-5%	

Note: Values in bold represent the baseline condition.

Table F-11: Sensitivity analysis results for the **zero-stress temperature**

Variables	Units	Range	Change in Zero-Stress T, °F			% Change from Base Line			Sensitivity Rating
			Paving Climate			Paving Climate			
			Cold	Normal	Hot	Cold	Normal	Hot	
MATERIALS INPUTS									
Cement Type	-	**Type I**	·	·	·	·	·	·	High
		Type II	-5.4	-11.0	-12.0	-7%	-10%	-9%	
		Type III	8.9	7.9	8.3	12%	7%	6%	
Blaine Value	m^2/kg	280	-2.2	-0.5	-1.2	-3%	0%	-1%	Low
		350	·	·	·	·	·	·	
		550	3.2	0.3	-0.9	4%	0%	-1%	
Activation Energy	J/mol	30,000	-0.3	-2.2	-2.1	0%	-2%	-2%	Low
		40,000	·	·	·	·	·	·	
		55,000	-0.1	3.0	3.1	0%	3%	2%	
Hydration time parameter, t	hours	10	3.7	3.6	2.0	5%	3%	2%	High
		13.7	·	·	·	·	·	·	
		35	-16.0	-9.9	-7.7	-21%	-9%	-6%	
Hydration slope parameter, b	-	0.365	-0.7	-5.4	-7.4	-1%	-5%	-6%	Moderate
		0.764	·	·	·	·	·	·	
		1.2	0.2	5.4	6.1	0%	5%	5%	
Ultimate degree of hydration. a_u	-	0.65	-1.6	-1.9	-2.8	-2%	-2%	-2%	High
		0.72	·	·	·	·	·	·	
		1.00	7.6	9.6	10.0	10%	9%	8%	
Aggregate Type	**Limestone**		·	·	·	·	·	·	Low
	River Gravel		1.5	1.9	2.4	2%	2%	2%	
CTE	eμ/°F	4.0	0.0	0.0	0.0	0%	0%	0%	None
		6.0	·	·	·	·	·	·	
		8.5	0.0	0.0	0.0	0%	0%	0%	

Note: Values in bold represent the baseline condition.

Table F-12: Sensitivity analysis results for the **zero-stress temperature**

Variables	Units	Range	Change in Zero-Stress T, °F			% Change from Base Line			Sensitivity Rating
			Paving Climate			**Paving Climate**			
			Cold	Normal	Hot	Cold	Normal	Hot	
ENVIRONMENTAL									
Relative Humidity	%	30	-0.6	-0.7	-0.6	-1%	-1%	0%	None
(constant values)		**60**	·	·	·	·	·	·	
		100	0.5	0.5	0.4	1%	0%	0%	
Wind Speed	mph	**5**	·	·	·	·	·	·	Moderate
(constant values)		10	-1.4	-1.9	-2.4	-2%	-2%	-2%	
		25	-2.7	-3.6	-5.1	-4%	-3%	-4%	
Solar Radiation	W/m2	650	·	-1.4	-2.5	·	-2%	-3%	Moderate
		900	2.9	·	-1.4	4%	·	-1%	
		1250	6.8	3.7	-	9%	3%	1%	
Cloud Cover	%	0	2.2	3.1	2.8	3%	3%	2%	Moderate
		30	·	·	·	·	·	·	
		60	-2.2	-2.9	-3.2	-3%	-3%	-2%	
		100	-5.6	-7.3	-7.5	-7%	-7%	-6%	
Deep ground temperature	°C	16	0.0	-0.1	0.0	0%	0%	0%	None
		21	·	·	·	·	·	·	
		26	0.0	-0.1	0.0	0%	0%	0%	
CONSTRUCTION INPUTS									
Fresh Concrete Temperature	°F	Air- 10°F	-5.7	-4.9	-9.7	-8%	-5%	-8%	High
		At Air	·	·	·	·	·	·	
		Air+10°F	5.6	5.0	9.5	7%	5%	7%	
Base temperature	°F	Air- 10°F	-3.0	-2.5	-5.1	-4%	-2%	-4%	Moderate
		At Air	·	·	·	·	·	·	
		Air+10°F	2.9	2.5	4.9	4%	2%	4%	
White wash base	-	**No**	·	·	·	·	·	·	Low
		Yes	-1.1	-2.1	-1.5	-1%	-2%	-1%	
Curing method		None	1.5	2.0	2.5	2%	2%	2%	Low
		Single Coat CC	0.5	0.5	0.8	1%	0%	1%	
		Double Coat CC	·	·	·	·	·	·	
		Plastic Sheeting	2.0	0.7	0.4	3%	1%	0%	
Color of plastic sheet	-	**None**	·	·	·	·	·	·	High
		White	0.4	0.7	0.4	0%	1%	0%	
		Yellow	3.1	3.7	2.8	4%	3%	2%	
		Black	7.6	8.5	8.3	10%	8%	6%	
Blanket Thickness	inches	**None**	·	·	·	·	·	·	High
		0.75	4.4	4.5	4.2	6%	4%	3%	
		1.50	10.3	5.0	5.1	14%	5%	4%	

Note: Values in bold represent the baseline condition.

Table F-13: Results for the ratio $\mathbf{R_d = (T_{max} - T_{zs}) / T_{max}}$

Variables	Units	Range	R_d	
			Paving Climate	
			Normal	Hot
GENERAL INPUTS				
PCC Thickness	in	7	-4%	-7%
		10	-5%	-8%
		12	·	·
		18	-9%	-10%
Subbase Thickness	in	4	-6%	-8%
		8	·	·
		12	-6%	-8%
		24	-7%	-8%
Subbase Type	**Asphalt Concrete**		·	·
	Cement Stabilized		-7%	-8%
	Asphalt Stabilized		-7%	-8%
	Granular		-6%	-8%
	Existing PCCP		-6%	-9%
Subgrade Thickness	in	24	-6%	-8%
		40	·	·
		60	-6%	-8%
Average Ratio			**-6%**	**-8%**

Table F-14: Results for the ratio $\mathbf{R_d = (T_{max} - T_{zs}) / T_{max}}$

Variables	**Units**	**Range**	$\mathbf{R_d}$	
			Paving Climate	**Paving Climate**
			Normal	Normal
MIXTURE PROPORTION				
Cement Factor	Sacks	5.0	-5%	-8%
		6.0	·	·
		7.5	-7%	-9%
Water/cementitious ratio	-	0.35	-6%	-8%
		0.45	·	·
		0.55	-6%	-9%
Class C Ash Content	%	0	·	·
(CaO = 29%)		20	-5%	-8%
		35	-4%	-7%
Class F Ash Content	%	0	·	·
(CaO = 14%)		20	-6%	-7%
		35	-5%	-6%
Class F Ash Content	%	0	·	·
(CaO = 5%)		20	-6%	-7%
		35	-5%	-5%
GGBF Slag Content	%	0	·	·
		30	-6%	-8%
		50	-4%	-9%
Average Ratio			**-5%**	**-7%**

Table F-15: Results for the ratio $\mathbf{R_d = (T_{max} - T_{zs}) / T_{max}}$

Variables	Units	Range	R_d	
			Paving Climate	**Paving Climate**
			Normal	Normal
MATERIALS INPUTS				
Cement Type	-	**Type I**	·	·
		Type II	-5%	-7%
		Type III	-9%	-8%
Blaine Value	m^2/kg	280	-6%	-9%
		350	·	·
		550	-6%	-8%
Activation Energy	J/mol	30,000	-5%	-6%
		40,000	·	·
		55,000	-8%	-9%
Hydration time parameter, t	hours	10	-6%	-8%
		13.7	·	·
		35	-5%	-5%
Hydration slope parameter, b	-	0.365	-6%	-8%
		0.764	·	·
		1.2	-8%	-10%
Ultimate degree of hydration. a_u	-	0.65	-5%	-7%
		0.72	·	·
		1.00	-10%	-11%
Aggregate Type		**Limestone**	·	·
		River Gravel	-6%	-8%
CTE	eμ/°F	4.0	-6%	-8%
		6.0	·	·
		8.5	-6%	-8%
Average Ratio			**-7%**	**-8%**

Table F-16: Results for the ratio $\mathbf{R_d = (T_{max} – T_{zs}) / T_{max}}$

Variables	Units	Range	R_d	
			Paving Climate	**Paving Climate**
			Normal	Normal
ENVIRONMENTAL				
Relative Humidity	%	30	-6%	-8%
(constant values)		**60**	·	·
		100	-6%	-8%
Wind Speed	mph	**5**	·	·
(constant values)		10	-6%	-7%
		25	-5%	-7%
Solar Radiation	W/m2	650	-5%	-7%
		900	·	-7%
		1250	-6%	-8%
Cloud Cover	%	0	-6%	-9%
		30	·	·
		60	-6%	-7%
		100	-5%	-6%
Deep ground temperature	°C	16	-6%	-8%
		21	·	·
		26	-6%	-8%
Average Ratio			**-6%**	**-7%**
CONSTRUCTION INPUTS				
Fresh Concrete Temperature	°F	Air- 10°F	-6%	-12%
		At Air	·	·
		Air+10°F	-6%	-8%
Base temperature	°F	Air- 10°F	-6%	-8%
		At Air	·	·
		Air+10°F	-6%	-8%
White wash base	-	**No**	·	·
		Yes	-8%	-8%
Curing method		None	-6%	-8%
		Single Coat CC	-6%	-8%
		Double Coat CC		
Average Ratio			**-6%**	**-7%**

OVERALL AVERAGE	**-6%**	**-8%**

APPENDIX G

PavePro Layout and Results

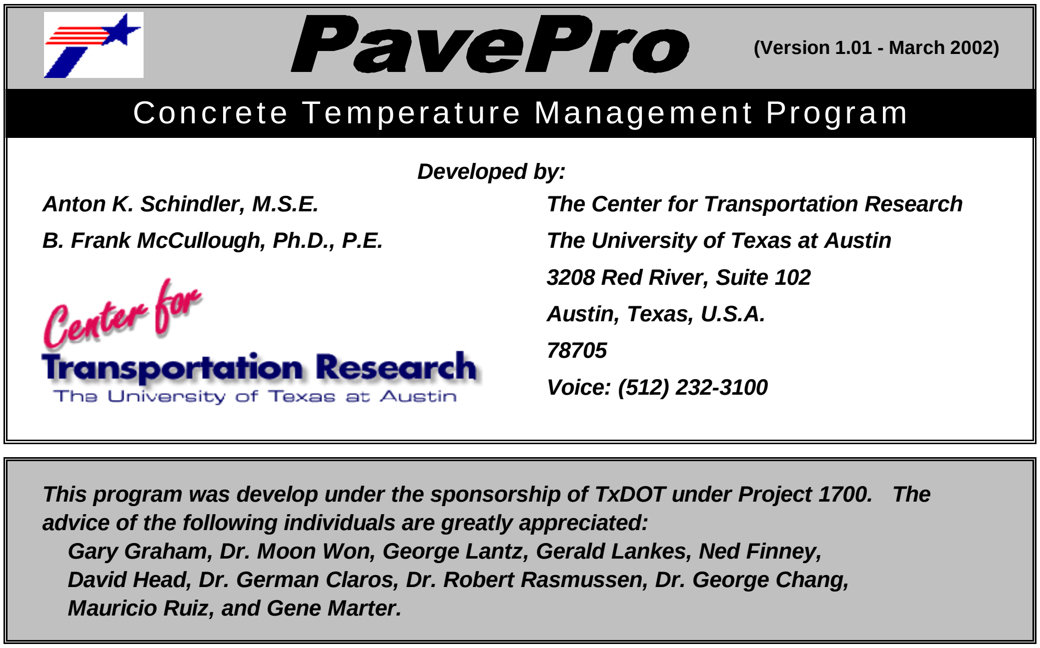

PavePro (Version 1.01 - March 2002)

Concrete Temperature Management Program

Developed by:

Anton K. Schindler, M.S.E.
B. Frank McCullough, Ph.D., P.E.

The Center for Transportation Research
The University of Texas at Austin
3208 Red River, Suite 102
Austin, Texas, U.S.A.
78705
Voice: (512) 232-3100

Center for Transportation Research
The University of Texas at Austin

This program was develop under the sponsorship of TxDOT under Project 1700. The advice of the following individuals are greatly appreciated:
Gary Graham, Dr. Moon Won, George Lantz, Gerald Lankes, Ned Finney, David Head, Dr. German Claros, Dr. Robert Rasmussen, Dr. George Chang, Mauricio Ruiz, and Gene Marter.

Figure G-1: PavePro - Title page

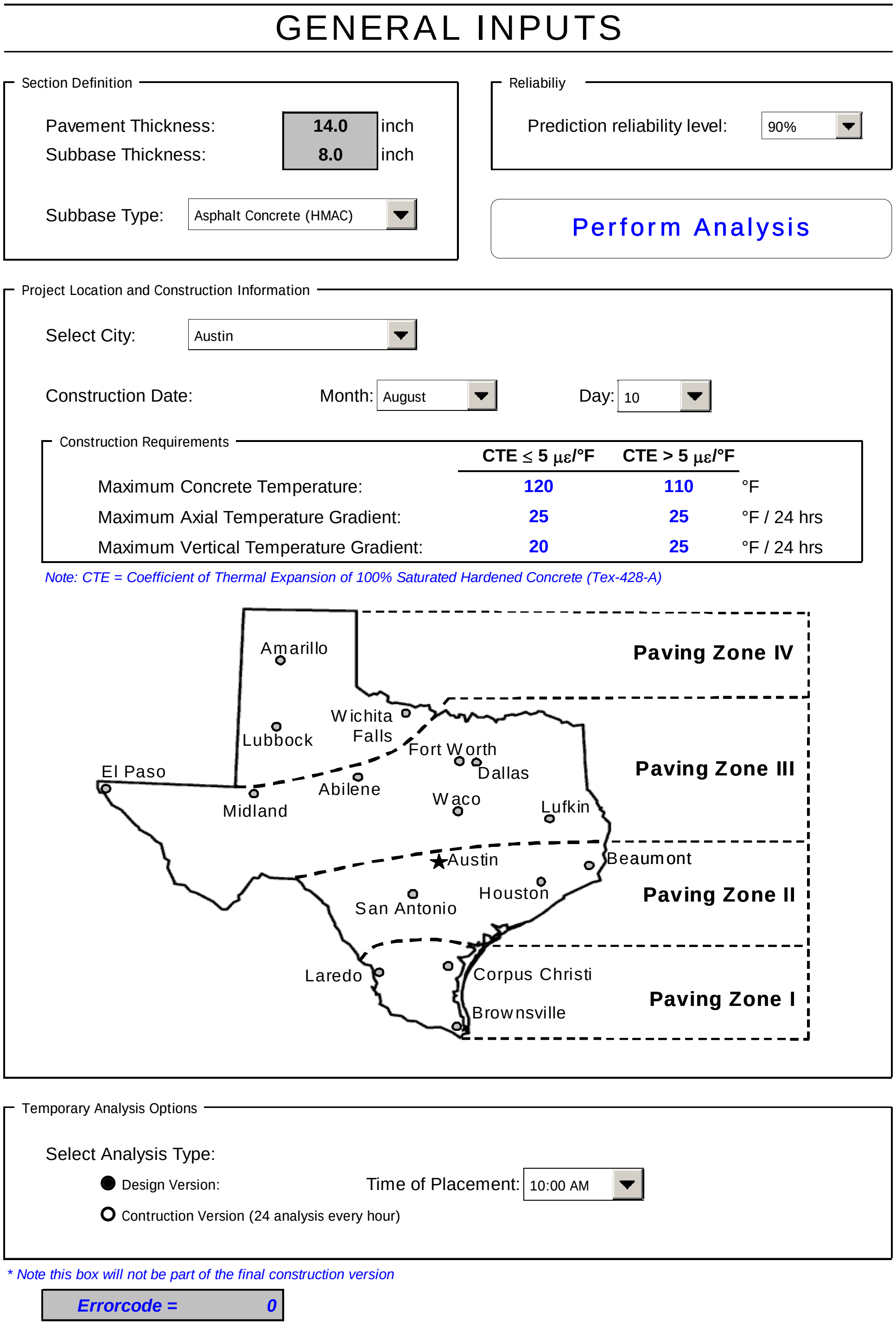

GENERAL INPUTS

Section Definition

Pavement Thickness: 14.0 inch

Subbase Thickness: 8.0 inch

Subbase Type: Asphalt Concrete (HMAC)

Reliabiliy

Prediction reliability level: 90%

Project Location and Construction Information

Select City: Austin

Construction Date: Month: August Day: 10

Construction Requirements

	CTE ≤ 5 με/°F	CTE > 5 με/°F	
Maximum Concrete Temperature:	120	110	°F
Maximum Axial Temperature Gradient:	25	25	°F / 24 hrs
Maximum Vertical Temperature Gradient:	20	25	°F / 24 hrs

Note: CTE = Coefficient of Thermal Expansion of 100% Saturated Hardened Concrete (Tex-428-A)

Temporary Analysis Options

Select Analysis Type:

● Design Version:

Time of Placement: 10:00 AM

○ Contruction Version (24 analysis every hour)

** Note this box will not be part of the final construction version*

Errorcode = 0

Figure G-2: PavePro - General Input screen

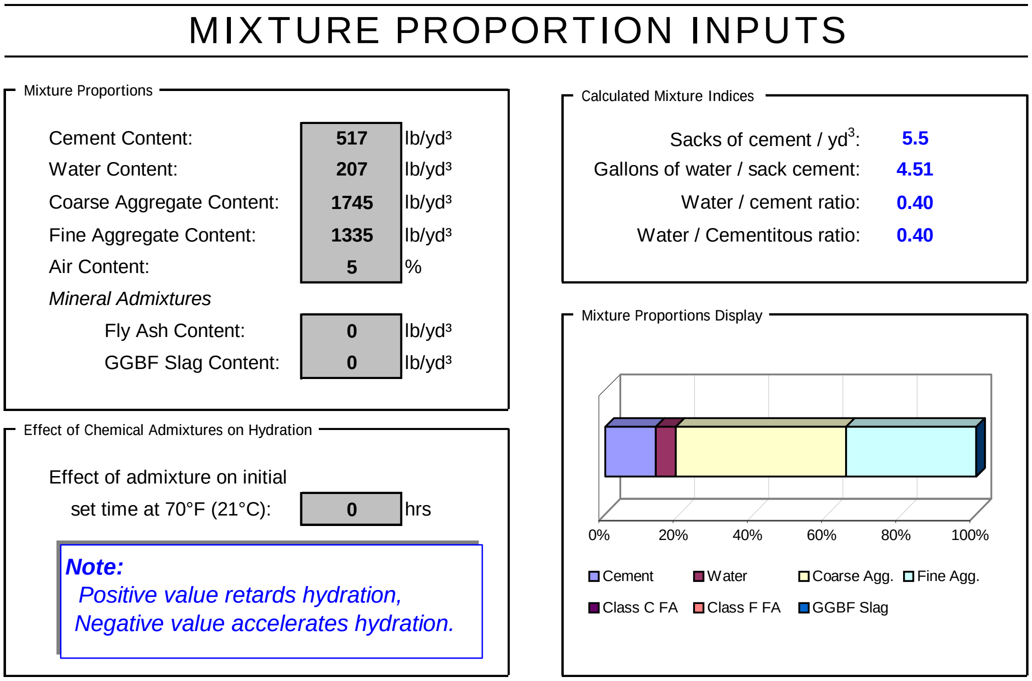

MIXTURE PROPORTION INPUTS

Mixture Proportions

Cement Content: **517** lb/yd^3
Water Content: **207** lb/yd^3
Coarse Aggregate Content: **1745** lb/yd^3
Fine Aggregate Content: **1335** lb/yd^3
Air Content: **5** %

Mineral Admixtures

Fly Ash Content: **0** lb/yd^3
GGBF Slag Content: **0** lb/yd^3

Effect of Chemical Admixtures on Hydration

Effect of admixture on initial set time at 70°F (21°C): **0** hrs

Note:
Positive value retards hydration,
Negative value accelerates hydration.

Calculated Mixture Indices

Sacks of cement / yd^3: **5.5**
Gallons of water / sack cement: **4.51**
Water / cement ratio: **0.40**
Water / Cementitous ratio: **0.40**

Mixture Proportions Display

Figure G-3: PavePro - Mixture Proportions Input screen

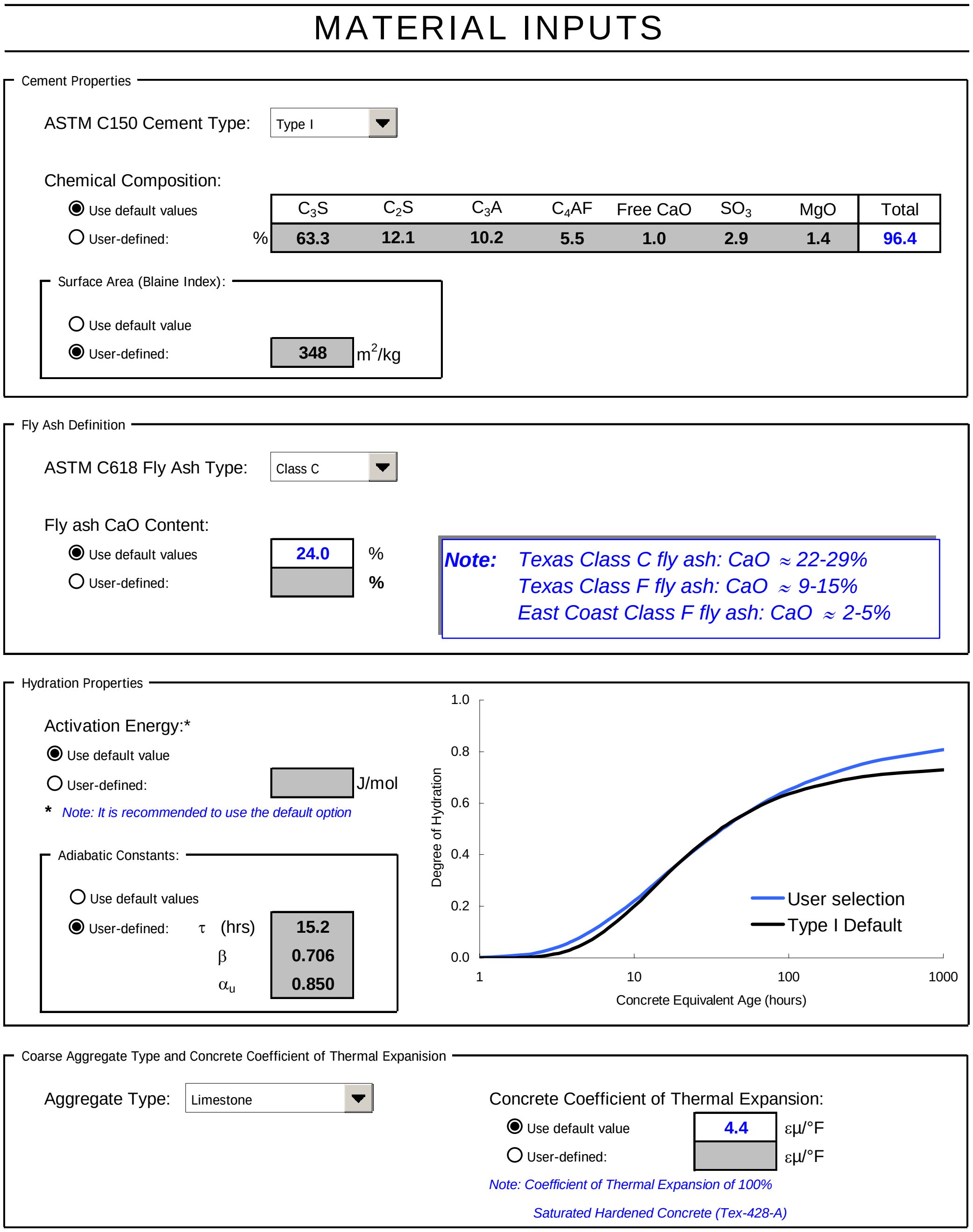

MATERIAL INPUTS

Cement Properties

ASTM C150 Cement Type: Type I

Chemical Composition:

● Use default values

○ User-defined:

	C_3S	C_2S	C_3A	C_4AF	Free CaO	SO_3	MgO	Total
%	63.3	12.1	10.2	5.5	1.0	2.9	1.4	96.4

Surface Area (Blaine Index):

○ Use default value

● User-defined: 348 m^2/kg

Fly Ash Definition

ASTM C618 Fly Ash Type: Class C

Fly ash CaO Content:

● Use default values 24.0 %

○ User-defined: %

Note: *Texas Class C fly ash: CaO ≈ 22-29%*
Texas Class F fly ash: CaO ≈ 9-15%
East Coast Class F fly ash: CaO ≈ 2-5%

Hydration Properties

Activation Energy:*

● Use default value

○ User-defined: J/mol

* *Note: It is recommended to use the default option*

Adiabatic Constants:

○ Use default values

● User-defined: τ (hrs) 15.2

β 0.706

α_u 0.850

Coarse Aggregate Type and Concrete Coefficient of Thermal Expansion

Aggregate Type: Limestone

Concrete Coefficient of Thermal Expansion:

● Use default value 4.4 εμ/°F

○ User-defined: εμ/°F

Note: Coefficient of Thermal Expansion of 100%

Saturated Hardened Concrete (Tex-428-A)

Figure G-4: PavePro - Materials Input screen

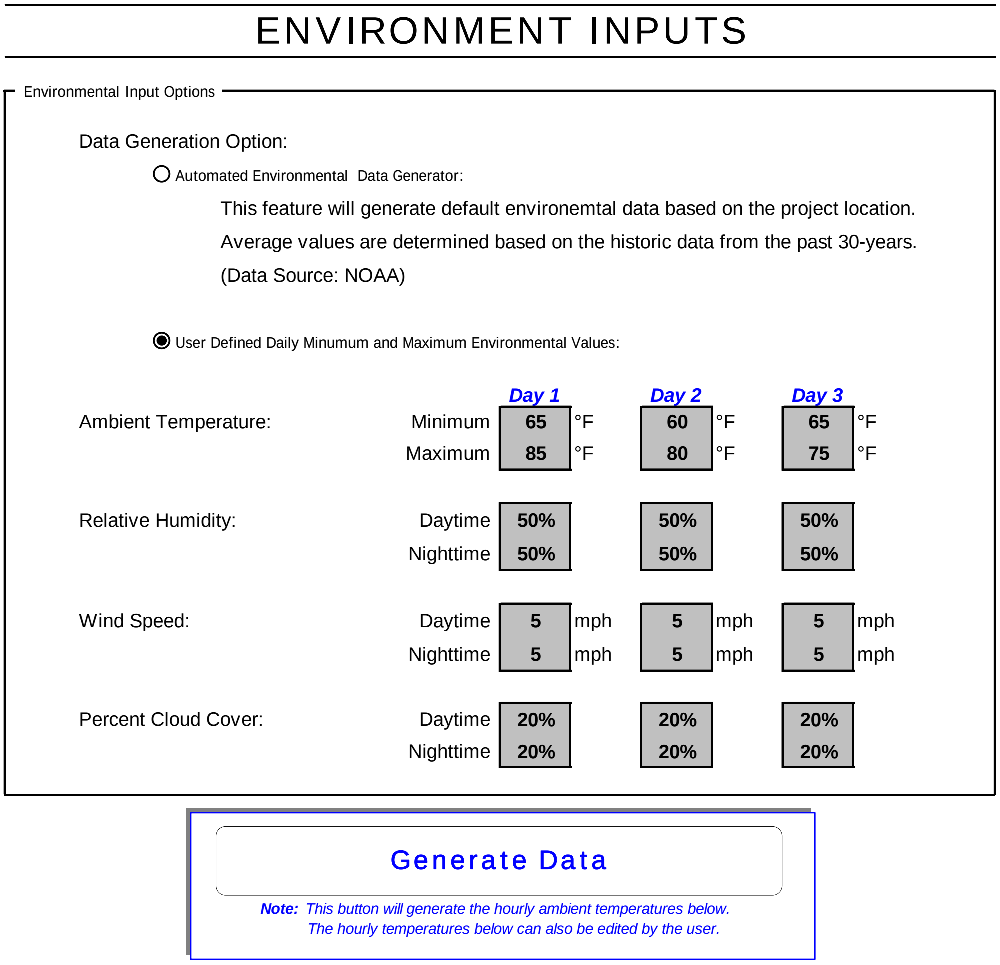

ENVIRONMENT INPUTS

Environmental Input Options

Data Generation Option:

○ Automated Environmental Data Generator:

This feature will generate default environemtal data based on the project location. Average values are determined based on the historic data from the past 30-years. (Data Source: NOAA)

● User Defined Daily Minumum and Maximum Environmental Values:

		Day 1	Day 2	Day 3
Ambient Temperature:	Minimum	65 °F	60 °F	65 °F
	Maximum	85 °F	80 °F	75 °F
Relative Humidity:	Daytime	50%	50%	50%
	Nighttime	50%	50%	50%
Wind Speed:	Daytime	5 mph	5 mph	5 mph
	Nighttime	5 mph	5 mph	5 mph
Percent Cloud Cover:	Daytime	20%	20%	20%
	Nighttime	20%	20%	20%

Note: *This button will generate the hourly ambient temperatures below. The hourly temperatures below can also be edited by the user.*

Figure G-5: PavePro - Environmental Input screen

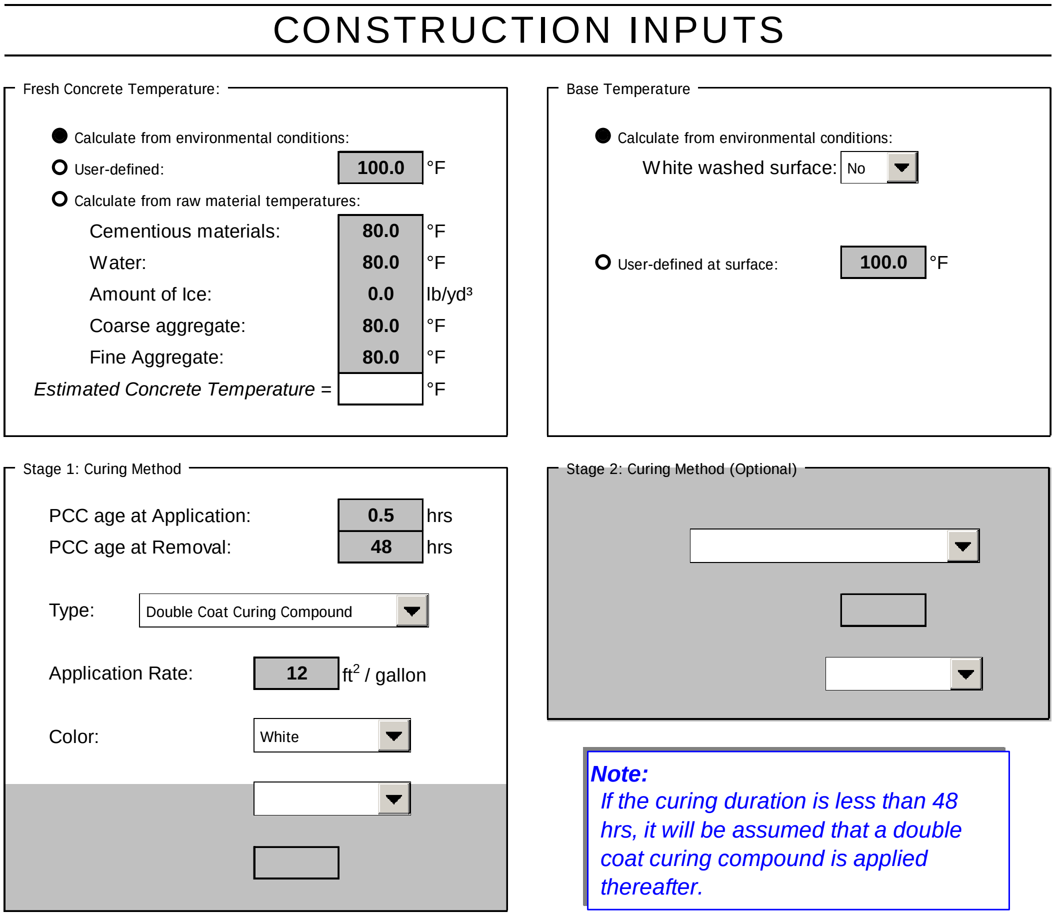

CONSTRUCTION INPUTS

Fresh Concrete Temperature:

● Calculate from environmental conditions:

○ User-defined: 100.0 °F

○ Calculate from raw material temperatures:

Cementious materials: 80.0 °F

Water: 80.0 °F

Amount of Ice: 0.0 lb/yd³

Coarse aggregate: 80.0 °F

Fine Aggregate: 80.0 °F

Estimated Concrete Temperature = °F

Base Temperature

● Calculate from environmental conditions:

White washed surface: No

○ User-defined at surface: 100.0 °F

Stage 1: Curing Method

PCC age at Application: 0.5 hrs

PCC age at Removal: 48 hrs

Type: Double Coat Curing Compound

Application Rate: 12 ft² / gallon

Color: White

Stage 2: Curing Method (Optional)

Note:
If the curing duration is less than 48 hrs, it will be assumed that a double coat curing compound is applied thereafter.

Figure G-7: PavePro - Construction Input screen

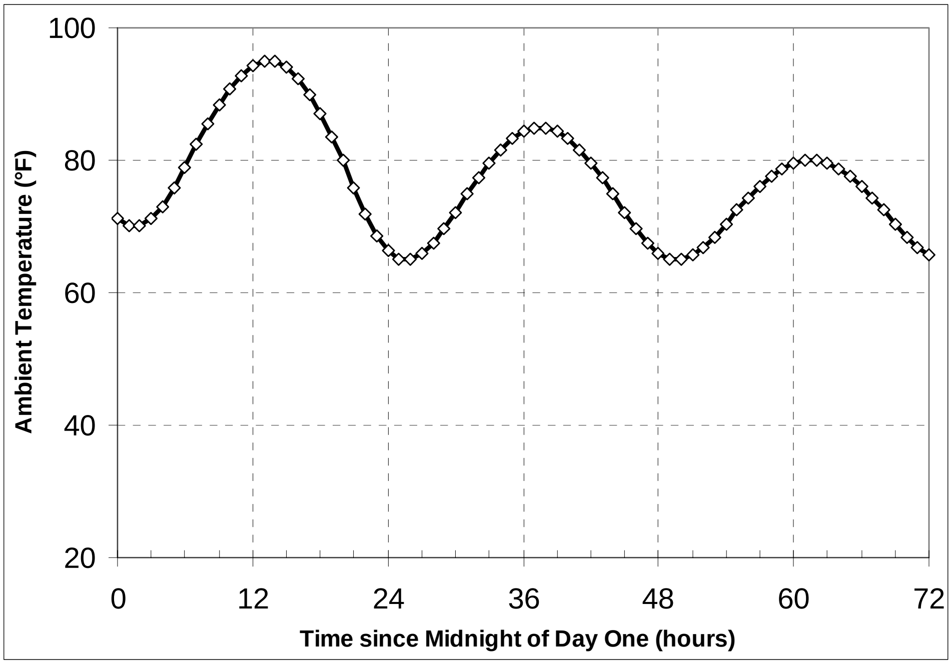

Figure G-6: PavePro - Ambient temperature review graph

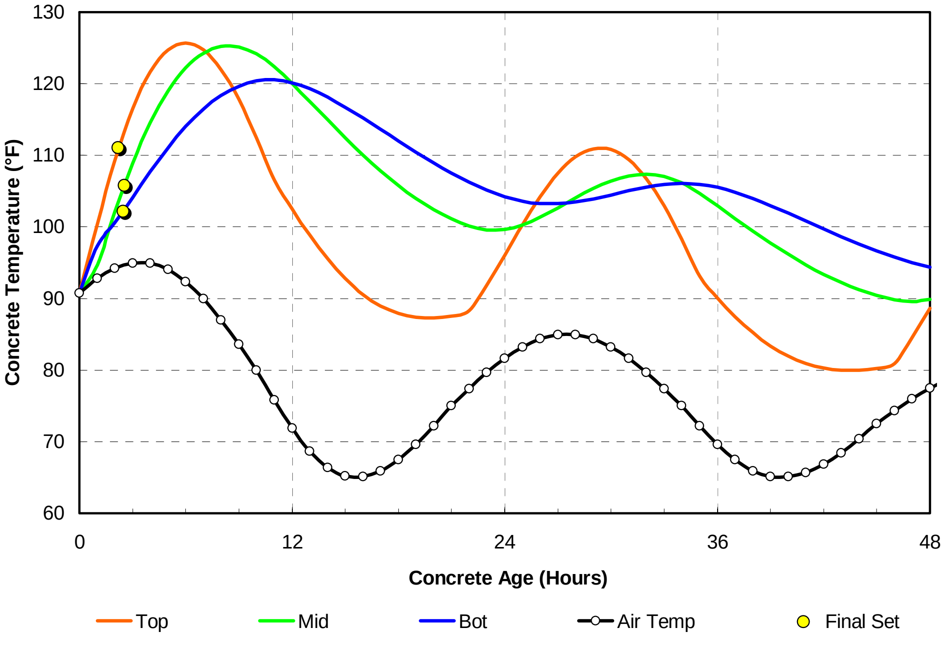

Figure G-8: PavePro – Predicted temperature history

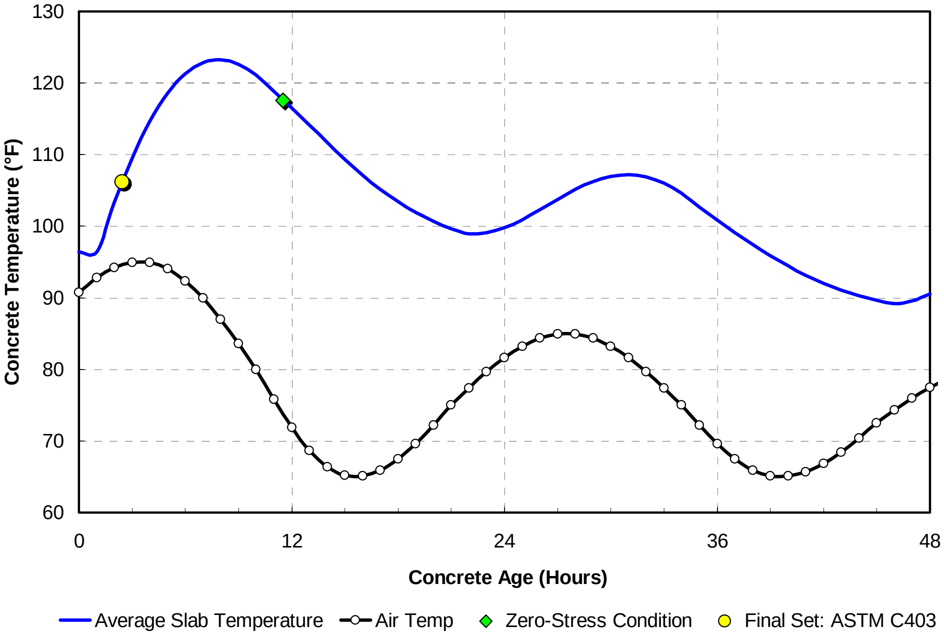

Figure G-9: PavePro – Average slab temperature and location of the zero-stress condition

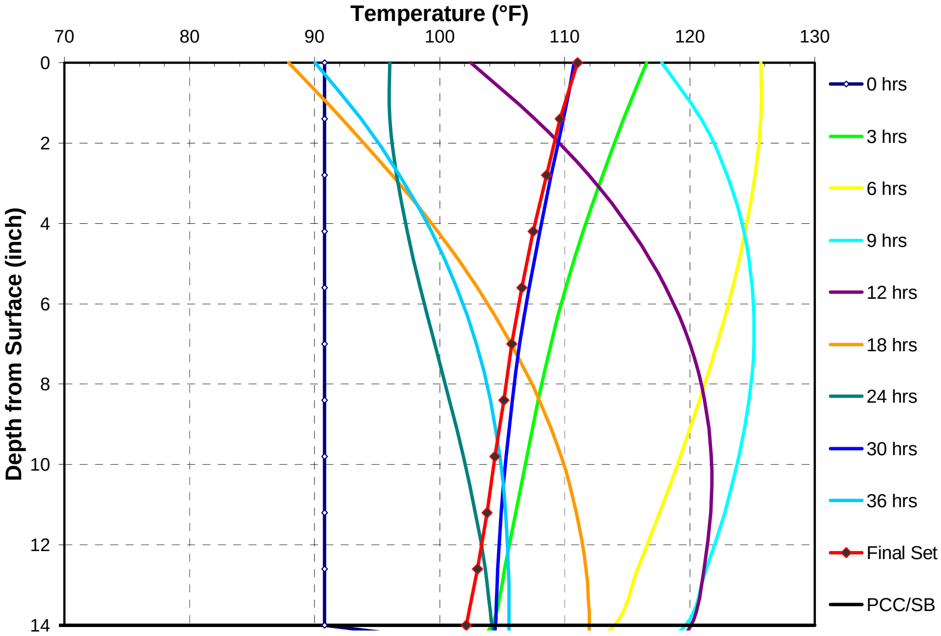

Figure G-10: PavePro – Predicted temperature distribution

APPENDIX H

Special Provision to Item 360

TxDOT Maximum In-Place Temperature Control Limits

SPECIAL PROVISION TO
ITEM 360
CONCRETE PAVEMENT

For this project, Item 360, “Concrete Pavement”, of the Standard Specifications, is hereby amended with respect to the clauses cited below and no other clauses or requirements of this Item are waived or changed hereby.

Article 360.8. Concrete Mixing and Placing, The following Subarticle is added:

(6) Maximum In-Place Concrete Temperature. During the period April 1st until October 31st, the maximum in place concrete temperature will be controlled and recorded over a minimum of 3 days. The Contractor shall develop a plan to assure that during the early-age hydration period, the in-place concrete temperature as measured at the mid-depth of the pavement shall not exceed the values listed in Table 1 or 2. The maximum in place temperature in Table 1 or 2 is determined by project location, as indicated by the Paving Zone shown in Figure 1, and by the Coefficient of Thermal Expansion (CTE) of the Hardened Concrete as tested in accordance with Tex-428-A. Table 3 provides a summary of the Paving Zones across the State of Texas.

A detailed plan, along with an analysis of the estimated in place concrete temperature development, shall be submitted to the Engineer for approval. No concrete shall be placed until this plan is approved. The plan may include a combination of the following:

1. Reducing the fresh concrete temperature. (The concrete temperature at the time of placement shall not exceed the limit specified in Article 360.8(3).)
2. Scheduling of activities at times to lower the heat of hydration
3. Selection of the cementitious materials to control the heat of hydration
   - Use of low heat cement, fly ash or GGBF slag

The Contractor shall furnish and install temperature recording devices at a minimum frequency of two (2) per 1000 linear foot of concrete, or per paving day. The time of the installation of the temperature recording devices will as be as determined by the Engineer.

Table 1: Current TxDOT Reinforcement Standards

Paving Zone	Maximum In Place Concrete Temperature (°F)		
	CTE ≤ 5.0	5.0 < CTE ≤ 6.5	CTE > 6.5
I	130	120	110
II	130	115	105
III	130	110	100
IV	122	105	na

Table 2: New Grade 70 Reinforcement Standard

Paving Zone	Maximum In Place Concrete Temperature (°F)		
	CTE ≤ 5.0	5.0 < CTE ≤ 6.5	CTE > 6.5
I	-	130	130
II	-	130	130
III	-	130	120
IV	130	120	120

Note: *na = not applicable

CTE = Coefficient of Thermal Expansion of 100% Saturated Hardened Concrete (Tex-428-A) in $1\text{x}10^{-6}$/°F.

Table 3: Summary of Paving Zones cross the State of Texas

Paving Zone	Combined Districts	Major Cities
I	Lower Coast / Lower Valley	Corpus Christi, Laredo, Brownsville
II	East coast / Lower South	Houston, San Antonio, Austin, Beaumont, Victoria
III	West, East, and Central Texas	Dallas, Forth Worth, El Paso, Waco, Lufkin, Abilene, Midland
IV	North Texas and Panhandle	Amarillo, Lubbock, Wichita Falls

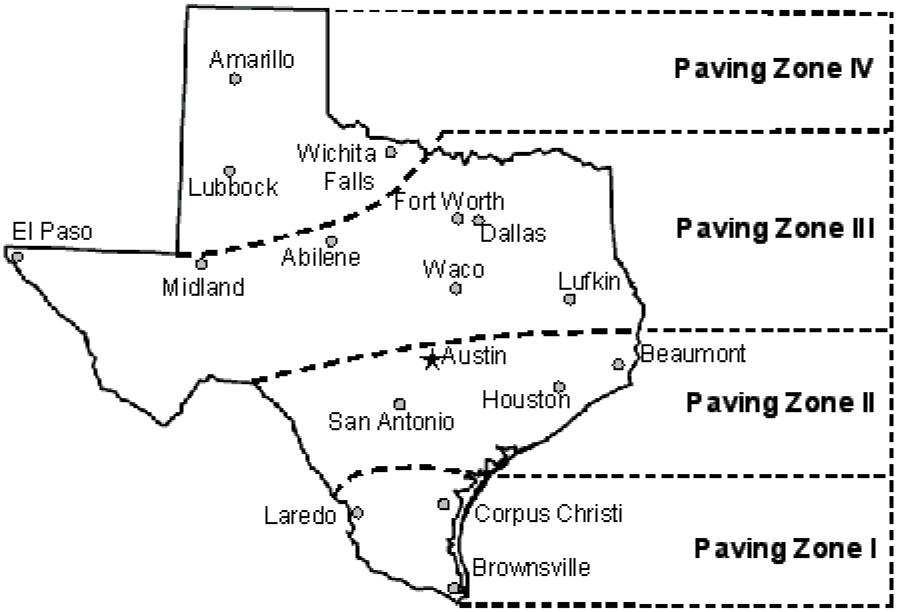

Figure 1: Paving Zones in Texas